

Newcastle
University

Molecular understanding of fungal cell
wall metabolism by gut *Bacteroides*

Ekaterina Buzun

A Thesis Submitted for the Degree of Doctor of Philosophy

2017 – 2021

Biosciences Institute
Faculty of Medical Sciences
Newcastle University

Abstract

The human gut is populated with a vast community of microbes, the microbiota. The Bacteroidetes play a prominent role in the breakdown of complex carbohydrates. Fungi are also normal members of the gut microbiota. Fungal cell wall proteins are extensively mannosylated, forming a highly branched matrix of mannan. Previous data from our lab show that the common gut bacterium, *Bacteroides thetaiotaomicron* (Bt) degrades cell wall mannan from *S. cerevisiae* via a selfish mechanism. Bt does this by releasing large oligosaccharides at the cell surface, which are transported into the periplasmic space to be further depolymerised.

Firstly, the degradation of mannan from a common human pathogen, *Candida albicans* was investigated. Here, novel enzymes from the Glycoside Hydrolase 130 family, which target β -1,2-mannosidic linkages found in *C. albicans* mannan, have been biochemically characterised. Bt was genetically manipulated to examine its ability to utilise mannan from *C. albicans*. This work demonstrated that degradation of *C. albicans* mannan in Bt requires an additional regulatory mechanism.

Secondly, I discovered that another gut Bacteroides, *B. salyersiae* (Bs), degrades yeast α -mannan in a mechanism contrasting to the 'selfish' strategy. Unlike Bt, Bs releases a range of smaller manno-oligosaccharides into the extracellular milieu, which are utilised as 'public goods' by other members of the gut microbiota. Biochemical characterisation of this alternative mechanism revealed that proteins orchestrating mannan breakdown contain signals, targeting them for the Bacteroidetes specific type 9 secretion system (T9SS). Our analysis revealed that Bs directs at least 109 proteins of diverse functions to the T9SS, implicating its role in a plethora of metabolic processes. This is the first description of T9SS in a human gut Bacteroides. This work demonstrates that members of the microbiota have developed multiple strategies for utilisation of the same carbon to survive in a highly populated human gut.

Acknowledgments

First of all, I would like to thank my supervisors, Dr Elisabeth Lowe and Prof. Janet Quinn, for giving me the opportunity to do this PhD, their supervision, and immense support throughout these years. I would also like to thank Dr Dave Bolam not only for his continuous scientific advice and patience but also his dramatic effort into teaching me how to do my shoelaces.

I also thank all past and current members of Newcastle University Glycolab and, in particular, Dr Lucy Crouch, Hannah Gibson and Maria Zakhour (who was only a transient member but still) for sharing all the ups and downs of life during a PhD with me. I would also like to thank Curtis Cottam for being a fantastic MRes student and generating very nice bioinformatics data, some of which is presented in Chapter 5 of this thesis.

I think Carl Morland deserves a separate paragraph as I can't express enough how grateful I am for the expertise and help I have received from him. I have not quite learnt to amplify DNA by simply looking at it and can only hope that one day I will become as proficient.

I should also say that without my friends and family a lot of it would not have been possible. First of all, I thank my mum and my sister for being there for me at any hour of the day and night. And, of course, my brother, Nikita, and his fiancée, Anastasia, for our dope wakeboarding trips and their emotional support throughout these years.

I am also very grateful to my friends: Valeria, Maria, Ekaterina, and Kristina, who, despite being miles away, built a fantastic support system and rang me frequently, greatly contributing to the stability of my mental health.

In the end, I would like to thank everyone for eating everything I have ever baked! You are all incredible people I am so lucky to know.

List of Abbreviations

OD ₆₀₀	Optical Density at wavelength 600 nm
BLAST	Basic Local Alignment Search Tool
BSA	Bovine serum albumin
CAZy	Carbohydrate-active enzymes database
CBM	Carbohydrate-binding modules
CE	Carbohydrate esterase
CTD	C-terminal domain
EDTA	Ethylenediaminetetraacetic acid
Glc	Glucose
GalA	Galacturonic acid
GH	Glycoside hydrolase
GlcNAc	N-acetylglucosamine
His	Polyhistidine tag
HPAEC	High-performance anion-exchange chromatography
HTCS	Hybrid Two Component System
IMAC	Immobilized metal-ion affinity chromatography
ITC	Isothermal titration calorimetry
LB	Luria-Bertani broth
Man	Mannose
Mnn1 mannan	Mannan from <i>mnn1 S. cerevisiae</i> strain
Mnn5 mannan	Mannan from <i>mnn5 S. cerevisiae</i> strain
Mnn2 mannan	Mannan from <i>mnn2 S. cerevisiae</i> strain
MS	Mass spectrometry

MUSCLE	Multiple Sequence Comparison by Log-Expectation
NCBI	National Center for Biotechnology Information
ORF	Open reading frame
PAD	Pulsed amperometric detection
PBS	Phosphate-buffered saline
PCR	Polymerase chain reaction
PL	Polysaccharide lyase
PUL	Polysaccharide utilisation loci
PULDB	Polysaccharide utilisation loci database
SDS-PAGE	Sodium dodecyl sulfate - polyacrylamide gel electrophoresis
SGBP	Surface glycan binding proteins
SP	Signal peptide
T9SS	Type 9 Secretion system
<i>tdk</i>	Thymidine kinase
TEMED	N,N,N',N'-Tetramethylethylenediamine
TLC	Thin layer chromatography
TYG	Tryptone yeast extract glucose

Table of Contents

Abstract	iii
Acknowledgments	iv
List of Abbreviations	v
Table of Contents	vii
List of Figures	xiii
List of Tables	xviii
Chapter 1: Introduction	1
1. 1 The Human gut microbiota.	1
1. 1. 1 Bacterial component of the microbiota.....	1
1. 1. 2 Fungal component of the microbiota (the mycobiota)	3
1. 1. 3 Bacteria-Fungi Interactions in the gut	6
1. 2 Carbohydrate-Degrading Systems.....	9
1. 2. 1 Starch utilisation system.....	10
1. 2. 2 SusC-SusD complex.....	11
1. 2. 3 Polysaccharide utilisation loci (PULs).....	12
1. 2. 4 Glycoside hydrolases	14
1. 2. 4. 1 Subsite nomenclature	15
1. 2. 4. 2 Catalytic mechanism	16
1. 2. 4. 3 Inverting mechanism.....	16
1. 2. 4. 4 Retaining mechanism.....	17
1. 2. 5 Regulation of PULs.....	18
1. 3 Metabolism of carbohydrates	19
1. 3. 1 Dietary carbohydrates	19
1. 3. 2 Host glycans.....	24
1. 3. 2. 1 N-linked glycans	24
1. 3. 2. 2 O-linked glycans	27
1. 4 Fungal cell wall	29
1. 4. 1 Structure of the cell wall.....	29
1. 4. 2 Recognition of the cell wall by the Immune system	33
1. 4. 2. 1 Immune recognition of α -mannan	33
1. 4. 2. 2 Immune recognition of β -mannan	35
1. 4. 2. 3 Immune recognition of the inner layer of the cell wall: β -glucan and chitin	35
1. 5 Utilisation of fungal cell wall polysaccharides by gut <i>Bacteroides</i>	37

1. 5. 1 Breakdown of β -glucan.....	37
1. 5. 2 Breakdown of fungal mannan by <i>B. thetaiotaomicron</i>	38
1. 5. 3 Fungal cell wall is a dynamic structure	42
1. 5. 3. 1 Remodelling in response to Carbon source	43
1. 5. 3. 2 Remodelling in response to low oxygen environment.....	43
1. 5. 3. 3 Remodelling in response to changes in pH	44
1. 6 Mannan degrading enzymes	45
1. 6. 1 Class I α -mannosidases: Glycoside Hydrolases 47.....	46
1. 6. 2 Class II α -mannosidases: Glycoside Hydrolases 38.....	47
1. 6. 3 Glycoside Hydrolases 92.....	48
1. 6. 4 Glycoside Hydrolases 125.....	49
1. 6. 5 Endo-acting α -mannanases	50
1. 6. 5. 1 Glycoside Hydrolases 99	50
1. 6. 5. 2 Glycoside Hydrolases 76	51
1. 6. 6 β -mannosidases.....	53
1. 7 Objectives.....	55
Chapter 2: Materials and Methods	56
2. 1 Bacterial strains and Plasmids	56
2. 2 Bacterial and Yeast Growth and Storage Conditions.....	59
2. 2. 1 Selective Media.....	59
2. 2. 2 Sterilisation	62
2. 2. 3 <i>E. coli</i> growth conditions.....	62
2. 2. 4 <i>Bacteroides spp.</i> growth conditions.....	62
2. 2. 5 Yeast growth conditions	63
2. 2. 6 Storage.....	63
2. 3 Molecular Biology.....	63
2. 3. 1 Centrifugation.....	63
2. 3. 2 Transformation of chemical competent <i>E. coli</i>	64
2. 3. 3 Propagation of plasmids	64
2. 3. 4 DNA isolation	65
2. 3. 5 Quantification of DNA.....	65
2. 3. 6 Polymerase Chain Reaction (PCR).....	65
2. 3. 7 Agarose gel electrophoresis	67
2. 3. 8 Purification of DNA fragments.....	68
2. 3. 8. 1 Purification of PCR products	68
2. 3. 8. 2 DNA gel extraction	68
2. 3. 9 Molecular cloning	69

2. 3. 9. 1 Digestion with Restriction Enzymes	69
2. 3. 9. 2 Ligation of vector and insert DNA	69
2. 3. 10 Automated DNA sequencing	69
2. 3. 11 Whole genome sequencing	70
2. 3. 12 Overexpression of recombinant proteins	70
2. 3. 13 Immobilised Metal Affinity Chromatography (IMAC)	71
2. 3. 14 Sodium Dodecyl Sulfate-Polyacrylamide Gel Electrophoresis (SDS-PAGE)	72
2. 3. 15 Quantification of proteins	74
2. 3. 16 Concentration of Proteins and Buffer Exchange	74
2. 3. 17 Genetic manipulations in <i>B. thetaiotaomicron</i>	74
2. 3. 17. 1 Construction of a deletion cassette	74
2. 3. 17. 2 Conjugations into <i>B. thetaiotaomicron</i>	76
2. 4 Biochemistry	79
2. 4. 1 Thin Layer Chromatography (TLC)	79
2. 4. 2 High-Performance Anion Exchange Chromatography (HPAEC)	80
2. 4. 3 Enzyme assays	81
2. 4. 4 D-Glucose/D-Fructose/D-Mannose detection kit	82
2. 4. 5 Preparation of substrates and oligosaccharides	83
2. 4. 5. 1 Extraction of mannans	83
2. 4. 5. 2 Generation and Purification of β -1,2-mannooligosaccharides	85
2. 4. 5. 3 Concentrating of samples by freeze drying	86
2. 4. 6 Analysis of in-gel proteins by Mass Spectrometry	86
2. 4. 6. 1 Sample preparation	86
2. 4. 6. 2 Sample analysis	86
2. 4. 7 Comparative proteomics	87
2. 4. 7. 1 Sample preparation	87
2. 4. 7. 2 Mass spectrometry	88
2. 4. 7. 3 Sample analysis	89
2. 4. 8 Isothermal Titration Calorimetry (ITC)	90
2. 4. 9 Affinity Gel Electrophoresis (NATIVE-PAGE)	90
2. 5 Microbiology	91
2. 5. 1 Culture preparation and monitoring	91
2. 5. 2 Cross-feeding experiments with conditioned media	92
2. 5. 3 Whole cell assays	93
2. 5. 4 Multi-species co-culture experiments	94
2. 5. 5 Real-time Quantitative PCR (qPCR)	95
2. 5. 6 Transmission Electron Microscopy of Outer Membrane Vesicles	98
2. 5. 6. 1 Purification of Outer Membrane vesicles (OMV)	98

2. 5. 6. 2 Transmission Electron Microscopy (TEM)	99
2. 6 Bioinformatics tools	99
Chapter 3: Degradation of mannan from <i>Candida albicans</i> by <i>Bacteroides thetaiotaomicron</i>	101
3. 1 Introduction	101
3. 2 Objectives	107
3. 3 Results	107
3. 3. 1 Characterisation of β -1,2 mannosidases from the Glycoside Hydrolase 130 family, BT4094 and orf19.6637(CaGH130).	107
3. 3. 2 Characterisation of β -mannosidases, BT3780 and BT4094, <i>in vivo</i>	116
3. 3. 2. 1 Construction and characterisation of $\Delta bt3780 + \Delta bt4094$ strain.	116
3. 3. 2. 2 Characterisation of Bt $\Delta pul1/2/3 + \Delta bt4094$ strain	122
3. 3. 3 Whole cell activity against mannan from <i>Candida albicans</i>	125
3. 3. 4 Characterisation of Mannan PUL4.....	128
3. 3. 5 Glycoside hydrolases 92 from Mannan PUL4	131
3. 3. 6 Characterisation of BT4072 ^{GH38}	132
3. 3. 7 Characterisation of enzymes from Mannan PUL4.....	139
3. 3. 8 <i>In vivo</i> characterisation of Mannan-PUL4	141
3. 3. 9 Mannan from <i>mnn1</i> , <i>mnn5</i> , and <i>mnn2 S. cerevisiae</i> mutants.....	144
3. 3. 10 Possible endo-acting mannanases in Bt $\Delta pul1/2/3/4$	147
3. 3 Discussion	150
Chapter 4: <i>Bacteroides salyersiae</i> deploys a non-selfish mechanism for degradation of mannan from <i>S. cerevisiae</i>	158
4. 1 Introduction	158
4. 2 Objectives	159
4. 3 Results	160
4. 3. 1 Growth analysis of <i>Bacteroides</i> spp on mannan from <i>S. cerevisiae</i>	160
4. 3. 2 <i>S. cerevisiae</i> mannan degradation by <i>B. salyersiae</i> occurs extracellularly	162
4. 3. 3 Activity of whole <i>B. salyersiae</i> cells against mannan from wild type, $\Delta mnn1$, and $\Delta mnn5 S. cerevisiae$ strains	163
4. 3. 4 Further analysis of manno-oligosaccharides generated by <i>B. salyersiae</i>	168
4. 3. 5 Identification of yeast α -mannan specific PULs in <i>B. salyersiae</i>	172
4. 3. 6 Domain analysis of GH76s: BS_04090 ^{GH76} , BS_04077 ^{GH76} , and BS_03668 ^{GH76}	176
4. 3. 7 Biochemical characterisation of Glycoside Hydrolases 76 from <i>Bacteroides salyersiae</i>	178

4. 3. 7. 1	Characterisation of BS_04090 ^{GH76}	180
4. 3. 7. 2	Characterisation of BS_03668 ^{GH76}	184
4. 3. 7. 3	Characterisation of Glycoside Hydrolases 38 (GH38) from <i>B. salyersiae</i>	188
4. 3. 8	Yeast α -mannan breakdown by <i>B. salyersiae</i>	198
4. 3. 8. 1	Activity of BS_04078 ^{GH92} , BS_04089 ^{GH125} , BS_04085 ^{GH38} , BS_01537 ^{GH38} , BS_04090 ^{GH76} against <i>mnn2</i> , <i>mnn5</i> , and <i>mnn1</i> mannan variants.	200
4. 3. 8. 2	Activity of BS_04078 ^{GH92} , BS_04089 ^{GH125} , BS_04085 ^{GH38} , BS_01537 ^{GH38} , BS_04090 ^{GH76} against α -mannan from wild type <i>S. cerevisiae</i>	205
4. 3. 9	<i>B. salyersiae</i> enables ‘sharing’ of mannan from <i>S. cerevisiae</i>	206
4. 3. 10	Cross-feeding of <i>S. cerevisiae</i> mannan between <i>B. salyersiae</i> and <i>B. xylanisolvens</i> <i>in vitro</i> . .	214
4. 3. 10. 1	Competition for mannose.....	215
4. 3. 10. 2	Competition for <i>S. cerevisiae</i> mannan	217
4. 3. 11	<i>In vitro</i> sharing of <i>S. cerevisiae</i> mannan between <i>B. thetaiotaomicron</i> and <i>B. salyersiae</i> , ‘selfish’ versus ‘non-selfish’	220
4. 3. 11. 1	Competition assay for mannose	221
4. 3. 11. 2	Competition for <i>S. cerevisiae</i> mannan	223
4. 4	Discussion	226
4. 4. 1	Mannan-degrading apparatus in <i>B. salyersiae</i>	229
4. 4. 2	Sharing of manno-oligosaccharides between gut <i>Bacteroides</i>	234
Chapter 5: Type 9 Secretion System in <i>B. salyersiae</i> and its role in mannan		
degradation		240
5. 1	Introduction.....	240
5. 1. 1	Type 9 secretion system complex	241
5. 1. 1. 1	T9SS in <i>Porphyromonas gingivalis</i>	241
5. 1. 1. 2	T9SS in <i>Flavobacterium johnsoniae</i>	242
5. 1. 2	Organisation and mechanism.....	242
5. 1. 3	Conserved C-terminal domains	244
5. 2	Objectives	246
5. 3	Results	247
5. 3. 1	Type 9 Secretion system in <i>B. salyersiae</i>	247
5. 3. 2	Proteins targeted for the secretion by the Type 9 system carry C-terminal domains.....	251
5. 3. 2. 1	Structural components	251
5. 3. 2. 2	Type A CTD-carrying proteins in <i>B. salyersiae</i> and other gut <i>Bacteroides</i>	253
5. 3. 2. 3	CTDs in Mannan PUL.....	256
5. 3. 3	Role of T9SS in yeast α -mannan breakdown.....	258
5. 3. 4	<i>B. salyersiae</i> produces Outer Membrane Vesicles (OMVs)	262

5. 3. 5 Biochemical characterisation of BS_04081 ^{unknown}	265
5. 3. 6 Biochemical characterisation of BS_04072 ^{unknown}	272
5. 4 Discussion	275
Chapter 6: Final Discussion	283
References	293
Appendix A	322

List of Figures

Figure 1. 1 Composition of the human gut microbiota. Bacterial diversity is determined by dietary alterations at different life stages.	2
Figure 1. 2 Distribution of microbial phyla in stool samples of healthy adults and their associated metabolic functions.	3
Figure 1. 3 Composition of the mycobiota. Panel a: Diversity of fungal genera across physiological sites.	5
Figure 1. 4 Summary of Bacteria-Fungi interactions in the human gut. Figure adapted from Richard and Sokol (2019).	8
Figure 1. 5 Diagram of Starch Utilisation system in Bt.	11
Figure 1. 6 Topologies of the active site of exo- and endo-acting glycoside hydrolases as indicated.	15
Figure 1. 7 Subsite nomenclature of a glycoside hydrolase.	15
Figure 1. 8 Inverting mechanism of glycoside hydrolases.	17
Figure 1. 9 Retaining mechanism of Glycoside Hydrolases.	18
Figure 1. 10 Schematic structures of dietary carbohydrates.	23
Figure 1. 11 Types of N-linked Glycans.	26
Figure 1. 12 Types of O-glycosylation.	29
Figure 1. 13 Structure of fungal cell wall. Panel a: diagram of multi-layered structure of cell wall.	32
Figure 1. 14 Summary on the recognition of fungal cell wall polysaccharides by the Pattern Recognition Receptors in the host.	37
Figure 1. 15 Three PULs upregulated in Bt in response to mannan from <i>S. cerevisiae</i> . Figure adapted from Cuskin et al. (2015).	40
Figure 1. 16 Selfish mechanism of mannan utilisation in Bt.	41
Figure 1. 17 Cell wall remodelling in response to carbon source, oxygen availability, and ambient pH.	45
Figure 1. 18 Schematic representation of N-glycan degradation by enzymes from the GH47 and GH38 families.	48
Figure 1. 19 Schematic representation of enzyme specificities from the GH92 (a), GH125 (b), and GH99 (c) and GH76 (d) families.	52
Figure 1. 20 Difference between Glycoside Hydrolases, Glycoside Phosphorylases, and Glycosyl Transferases.	54
Figure 2. 1 Sewing PCR to generate gene deletion fragments.	75

Figure 2. 2 Gene deletions in <i>B. thetaiotaomicron</i> ,	77
Figure 2. 3 Linker enzymes deployed by Mannose detection kit to monitor mannose release.	82
Figure 3. 1 Alignment of GH130s.	105
Figure 3. 2 Overlay of the active site of β -mannosidase BT3780 and β -mannoside phosphorylase BF0772.	106
Figure 3. 3 SDS-PAGE analysis of recombinant GH130s.	108
Figure 3. 4 Activity of BT3780 (a-b), BT4094 (c-d), CaGH130 (e-f) on mannan from <i>C. albicans</i>	110
Figure 3. 5 Activity of BT3780, BT4094, and CaGH130 against β -1,2-mannosides from <i>C. albicans</i> mannan.	112
Figure 3. 6 Activity of BT4094 and CaGH130 against β -1,2 and β -1,4 linked mannooligosaccharides.	113
Figure 3. 7 End-point reactions with BT3780, CaGH130, and BT4094 against <i>C. albicans</i> mannan.	115
Figure 3. 8 Kinetics of BT4094 and CaGH130 against mannan from <i>C. albicans</i>	116
Figure 3. 9 Construction of $\Delta bt4094$ and $\Delta bt4094+\Delta bt3780$ strains.	118
Figure 3. 10 Growth curves of WT Bt; $\Delta bt4094$; $\Delta bt3780$; $\Delta bt4094+\Delta bt3780$ strains on mannan from <i>Candida albicans</i>	119
Figure 3. 11 Biochemical analysis of the $\Delta bt3780+\Delta bt4094$ culture supernatant.	121
Figure 3. 12 Growth of Bt $\Delta pul1/2/3$ on mannan from <i>C. albicans</i> and <i>S. cerevisiae</i>	122
Figure 3. 13 Growths of Bt strains: WT Bt, $\Delta pul3$, $\Delta bt3780+\Delta bt4094$, $\Delta pul2$, $\Delta pul1/2/3$, $\Delta pul1/2/3+\Delta bt4094$	125
Figure 3. 14 Activity of the wild type Bt whole cells on mannan from <i>C. albicans</i>	127
Figure 3. 16 SDS-PAGE gel of recombinant proteins from the mannan PUL-4.	129
Figure 3. 17 Activity of GH92s from the MAN-PUL4 against α -linked mannobiose substrates and yeast mannan.	132
Figure 3. 18 Phylogenetic tree of characterised GH38s.	134
Figure 3. 19 Activity of BT4072 on α -linked mannobiose substrates.	135
Figure 3. 20 Schematic illustration of High Mannose N-glycan (HMNG) found in Ribonuclease B.	137
Figure 3. 21 RNase B degradation by α -mannosidases: BT3990 ^{GH92} ; BT3991 ^{GH92} , and BT4072 ^{GH38}	139
Figure 3. 22 TLC of one pot reaction.	140

Figure 3. 23 Growths of WT Bt, Bt $\Delta pul4$, Bt $\Delta pul1/2/3/4$, and Bt $\Delta pul1/2/3$ on mannan from <i>Candida albicans</i> .	142
Figure 3. 24 Growth analysis of Bt WT, Bt $\Delta pul1/2/3/4$, and Bt $\Delta pul1/2/3$ on mannan from <i>S. cerevisiae</i> .	143
Figure 3. 25 Architecture of mannan variants extracted from the wild type, <i>mnn1</i> , <i>mnn5</i> , and <i>mnn2</i> <i>S. cerevisiae</i> strains.	144
Figure 3. 26 Growth analysis of Bt $\Delta pul1/2/3/4$ on indicated <i>S. cerevisiae</i> mannan variants.	146
Figure 3. 27 Analysis of $\Delta pul1/2/3/4$ growth on α -mannan variants.	147
Figure 3. 28 Expression of GH76s in Bt $\Delta pul1/2/3/4$ and Bt WT in response to <i>S. cerevisiae</i> mannan.	150
Figure 4. 1 Growth of <i>Bacteroides spp.</i> on mannan from <i>S. cerevisiae</i> .	161
Figure 4. 2 Growth analysis of <i>B. salyersiae</i> on <i>S. cerevisiae</i> mannan.	163
Figure 4. 3 Activity of whole <i>B. salyersiae</i> cells against <i>S. cerevisiae</i> mannan.	165
Figure 4. 4 HPAEC-PAD analysis of the whole cell assay.	166
Figure 4. 5 Activity of whole <i>B. salyersiae</i> cells against <i>mnn1</i> <i>S. cerevisiae</i> mannan.	167
Figure 4. 6 Activity of whole <i>B. salyersiae</i> cells against <i>mnn5</i> <i>S. cerevisiae</i> mannan.	168
Figure 4. 7 Diagrammatic representation of exo-mannosidase degradation assay.	169
Figure 4. 8 Exo-mannosidase degradation assay of <i>B. salyersiae</i> supernatant.	171
Figure 4. 9 Polysaccharide Utilisation Loci (PULs) from <i>B. salyersiae</i> WAL 10018.	173
Figure 4. 10 Protein profile of <i>B. salyersiae</i> in response to yeast mannan.	174
Figure 4. 11 Analysis of GH76s from <i>B. salyersiae</i> .	178
Figure 4. 12 SDS-PAGE analysis of BS_04090 and BS_03668.	180
Figure 4. 13 TLC analysis of BS_04090 and BS_03301 assayed against different types of yeast mannan.	182
Figure 4. 14 Time course assay with BS_04090 against unbranched α -1,6-linked backbone from <i>mnn2</i> <i>S. cerevisiae</i> strain.	184
Figure 4. 15 Activity of BS_03668 on yeast mannan.	186
Figure 4. 16 Activity of BS_03668 against undecorated α -1,6-mannan from <i>mnn2</i> <i>S. cerevisiae</i> (a) and α -1,6 manno-tetraose (b).	187
Figure 4. 17 SDS-PAGE analysis of BS_04085 and BS_01537.	189
Figure 4. 18 Activity of GH38s, BS_04085 and BS_01537, against a range of substrates.	190
Figure 4. 19 Activity of GH38s, BS_04085 and BS_01537, against mannan from <i>mnn1</i> , <i>mnn5</i> , <i>mnn2</i> <i>S. cerevisiae</i> strains and wild type <i>S. cerevisiae</i> and <i>C. albicans</i> .	192

Figure 4. 20 Kinetic analysis of the two GH38s from <i>B. salyersiae</i>	194
Figure 4. 21 Kinetic analysis of GH38s: BS_01537 and BS_04085 against α -linked mannobioses	195
Figure 4. 22 Activities of BS_04085 and BS_01537 against mannan substrates.	198
Figure 4. 23 SDS-PAGE analysis of BS_04078 ^{GH92} and BS_04089 ^{GH125}	199
Figure 4. 24 Activity of BS_04078 ^{GH92} and BS_04089 ^{GH125} against α -linked mannobioses.	200
Figure 4. 25 Enzymatic degradation of mnn2 mannan.....	201
Figure 4. 26 Enzymatic degradation of mnn5 mannan.....	203
Figure 4. 27 Enzymatic degradation of mnn1 mannan.....	204
Figure 4. 28 Enzymatic degradation of mannan from wild type <i>S. cerevisiae</i>	206
Figure 4. 29 Utilisation of <i>B. salyersiae</i> -digested <i>S. cerevisiae</i> mannan by <i>Bacteroides</i> strains. .	208
Figure 4. 30 Utilisation of Bt-digested α -mannan but <i>Bacteroides species</i>	209
Figure 4. 31 Utilisation of either native or pre-digested <i>S. cerevisiae</i> mannan by <i>Bacteroides species</i>	212
Figure 4. 32 Mannose concentration in conditioned media before and after bacterial growth.	214
Figure 4. 33 Sharing of mannose between <i>B. salyersiae</i> and <i>B. xylanisolvans</i>	216
Figure 4. 34 Sharing of Mannan from <i>S. cerevisiae</i> between <i>B. salyersiae</i> and <i>B. xylanisolvans</i> . 218	
Figure 4. 35 Analysis of cell free spent media.....	220
Figure 4. 36 Competition for mannose between <i>B. salyersiae</i> and <i>B. thetaiotaomicron</i>	222
Figure 4. 37 Competition for mannan between <i>B. salyersiae</i> and <i>B. thetaiotaomicron</i>	224
Figure 4. 38 Analysis of cell free supernatant taken from Bt-Bs co-culture on mannan from <i>S. cerevisiae</i>	226
Figure 4. 39 Phylogenetic analysis of mannosidases from Bs.	233
Figure 4. 40 Structural organisation of Mannan PUL 2 in <i>B. thetaiotaomicron</i> VPI-5482 and its similarity with PULs found in <i>B. ovatus</i> ATCC 8483 and <i>B. xylanisolvans</i> DSM 18836.	237
Figure 4. 41 Structural organisation of Mannan PUL 1 and Mannan PUL 3 in <i>B. thetaiotaomicron</i> VPI-5482.....	238
Figure 4. 42 Structural organisation of a genetic cluster shared between <i>B. fingoldii</i> DSM 17565, <i>B. xylanisolvans</i> DSM 18836, and <i>B. ovatus</i> . ATCC 8483	239
Figure 5. 1 Structural organisation of the Type 9 Secretion System in <i>P. gingivalis</i>	241
Figure 5. 2 Type 9 Secretion System associated C-terminal domains.....	246
Figure 5. 3 Proteome of <i>B. salyersiae</i> in response to yeast α -mannan.	250

Figure 5. 4 Diagram of T9SS in <i>B. salyersiae</i>	251
Figure 5. 5 CTDs in T9SS structural proteins.....	253
Figure 5. 6 Number of proteins, containing Type A (TIGR04183) CTDs, among a range of Bacteroidetes.....	255
Figure 5. 7 T9SS CTD in <i>B. salyersiae</i> Mannan PUL -1.....	257
Figure 5. 8 Growth of <i>B. salyersiae</i> on mannan from <i>S. cerevisiae</i>	259
Figure 5. 9 Mass spectrometric analysis of proteins found in cell free supernatant. Bands were analysed with MALDI-TOF.....	261
Figure 5. 10 <i>B. salyersiae</i> produces OMVs in response to glucose (a) or yeast mannan (b).	264
Figure 5. 11 Analysis of BS_04081 ^{unknown} from <i>B. salyersiae</i>	266
Figure 5. 12 NATIVE-PAGE affinity gels of BS_04081 against <i>S. cerevisiae</i> mannan variants. .	269
Figure 5. 13 Binding of BS_04081 to mannan from wild type, mnn1, mnn5, and mnn2 <i>S. cerevisiae</i> strains by ITC.	271
Figure 5. 14 Analysis of BS_04072 ^{unknown}	273
Figure 5. 15 NATIVE-PAGE affinity gel of BS_04072 against 0.1% (w/v) yeast mannan.....	274
Figure 6. 1 Summary of utilisation of fungal mannan between gut <i>Bacteroides</i>	292

List of Tables

Table 2. 1 Bacterial strains and mutants used in this study. Genotypes and the origin of the strains are indicated.	59
Table 2. 2 Vectors used in this study.	59
Table 2. 3 Media routinely used throughout this study.	61
Table 2. 4 Selective antibiotics used. Working concentrations are indicated.	61
Table 2. 5 Standard PCR reaction.	66
Table 2. 6 Standard PCR thermocycler program.	67
Table 2. 7 Buffers used for agarose gel electrophoresis.	68
Table 2. 8 SDS-PAGE gel preparation.	73
Table 2. 9 SDS-PAGE gel Running buffer	73
Table 2. 10 Composition of the TLC running buffer and Orcinol stain.	80
Table 2. 11 Composition of a standard reaction for a linked assay.	83
Table 2. 12 Components of 2X Fehling reagent and 0.02 M Citrate buffer used for mannan extractions.	85
Table 2. 13 Composition of NATIVE-PAGE affinity gels and buffers	91
Table 2. 14 qPCR primers designed for species-specific genetic markers.	96
Table 2. 15 qPCR program and parameters used throughout this project.	97
Table 2. 16 qPCR primers used to determine gene expression.	98
Table 2. 17 List of Bioinformatics tools used throughout this study.	100
Table 3. 1 Table of molecular weight, GH-family, and known functions of proteins in Mannan PUL-4.	130
Table 3. 2 GH76 in Bt. Bt encodes 9 GH76, located in indicated PULs. Signal peptide was assessed with SignalP 5.0. “√” – genes present, “✗” – genes deleted.	149
Table 4. 1 Table of upregulated proteins in <i>B. salyersiae</i> in response to <i>S. cerevisiae</i> mannan.	175
Table 4. 2 Kinetic parameters of BS_01537 ^{GH38} and BS_04085 ^{GH38}	196
Table 5. 1 Table of homologues of structural T9SS proteins found in <i>B. salyersiae</i> WAL 10018.	248
Table 5. 2 Table of thermodynamic parameters of BS_04081 against different mannan substrates.	272

Chapter 1: Introduction

1. 1 The Human gut microbiota.

1. 1. 1 Bacterial component of the microbiota

The human gut is vastly populated with microbes. The microbiota is composed of Bacteria, Archaea, and Eukarya. The Human Microbiome Project established that the bacterial community of the gut microbiota is represented by two dominant phyla: Firmicutes, Bacteroidetes, and three minor: Actinobacteria, Proteobacteria, and Verrucomicrobia (Figure 1. 1) (Turnbaugh et al., 2007). While the composition at the phylum level is conserved within the population, the combination of constituent species is highly variable between individuals (Figure 1. 1) (Lozupone et al., 2012, Ottman et al., 2012). The microbial diversity is also shaped by the age, gender, diet, lifestyle, and environmental factors (Figure 1. 1) (Muegge et al., 2011, Lozupone et al., 2012, Singh et al., 2017). It has been suggested that despite being diverse at the species level, the host specifically selects for a set of bacterial phyla whose presence provides beneficial attributes and promotes its fitness (Arumugam et al., 2011). Microbial disbalance in the gut has been strongly linked with diseases ranging from inflammatory bowel diseases, obesity, food allergies, to autoimmune diseases such as Rheumatoid arthritis and Alzheimer's disease and cancer (Lloyd-Price et al., 2019, Zhou et al., 2019, Jackson et al., 2018)

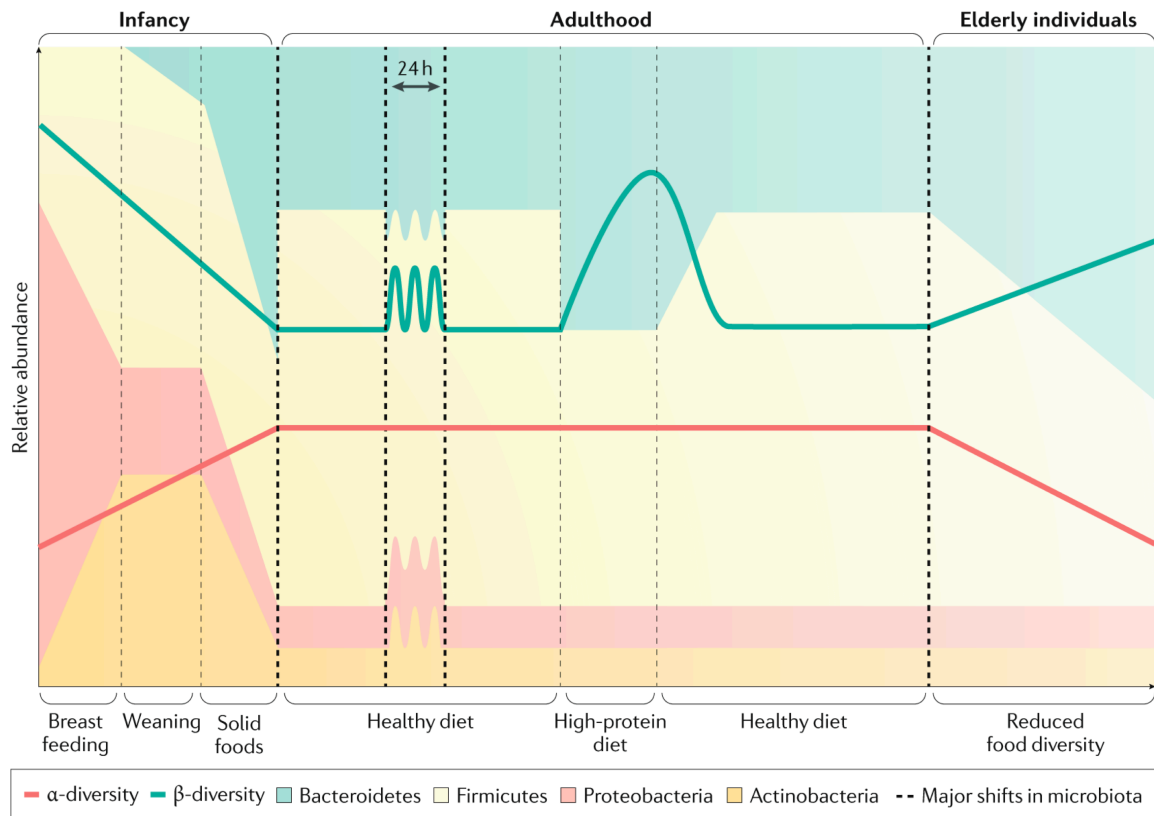


Figure 1. 1 Composition of the human gut microbiota. Bacterial diversity is determined by dietary alterations at different life stages. Figure adapted from Zmora et al. (2019).

The gut microbiota performs a number of physiological roles, one of which is digestion of complex carbohydrates (Figure 1. 2) (Huttenhower et al., 2012).

Human ability to digest dietary carbohydrates is limited to starch, sucrose, and lactose. In contrast, some microbes possess an extensive number of Carbohydrate Active enzymes (CAZymes), conferring a huge catabolic potential to degrade polysaccharides of exogenous and endogenous origins, producing short chain fatty Acids (SCFAs) as by-products (Koropatkin et al., 2012, Martens et al., 2009a, Kaoutari et al., 2013). The three most abundant SCFAs are butyrate, propionate, and acetate. Butyrate accumulates in the gut polarises the immune response towards an anti-inflammatory state, induces proliferation of colonocytes, and reduces recruitment of immune cells to the lining of the gut (Koh et al., 2016).

Propionate is directed to the liver, where it contributes to lipogenesis, while acetate is circulated in the periphery, performing a range of physiological roles and dictating central homeostasis (Koh et al., 2016).

Therefore, digestion of complex carbohydrates by the gut microbiota provides a range of benefits that are relevant to human health.

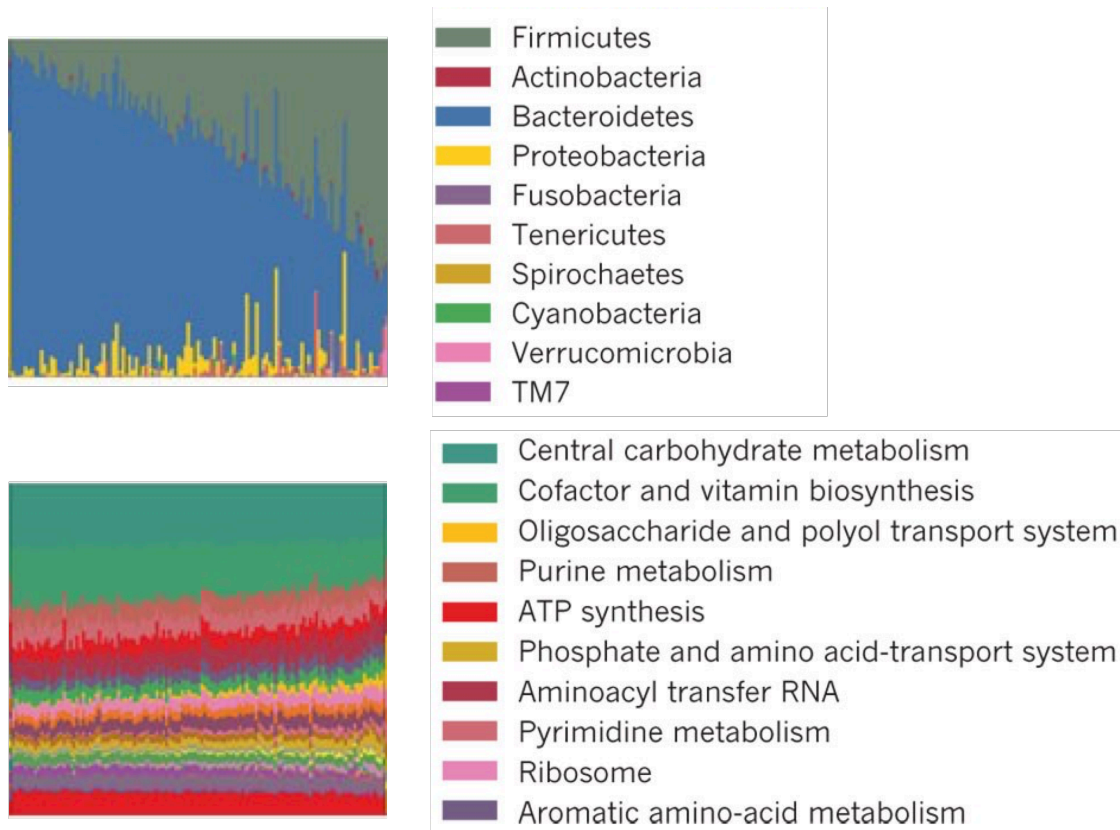


Figure 1. 2 Distribution of microbial phyla in stool samples of healthy adults and their associated metabolic functions. Figure adapted from Huttenhower et al. (2012)

1. 1. 2 Fungal component of the microbiota (the mycobiota)

Though understudied in comparison to bacteria, fungi are also normal residents of the microbiota (Figure 1. 3 a). Phylogenetic typing using samples from the Human Microbiome Project revealed that fungal diversity in the human gut is overall lower

than bacterial, showing high variability between individuals (Nash et al., 2017). In addition, fungal composition changes over time within a single host and is also determined by the age and diet (Nash et al., 2017, Hoffmann et al., 2013). Fungal overgrowth is highly associated with inflammation of the bowel, colorectal cancer, and other disease states (Richard and Sokol, 2019). Human metagenomes demonstrate that the mycobiota is mostly represented by the members of the Ascomycota phylum, where the most prevalent species are members of *Saccharomyces* and *Candida* genera, followed by *Malassezia* and *Cladosporium* (Figure 1. 3 b) (Hoffmann et al., 2013, Nash et al., 2017). The minor proportion was represented by species from *Cyberlindnera*, *Pichia*, *Debaromyces*, *Galactomyces*, and *Clavispora* genera, however their abundance varied between individuals (Figure 1. 3 b) (Nash et al., 2017). Auchtung and colleagues proposed that fungi could be only transient members of the gut microbiota and their presence in the large intestine is modulated by their abundance in the oral mucosa (Auchtung et al., 2018). Eliminating fungi from the diet or brushing teeth straight after a meal decreased overall fungal population in the large intestine (Auchtung et al., 2018).

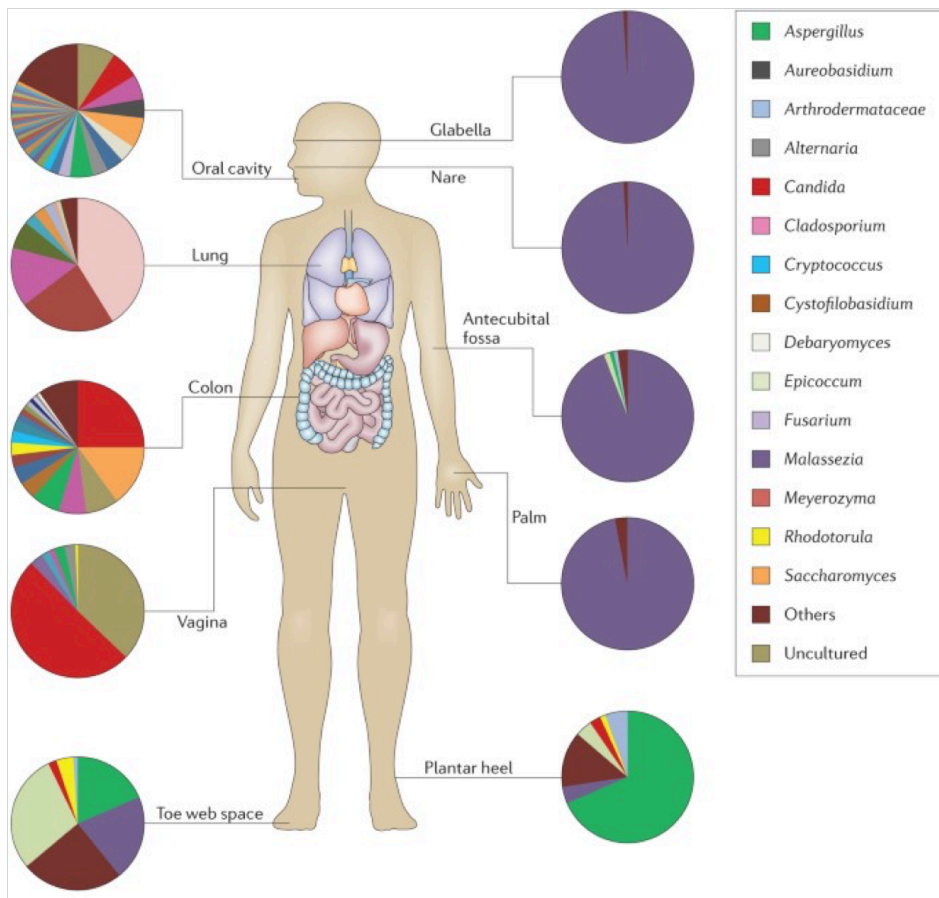
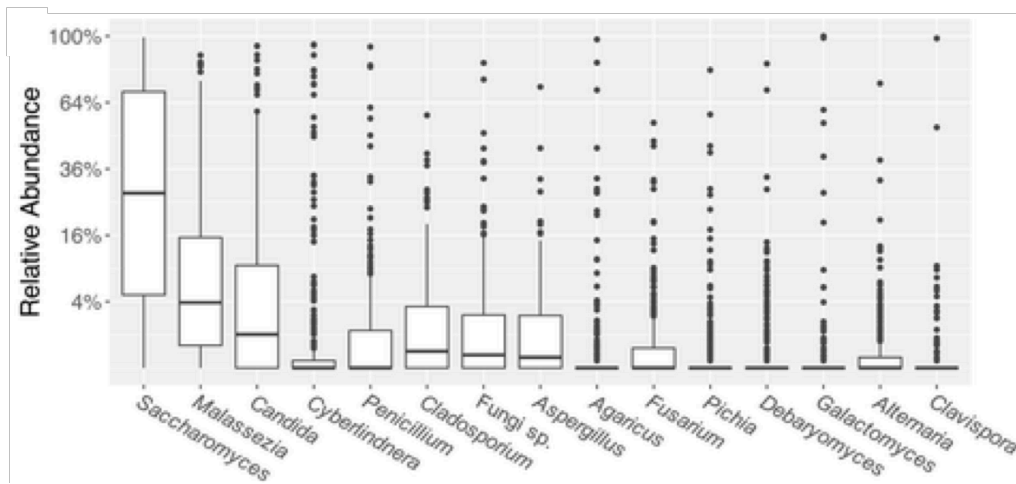
a**b**

Figure 1. 3 Composition of the mycobiota. Panel a: Diversity of fungal genera across physiological sites. Figure was adapted from Underhill and Iliev (2014). Panel b: Abundance of fungal genera in the stool samples from HMP volunteers. Figure adapted from Nash et al. (2017).

1. 1. 3 Bacteria-Fungi Interactions in the gut

The gastrointestinal (GI) tract can act as a reservoir of *C. albicans* strains which may escape and cause an invasive systemic disease in susceptible individuals. *Candida* strains isolated from patients with candidemia shared close similarity to those thriving in the large intestine of these patients (Miranda et al., 2009). In addition to *C. albicans* overgrowth, pathogenesis of Crohn's disease correlates with microbial dysbiosis and is associated with decreased abundance of *Bacteroides species* and, in contrast, increased prevalence of pathogenic *E. coli*, *Serratia*, and *Ruminococcus species* (Hoarau et al., 2016). Mice are naturally colonised with *C. tropicalis* and a broad-spectrum antibiotic treatment is required to achieve *C. albicans* colonisation, which is then reversed when commensal bacteria are reintroduced (Fan et al., 2015). This indicates that gut bacteria play a role in modulating fungal survival in the gut. Murine models also demonstrate that *C. albicans* is able to disseminate from the gut and infect other organs (Koh et al., 2008, Vautier et al., 2012). Moreover, the presence of *C. albicans* exacerbates the underlying inflammation of Dextran Sodium Sulphate (DSS) induced colitis models, which is used to mimic human IBD, by elevating TNF- α and IL-6 expression (Panpetch et al., 2020).

Bacterial and fungal components of the microbiota actively interact with each other, modulating each other's fitness in the gut. The presence of *B. thetaiotaomicron*, *B. producta* and *L. reuteri* but not *B. fragilis* was sufficient to completely eliminate *C. albicans* growth in the antibiotic-treated mouse model of *C. albicans* colonisation discussed above (Fan et al., 2015). These bacteria exert their fungicidal effect through the generation of an antimicrobial peptide, LL-37 (Fan et al., 2015). Antifungal action against *C. albicans* is also deployed by *S.*

marcescens, which injects toxic effectors via the Type 6 Secretion System (T6SS) resulting in fungal death (Trunk et al., 2018). Components of the T6SS are also present in gut *Bacteroides*, implicating their potential in antifungal immunity (Verster et al., 2017, Wexler et al., 2016). Another example of bacteria-fungi interactions was demonstrated by Graham and colleagues, where *Enterococcus faecalis* was shown to secrete a soluble protein, EntV, which directly disintegrates *C. albicans* biofilms and precludes its virulence via inhibition of filamentation (Graham et al., 2017). *L. rhamnosus* was also shown to reduce the ability of *C. albicans* to form hyphae and invade the epithelial barrier in gut-on-chip models, whose immune response promoted epithelial shedding and ultimate death of *C. albicans* (Maurer et al., 2019, Graf et al., 2019).

Bacterial diversity was shown to impact on fungal composition of ethnically distinct cohorts, such that presence of *Prevotella species* in the Indian population correlated with high levels of *Candida spp*, whereas abundance of *Bacteroides species* in the Japanese population was associated with the presence of *Saccharomyces spp* (Pareek et al., 2019). Here it was also found that *P. copri* failed to colonise germ free mice unless they were pre-colonised with *C. albicans*, indicating a mutualistic relationship between these two species (Pareek et al., 2019).

The ecosystem of the human gut is highly dynamic, where the interactions between fungal and bacterial species (Figure 1. 4) are dictated by a range of biological factors such as the diet, lifestyle, genetic profile, age and others.

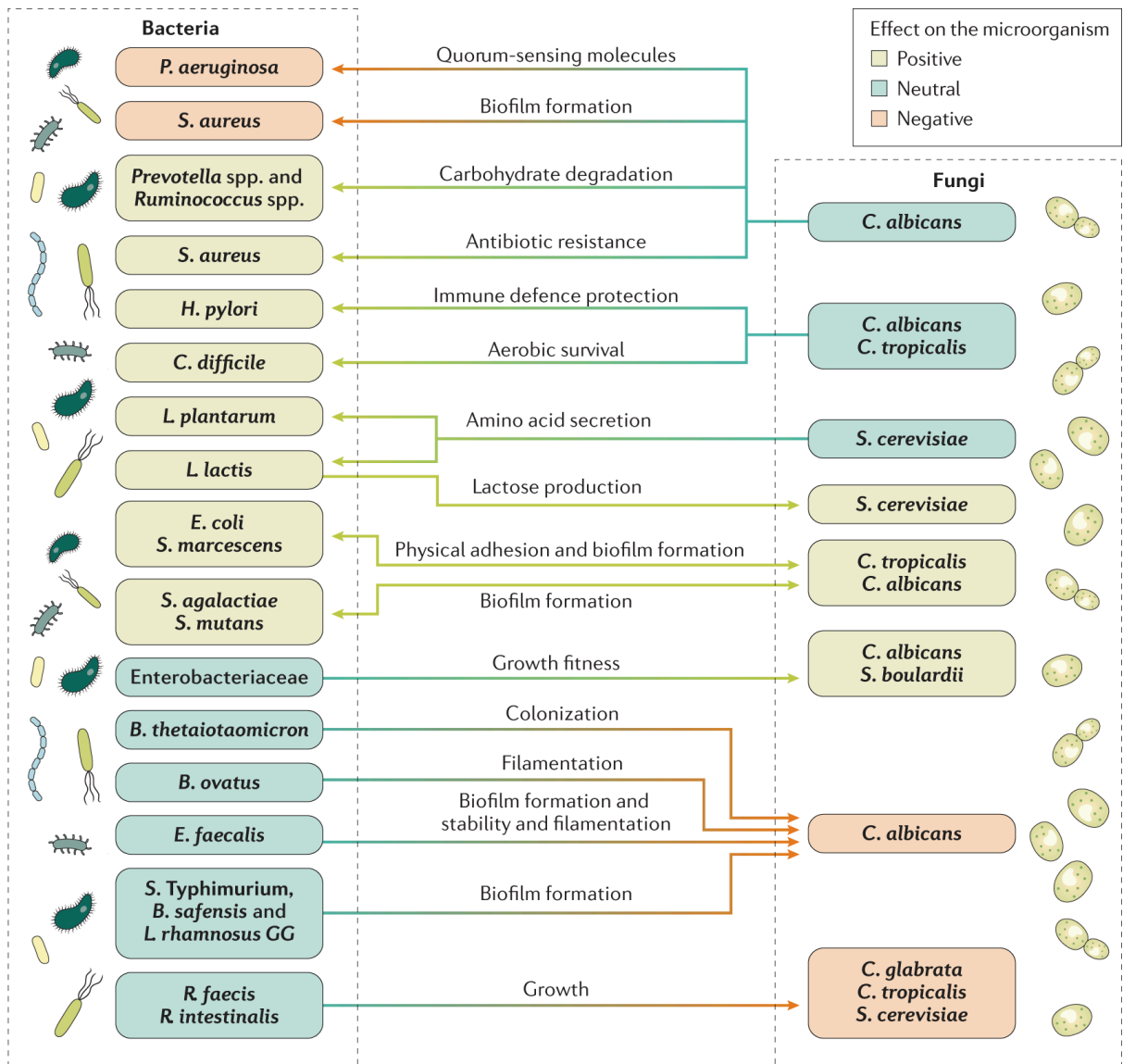


Figure 1. 4 Summary of Bacteria-Fungi interactions in the human gut. Figure adapted from Richard and Sokol (2019). The interactions between Bacterial and Fungal species can be unidirectional (single-headed arrow) or bidirectional (double-headed arrow). Positive interactions (green boxes) indicate that the presence of one species promotes survival of the other. Negative interactions (red boxes) indicate that the presence of the species limits the growth of the other. Neutral (blue boxes) shows that the presence of the species is unaffected by the presence of the interacting species.

1. 2 Carbohydrate-Degrading Systems

As mentioned above the primary role of the gut microbiota is to digest complex carbohydrates inaccessible to the host. The gut microbiota possesses an extensive repertoire of proteins dedicated to the degradation of glycans of dietary, mammalian, and microbial origins. The composition of these glycans induces differential expression of genes necessary for their utilisation, shaping microbial diversity in the gut (Sonnenburg et al., 2005, Martens et al., 2008, Marcobal et al., 2011). While the role of Firmicutes and Actinobacteria in the degradation of complex carbohydrates is less understood, *Bacteroides* are thought to act as glycan-degrading generalists, deploying a variety of strategies to deconstruct complex substrates. *Bacteroides* rapidly adjust their transcriptome in response to dietary changes and display a preferential hierarchy towards certain carbohydrates, utilisation of which is prioritised over others (Rogers et al., 2013, Martens et al., 2008). Moreover, the host favours the presence of *Bacteroides* spp. such as *B. thetaiotamicron* (Bt) by specifically fucosylating the ileal epithelium, thereby creating a niche for its survival (Hooper et al., 1999). In return, the by-products of glycan metabolism fortify the integrity of the epithelial barrier, increase angiogenesis, educate the immune system towards an anti-inflammatory state and a range of other physiological benefits (Bry et al., 1996, Hooper et al., 1999).

The systems mediating degradation of complex carbohydrates are usually grouped into distinct genetic clusters, termed Polysaccharide Utilisation Loci (PULs). These usually contain binding and transport proteins, CAZymes, and signal transduction systems. The discovery of PULs, their structural organisation, diversity, and regulation is discussed in this section.

1. 2. 1 Starch utilisation system

Salyers and colleagues first demonstrated that Bt utilises amylose, amylopectin, and pullulan using a genetic cluster composed of 8 genes, *susRABCDEFG* (Anderson and Salyers, 1989a, Anderson and Salyers, 1989b). These assembled into a transmembrane complex, which they called a starch utilisation system (Sus) (Figure 1. 5). In this system, SusR was identified to function as a transmembrane regulator, which controls expression of the Sus operon in response to extracellular malto-oligosaccharides (D'elia and Salyers, 1996b, Cho et al., 2001). An endo-acting α -1,4 glucanase, SusG, was shown to orchestrate starch metabolism and acquisition at the cell surface (Shipman et al., 1999, Koropatkin and Smith, 2010). Long oligosaccharides are then captured by SusEF binding proteins and transported to the periplasmic space through the SusCD complex, where they are further processed into simpler units by α -amylase, SusA, and α -glucosidase, SusB (Figure 1. 5) (Reeves et al., 1997, D'elia and Salyers, 1996a, Koropatkin et al., 2008, Tuson et al., 2018)

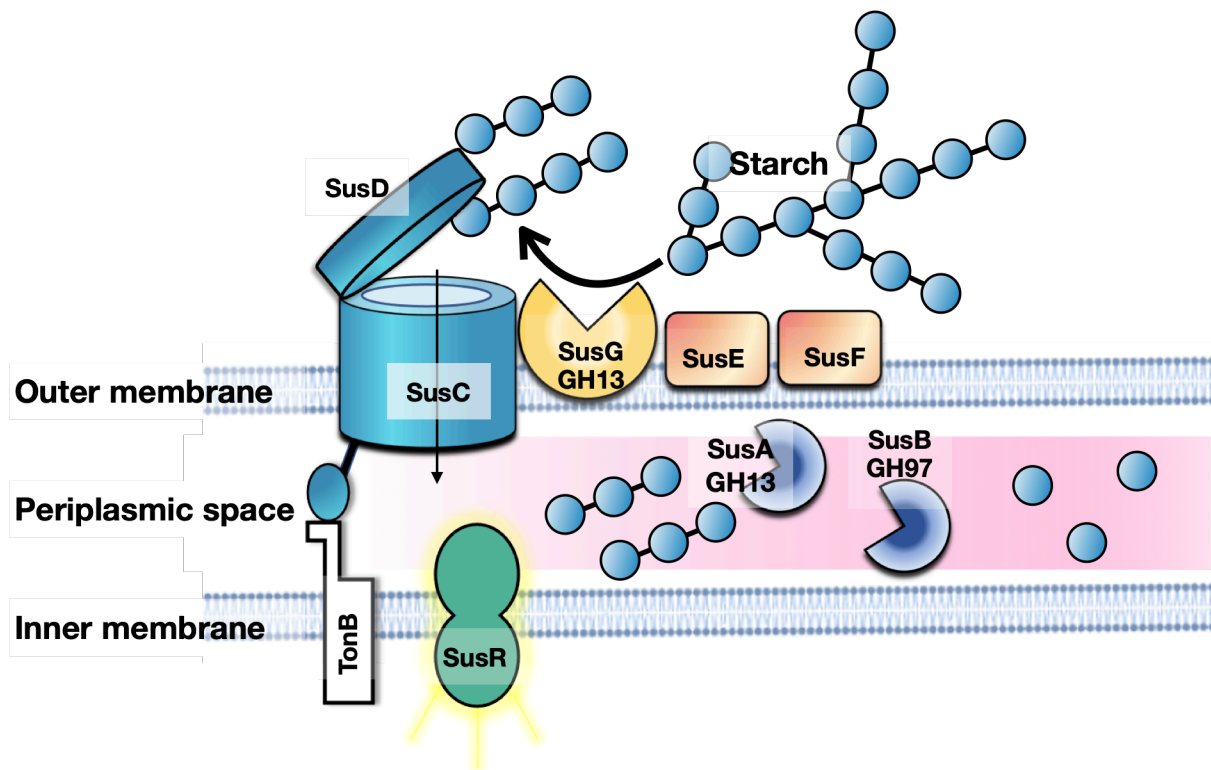


Figure 1. 5 Diagram of Starch Utilisation system in Bt. SusG (GH13) is a surface neopullulanase which initiates starch breakdown. SusEF are surface binding proteins. SusCD complex mediates import of oligosaccharides into the periplasmic space, where they are further depolymerised into glucose by SusA (GH13) and SusB (GH97). SusR functions as a signal transducer and controls expression of proteins in the system.

1. 2. 2 SusC-SusD complex

SusC and D proteins closely associate with each other, mediating transport of oligosaccharides in a 'pedal-bin' mechanism (Glenwright et al., 2017). SusC is a TonB-dependent transporter (TBDT) which is composed of a 22 stranded transmembrane β -barrel and a globular plug domain, forming a malleable pore in the outer membrane (Noinaj et al., 2010, Glenwright et al., 2017, Gray et al., 2021). Structural investigations into the mechanism of action of SusC-like proteins revealed that, unlike other TBDTs, they also contain an N-terminal extension domain (NTE) (Gray et al., 2021). Deletion of the NTE in BT1763 precludes

growth of Bt on levan, β -2,6-fructan (Gray et al., 2021). The NTE may play a role in substrate recognition however its exact function is currently unknown.

The SusD lipoprotein is attached to the SusC via two hinge loops, which mediate the opening and the closure of the complex, hence the “pedal bin” mechanism (Glenwright et al., 2017). SusDs function as surface glycan binding proteins (SGBPs) and display specificity for oligosaccharides of a certain size range (Gray et al., 2021, Koropatkin et al., 2008). In the absence of a substrate, the SusCD complex exists in an open state. Upon glycan binding the SusD lid closes, leading to a conformational change, facilitating glycan uptake into the periplasmic space through the SusC pore with the energy provided by the interaction with TonB (Glenwright et al., 2017, Gray et al., 2021). Interestingly, oligosaccharides shorter than 4 units do not seem to require active transport and can move freely through the open SusCD complex (Gray et al., 2021)

Bt is predicted to encode at least 209 homologues of SusC-SusD proteins, grouped into at least 101 pairs (Martens et al., 2009a, Xu et al., 2007). Based on the requirement that a glycan-degrading cluster is defined by at least 1 pair of SusCD homologues, 88 putative Polysaccharide Utilisation Loci (PULs) have been identified (Martens et al., 2008). These encompassed approximately 900 genes that were differentially regulated in response to a diversity of carbon sources (Martens et al., 2008, Sonnenburg et al., 2005, Sonnenburg et al., 2010).

1. 2. 3 Polysaccharide utilisation loci (PULs)

Polysaccharide Utilisation Loci (PULs) of varying lengths have been characterised (Martens et al., 2008, Ndeh et al., 2017, Luis et al., 2018). A PUL includes a pair of SusCD-like proteins, SGBPs, a regulator, and Carbohydrate Active enzymes

(CAZymes). CAZymes are grouped into distinct families based on their sequence similarity and include glycoside hydrolases (GH), Polysaccharide Lyases (PL), Carbohydrate Esterases (CE), and Lytic Polysaccharide Monooxygenases (LPMO) (Cantarel et al., 2009, Lombard et al., 2014). Members of each family are catalogued in the CAZy database (<http://www.cazy.org>), which is regularly updated. Currently the CAZy database lists 170 and 41 GH and PL families, respectively.

It has been assumed that each PUL targets a specific glycan structure, however as later discussed in Section 1.3, several PULs from one or even multiple species are required to work in concert to degrade more complex glycan structures. The structural organisation of PULs is retained across other Bacteroidetes and these have been collected in the PULDB database (<http://www.cazy.org/PULDB/>), which comprises both predicted and experimentally characterised PULs across approximately 900 genomes, encompassing 150,000 CAZyme modules (Terrapon et al., 2018, Xu et al., 2007). Analysis of these PULs revealed that about a half of them contained CAZymes of unknown functions, whereas the other half contained at least 2 PULs of identical compositions and 10% of these PULs were unique (Lapébie et al., 2019). Not all CAZymes were associated with a PUL but, overall, it was estimated that a few thousand enzyme combinations are required to break down all possible glycans (Lapébie et al., 2019). The occurrence of PULs was more frequent in *Bacteroides* genus compared to other Bacteroidetes, and in line with this, Bt was estimated to dedicate almost a quarter of its genome to glycan metabolism (Xu et al., 2007, Lapébie et al., 2019). Bt was predicted to encode at least 230 GHs, but new families are frequently found (Xu et al., 2007).

1. 2. 4 Glycoside hydrolases

Glycoside hydrolases are divided into families based on sequence similarity (Henrissat et al., 1995, Henrissat, 1991, Cantarel et al., 2009). It is common that GHs from the same family can display different substrate specificities, whereas enzymes targeting the same substrate are placed in different families. Most but not all GHs are further grouped into 14 clans, GH-A to GH-N. Families within an individual clan share a common evolutionary ancestor, structural folds, and the catalytic mechanism, with the exception of GH23 and GH97 (Naumoff, 2011, Henrissat and Davies, 1997).

Glycoside hydrolases differ in their ability to process carbohydrates and therefore are separated into exo- or endo-acting, which is determined by the topology of the active site (Figure 1. 6) (Henrissat and Davies, 1997). Exo-acting enzymes possess a pocket topology (Figure 1. 6 a), which allows for the removal of a terminal sugar unit from the non-reducing end of a polysaccharide, generating a pool of monosaccharides (Davies and Henrissat, 1995, Henrissat and Davies, 1997). Endo-acting enzymes produce a range of oligosaccharides of varying length and have active sites of either open cleft or tunnel topologies (Figure 1. 6 b, c) (Davies and Henrissat, 1995). The open cleft facilitates contact of the enzyme with sugar units surrounding the scissile bond. The tunnel topology has evolved from the open cleft structure but developed distinct loops, which confer tight binding with the substrate (Davies and Henrissat, 1995). Exo- and endo-acting enzymes usually work in concert, where endo-acting enzymes depolymerise complex polysaccharides, making accessible structures to the exo-acting enzymes or vice versa.

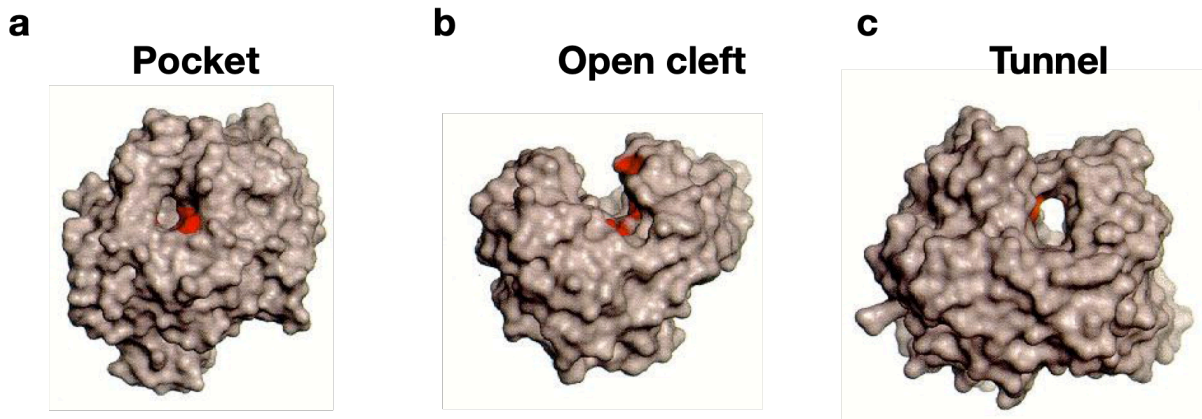


Figure 1. 6 Topologies of the active site of exo- and endo-acting glycoside hydrolases as indicated. Figure adapted from (Davies and Henrissat, 1995)

1. 2. 4. 1 Subsite nomenclature

Glycoside hydrolases typically cleave glycosidic bonds from the non-reducing ends. A subsite of a GH comprises all amino acids which interact with sugars on either of the sides of the scissile glycosidic bond. Davis and colleagues proposed a system where the subsites, which recognise sugars from the non-reducing end are given the increasingly negative numbers, while the ones recognising sugars towards the reducing end of the polysaccharide are given the increasingly positive numbers (Figure 1. 7). In this nomenclature the scissile bond is located between -1 and +1 subsites (Figure 1. 7) (Davies et al., 1997).

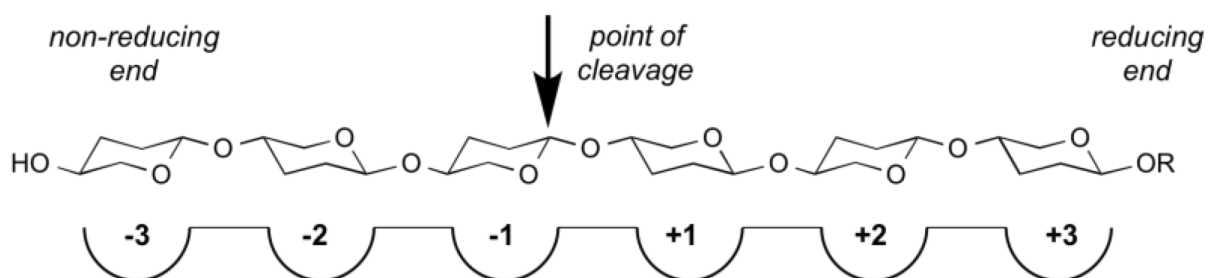


Figure 1. 7 Subsite nomenclature of a glycoside hydrolase. Reducing and non-reducing ends, which respective subsite are indicated. Figure adapted from

Cazypedia.org, <http://www.cazypedia.org>, accessed on 04.03.2021.

1. 2. 4. 2 Catalytic mechanism

Glycosidic bonds are very stable with a half-life of over a million years and yet Glycoside hydrolases are very efficient at their hydrolysis. This is achieved by the distortion of the glycoside at the -1 subsite into a half chair 3H_4 or 4H_3 or boat ${}^{2,5}B$ or $B_{2,5}$ sugar conformations (Davies and Henrissat, 1995, Ardèvol and Rovira, 2015).

Glycoside hydrolases exhibit two main mechanisms of glycosidic bond hydrolysis, resulting in either inversion ($\alpha \rightarrow \beta$; $\beta \rightarrow \alpha$) or retention ($\alpha \rightarrow \alpha$ or $\beta \rightarrow \beta$) of the anomeric carbon (C1) configuration. Both inverting and retaining reactions require two catalytic carboxylates and pass through an oxocarbenium ion-like intermediate state. The transition state determines the energy level required for bond hydrolysis and is stabilised by the positive charge between the anomeric carbon (C1) and the ring oxygen (Davies and Henrissat, 1995). Some enzymes from the families GH18, GH20, GH55, GH84, GH85 and GH103 have been reported to operate via substrate-assisted catalysis, where oxygen on C₂ of the sugar at the -1 subsite acts as a nucleophile and forms an oxazoline intermediate (Vuong and Wilson, 2010).

1. 2. 4. 3 Inverting mechanism

Inverting glycoside hydrolases display a single displacement mechanism, where a general base removes a proton from a water molecule, generating a hydroxyl ion and activating the nucleophilic attack on the anomeric carbon (Figure 1. 8). In turn, a general acid donates a proton to facilitate displacement of the leaving group (Figure 1. 8). The two catalytic carboxylates, usually Glutamate and Aspartate, are

positioned 6-11 Å apart to accommodate a water molecule and the substrate in the active site (Zechel and Withers, 2000, Rye and Withers, 2000).

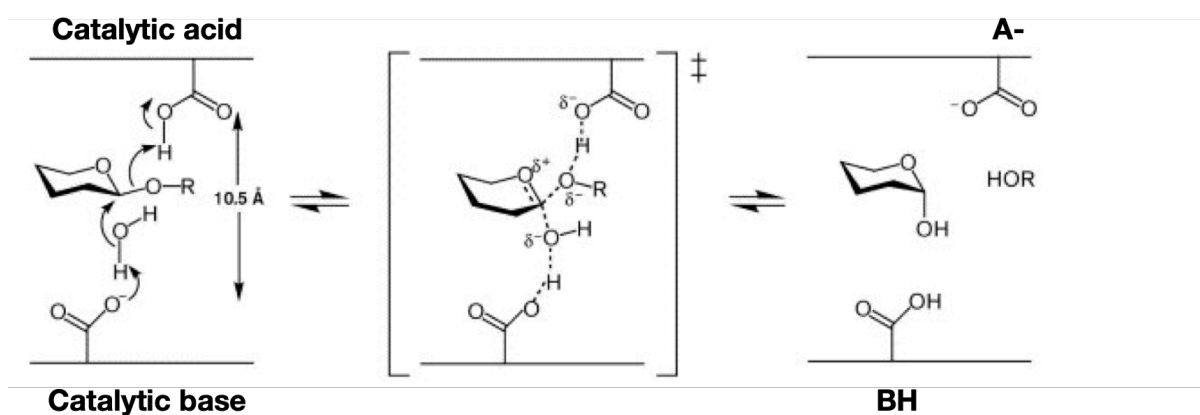


Figure 1. 8 Inverting mechanism of glycoside hydrolases. Oxocarbenium ion-like transition state is shown in brackets, catalytic acid/base carboxylates are indicated. Mechanism results in inversion of C1 conformation. Figure adapted from Rye et al. (2000).

1. 2. 4. 4 Retaining mechanism

Retaining enzymes operate in a double-displacement mechanism, which involves two amino acid residues where one functions as a general acid/base and the other as a nucleophile, usually glutamate or aspartate, located 5.5 Å apart (Davies and Henrissat, 1995, Ardèvol and Rovira, 2015). This is a two-step reaction, which passes through glycosylation and deglycosylation steps (Figure 1. 9). In the first phase the catalytic amino acid attacks the anomeric centre of the glycoside, acting as a nucleophile. The second residue acts as an acid, donating a proton to the glycosidic oxygen, forming a glycosyl enzyme intermediate. In the second step, the proton donating acid functions as a base and removes a proton from a water molecule, inducing a nucleophilic attack on the anomeric centre and displacing the sugar (Figure 1. 9) (Zechel and Withers, 2000, Rye and Withers, 2000). This mechanism is deployed by the largest clan of glycoside hydrolases, GH-A, which process β-glycosidic bonds (Naumoff, 2011).

1. Glycosylation step

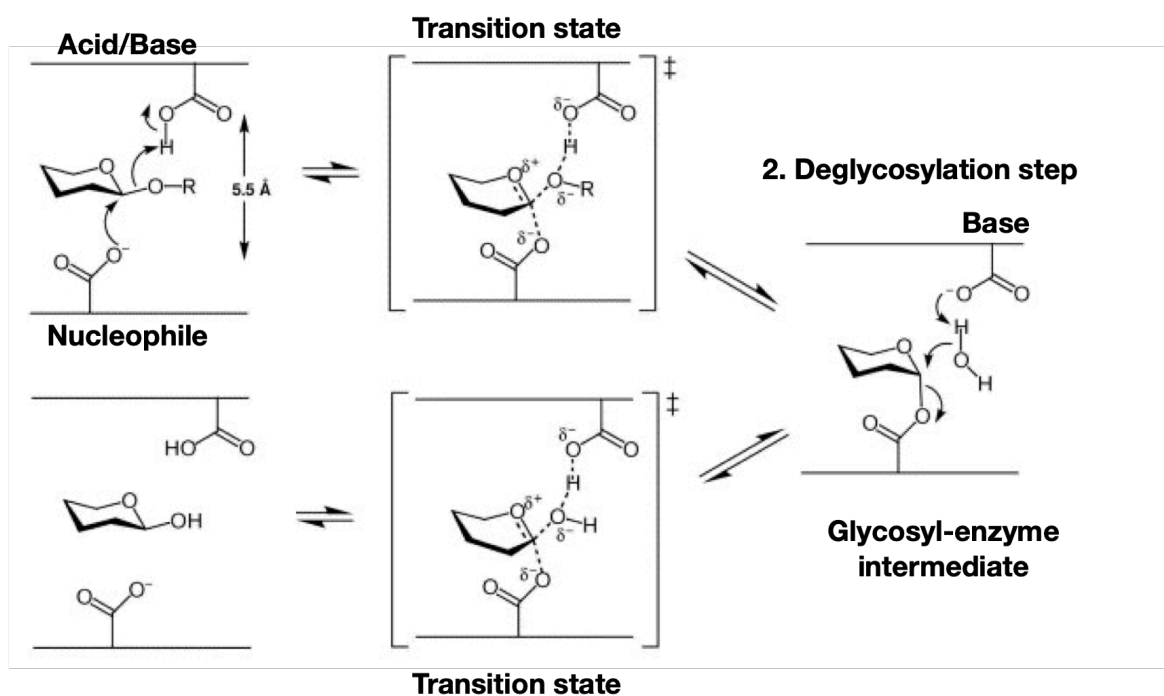


Figure 1. Retaining mechanism of Glycoside Hydrolases. Transitions states, Glycosyl-enzyme intermediate, Acid/base and nucleophile residues are indicated. Process is mediated in a two-step reaction, resulting in retention of C1 conformation. Figure adapted from Rye et al. (2000).

1. 2. 5 Regulation of PULs

Expression of PULs is typically regulated via 3 mechanisms: 1) SusR-like regulators; 2) Hybrid Two Component Systems (HTCS); 3) Extra-cytoplasmic (ECF) sigma/Anti-sigma factors (Ravcheev et al., 2013). Regulation through SusR is rare, and most PULs are regulated via HTCS or ECF- σ /anti- σ pairs (Martens et al., 2009b, Sonnenburg et al., 2006). Interestingly, PULs mediating degradation of host glycans such as mucins are regulated with ECF- σ /anti- σ pairs, whilst those targeting plant polysaccharides typically use HTCS (Martens et al., 2011, Martens et al., 2008). In the ECF- σ /anti- σ systems, anti- σ interacts with the TonB box of a SusC-like proteins in the periplasm but it is also coupled with ECF- σ at the

cytoplasmic face of the inner membrane, repressing transcriptional activation. Inducible conditions cause a conformational change in the SusC-anti- σ complex, releasing ECF- σ , which modulates gene expression (Martens et al., 2009b). HTCS are composed of a periplasmic sensor domain, transmembrane helix, and a cytoplasmic Histidine Kinase, receiver domain and AraH-like DNA-binding domain in a single polypeptide (Townsend et al., 2013) Glycan fragment binding induces a conformational change, which triggers autophosphorylation of the cytoplasmic domains, resulting in differential transcription of the target genes (Lowe et al., 2012).

1. 3 Metabolism of carbohydrates

1. 3. 1 Dietary carbohydrates

Plant cell wall is composed of a variety of sugars, forming highly complex polymers (Figure 1. 10). These include cellulose, followed by pectins such as rhamnogalacturonan II, and hemicellulose, comprising of xylan, xyloglucan, galacto- and gluco-mannan, and mixed linkage β -glucan (Lattimer and Haub, 2010, Cosgrove, 2005). Plant glycans also include storage molecules such as resistant starch and fructans. Dietary fibre differentially regulates microbial diversity in the gut, where glycan content is able to select for a certain subset of species, inhibiting proliferation of others (Patnode et al., 2019).

A significant proportion of plant carbohydrates comes in the form of insoluble fructans such as inulin and levan. These are differentially utilised by a range of gut *Bacteroides*, but generally, *B. thetaiotaomicron* displays a strong preference for levan, whereas others such as *B. caccae*, *B. ovatus*, and *B. fragilis* are tuned to

degrade inulin (Sonnenburg et al., 2010). Inulin and levan are homopolymers of fructose composed of repeating β -2,1 or β -2,6 units, respectively, (Figure 1. 10) and their degradation does not require a sophisticated enzymatic machinery. Fructan utilisation PULs comprise 9 proteins, some of which bind and transport fructo-oligosaccharides and only 3 act as depolymerising enzymes (Sonnenburg et al., 2010). Similarly, *B. ovatus* and *B. fragilis* orchestrate degradation of plant β -mannans (Figure 1. 10), such as galactomannan, using a small locus, comprising of 2 endo- and 1 exo-acting enzymes (Bågenholm et al., 2017, Reddy et al., 2016, Kawaguchi et al., 2014). In contrast, heparin and heparan sulphate are more complex polysaccharides, which are composed of repeating units of Glucuronic Acid (GlcA) or Iduronic Acid (IdoA) alternating with D-glucosamine (GlcN) (Figure 1. 10). Moreover, all units within these polysaccharides are differentially sulphated, resulting in highly negatively charged hydrophilic molecules, which are produced as part of the extracellular matrix by mammalian cells. Unlike fructans, deconstruction of this group of polysaccharides involves a PUL composed of 15 proteins, including enzymes which can de-sulphate and cleave glycosidic bonds between amino and uronic sugars (Cartmell et al., 2017). The complexity of dietary glycans reflects the complexity of the enzymatic apparatus necessary for its utilisation. Pectins, such as rhamnogalacturonan-I (RGI) and rhamnogalacturonan-II (RGII) form highly branched molecules, whose degree of polymerisation and oligosaccharide decorations is dependent on the plant species and can involve up to 13 different sugars linked with numerous glycosidic bonds (Figure 1. 10) (Luis et al., 2018, Ndeh et al., 2017). Depolymerisation of such complex polymers requires at least 30 different enzymes grouped into 5 separate genetic clusters in Bt (Ndeh et al., 2017, Luis et al., 2018). Elements of pectin-

degrading systems are retained in other *Bacteroides species*, and, given the complexity of pectic polymers, species have been suggested to cooperate to deconstruct them.

Production of carbohydrate-degrading enzymes comes at a huge metabolic cost, therefore a proportion of bacterial species deploy a 'selfish' strategy for glycan metabolism. PULs are usually organised to contain a surface-localised endo-acting enzyme, which initiates glycan breakdown and produces a pool of oligosaccharides, depolymerisation of which is then completed intracellularly. In this type of strategy, species often display a specific preference for the substrate and do not share glycan intermediates with other species (Sonnenburg et al., 2010, Cuskin et al., 2015b, La Rosa et al., 2019). However, the strategy of utilisation of the same substrate is not necessarily conserved. As for example, *B. caccae* outcompetes *Bt* and does not permit sharing of inulin with other members of the gut microbiota, whereas *B. ovatus* cooperates with *B. vulgatus* during growth on inulin, helping to generate a pool of fructo-oligosaccharides in return for reciprocal benefits (Rakoff-Nahoum et al., 2016, Sonnenburg et al., 2010). *B. ovatus* adopts a similar 'sharing' model for the degradation of xylan, the main plant cell wall polysaccharide. However, the degree of xylan complexity dictates the mechanism for its utilisation, where more simple structures such as those released from wheat arabinoxylan and birch glucuronoxylan (Figure 1. 10) can be shared with *Bifidobacterium adolescentis* (Rogowski et al., 2015). *B. ovatus* also liberates oligosaccharides from more complex corn glucuronoarabinoxylan (Figure 1. 10), but these are not consumed by *B. adolescentis* due to the lack of the appropriate apparatus, but it is possible that these are utilised by other members of the microbiota (Rogowski et al., 2015). In contrast, *B. ovatus* deploys a 'selfish'

manner to degrade xyloglucans (Larsbrink et al., 2014). *B. ovatus* possesses a few distinct xylan-specific PULs, whose expression is determined by the complexity of the xylan substrate (Rogowski et al., 2015). The inter-phylum competition for the same carbon source was demonstrated by La Rosa et al. (2019), where an avid β -mannan (Figure 1. 10) user, *Roseburia intestinalis* from the Firmicutes phylum, deploys a 'selfish' mechanism, but at the same time permits sharing with *B. ovatus* while β -mannan is in excess. In nutrient-depleted conditions, the sharing ceases and *R. intestinalis* outcompetes *B. ovatus* (La Rosa et al., 2019).

Interestingly, while being able to degrade the most complex polysaccharides and possessing such a dramatic saccharolytic potential, human gut *Bacteroides* are incapable of breaking down crystalline cellulose (Figure 1. 10) (Martens et al., 2011). In contrast, this function has been designated to Bacteroidetes phylotype *AC2a*, inhabiting cow rumen and closely similar to a strain isolated from tammar wallaby, whose diet primarily consists of lignocellulose. Unlike β -glucan PULs in human gut *Bacteroides*, the PUL orchestrating cellulose degradation in *AC2a* produces two endo-acting enzymes localised to the cell surface, which cooperate to complement each other (Naas et al., 2015, Naas et al., 2014).

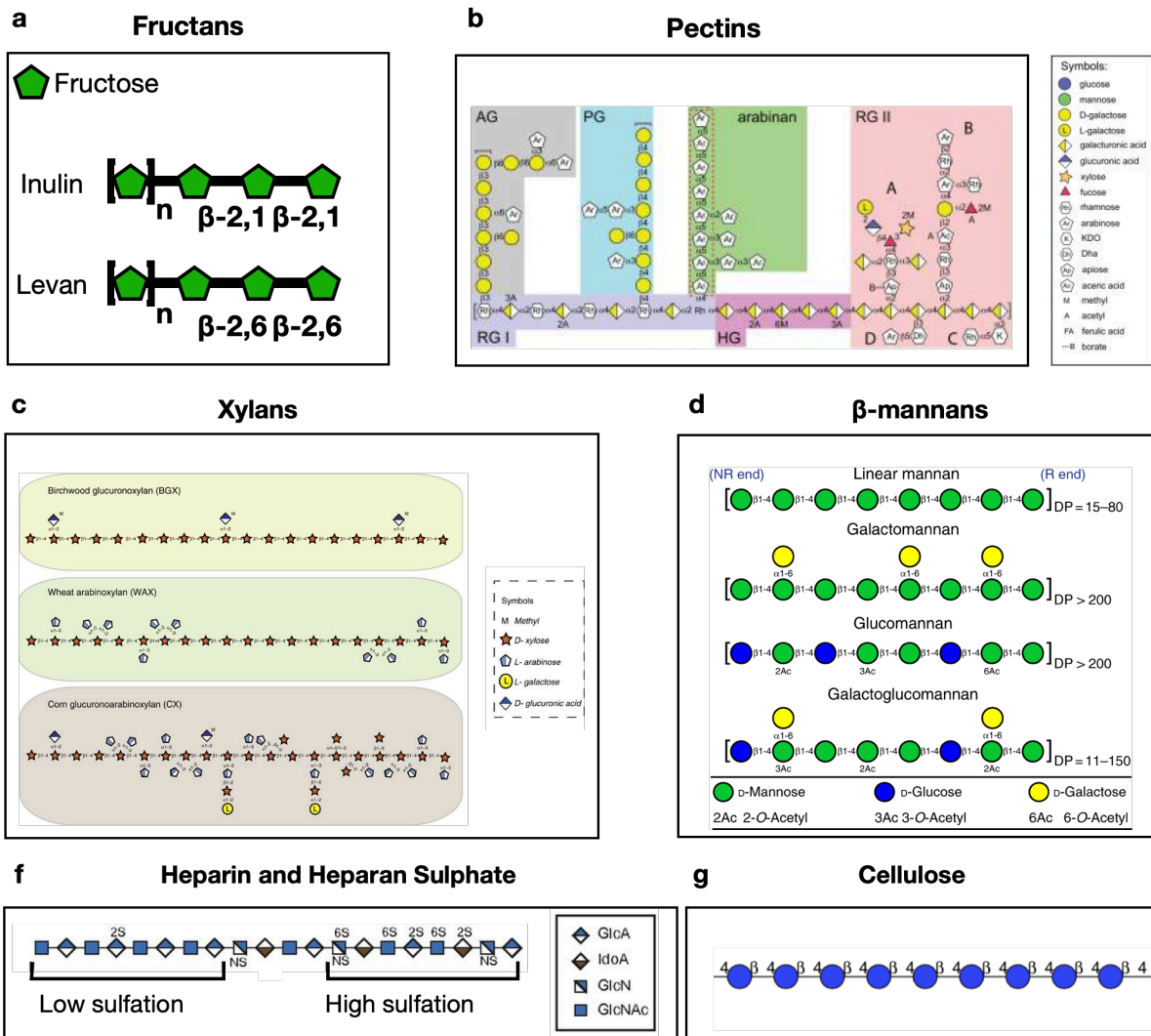


Figure 1. 10 Schematic structures of dietary carbohydrates. Panel a: structure of inulin and levan; Panel b: structure of pectins, figure adapted from Martens et al. (2011); Panel c: structure of birch glucuronoxylan, wheat arabinoxylan, and corn glucuronoarabinoxylan, figure taken from Rogowski et al. (2015); panel d: structure of plant β -mannans, figure adapted from La Rosa et al. (2019); Panel f: structure of heparin and heparan sulphate, adapted from Cartmell et al. (2017); Panel g: structure of cellulose, taken from Larsbrink and Mckee (2020). Monosaccharides are represented with appropriate symbols as per Consortium for Functional Glycomics format Raman et al. (2006)

1. 3. 2 Host glycans

In addition to dietary carbohydrates, the gut microbiota is able to degrade glycans which are derived from the host (Martens et al., 2008). Degradation of highly sulphated glycosaminoglycans (GAGs), which include chondroitin sulphate, dermatan sulphate as well as hyaluronic acid, is mediated by a single PUL, which is strikingly enriched with sulfatases and Polysaccharide Lyases (PLs) capable to cleave glycosidic bonds between uronic sugars (Ndeh et al., 2020). GAGs are highly preferable substrates for Bt maybe due to the fact that they are produced as free molecules, composing the synovial fluid and cartilage, and the extracellular matrix (Pudlo et al., 2015, Rogers et al., 2013). All host proteins, however, are highly decorated with glycans. Glycosylation is the primary mode of post-translational modification, determining protein folding, stability, and cellular localisation (Wang et al., 2014, Blom et al., 2004). Glycans are usually N- or O-bound to the Asparagine or Serine/Threonine residues of a protein, respectively (Blom et al., 2004).

1. 3. 2. 1 N-linked glycans

N-glycans decorate proteins such as α -1-acid-glycoprotein and albumin, ribonuclease B, lactoferrin, α -antitrypsin, all immunoglobulins (Goonatilleke et al., 2019). N-glycosylation begins with covalent attachment of the pentasaccharide core ($\text{Man}_3\text{GlcNAc}_2$) to Asparagine (Asn) residues of a protein (Chung et al., 2017, Wang et al., 2014). The core is then further modified, splitting N-glycans into three groups: 1) High mannose; 2) Complex; 3) Hybrid (Figure 1. 11) (Chung et al., 2017, Higel et al., 2016). The core of High Mannose N-glycans (HMNG) is extended by mannose moieties linked by different glycosidic bonds, forming Man_5 -

GlcNAc_2 in mammals (Figure 1. 11 b). In yeast, the core is further decorated with up to several hundreds of mannose units, producing a highly complex hypermannose N-glycan (Figure 1. 11 b) (Chung et al., 2017, Ballou et al., 1974). Complex N-glycans display heterogeneity but generally $\text{Man}_3\text{GlcNAc}_2$ is extended with β -1,2-linked N-acetyl glucosamine (GlcNAc) followed by galactose via β -1,4 linkage, forming LacNAc antennae, which are commonly terminated with α -2,3 or α -2,6-linked Sialic Acid (Neu5Ac). In this type of N-glycans the core GlcNAc can also be decorated with α -1,6 or α -1,3 linked fucose (Figure 1. 11 c) (Chung et al., 2017). Hybrid N-glycans possess elements of both HMNG and Complex N-glycans, where LacNAc antennae capped with sialic acid are attached to one of the core mannose moieties and the second mannose residue is mildly decorated with additional mannoses. In plants, complex N-glycans contain a characteristic β -1,2-xylose side chain and the core GlcNAc can be decorated with α -1,3-linked fucose (Figure 1. 11 d) (Chung et al., 2017, Higel et al., 2016).

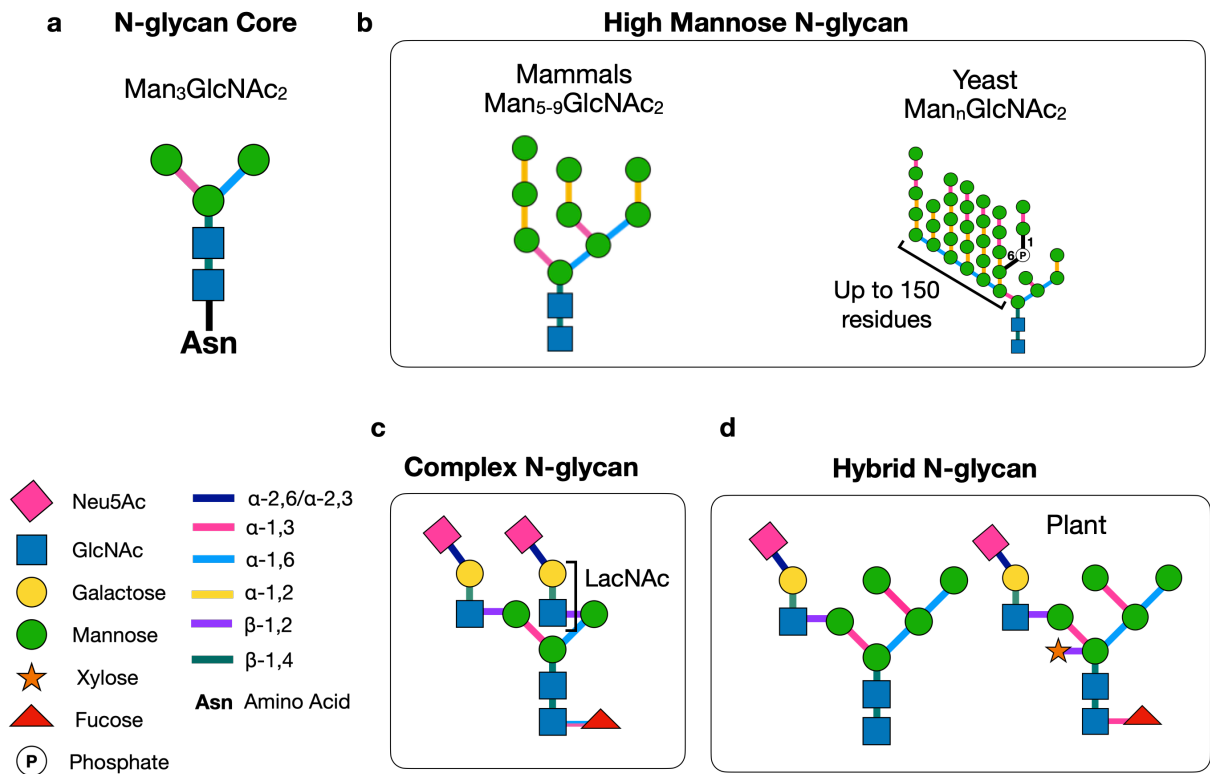


Figure 1. 11 Types of N-linked Glycans. Panel a: N-glycans core Man₃GlcNAc₂. Panel b: Mammalian and yeast High Mannose N-glycans. Panel c: structure of Complex N-glycan. Panel d: diagram of Hybrid N-glycans.

The composition and heterogeneity of N-glycans highlights the complexity of the mechanisms required for their utilisation. Bt was shown to dedicate multiple genetic loci to the degradation of complex N-glycans, expression of which was orchestrated by the dominant PUL. These loci combine into a system, where surface enzymes can de-sialate and release the entire N-glycan from the protein to be further depolymerised by a diversity of enzymes intracellularly (Briliūtė et al., 2019). Whilst this is specific for complex and Hybrid N-glycans, Bt dedicates a separate degradome to process HMNG (Cuskin et al., 2015b). In addition to Bacteroides, species of *Bifidobacterium* genus, *B. infantis* and *B. longum*, commonly associated with infant gut microbiota, produce similar endo-processive

enzymes which cleave complex as well as high-mannose N-glycans from a range of glycoproteins, including those found in Human Milk (Garrido et al., 2012).

1. 3. 2. 2 O-linked glycans

O-glycosylation of proteins occurs at serine (Ser) or threonine (Thr) residues (Figure 1. 5) (Joshi et al., 2018, Wang et al., 2014, Blom et al., 2004). O-glycosylation of proteins is highly diverse and can initiate with O-mannose, O-GalNAc, O-galactose, O-xylose, O-fucose, O-glucose, O-GlcNAc (Figure 1. 12 a) (Joshi et al., 2018).

O-mannosylation is restricted to yeast and the core mannose is linked to the protein backbone, which is then elongated by repeating α -1,2 mannosyl residues to form a linear polymer (Figure 1. 12 b) (Mora-Montes et al., 2009). Intestinal mucins are heavily decorated with O-glycans, which constitute up to 80% of the total weight of mucin glycoproteins (Blom et al., 2004, Larsson et al., 2009). O-glycosylation is initiated by the attachment of N-acetyl galactosamine (GalNAc), which is then extended into a poly LacNAc chain (GlcNAc-galactose units), which are then capped with α -linked sialic acid, galactose, GlcNAc, or GalNAc moieties (Figure 1. 12 c) (Joshi et al., 2018, Brockhausen and Stanley, 2015). Decoration patterns of mucins vary dramatically and Gal and GlcNAc moieties can be further modified with sulfation, resulting in gel-like macromolecules (Figure 1. 12 c) (Larsson et al., 2009). Sulphation usually precludes enzymatic degradation, despite this gut bacteria have developed a system to overcome this problem, allowing them to thrive on mucosal glycans (Derrien et al., 2004, Pudlo et al., 2015, Martens et al., 2008). Recently it was shown that 3 *Bacteroides* species: *Bt*, *B. fragilis*, and *B. caccae* as well as *Akkermansia muciniphila* release polyLacNAc chains of varying lengths from mucin glycoproteins using surface-localised endo-

β -galactosidases (Crouch et al., 2019). In addition to mucins, human milk is enriched in O-glycans, which decorate glycoproteins such as casein. In addition, Human milk oligosaccharides (HMOs) share structural similarity to mucin O-glycans. HMOs upregulate a range of genetic loci, which overlap with mucin and HMNG metabolism, in *B. fragilis* and Bt (Marcobal et al., 2011). The terminal sialic acid caps render protection to glycans against unspecific degradation, and interestingly, Bt removes sialic acid caps from HMOs but does not utilise it due to the lack of the necessary system (Marcobal et al., 2011). Free sialic acid is rapidly consumed by *B. fragilis* but also presumably by other members of the infant gut microbiota (Marcobal et al., 2011). This strongly indicates that once sialic acid has been removed from HMOs, other *Bacteroides* can probably participate in their depolymerisation. In addition to *Bacteroides*, *Bifidobacterium* possess HMO degrading enzymes, which allow them to share glycosyl-intermediates with each other (Lawson et al., 2020). O-glycans are a low priority substrate and their utilisation is rapidly repressed in the presence of other dietary sources (Pudlo et al., 2015). This behaviour, however, is not conserved in other *Bacteroides*, as for example *B. massiliensis* preferentially selects O-glycans over other substrates such as starch (Pudlo et al., 2015).

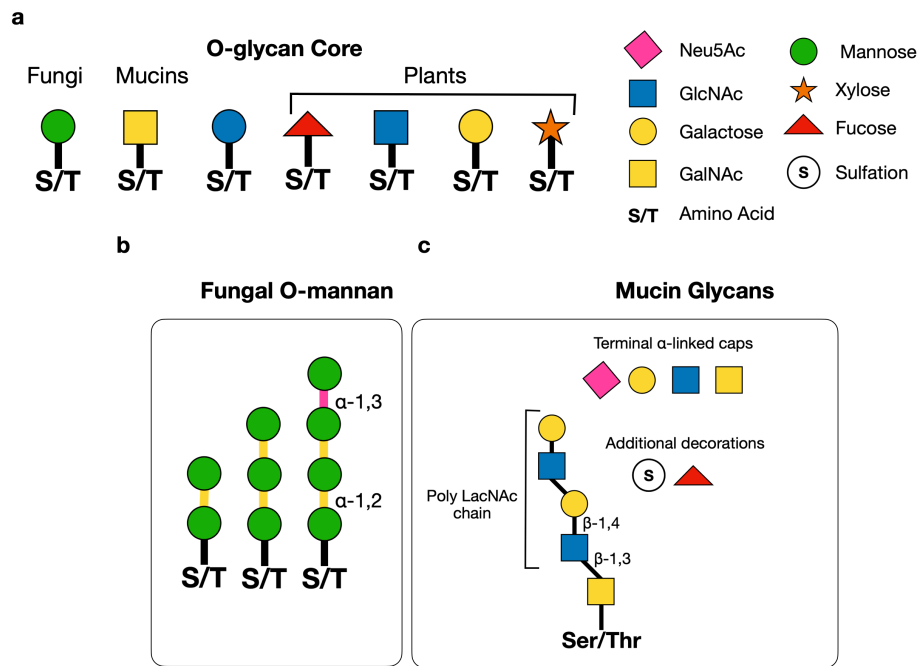


Figure 1. 12 Types of O-glycosylation. Panel a: Variety of O-glycan cores. Panel b: Structure of fungal O-mannans. Panel c: Decoration of mucin glycoproteins in the intestinal tract.

1. 4 Fungal cell wall

Alongside dietary and host glycans, other microbes inhabiting the gut can provide a source of nutrients for glycan degraders such as *Bacteroides*. The yeast cell wall is composed of multiple layers of polysaccharides: chitin, β -glucan, and mannan, which create a shield, conferring protection against oxidative and osmotic stress, determining cell wall rigidity and also defining recognition of the fungus by the immune system (Levin, 2011, Klis et al., 2006, Netea et al., 2008).

1. 4. 1 Structure of the cell wall

The fungal cell wall can be divided into three separate sugar layers. In *Saccharomyces* and *Candida spp*, the innermost layer is composed of a β -1,4-GlcNAc polymer, chitin (Figure 1. 13 a, b). This is then decorated with a layer of β -1,3-glucan crosslinked via β -1,6 bonds (Klis et al., 2006, Gow et al., 2017). The

outer layer is composed of a matrix of highly mannosylated cell wall proteins (CWP), covalently attached to β -1,6-glucan (Figure 1. 13 a, b) (Hall and Gow, 2013). Most of these CWP are GPI-anchored, some however can be attached via Protein internal repeats (Pir) and perform a diversity of functions (Gow et al., 2017). There are at least 66 CWP in *S. cerevisiae*, whereas some *Candida* species possess hundreds of such proteins (De Groot et al., 2003). Expression of these proteins is tightly regulated, and they determine adaptation to stress, morphogenesis, and virulence (Gow et al., 2017)

Mannosylation of the cell wall is primarily N-linked but O-bound mannans also exist. N-mannans possess an N-glycan core, which is then elongated with up to 200 α -1,6-linked mannose moieties, forming a linear backbone. A range of mannosyltransferases then extends the backbone with α -1,2 and α -1,3-linked mannan sidechains (Figure 1. 13 c) (Ballou et al., 1974). In *Saccharomyces spp.*, the number of mannose residues in the side chain is dependent on the strain, however the longest was discovered to be a pentasaccharide, consisting of man- α 1,2-man- α 1,2-a1,3-man- α 1,3-man (Ballou et al., 1974). In addition, linear side chains are decorated with phosphates via phosphodiester linkage and elongated with α -1,3 mannobiose or mannotriose (Figure 1. 13 c) (Ballou, 1976, Corbacho et al., 2010, Karson and Ballou, 1978). O-mannans are short linear polymers composed of either α -1,3 or α -1,2-linked mannosyl residues (Figure 1. 13 d) (Ballou, 1990).

The architecture of mannan from *Candida spp.* is more complex. Whilst retaining the overall α -1,6, α -1,2, α -1,3 oligomannose organisation, the branches are also capped with β -1,2 mannosides (Figure 1. 13 e) (Kobayashi et al., 1994). β -

mannosylation of the sidechains is highly heterogeneous and depends on the serotypes and strain of *Candida species* (Yan et al., 2020).

The acid stable (not linked with phosphodiester linkages) mannan of *C. albicans* serotype A can contain up to four β -1,2-mannosyl residues, capping either α -1,2 or α -1,3 linked sidechains, extending them to manno-octaoses in some places (Figure 1. 13 e) (Shibata et al., 1992, Yan et al., 2020). None or a single β -mannosylation also occurs (Yan et al., 2020, Shibata et al., 2007). In contrast, *C. albicans* serotype B lacks β -mannosylation in the acid stable mannan (Mille et al., 2008). The differentiation between serotypes relies on the sensitivity of *C. albicans* to 5-fluorocytosine, where B is resistant, and A is not (Mercure et al., 1996). The serotype B is a lot less virulent and less common than the serotype A, and majority of clinical isolates, including the laboratory strain SC5314, belong to the Serotype A (Mercure et al., 1996, Odds et al., 2004). $^1\text{H-NMR}$ structure of mannan from *C. albicans* from both serotypes shows that, in addition to β -mannan, some sidechains have ubiquitous α -1,6-linked mannosyl units attached (Figure 1. 13 e) (Shibata et al., 2007, Yan et al., 2020). Patterns of β -mannosylation are highly variable across *Candida* spp and, for example, *Candida auris* and *Candida haemulonii* only scarcely distribute β -mannoses in their cell walls (Yan et al., 2020). Interestingly, regardless of the serotype, all *C. albicans* species retain β -mannosylation of phosphomannan and phospholipomannan, where a single mannose unit is linked to a phosphate moiety and then elongated to form β -mannooligosaccharides (Figure 1. 13 d, e) (Kobayashi et al., 1994). Recently it has been shown that, while forming three visibly separate layers, all layers in the cell wall are intertwined, where some mannosylated proteins are embedded into

the glucan layer, forming an extremely complex multi-polysaccharide matrix
(Figure 1. 13 b) (Lenardon et al., 2020)

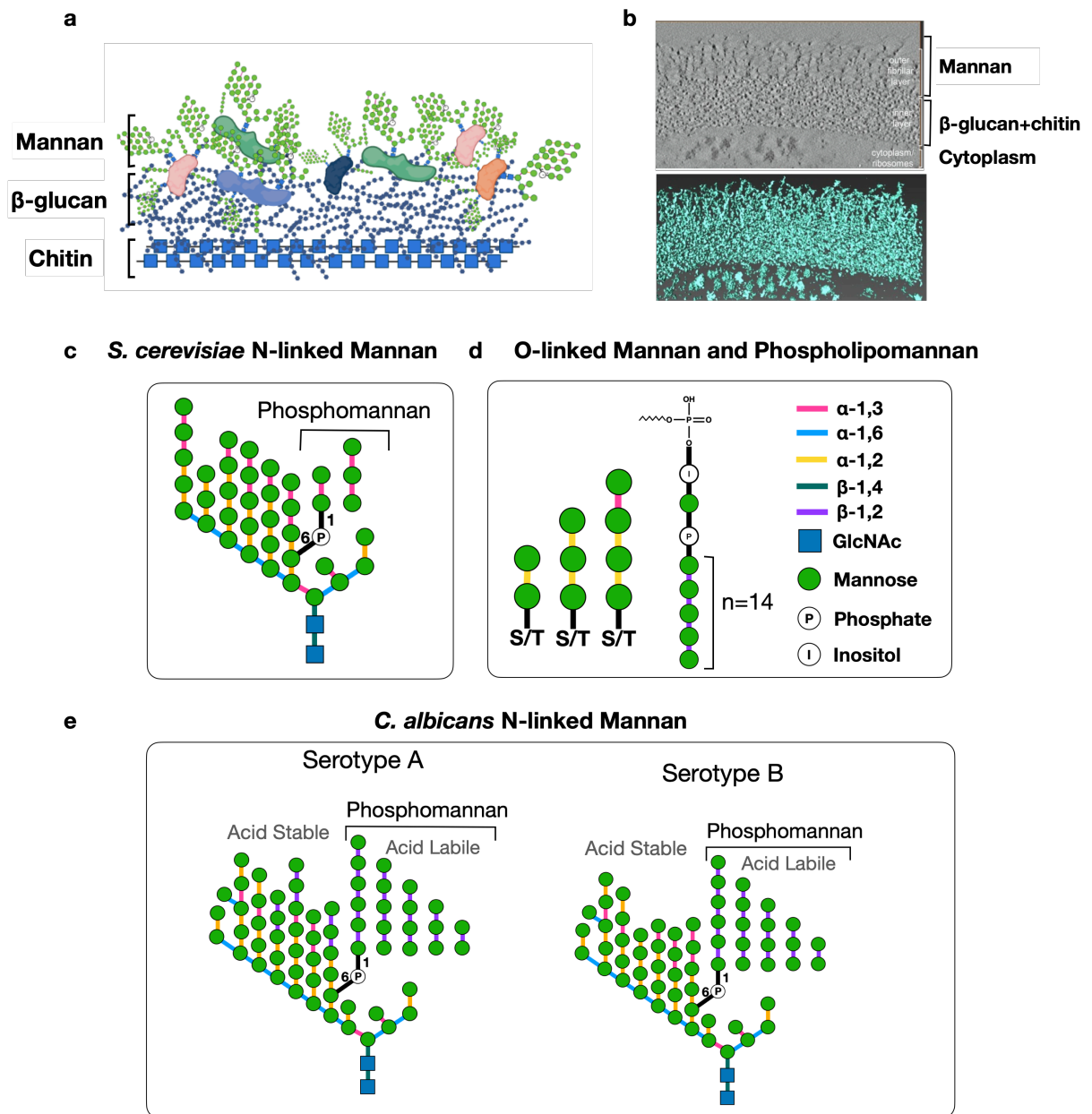


Figure 1. 13 Structure of fungal cell wall. Panel a: diagram of multi-layered structure of cell wall.

Panel b: top picture – 2D optimised tomogram of *C. albicans* cell wall; bottom picture:

reconstructed 3D model of *C. albicans* cell wall, pictured adapted from Lenardon et al. (2020).

Panel c: diagram of N-linked mannan in *S. cerevisiae* cell wall. Panel d: diagram of O-linked

mannan in both *S. cerevisiae* and *C. albicans* and phospholipomannan from *C. albicans*. Panel e:

diagram of N-linked mannan in *C. albicans* serotype A and B.

1. 4. 2 Recognition of the cell wall by the Immune system

Polysaccharide constituents of the cell wall define fungal recognition by the immune system and thus determine their survival in the host. The first line defence against fungal invasions relies on phagocytosis by neutrophils and macrophages as well as dendritic cells, which activate the adaptive immune response (Erwig and Gow, 2016, Swidergall, 2019). This is dependent on the interplay between a range of Pattern Recognition Receptors (PRR) expressed by these immune cells, which carefully examine the epitopes presented by fungal cells (Figure 1. 14) (Erwig and Gow, 2016, Swidergall, 2019). Signalling of these receptors polarises the immune system towards either inflammatory or tolerogenic states. *In vivo* models using knock out mice highlight the complexity of this interplay as usually the phenotype associated with a set of genetic manipulations *in vitro* or *ex vivo* is often unattainable *in vivo* and vice versa.

1. 4. 2. 1 Immune recognition of α -mannan

N-linked mannan is thought to be recognised through its terminal α -1,2 α -1,3 residues by the mannose receptor (CD206) located on a range of immune cells such as macrophages, dendritic cells (DCs), and endothelial cells (Kéry et al., 1992). *C. albicans* strains deficient in N-glycans elicit only 20% of the total pro-inflammatory response in human monocytes *in vitro* and display a highly attenuated virulence *in vivo*, resulting in 90% survival rates (Netea et al., 2006). However, the loss of this receptor is not critical, as mice deficient in CD206 do not exhibit abnormal defence responses to systemic *Candida* infection and their

macrophages are still able to perform efficient phagocytosis (Lee et al., 2003). Dendritic cell receptor, Dectin-2 (CLEC6A) (Figure 1. 14) is a central α -mannan receptor and its deletion exacerbated fungal burden in mice, bone marrow derived dendritic cells from these mice failed to respond to both purified mannan and whole *C. albicans* cells (Saijo et al., 2010, Ifrim et al., 2016, Mcgreal et al., 2006). Moreover, Dectin-2 associates with Fc γ R to polarise naïve CD4⁺ cells towards TH17 phenotype, central to the antifungal defence (Saijo et al., 2010). Another dendritic cell receptor, DC-SIGN (Figure 1. 14), has shown specificity for the α -linked epitopes in N-mannan from *Candida spp* but not *S. cerevisiae* (Guo et al., 2004, Cambi et al., 2008).

The role of O-linked mannan in the host antifungal response is thought to be less important (Netea et al., 2006). O-mannan is recognised by Toll-like receptor 4 (TLR4) (Figure 1. 14), however strains lacking O-mannan were still highly immunogenic and were eagerly phagocytosed (Netea et al., 2006). Involvement of TLR4 in antifungal responses remains unclear, as this receptor primarily orchestrates antibacterial defence mechanisms, recognising GlcNAc and 3-deoxy-3-manno-2-octulosonic acid components of bacterial lipopolysaccharide (LPS) (Cochet and Peri, 2017).

In addition to acting as epitopes for innate PPRs, α -mannan generates a pool of antibodies, which serve as biomarkers of Chron's disease (CD) (Israeli et al., 2005). Terminal man- α 1,3-man- α 1,2 decorations have been shown to induce production of Anti-*Saccharomyces cerevisiae* antibodies (ASCA) (Young et al., 1998). These are also detected in sera of CD patients upon stimulation with mannan from *C. albicans* (Standaert-Vitse et al., 2006).

1. 4. 2. 2 Immune recognition of β -mannan

β -1,2 mannoooligosaccharides from *Candida* cell wall are recognised via Galectin-3 (Figure 1. 14), which is expressed by an array of immune cells including macrophages and epithelial cells (Fradin et al., 2000, Kohatsu et al., 2006).

Kohatsu et al. showed that activation of Galectin 3 required oligosaccharides where β -1,2-mannosides were linked to the underlying α -mannan or phosphate (Kohatsu et al., 2006). Interestingly, while being attached to macrophages stimulation of Galectin 3 induced TNF- α production, however in assays using recombinant protein, binding of Galectin 3 to *C. albicans* cells resulted in cell death (Kohatsu et al., 2006). This fungicidal effect of the recombinant protein was found to be dependent on its interaction with capping β -1,2 mannosides, which are attached to the branches of the cell wall via either phosphodiester or α -1,2 but not α -1,3 glycosidic bonds (Kohatsu et al., 2006).

1. 4. 2. 3 Immune recognition of the inner layer of the cell wall: β -glucan and chitin

The inner layer of the fungal cell wall composed of chitin and β -1,3-glucan is extensively masked by mannoproteins (Figure 1. 14). Despite being exposed only at the scars of budding yeast and not filamentous cells, it evokes a potent immune response *ex vivo* via interaction with Dectin-1 receptor (Figure 1. 14) (Brown et al., 2003, Gantner et al., 2005). Netea et al. (2006) showed that in the absence of N- or O-linked mannan, the residual inflammatory response was mediated via recognition of the β -1,3-glucan layer by Dectin-1 receptor. However, *in vivo* experiments with Dectin-1 knock out mice suggested that the loss of this receptor on its own is not sufficient to exacerbate fungal infection as these mice developed a normal immune response (Saijo et al., 2007). Activation of Dectin-1 leads to

production of TNF- α and was suggested to require co-stimulation with TLR2 (Brown et al., 2003, Gantner et al., 2003). Interestingly, Dectin-1 cooperates with a β -mannan recognising receptor, galectin 3, to mount the TNF- α response in the presence of *C. albicans* but not *S. cerevisiae* (Esteban et al., 2011). Carriage of a Single Nucleotide Polymorphism (SNP) in CLEC7a allele results in defective Dectin-1 signalling in the gut and was found to be strongly associated with spontaneous ulcerative colitis refractory to treatment (Iliev et al., 2012).

The exact recognition of chitin epitopes, which are also exposed at the bud scars along with β -glucan, is not well described. GlcNAc fragments but not long polymers can be recognised by the TLR2 on murine macrophages *in vitro* and *in vivo*, contributing to the TH-17 mediated anti-fungal immunity (Da Silva et al., 2008). Determination of the crystal structure of the TLR2 revealed that oligomers of at least 6 GlcNAc residues are required to facilitate an inflammatory response (Fuchs et al., 2018). Interestingly, the authors suggested that chito-oligosaccharides shorter than 5 units may polarise receptor signalling towards an anti-inflammatory phenotype (Fuchs et al., 2018). Due to the discrete position of the chitin layer in the cell wall, exposure of these epitopes will be dictated by the overall architecture of the cell wall.

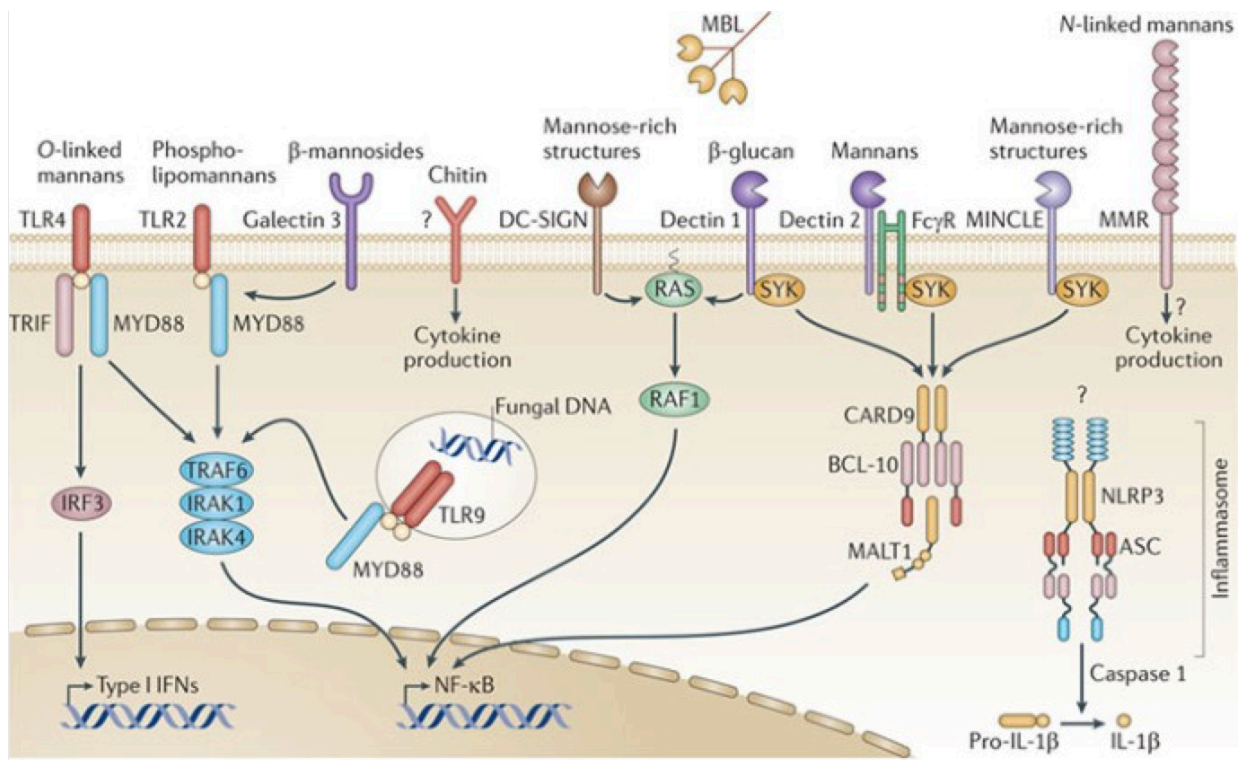


Figure 1. 14 Summary on the recognition of fungal cell wall polysaccharides by the Pattern Recognition Receptors in the host. Each epitope and its appropriate PRR are indicated in the figure. N-mannan is recognised by mannose receptor (MMR), DC-SIGN, MINCLE, and Dectin-2- Fc γ R receptors; O-mannan is recognised by TLR4; β -mannan is recognised by Galectin 3, which associates with TLR2; recognition β -glucan is sensed via Dectin-1; chitin is sensed via an unknown receptor, possibly TLR2. Figure adapted from Gow et al. (2012).

1. 5 Utilisation of fungal cell wall polysaccharides by gut *Bacteroides*

1. 5. 1 Breakdown of β -glucan

Members of gut *Bacteroides* are well accustomed to digest β -glucan. Mixed linkage β -1,4/1,3 glucan is a common component of oats and barley, whereas a β -1,3-linked homopolymer, which can be differentially decorated with β -1,6 units, is found in microbial cell walls. *B. ovatus* was first discovered to process barley β -glucans using a surface-endo-glucanase, which also displayed activity on all other

types of β -glucans such laminarin and yeast glucan (Tamura et al., 2017). The β -glucan PUL was found to be retained in all strain of *B. xylanisolvens* and *B. uniformis* and some strains of *B. fingoldii* and *B. cellulosilyticus* and was also detected at least once in 90% of human gut metagenomes (Tamura et al., 2017). Organisation of fungal β -glucan is relatively specific as it is composed of long β -1,3-linked polymers, cross-linked with β -1,6 bridges. Interestingly, while being unable to utilise barley β -glucan, Bt possesses a PUL strictly specific for fungal β -1,6 glucan (Martens et al., 2011, Temple et al., 2017). Structural organisation of this PUL is distinct from barley β -glucan PUL as it contains an endo- β -1,6-glucanase, which displays a strict specificity long β -1,6 polymers (pustulan) only (Temple et al., 2017). Analysis of other *Bacteroides* genomes revealed that homologous PULs were also present in *B. ovatus*, and *B. xylanisolvens* and some *B. fingoldii* strains as well as a small number of Bacteroidetes (Temple et al., 2017). These data suggest that gut *Bacteroides* are capable of modifying fungal cell wall, however as discussed in Section 1.4, the β -glucan layer is masked by the matrix of mannan and is only available at the bud scars of dividing yeast, suggesting its accessibility is most likely limited.

1. 5. 2 Breakdown of fungal mannan by *B. thetaiotaomicron*

Bt was shown to upregulate three specific PULs in response to α -mannan from *S. cerevisiae* (Figure 1. 15) (Martens et al., 2011, Martens et al., 2008, Cuskin et al., 2015b). These three PULs were confined to the utilisation of hypermannose N-glycan, and the degradation of HMNG or fungal β -1,6-glucan is orchestrated by two additional distinct PULs. Mannan-specific PULs were annotated as MAN-PUL1, MAN-PUL2, and MAN-PUL3, where proteins assembled a machinery where surface endo-mannanases cleave large oligosaccharides from yeast

mannan, which are then transported into the periplasmic space and further depolymerised into smaller fragments (Figure 1. 16) (Cuskin et al., 2015b). MAN-PUL2 plays a central role in mannan degradation and its deletion aborted ability of Bt to grow on yeast mannan, while Bt strain lacking MAN-PUL1/3 displayed a defective growth profile. Interestingly, *in vivo* assays showed that Bt strain $\Delta pul1/2/3$ was able to outcompete wild type Bt when mice were fed polysaccharide free diet. However, when glycans were reintroduced into the diet, the opposite was observed (Cuskin et al., 2015b). Elements of mannan PULs were detected in at least 60% of human metagenomes (Cuskin et al., 2015b). All sequenced Bt strains possess three mannan PULs and display robust growth on mannan from *S. cerevisiae*, *C. albicans* and *S. pombe*, whereas fragments of MAN-PUL1 and MAN-PUL2 were found in other gut Bacteroides, such as *Bacteroides ovatus* and *Bacteroides xylanisolvens* (Cuskin et al., 2015b). Genome analysis revealed that *B. xylanisolvens* strains *NLAE- zI- P732*; *-P352*; *-P393*; *-P736*; *P727* isolated from pigs have inherited MAN-PUL-1 from Bt via conjugative transposition, however most *B. xylanisolvens* or *B. ovatus* strains were unable to grow on branched fungal mannan but displayed growth on simplified mannan variants (Cuskin et al., 2015b).

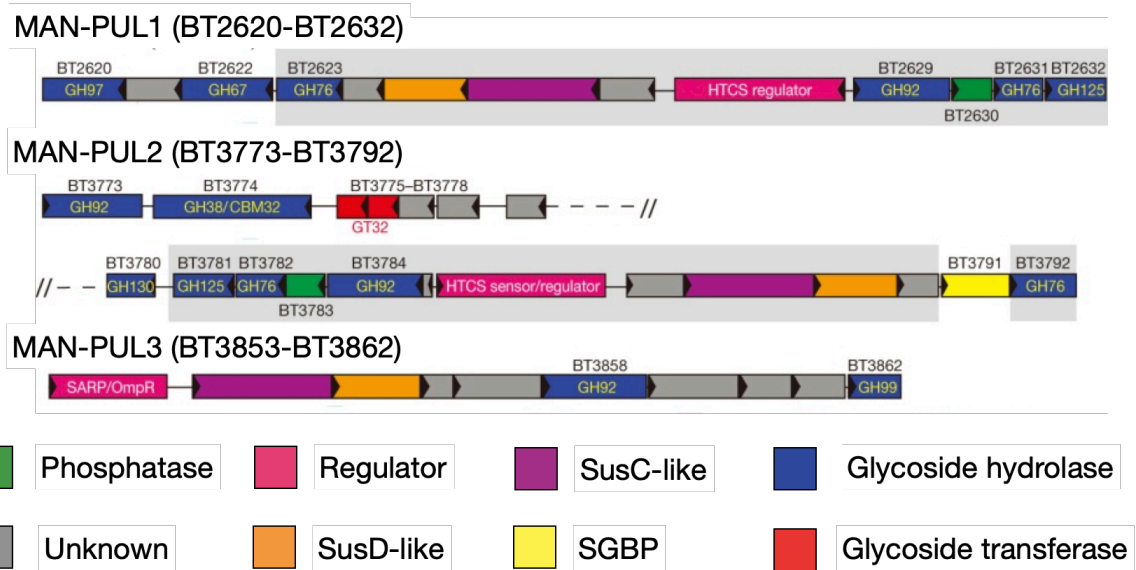


Figure 1. 15 Three PULs upregulated in *Bt* in response to mannan from *S. cerevisiae*. Figure adapted from Cuskin et al. (2015).

The enzymatic apparatus of mannan depolymerisation in *Bt* involves 12 α -mannan specific exo- and endo-acting enzymes from 5 different GH families (Figure 1. 15). The surface endo-acting mannosidase BT3862 (GH99) alleviates steric constraints by cleaving internal α -1,2 bonds, releasing α -1,3 disaccharides from mannan sidechains. Non-mannan PUL encoded GH92s likely also contribute to the removal of some side chains enabling the surface endo α -1,6 mannanases from family GH76 (BT3792 and BT2623), which require undecorated mannan to act (Figure 1. 16). These enzymes produce branched oligosaccharides that are transported into the periplasm and degraded intracellularly by an array of periplasmic enzymes: 4 GH92s, 2 GH76s, 3 GH125s, and a GH38 (Figure 1. 16). The GH38, BT3774, is crucial for mannan depolymerisation and *Bt* mutants $\Delta bt3774$ display a defective phenotype (Cuskin et al., 2015b). In addition to α -mannan degrading enzymes, MAN-PUL2 encloses a GH130, BT3780, which was able to remove β -1,2-mannosyl caps from *C. albicans* mannan, suggested to

expose the α -mannan component of *C. albicans* cell wall (Figure 1. 13 e and Figure 1. 16) (Cuskin et al., 2015a).

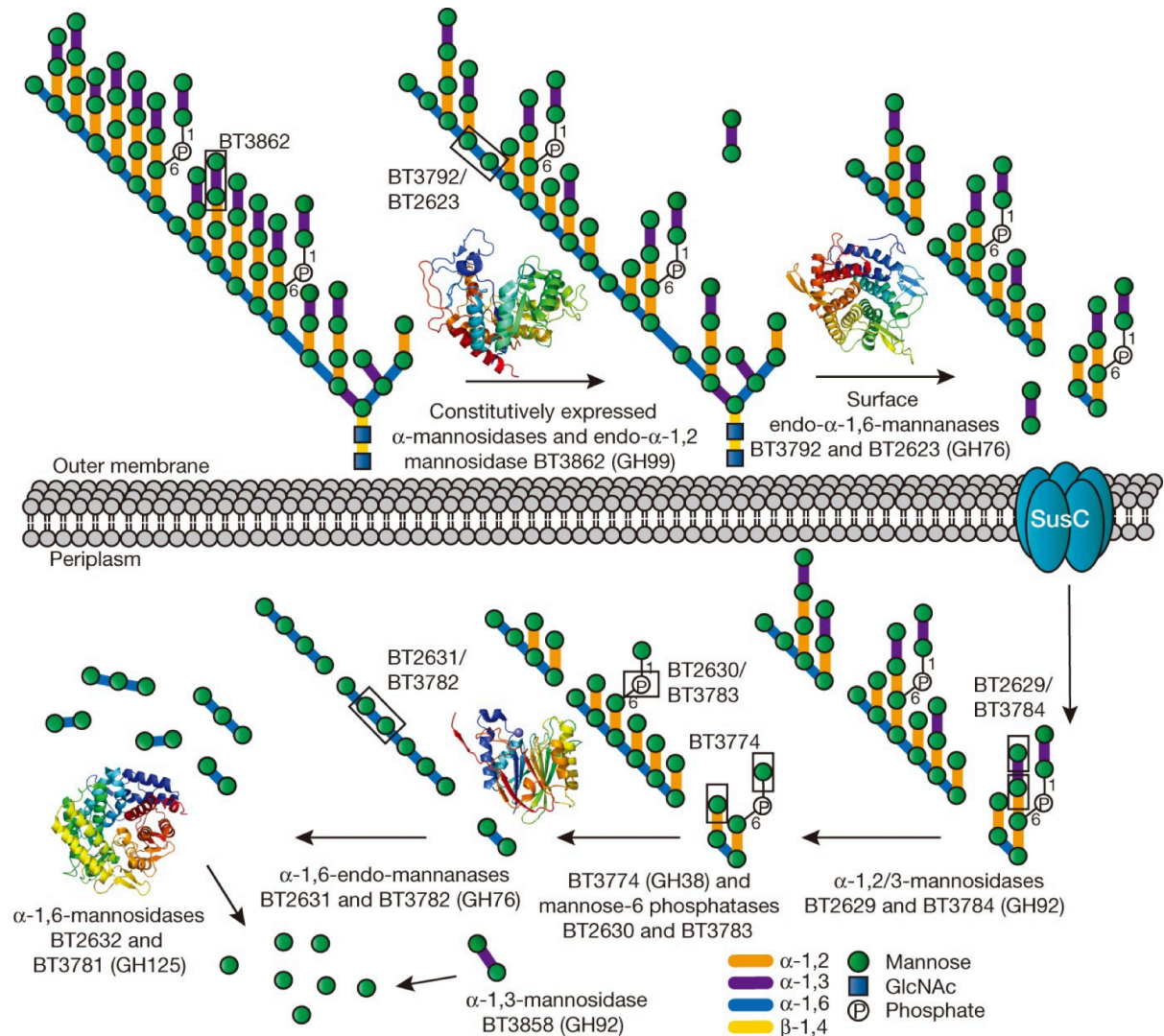


Figure 1. 16 Selfish mechanism of mannan utilisation in *Bt*. Surface endo-mannanases GH99 and GH76s cleave large oligosaccharides from yeast mannan and transport them into the periplasmic space. Mannan fragments are further degraded by a number of periplasmic enzymes as indicated. Figure adapted from Cuskin et al. (2015).

As discussed in Section 1.3, production of such an extensive repertoire of proteins will require a significant amount of energy and, given the conservation of mannan PULs in other gut *Bacteroides*, it would be logical to predict that multiple species

may cooperate to degrade yeast mannan. Bt, however, deployed a “selfish” mechanism of mannan utilisation and did not promote growth of mannan non-degrading species (Cuskin et al., 2015b). This behaviour indicates that fungal mannan is such a limited substrate in the gut, which forced Bt to develop a highly competitive strategy for its utilisation. The structural similarity of PULs in other *Bacteroides* to mannan PULs in Bt leads to a conclusion that all of them would use a ‘selfish’ strategy for mannan breakdown. Considering the competitiveness of Bt, it is unclear why these species would retain degrading systems, which they will unlikely be able to use, and logically, these genes should be lost under the evolutionary pressure. Cuskin et al. (2015b) also showed that some strains of *B. salyersiae* were able to grow to a higher OD₆₀₀ than Bt, despite not sharing structural synteny with mannan PULs. The ability of *B. salyersiae* to utilise yeast mannan was not addressed in this study, and therefore it is currently unknown how this bacterium implements mannan breakdown and what strategy is deployed.

The degradation of fungal mannan will firstly reflect on the availability of β -glucan to Bt as well as other gut *Bacteroides*. It will also modify the epitopes fungi present to the immune system, most likely altering the immune response. However, whether this contributes to fungal survival and commensalism in the gut or, inversely, the pathogenesis is unknown.

1. 5. 3 Fungal cell wall is a dynamic structure

Adding another level of complexity, the structure of the fungal cell wall is malleable and responds to environmental changes such as alterations in temperature, pH, a food source, and oxygen availability by reorganising its sugar layers. The amount

of mannan or β -glucan that can be released from the fungal cell wall by gut bacteria is currently unknown. It is similarly unknown how this enzymatic degradation impacts on fungal physiology. Given the flexibility of the fungal cell wall, as discussed below, it is not in question, that live fungi would respond to the degradation of their own cell wall by the alien microbes.

1. 5. 3. 1 Remodelling in response to Carbon source

Fungi are often grown in glucose rich media in laboratory conditions. However, glucose availability is highly limited at physiological sites other than blood. In the gastrointestinal or urogenital tracts, *C. albicans* survives using lactate as a primary carbon source, which accumulates in the milieu as a by-product of microbial metabolism (Ene et al., 2012, Ballou et al., 2016). Lactate grown *C. albicans* cells develop thinner cell walls, where the thickness of the β -glucan and chitin layers is reduced by about 50%, mannan matrix condenses as fibrils become scarcely distributed around cell periphery (Figure 1. 17 a) (Ene et al., 2012). This lactate mediated cell wall re-organisation is reversible and results in reduced exposure of β -glucan in *Candida spp* but not in *S. cerevisiae* (Figure 1. 17 a) (Ballou et al., 2016). The total amount of the cell wall constituents (Mannose, Glucose, GlcNAc) remains unchanged, suggesting that the cell wall re-modelling is a result of rearrangement of the glycosidic bonds.

1. 5. 3. 2 Remodelling in response to low oxygen environment

The human gut is strictly anaerobic to allow for the survival of the resident microbiota.

Pradhan et al. (2018) showed that, similar to changes in the carbon source, *C. albicans* re-arranges its cell wall in response to low oxygen concentrations.

Hypoxia halved the thickness of all three cell wall layers and was associated with decreased exposure of β -glucan (Figure 1. 17 b) (Pradhan et al., 2018). This process was retained in pathogenic clinical isolates but not in *Candida glabrata*. Moreover, hypoxic environment of the gut has been suggested to polarise *C. albicans* towards a less virulent, commensalism-associated phenotype (Pradhan et al., 2018).

1. 5. 3. 3 Remodelling in response to changes in pH

pH of the gastro-intestinal tract is highly variable and shifts from being highly acidic in the stomach (pH 2) to mildly acidic in the small intestine (pH 5) to mildly alkaline in the colon (pH 7.7) (Evans et al., 1988). *S. cerevisiae* masks β -glucan layer in response to low environmental pH, via enhanced incorporation of CWP in the cell wall (Kapteyn et al., 2001). In contrast, *C. albicans* reveals its β -glucan layer in acidic pH and condenses its mannan fibrils (Figure 1. 17 c) (Sherrington et al., 2017). In both *S. cerevisiae* and *C. albicans*, acidic environment also promotes unmasking of chitin at the bud scars by suppression of Cht2 chitinase activity, regulated by Rim 101 (Figure 1. 17 c) (Sherrington et al., 2017, Kapteyn et al., 2001).

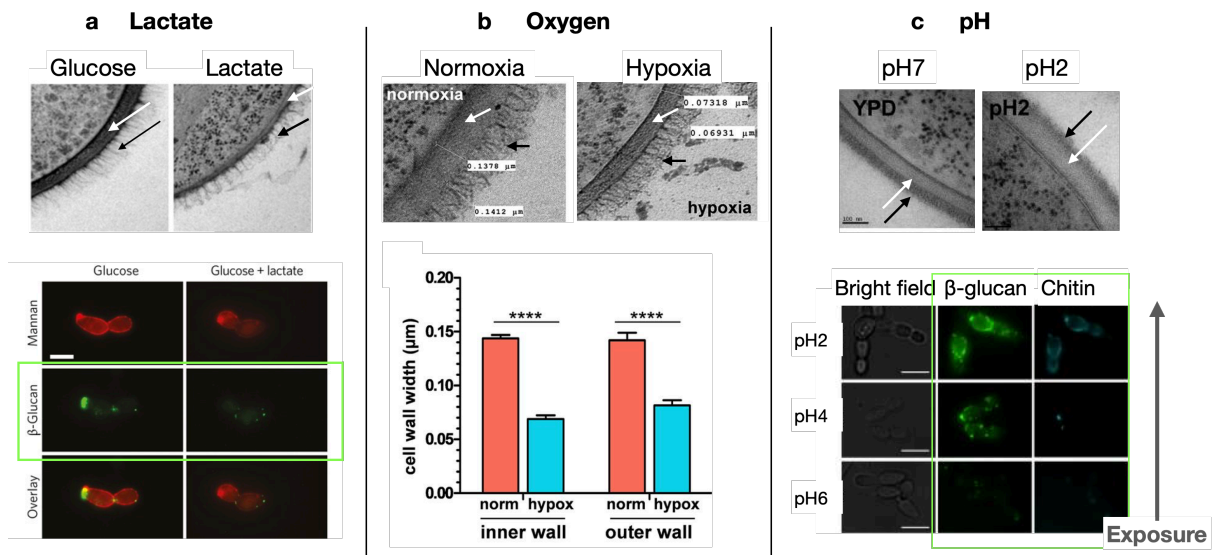


Figure 1. 17 Cell wall remodelling in response to carbon source, oxygen availability, and ambient pH. In all panels black and white arrows indicate mannan and inner layers, respectively. Panel a: top picture TEM of *C. albicans* cell wall in response to glucose or lactate, adapted from Ene et al. (2012); bottom picture: exposure of mannan and β -glucan (green box) in lactate grown *C. albicans*, adapted from Ballou et al. (2016). Panel b: Cell wall changes in *C. albicans* cell wall in response to hypoxia, adapted from Pradhan et al. (2018). Panel c: Changes in *C. albicans* cell wall in response to low pH, increasing exposure of β -glucan and chitin in low pH is shown in a green box, adapted from Sherrington et al. (2017).

1. 6 Mannan degrading enzymes

α -Mannosidases are exo-acting enzymes which remove mannose from the non-reducing end from complex manno-polymers, usually N-glycans. Maturation of N-glycans occurs in the Endoplasmic Reticulum (ER), Golgi, and the cytoplasm and is critical for homeostasis, as aberrant N-glycosylation has been associated with oncogenesis and tumour metastasis (Couldrey and E Green, 2000). Originally, mannosidases were split into two classes I and II, represented by the families GH47 and GH38, respectively. However, other families of mannosidases have been characterised and to date exo-acting α -mannosidases are grouped into four

enzyme families: GH47, GH38, GH92, GH125 (Herscovics, 2001). Endo-acting mannanases are represented with 2 families: GH76 and GH99. These display divergent structural folds and operate via different catalytic mechanisms. All α -mannosidases, except for the members of the GH125 family, display dependence on divalent cation and require either Ca^{2+} , Zn^{2+} , Mg^{+2} for activity (Jelinek-Kelly and Herscovics, 1988, Zhu et al., 2010, Gregg et al., 2011, Venkatesan et al., 2009).

1. 6. 1 Class I α -mannosidases: Glycoside Hydrolases 47.

Class I α -mannosidases are representative of the GH47 family. In mammals and yeast, these display α -1,2-mannosidic activity and localise to the ER and the Golgi, where they process high mannose N-glycans (HMNG) (Figure 1. 18 a) (Herscovics, 2001). Mammalian and yeast ER GH47s modify $\text{Man}_9\text{GlcNAc}_2$ N-glycan precursor to $\text{Man}_{7-8}\text{GlcNAc}_2$, and thus monitor glycosylation of proteins (Figure 1. 18 a) (Herscovics, 2001, Jelinek-Kelly and Herscovics, 1988). Golgi GH47s exhibit specificity for α -1,2-linkage, trimming HMNG $\text{Man}_8\text{GlcNAc}_2$ to $\text{Man}_5\text{GlcNAc}_2$, which could then be used to generate a core for Complex and Hybrid N-glycans (Figure 1. 18 a) (Maruyama et al., 1994, Herscovics, 2001). There are three types of such GH47s: IA, IB, IC, which are differentially expressed depending on the cell type and the tissue. Overall, proteins within this family operate via a single displacement inverting mechanism (Vallée et al., 2000). Binding of calcium ions stabilises glycosyl-enzyme intermediate and is critical for the activity of GH47 (Vallée et al., 2000).

1. 6. 2 Class II α -mannosidases: Glycoside Hydrolases 38

GH38s are exo-acting mannosidases which usually modify $\text{Man}_5\text{GlcNAc}_2$, producing $\text{Man}_3\text{GlcNAc}_2$ core of N-glycans (Figure 1. 18 b). In humans, the autosomal recessive mutation in *MAN2B1* producing a dysfunctional lysosomal GH38 results in a severe neurodegenerative disorder, α -mannosidosis (Cathey et al., 2019).

GH38s of subgroup 2A are localised to the Golgi, where they display dual specificity towards α -1,6 and α -1,3-mannosidic bonds (Suits et al., 2010). Glogi GH38s define maturation of Hybrid and Complex N-glycans and display requirement for β -1,2 GlcNAc on the terminal core mannose moiety to produce a $\text{GlcNAcMan}_3\text{GlcNAc}_2$ (Figure 1. 18 b) (Van Den Elsen et al., 2001). Lysosomal mannosidases are split into two groups: 2B1 hydrolysing α -1,2, α -1,3, α -1,6-mannosidic bonds, and 2B2, which exhibit strict specificity for α -1,6-linkages, activity of these mannosidases does not require recognition of GlcNAc residues in the N-glycan (Park et al., 2005). BT3774, characterised by Cuskin et al. (2015), is the only GH38, which displays specificity for highly branched manno-polymers, such as yeast mannan (Figure 1. 18 b). The CAZy database (Cazy.org) lists 6144 ORF encoding for putative GH38s across Bacteria, Eukaryota, and Archaea, only 44 of which have been assigned activity. GH38s operate through a double-displacement mechanism with retention of the anomeric carbon configuration (Heikinheimo et al., 2003, Numao et al., 2003).

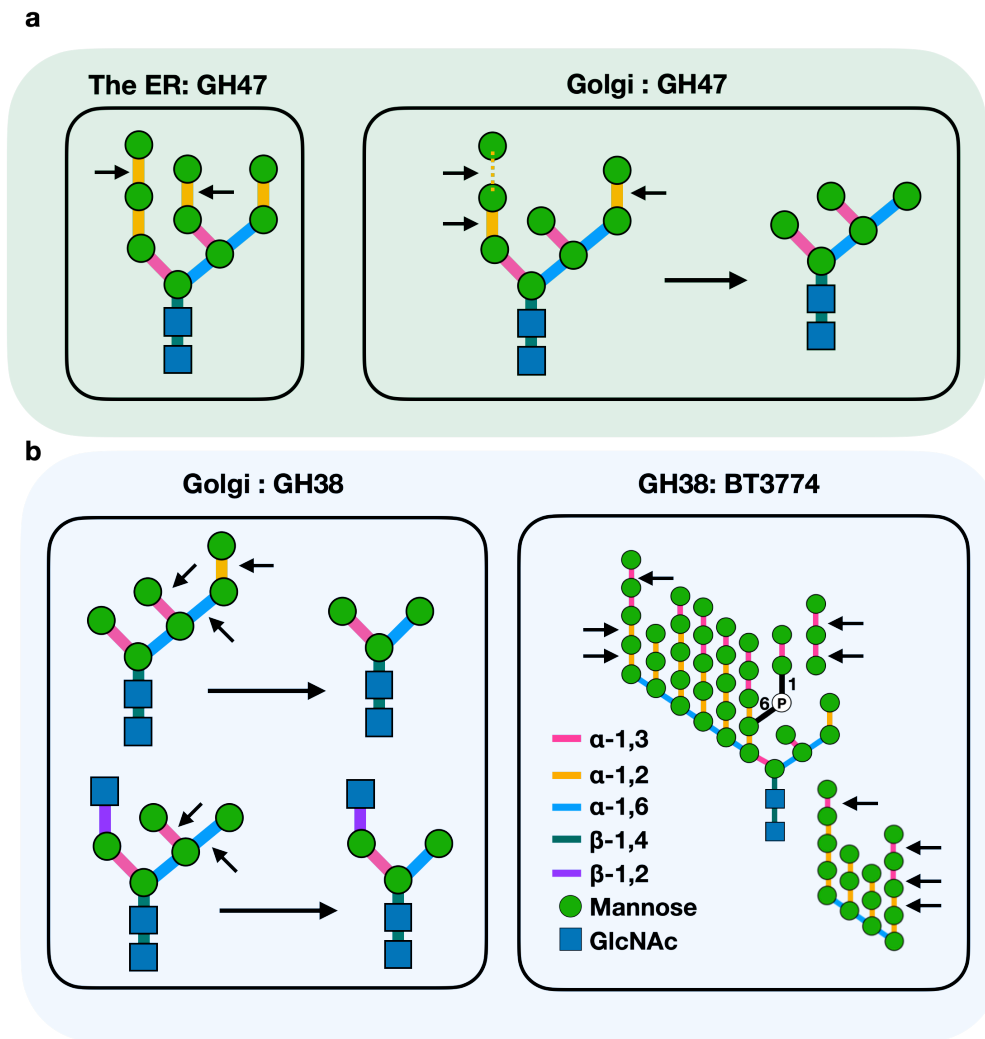


Figure 1. 18 Schematic representation of N-glycan degradation by enzymes from the GH47 and GH38 families. Cellular localisation and bonds targeted by the enzymes at the respective sites are indicated.

1. 6. 3 Glycoside Hydrolases 92.

GH92 are exo-acting α -mannosidases, displaying specificities for a wide range of substrates. Zhu et al. (2010) characterised 22 out of 23 GH92s from Bt, demonstrating that they target α -1,2; α -1,3; α -1,4; and α -1,6-mannosidic bonds. While α -1,2; α -1,3; and α -1,6 mannosidic linkages are found in a variety of substrates such as high mannose, complex, or hybrid N-glycans and yeast mannan, α -1,4 mannosidic linkage is rare in nature. One study suggested that α -

1,4-mannosides cap side chains of mannan from a soil yeast *Gilmaniella spp* (Chen et al., 2016). GH92s from Bt cooperate to depolymerise complex substrates such as yeast mannan (Figure 1. 19 a). Deconstruction of HMNG also requires sequential activity GH92s, where BT3990 removes terminal α -1,2 mannose moieties from $\text{Man}_9\text{GlcNAc}_2$, exposing α -1,3 and α -1,6 linkages to BT3991 and BT3994, respectively (Figure 1. 19 a). BT3994 is unable to hydrolyse α -1,6 bonds unless one of the GlcNAc moieties in the N-glycan core is present (Figure 1. 19 a) (Cuskin et al., 2015a, Zhu et al., 2010). GH92s exhibit inversion of the anomeric carbon via a single displacement mechanism, where the calcium ion interacts with the incoming water molecule and stabilises glycoside-enzyme transition state (Zhu et al., 2010)

Transcriptional profiling showed that Bt expresses a range of GH92s *in vivo* in mice, even when the diet lacks yeast α -mannan, indicating that these are deployed to modify yhost N-glycans (Martens et al., 2008). In addition, low expression of a variety of GH92s is driven *in vitro* in the presence of galactose, lactose, or Human Milk Oligosaccharides (Marcobal et al., 2011).

1. 6. 4 Glycoside Hydrolases 125

GH125 is a recently identified family of exo-acting α -mannosidases, which were first characterised in *Clostridium perfringens* (CpGH125) and *Streptococcus pneumoniae* (SpGH125) (Gregg et al., 2011). These enzymes exhibit a strict specificity for linear α -1,6-linked manno-polymers, such as yeast mannan backbone (Figure 1. 19 b). This is driven by the specific pocket topology of the active site, which tightly encloses sugars from both reducing and non-reducing ends (Gregg et al., 2011). GH125s operate via an inverting mechanism and,

unlike in other mannosidases, catalytic mechanism of GH125s does not require a metal cation to stabilise glycosyl-enzyme intermediate (Alonso-Gil et al., 2017). Phylogenetic analysis of GH125 showed that the catalytic residues are highly conserved in other proteins from this family, which are separated into three clusters split between Bacteroidetes, Firmicutes, and Fungi (Gregg et al., 2011).

1. 6. 5 Endo-acting α -mannanases

1. 6. 5. 1 Glycoside Hydrolases 99

Mammalian GH99s are mostly present in the Golgi, where they mediate maturation of N-glycans. In mammals, N-glycosylation is initiated with $\text{Glc}_3\text{Man}_9\text{GlcNAc}$ pre-cursor, which is conventionally trimmed by glucosidases in the ER to generate $\text{Man}_9\text{GlcNAc}_2$ (Figure 1. 19 c) (Roth et al., 2003). Inhibition of this pathway directs glycans to the alternative mechanism of maturation, where a Golgi GH99 acts as an endo- α -1,2-mannanase and deglycosylates $\text{Glc}_{1-3}\text{Man}_9\text{GlcNAc}_2$ precursor into $\text{Man}_9\text{GlcNAc}_2$, releasing $\text{Glc-}\alpha$ -1,3-Man disaccharide or $\text{Glc}_{2-3}\text{Man}$ oligosaccharides (Roth et al., 2003, Spiro et al., 1997). Bacterial GH99s have only been characterised in *Shewanella amazonensis*, *B. thetaiotaomicron*, and *B. xylanisolvens* (Matsuda et al., 2011, Thompson et al., 2012). Unlike other characterised GH99s, *Bacteroides* enzymes preferentially release α -1,3-mannobiose from hypermannose N-glycans such as yeast mannan (Figure 1. 19 c) (Thompson et al., 2012). Investigations into the crystal structure of these enzymes suggested that they operate via substrate-assisted catalysis with retaining of anomeric configuration and do not require a metal cation for hydrolysis (Thompson et al., 2012).

1. 6. 5. 2 Glycoside Hydrolases 76

Characterised proteins from the GH76 family comprise endo-acting mannanases, which process long linear α -1,6-linked mannose polymers found in the backbone of fungal mannan into smaller manno-oligosaccharides (Figure 1. 19 d). Enzymes from this family are mainly of fungal or bacterial origins. Endo-processivity of these enzymes is conferred by the curved cleft-shaped active site, allowing for the incorporation of long oligosaccharides between 3 and 8 sugars (Nakajima et al., 1976, Cuskin et al., 2015b). GH76s operate through a double displacement retaining mechanism, and do not require metals to stabilise the $S_{2,5}$ transition state (Nakajima et al., 1976, Cuskin et al., 2015b, Thompson et al., 2015). GH76s usually act on linear substrates after removal of α -1,2; α -1,3 side chains by GH92s. Recently, a GH76 from a Bt strain isolated from cattle has been shown to hydrolyse branched manno-oligosaccharides (Jones et al., 2020). Investigation into the structure of this enzyme revealed that the cleft-shape of the active site expands to accommodate sidechain sugars, decorating -1 and +2 subsites, suggesting that it is capable of hydrolysing α -1,6-linked manno-polymers containing α -1,2-linked branchpoints (Jones et al., 2020).

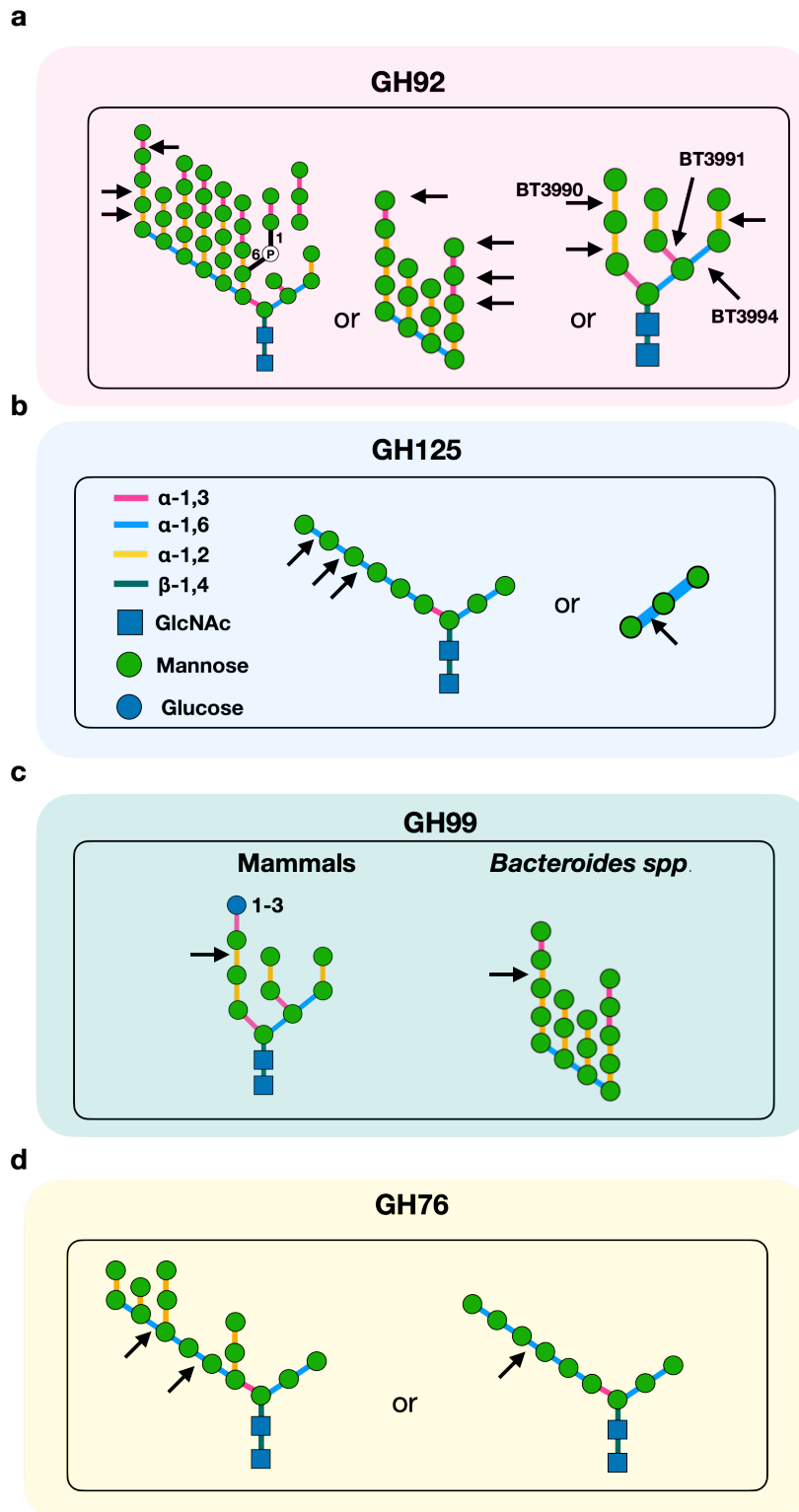


Figure 1. 19 Schematic representation of enzyme specificities from the GH92 (a), GH125 (b), and GH99 (c) and GH76 (d) families. Bonds targeted by each family are indicated with arrows.

1. 6. 6 β -mannosidases

β -1,4 mannosidic linkages compose a diversity of substrates, such as plant galacto- and gluco-mannans as well as the core of mammalian N-glycan (Figure 1. 11), while β -1,2-linked mannan is rare in nature and is only found in *Candida* and *Leishmania species*. *Candida species* decorate their cell walls with β -1,2-mannosyl caps, which serve as epitopes for immune recognition (Mora-Montes et al., 2009). In contrast, *Leishmania species* accumulate β -1,2 manno oligomers of 4-10 units long intracellularly and deplete them in nutrient scarce conditions. These also allow to resist oxidative stress inside macrophages and are associated with virulent states (Ralton et al., 2003). Metabolism of these β -1,2 manno-oligomers is orchestrated by the enzymes from the Glycosyltransferase GT 108 family, which display a dual β -1,2-mannoside-phosphorylase and mannosyltransferase activity (Sernee et al., 2019). These enzymes will not be discussed further in this thesis.

Catabolism of β -1,2-mannosidic bonds found in *C. albicans* is performed by the enzymes from the Glycoside Hydrolase 130 family (Cuskin et al., 2015a). This family is mostly composed of β -mannoside-phosphorylases but Cuskin and colleagues have shown that some enzymes in this family display hydrolase activity (Cuskin et al., 2015a). Mannoside-phosphorylases cleave glycosidic bonds using inorganic phosphate as a nucleophile, producing sugar-1-phosphate as a result (Figure 1. 20). These enzymes are also capable of reverse phosphorolysis, where sugar-1-phosphate can be utilised as both a donor substrate and a carbohydrate acceptor (Chiku et al., 2014, O'Neill and Field, 2015). Phosphorylases are divided into 4 groups based on linkage specificity: 1) Glc- β 1,4-Man; 2) Man- β 1,4-Man; 3) Man- β 1,4-GlcNAc; 4) Man- β 1,2-Man (Chiku et al., 2014). The phosphorylase

activity of these enzymes is dictated by the three basic amino acid residues (Arginines) and, in contrast, glycoside hydrolases were found to lack these residues and their activity is determined by the two Glutamate residues (Cuskin et al., 2015a, Ladevèze et al., 2013). BT3780 from MAN-PUL2 was characterised to possess such glycoside hydrolase activity as well as a critical Lysine residue (Lys199 in BT3780) positioned in the active site, which determined its β -1,2 mannosidic activity against β -mannan from *C. albicans* cell wall (Cuskin et al., 2015a, Chiku et al., 2014). This enzyme was suggested to expose *C. albicans* α -mannan for further depolymerisation by the enzymes in MAN-PUL1/2/3. Analysis of human faecal metagenomes showed that the abundance of GH130s from bacterial origin could be associated with Inflammatory Bowel Diseases (IBD), implicating the role of gut microbiota in fine-tuning inflammatory states (Ladevèze et al., 2013).

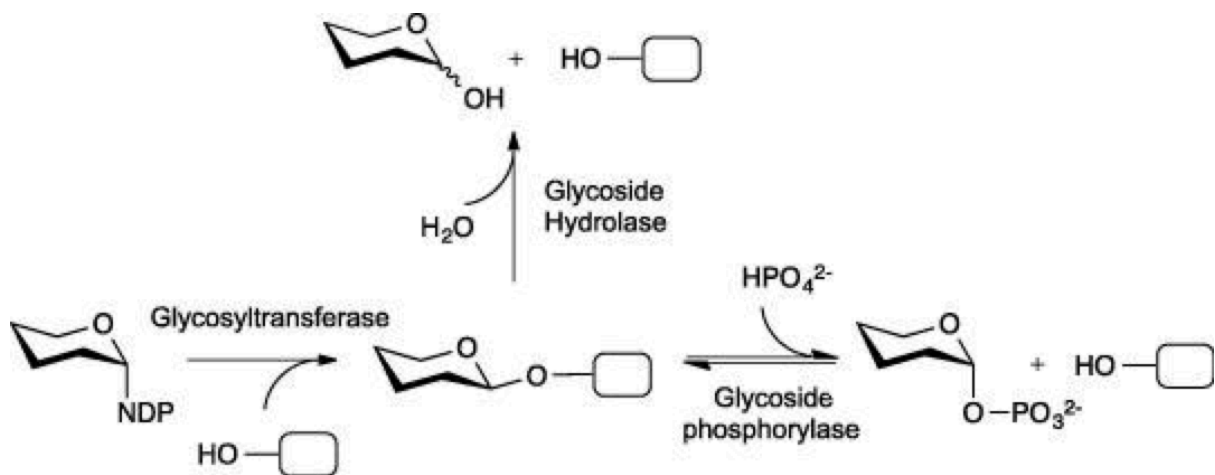


Figure 1. 20 Difference between Glycoside Hydrolases, Glycoside Phosphorylases, and Glycosyl Transferases. Glycoside phosphorylases use phosphate to produce sugar-1-phosphate, whereas use water as a nucleophile. NDP stands for nucleotide diphosphate, figure adapted from (O'Neill and Field, 2015)

1.7 Objectives

The interactions between fungal and bacterial members of the gut microbiota are still understudied. This project aimed to investigate how bacterial degradation of fungal glycans may play a role in these inter-species interactions. This was pursued through two main aims:

1. How does *B. thetaiotaomicron* degrade mannan from *C. albicans*? Previous work has dissected the mechanism of how Bt breaks down *S. cerevisiae* mannan and identified an enzyme able to hydrolyse the β -1,2-mannosidic linkages which distinguish *C. albicans* mannan from *S. cerevisiae*. It is not known, however, if other enzymes outside the previously characterised MAN-PULs contribute to the degradation of *C. albicans* mannan by Bt.
2. Is the 'selfish' route the only mechanism by which fungal α -mannan can be degraded? In addition to being a source of nutrients for *Bacteroides* species such as Bt, the immunogenic nature of fungal cell wall glycans means that the release of breakdown fragments may have implications for host health. As discussed above, networks of glycan degradation have been identified for many other complex carbohydrates such as xylans and fructans. However, it still remains unknown whether fungal mannan is utilised solely in a 'selfish' manner or whether it can be shared between gut *Bacteroides* other than Bt.

Chapter 2: Materials and Methods

2. 1 Bacterial strains and Plasmids

Escherichia coli and *Bacteroides spp.* strains as well as *B. thetaiotaomicron* mutants used in this study are listed in Table 2. 1. Plasmids routinely used in this study are listed in Table 2. 2. Plasmids used to introduce mutations into Bt are also listed in Table 2. 2.

Name	Genotype	Description	Reference
Tuner™(DE3)	F ⁻ <i>ompT hsdSB</i> (r _B ⁻ m _B ⁻) <i>gal dcm lacY1</i> (DE3)	Protein expression	Novagen
One Shot™TOP10	F ⁻ <i>mcrA</i> Δ(<i>mrr-hsdRMS-mcrBC</i>) ϕ80/ <i>lacZ</i> ΔM15 Δ <i>lacX74 recA1 araD139</i> Δ(<i>ara, leu</i>)7697 <i>galU galK rpsL</i> (STR ^R) <i>endA1 nupG</i> λ-	DNA ligation and replication	Invitrogen
CC118 λ-pir	Δ(<i>ara-leu</i>) <i>araD</i> Δ <i>lacX74 galE galK phoA20 thi-1 rpsE rpoB argE</i> (Am) <i>recA1</i> λ <i>pir</i>	pExchange plasmid propagation and cloning	Herrero et al. (1990)
S17.1 λ-pir	<i>recA pro hsdR</i> RP4-2 (Tc::Mu;Km::Tn7) (λ <i>pir</i>)	Conjugations of pExchange plasmid, used for gene deletions	Skorupski and Taylor (1996)
<i>B. thetaiotaomicron</i> (Bt)	VPI-5482	Type strain, human isolate	Martens lab, Centre for Microbial systems, University of Michigan
<i>B. thetaiotaomicron</i> Δ <i>tdk</i>	VPI-5482 - Δ <i>tdk</i>	Bt without a functional thymidine kinase	
<i>B. salyersiae</i>	DSM 18765/WAL 10018,	Type strain, human isolate	

Name	Genotype	Description	Reference
<i>B. caccae</i>	ATCC 43185	Type strain, human isolate	
<i>B. cellulosilyticus</i>	DSM 14838	Type strain, human isolate	
<i>B. cellulosilyticus</i>	WH2	Human isolate	
<i>B. eggerthii</i>	DSM 20697	Type strain, human isolate	
<i>B. finegoldii</i>	DSM 17565	Type strain, human isolate	
<i>B. finegoldii</i>	CL09T03C10	Possesses Type 6 secretion system (T6SS), human isolate	
<i>B. fragilis</i>	ATCC 25285	Type strain, human isolate	
<i>B. intestinalis</i>	DSM 17393	Type strain, human isolate	
<i>B. ovatus</i>	ATCC 8483	Type strain, human isolate	
<i>B. ovatus</i>	CL02T12C04	Possesses T6SS, human isolate	
<i>B. stercoris</i>	ATCC 43183	Type strain, human isolate	
<i>B. uniformis</i>	ATCC 8492	Type strain, human isolate	
<i>B. vulgatus</i>	ATCC 8482	Type strain, human isolate	
<i>B. xylanisolvens</i>	DSM 18836	Type strain, human isolate	
<i>B. xylanisolvens</i>	NLAE-zl-p352	Porcine isolate	
<i>B. clarus</i>	DSM 22519	Type strain, human isolate	
<i>B. dorei</i>	DSM 17855	Type strain, human isolate	
<i>B. fluxus</i>	DSM 22534	Type strain, human isolate	

Name	Genotype	Description	Reference
<i>B. plebius</i>	DSM 17135	Type strain, human isolate	
<i>Bt</i> Δ <i>bt3780</i>	Δ <i>bt3780</i>	Bt with a deletion of <i>bt3780</i>	Available in Lowe Lab, Newcastle University
<i>Bt</i> Δ <i>pul2</i>	Δ <i>bt3773-bt3792</i>	Bt with a deletion of <i>bt3773-bt3792</i> operon	Cuskin et al. (2015b)
<i>Bt</i> Δ <i>pul3</i>	Δ <i>bt3853-3862</i>	Bt with a deletion of <i>bt3853-bt3862</i> operon	
<i>Bt</i> Δ <i>pul1/2/3</i>	Δ <i>bt2620-bt2632+\Delta<i>bt3773-bt3792+\Delta<i>bt3853-bt3862</i></i></i>	Bt with a deletion of <i>bt2620-32</i> , <i>bt3773-92</i> , and <i>bt3853-62</i> operons	
<i>Bt</i> Δ <i>bt4094</i>	Δ <i>bt4094</i>	Bt with a deletion of <i>bt4094</i>	Generated in this study
<i>Bt</i> Δ <i>bt3780+\Delta<i>bt4094</i></i>	Δ <i>bt3780+\Delta<i>bt4094</i></i>	Bt with a deletion of <i>bt4094</i> and <i>bt3780</i>	
<i>Bt</i> Δ <i>pul1/2/3+\Delta<i>bt4094</i></i>	Δ <i>bt2620-32+\Delta<i>bt3773-92+\Delta<i>bt3853-62+\Delta<i>bt4094</i></i></i></i>	Bt with a deletion of <i>bt2620-32</i> , <i>bt3773-92</i> , and <i>bt3853-62</i> operons and <i>bt4094</i>	
<i>Bt</i> Δ <i>pul4</i>	Δ <i>bt4072-96</i>	Bt with a deletion of <i>bt4072-bt4096</i> operon	
<i>Bt</i> Δ <i>pul1/2/3/4</i>	Δ <i>bt2620-bt2632+\Delta<i>bt3773-bt3792+\Delta<i>bt3853-bt3862+\Delta<i>bt4072-96</i></i></i></i>	Bt with a deletion of <i>bt2620-32</i> , <i>bt3773-92</i> , <i>bt3853-62</i> , <i>bt4072-96</i> operons	
<i>C. albicans</i>	SC5314	Wild type	Quinn Lab, Biosciences Institute, Newcastle University
<i>S. cerevisiae</i>	Δ <i>mnn1</i>	<i>S. cerevisiae</i> strain lacking MNN1,	

Name	Genotype	Description	Reference
		produces truncated mannan	Provided by Dr Peter Banks, Bio Screening facility, Newcastle University.
<i>S. cerevisiae</i>	$\Delta mnn5$	<i>S. cerevisiae</i> strain with low MNN2 expression, produces truncated mannan	
<i>S. cerevisiae</i>	$\Delta mnn2$	<i>S. cerevisiae</i> strain which lacks MNN2, truncated mannan	

Table 2. 1 Bacterial strains and mutants used in this study. Genotypes and the origin of the strains are indicated.

Plasmid	Features	Reference
pET28a-b	Kan ^r , T7 promoter, lac, lacI ^q , integrated His-tag	Novagen
pExchange-tdk	Bla ^r , Erm ^r , tdk (BT227), suicide vector	Koropatkin et al. (2008)
pExchange-tdk-bt4094KO	pExchange-tdk, carrying bt4094 deletion cassette	Generated in this study
pExchange-tdk-pul4KO	pExchange-tdk, carrying a deletion cassette for bt4072-96	

Table 2. 2 Vectors used in this study.

2. 2 Bacterial and Yeast Growth and Storage Conditions

2. 2. 1 Selective Media

Bacterial and yeast cultures were cultured in media listed in Table 2. 3. Defined medium was used to culture *Bacteroides* species other than *B. thetaiotaomicron* (Appendix A).

A range of antibiotics were used for the selection of desired transformants or appropriate bacterial species, which are listed in table Table 2. 4.

Media	Component	Amount per litre	Details
Luria Broth (LB)	LB powder (Sigma-Aldrich)	25 g	Dissolved in MilliQ water, pH adjusted to 7.2 with NaOH, Autoclaved
	NaCl 10 g l ⁻¹		
	Tryptone 10 g l ⁻¹		
	Yeast extract 5 g l ⁻¹		
Tryptone Yeast Extract Glucose (TYG)	Tryptone Peptone	10 g	Prepared in MilliQ water, autoclaved before use and supplemented with 0.1% (v/v) Hematin-Histidine
	Yeast Extract	5 g	
	Glucose	2 g	
	Cysteine (Free base)	0.5 g	
	1 M KPO ₄ pH 7.2	100 ml	
	Vitamin K solution, 1 mg ml ⁻¹	1 ml	
	TYG salts (MgSO ₄ 0.5 g l ⁻¹ , NaHCO ₃ 10 g l ⁻¹ , NaCl 2 g l ⁻¹)	40 ml	
	0.8% CaCl ₂	1 ml	
	FeSO ₄ , 0.4 mg ml ⁻¹	1 ml	
	Resazurin, 0.25 mg ml ⁻¹	4ml	
Minimal Medium (MM)	NH ₄ SO ₄	1 g	Prepared in MilliQ water, autoclaved, supplemented with 0.1% (v/v) Hematin-Histidine
	Na ₂ CO ₃	1 g	
	Cysteine (Free base)	0.5 g	
	1 M KPO ₄ pH 7.2	100 ml	
	Vitamin K solution, 1 mg ml ⁻¹	1 ml	
	FeSO ₄ , 0.4 mg ml ⁻¹	10 ml	

Media	Component	Amount per litre	Details
	Vitamin B12, 0.01 mg ml ⁻¹	0.5 ml	
	Mineral Salts for defined medium (NaCl 18 g l ⁻¹ , CaCl ₂ 0.53 g l ⁻¹ , MgCl ₂ 0.4 g l ⁻¹ , MnCl ₂ 0.2 g l ⁻¹ , CoCl ₂ 0.2 g l ⁻¹)	50 ml	
	Resazurin, 0.25 mg ml ⁻¹	4ml	
Brain-Heart Infusion (BHI)	BHI powder (Sigma-Aldrich)	37.5 g	Prepared in MilliQ water, supplemented with 0.1% (v/v) Hematin-Histidine
Hematin-Histidine	1.9 mM Hematin in 0.2 M Histidine	Adjust pH to 8 with 10 M NaOH, dissolve with shaking overnight at 37°C	
Yeast extract Peptone Tryptone Dextrose (YPD) medium	YPD powder (Sigma-Aldrich)	50 g	Dissolved in MilliQ water and autoclaved

Table 2. 3 Media routinely used throughout this study.

Antibiotic	Working concentration (µg ml ⁻¹)	Storage	Application
Ampicillin	100	-20 °C	pExchange-tdk
Kanamycin	10	-20 °C	pET28a-b
Gentamycin	200	Prepared when necessary	pExchange-tdk
Erythromycin	25	Prepared when necessary	pExchange-tdk
5-fluoro-2'-deoxyuridine (FUdR)	200	Prepared when necessary	Conjugations

Table 2. 4 Selective antibiotics used. Working concentrations are indicated.

2. 2. 2 Sterilisation

All solutions, media, and glassware were sterilised by autoclaving using an Astell Hearson 2000 Series Autoclave or a Prestige[®] Medical Series 2100 Clinical Autoclave at 121°C, 32 or 15 lb / inch² for 20 min.

Solutions were also filter sterilised using sterile Millipore filter disc (0.22 µm pore size) (Supor[®] Acrodisc[®] 3.2) and a suitable sterile syringe (Plastipak[®], Becton Dickinson).

2. 2. 3 *E. coli* growth conditions

E. coli strains listed in Table 2. 1 were grown in LB Medium (Table 2. 3) with agitation at 150-180 rpm. For growth on solid medium 2% (w/v) Bacteriological agar (Sigma, UK) was added to the medium prior to autoclaving. Plates were prepared with 25 ml of molten LB-Agar and sterile plastic Petri dishes (ThermoFisher, UK). Relevant antibiotic was added as indicated in Table 2. 4.

2. 2. 4 *Bacteroides spp.* growth conditions

Bacteroides spp. listed in Table 2. 1 were routinely grown in Tryptone-Yeast extract-Glucose (TYG) (Table 2. 3) medium at 37 °C under anaerobic conditions using an A35 anaerobic cabinet (Don Whitley Scientific, UK).

For all experiments in Chapter 3 *B. thetaiotaomicron* was grown in Minimal Media containing 10 mg ml⁻¹ carbon source. In Chapter 4 and 5, *B. salyersiae* and other *Bacteroides spp.* were grown in Defined medium (Appendix A) supplemented with 10 mg ml⁻¹ substrate, unless specified otherwise.

For growth on solid medium 2% (w/v) Bacteriological agar (Sigma) was added to TYG or Brain Heart Infusion media (Table 2. 3) prior to autoclaving. Plates were

prepared with 25 ml of molten Media-Agar and sterile plastic Petri dishes (ThermoFisher, UK).

2. 2. 5 Yeast growth conditions

C. albicans or *S. cerevisiae* were routinely grown in Yeast extract-tryptone Peptone-Dextrose (YPD) at 30 °C with shaking at 150-180 rpm. For growth on solid medium, 2% (w/v) Bacteriological agar (Sigma) was added to YPD prior to autoclaving, 25 ml was poured into sterile Petri dishes (ThermoFisher).

2. 2. 6 Storage

Stocks of all bacterial and yeast strains were stored in 25% (v/v) glycerol at -80 °C in cryovials. Bacterial DNA and plasmids were stored in Elution Buffer (10 mM Tris-Cl 0.1 mM EDTA) (QIAGEN) at -20 °C in Eppendorf tubes.

2. 3 Molecular Biology

2. 3. 1 Centrifugation

Bacterial cultures 100-1000 ml were centrifuged at 5,000 rpm in 500 ml centrifuge tubes (Nalgene) for 10 minutes using a Beckman J2-21 centrifuge with a JA-10 rotor at 4 °C. Yeast cultures 100-1000ml were centrifuged in the same conditions but at 3,000 rpm. Bacterial cultures of 50 ml were centrifuged at 15,000 rpm for 30 minutes in 50 ml centrifuge tubes (Nalgene) using a Beckman J2-21 centrifuge with a JA-25.5 rotor at 4 °C.

Cultures of 2-50 ml were harvested by centrifugation at 5,000 rpm in 25 ml universal tubes (Sterilin) using Hettich Mikro 220R benchtop centrifuge with fixed

angle rotor at 4 °C. Reactions < 2 ml were centrifuged in Eppendorf tubes (2 or 1.5 ml) at 13,000 rpm using a Heraeus Instruments Biofuge pico benchtop centrifuge.

For buffer displacement, ultrafiltration, and concentration of protein solutions were centrifuged in Harrier 18/80R centrifuge with swing out rotor at 4,000 rpm at 4 °C. The centrifugation time was dependent of the sample.

2. 3. 2 Transformation of chemical competent *E. coli*

Competent *E. coli* were prepared by Carl Morland and stored in 100 µl aliquots at -80 °C. Competent *E. coli* strains are listed in Table 2. 1

An aliquot was thawed on ice, mixed with 2 µl of plasmid DNA, and incubated on ice for 20-30 minutes. Cells were then heat-shocked at 42 °C for 2 minutes and returned on ice. For plasmid propagation or protein expression, cells were plated out on solid LB-Agar medium, containing appropriate antibiotic.

Transformation of ligation mixtures required a recovery step prior to plating on solid medium. Heat shocked cells were mixed with 500-1000 µl of LB and incubated 37 °C with agitation at 180 rpm for 1 h. Cells were then harvested by centrifugation at 5000 rpm, pellet was resuspended in 100 µl of sterile LB, and plated out on LB-Agar, containing appropriate antibiotic. Plates were incubated inverted at 37 °C for 16 h.

2. 3. 3 Propagation of plasmids

Transformed *E. coli* Top 10 for pET28a-b vectors and CC118 for pExchange-tdk were cultured from a single colony in 5 ml LB with appropriate antibiotic with

shaking at 150-180 rpm at 37 °C for 16 h. The pellet was collected by centrifugation at 5,000 rpm.

2. 3. 4 DNA isolation

Plasmid DNA was purified with QIAspin Prep Kit (QIAGEN) as per manufacturers instructions. Genomic DNA from *Bacteroides spp.* was extracted from 1-2 ml of culture using Sigma GenElute™ Bacterial Genomic DNA Kit (Sigma) as per manufacturer's instructions

2. 3. 5 Quantification of DNA

DNA concentration was determined with NanoDrop 2000 UV-Vis spectrophotometer (Thermo Fisher Scientific) by measuring the absorbance at 260 nm, using EB buffer (QIAGEN) or Elution buffer (Sigma) as blanks. 2 µl aliquots were used to determine DNA concentration.

In multi-species co-culture experiments, genomic DNA concentration was measured from 1 µl samples with Qubit 4 Fluorometer (ThermoFisher) and 1X dsDNA High Sensitivity Assay Kit (ThermoFisher) as per manufacturers instructions, using the standard curve provided in the kit.

2. 3. 6 Polymerase Chain Reaction (PCR)

The polymerase chain reaction (PCR) developed by Mullis and Faloona (1987) was used to amplify target DNA fragments and construct deletion cassettes for genetic knockouts. The technique requires a thermostable DNA polymerase, a DNA template, two oligonucleotide primers that are complementary to each strand of the target DNA fragment, and dNTPs. Dimethyl Sulfoxide (DMSO) (Sigma) were

added to increase primer binding to the DNA template. The reactions were performed using a PHC-3 thermocycler (Biorad, USA).

Primers of 20-25 bases were designed to flank the sides of a desired gene. The G/C content of each primer was maintained at approximately 40 % and where possible G/C flanked the ends of each primer to increase annealing and amplification efficiency. Where necessary restriction sites were included in the 5' end of each primer, preceded with a 6-base overhang to allow restriction enzymes to cut the fragment. Primers were manufactured by MWG-Biotech (Germany) and lyophilised. Primers were resuspended in sterile water to obtain 100 pmol μl^{-1} . PCR reactions were performed with Kod Hot Start DNA Polymerase Kit (Merck, UK) in 0.2/0.5 ml Eppendorf tubes. Ingredients are listed in Table 2. 5 and the standard thermocycler program is summarised in Table 2. 6. Negative controls, lacking a DNA template, were also included.

Component	Volume
KOD Hot start DNA polymerase	1 μl
10 × Buffer for KOD DNA Polymerase	5 μl
MgCl ₂ (25 mM)	3 μl
dNTPs (2 mM each)	5 μl
Oligonucleotide primer forward (5 μM)	5 μl
Oligonucleotide primer reverse (5 μM)	5 μl
DMSO (100 %)	2 μl
DNA template	1 μl (~ 100 ng)
PCR Grade Water	Up to 50 μl

Table 2. 5 Standard PCR reaction. Hot start DNA polymerase, 10X Buffer, dNTPs, and MgCl₂

were provided in the Hit start DNA polymerase kit (Merck, UK)

Temperature	Time	Number of cycles	Description
95 °C	1 min	1	Initial denaturation
95 °C	1 min		Denaturation
50-55 °C	30 sec	36	Annealing
68 °C	1 min per kb fragment size		Elongation
68 °C	10 min	1	Final Elongation
4 °C	∞		Storage

Table 2. 6 Standard PCR thermocycler program.

2. 3. 7 Agarose gel electrophoresis

Sizes of linear DNA fragments can be determined with gel electrophoresis through submerged horizontal gels (Brody and Kern, 2004). Agarose gels were prepared by dissolving 0.4-0.5 g (0.8-1% w/v) of agarose in 40 ml of 1X TBE buffer (89 mM Tris-borate and 2 mM EDTA, pH 8.3). The suspension was boiled to dissolve agarose, cooled, and 0.5 µg ml⁻¹ of ethidium bromide was added to allow for visualisation of DNA under UV light. Gels were poured in mini-gel trays and complete with a comb to create wells (Applied Biosystems). Set gels were submerged in TBE buffer and the samples were loaded and run at 30-70 Volts for 1 hour using Bromma 2197 Power Pack (Biorad, USA). Samples were mixed 10:1 with 10X loading buffer (0.25 % bromophenol blue, 50 % v/v glycerol, 10X TBE) to sink into the wells. 5µl of DNA Hyperladder™ I (Bioline) was run alongside to determine DNA sizes. All reagents are listed in Table 2. 7.

The size of linear DNA fragments was determined by comparison to the standards of a known length in the DNA ladder based on their electrophoretic motility. Migration rate through the agarose gel is inversely proportional to the Log_{10} of the size of the oligonucleotide fragments.

Gels were visualised with Gel Doc 1000 (Bio-Rad, USA) and Molecular Analyst™/PC windows Software. Photographs were printed with a Video Copy Processor P68B (Mitsubishi) on thermal paper (Mitsubishi).

Buffer	Composition	Amount
10X TBE (pH 8.3)	Tris-base	108 g l ⁻¹
	Boric acid	55 g l ⁻¹
	0.5 M EDTA pH 8.0	40 ml
DNA loading buffer	Bromophenol Blue	0.25%
	Glycerol	50%
	TBE	10X

Table 2. 7 Buffers used for agarose gel electrophoresis.

2. 3. 8 Purification of DNA fragments

2. 3. 8. 1 Purification of PCR products

PCR products were purified with QIAquick PCR purification Kit (QIAGEN) as per manufacturer's instructions.

2. 3. 8. 2 DNA gel extraction

For molecular cloning, linearised DNA fragments, such as endonuclease digested vector or insert, were resolved by gel electrophoresis on 0.8% (w/v) high purity Seachem Gold™ Agarose prepared in 1X TBE buffer (Table 2. 7). Bands of

appropriate size were excised from the gel and extracted using Gel Extraction Kit (QIAGEN) as per manufacturer's instructions.

2. 3. 9 Molecular cloning

2. 3. 9. 1 Digestion with Restriction Enzymes

One µg of DNA was incubated with 1 unit of appropriate endonuclease in 1X or 2X of appropriate buffer. 20-50 µl reactions were incubated at 37 °C for 1 hour.

Digested fragments were purified with QIAquick PCR purification Kit (QIAGEN) as per manufacturer's instructions and analysed with gel electrophoresis.

2. 3. 9. 2 Ligation of vector and insert DNA

Digested fragments were ligated with Rapid DNA ligase kit (ThermoFisher). The ratio of insert to vector was calculated using NEBioCalculator

(<https://nebiocalculator.neb.com/#!/ligation>), which uses the following formula:

$$\text{Amount of insert (ng)} = \left(\frac{\text{Insert length (bp)}}{\text{Vector length (bp)}} \right) \times \text{Amount of vector (ng)}$$

20 µl reactions were prepared in with 1 unit of Rapid ligase and 1X Ligation Buffer, where the molar ratio of insert:vector was routinely taken at 3:1 but could be adjusted depending on the insert size. Ligations were incubated at room temperature for 1 hour, then 5 µl was transformed into Top10 or CC118 chemically competent *E. coli* (Section 2.3.2).

2. 3. 10 Automated DNA sequencing

Sequencing of DNA fragments was performed by MWG-Biotech (Germany) as a value read service. Each clone was sequenced in the forward and reverse

directions, using standard sequencing primers T7 (TAATACGACTCACTATAGGG) and T7term (CTAGTTATTGCTCAGCGGT) for cloning into pET28a-b. Sequencing was performed with custom primers when cloning into pExchange. Total of 100 ng of DNA (10 µl) was required for a single reaction. Sequencing results were aligned and compared to the original gene in Clustal Omega (<https://www.ebi.ac.uk/Tools/msa/clustalo/>).

2. 3. 11 Whole genome sequencing

In chapter 3, Bt strains Bt Δ *pul1/2/3*; Bt Δ *pul1/2/3*+ Δ *bt4094*; and Bt Δ *pul1/2/3/4* were sent off for whole genome sequencing to confirm genotypes. This was performed Illumina Sequencing by Microbes NG (University of Birmingham, UK) as a paid service. Contigs were aligned and compared to *B. thetaiotaomicon* VPI-5482 as a reference genome by the Bioinformatics Unit, Newcastle University to confirm that the appropriate genetic mutations were present.

2. 3. 12 Overexpression of recombinant proteins

Expression plasmids, carrying the sequence corresponding to the protein of interest, were transformed into TUNER *E. coli* (Section 2.3.2). These cells were then resuspended in 5 ml of LB broth and used to inoculate 1 l of LB broth in conical flasks, containing appropriate antibiotic. The culture was grown to OD₆₀₀ of 0.6 at 37 °C with shaking at 180 rpm. The cultures were then cooled and 1 ml of 0.2 M of isopropylthio- β -D-galactoside (IPTG) was added and the cultures were incubated at 16 °C at 180 rpm for 16 h. Addition of IPTG induces protein expression controlled by *lacO* in *lacI^q* carrying plasmids.

Cells were harvested by centrifugation at 5,000 rpm for 10 minutes (Section 2.3.1). Pellets from 1 l cultures were resuspended in 10 ml of TALON (50 mM Tris-

HCl, 300 mM NaCl, pH8.0) buffer. If the protein was not purified immediately, pellets were stored at -20 °C.

To produce cell free extracts, resuspended pellets were placed on ice and sonicated for 2 minutes using a B. Braun Labsonic U sonicator set at low intensity (~42 watts and 0.5 second cycling). Cells were pelleted by centrifugation at 15,000 rpm for 30 minutes (Section 2.3.1). Cell lysate (supernatant) was collected and used for protein purification with Immobilised Metal Affinity Chromatography (IMAC). Cell debris were resuspended in TALON buffer and was analysed with SDS-PAGE alongside other IMAC fractions.

2. 3. 13 Immobilised Metal Affinity Chromatography (IMAC)

Pet28a-b vectors are designed to contain a hexa-Histidine tag, which interacts with transition metals immobilised in a column, to allow for purification of proteins with IMAC. This interaction can be displaced with an imidazole gradient to elute proteins from the column. The purification procedure was performed in TALON buffer (50 mM Tris-HCl, 300 mM NaCl, pH 8.0).

TALON™ (Clontech Laboratories Inc.) resin, containing cobalt ions, was pipetted into a column and left to settle, forming a 3 cm bed. Columns were equilibrated with 10 volumes of TALON buffer. Cell free extracts (5-20 ml) were poured through the column and the eluent was collected. Columns were washed with 20 ml of TALON buffer to remove unbound proteins. The protein was eluted with 5 ml of 10 mM Imidazole in TALON buffer followed by 2 x 5 ml of 100 mM Imidazole in TALON buffer, three fractions were collected. All fractions were analysed with SDS-PAGE.

2. 3. 14 Sodium Dodecyl Sulfate-Polyacrylamide Gel Electrophoresis (SDS-PAGE)

Proteins were visualised by SDS-PAGE as described by Laemmli (1970) to assess the size, relative purity and expression level of a protein.

Routinely, 12.5 % polyacrylamide gels, unless stated otherwise, were prepared using the AE-6450 apparatus from ATTO Corporation (Genetic Research Instruments), which is composed of 2 12 cm x 10 cm glass plates sealed by a rubber gasket. The composition of polyacrylamide gels and the SDS-PAGE running buffer is summarised in Table 2. 8 and 2. 9, respectively. The resolving gel (Table 2. 8) was poured into the plates and covered with 100% ethanol and left to polymerise. The ethanol was then removed and the stacking gel (Table 2. 8) was then poured on top of the resolving gel, a comb was added to create wells, and the gel was left to polymerise. Before use, the comb and rubber seal were removed and the gel affixed within the gel tank, which was filled with SDS-PAGE running buffer (Table 2. 9).

The loading buffer (Table 2. 9) was added to samples (1:2 v/v), 20 µl samples were boiled for 2 minutes to denature the proteins and loaded into the gel.

Molecular weight standard SigmaMarker™ wide range ladder (Sigma) was loaded alongside and used to assess protein size. Gels were run at a current of 35 A per gel.

After electrophoresis, proteins were visualised with InstantBlue™ stain (Expedeon) for at least 15 minutes, the gels were destained in distilled water for 16 hours. Gels were photographed using a Bio-Rad Gel Doc 1000, Molecular Analyst™/PC windows Software). Photographs were printed with a Video Copy Processor P68B (Mitubishi) on thermal paper (Mitubishi).

Component	Reagent	Volume per gel
Resolving gel	0.75 M Tris-HCl, pH 8.8, 0.2 % SDS	2.35 ml
	40 % Acrylamide (BDH Electran acrylamide, 3% (w/v) bisacrylamide)	1.45 ml
	d. d. H ₂ O	0.875 ml
	10 % (w/v) Ammonium persulfate	22.5 µl
	TEMED	7.5 µl
Stacking gel	0.25 M Tris-HCl, pH 8.8, 0.2 % SDS	0.938 ml
	40 % Acrylamide (BDH Electran acrylamide, 3% (w/v) bisacrylamide)	0.188 ml
	d. d. H ₂ O	0.75 ml
	10 % (w/v) Ammonium persulfate	15 µl
	TEMED	5 µl

Table 2. 8 SDS-PAGE gel preparation

Component	Reagent	Volume or concentration
Running Buffer (for 1 l)	32 mM Tris/190 mM glycine, pH 8.3	350 ml
	SDS	0.1% (w/v)
Loading buffer (for 10 ml)	SDS	10 % (w/v)
	0.25 M Tris-HCl, pH 8.8	5 ml
	Glycerol	25 % (w/v)
	β-mercaptoethanol	2.5 ml
	Bromophenol blue dye	0.1 % (v/v)

Table 2. 9 SDS-PAGE gel Running buffer

2. 3. 15 Quantification of proteins

Protein concentration was determined using a NanoDrop 2000 UV-Vis spectrophotometer (Thermo Fisher, USA) and the Beer-Lambert's equation: $A = \epsilon l C$, where A = absorbance 280 nm – absorbance at 320 nm; ϵ = extinction coefficient ($M^{-1}cm^{-1}$), l = length of light path (cm), and C = concentration of sample (M).

2. 3. 16 Concentration of Proteins and Buffer Exchange

Protein solutions were concentrated using 20 ml Vivaspin[®] concentrator columns (Sartorius Stedim Biotech) with appropriate 10, 30, or 100 kDa molecular weight cut off membranes

When necessary PD-10 desalting columns (GE Healthcare) were utilised as per manufacturer's instructions. The buffer exchange for larger volumes was performed with dialysis into 4 l of 50 mM HEPES 150 mM NaCl using 13.5 kDa cut off dialysis tubing with stirring at 4 °C for 16 hours.

2. 3. 17 Genetic manipulations in *B. thetaiotaomicron*

2. 3. 17. 1 Construction of a deletion cassette

For each deletion, flanking regions of ~1KB upstream and downstream of a gene of interest were identified, and the appropriate primers of 20-25 bases were constructed (Figure 2. 1). Primers distal to the gene of interest (Primer 1 and 4) were designed to contain restriction sequences compatible with cloning sites in pExchange-tdk vector (Figure 2. 1 a). One of the proximal primers, located directly after the stop codon of the gene of interest, contained a sequence complementary to the 5' end of the Flank 1 (Figure 2. 1 a). Each flanking region was amplified with

PCR (Section 2.3.5) and analysed with gel electrophoresis (Section 2.3.6). A sewing PCR was then performed using Primer 1 and Primer 2 (Figure 2. 1 b), producing a 2kB deletion cassette (Figure 2. 1 c). This was then ligated into pExchange-tdk using appropriate restriction sites (Section 2.3.8). The plasmid was then propagated in CC118 *E. coli*, presence of appropriate deletion cassettes in isolated clones was confirmed by sequencing using primers 1 and 4.

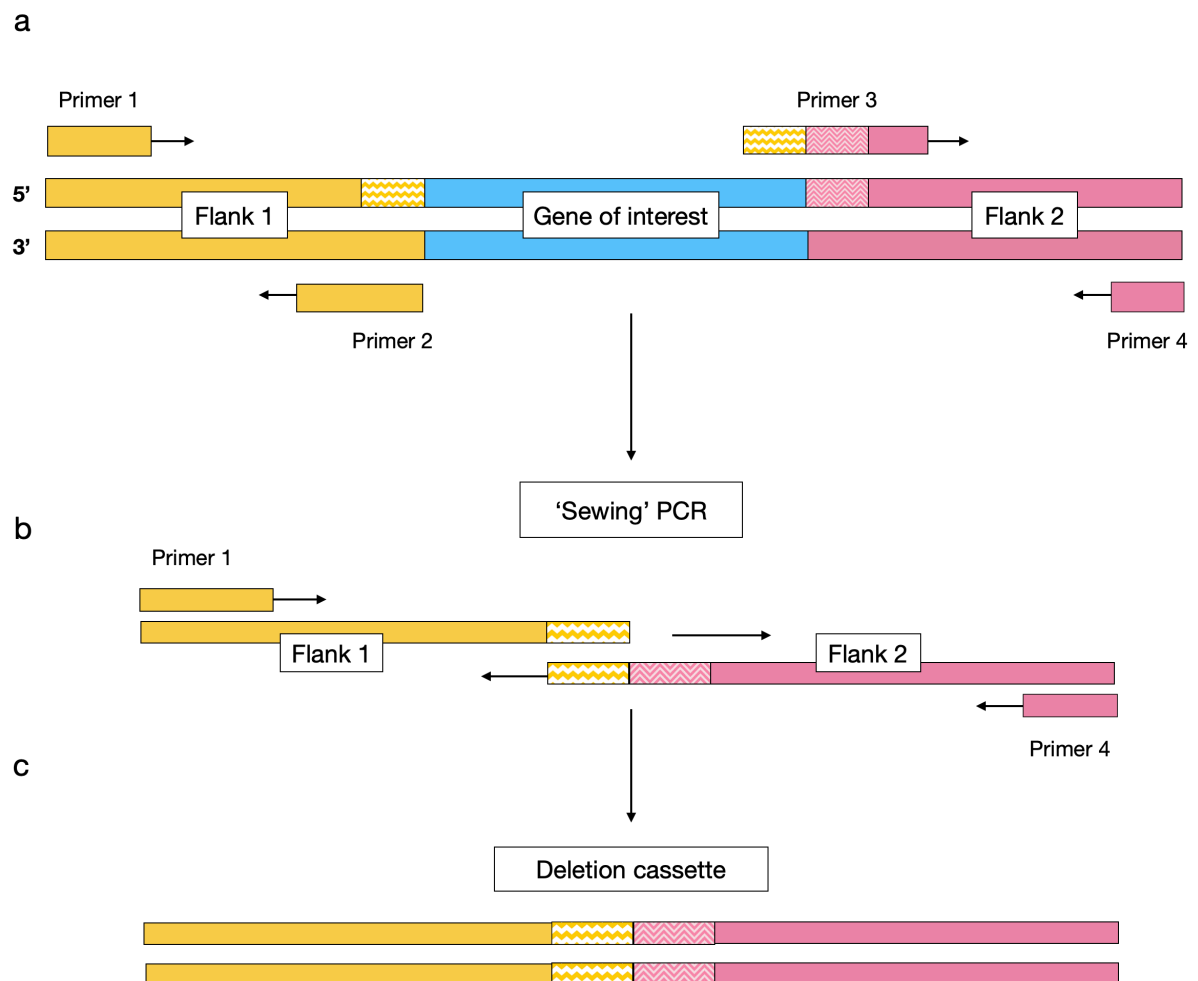


Figure 2. 1 Sewing PCR to generate gene deletion fragments. Panel a: primer design. Primer 1 and Primer 4 were designed to contain appropriate restriction sites. Primer 3 was designed to contain a region complementary to the 5' end of flank 1. Two 1000 bp regions flanking the gene of interest, Flank 1 and 2, were amplified by PCR. Panel b: Flank 1 and Flank 2 were ligated with sewing PCR using Primer 1 and Primer 4. Panel c: 2 kb product of the sewing PCR used to introduce deletions.

2. 3. 17. 2 Conjugations into *B. thtaiotaomicron*

The gene deletion procedure is an adaptation of the standard counter-selectable allelic exchange procedure employed in bacterial genetics, which was modified by E. Martens. The process involves a counter-selectable suicide vector, pExchange-tdk, and *B. thtaiotaomicron* Δtdk strain, which lacks a functional thymidine kinase (Tdk-BT2275). This enzyme participates in the pyrimidine salvage pathway. Wild type Bt displays sensitivity to a toxic compound 5fluoro-2-deoxy-uridine (FUdR), which interferes with de novo synthesis of thymidine. *B. thtaiotaomicron* Δtdk is resistant to FudR and pExchange-tdk, carries a copy of Bt2275 and its promoter. The deletion involves two recombination events (Figure 2. 2)

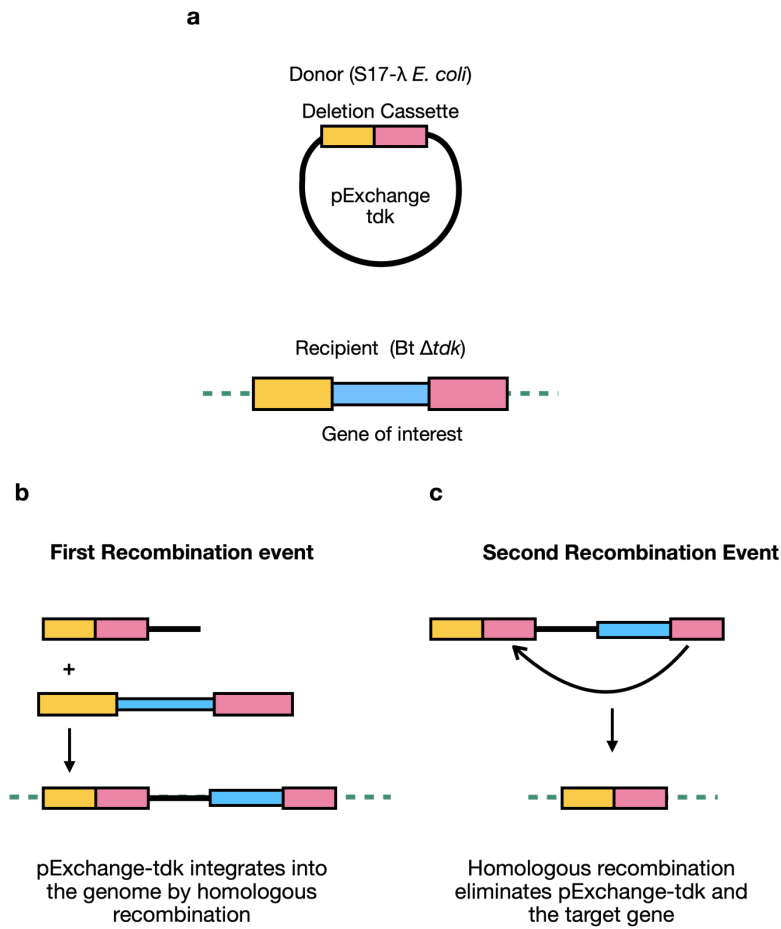


Figure 2. 2 Gene deletions in *B. thtaiotaomicron*, a: the process requires a donor strain, S17- λ *E. coli*, carrying a pExchange-tdk with a deletion cassette, and a recipient Bt Δtdk , encoding the target gene. Gene deletion involves two recombination events: b: plasmid is integrated into the genome via homologous recombination and c; plasmid is expelled from the genome by the second recombination event.

S17- λ *E. coli* (donor) and Bt Δtdk (recipient) were cultured overnight in 5 ml of LB broth with ampicillin, and TYG media, respectively. The donor and recipient strains were inoculated into fresh respective media and grown for further 3-4h at 37°C, static for Bt and shaking at 180 rpm for *E. coli*. The cells were pelleted by centrifugation at 5,000 rpm for 5 mins and resuspended in 0.5 ml of fresh TYG. Cells were then combined in equal amounts, spread out evenly on BHI pates without antibiotic, and incubated agar side down at 37 °C for at least 24 hours.

This allows for the conjugation to occur, where *E. coli* grows first, creating an anaerobic niche underneath for Bt to grow. Bacterial mass was then scraped from the plate and resuspended in 5 ml of TYG. The stock and 3 x 10-fold serial dilutions were then plated onto BHI-blood agar containing gentamycin ($200 \mu\text{g ml}^{-1}$) and erythromycin ($25 \mu\text{g ml}^{-1}$) and grown anaerobically at 37°C for 2 days. Gentamycin kills *E. coli* and erythromycin allows for the selection of the recipient Bt, carrying pExchange-tdk plasmid.

Following this, 10 individual colonies were re-streaked onto BHI + erythromycin + gentamycin plates and grown for another 2 days anaerobically at 37°C . Each colony represents a single recombinant strain of Bt, containing a modified pExchange-tdk plasmid. 10 single colonies were picked and cultured in 5 ml of TYG media anaerobically at 37°C overnight. This step encourages the second recombination event to occur, which will expel pExchange plasmid from the genome. All 10 cultures were then pooled together in equal amounts. The stock and 2 of the 10-fold dilutions were plated on BHI, containing FUdR ($200 \mu\text{g ml}^{-1}$). These were then incubated anaerobically at 37°C for 3 days. This step selects for either recombinant mutants with a desired deletion or a genetically wild-type strain. Further 10 FUdR resistant colonies were re-streaked onto new BHI-blood FUdR plates and again grown for 2 days. 10 individual colonies were then picked and cultured in 5 ml of TYG anaerobically at 37°C overnight. These were stored at -80°C in 25% glycerol (Section 2.2.5) and genomic DNA was extracted as described in Section 2.3.7.1.

The presence of appropriate deletions was assessed with PCR and the primers specific for the deletion cassette (Figure 2. 1). The wild-type strain was tested alongside, which would generate a PCR product, comprising of the target gene

(500-2000 bp) plus the length of both flanks (1000 bp each). Any successful knockouts will lack the target gene, producing a 2000 bp fragment. Genotypes were confirmed by automated sequencing (Section 2.3.8).

2. 4 Biochemistry

2. 4. 1 Thin Layer Chromatography (TLC)

Thin layer chromatography is a solvent-based chromatography used to analyse glycans. Different molecules migrate at different rates through the solvent due to the differences in ionisation state, solubility and structure. Smaller and more hydrophobic compounds will migrate faster than larger complexes.

A solution of 1-butanol/ acetic acid/ water at 2:1:1 (mobile phase or solvent) was used as a running buffer (Table 2. 10) in a glass chromatography tank (23 cm x 23 cm x 7.5 cm), which was sealed tightly and left to equilibrate 1 hour prior to use. Silica-coated foil plates (Silica gel 60, 20cm x 20cm, Merck) were used as a stationary phase. The plates were cut to an appropriate size with a height of at least 10 cm and a line was drawn 1 cm from the bottom edge of the plate.

Samples of 3-12 µl were loaded onto the plates 1 cm apart from each other along the appropriate known sugar standards. The plates were then put into the equilibrated tanks and left to run until the solvent front was 1cm away from the top of the plate. For better separation of sugars with similar sizes, plates were taken out, dried, and returned to the tank until the solvent was 1cm away until the top of the plate.

To visualise sugars, plates were immersed into Orcinol stain (Table 2. 10).

Acetylated sugars were visualised with Diphenylamine-aniline-phosphoric acid stain (Diphenylamine 1.7% w/v, Aniline 1.7%, Ethyl acetate 85% v/v, hydrochloric

Acid 2% v/v, Phosphoric acid 11% v/v). Plates were dried and developed by heating to 100°C.

Component	Reagent	Volume per litre
Running buffer	1-Butanol	500 ml
	Glacial Acetic acid	250 ml
	H ₂ O	250 ml
Orcinol Stain	Sulphuric acid	36 ml
	100% Ethanol	700 ml
	H ₂ O	260 ml
	Orcinol monohydrate	10 g

Table 2. 10 Composition of the TLC running buffer and Orcinol stain.

2. 4. 2 High-Performance Anion Exchange Chromatography (HPAEC)

Sugars were separated by High Performance Anion Exchange Chromatography with Pulsed Amperometric Detection (HPAEC-PAD). The fully automated system (ICS-3000 gradient pump, detector compartment, detector, auto sampler) had a loop size of 100 µl. Monosaccharides were separated with CarboPAC™ PA-20 anion exchange column (ThermoFisher) equipped with a CarboPac™ PA-20 guard column, and eluted isocratically with 20mM NaOH. Oligosaccharides were separated with CarboPAC™ PA-200 anion exchange column (ThermoFisher) equipped with a CarboPac™ PA-200 guard column and eluted with a Sodium Acetate gradient.

The program settings were 0-10 minutes with 100 mM NaOH, 10-25 minutes 100 mM NaOH with linear gradient of 0-33 mM Sodium Acetate, unless specified. This was followed by a wash with 500 mM Sodium Acetate and 500 mM NaOH for another 10 minutes. Data were collected using Chromeleon™ Chromatography

Management system V 6.8 (Dionex) via a Chromeleon™ Server (Dionex) and processed in Prism 9.0 (GraphPad).

Samples were boiled for 10 mins, centrifuged 13,000 rpm for 10 mins, and diluted 1:10 in distilled water in HPLC Vials. Peaks corresponding to different sugars were identified using appropriate standards. A glucose standard at 50 μM was routinely tested before and after sample analysis.

2. 4. 3 Enzyme assays

All enzyme assays were performed at standard conditions using 1-2 μM enzyme and 4-5 mg ml^{-1} substrate in 50 mM MOPS 2 mM CaCl_2 at 37 °C for 16 h, unless stated otherwise.

For catalytic activity assays, all reactions were pre-warmed to 37 °C and initiated by the addition of appropriately diluted enzyme. Data was processed in Prism 9.0 (GraphPad) and the kinetic parameters (K_m , k_{cat} , V_{max}) were determined with Michaelis-Menten non-linear regression, using appropriate enzyme concentrations. V_{max} is a maximum rate of enzyme when substrate is in excess; K_m is the concentration of substrate at which the reaction rate is half V_{max} , k_{cat} is the catalytic efficiency of the enzyme, showing a number of substrate molecules turned over by one enzyme molecule per unit of time. If it was not possible to determine these parameters from a non-linear regression, a simple linear regression was used instead, and k_{cat}/K_m were determined from the slope divided by the enzyme concentration.

2. 4. 4 D-Glucose/D-Fructose/D-Mannose detection kit

Mannose release was monitored using a Mannose detection Kit (Megazyme, Portugal). This kit is based on a linked assay, where mannose is converted to mannose-6-phosphate, which is rapidly modified to glucose-6-phosphate to be oxidised by Glucose-6-phosphate dehydrogenase, resulting in reduction of NADP⁺ to NADPH (Figure 2. 3). Formation of NADPH is directly proportional to the amount of sugar released and can be continuously monitored spectrophotometrically at 340 nm. Extinction coefficient of NADPH $\epsilon = 6230 \text{ M}^{-1} \text{ cm}^{-1}$ was used to determine concentration of mannose using Beer-Lambert's law $A = \epsilon C l$, where $A =$ at 340 nm; $\epsilon = 6230 \text{ M}^{-1} \text{ cm}^{-1}$, $l =$ length of light path (1 cm), and $C =$ concentration of sample (M).

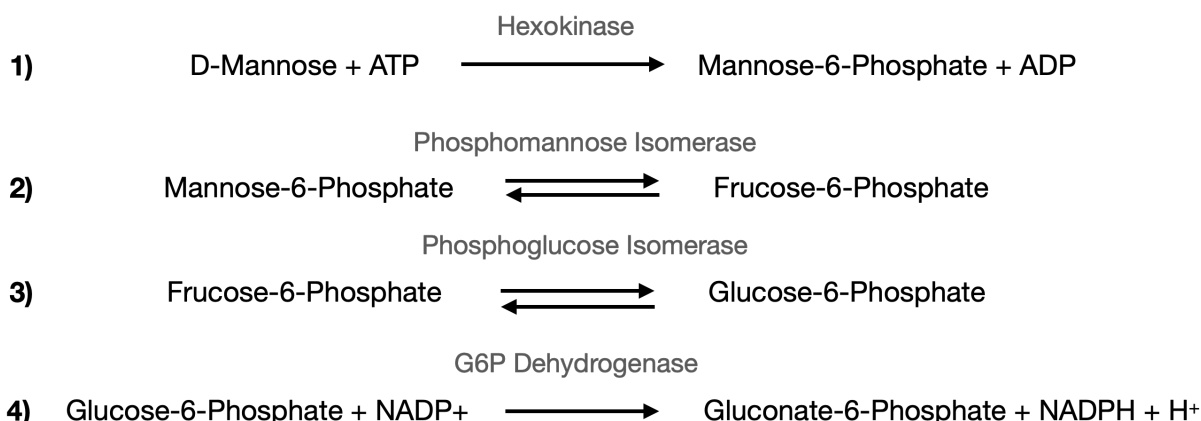


Figure 2. 3 Linker enzymes deployed by Mannose detection kit to monitor mannose release.

Enzymes catalysing appropriate reactions are indicated.

Reactions were performed in glass cuvettes to monitor NADH release using a Biotech Ultrospec 4000, UV/vis spectrophotometer at 37 °C.

All reactions were carried out at 37 °C in the specified buffer. Glass cuvettes were used and NADPH release monitored using a Biotech Ultrospec 4000, UV/vis

spectrophotometer. Assays were prepared according to manufacturer's instructions; components of an assay are listed in Table 2. 11.

Component	Volume
Buffer 1 or 50 mM MOPS 2mM CaCl ₂	50 µl
NADP ⁺ + ATP	50 µl
Hexokinase + Glucose-6-Phosphate Dehydrogenase	5 µl
Phosphoglucose Isomerase	5 µl
Phosphomannose Isomerase	5 µl
Substrate	Variable
Enzyme (appropriately diluted)	Variable
Sterile Water	Up to 500 µl

Table 2. 11 Composition of a standard reaction for a linked assay.

Buffer 1, enzymes, and NADP⁺ were provided in the Mannose detection kit (Megazyme).

2. 4. 5 Preparation of substrates and oligosaccharides

2. 4. 5. 1 Extraction of mannans

The method of mannan purification was adapted from Kocourek and Ballou (1969) 1 ml of overnight culture of *C. albicans* SC5315 or *S. cerevisiae* $\Delta mnn1$; $\Delta mnn5$; $\Delta mnn2$ strains was inoculated into 1 l of YPD medium and grown for up to 2 days with shaking at 180 rpm at 30 °C. Cells were harvested by centrifugation at 3000 rpm for 10 min (Section 2.3.1). Approximately, 8 l of yeast culture produced 100 g of pellet. If not used immediately for mannan extraction, pellet was stored at -20 °C.

100 g of pellet was resuspended in 50 ml of 0.02 M Citrate Buffer pH 7.0 (Table 2. 12) and autoclaved for 90 mins (Section 2.2.2). The mixture was centrifuged at 5000 rpm for 10 min and the supernatant was collected. The pellet was again resuspended in 75 ml of 0.02 M Citrate buffer pH 7.0 and autoclaved for 90 minutes. The supernatant was again harvested by centrifugation at 5,000 rpm for 10 minutes and combined with the previous extract. The supernatant extract contains polysaccharides which were released from the cell wall during autoclaving. If not used immediately for mannan precipitation, supernatant can be stored at 4 °C overnight.

2X Fehling reagent stock was prepared as described in Table 2. 12. A volume of Fehling reagent, equal to that of the supernatant extract, was heated to 40 °C and the supernatant was carefully added with vigorous stirring, resulting in a formation of a light-blue precipitate. The mixture was left stirring at 40 °C for 1 hour. The resulting polysaccharide-copper precipitate was collected by centrifugation at 5000 rpm for 10 minutes. The supernatant was disposed of according to the University protocol for the management of hazardous waste. The pellet was dissolved in 8 ml of 3 M HCl to disrupt the copper complexes, producing a light green solution. This was then poured slowly with vigorous stirring into 100 ml of methanol acetic acid solution (8:1 v/v) and left stirring for up to 1 hour, causing mannan to precipitate. Mannan was collected by centrifugation at 10,000 rpm for 10 min (Section 2.3.1) and the pellet was washed at least three times with methanol acetic acid solution (8:1 v/v) or until the supernatant was colourless to wash off residual copper. The white precipitate was then washed with methanol and left to dry overnight at room temperature for 16 h. Dried pellet was resuspended in distilled water and dialysed into 4 l of distilled water using 13.5

kDa dialysis tubing with stirring at room temperature for 16 h, water was then changed and mannan was dialysed for one more day. The solution was freeze dried and stored at room temperature in powder form. The yield was dependent of the strain and the species, 100 g of yeast pellet generated approximately 0.5 g of mannan,

Reagent	Components	Amount per litre	Preparation Procedure
2X Fehling Reagent	CuSO ₄	70 g (7%)	Gradually dissolve all ingredients in distilled water with stirring
	Potassium Sodium Tartrate (Rochelle's salt)	350 g (35%)	
	NaOH	50 g (5%)	
0.02M Citrate Buffer pH 7.0	Sodium Citrate	5.8 g	Dissolve in distilled water, pH is self-adjusting.
	Citric Acid	75 mg	

Table 2. 12 Components of 2X Fehling reagent and 0.02 M Citrate buffer used for mannan extractions.

2. 4. 5. 2 Generation and Purification of β -1,2-mannooligosaccharides

β -1,2-mannooligosaccharides were released from mannan purified from *C. albicans* SC5315 with mild acid hydrolysis. The procedure involved boiling 10 mg ml⁻¹ of *C. albicans* mannan at 100 °C in 10 mM HCl for 1 hour. The reaction was neutralised with NaOH until neutral pH was obtained, samples were analysed with TLC (Section 2.4.1). Samples were then freeze dried, resuspended in water, and purified by size exclusion chromatography using P2 Bio-gel (Bio-Rad) matrix packed in two Glass Econo-Columns (2.5cm X 80cm) with a flow adaptor (Bio-Rad) at 0.2 ml min⁻¹. Columns were equilibrated with degassed distilled water and oligosaccharides were eluted with distilled water. Fractions of 1.8-2 ml were collected and assessed for the presence of sugars with TLC. Fractions containing

sugars of approximately the same size were pooled, freeze dried, resuspended in 0.5 ml of water and stored at -20 °C. Concentration of oligosaccharides was determined with a Mannose detection kit (Section 2.4.4). and an enzyme with a known β -1,2-mannosidase activity.

2. 4. 5. 3 Concentrating of samples by freeze drying

Purified mannan or oligosaccharides were frozen to -80 °C and then lyophilised in a Christ Alpha 1-2 Freeze Drier at -60 °C.

2. 4. 6 Analysis of in-gel proteins by Mass Spectrometry

Mass Spectrometry analysis of in-gel proteins presented in Chapter 5 was performed by the Metabolomics and Proteomics facility, Department of Biology (University of York, UK)

2. 4. 6. 1 Sample preparation

B. salyersiae was grown in 15 ml of defined medium (Appendix A) with 10 mg ml⁻¹ mannan from *S. cerevisiae* (Sigma) anaerobically at 37 °C (Section 2.2.3) and aliquots were collected hourly for 14 hours. Supernatant was separated by centrifugation at 13000 rpm for 2 minutes (Section 2.3.1) and concentrated 5 times with Vivaspin[®] 20 concentrator tubes with 30 kDa cut off (Section 2.3.12), 20 μ l was analysed with SDS-PAGE gel (Section 2.3.11). Desired protein bands were excised from the gel and sent to the University of York (<https://www.york.ac.uk/biology/technology-facility/proteomics/>) for analysis.

2. 4. 6. 2 Sample analysis.

This was performed as a paid service but briefly, proteins were in-gel digested with trypsin and the resulting peptides were analysed with Matrix Assisted Laser Desorption Ionization Tandem Time-of-Flight (MALDI-TOF) mass spectrometry.

Mass spectral data was searched against *B. salyersiae* CL02T12C01 genome available in the NCBI database using Mascot search program. Threshold for the associated expect value was set to 0.05, fragment mass tolerance was set at 0.5 Da, a minimum of 2 matched peptides was required for protein identification.

2. 4. 7 Comparative proteomics

2. 4. 7. 1 Sample preparation

B. salyersiae was grown in 10 ml of defined medium (Appendix A) with 10 mg ml⁻¹ mannan from *S. cerevisiae* or glucose to mid exponential phase OD₆₀₀ = 0.8 anaerobically at 37 °C. Respective mannan and glucose cultures were produced in triplicates. Cells were pelleted by centrifugation at 5000 rpm for 10 minutes (Section 2.3.1), supernatant was collected and stored at -20 °C. Pellets were washed in 10 ml of sterile PBS three times and stored frozen at -20 °C until required.

Comparative proteomics presented in Chapters 4 and 5 were performed by Dr Tiaan Heunis, Biosciences Institute, Newcastle University, as a collaboration.

Briefly, *B. salyersiae* cells were suspended in 5% SDS in 50 mM triethylammonium bicarbonate (TEAB) pH 7.5. and sonicated using an ultrasonic homogenizer (Hielscher) for 1 minute. The cell extract was collected by centrifugation at 10,000 x g for 5 minutes. Protein concentration was determined using a bicinchoninic acid (BCA) protein assay (Thermo Scientific). A total of 30 µg protein for the whole cell lysate was used for analysis and the sample preparation was performed using the suspension trapping (S-Trap) sample preparation method, as recommended by the supplier ProtiFi™ (Huntington NY). Samples were digested with trypsin in 50 mM TEAB (1:10 ration of trypsin: protein) for 2

hours at 47 °C using a thermomixer (Eppendorf). Peptides were eluted with 50 mM TEAB pH 8.0 and centrifugation at 1000 g for 1 minute. Elution steps were repeated using 0.2% formic acid and 0.2% formic acid in 50% acetonitrile, respectively. The three eluates from each sample were combined and dried using a speed-vac before storage at -80°C.

2. 4. 7. 2 Mass spectrometry

Each sample was independently analysed on an Orbitrap Fusion Lumos Tribrid mass spectrometer (Thermo Fisher Scientific), connected to an UltiMate 3000 RSLCnano System (Thermo Fisher Scientific). Peptides (1 µg) were injected on a PepMap 100 C18 LC trap column (300 µm ID × 5 mm, 5 µm, 100 Å) followed by separation on an EASY-Spray nanoLC C18 column (75 µm ID × 50 cm, 2 µm, 100 Å) at a flow rate of 250 nl min⁻¹. Solvent A was water containing 0.1% formic acid, and solvent B was 80% acetonitrile containing 0.1% formic acid. The gradient used for analysis of proteome samples was as follows: solvent B was maintained at 2% for 5 min, followed by an increase from 2 to 35% B in 120 min, 35-90% B in 0.5 min, maintained at 90% B for 4 min, followed by a decrease to 3% in 0.5 min and equilibration at 2% for 10 min. The Orbitrap Fusion Lumos was operated in positive-ion data-dependent mode. The precursor ion scan (full scan) was performed in the Orbitrap in the range of 400-1,600 m/z with a resolution of 120,000 at 200 m/z, an automatic gain control (AGC) target of 4×10^5 and an ion injection time of 50 ms. MS/MS spectra were acquired in the linear ion trap (IT) using Rapid scan mode after high-energy collisional dissociation (HCD) fragmentation. An HCD collision energy of 30% was used, the AGC target was set to 1×10^4 and dynamic injection time mode was allowed. The number of MS/MS events between full scans was determined on-the-fly to maintain a 3 s fixed duty cycle. Dynamic exclusion of ions

within a ± 10 ppm m/z window was implemented using a 35 s exclusion duration. An electrospray voltage of 2.0 kV and capillary temperature of 275°C, with no sheath and auxiliary gas flow, was used.

2. 4. 7. 3 Sample analysis

Mass spectral data were analysed using MaxQuant 1.6.14.0, and searched against the Uniprot *Bacteroides salyersiae* CL02T12C01 proteome database (UP000005150). Peak list generation was performed within MaxQuant and searches were performed using default parameters and the built-in Andromeda search engine. The enzyme specificity was set to consider fully tryptic peptides, and two missed cleavages were allowed. Oxidation of methionine, N-terminal acetylation and deamidation of asparagine and glutamine were allowed as variable modifications. Carbamidomethylation of cysteine was allowed as a fixed modification. A protein and peptide false discovery rate (FDR) of less than 1% was employed in MaxQuant. Proteins that contained similar peptides and that could not be differentiated on the basis of MS/MS analysis alone were grouped to satisfy the principles of parsimony. Statistical analysis was conducted by Dr Tiaan Heunis, Biosciences Institute, Newcastle University in the R statistical programming language using the MSstats package. At least 2 peptides of the same protein were required to be detected in all tested glucose- and mannan-grown samples to qualify for the statistical analysis. To determine the relative abundance of proteins, obtained data were normalised to the glucose samples, \log_2 value ≥ 2 was taken as a cut off for upregulation, proteins with \log_2 value ≤ -2 were counted as downregulated.

2. 4. 8 Isothermal Titration Calorimetry (ITC)

Binding of proteins to glycans and the thermodynamic parameters can be quantified with ITC. Formation of protein-ligand complexes either generates or absorbs heat, resulting in exothermic or endothermic reactions, respectively. MicroCal™ VP-Isothermal Titration Calorimeter measures the amount of energy required to maintain the temperature of the reaction cell relative to the reference cell and therefore provides a readout of the amount of heat released or absorbed.

Recombinant proteins were dialysed into 50 mM HEPES 150 mM NaCl, pH 7.0 (Section 2.3.12) and substrates were prepared in the same dialysis buffer.

Titration were performed at 25 °C and 307 rpm with 27 injections at regular intervals of 10 µl of ligand into the cell containing 25 µM of protein. The concentration of ligand was adjusted depending on the conditions to obtain a titration curve. The curve was analysed with non-linear regression and was fitted to a model where number of binding sites was equal to 1. The thermodynamic parameters: association constant (K_a), binding enthalpy (ΔH), and Gibbs free energy (ΔG) were estimated from the titration curve using Microcal PEAQ-ITC software v1.30 (Malvern Panalytical). Standard thermodynamic equation $\Delta G = \Delta H - T\Delta S$ was used to calculate the entropy change ($T\Delta S$).

2. 4. 9 Affinity Gel Electrophoresis (NATIVE-PAGE)

Binding of proteins to glycans can also be analysed with affinity gel electrophoresis. Formation of ligand-protein complexes distorts migration of the protein through the polyacrylamide matrix. Similar to what was described for SDS-PAGE (Section 2.3.11), an AE-6450 apparatus from ATTO Corporation was applied, using a native polyacrylamide gels containing soluble substrates Table 2.

13). The ligands were added at 0.1% (w/v) prior to polymerisation, water was used as a negative control. 5 µg of protein was mixed with 5 µl of loading buffer (Table 2. 13), loaded onto a gel and run at 10 mA per gel at room temperature. Gels with and without ligands were run in the same gel box with identical samples loaded on each. Mixture of oligomers of BSA (15 µg) was used as a negative, non-interacting control. Proteins were stained and visualised as described for SDS-PAGE (Section 2.3.11)

Component	Composition	Amount
10X Native buffer	Tris base (0.25 M)	30 g l ⁻¹
	Glycine (2.5 M)	187 g l ⁻¹
DNA loading buffer	Bromophenol Blue	0.0025%
	Glycerol	5%
		Amount per gel
Native gel	d H ₂ O	6.06 ml
	10X Native buffer	1 ml
	40 % Acrylamide (BDH Electran acrylamide, 3% (w/v) bisacrylamide)	1.9 ml
	10 % (w/v) Ammonium persulfate	50 µl
	TEMED	10 µl
	Substrate 1% (w/v) or water	1 ml

Table 2. 13 Composition of NATIVE-PAGE affinity gels and buffers

2. 5 Microbiology

2. 5. 1 Culture preparation and monitoring.

Bacterial cultures were routinely prepared by inoculation of 5 ml of rich TYG medium (Section 2.2.1) with 20 µl of a glycerol stock of desired species and grown to stationary phase for at least 14 hours in controlled anaerobic conditions inside the A35 anaerobic chamber (Don Whitley Scientific) at 37 °C to produce active

bacterial cultures. These were then used to inoculate defined or minimal media using 5 μ l per 200 μ l for the growth experiments in the plate reader and 5-10% cell density in all other experiments.

Bacterial cultures were prepared in 96 well Corning® Costar® culture plates (Sigma-Aldrich) and monitored with an Epoch microplate spectrometer (Biotek Instruments Ltd.) inside of the anaerobic chamber. The plate reader collected OD₆₀₀ at 15-minute intervals to generate a growth curve. Each growth condition was prepared in triplicates, data were averaged to produce a standard error of mean. A control containing media without bacterial inoculum was run to ensure no contamination has occurred throughout the growth period. Background absorbance of the control was taken as a baseline and subtracted from all samples. Data were analysed in Prism 9.0 (GraphPad).

Cultures larger than 200 μ l and co-cultures were performed in 10 ml sterile glass tubes and 50 ml conical flasks, respectively, which were plugged with cotton wool, preventing contamination. Tubes were placed in the anaerobic chamber and OD₆₀₀ was monitored using a manual CO 75000 spectrophotometer (Sigma).

2. 5. 2 Cross-feeding experiments with conditioned media

A set of growth experiments in Chapter 4 utilised conditioned media. This was prepared by growing *B. salyersiae* or *B. thetaiotaomicron* in defined medium (Appendix A) with 15 mg ml⁻¹ mannan from *S. cerevisiae* (Sigma) to the mid exponential phase OD₆₀₀ = 0.6-0.8 anaerobically at 37 °C. Cells were separated by centrifugation at 5000 rpm for 10 minutes, supernatant was then collected and autoclaved (Section 2.2.2) and stored at -20 °C until required.

Supernatant was defrosted and filter sterilised with 0.2 µl Millipore filter disc (Section 2.2.2) and diluted 1:2 with sterile 2X defined medium (Appendix A) to produce conditioned media. *Bacteroides spp.* were grown as described in Section 2.4.1 and inoculated (2.5 % v/v) into 200 µl of conditioned media. Assays were prepared in 96 well plates in triplicates and monitored using an automatic plate reader as described in Section 2.4.1.

2. 5. 3 Whole cell assays

Whole cell assays were deployed to assess enzymatic activity at the cell surface. Cells of *Bacteroides spp.* remain structurally intact but metabolically inactive in the presence of oxygen and thus, the activity of the CAZymes presented on the cell surface can be assessed as these enzymes do not require ATP. Enzymes could be removed from the cell surface with Proteinase K, while lysed cells could be used to assess activity of all enzymes expressed in the cytosol, periplasm, and the cell surface.

B. thetiaiotaomicron or *B. salyersiae* were grown in 10 ml of defined medium (Appendix A) containing 10 mg ml⁻¹ substrate, unless stated otherwise, to the mid exponential phase OD₆₀₀ = 0.8 anaerobically at 37 °C (Section 2.2.3). Cells were collected by centrifugation at 5000 rpm for 10 minutes at 4 °C (Section 2.3.1), washed 10 ml of PBS 3 times, resuspended in 1.5 ml of PBS, and kept on ice. A fraction of cells was treated with 2 mg ml⁻¹ Proteinase K (Sigma) at 37 °C for 2 hours. Cells were washed with PBS three times with centrifugation at 13000 rpm for 2 minutes to wash off Proteinase K. A fraction of whole cells and the Proteinase K treated cells was lysed with BugBuster (Merck) to investigate intracellular enzymatic activity. All samples were incubated with 10 mg ml⁻¹ substrate or PBS as a negative control, unless stated otherwise, at 37 °C.

Substrate resuspended in PBS but without cells was also included as a control. Aliquots were collected at regular intervals; reactions were stopped by boiling at 100 °C for at least 10 minutes, supernatant was separated by centrifugation at 13000 rpm for 2 minutes and stored at 4 °C prior to analysis. All samples were analysed with TLC (Section 2. 4. 1) and HPAEC-PAD (Section 2. 4. 2), when appropriate, to assess activity of the cells.

2. 5. 4 Multi-species co-culture experiments

Active overnight cultures were inoculated at 5 % v/v into 10 ml of defined medium with 10 mg ml⁻¹ glucose and grown to the mid exponential phase OD₆₀₀ = 0.7 to obtain the same cell density. Cells were collected by centrifugation at 5000 rpm and washed with sterile PBS three times to wash off residual glucose and resuspended in 10 ml of PBS. These were then used to inoculate defined medium with 10 mg ml⁻¹ substrate at 5% v/v ratio and placed in the anaerobic cabinet. OD₆₀₀ was monitored manually using CO 7500 spectrophotometer (Sigma). Each experimental condition was performed in triplicate, monocultures were also included to monitor growth phases.

Co-culture samples were collected from appropriate growth phases. Cells were centrifuged at 13000 rpm for 2 minutes. Cells and supernatant were separated and stored at -20 °C until required. Simultaneously, 100 µl of the culture was reserved and used to perform 10- fold serial dilutions into sterile TYG medium in a sterile 96 well Corning® Costar® culture plate. 10 µl of appropriate six of the 10- fold serial dilutions were spread out on TYG plates without antibiotic and incubated anaerobically at 37 °C for 2 days. Colonies were counted in each dilution to determine CFU ml⁻¹ for each time point and culture. To determine abundance of each *Bacteroides species* in co-cultures, genomic DNA was

extracted from frozen cells with GenElute™ Bacterial Genomic DNA Kit (Sigma Aldrich) and used to differentiate between species with qPCR analysis using species specific genes as genetic markers. Unique, species specific, qPCR primers were designed with ID Primer Quest tool (Section 2. 6), and are listed in Table 2. 14 This was then used to calculate CFU ml⁻¹ of each species in co-culture. Supernatant was analysed with TLC (Section 2. 4. 1).

2. 5. 5 Real-time Quantitative PCR (qPCR)

Genomic DNA harvested in co-culture experiments (Section 2.4.5) were analysed with qPCR to determine abundance of each species using primers specific to genes unique to each species (Table 2. 14). qPCR relies on a dye which binds DNA and releases measurable light during its amplification. In this project SYBR Green I master mix (Roche) or Luna® Universal qPCR Master Mix (New England Biolabs), which also contains SYBR Green to act as an intercalating dye, which absorbs light at 497 nm and emits light at 520 nm when intercalated into double stranded DNA. Light emission at 520 nm is detected during each cycle and a quantification cycle (C_q) is determined when the fluorescence signal from the sample exceeds the background fluorescence. This is then used to determine abundance of DNA in each sample, a low C_q value means that fewer cycles required to detect amplification, whilst a high C_q value shows that more cycles were required.

Species	Gene	Direction	Primer Sequence
<i>B. thetaiotaomicron</i>	<i>Bt3780</i> (GH130)	Forward	TCACCTGTTTCCCATTGACA
		Reverse	AGACCCCGGTATTTTATCCG
<i>B. salyersiae</i>	<i>Bs_04085</i> (GH38)	Forward	TTCTTTGCCGGTGTTTAC
		Reverse	CGTCATCAACCGCCTTATC
<i>B. xylanisolvens</i>	<i>Bxy_2930</i> (GH10)	Forward	GCATGGAACTTGGATGTAG
		Reverse	TTCGGGAGTAAGAGGAATAG

Table 2. 14 qPCR primers designed for species-specific genetic markers.

Prior to analysis concentration of the gDNA extracted from all co-culture samples was measured from 1 µl aliquots with Qubit 4 Fluorometer (ThermoFisher) and 1X dsDNA High Sensitivity Assay Kit (ThermoFisher) as per manufactures instructions, using the standard curve provided in the kit. Concentration of genomic DNA, extracted from appropriate *Bacteroides spp.* grown in monoculture on rich medium, was also quantified the same way and diluted to contain 20, 10, 1, 0.1, 0.01, or 0.001 ng µl⁻¹, generating a standard curve. This was always included in each qPCR run to extrapolate DNA concentrations in the samples. Samples were diluted to contain 10 ng µl⁻¹ of DNA.

A standard qPCR reaction was performed using 5 µl of SYBR Green I Master Mix (Roche) or Luna[®] Universal qPCR Master Mix (NEB), 1 µl of 10 µM primer mix (Forward+Reverse), 3 µl of PCR grade water, and 2 µl gDNA (Sample or Standard curve). qPCR was conducted using a LightCycler[®] 96 (Roche) with a program given in Table 2. 15.

Step	Process	Temperature (°C)	Time (s)
1	Initial Denaturation	95	600
2	Denaturation	95	10
3	Annealing	58	10
4	Elongation	72	10
5	Measurement	72	-

Table 2. 15 qPCR program and parameters used throughout this project. Steps 2-5 were repeated 50 times, the measurement was taken by exciting samples at 497 nm and measuring light emission at 520 nm.

To determine relative gene expression, Bt was grown in 5ml of minimal media with 10 mg ml⁻¹ *S. cerevisiae* mannan or glucose (Section 2. 4. 1). Cells from the mid-exponential phase OD₆₀₀=0.8 were harvested by centrifugation at 5,0000 rpm and resuspended in RNAprotect Bacteria Reagent (QIAGEN) and stored at -20 °C until required. RNA was extracted with RNeasy mini kit (QIAGEN) and was converted into cDNA with Quanti Tec Reverse Transcription kit (QIAGEN) as per manufactures instructions. 5 µl of cDNA was used in 20 µl reactions as described above. qPCR primers specific for each gene of interest were designed in IDT Primer Quest Tool (Section 2. 6) and are listed in Table 2. 16

Gene	Primer direction	Primer Sequence
16 S	Forward	GGTAGTCCACACAGTAAACGATGAA
	Reverse	CCCGTCAATTCCTTTGAGTTTC
bt3521	Forward	ATGTGGTGGACAGTTACA
	Reverse	CTCTGAGCCATACCATACA
bt2949	Forward	GAATGGTCCGGATGCTTTG
	Reverse	CGGCACTCGTAGGTAAA
bt3501	Forward	CAGGGAACATTTGGAGAAG
	Reverse	CTTGTAGCGGCATAGTTG
bt3301	Forward	GCTGCCCTACTCTATCAA
	Reverse	TCTCCTGTGTCAGTTGTAA

Table 2. 16 qPCR primers used to determine gene expression

2. 5. 6 Transmission Electron Microscopy of Outer Membrane Vesicles

2. 5. 6. 1 Purification of Outer Membrane vesicles (OMV)

B. salyersiae was grown in 50 ml of defined medium (Appendix A) containing either 10 mg ml⁻¹ mannan from *S. cerevisiae* or glucose anaerobically at 37 °C for 16 hours (Section 2.4.1). Cultures were centrifuged at 10000 rpm for 20 minutes (Section 2.3.1), supernatant was collected, and filter sterilised with 0.2 µm Millipore membrane (Section 2.2.2). The filtrate was then ultracentrifuged using 26.3 ml polycarbonate tubes Brom Backman Coulter and 70 Ti rotor with Beckman Coulter Optima L-90K ultracentrifuge at 100,000 g for 2 hours. The supernatant was discarded, and the vesicle pellet was resuspended in 100 µl of sterile PBS and stored at 4 °C before analysis.

2. 5. 6. 2 Transmission Electron Microscopy (TEM)

This was performed by Tracey Davey in the EM Research Services unit, Newcastle University.

Briefly, samples were soaked onto carbon-coated copper grids and negatively stained with 2 % aqueous uranyl acetate for 15 mins and analysed with Hitachi HT7800 120 kV Transmission Electron Microscope. Pictures were taken at 100 kV accelerating voltage with 20000 x magnification. The diameters of vesicles were measured using a scale bar provided using Fiji.

2. 6 Bioinformatics tools

Bioinformatics tools used throughout this project are listed in Table 2. 17

Bioinformatic Tool	Server	Description
Primers design & Molecular cloning	IDT PrimeQuest	Primer design for qPCR assays (Owczarzy et al., 2008).
	KEGG	Collection of databases of different biological systems used to search <i>B. thetaiotaomicron</i> DNA and protein sequences (Kanehisa et al., 2002).
	NEBcutter	Analysis of restriction sites in DNA sequences (Vincze et al., 2003).
	Signal P 5.0	Prediction of signal peptides in Gram-negative or Gram-positive bacteria (Almagro Armenteros et al., 2019).
Protein parameters	ProtParam	Calculation of protein parameters based on amino acid sequence: molecular weight, isoelectric point and extinction coefficient (Gasteiger et al., 2005).
Analysis of DNA or Amino Acid sequences	BLAST	The query sequence is compared to a database of non-redundant protein sequences ((Johnson et al., 2008).
	InterPro	Database used to identify organisation of domains in a protein, using its amino acid sequence (Mitchell et al., 2019).

Bioinformatic Tool	Server	Description
	Smart	Also used to predict domain organisation in a protein based on its amino acid sequence (Schultz et al., 2000).
	IMG	Database of microbial genomes, which computes a full list of closest homologues/orthologues (Markowitz et al., 2012).
	CAZy	Collection of all carbohydrate active enzymes found across all domains of life grouped into respective classes and families (Lombard et al., 2014).
	PUL DB	Collection of literature derived PULs across the Bacteroidetes phylum (Terrapon et al., 2018).
Phylogenetic analyses	MUSCLE	Multiple alignment of protein sequences (Edgar, 2004).
	MegaX	Used to construct phylogenetic trees using alignments in MUSCLE (Hall, 2013).
	Clustal Omega	Routinely used to align multiple DNA and Amino Acid sequences (Sievers and Higgins, 2018).
	Phylogeny.fr	Drawing of phylogenetic trees (Dereeper et al., 2008)

Table 2. 17 List of Bioinformatics tools used throughout this study.

Chapter 3: Degradation of mannan from *Candida albicans* by *Bacteroides thetaiotaomicron*

3. 1 Introduction

As previously discussed, *B. thetaiotaomicron* possesses an extensive repertoire of proteins that degrade yeast mannan (Cuskin et al., 2015b). These were grouped into MAN-PUL1, MAN-PUL2, and MAN-PUL3 and are upregulated in Bt in response to mannan from both *S. cerevisiae* and *C. albicans* (Martens et al., 2008, Cuskin et al., 2015b). Bt degrades mannan in a 'selfish' mechanism, where large oligosaccharides are released and transported into the periplasmic space to be further depolymerised (Cuskin et al., 2015b). Genome analysis showed that mannan metabolism was restricted to *Bacteroides* and *Parabacteroides* species, where all Bt strains contained three mannan PULs, displaying robust growth. Elements of MAN-PUL1 and MAN-PUL2 but not MAN-PUL3 were also found in a range of *B. xylanisolvens* (Bx) and *B. ovatus* (Bo) strains. Bx and Bo strains could only utilise mannan variants, which lack extensive decorations of the sidechains, but not mannan from the wild-type yeast. In the inter-species competition assays Bt did not share, positioning itself as a primary mannan user. Unlike mannan from *S. cerevisiae*, the sidechains of mannan from *C. albicans* are capped with repeating β -1,2-mannosyl units, essential for immune recognition of this common human pathogen (Kohatsu et al., 2006). Another study by Cuskin et al. (2015a) revealed that, in addition to α -mannan degrading enzymes, MAN-PUL2 in Bt also contains an enzyme, BT3780, which specifically targets β -1,2-mannosidic linkage found in *C. albicans* mannan. BT3780 belongs to the

glycoside hydrolase 130 (GH130) family comprised of β -mannoside phosphorylases, which use phosphate to cleave β -1,2 or β -1,4-mannosidic bonds. In UhgMP this mechanism was shown to be mediated through three highly conserved residues (Arg150, Arg168, and Asn151), which stabilise phosphate allowing it to act as a nucleophile (Ladevèze et al., 2013). Unlike glycoside phosphorylases, BT3780 and a subset of other proteins in the GH130 family were discovered to lack these phosphate-interacting residues, indicating that these enzymes deploy a different enzymatic mechanism. The crystal structure of BT3780 revealed that the recognition of the sugar at the +1 subsite is mediated by Lys199, Arg89, and Glu141, where Lys199 interacts with O_2 , O_6 and the endocyclic oxygen of Man₂, thus conferring specificity for Man- β 1,2-Man linkages (Figure 3. 1 and Figure 3. 2) (Cuskin et al., 2015a). This lysine residue was conserved in another GH130 from *B. ovatus*, BACOVA_03624, which also utilised water as a nucleophile and displayed β -1,2-mannosidic activity (Cuskin et al., 2015a). Another subset of GH130s from *Thermoanaerobacter sp.*, Teth514_1788 and Teth514_1789, which displayed glycoside phosphorylase activity against β -1,2-oligomannan, also retain this lysine residue at the same position (Figure 3. 1), demonstrating that Lys199 acts as a specificity determinant (Chiku et al., 2014).

BT4094	SPDSTTVFYCPMRQDSVAWESSDTFNPAATIYD--GKVVVLYRAEDNSA-----	95
Dfer_3176	SPDSTTRFFCPMNKREVWESNDTFNPAATMKN--GKIVVLYRAEDKAG-----	92
BT3780	SPIENTKFYCPMTQDYVAVESNDTFNPAATLHD--GKIVVLYRAEDKSG-----	95
BACOVA_03907	SPIENTKFYCPMTKDISIAWESNDTFNPAATLYN--GEIVVLYRAEDKSG-----	98
C.auris_QEO19388.1	EPN-----PDNEWEEAYVYNASAIVID--DRVYLLYRAQDEN-----	74
C.albicans_CR05750WA	KPD-----PNVEWESSYLYNATAIVID--DKVFMLYRAQNKD-----	72
C.dublinsiensis_CAX40110.1	KPD-----PNVEWESGYLYNATAIVVD--DKVFMLYRAQNKD-----	72
RIL182_01099	NPYF-----M---ERLGINAVMNSGAIELN--GKYLVARLEGNDR-----	92
RaMP1	NPFY-----Q---ERLGINAVFNAGAIKLN--DRYCLVARVEGNDR-----	92
UNK1	NPHL-----M---ERQGINAAFNNSGAMYWN--GKYLLAVRVEGVDR-----	94
BT3028	NPYL-----M---ERFGINAVFNAGAIKFN--GKYLVMARVEGHDR-----	94
BS_03992	NPFL-----M---ERFGINGTFNAGAIKWD--GKYIMVVRVEGNDR-----	95
BF9343_0737	NPFL-----M---ERIGMNATLNAGAIKWD--GKYLMLVRVEGADR-----	94
RIL182_01100	GRNP-----VKG----VARIFNSAVMPYE--DGFIVGVRGEQTNG-----	71
BT1033	GRYH-----IPS----SNSIFNSAVVPPK--DGFAGVFRCDNKAV-----	62
BS_00404	GRYH-----IPS----SNSIFNSAVVPPG--DGFAGVFRCDNKAV-----	63
UhgbMP	PRDL-----LPT----SNSIFNSAVVPPG--DGFAGVFRCDTTSR-----	65
Rumal_0099	PRDQ-----LPT----SNSIFNSAVVPESEKGFAGVFRVDDKCR-----	73
Teth514_1789	SPIK-----E---HEWEKEAVFNAAVIYEG--NKFHLFYRASNKF-----	49
Teth514_1788	MPKA-----E---NEWERAAVFNATAIYDN--GLFHLYRATDIGP-----	49
BS_01732	TPRD-----IQPSMEGLVIECLLNPGVFYFR--NKIGLLLVAERPLQKENFISFPI	67
	* * *	
BT4094	-MTVPVFYPADDNQKELEWPGGCEDP RVAVT-EDGLYVMLYTQWNR-----	162
Dfer_3176	-RKEPVLFP AEDSQKAN EWPGGCEDP RVAVT-EDGLYVV IYTQWNK-----	159
BT3780	-EKTVPVFPDNDTQKLEWPGGCEDP RIAVT-AEGLYVMYTQWNR-----	162
BACOVA_03907	-EKTVPVFPDNDSDQKELEWPGGCEDP RIAVT-DDGLYVMYTQWNR-----	165
C.auris_QEO19388.1	-YHKPIIYPTD---SYEFPGGCEDP RIVRDPISKRFIVTYTAYDG-----	133
C.albicans_CR05750WA	-HKKPVITATE---SYEQGGGCEDP RIVRDPVSKLFFVVTYSYDR-----	131
C.dublinsiensis_CAX40110.1	-HKKPVITATE---SYEQGGGCEDP RIVRDPVSKLFFVVTYSYDR-----	131
RIL182_01099	FWDYPIILLPD---TC-PEETNVYDMRLTKH-EDGYIYGVCSESDDTT-----	152
RaMP1	FRQYPVCLPA---LT-DDEITNVYDMRLTQH-EDGWYIGVFCVEKSA-G-----	151
UNK1	FWDYPIITMPE---TD-RPDTNVYDMRLTNH-EDGYIYGLFCTERKDLNH-----	155
BT3028	FWEYVQLPD---LY-PEETNVYDMRLTKH-EDGWYIGIFCSESDDPA-----	155
BS_03992	FIDYVVAIPE---TE-NPDINIYDMRLTAH-EDGWYIGIFCSEKDPDA-----	156
BF9343_0737	FWEYVTLPE---DV-VPATNVYDMRLTAH-EDGWYIGIFCAERHDDNA-----	155
RIL182_01100	DENKINFVDE---EGKPFMPRYAYDP RLKVKV-EDTY-YIWCQDFY-----	129
BT1033	SHEPIQFKAG---NTEMIESEYKYDPRVTWI-EDRY-WVTWCNGYH-----	120
BS_00404	NHEPIRFKAG---NTEMIESEYKYDPRVTWI-EDRY-WITWCNGYH-----	121
UhgbMP	KEEPLKFQCD---DEEIGTWVYGYDPRVCFI-EDRY-YVTWCNGYH-----	123
Rumal_0099	NPDRIVFEQAEKSTEEVNWQWGYDPRVCFI-EDRF-WVTWCNAYG-----	134
Teth514_1789	F-DKPVLVGE---IP-QEAWGVEDPRITKI-DNKY-YMLYTGFGG---RDW-----	120
Teth514_1788	L-DKPVMSNE---TE-QELRGL EDP RIVKI-DGIY-YMMYTGFGD---RFQ-----	114
BS_01732	LEGTNRLFGN---NE-YSSFGIEDCRVVTQI-GDEY-YLTYTSVSS---K-----	161
	* * :	
BT4094	-----KQARLAVATSRDLQIWEKYGPAFAKAYG-----G--RFFDEFS	198
Dfer_3176	-----DKARLGVATSRDLLKWKQGPFAKAYG-----G--KFNNIWT	195
BT3780	-----HIPRLAIATSRNLKDWTKHGPAFAKAYD-----G--KFFNLGC	198
BACOVA_03907	-----HVPRLAVATSRNLKDWTKHGPAFAKAFD-----G--KFFNLGC	201
C.auris_QEO19388.1	-----YLARLCAVESMDLFTWRKYPPIIKDDNFNEIANGLDGNQFIRHAW	179
C.albicans_CR05750WA	-----ITARLCVATSEDLFHWTKHGPIVP-PYWQDIAVASNGTNMIRNNWS	176
C.dublinsiensis_CAX40110.1	-----ITARLCVATSEDLFHWTKHGPIVP-PYWQDIAVESNGKNLIRNNWS	176
RIL182_01099	-----VNDLSAAVAAGIVRTKDLKNWERLPNLVTLNSP-----QQ	188
RaMP1	-----TADLSEAVASAGIARTKDLTNWERLPDLVTLRSP-----QQ	187
UNK1	-----PN-DTSAAEQCIARTKDLITWERLPDLVITY-SG-----QQ	190
BT3028	-----PAGDLTSAIAAAGIIRSRDLKNWERLPNLVSQ---S-----QQ	190
BS_03992	-----PEGDLSAAIATAGIVRTKDLKNWERLPDLKSK---S-----QQ	191
BF9343_0737	-----PIGDLSSATATAGIARTKDLKNWERLPDLKTK---S-----QQ	190
RIL182_01100	-----G-AAIGMAKTDFKTFTRIENPFLP-----FN	155
BT1033	-----G-PTIGIAYTFDFVDFQCENAFLP-----FN	146
BS_00404	-----G-PTIGIAYTFDFKFFQCENAFLP-----FN	147
UhgbMP	-----G-PTIGVAYTFDFETFHQLENAFIP-----FN	149
Rumal_0099	-----WKPTIGVAYTFDFKTFYQCENAFLP-----FN	161
Teth514_1789	-----LDFRICMWSDDLKNWKGHRIVLDE-----PN	147
Teth514_1788	-----DDYRICLATSKNLDWERKGVVLDE-----PN	141
BS_01732	-----GVGVLKKTGDWNGNYTELGLIFPP-----HN	187
	: : :	

BT4094 X SASIVTKLVGDKQVI AKIDGKYWMY WGE -----K FVNVA TSTDLINWEPMLD 246
Dfer_3176 X S G S I L T K L V G D R Q V I A K V N G K Y W L Y F G E -----A N V N I A T S T D L L N W E P V V D 243
BT3780 X S G S I L T E V V N G K Q V I K K I D G K Y F M Y W G E -----E H V F A A T S E D L V N W T P Y V N 246
BACOVA_03907 X S G S I L T E V V N G K Q V I K K V N G K Y F M Y W G E -----E H V F A A T S D D L I H W T P I V N 249
C.auris_QEO19388.1 X S G A I F V E R -----H K D G H Y M I W G E -----S G F Y L A K S K L V H W T I A D N 219
C.albicans_CR05750WA X S G S I F T E K -----A P D G K Y Y M I W G D -----S E L H L A E S V D L V N W N L T N N 216
C.dublinsiensis_CAX40110.1 X S G A I F T E R -----A P D G K Y Y M I W G D -----S E L H L A E S M D L V N W K L T N N 216
RIL182_01099 R N V V L H P E -----F V D G K Y A F Y T R P M D D F I E T -G S G -G G I G F L C D D I T H A V I D E E 237
RaMP1 R N V T L L P E -----F V D G K Y A F Y T R P M D G F I E T -G S G -G G I G F L A D D I T H A V I D E E 236
UNK1 R N V V L H P E -----F I D G K Y G L F T R P Q D G F I S V -G A G -G G I G W G L V D M T R A E V K S E 239
BT3028 R N V V L H P E -----F V D G K Y A L Y T R P Q D G F I D A -G S G -G G I S W A L I D D I T H A V I K K E 239
BS_03992 R N V V L H P E -----F V N G K Y A L Y T R P Q D G F I D A -G S G -G G I G W A L I D D I E H A E I K E E 240
BF9343_0737 R N V V L H P E -----F V D G K Y A L Y T R P Q D G F I D T -G S G -G G I G W A L I D D I T H A E V G E E 239
RIL182_01100 R N A V L F P R -----K I N G N F M L L S R P S D S G H T P F ---G D I F V S E S P D L T Y W G K H R H 202
BT1033 R N G V L F P Q -----K I D G K Y A M L S R P S D N G H T P F ---G D I Y I S Y S P M K M Y W G E H R C 193
BS_00404 R N G V L F P Q -----K I N G K Y A M L S R P S D N G H T P F ---G D I Y I S Y S P M K M Y W G E H R S 194
UhgbMP R N G V L F P R -----K I N G R F A M L S R P S D N G H T P F ---G D I F Y S E S P M E F W G R H R H 196
Rumal_0099 R N G V L F P R -----K I N G K Y V M F S R P S D S G H T P F ---G D M F I S Q S P M K M Y W G E H R H 208
Teth514_1789 X D A A L L S E -----K I N G K Y V L F H R R M -----P D I W I A Y S D D L V N W Y N H K I 187
Teth514_1788 X D A S L F P E -----K I N G K Y V M L H R R Y -----P D I W I A F S D D L K N W Y D H K P 181
BS_01732 X D C A I F E E -----K I N G L Y Y A L H R P S S P -----E I G N Y M W I A E S P D L V H W G N H K C 233
.: . . . * :

BT4094 E K G D F L K V I T P R ---E G K F D S D L T E C G P P A I M T D K G -----I L L L Y N G K N K S G A E G D T L 297
Dfer_3176 S K G D L I N L I S P R ---K G Y F D S N L T E C G P P A I L T D K G -----I V L L Y N G K N D K G E D G D K R 294
BT3780 T D G S L R K L F S P R ---D G H F D S Q L T E C G P P A I Y T P K G -----I V L L Y N G K N S A -R G D K R 296
BACOVA_03907 I D G S L K K L F S P R ---D G Y F D S H L T E C G P P A I Y T P K G -----I V L L Y N G K N H S G -R G D K R 299
C.auris_QEO19388.1 Y -----T I G ---K F N W Q D R L I E P G P A I K M D T G N R H Q N Y I I L F Y N S S T ---I G G G P 264
C.albicans_CR05750WA S A N W ---N T W A K A ---I F T R E N K L L E S G P A P V K M A G N ---A N Q W I F V Y N A A T ---T G G G D 264
C.dublinsiensis_CAX40110.1 S V N W ---N T W A K A ---I F I R E N K L L E S G P A P V K M A G K ---S N Q W I F V Y N A A T ---T G G G D 264
RIL182_01099 K -----M T S L R K ---Y H T T E A K N G A G A T P I K T D K G -----W I H I A H G V R N T A ----- 277
RaMP1 R -----M T S I R R ---Y H T I T E S K N G A G A T P I K T E R G -----W L N I A H G V R N T A ----- 276
UNK1 V -----I V D G K V ---Y H T I K E V K N G Q G P A I K T A E G -----W L N L A H G V R N T A ----- 279
BT3028 I -----V I E Q R H ---Y H T I K E V K N G E G P H P I K T P Q G -----W L H L A H G V R N C A ----- 279
BS_03992 T -----I N F R Y ---Y H T I K E L K N G E G P H P I K T S K G -----W L H L A H G V R G C A ----- 280
BF9343_0737 K -----I I D K R Y ---Y H T I K E V K N G E G P H P I K T P Q G -----W L H L A H G V R N C A ----- 279
RIL182_01100 V -----M -G K G ---S E W W E S L K I G G G A A P I E T S E G -----W L L F Y H G V S G T C ----- 240
BT1033 V -----M -K V T P P F E S A W Q C T K I G A G S V P F L T D E G -----W L L F Y H G V I T T C ----- 234
BS_00404 V -----M -K V T P P F E S A W Q C T K I G A G S V P F L T E E G -----W L M F Y H G V I T T C ----- 235
UhgbMP V -----M -S P A A F E V S A W Q C T K I G A G P I P V E T P E G -----W L L I Y H G V L H S C ----- 237
Rumal_0099 V -----M -G P L ---R A W E S K I G A G P I P I E T S E G -----W L C F Y H G V L E S C ----- 245
Teth514_1789 I -----M -S P K ---S H T W E S K K I G I A G P P I K R E D G -----W L L I Y H G V D N N ----- 224
Teth514_1788 I -----L -K P I ---P N T W E S A R V G I G G P P I K T K D G -----W F L I Y H A A D N ----- 218
BS_01732 I -----A -C T R ---A G K F D S A R L G A G A P V K T E K G -----W L V I Y H G A T I E ----- 270
.

BT4094 Y T A N S Y C A G Q A L F D A K D P T -K L I D R L D K P F Y I P E S D F E K S G Q Y P A G T V F I E G L V F H N --Q 354
Dfer_3176 F T P N S Y C A G Q V L F D K N D P T -K V L A R L D T P F F R P M E P F E K S G Q Y V A G T V F I E G M V Y H K --K 351
BT3780 Y T A N V Y A A G Q A L F D A N D P T -R F I T R L D E P F F R P M D S F E K S G Q Y V D G T V F I E G M V Y Y K --D 353
BACOVA_03907 Y T A N V Y A A G Q A L F D A N D P T -R F I T R L D E P F F R P M D S F E K S G Q Y V D G T V F I E G M V Y F K --N 356
C.auris_QEO19388.1 Y P K G T Y T I S Q M L V D Y N I K D G P V A R L E K P I L V P E D A N E V N G Q -V D K V V F T E G V V Q F K --G 321
C.albicans_CR05750WA L P K N A Y T V N Q M L I D Y N D I R K G P V A R L E Q P V L K P E S A N E R E G Q -V N Q V V F C E G L V Q F K --G 321
C.dublinsiensis_CAX40110.1 L P K N A Y T V N Q M L V D Y N D I H K G P V A R L E Q P V L K P E S A N E K E G Q -V N Q V V F C E G L V Q F K --G 321
RIL182_01099 -A G L R Y V I Y A F A T D L N D P S -K V I A E P S G L L I G P R G -E E R V G D -V S N V V F T N G A I V D N -N N 332
RaMP1 -A G L R Y V I Y C F V T D L S E P W -K V I A E P G G Y L I A P F K -D E R V G D -V S N V V F T N G A I V D D -N G 331
UNK1 -A G L R Y V L Y M F M T E L E R P W -V V T H R P A G H F I A P H G -A E R V G D -V S N V A F S N G W I A N E -K N 334
BT3028 -A G L R Y V L Y L Y M T S L D D P R -K V I A Q P G G Y F M A P V G -E E R T G D -V S N V L F S N G W I A D E -D G 334
BS_03992 -A G L R Y V L Y L Y L T D L K H P E -K I I A E P A G Y F M A P I G -M E R I G D -V S N V L F C N G W I P D E -D G 335
BF9343_0737 -A G L R Y V L Y M Y M T S L D D P T -R L I A S P A G Y F M A P V G -E E R I G D -V S N V L F S N G W I A D D -D G 334
RIL182_01100 -N G Y V Y S I G G A I L D I D N P S -I V K Y R C E T F L L T P E E W Y E E R G F -V P N V C F P C A T I H D S E S G 297
BT1033 -N G F R Y S M G A A I L D R D N P D -K V L Y R T R E Y L L A P A A P Y E L Q G D -V P N V V F P C A A L Q D G --E 289
BS_00404 -N G Y V Y S F G S A L L D L D P E W -K V K F R S G P Y L L A P R E P Y E C M G D -V P N V C F P C A A L H D N E T G 294
UhgbMP -N G F V Y S F S A C I L D K D E P W -K V K Y R C A E Y L L S P Q K I Y E C V G D -V Q N V T F P C A T I V D A D T G 302
Rumal_0099 ---N V Y R L G A V L L D L K D P S -K V I A R Q K E P I L E P E L D W E I N G L -V P N V V F S C G A V E V N --D 277
Teth514_1789 ---N V Y R L G A V L L D L E D P S -K V I A R Q K E P I L E P E L G W E K E G Y -I P N V V F S C G N A V K D --D 271
Teth514_1788 ---N R Y C L G A L L L D I N D P S -V V I A R S E S P I M E P E T S Y E K M G F -F G D V I F T N G Q L V N G --D 323
BS_01732 * . . . * * * * *

BT4094	KWYLYYGCA	D	SRVAVAVYDPFKK	-----	377
Dfer_3176	KWLLYYGCA	D	SRVGVAEFDPSRKA	-----PGDPIP	382
BT3780	KWYLYYGCA	D	SKVGMAIYNPKKPA	-----AADPLP	383
BACOVA_03907	KWYLYYGCA	D	SKVGVAVYDPKRP	-----KADPLP	386
C.auris_QE019388.1	KWFLYYGQ	G	SKLAVATCPAN	-----	342
C.albicans_CR05750WA	QWFLYFGQ	G	SELGVAIAPVN	-----	342
C.dublinsiensis_CAX40110.1	QWFMFYFGQ	G	SELGVAIAPVN	-----	342
RIL182_01099	EVFIYYASS	D	TRMHVATTTVDKLV	DYVFNT	392
RaMP1	DVYIYYASS	D	TRLHVAVSSIDKLL	DYAFNTPADAL	386
UNK1	EVFIYYASS	D	TRMHVATSTVEKLI	DYCKNTPEDGL	393
BT3028	TVYIYYASS	D	TRMHVATSTIERLI	DYCRHTPEDRL	394
BS_03992	TVFIYYASS	D	TRMHVAVSTIDQL	LDYCLNTPDGL	395
BF9343_0737	KVFIYYASS	D	TRMHVATSTIERLV	DYCLHTPQDGF	390
RIL182_01100	KIAIYYGAA	D	SYVGLAFTELDDI	DIYIKENSVVTP	340
BT1033	RVAVYYGAA	D	TVVGMAFGYIQEI	IDFTKRTSII	322
BS_00404	RVAVYYGAA	D	TVVGMAFGYIADI	IEFIKKTNIV	323
UhgbMP	RIAIYYGCA	D	TVTGLAFGYIPEI	IEFTKRTSII	327
Rumal_0099	RIAIYYGCA	D	TCVSMAFTTVDV	DVVDYVVKSH	335
Teth514_1789	MYVYYGAA	D	THIGVAVIEKEK	VKVF	302
Teth514_1788	TIYVYYGAA	D	TVIGVAILEMKD	IKF	296
BS_01732	ELIYYGAA	D	EVICGAKASIT	SILRSLGF	352

Figure 3. 1 Alignment of GH130s. Amino Acid sequences were retrieved from IMG and aligned in Clustal Omega (<https://www.ebi.ac.uk/Tools/msa/clustalo/>). Red and Black indicate glycoside hydrolases and Glycoside Phosphorylases, respectively. Residues highlighted in yellow mediate substrate binding, catalytic residues of glycoside hydrolases are shown in magenta, residues specific for glycoside phosphorylases are shown in cyan, critical lysine residue, determining β -1,2 specificity is shown in green.

Unpublished data from Dr. Fiona Cuskin and Dr Elisabeth Lowe showed that *Δbt3780* strain was still able to grow in *C. albicans* mannan, though to a lower OD₆₀₀ (data not shown). This suggested that there are other enzymes which can hydrolyse β -1,2 mannan. Bioinformatics analysis of the Bt genome revealed three additional GH130 enzymes: BT1033, BT3028, and BT4094. BT1033 has been characterised as a Man- β -1,4-GlcNAc phosphorylase (Nihira et al., 2013). Alignment of BT3028 and BT4094 indicates that BT3028 is likely to be a Man- β -1,4-Glc phosphorylase, whereas BT4094, which shares 64% identity to BT3780, retains the critical lysine residue, suggesting that it is likely to be a β -1,2-mannosidase (Figure 3. 1). Using PULDB (Terrapon et al., 2018), it was established that BT4094 is encoded in an uncharacterised PUL 74, enclosing genes bt4069-bt4096, which also could contribute to the degradation of C.

albicans mannan in Bt. Moreover, during the bioinformatics analyses, we identified homologues GH130s in some fungi, including *C. albicans*, *C. auris*, and *C. dubliniensis* (Figure 3. 1). Aligning these sequences also showed conservation of Lys199 and other active site residues, suggesting that some *Candida species* are able to hydrolyse their own cell wall.

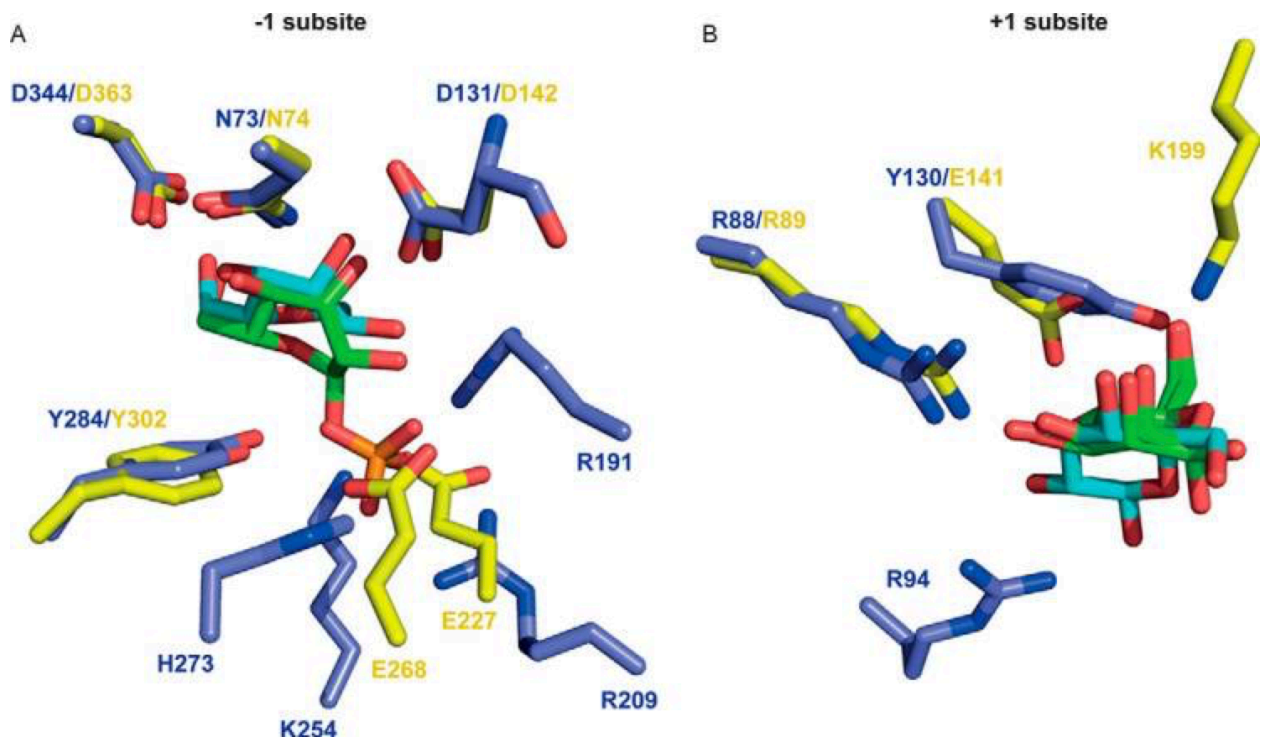


Figure 3. 2 Overlay of the active site of β -mannosidase BT3780 and β -mannoside phosphorylase BF0772. Residues shown in yellow belong to BT3780, residues in blue – BF0772. Mannobiose is shown in green, Man-Glc – cyan, phosphate shown in orange. Figure adapted from Cuskin et al. (2015a)

Znaidi et al. (2018) showed that adaptation of *C. albicans* to the mammalian gut is reliant on the activation of Crz2 transcription factor. This transcription factor was shown to induce differential expression of an array of cell surface and cell-wall

remodelling genes (Znaidi et al 2018). One of the downregulated genes identified was orf19.6637 (CR05750WA), which encodes for the GH130 enzyme identified above (Figure 3. 1), suggesting that the alterations in the cell wall structure maybe linked to colonisation of the gut. The aims of this work were: 1) to investigate whether the conserved lysine residue confers the specificity for β -1,2-mannosides in the fungal homologues of BT3780; 2) establish if BT4094 is responsible for the ability of Bt to utilise *C. albicans* mannan; 3) investigate whether the genetic locus bt4069-bt4096 contributes to the degradation of *C. albicans* mannan in Bt.

3. 2 Objectives

1. Perform biochemical characterisation of BT4094 and orf19.6637 (named hereafter CaGH130)
2. Investigate the biological role of BT4094 and its PUL (BT4072-BT4096)
3. Characterise mechanism of *C. albicans* mannan breakdown by *B. thetaiotaomicron*

3. 3 Results

3. 3. 1 Characterisation of β -1,2 mannosidases from the Glycoside Hydrolase 130 family, BT4094 and orf19.6637(CaGH130).

As discussed above, the specificity for β -1,2-mannosidic linkage is dictated by Lys199 in the active site of BT3780 (Figure 3. 2). To investigate if Lys199 acts as a determinant of β -1,2-mannosidic activity in other uncharacterised enzymes in this family, genes for BT4094 and CaGH130 from *B. thetaiotaomicron* and *C. albicans*, respectively, were cloned into pET-28a vector. Recombinant proteins were

expressed in TUNER cells and purified with Immobilised Metal Affinity Chromatography (IMAC). Fractions were analysed with SDS-PAGE, soluble BT4094, CaGH130, and BT3780 proteins of correct molecular weight were obtained (Figure 3. 3).

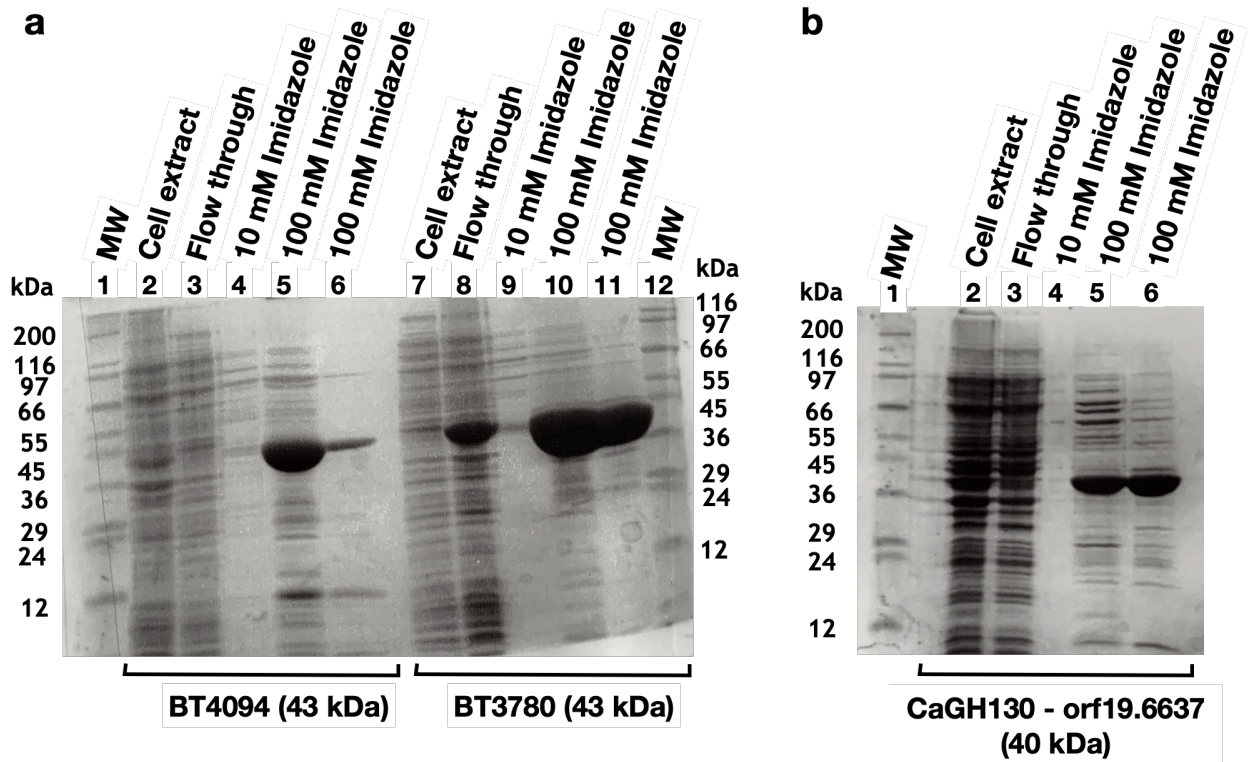


Figure 3. 3 SDS-PAGE analysis of recombinant GH130s. Indicated fraction were collected and resolved on 12.5% SDS-PAGE gels. Wide molecular weight ladder (Sigma, UK) was used to identify sizes. Soluble proteins were eluted with 100 mM imidazole in TALON buffer (20 mM Tris-HCl 300 mM NaCl). Panel a: purification of recombinant BT4094 (lanes 2-6) and BT3780 (lanes 7-11), soluble proteins were obtained, Panel b: purification of recombinant CaGH130, soluble protein lanes 5-6

Cuskin et al. (2015a) showed that BT3780 displays activity against mannan from *C. albicans*, to confirm the hydrolase activities of BT4094 and CaGH130, they were assayed against mannan from *C. albicans*. Both, BT4094 and CaGH130 at 1 μ M were incubated with 1 mg ml⁻¹ mannan purified from *C. albicans* strain SC5314, as described in Methods, at 37°C in 50 mM MOPS 2 mM CaCl₂. BT3780

was assayed alongside for comparison. Aliquots were collected at regular intervals; reactions were stopped by boiling and analysed with Thin Layer Chromatography (TLC). Both BT4094 and CaGH130 released mannose from *C. albicans* mannan (Figure 3. 4 c-f), but at a slower rate compared to BT3780 (Figure 3. 4 a). Reactions were then further analysed with HPAEC-PAD. Retention time of the peak produced by BT4094, CaGH130, BT3780 on CarboPac PA20 (ThermoFisher, UK) column corresponded to the one seen in the mannose standard (Figure 3. 4 b, d, f). These analyses confirmed that BT4094 and CaGH130 display glycosyl hydrolase activity against mannan from *C. albicans*, consistent with what was shown for BT3780 by Cuskin et al. (2015a). Neither BT4094 nor CaGH130 displayed activity on 4-Nitrophenyl β D-mannose (PNP- β -mannose) (data not shown)

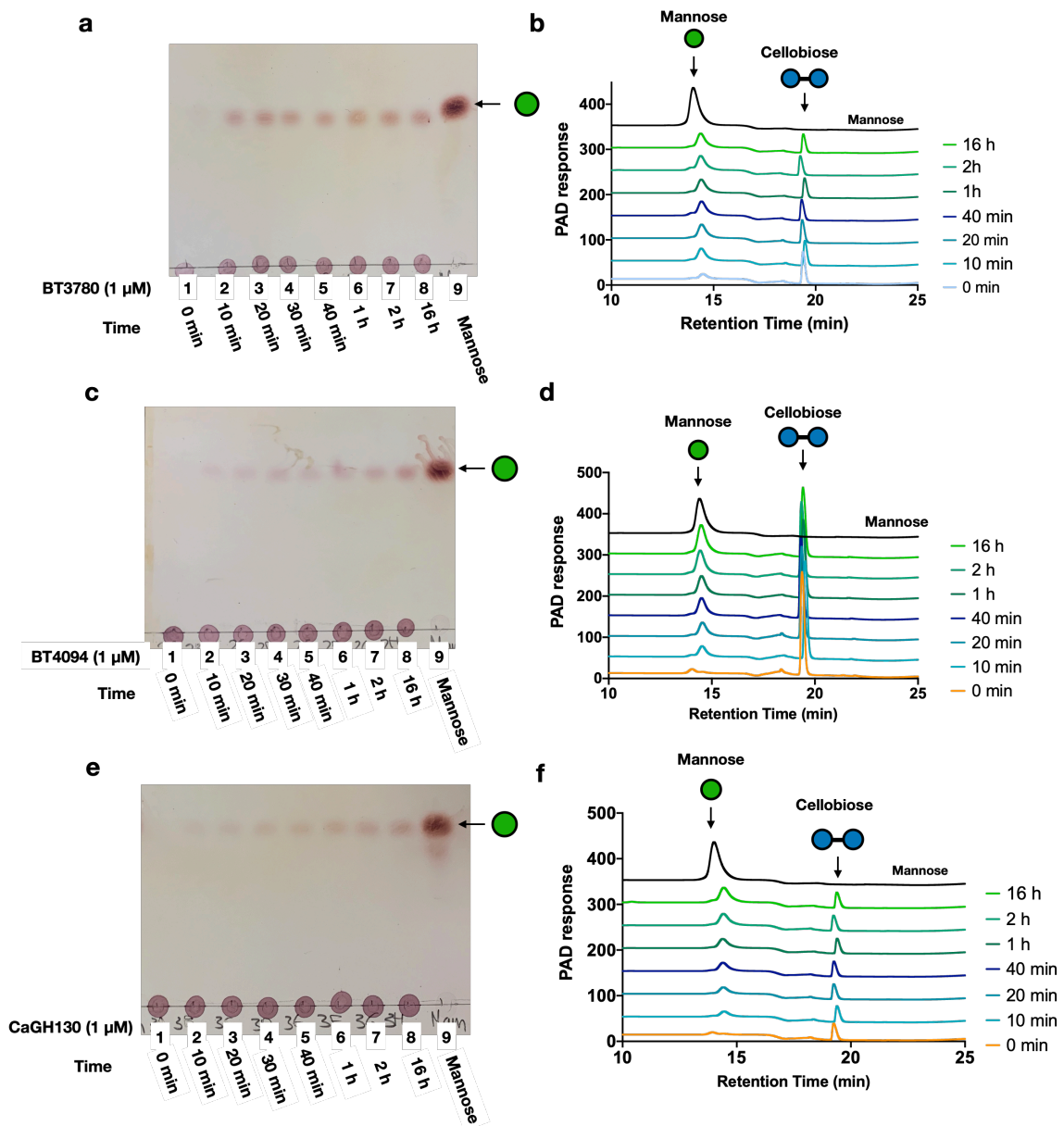


Figure 3. 4 Activity of BT3780 (a-b), BT4094 (c-d), CaGH130 (e-f) on mannan from *C. albicans*. Enzymes at 1 μM were assayed against 1 mg ml^{-1} mannan from *C. albicans*. Aliquots at specified time points were collected and stopped by boiling. Reactions were diluted 1:10 in distilled water prior to HPAEC-PAD analysis on CarboPac PA20 column, with 0-25 mM NaAc gradient, cellobiose was included as an internal standard. Panel a, c, e: TLC of BT3780, BT4094, CaGH130 against *C. albicans* mannan, respectively; Panel b, d, f: HPAEC-PAD of BT3780, BT4094, CaGH130 against *C. albicans* mannan, respectively.

Enzymatic activity of BT3780, BT4094, and CaGH130 against *C. albicans* mannan was further assessed. It was previously shown that BT3780 displays activity against β -1,2 mannoooligosaccharides, that uniquely cap the sidechains of *C. albicans* mannan. These are not commercially available but can be released from phosphomannan upon mild acid hydrolysis (Figure 3. 5). *C. albicans* mannan was treated with 10 mM HCl at 95 °C for 1 hour, reaction was then neutralised with NaOH. Acid hydrolysed mannan was then incubated with 1 μ M BT3780, BT4094, or CaGH130 overnight, reactions were analysed with TLC. Mild acid hydrolysis released a pool of β -oligosaccharides from *C. albicans* mannan (Figure 3. 5 b lane 1). All three enzymes degraded β -oligosaccharides into mannose (Figure 3. 5 b lane 2-4). HPAEC-PAD analysis showed that addition of enzymes resolved β -oligosaccharides, producing a single peak corresponding to mannose standard (Figure 3. 5 c). This demonstrates that BT3780, BT4094, and CaGH130 display activity against β -1,2-mannosides in mannan from *C. albicans*, confirming β -mannosidic activity of BT4094 and CaGH130.

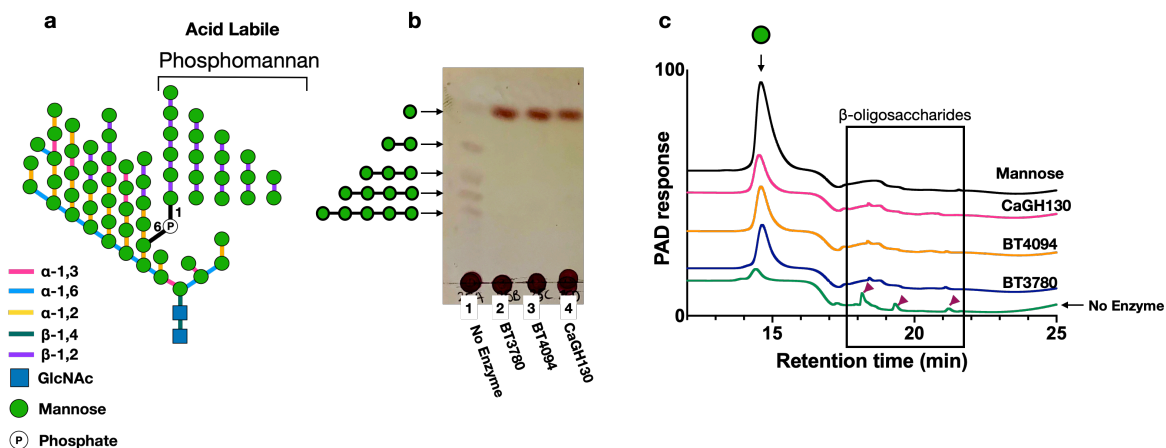


Figure 3. 5 Activity of BT3780, BT4094, and CaGH130 against β -1,2-mannosides from *C. albicans* mannan. β -oligosaccharides were released from *C. albicans* mannan mild acid hydrolysis.

Enzymes at 1 μ M were incubated with hydrolysed mannan overnight. Panel a: Diagram of *C.*

albicans mannan: α -1,6-linked backbone is decorated with α -1,2 and α -1,3 linked sidechains

capped with β -1,2-mannosides, β -1,2-oligosaccharides are released from mannan with mild acid

hydrolysis; Panel b: TLC analysis: lane 1 oligosaccharides released from *C. albicans* mannan, lane

2, 3, 4 activity of BT3780, BT4094, and CaGH130, respectively, degrade oligosaccharides into

mannose. Panel c: HPAEC-PAD analysis on CarboPAC PA20 column using 0-50 mM NaAc

gradient, reactions were diluted 1:20 prior to analysis, 30 μ M mannose was run as standard.

To investigate the specificity of BT4094 and CaGH130, β -1,2-oligosaccharides

were purified with P2 Bio-gel size exclusion columns (Bio-Rad, USA). Individual

fractions were analysed with TLC and freeze-dried. As a result, β -1,2-linked

mannobiose, mannotriose, and mannotetraose were purified, mannosidic linkage

was confirmed with recombinant BT3780 and the concentration of each substrate

was determined in a continuous assay using the Mannose Detection Kit

(Megazyme, Portugal).

BT4094 and CaGH130 were tested against β -1,2-mannosides or β -1,4-

mannosides (Magazyme, Portugal) overnight. Reactions were analysed with TLC.

BT4094 and CaGH130 did not display activity against β -1,4-linked substrates but

were able to degrade β -1,2-linked oligosaccharides into mannose and not mannophosphate (Figure 3. 6). This confirmed that both BT4094 and CaGH130 act as β -1,2 mannosidases, exhibiting glycoside hydrolase and not glycoside phosphorylase activities.

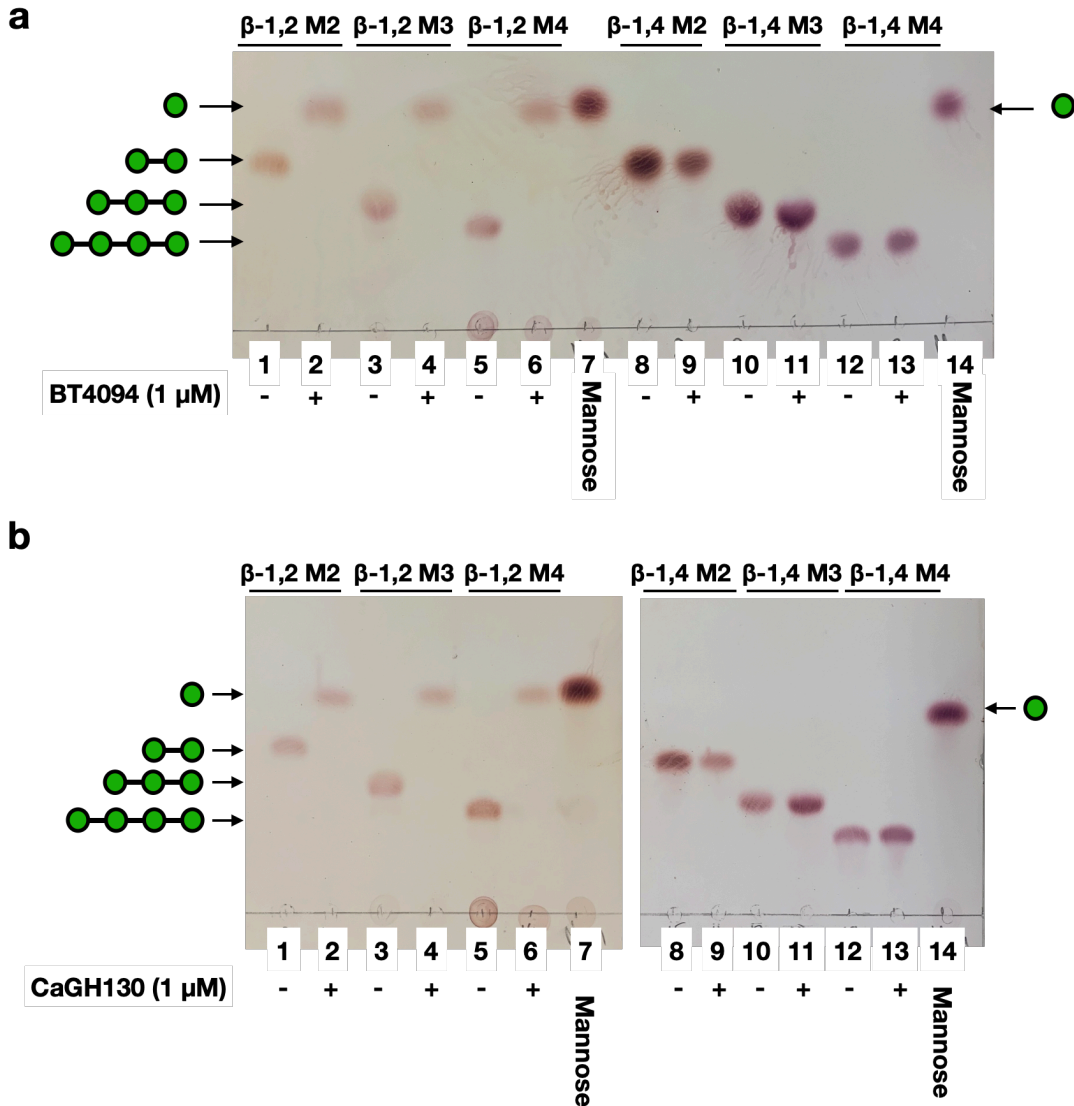


Figure 3. 6 Activity of BT4094 and CaGH130 against β -1,2 and β -1,4 linked manno-oligosaccharides. Enzymes were incubated with 1 mM of β -1,2 or β -1,4 linked manno-oligosaccharides in 50 mM Phosphate buffer at 37 °C overnight. Panel a: BT4094 against manno-oligosaccharides; Panel b: CaGH130 against manno-oligosaccharides. In each lane ‘+’ and ‘-’ indicate with and without enzyme, respectively. Mannose is shown as a green circle.

The amount of mannose released by each GH130 from *C. albicans* mannan was then assessed. This was performed using a continuous spectrophotometric linked assay system, mannose detection kit, where production of free mannose is directly proportional to the amount of reduced NADPH, whose formation is measured at 340 nm. To assess available substrate, excess enzyme concentration is used with a limited amount of substrate to ensure the reaction runs to completion. BT3780, BT4094, CaGH130 were assayed at 10 μ M against 10 μ g *C. albicans* mannan in a continuous assay, reactions were run to completion. This showed that BT3780 released 30 μ M of mannose, while BT4094 and CaGH130 could only release half of this amount, 17 and 12 μ M, respectively (Figure 3. 7 a). To investigate this further, enzymes were assayed in two sequential reactions, where BT3780 was followed by either BT4094 or CaGH130 and vice versa. In a set of reactions where BT3780 was applied first, approximately 30 μ M of mannose was consistently released from 10 μ g of *C. albicans* mannan (Figure 3. 7 b and c). Neither BT4094 nor CaGH130 displayed activity on *C. albicans* mannan after BT3780 had completed its reaction (Figure 3. 7 b and c). The enzyme order was then swapped. CaGH130 released 10 μ M of mannose and, when BT3780 was added, additional 17 μ M of mannose was formed (Figure 3. 7 b). The same trend was observed when BT4094 was used first, releasing 17 μ M of mannose from *C. albicans* mannan, and after completion of this reaction additional 12 μ M was produced by BT3780 (Figure 3. 7 c). These assays indicate that BT3780 removes a greater amount of β -mannan from *C. albicans* mannan than BT4094 or CaGH130. It is possible that BT3780 is capable of cleaving β -mannoses linked to the underlining α -mannan, while BT4094 and CaGH130 are

not. However, it is also possible that despite displaying activity on *C. albicans* β -mannan, it might not be a preferred substrate for BT4094.

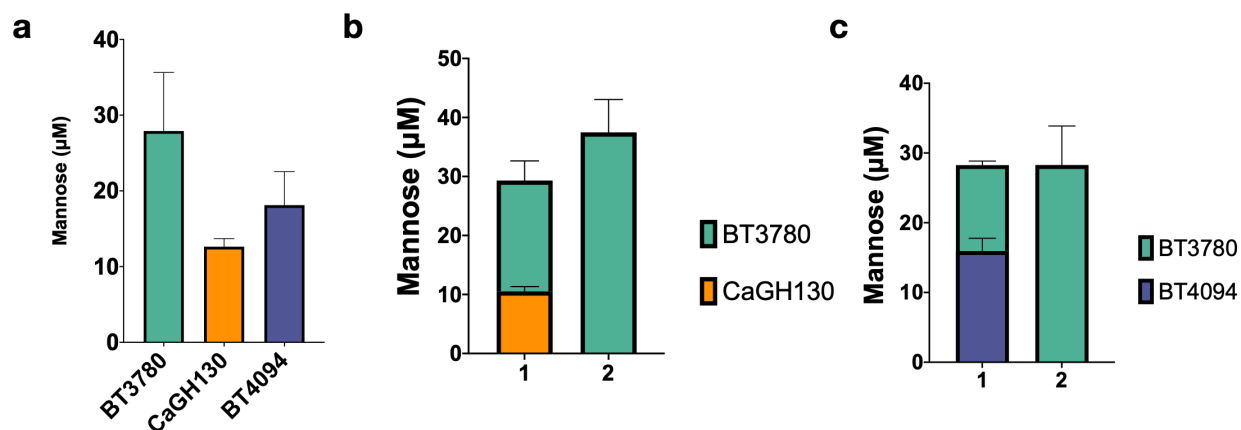
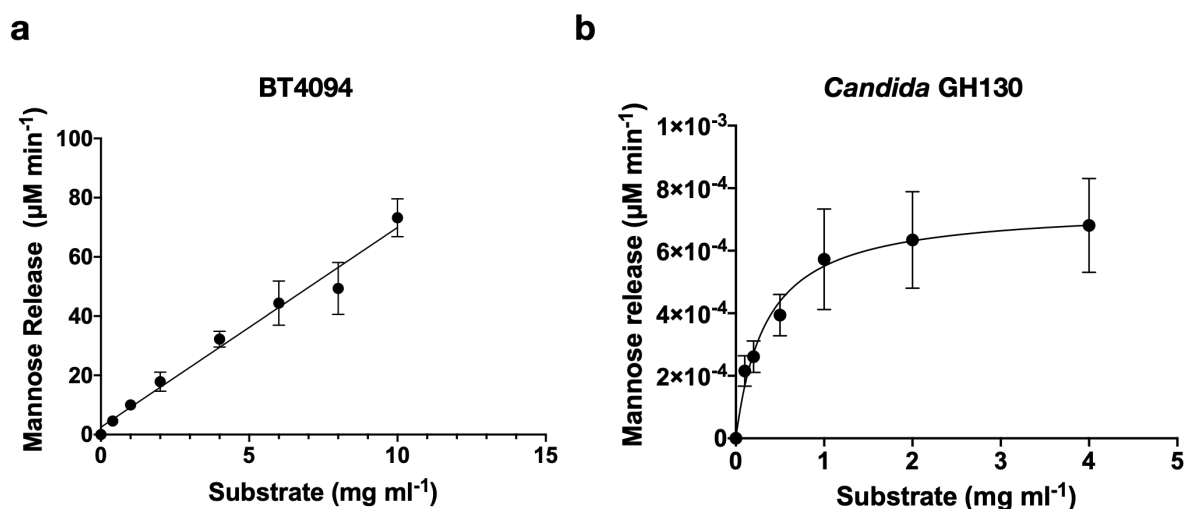


Figure 3. 7 End-point reactions with BT3780, CaGH130, and BT4094 against *C. albicans* mannan. Enzymes at 10 μ M were tested against 10 μ g of mannan, continuous mannose release was monitored spectrophotometrically at 340 nm at 37 °C. Panel a: amount of mannose released from *C. albicans* mannan by BT3780, BT4094, and CaGH130. Panel b: Sequential assay with BT3780 and CaGH130. Column 1: CaGH130 followed by BT3780, column 2: BT3780 followed by CaGH130; Panel c: sequential assay with BT4094 and Bt3780. Column 1: BT4094 followed by BT3780, column 2: BT3780 followed by BT4094. Error bars show SE of three biological repeats.

To complete the biochemical characterisation of the two GH130s, their kinetic parameters were assessed. Both BT4094 and CaGH130 were assayed against *C. albicans* mannan at a range of concentrations using the mannose detection kit. This showed that CaGH130 displayed a strong affinity for *C. albicans* mannan, as indicated by its low $K_m=0.34$ mg ml⁻¹, while it was not possible to determine K_m for BT4094, which does not begin to saturate when substrate is at 10 mg ml⁻¹ (Figure 3. 8). In contrast, BT4094 possesses a higher catalytic efficiency (k_{cat}) than CaGH130, which is reflected by the difference between their k_{cat}/K_m (Figure 3. 8). This indicates that, while both being able to degrade cell wall mannan from *C.*

albicans, BT4094 and CaGH130 most likely perform two biologically distinct functions.



Enzyme	Substrate	K_m (mg ml^{-1})	k_{cat} (min^{-1})	k_{cat}/K_m ($\text{min}^{-1} \text{mg}^{-1} \text{ml}$)
BT4094	<i>C. albicans</i> mannan	n.d	n.d	6.74
CaGH130	<i>C. albicans</i> mannan	0.34 ± 0.1	7×10^{-4}	0.002

Figure 3. 8 Kinetics of BT4094 and CaGH130 against mannan from *C. albicans*. BT4094 and CaGH130 were assayed against *C. albicans* mannan at a range of concentrations. Panel a: BT4094 vs *C. albicans* mannan, simple linear regression was used to determine k_{cat}/K_m . Panel b: CaGH130 vs *C. albicans* mannan. For CGH130 K_m and k_{cat} were determined with Michaelis-Menton equation, for BT4094 k_{cat}/K_m was calculated from the linear fit. Assays were performed in triplicates, \pm shows SE, n.d stands for not determined. Data are representative of three technical repeats.

3. 3. 2 Characterisation of β -mannosidases, BT3780 and BT4094, *in vivo*.

3. 3. 2. 1 Construction and characterisation of $\Delta bt3780 + \Delta bt4094$ strain.

To determine if BT4094 contributes to the ability of Bt to degrade *C. albicans* mannan, Bt strains lacking either BT4094 or BT4094 together with BT3780 were

constructed. Briefly, regions of 1000 bases flanking *bt4094* gene were amplified by PCR, these were then joined together by a sewing PCR to generate a 2 kB deletion cassette (Figure 3. 9 b). The cassette was then cloned into pExchange plasmid (Figure 3. 9 c) and transformed into S17-1λ *E. coli* cells. Plasmid was then conjugated into Bt Δtdk strain as described in Methods to generate $\Delta bt4094$ strain, deletion was confirmed by PCR (Figure 3. 9 d) and sequencing. Deletion in Bt involves two recombination events, mediated by the counter-selectable pExchange vector, carrying erythromycin resistance gene, and the absence of a functional thymidine kinase (tdk) in Bt, which allows for de novo synthesis of thymidine in Bt. To generate $\Delta bt4094+\Delta bt3780$ strain, *bt4094* was deleted from $\Delta bt3780$ (previously constructed by Dr. E Lowe) strain using the same protocol, similarly deletion was confirmed by PCR (Figure 3. 9 e) and sequencing.

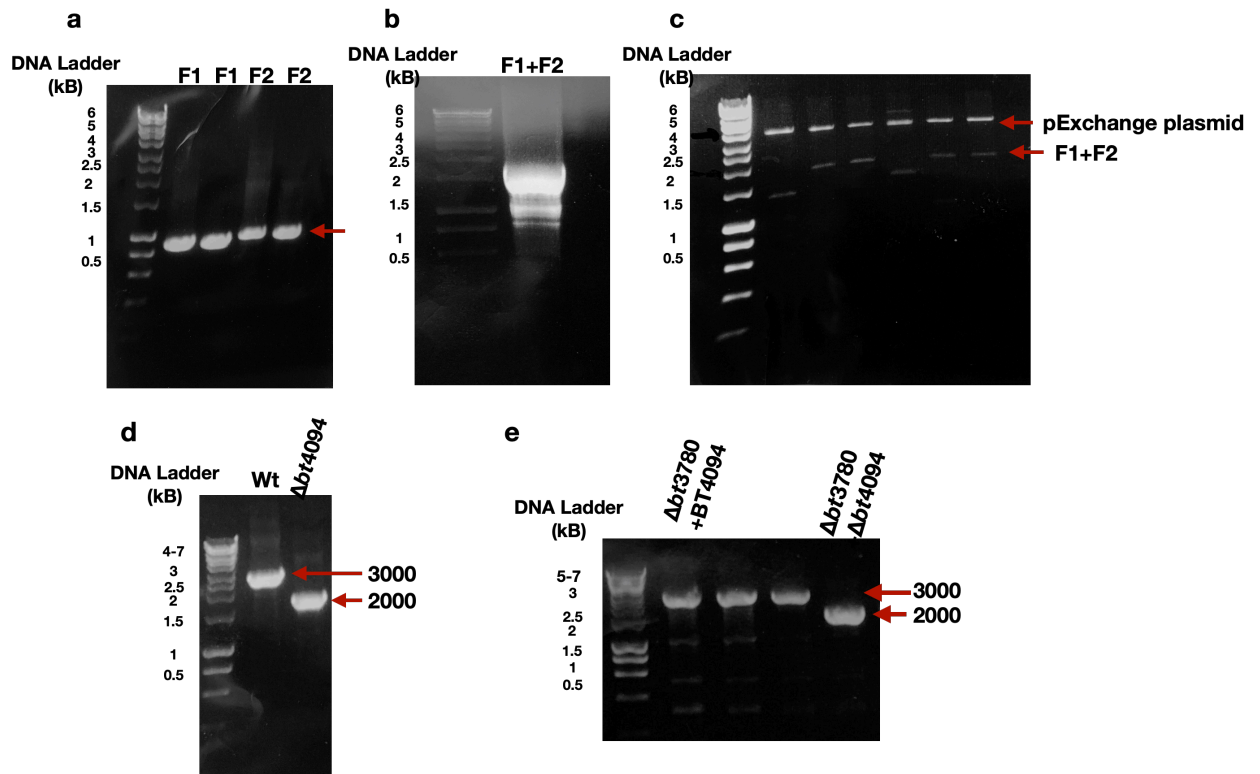


Figure 3. 9 Construction of $\Delta bt4094$ and $\Delta bt4094+\Delta bt3780$ strains. Panel a: 1000 bases regions flanking *bt4094* were amplified with PCR Panel b: Flank 1 and Flank 2 regions were annealed together with sewing PCR generating 2 kb deletion cassette. Panel c: 2kb deletion cassette was cloned into pExchange vector. Panel d: pExchange vector containing *bt4094* deletion cassette was conjugated into *Bt-tdk-* to create $\Delta bt4094$ strain. 3 kb PCR product is produced in a reaction using WT genomic DNA and 2 kb PCR product (lacking *bt4094* gene -1000 bases) was obtained with genomic DNA extracted from $\Delta bt4094$ strain. Panel e: pExchange vector containing *bt4094* deletion cassette was conjugated into $\Delta bt3780-tdk-$ strain to generate $\Delta bt4094+\Delta bt3780$ strain.

Strains $\Delta bt3780$; $\Delta bt4094$; and $\Delta bt4094+\Delta bt3780$ were then grown anaerobically on 10 mg ml^{-1} *Candida* mannan at 37°C , change in absorbance at 590 nm was recorded every 15 min for 48 h by an automatic plate reader (Biotek). A single deletion of BT4094 had very little effect, whereas $\Delta bt3780$ displayed a defective phenotype (Figure 3. 10 a), suggesting that BT3780 is the primary enzyme, contributing to removal of β -1,2-mannose from *C. albicans* mannan. Deletion of both BT4094 and BT3780 ($\Delta bt4094+\Delta bt3780$ strain) did not abort the ability of the

strain to grow on *C. albicans* mannan (Figure 3. 10 a). This indicated that enzymes other than BT3780 and BT4094 are also involved in mannan depolymerisation.

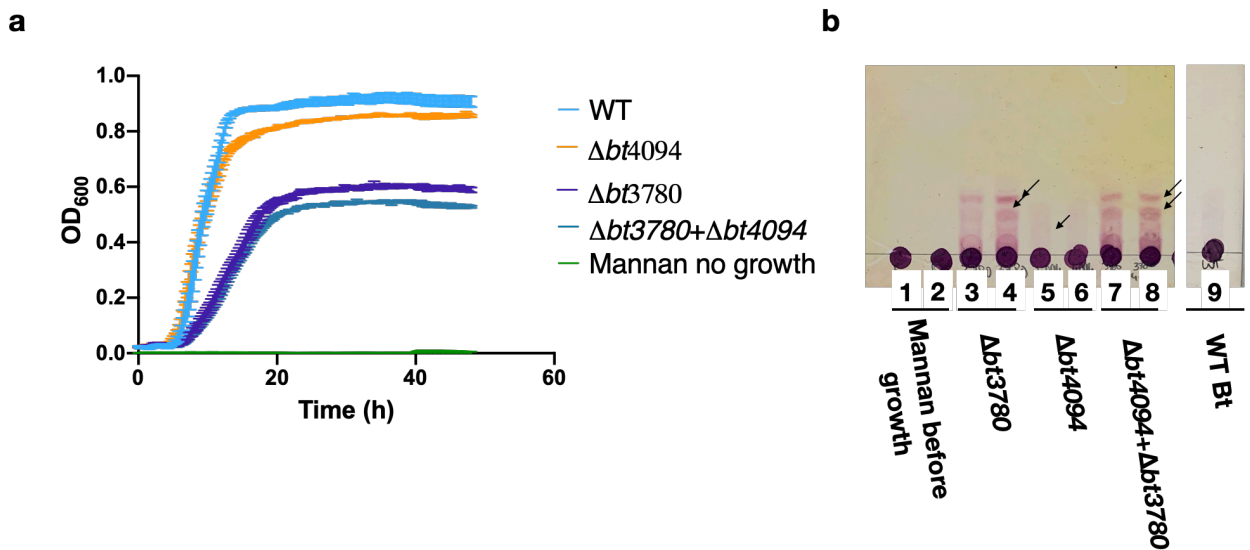


Figure 3. 10 Growth curves of WT Bt; $\Delta bt4094$; $\Delta bt3780$; $\Delta bt4094+\Delta bt3780$ strains on mannan from *Candida albicans*. Strains were grown in minimal media *C. albicans* mannan anaerobically at 37 °C for 48 h. Traces: WT Bt - blue, $\Delta bt4094$ - orange, $\Delta bt3780$ - purple, $\Delta bt4094+\Delta bt3780$ - teal, mannan no growth - green. Error bars show SE from three technical replicates. Data set is a representative of three biological replicates. (b) TLC of spent media from the stationary phase post WT Bt; $\Delta bt494$; $\Delta bt3780$; $\Delta bt4094+\Delta bt3780$ growths. Lane 1: *C. albicans* mannan without bacterial growth, lane 2: spent media taken post $\Delta bt3780$ growth, lane 3 media post $\Delta bt4094$ growth, lane 4 media post $\Delta bt4094+\Delta bt3780$ growth. Arrows indicate oligosaccharides that were found in the culture supernatant.

Spent media from the stationary phase was analysed on TLC. The analysis showed that the strain $\Delta bt4094+\Delta bt3780$ releases large oligosaccharides in the media (Figure 3. 10 b). 10 μ l of culture supernatant from the stationary phase was then incubated with recombinant BT3780 or BT4094 overnight. Reactions were then analysed with TLC. This showed that the large oligosaccharides from the supernatants were resolved into mannose by both BT4094 and BT3780 (Figure 3. 11 a, b). Assays were also further analysed with HPAEC-PAD. Peaks suggestive

of oligosaccharides were eluted from the culture supernatant between 34-37min of retention time (Figure 3. 11 c). Addition of BT3780 resolved these oligosaccharides producing a single peak, which corresponded to the mannose standard (Figure 3. 11 c). These data indicate that strains $\Delta bt4094+\Delta bt3780$ and $\Delta bt3780$ release β -1,2-oligosaccharides into the culture supernatant. This also suggests the presence of an endo-mannanase which can remove β -1,2 mannosyl caps from *C. albicans* mannan to expose the α -mannan component of the cell wall, which could then be disassembled by the enzymes encoded in MAN-PUL1, MAN-PUL2, MAN-PUL3.

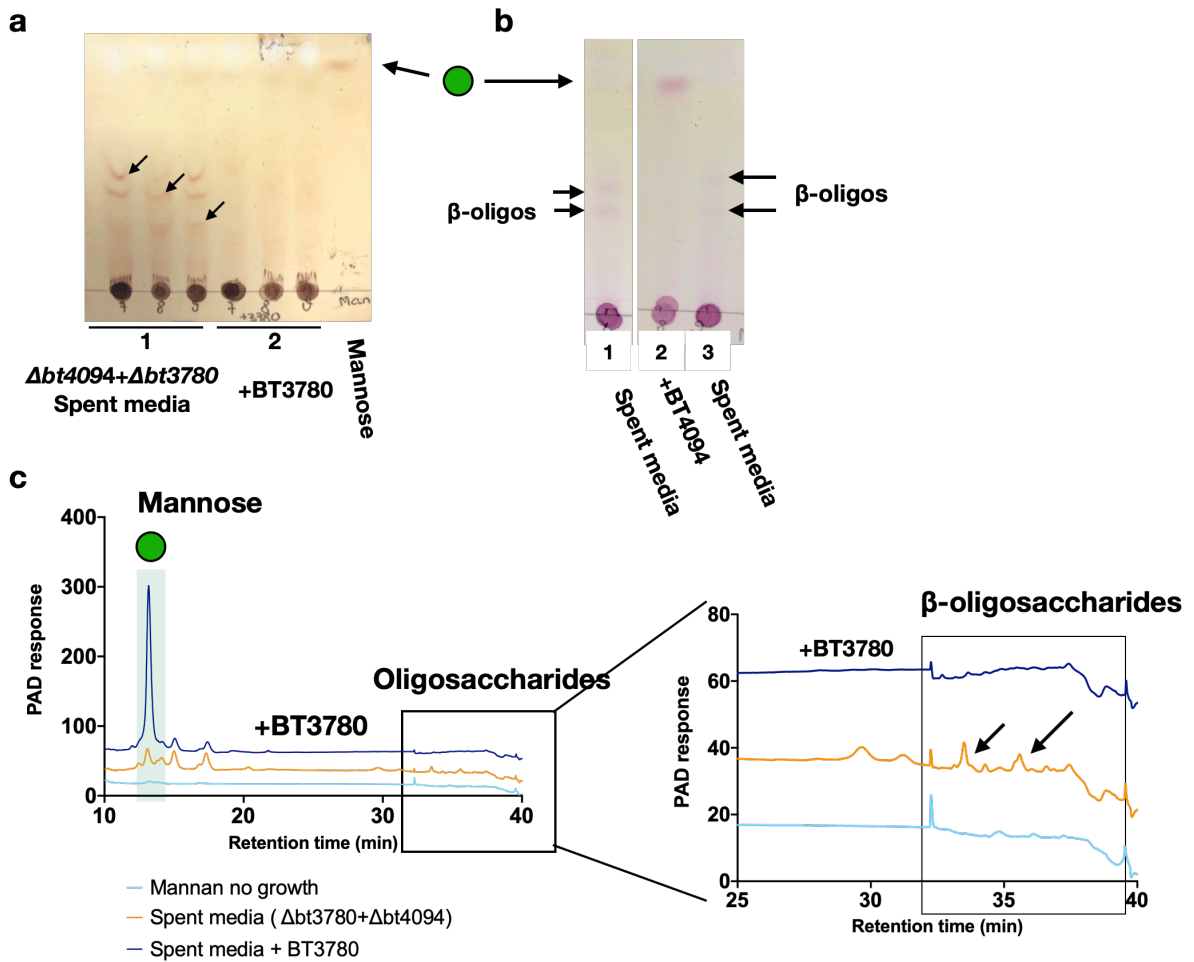


Figure 3. 11 Biochemical analysis of the $\Delta bt3780+\Delta bt4094$ culture supernatant. Culture supernatant was incubated with BT3780 and BT4094. Panel a: lane 1 oligosaccharides detected in the culture supernatant from $\Delta bt3780+\Delta bt4094$ marked with black arrows, lanes 2 oligosaccharides resolved by BT3780. (b) lane 1 and 3: oligosaccharides found in $\Delta bt3780+\Delta bt4094$ supernatant; lane 2 oligosaccharides degraded with BT4094. Panel c: HPAEC-PAD analysis of $\Delta bt3780+\Delta bt4094$ supernatant (orange trace), samples were analysed with CarboPac PA200 column, oligosaccharides were eluted with NaAc gradient and detected between 34-37 min of retention time. BT3780 treatment (navy trace) results in a single mannose peak (shaded).

3. 3. 2. 2 Characterisation of Bt $\Delta pul1/2/3 + \Delta bt4094$ strain

As previously shown in Cuskin et al. (2015b), Bt $\Delta pul1/2/3$ ($\Delta bt2620$ - $bt2632 + \Delta bt3773$ - $bt3792 + \Delta bt3853$ - $bt3862$) could not grow on α -mannan from *S. cerevisiae*. Growth of Bt $\Delta pul1/2/3$ was then assessed on mannan from *C. albicans*. Bt $\Delta pul1/2/3$ was grown on mannan from *C. albicans* for 48 h. This showed that despite not being able to utilise mannan from *S. cerevisiae*, Bt $\Delta pul1/2/3$ could still grow on mannan from *C. albicans*, whilst displaying a severely defective phenotype (Figure 3. 12).

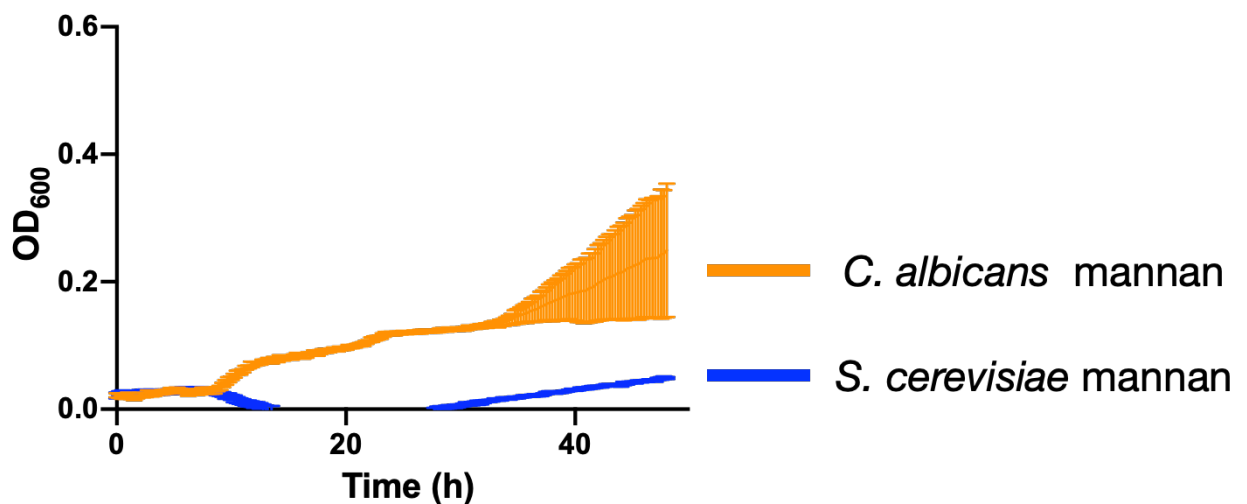


Figure 3. 12 Growth of Bt $\Delta pul1/2/3$ on mannan from *C. albicans* and *S. cerevisiae*. Bt $\Delta pul1/2/3$ was grown in minimal media with 10 mg ml⁻¹ mannan from *C. albicans* or *S. cerevisiae* anaerobically at 37 °C for 48h. Blue trace: growth of Bt $\Delta pul1/2/3$ on *S. cerevisiae* mannan; Orange trace: growth of Bt $\Delta pul1/2/3$ on *C. albicans* mannan. Mean and error bars are generated from three technical replicates. Data set is representative of at least three independent experiments.

We hypothesised that this residual growth of Bt $\Delta pul1/2/3$ was driven by the activity of the additional β -mannosidase, BT4094, located outside the three mannan PULs. To investigate further, a strain Bt $\Delta pul1/2/3 + \Delta bt4094$, lacking the

three mannan PULs and BT4094, was engineered. This was done by conjugating pExchange plasmid, containing $\Delta bt4094$ deletion cassette (Figure 3. 9 c), into $\Delta pul1/2/3$ strain previously constructed by Dr. Elisabeth Lowe, the resulting genotype was confirmed by sequencing. Bt $\Delta pul1/2/3+\Delta bt4094$ was grown anaerobically on *C. albicans* mannan for 48 h. Strains previously constructed in the lab: $\Delta pul1/2/3$, $\Delta pul2$, $\Delta pul3$, and $\Delta bt4094+\Delta bt3780$ were grown alongside and used as controls. Deletion of MAN-PUL3 alone did not affect the ability to grow on *C. albicans* mannan, while deletion MAN-PUL2 resulted in a significant growth defect (Figure 3. 13 a). This demonstrates that MAN-PUL2, which includes BT3780, remains central in utilisation of mannan from *C. albicans*, whereas absence of the MAN-PUL3 could be compensated by other mannan PULs. TLC analysis of spent media from stationary phase of both $\Delta pul2$ and $\Delta pul3$ showed that the strains did not release by-products into the culture supernatant (Figure 3. 13 c). This is consistent with the 'selfish' mechanism described by Cuskin et al. (2015).

Interestingly, deletion of BT4094 in the background of the three mannan PULs resulted in a more severe growth defect compared to that seen with Bt $\Delta pul1/2/3$ however the strain was still able to grow on *C. albicans* mannan (Figure 3. 13 b). TLC analysis of spent media showed that the strain released oligosaccharides into the culture supernatant (Figure 3. 13 panel d lane 13). Bt $\Delta pul1/2/3+\Delta bt4094$ was then grown in 5 ml of minimal media with *C. albicans* mannan, aliquots were collected every hour for 10 h and boiled. Samples were then analysed with TLC. This time course assay showed that a faint ladder, suggestive of oligosaccharides, started to appear in the culture supernatant 5 hours ($OD_{590}=0.4$) into growth, and as the growth continued bands became more intense (Figure 3. 13 d). These

oligosaccharides were refractory to the degradation by recombinant α - (BT3774, BT3858, BT2632) or β -mannosidases (BT4094, BT3780) (data not shown). These data indicate that while being a β -mannosidase targeting mannosidic linkages in mannan from *C. albicans*, BT4094 did not mediate residual growth of the mutant strain $\Delta pul1/2/3$ on mannan from *Candida albicans* and other enzymes are involved.

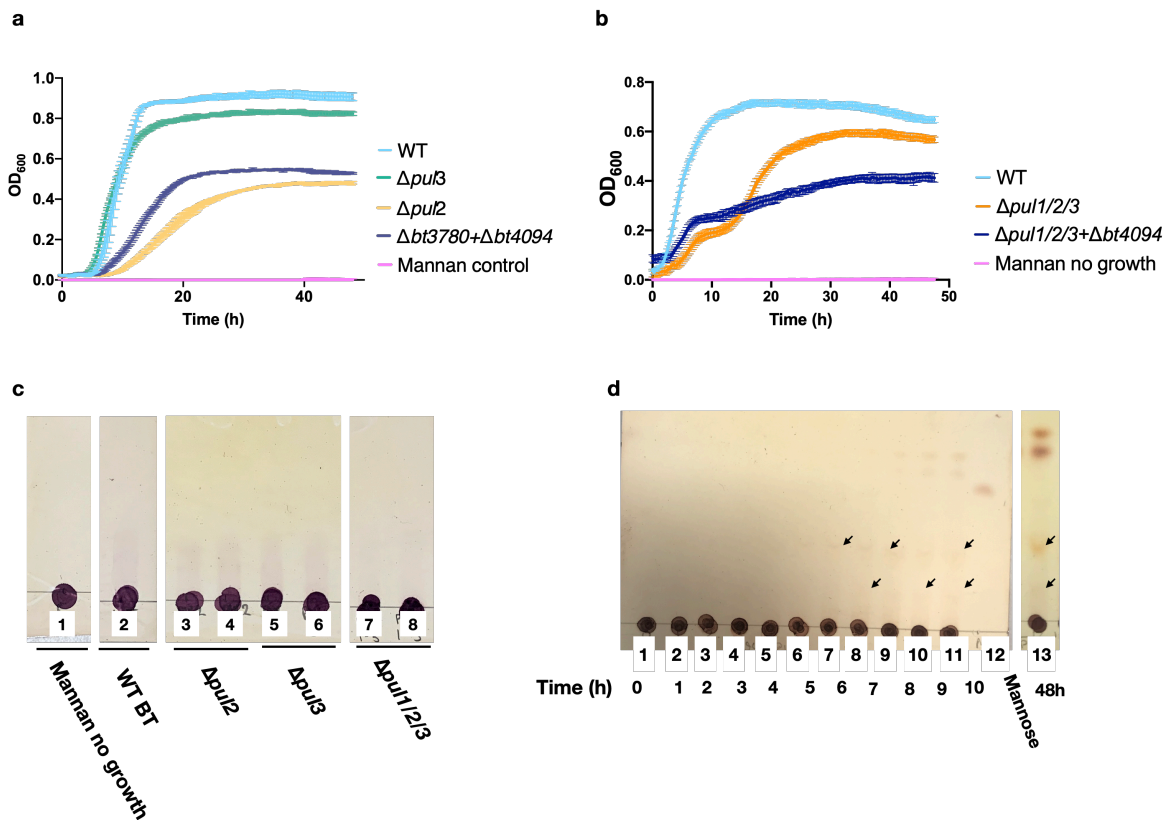


Figure 3. 13 Growths of Bt strains: WT Bt, $\Delta pul3$, $\Delta bt3780+\Delta bt4094$, $\Delta pul2$, $\Delta pul1/2/3$, $\Delta pul1/2/3+\Delta bt4094$. Strains were grown on 10 mg ml⁻¹ mannan from *C. albicans* anaerobically at 37 °C for 48 h. Error bars show SE from triplicates. Data set is representative of at least three independent experiments. Panel a Traces: WT Bt shown in light blue; $\Delta pul3$ green, $\Delta bt4094+\Delta bt3780$ in purple, $\Delta pul2$ in yellow, mannan without bacterial growth in magenta. Panel b: traces: WT Bt shown in sky blue, $\Delta pul1/2/3$ in tangerine, $\Delta pul1/2/3+\Delta bt4094$ in midnight blue, mannan before growth in magenta. Panels c: TLC analysis of spent media taken post growth of indicated strains. Panel d: TLC analysis of spent media of $\Delta pul1/2/3+\Delta bt4094$ at indicated time points.

3. 3. 3 Whole cell activity against mannan from *Candida albicans*

As previously established, Bt degrades mannan from *S. cerevisiae* in a selfish manner. It was then investigated whether Bt deploys a different mechanism for degradation of mannan from *C. albicans*. Bt WT was grown on 5 mg ml⁻¹ *C.*

albicans mannan, cells were harvested from the mid-exponential phase ($OD_{590}=0.7$), washed and resuspended in 1.5 ml PBS. A fraction of cells was treated with proteinase K to degrade proteins located on the cell surface. Another fraction of cells was treated with BugBuster, a detergent which lyses the cells, to examine activity of intracellular enzymes. Cells at equal amounts were incubated with 5 mg ml^{-1} of *C. albicans* mannan at 37°C . Samples were collected at regular intervals, reactions were stopped by boiling. Supernatant was analysed with TLC. These assays demonstrated that whole Bt cells cleaved long oligosaccharides from *C. albicans* mannan from the 1h incubation time point onwards, which were then gradually degraded into mannose (Figure 3. 14 a lanes 1-5). Bands corresponding to these oligosaccharides were much less visible in the proteinase K-treated cells (Figure 3. 14 a lanes 6-9) and were not detectable at 1-3h time points after cell lysis (Figure 3. 14 a lanes 11-13 ; lanes 17-21). A number of controls were also included: cells incubated with PBS without a carbon source and substrate resuspended in PBS (Figure 3. 14 panel b). These data indicate that degradation of mannan from *C. albicans* is initiated by the enzymes expressed on the surface of Bt. The ladder of oligosaccharides produced by the whole cells (Figure 3. 14 a lanes 2-5) is suggestive of a disaccharide and a trisaccharide, which are then gradually processed into mannose at the cell surface. It also implies that Bt uses a mechanism alternative to the one for utilisation of mannan from *S. cerevisiae* to degrade mannan from *C. albicans* and needs to be investigated further.

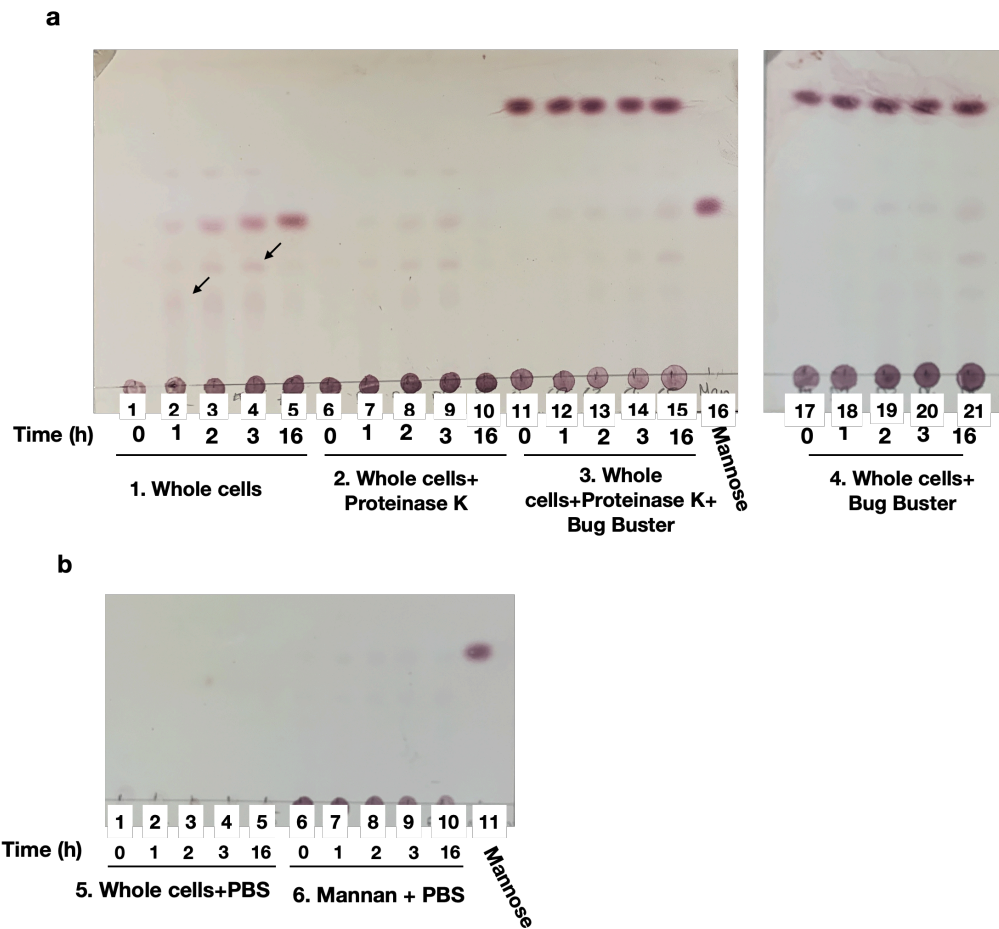


Figure 3. 14 Activity of the wild type Bt whole cells on mannan from *C. albicans*. Wild type Bt was grown on *C. albicans* mannan, cells were collected from the mid exponential phase ($OD_{590} = 0.6 - 0.8$) and washed. A fraction of cells was treated with Proteinase K (2 mg ml^{-1}) for 2 h at 37°C . Another fraction of cells was lysed with BugBuster. Cells were then incubated with 5 mg ml^{-1} *C. albicans* mannan, and aliquots were taken indicated time points. Panel (a) 1 Activity of whole cells on *C. albicans* mannan (lanes 1-5) arrows indicate oligosaccharides; 2 Activity of whole cells treated with Proteinase K on *C. albicans* mannan (lanes 6-10); 3 Activity of proteinase K treated cells lysed with BugBuster on *C. albicans* mannan (11-15); 4 Activity of whole cells lysed with BugBuster on *C. albicans* mannan (17-20); Panel (b) Controls: 5 Activity of whole cells without substrate (PBS) (lanes 1-5); 6 *C. albicans* mannan without added cells (lanes 6-10)

3. 3. 4 Characterisation of Mannan PUL4

Using the Cazy database PULDB (Terrapon et al., 2018), it was identified that BT4094 is predicted to form a part of PUL 74 which was identified by Martens et al. (2018) where bt4080-bt4084 were upregulated in response to a fraction of porcine mucosal glycans but bt4094 was not directly upregulated (Figure 3. 15). In addition to β -mannosidase BT4094, this PUL contains two pairs of SusCD complexes, a number of unknown proteins, GH92s, and a GH38, which are α -mannosidase families known to orchestrate α -mannan degradation. A general requirement for a genetic cluster to qualify as a PUL is the presence of a SusC-SusD pair. The genetic cluster bt4069-bt4096 was predicted to contain two SusC-SusD pairs and a pair of SusC-SusD which was separated by two proteins of unknown function. Moreover, given the the lack of data showing co-ordinated regulation for the whole PUL, it might be the case that these genes form multiple smaller loci.

Analysis of amino acid sequences of unknown proteins with SMART

(<http://smart.embl-heidelberg.de>) and InterPro showed that BT4079 contained a Glycoside Hydrolase Superfamily domain, suggesting that it could act as a GH, but other than that was not informative. Analysis with BLAST showed these proteins were not homologous to other proteins in Bt. An appropriate gene of each individual protein within the new PUL were cloned into a separate pET28a-vector by a biotechnology company, NZYtech (Portugal). Each gene was cloned into the vector to contain a C-terminal poly-Histidine tag, allowing for the purification by IMAC (Chapter 2 Section 2. 3. 13).

Proteins were expressed in TUNER, purified with IMAC, 100 mM Imidazole elutions were analysed with SDS-PAGE. With the exception of BT4084 and

BT4078, soluble proteins of appropriate sizes were obtained (Figure 3. 16). Protein sizes are summarised in Table 3. 1.

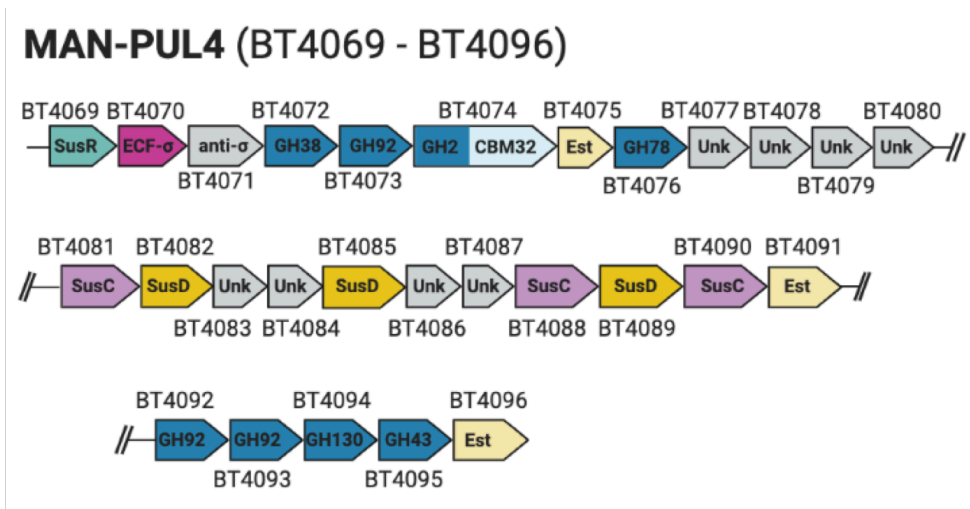


Figure 3. 15 Diagram of potential Mannan-PUL4 (BT4069-BT4096) as predicted by PULDB. GH: glycoside hydrolase; Unk: function unknown; est: esterase; CBM: carbohydrate binding module; SusC-SusD: transport proteins; SusR-ECF- σ /anti- σ : regulators.

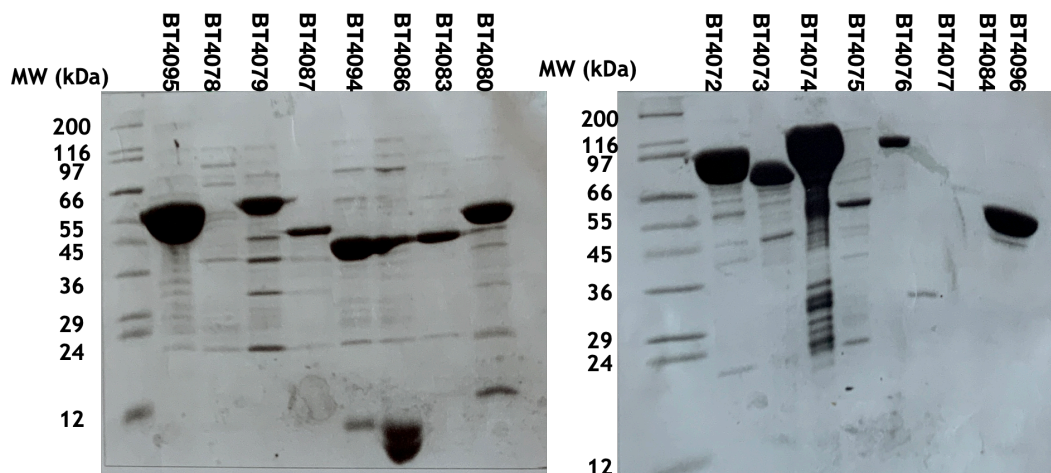


Figure 3. 16 SDS-PAGE gel of recombinant proteins from the mannan PUL-4. Proteins were purified with IMAC. 100 mM imidazole elutions were resolved on 12.5% SDS-PAGE gel. Wide-range molecular weight marker (Sigma, UK) was used to determine protein sizes.

Locus tag	MW (kDa)	GH Family	Activity/Substrate
BT4071	8.8	-	Anti-sigma
BT4072	97	GH38	α -1,2 mannosidase/HMNG
BT4073	88	GH92	α -1,4 α -1,2- mannosidase
BT4074	116	GH2	β -?-mannosidase/PNP- β -man
BT4075	55	-	Esterase/roxatidine acetate (Zimmermann et al 2019)
BT4076	101	GH78	Unknown
BT4077	33	Unknown	Unknown
BT4078	26	Unknown	Unknown
BT4079	69	Unknown	Unknown
BT4080	51	Unknown	Unknown
BT4081	116	SusC	
BT4082	78	SusD	
BT4083	40	Unknown	Unknown
BT4084	51	Unknown	Unknown
BT4085	71	SusD	
BT4086	17	Unknown	Unknown
BT4087	40	Unknown	Unknown
BT4088	117	SusC	-
BT4089	68	SusD	-
BT4090	116	SusC	-
BT4091	74	-	Esterase/Diflorasone (Zimmermann et al 2019)
BT4092	86	GH92	α -1,2 mannosidase/ yeast mannan
BT4093	81	GH92	α -1,4 mannosidase
BT4094	43	GH130	β -1,2 mannosidase/ <i>C. albicans</i> mannan
BT4095	58	GH43	Unknown
BT4096	53	-	Esterase/Diltiazem (Zimmermann et al 2019)

Table 3. 1 Table of molecular weight, GH-family, and known functions of proteins in Mannan PUL-

4.

3. 3. 5 Glycoside hydrolases 92 from Mannan PUL4

MAN-PUL4 was predicted to contain 3 GH92s: BT4092, BT4073, BT4093. These GH92s were previously characterised by Zhu et al. (2010). All GH92s were shown to be Ca^{+2} dependent therefore all reactions were carried out in 50mM MOPS containing 2mM CaCl_2 ,

BT4092^{GH92}, BT4093^{GH92}, BT4073^{GH92} at 1 μM were tested against 1 mM α -linked manno- β -D-glucopyranoside substrates and 1 mg ml⁻¹ mannan from *S. cerevisiae*, *C. albicans*, and *Gilmaniella spp.* overnight. In line with data from Zhu et al. (2010), BT4092 was active against α -1,2-mannobiose (Figure 3. 17 a) as well as mannan from both *S. cerevisiae* and *C. albicans* (Figure 3. 17 d). This indicates that a fraction of sidechains in mannan from *C. albicans* lack β -mannosylation. Both BT4073 and BT4093 could hydrolyse α -1,4-mannosidic linkage (Figure 3. 17 b and c), however BT4073 and BT4093 also showed incomplete activity on α -1,2- and α -1,3 linked disaccharides (Figure 3. 17 b and c). Neither BT4093 nor BT4073 were active on mannan from *S. cerevisiae* (Figure 3. 17 c). Interestingly BT4093 but not BT4073 displayed activity on mannan extracted from a soil yeast *Gilmaniella spp* (Figure 3. 17 f), which was provided as a gift by Jiangsu Key lab (Nanjing, China) to Dr. Fiona Cuskin. Chen et al. (2016) performed NMR analysis of mannan from *Gilmaniella spp*, which was able to identify that its sidechains were capped with α -1,4-mannosyl linkages. This is the only study to date that reports α -1,4-mannosidic bonds to be found in nature (Chen et al., 2016).

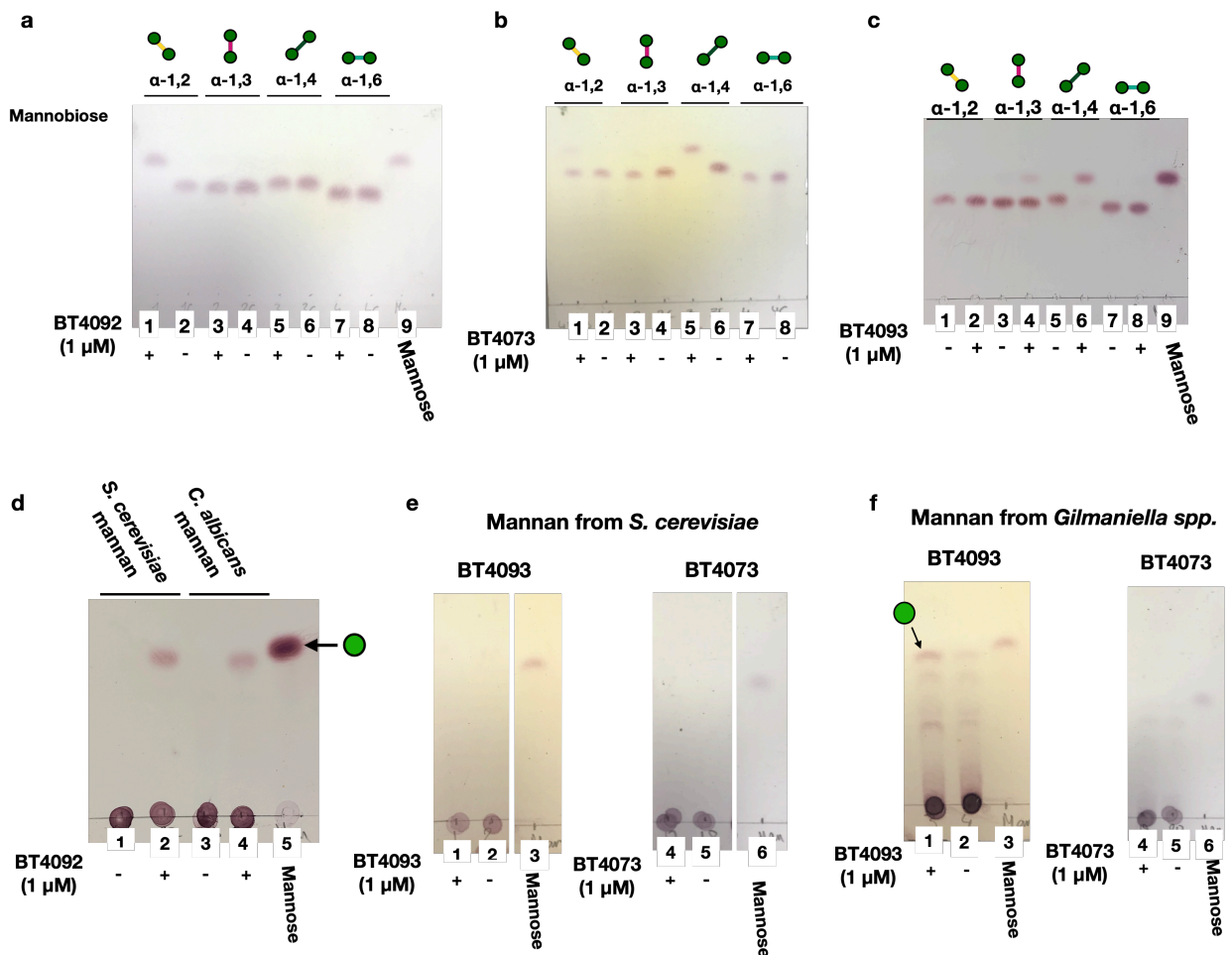


Figure 3. 17 Activity of GH92s from the MAN-PUL4 against α -linked mannosidase substrates and yeast mannan. Enzymes 1 μ M were assayed against 1 mM α -1,2- α -1,3- α -1,4- and α -1,6- mannosidase substrates as well as 1 mg ml⁻¹ yeast mannan substrates overnight. Panel a: BT4092 displays activity α -1,2 mannosidase; Panel b: BT4073 displays activity on α -1,4-mannosidase and trace activity on α -1,2-mannosidase; Panel c: BT4093 is active against α -1,4-mannosidase, trace on α -1,3-mannosidase; Panel d: BT4092 releases mannose from mannan from both *S. cerevisiae* and *C. albicans*; Panel e: BT4093 and BT4073 do not show activity on mannan from *S. cerevisiae*; Panel f: BT4093 but not BT4073 releases mannose from *Gilmaniella spp.* mannan.

3. 3. 6 Characterisation of BT4072^{GH38}

BT4073 is flanked by BT4072 and BT4074 in MAN-PUL4 (Figure 3. 15). BT4072 is predicted to belong to the GH38 family. Bt genome encodes only two GH38s:

BT4072 and BT3774, a previously characterised α -1,3- and α -1,2-mannosidase from MAN-PUL2 (Cuskin et al., 2015b).

The amino acid sequence of BT4072 was aligned with other characterised GH38s listed in Cazy.org database, using Clustal Omega. Phylogenetic analysis was carried out in phylogeny.fr (<http://www.phylogeny.fr>). This showed that BT4072 was not homologous to any of the characterised GH38s, sharing 20 % identity with BT3774. Phylogenetic analysis showed that BT4072 positions on the same branch with a GH38 from *Streptococcus pyogenes* (Spy1604) (Figure 3. 18).

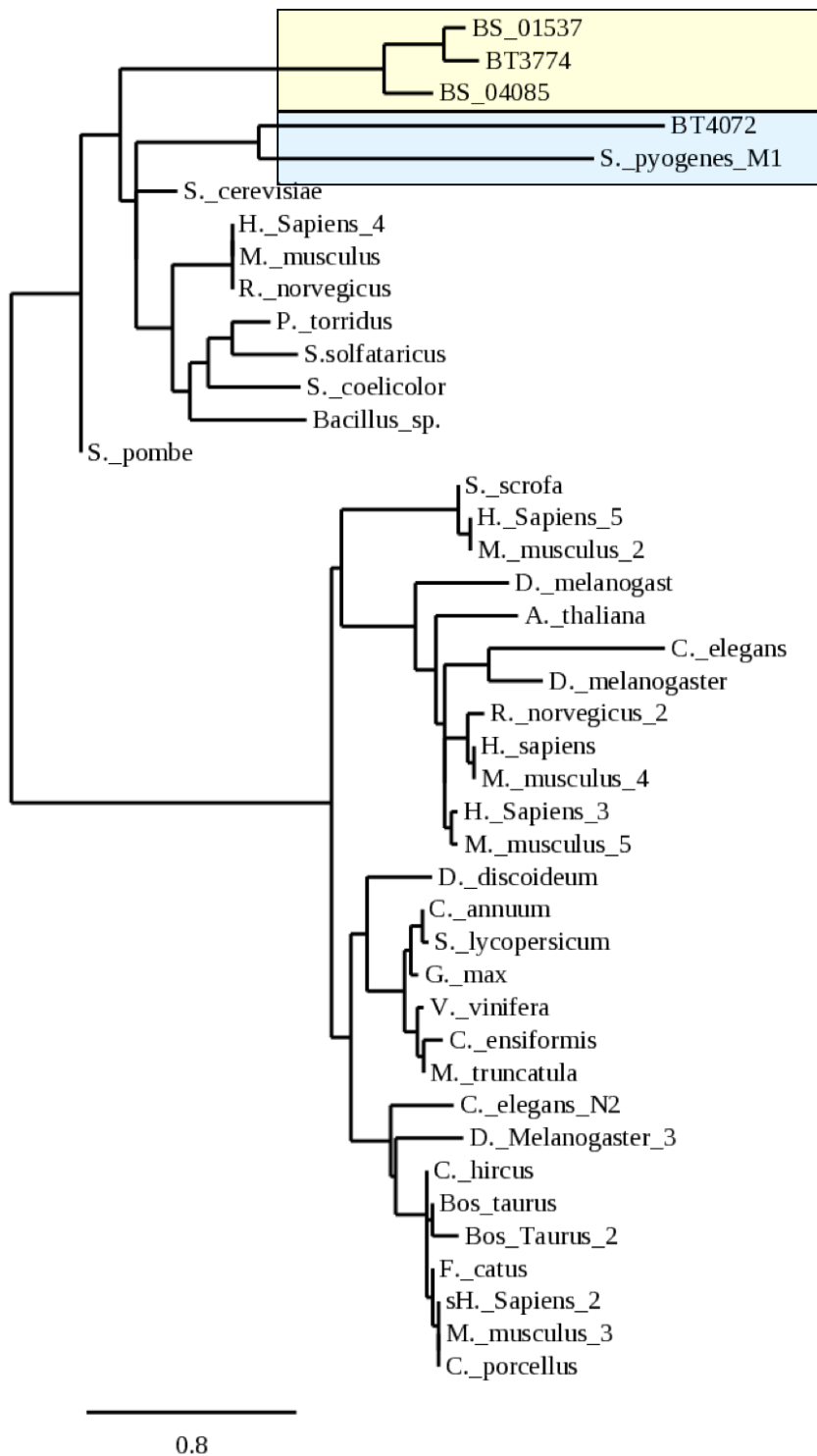


Figure 3. 18 Phylogenetic tree of characterised GH38s. The tree was constructed using phylogeny.fr, BT4072 positions on the same branch with a GH38 from *S. pyogenes*, blue box, BT3774 -yellow box.

GH38s are metal dependent enzymes, and the majority of the GH38s require Zn^{+2} for activity (Suits et al., 2010), however BT3774 showed preference for Ca^{+2}

(Cuskin et al., 2015b), therefore all initial reactions with BT4072 were carried out in 50 mM MOPS containing 2 mM CaCl₂.

BT4072 was assayed against 4 types of α -linked mannosiose substrates overnight. Reactions were analysed with TLC. BT4072 displayed specificity for α -1,2-mannosidic linkage (Figure 3.). α -1,2-mannosidase activity was further investigated and 1 μ M enzyme was tested against 5 mg ml⁻¹ mannan from *S. cerevisiae* and *C. albicans*, BT4072 did not display activity (data not shown).

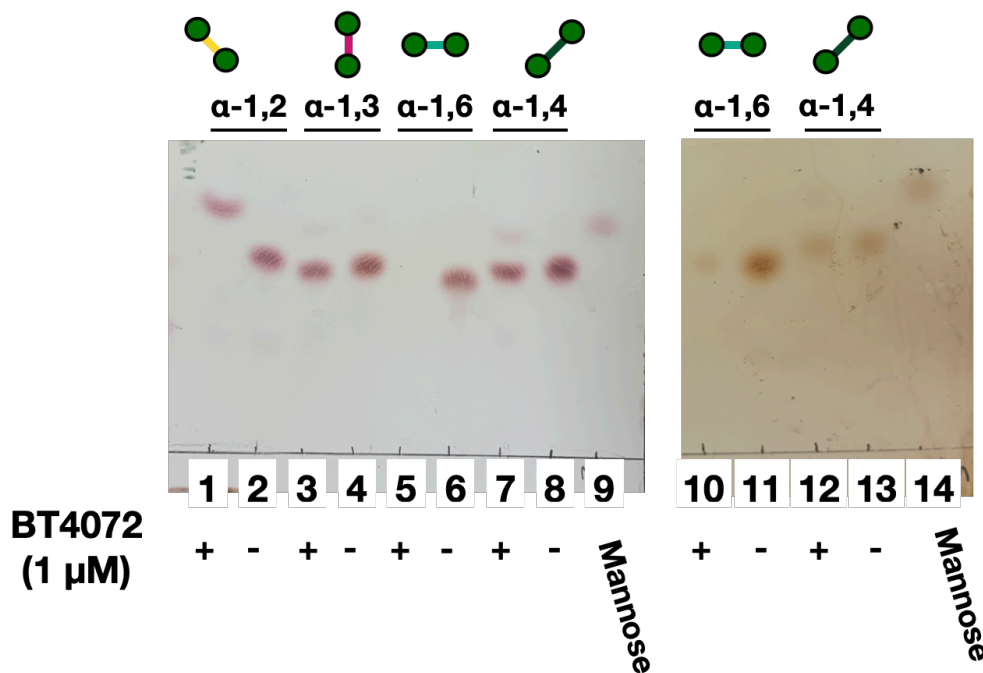


Figure 3. 19 Activity of BT4072 on α -linked mannosiose substrates. BT4072 was assayed with 1 mM of α -1,2- α -1,3- α -1,4 and α -1,6 mannosiose overnight at 37 °C. BT4072 shows activity on α -1,2 mannosiose and trace activity on α -1,4-mannosiose

S. pyogenes GH38 was previously characterised as α -1,3-mannosidase, which deconstructs Man₅GlcNAc₂ to Man₃₋₄GlcNAc₂, once α -1,2 decorations of High Mannose N-glycan (HMNG) have been removed (Figure 3.) (Suits et al., 2010). Given the activity of BT4072 against α -1,2-mannosiose, it was then investigated if BT4072 can act on HMNG from RNaseB (Sigma, UK). 1 μ M enzyme was

incubated with 10 mg ml⁻¹ RNaseB overnight, reaction was analysed with TLC. Diphenylaniline (DPA) stain was used to visualise HMNG to stain substrates containing acetylated sugars, such as GlcNAc or Sialic Acid. BT4072 liberated mannose from RNase B, suggesting that the enzyme can hydrolyse α -1,2-linkages found in RNaseB HMNG (Figure 3. 19 lane 2)

Degradation of HMNG in Bt is orchestrated by a PUL distinct from three mannan PULs (Cuskin et al 2015). Bt HMNG PUL contains an endo-acting BT3987^{GH18} localised to the cell surface, and 3 GH92s: BT3990, BT3991, BT3994. BT3987^{GH18} releases Man₉GlcNAc from the surface of the glycoprotein by targeting β -1,4-glycosidic linkage found between the two GlcNAcs at the core of the glycan (Figure 3.). Further degradation of Man₉GlcNAc is mediated by BT3990^{GH92} and BT3991^{GH92}, cleaving α -1,2 and α -1,3-mannosyl linkages, respectively, to generate Man₃GlcNAc (Zhu et al., 2010, Cuskin et al., 2015b) (Figure 3.). BT3987^{GH18}, BT3990^{GH92}, and BT3991^{GH92} were used to assess activity of BT4072 on HMNG.

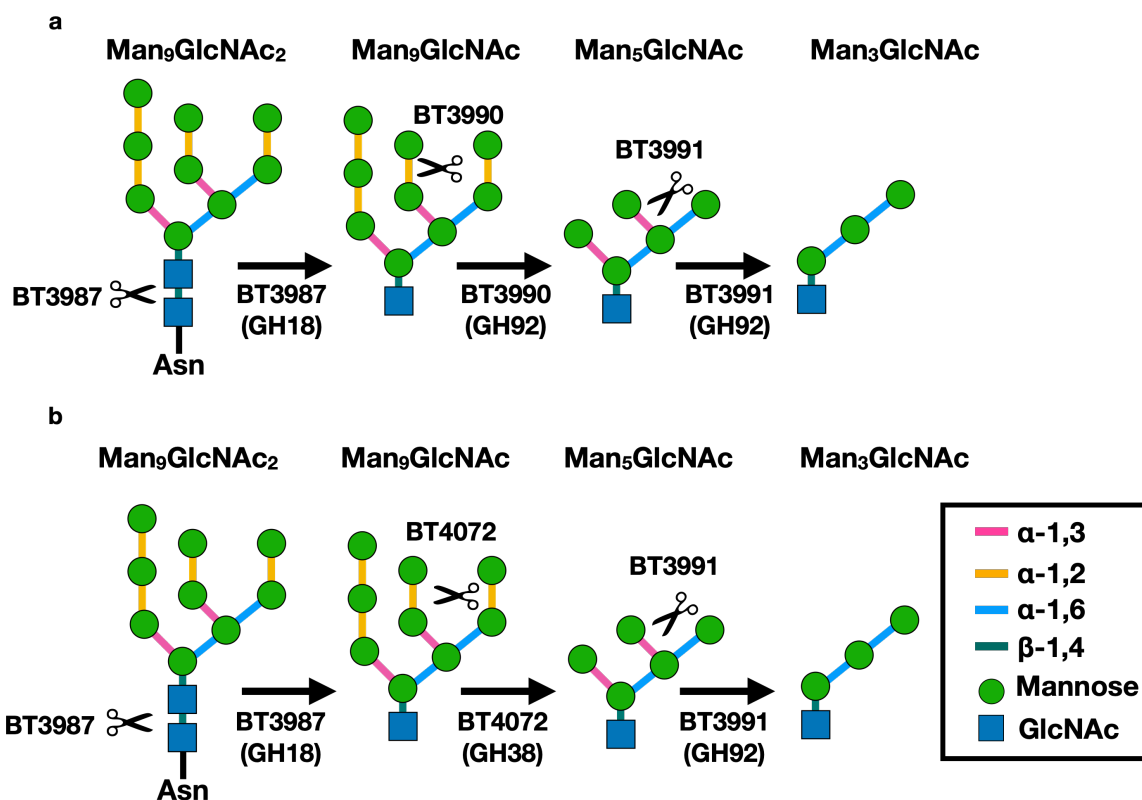


Figure 3. 20 Schematic illustration of High Mannose N-glycan (HMNG) found in Ribonuclease B. Mannose is labelled by a green circle, GlcNAc is shown with a blue square (a) Man₅₋₉GlcNAc is liberated from the glycoprotein by BT3987^{GH18}, GH92 α-1,2-mannosidase BT3990 degrades Man₅₋₉GlcNAc to Man₅GlcNAc, GH92 α-1,3-mannosidase BT3991 produces Man₃GlcNAc (b) Proposed model for BT4072^{GH38} activity on HMNG.

Assays containing 10 mg ml⁻¹ RNaseB and a range of enzyme cocktails comprising of various combinations of BT3987^{GH18}, BT3990^{GH92}, BT3991^{GH92}, and BT4072^{GH38} (as indicated) all at 5 μM were incubated overnight. Reactions were analysed with TLC and DPA stain was used to visualise glycans. N-glycan release from RNaseB by BT3987^{GH18} was indicated by the ladder produced (Figure 3. 19 lane 3). Mannose was generated by both BT3990^{GH92} and BT3991^{GH92}, lane 5 and 9, respectively (Figure 3. 21). The combination of BT3987^{GH18} and BT3990^{GH92} produced mannose and Man₅GlcNAc, as the ladder generated by BT3987 resolved into one clear band (Figure 3. 19 ane 7). This band

then underwent a visible shift (Figure 3. 19 lane 14) when BT3991^{GH92} was co-incubated with BT3987^{GH18} and BT3991^{GH92} cocktail, yielding mannose and Man₃GlcNAc (Figure 3. 19 lane 13). This model was then used to assess the specificity of BT4072.

Similarly to what was observed in lane 7 with BT3990^{GH92}, the ladder generated by BT3987^{GH18} also resolved into one distinctive band post BT4072^{GH38} treatment (Figure 3. 19). This band then again shifted (Figure 3. 19 lane 13) when BT3991^{GH92} was tested along with BT3987^{GH18} and BT4072^{GH38}. A control reaction was also set up where all 4 enzymes: BT3987^{GH18}, BT3991^{GH92}, BT3990^{GH92}, and BT4072^{GH38} were added simultaneously, which did not trigger any further band movements, indicating that further degradation did not occur (Figure 3. 19 lane 15). This analysis shows that BT4072^{GH38} acts as an α -mannosidase, which can remove α -1,2-linked mannoses from the HMNG to produce Man₆GlcNAc, making the underlying α -1,3-mannosidic bonds accessible to BT3991^{GH92} (Figure 3.). This suggests that BT4072^{GH38} displays a similar α -1,2-mannosidic activity to BT3990^{GH92}.

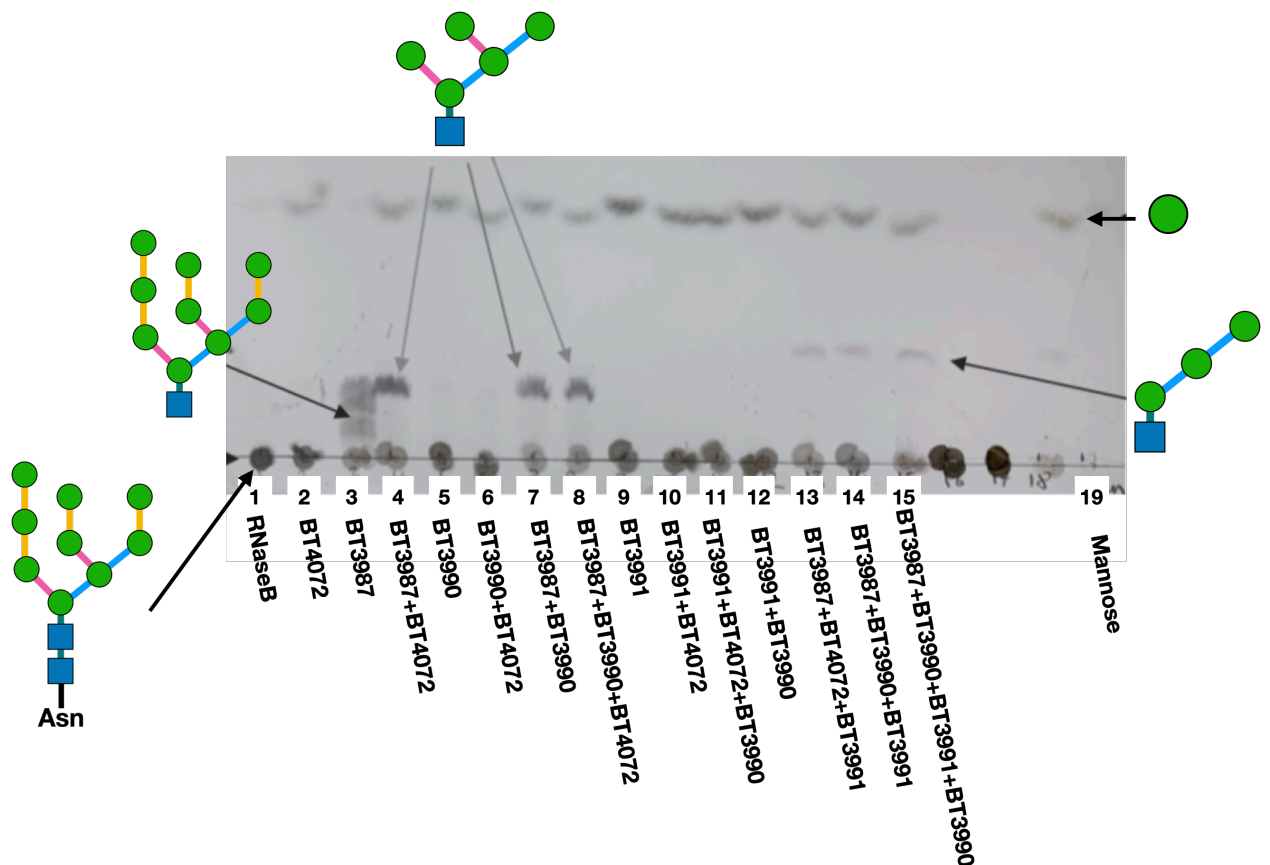


Figure 3. 19 RNase B degradation by α -mannosidases: BT3990^{GH92}; BT3991^{GH92}, and BT4072^{GH38}. Enzymes BT3987^{GH18}, BT3990^{GH92}, BT3991^{GH92}, and BT4072^{GH38} were tested against RNase B overnight 37 °C. Mannose – green circle, GlcNAc – Blue square, respectively. Lane 1: undigested RNase B; lane 2 BT4072^{GH38} releases mannose from RNase B; lane 3 BT3987^{GH18} releases Man₉GlcNAc from RNase B; lane 4 activity of BT4072^{GH38} on Man₅₋₉GlcNAc; lane 5 BT3990^{GH92} releases mannose from RNase B; lane 6 BT3990^{GH92} and BT4072^{GH38} against RNase B; lane 7; BT3990^{GH92} acts on Man₉GlcNAc; lane 13 BT3991^{GH92} and BT4072^{GH38} degrade Man₅₋₉GlcNAc; lane 14 BT3990^{GH92} and BT3991^{GH92} act on Man₉GlcNAc, lane 15 BT4072^{GH38}, BT3991^{GH92}, and BT3990^{GH92} against Man₉GlcNAc.

3. 3. 7 Characterisation of enzymes from Mannan PUL4

To investigate whether any of the remaining proteins in MAN-PUL4 were able to degrade *C. albicans* mannan more effectively, 9 proteins from the MAN-PUL4 (BT4095, BT4072, BT4086, BT4076, BT4077, BT4079, BT4080, BT4075,

BT4074), at concentrations ranging between 1-10 μM were combined into one reaction and assayed against 1 mg ml⁻¹ *C. albicans* mannan. Proteins were also mixed in different combinations in an attempt to reveal activity. All reactions were carried out overnight and analysed with TLC. Figure 3. 22 a shows that bands suggestive of sugars were released from *C. albicans* mannan by BT4074. Addition of mannose standard to these reactions revealed that both products resolved on a different level to mannose (data not shown), however it was not possible to identify these sugars. The rest of the assayed proteins did not display activity against *C. albicans* mannan (Figure 3. 20).

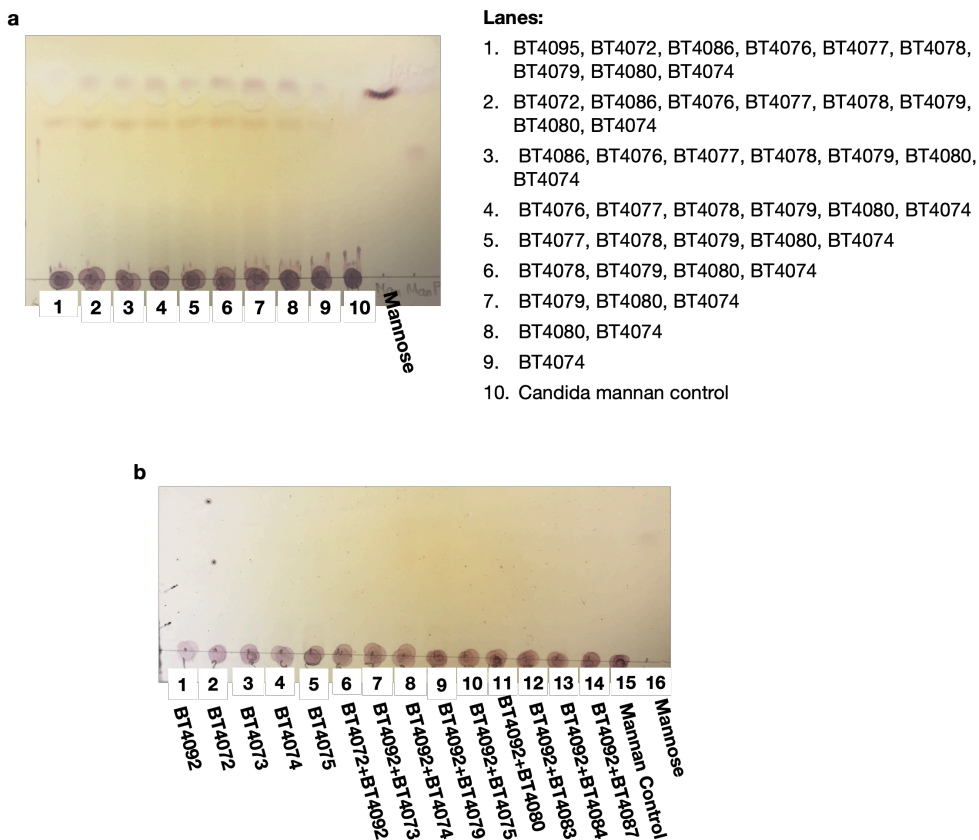


Figure 3. 20 TLC of one pot reaction. Proteins at 1-5 μM were combined into a set of reactions (Panel a and b) and tested against mannan from *C. albicans* (1 mg ml⁻¹) overnight 37 °C. None of the proteins displayed enzymatic activity against mannan.

3. 3. 8 *In vivo* characterisation of Mannan-PUL4

With the exception of BT4094, recombinant proteins from MAN-PUL-4 did not display activity on mannan from *C. albicans*, therefore, to investigate if it contributes to *C. albicans* mannan degradation *in vivo*, a set of new deletions was introduced into Bt. Bt strains lacking MAN-PUL4 and MAN-PUL1/2/3/4 were created as described in Methods. Briefly, 1000 kb regions upstream and downstream of MAN-PUL4 were amplified and stitched together with a sewing PCR to generate a 2 kb deletion cassette. The deletion cassette was then cloned into pExchange vector and conjugated into Bt Δtdk strain or $\Delta pul1/2/3$ strain, to construct $\Delta pul4$ and $\Delta pul1/2/3/4$ strains, respectively. Genotypes were confirmed by PCR and sequencing.

The ability of the newly generated strains $\Delta pul4$ and $\Delta pul1/2/3/4$ to utilise *C. albicans* mannan was then assessed. Deletion of MAN-PUL4 alone did not affect the growth of Bt on *C. albicans* mannan, as Bt $\Delta pul4$ displayed growth similar to the one seen with the wild-type Bt (Figure 3. 21 a). Unexpectedly, deletion of MAN-PUL4 in the strain $\Delta pul1/2/3$ partially rescued the previously seen phenotype as the strain $\Delta pul1/2/3/4$ displayed robust growth on mannan from *C. albicans* (Figure 3. 21). Interestingly, the growth phenotype of $\Delta pul1/2/3/4$ resembled the phenotype of $\Delta pul-2$ strain (Figure 3. 13 a).

Cell-free spent media taken from the stationary phase of $\Delta pul1/2/3/4$ was then analysed with TLC, which revealed that the strain liberated a ladder of oligosaccharides (Figure 3. 21 b). These data indicate that the residual growth of $\Delta pul1/2/3$ strain on mannan from *C. albicans* is not mediated by the activity of MAN-PUL4, strongly suggesting that an additional locus or loci orchestrate breakdown of *C. albicans* mannan. These data also suggest that MAN-PUL4 may

contain a regulator for this putative locus and thus deletion of the MAN-PUL4 in $\Delta pul1/2/3$ strain enhanced its expression, giving rise to a new phenotype. This was an unexpected result and the genomes of the new strains $\Delta pul1/2/3/4$ and $\Delta pul4$ were sequenced by MicrobesNG (Birmingham, UK) to confirm that other mutations had not been introduced. Sequencing confirmed that the appropriate deletions were present and random recombination events did not occur. This supports the hypothesis that deletion of the MAN-PUL4 in $\Delta pul1/2/3$ triggered upregulation of an additional locus in the genome, permitting growth of $\Delta pul1/2/3/4$ strain on mannan from *C. albicans*.

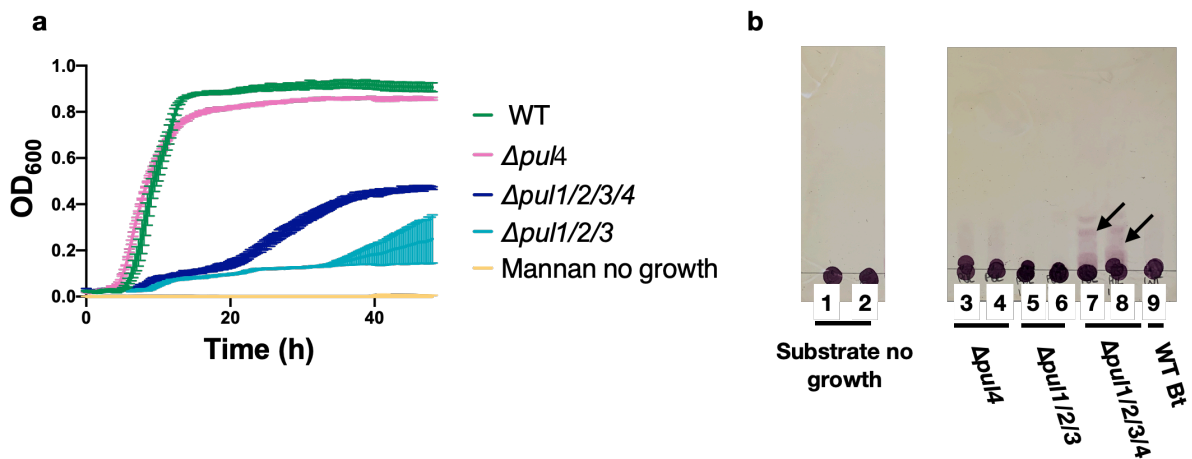


Figure 3. 21 Growths of WT Bt, Bt $\Delta pul4$, Bt $\Delta pul1/2/3/4$, and Bt $\Delta pul1/2/3$ on mannan from *Candida albicans*. Strains were grown on 10 mg ml⁻¹ mannan in minimal media anaerobically 37 °C for 48h. Mean and error bars were generated from three technical replicates; the data set is representative of at least three biological replicates. Growth curves were normalised to background mannan OD₆₀₀. Panel a: traces: WT Bt – green; Bt $\Delta pul4$ – pink; Bt $\Delta pul1/2/3/4$ – navy, Bt $\Delta pul1/2/3$ – teal, mannan without bacterial growth – mustard. Panel b: TLC analysis of cell free supernatant from the stationary phase after growth of indicated strains. Arrows in lanes 7-8 indicate oligosaccharides found in spent media of Bt $\Delta pul1/2/3/4$ strain.

It was then investigated if deletion of MAN-PUL4 restored growth of Bt $\Delta pul1/2/3$ on mannan from *S. cerevisiae*. The strain $\Delta pul1/2/3/4$ was grown alongside $\Delta pul1/2/3$ on *S. cerevisiae* mannan. Unexpectedly Bt $\Delta pul1/2/3/4$ displayed robust growth on *S. cerevisiae* mannan, which was preceded by an 18-hour lag phase (Figure 3. 22 a). Consistent with previous data, $\Delta pul1/2/3$ did not grow on mannan from *S. cerevisiae* (Figure 3. 22 a). Supernatant from the stationary phase was analysed with TLC. This did not reveal any extracellular activity (Figure 3. 22 b)

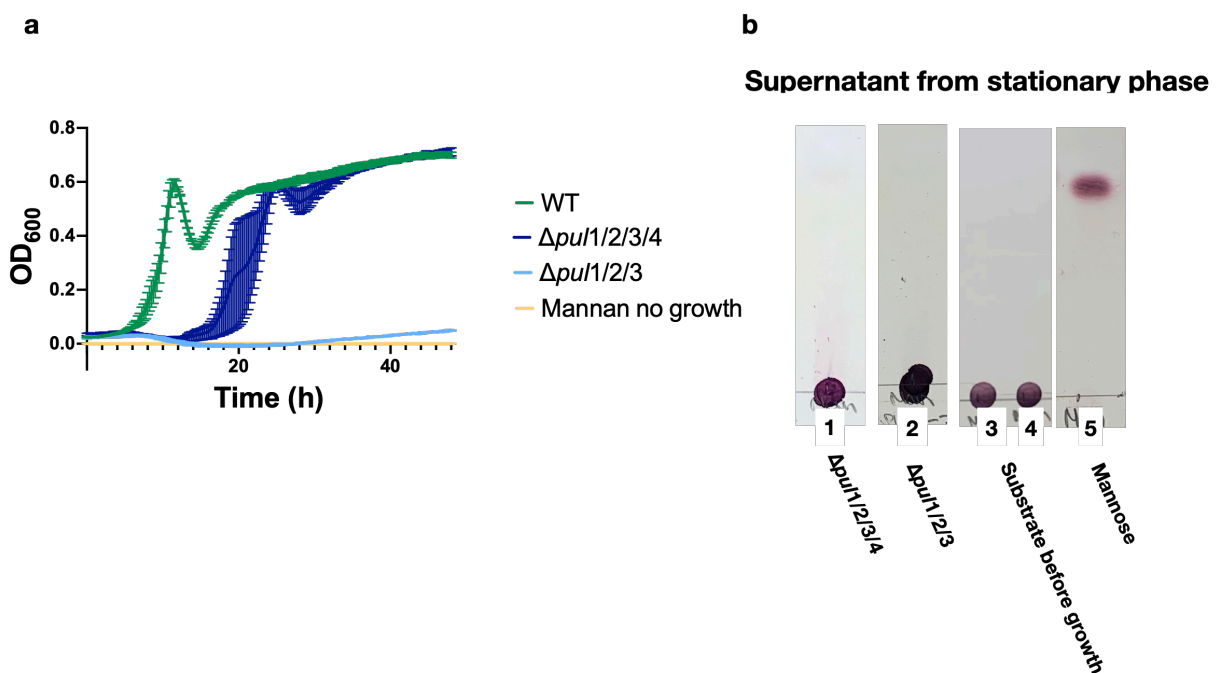


Figure 3. 22 Growth analysis of Bt WT, Bt $\Delta pul1/2/3/4$, and Bt $\Delta pul1/2/3$ on mannan from *S. cerevisiae*. Strains were grown in minimal media with 10 mg ml⁻¹ mannan at 37 °C for 48 hours. Mean and error bars were generated from 3 biological repeats. Curves were normalised to mannan. Panel a: traces: WT – green; $\Delta pul1/2/3/4$ – navy; $\Delta pul1/2/3$ – sky blue; mannan without bacterial growth – mustard. Panel b: TLC analysis of the cell free supernatant from WT, $\Delta pul1/2/3/4$, and $\Delta pul1/2/3$ strains at stationary phases.

3. 3. 9 Mannan from *mnn1*, *mnn5*, and *mnn2* *S. cerevisiae* mutants

Less complex yeast mannan variants were used to further explore the unexpected phenotype of $\Delta pul1/2/3/4$ strain. Ballou and co-workers (Raschke et al., 1973, Ballou et al., 1980) have created a library of deletion strains in *S. cerevisiae*, lacking various mannosyltransferases, which produce mannan with different sidechain decorations. Here, mannan from *mnn1*, *mnn5*, and *mnn2* strains was used (Figure 3. 23). The *mnn1* strain is defective in MNN1 α -1,3-mannosyltransferase and therefore lacks α -1,3-linked mannoses in the side chains; *mnn5* mutant produces α -1,6 backbone with a single α -1,2-linked mannose attached due to low activity of α -1,2-mannosyltransferase II, which extends the side chains; mannan from *mnn2* strain is composed of a long α -1,6-linked backbone as the strain does not possess an α -1,2-transferase to initiate side chain biogenesis (Ballou et al., 1980, Raschke et al., 1973). Schematically, mannan variants produced by the three strains are shown in Figure 3. 23. Mannan extraction was performed from appropriate yeast strains as described in Methods.

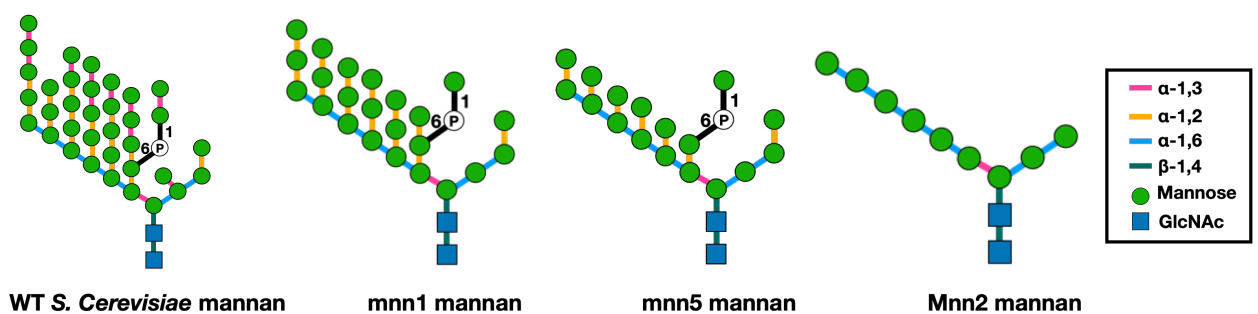


Figure 3. 23 Architecture of mannan variants extracted from the wild type, *mnn1*, *mnn5*, and *mnn2* *S. cerevisiae* strains. Wild type mannan is shown for comparison. *Mnn1* mannan is composed of α -1,6-backbone with two α -1,2-linked mannoses attached. *Mnn5* mannan retains a single α -1,2-linked mannose attached to the α -1,6-mannan backbone. *Mnn2* mannan contains linear α -1,6-linked mannan backbone. *Mnn1* and *mnn5* mannan retains phosphomannan, whereas *mnn2* mannan does not.

$\Delta pul1/2/3/4$ was grown on 10 mg ml^{-1} mannan from *mnn1*, *mnn5*, *mnn2*, and the wild type *S. cerevisiae* for 48 h. $\Delta pul1/2/3/4$ grew on mannan from the wild type *S. cerevisiae* (Figure 3. 24 a). Unexpectedly, when this strain was grown on less branched *mnn1* and *mnn5* mannan variants, it displayed a growth defect but was still able to grow (Figure 3. 24 b-c). Interestingly, $\Delta pul1/2/3/4$ was able to robustly use *mnn2* mannan, composed of a linear α -1,6 mannan backbone, but exhibited a 12-h lag phase (Figure 3. 24 d). Analysis of culture supernatant from the stationary phase with TLC showed that a ladder of oligosaccharides was released into the media when $\Delta pul1/2/3/4$ was cultured on *mnn2* but not on *mnn1* or *mnn5* α -mannan (Figure 3. 25 a). Cells from these cultures were also collected, washed, and incubated overnight with all four mannan variants, as demonstrated in Figure 3. 25. Whole cell assays showed that $\Delta pul1/2/3/4$ was able to liberate a ladder of oligosaccharides from *mnn2* mannan and mannose from other more complex mannan polymers (Figure 3. 25 b-e). Activity of the cells was independent of the mannan variant the strain was grown on. These data indicate that, despite lacking the main mannan degrading apparatus, $\Delta pul1/2/3/4$ is still able to utilise less complex mannan variants. Combined with the activity of the whole cells, these data suggest that Bt $\Delta pul1/2/3/4$ possesses exo-acting mannosidases, which allow for depolymerisation of complex mannan polymers. The ladder of oligosaccharides generated in response to *mnn2* mannan indicates the presence of a functional endo-acting surface mannanase, which breaks down α -1,6 linked backbone. Due to a limited substrate availability, it was not possible to repeat the same set of experiments with $\Delta pul1/2/3$ strain.

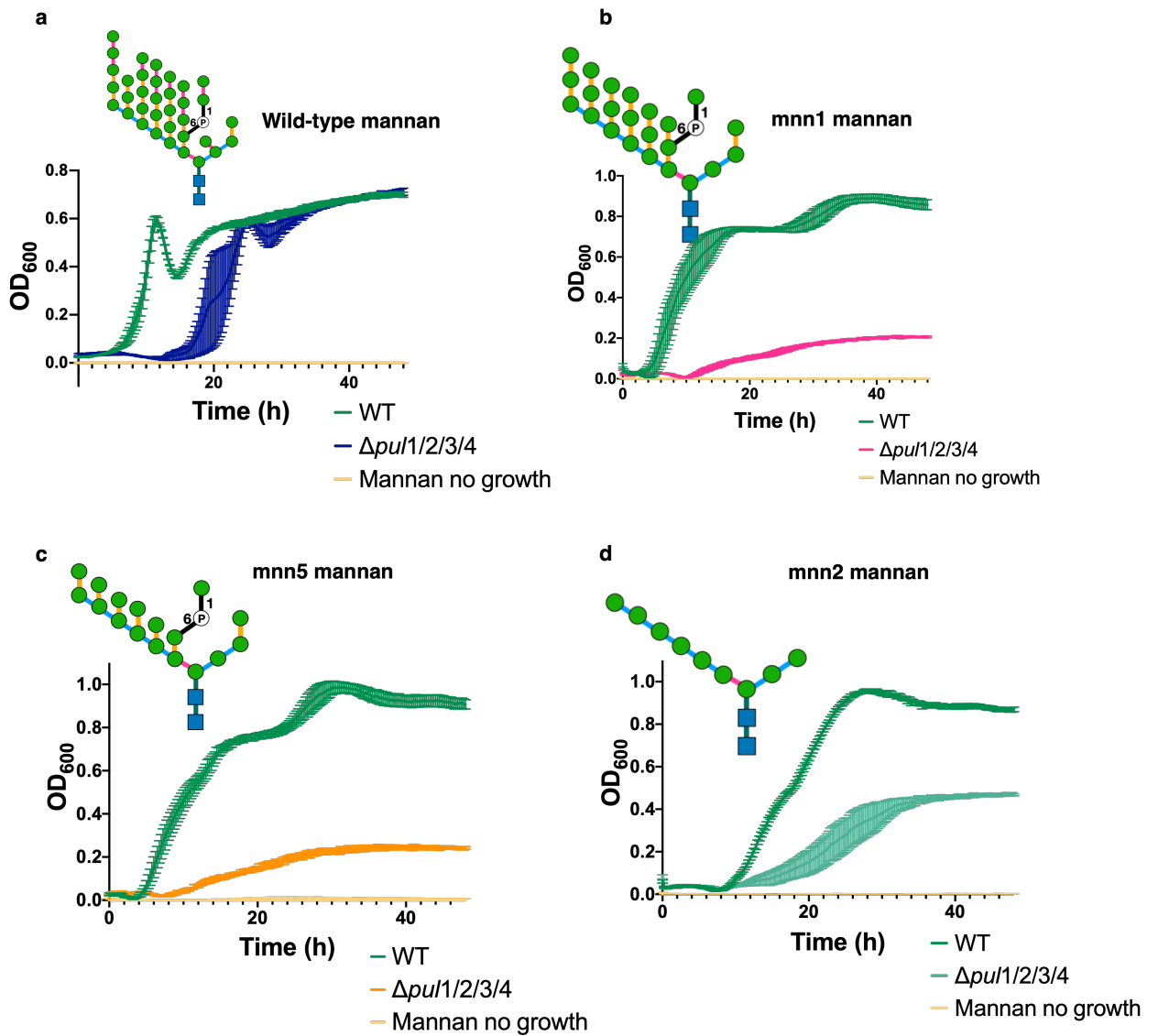


Figure 3. 24 Growth analysis of *Bt* $\Delta pul1//2/3/4$ on indicated *S. cerevisiae* mannan variants. Bacteria was grown on 10 mg ml^{-1} substrate in minimal media anaerobically at 37°C for 48 h. Mean and error bars were generated from three biological replicates, data are representative of three independent experiments. Curves were normalised to mannan OD_{600} shown in mustard. Panel a: growth of $\Delta pul1//2/3/4$ on wild type mannan (navy); panel b: $\Delta pul1//2/3/4$ vs mnn1 mannan (pink); panel c: $\Delta pul1//2/3/4$ vs mnn5 mannan (orange), panel d: $\Delta pul1//2/3/4$ vs mnn2 mannan (teal). WT *Bt* is shown in green in all panels.

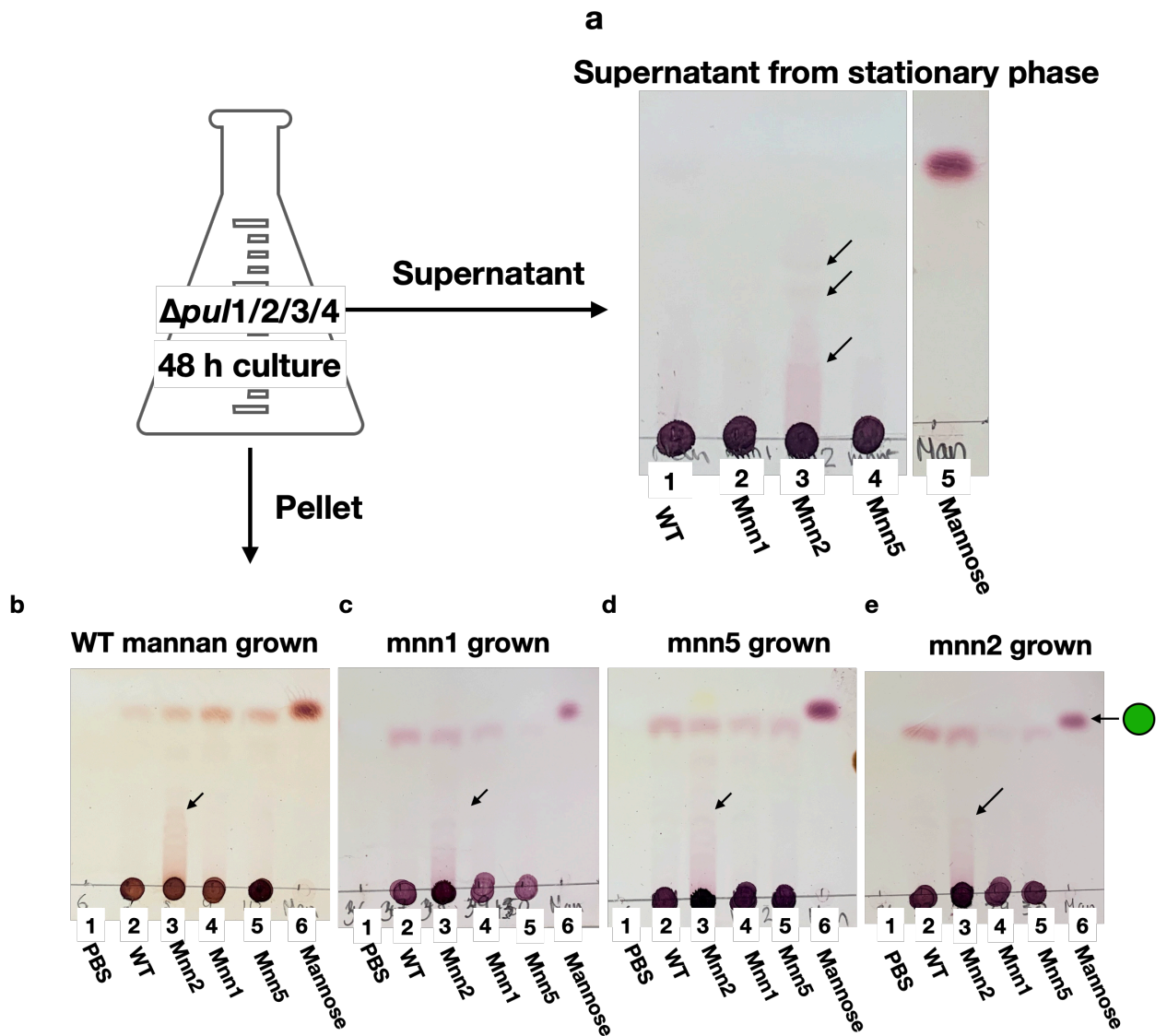


Figure 3. 25 Analysis of $\Delta pul1/2/3/4$ growth on α -mannan variants. Panel a: TLC analysis of spent media taken from stationary phase after growths shown in Figure 3.26. Panels b-e, activity of $\Delta pul1/2/3/4$ cells collected after growths on WT (b), mnn1 (c), mnn5 (d), mnn2 (e) mannan variants shown in Figure 3.26 against indicated mannan substrates. Arrows show oligosaccharides, mannose is shown as a green circle. Data are representative of 2 technical repeats.

3. 3. 10 Possible endo-acting mannanases in Bt $\Delta pul1/2/3/4$

The ability of $\Delta pul1/2/3/4$ to grow on both *C. albicans* and mnn2 mannan was highly unexpected. Previous transcriptomics analysis by Martens et al. (2008) identified that three PULs were upregulated in Bt in response to α -mannan. These

were characterised by Cuskin et al. (2015b). Martens et al. (2008) also showed that α -mannan induced low expression of the bt2559-bt2260 SusCD pair, but the activation of this complex was stronger in response to LacNAc or porcine mucins. Moreover, this pair is located in a literature-derived PUL, which is not predicted to contain enzymes. Analysis of nearby proteins did not reveal any potential mannan specific enzymes. However, combined data presented in this chapter suggested that degradation of mannan from *C. albicans* requires additional enzymes. Growth of Bt $\Delta pul1/2/3/4$ on mnn2 mannan suggested that an additional α -1,6 endo-mannanase is expressed on the cell surface.

Bt encodes nine α -1,6 endo-mannanases, four of which (BT2623 and BT2631, BT3782 and BT3792) are located in MAN-PUL1 and MAN-PUL2, respectively (Table 3. 2). The remaining five (BT3501, BT3521, BT3524, BT2949, BT3301) encoded outside three mannan PULs (Table 3. 2). The gene region BT2620-BT3532 is a possible mannan PUL, as it contains two GH76 endo-mannanases (BT3521 and BT3524) two GH92 α -mannosidases (BT3530 and BT3527) and one GH125 α -1,6-mannosidase, BT3528. The extensive analysis of GH92s from Bt previously conducted in our lab showed that the two GH92: BT3530 and BT3527 display activity against yeast α -mannan (Zhu et al., 2010). SignalP analysis of both GH76s, BT3524 and BT3521, showed that they carry SPI and SPII N-terminal signals, respectively. This suggested that BT3521 could act as a surface mannanase. The two other candidates for possible endo-mannanases could be BT3301 and BT2949, both of which contain SPII sites, indicating that they are probably localised to the cell surface. BT3301 displayed activity on linear α -1,6-backbone of yeast α -mannan but not against branched mannan variants (Chapter

4). The PUL containing BT2949, also encodes for BT2948, GH92, previously characterised in our lab to be active against yeast α -mannan (Zhu et al., 2010)

GH76	PUL	Signal Peptide	WT Bt	Bt $\Delta pul1/2/3/4$
BT2623	MAN-PUL-1	I	✓	✗
BT2631	MAN-PUL-1	I	✓	✗
BT3782	MAN-PUL-2	I	✓	✗
BT3792	MAN-PUL-2	II	✓	✗
BT3501	Predicted PUL-59	II	✓	✓
BT3521	Predicted PUL-60	II	✓	✓
BT3524	Predicted PUL-60	I	✓	✓
BT2949	Predicted PUL-40	II	✓	✓
BT3301	Predicted PUL-53	II	✓	✓

Table 3. 2 GH76 in Bt. Bt encodes 9 GH76, located in indicated PULs. Signal peptide was assessed with SignalP 5.0. “✓” – genes present, “✗” – genes deleted.

To test whether any of these GH76 mediated mannan breakdown in $\Delta pul1/2/3/4$, their expression was quantified by qPCR. WT Bt and Bt $\Delta pul1/2/3/4$ were grown in minimal media on *S. cerevisiae* mannan or glucose to mid-exponential phase (OD_{600} = 0.6-0.8). Cells were collected and RNA was extracted with RNeasy Mini Kit (Qiagen, Germany). RNA was converted to cDNA with QuantiTec Reverse transcription kit (Qiagen, Germany). The relative levels of expression of bt3501, bt3521, bt2949, bt3301 were determined by qPCR using primers specific for each gene and compared to glucose-grown cells. This analysis showed that none of these GH76 were significantly upregulated in $\Delta pul1/2/3/4$ in response to *S. cerevisiae* mannan (Figure 3.). This indicates that these enzymes are not

upregulated in $\Delta pul1/2/3/4$ and it still remains unclear, which enzymes are contributing to mannan breakdown in this strain.

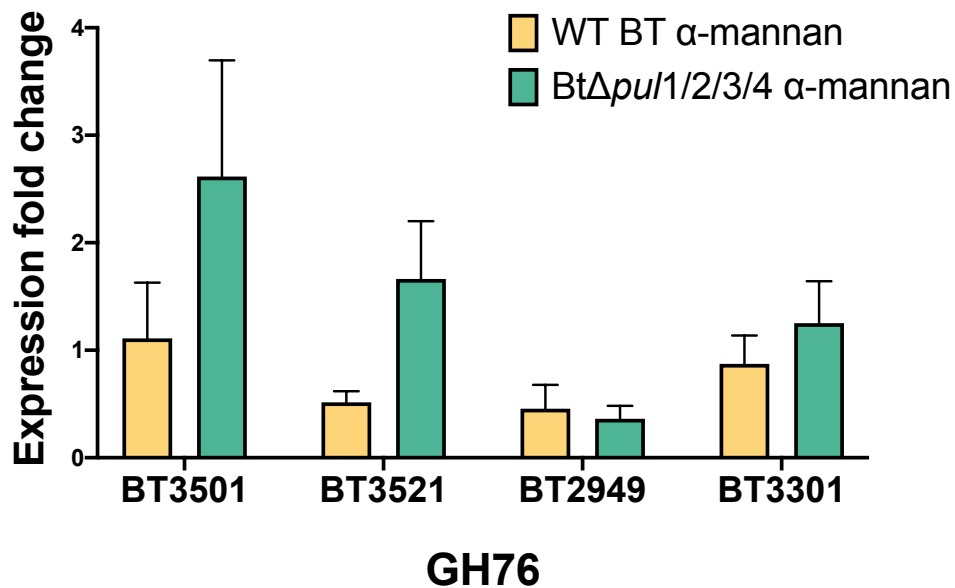


Figure 3. 28 Expression of GH76s in Bt $\Delta pul1/2/3/4$ and Bt WT in response to *S. cerevisiae* mannan. Expression levels shown are relative to glucose-grown cells. $\Delta pul1/2/3/4$ is shown in green, WT Bt is in yellow, error bars show SE from 3 biological replicates.

3. 3 Discussion

This chapter aimed to characterise the breakdown of *C. albicans* mannan by Bt. This process involves enzymes from the GH130 family to remove the β -mannosidic linkage which uniquely cap this mannan. The GH130 family is comprised of exo- β -mannoside phosphorylases and exo- β -mannosidases. Phosphorylases use phosphate to initiate nucleophilic attack at C1 of Man₁ at the -1 subsite to cleave glycosidic bonds. This mechanism is mediated by the three highly conserved basic amino acid residues (Ladevèze et al., 2015). Glycoside hydrolases lack these three basic amino acids to interact with the phosphate but contain lysine at the active site, which was suggested to interact with O₂ of Man₂

and allow water to act as a nucleophile. This lysine residue also acts as a specificity determinant for β -1,2-mannosides (Cuskin et al., 2015a).

Two additional glycoside hydrolases, BT4094 and CaGH130, from the GH130 family were biochemically characterised in this chapter. Both BT4094 and CaGH130 were able to hydrolyse β -1,2-mannooligosaccharides, released from *C. albicans* mannan, into mannose, in a similar manner to BT3780. However, despite this, all three GH130s exhibited different enzymatic activity against complex β -1,2-mannosyl substrates, such as mannan from *C. albicans*. The spectrophotometric assays indicated that BT3780 acts as a broad specificity β -1,2-mannosidase, whereas BT4094 and CaGH130 display narrower specificities against β -mannan. Generally, enzymes from the GH130 family can recognise a range of sugars at the +1 subsite, which could be glucose, mannose, or GlcNAc. The crystal structure of BT3780 showed Lys199 determines β -1,2-mannosidic activity, as it recognises mannose at the +1 subsite (Cuskin et al., 2015a). In BT3780, three main residues, Lys199, Arg89, and Glu141 interact with O₂, O₃, O₄, and O₆, of Man₂ (Cuskin et al., 2015a), indicating that BT3780 lacks interactions with O₁ and therefore can recognise mannose in both β - and α - configurations. This suggests that BT3780 is probably capable of removing β -mannosyl caps from *C. albicans* mannan. It is possible that BT4094 and CaGH130 can only cleave glycosidic bonds between sugars in β -configuration but both proteins possess identical Lys199, Arg89, and Glu141, suggesting that narrow specificity of these enzymes for *C. albicans* mannan is mediated by other structural residues. However, the overlay of a predicted structure of BT4094 with BT3780 did not reveal any obvious differences. Activity of BT4094 and CaGH130 could be further analysed with small manno-oligosaccharides such as man- β 1,2-man- α 1,2-man or mannan from *C. albicans*

strains, which contains a single β -1,2 mannose attached to α -mannan in the acid stable mannan, such as that found in *Cabmt4* strains (Mille et al., 2008). In addition, *C. albicans* deficient in BMT5 and BMT6 produce cells walls with aberrant β -mannosylation of phospholipomannan (PLM) (Mille et al., 2012, Murciano et al., 2011). Therefore, it would be interesting to examine whether any of these enzymes display preference for acid stable or acid labile β -mannan of the cell wall. A crystal structure of both BT4094 and CaGH130 may provide further understanding of substrate recognition.

Analysis of kinetic parameters of BT4094 and CaGH130 suggested that these two enzymes probably perform two biologically distinct roles. Indeed, BT4094 contains a S_{PII} cleavage site, indicating that it is probably located on the cell surface, and is likely to be one of the enzymes which produces extracellular mannose in assays with whole Bt cells. In contrast, CaGH130 lacks a signal peptide, suggesting that it performs its function intracellularly. An extensive transcriptomic analysis by Azadmanesh et al. (2017) and Witchley et al. (2019) showed that this enzyme is upregulated in hypha inducing conditions. Hyphal morphology is usually associated with virulence, however an extensive screen of *C. albicans* deletion strains showed that the absence of orf19.6637 did not result in defective virulence, morphogenesis, or proliferation (Noble et al., 2010). Another study showed that orf19.6637 is down regulated upon adaptation of *C. albicans* to the anaerobic environment of murine gut (Znaidi et al., 2018). In *C. albicans* formation of hyphae is a stress response mechanism, which is triggered by changes in nutritional or environmental cues, and results in extensive cell wall reorganisation (Ballou et al., 2016, Sherrington et al., 2017, Pradhan et al., 2018). This therefore suggests that orf19.6637 can potentially modulate mannosylation of glycoproteins intracellularly,

contributing to the process of cell wall remodelling, however its exact function needs to be further investigated.

The second part of this chapter attempted to characterise the role of two β -mannosidases from Bt in the breakdown of *C. albicans* mannan. Deletion of BT4094 did not result in a defective phenotype *in vivo*, demonstrating that the loss of this enzyme is not critical and could be compensated by BT3780. In contrast, Bt strain lacking BT3780 displayed a growth defect, suggesting that BT3780 is one of the key enzymes driving *C. albicans* mannan depolymerisation in Bt.

Unexpectedly, simultaneous deletion of both β -mannosidases, BT3780 and BT4094, did not completely abort the ability of Bt to utilise *C. albicans* mannan but only slightly reduced it. Analysis of the supernatant from the stationary phase revealed that the strain $\Delta bt3780 + \Delta bt4094$ liberates a ladder of β -mannooligosaccharides. A similar ladder was generated in the whole cell assays. This ladder of oligosaccharides was retained in the extracellular milieu even when all four mannan PULs were deleted. Combined, this suggests the presence of an additional putative endo-acting mannanase, which can cleave β -1,2-mannooligosaccharides from *C. albicans* mannan. This putative enzyme is not encoded in PUL-4 or three characterised mannan PULs. To date, any of the GH families are not known to contain enzymes with such activity, making it difficult to identify potential candidates. It is also possible that β -mannooligosaccharides can be released from mannan with an uncharacterised enzyme from the GH99 family. Attempted degradation of *C. albicans* mannan using enzymes from MAN-PUL1, MAN-PUL2, MAN-PUL3 in various cocktails were not sufficient to expose the α -1,6 backbone for endo-mannanases. The architecture of *C. albicans* mannan is

more complex compared to *S. cerevisiae* α -mannan. Ballou et al. (1974) suggested that the longest sidechain in *S. cerevisiae* mannan is a pentasaccharide composed of man- α 1,3-man- α 1,3-man- α 1,2-man- α 1,2-man, whereas in *C. albicans* sidechains are decorated with β -1,2 mannosyl caps, extending them up to an octasaccharide at some branch points (Shibata et al., 2007). Moreover, some α -1,3 sidechains within the matrix are capped with single α -1,6-mannosides (Shibata et al., 2007). It is possible that these features sterically restrict mannan from degradation by the enzymes in MAN-PUL1-2-3 and, thus, making it possible that depolymerisation of *C. albicans* mannan requires a more extensive repertoire of enzymes.

Experimental data indicated that MAN-PUL2, encoding BT3780, plays a crucial role in *C. albicans* mannan breakdown, as its deletion resulted in a profound growth defect. However, Bt strain lacking three mannan PULs was still able to utilise *C. albicans* mannan. The second β -mannosidase, BT4094, is enclosed in a completely different PUL in the genome of Bt. This PUL was hypothesised to mediate the residual growth of $\Delta pul1/2/3$ on *C. albicans* mannan. Surprisingly, deletion of PUL-4 in the background of three mannan PULs partially rescued a previously defective phenotype of $\Delta pul1/2/3$. The restored ability of the new $\Delta pul1/2/3/4$ strain to grow on mannan from *C. albicans* and *S. cerevisiae* was highly unexpected but suggested that mannan breakdown could be mediated by an additional putative locus. It was hypothesised that this additional locus would contain an endo acting GH76, which we attempted to identify by qPCR. This however showed that none of the GH76 grouped in known PULs were upregulated in $\Delta pul1/2/3/4$ in response to mannan. Comparative proteomics or transcriptomics might be able to identify this additional PUL.

These data also suggested that MAN-PUL4 contains a regulator for this putative locus. Regulation of PUL expression in *Bacteroides* spp. occurs via 3 known mechanisms. In starch utilisation system (Sus), constitutively expressed SusR controls transcription of structural proteins within the system by enhancing their expression in response to maltose and longer glucose polymers (D'elia and Salyers, 1996b, Cho et al., 2001). Mucin O-glycan degrading PULs are regulated by sigma factor (ECF- σ)/ anti- σ factor pairs, where the extracytoplasmic sigma factor is repressed by a transmembrane anti- σ factor, which interacts with SusC (Martens et al., 2008). In inducible conditions, TBDT undergoes a conformational change and releases sigma-factor, which then controls gene expression (Davis et al., 2017). Some PULs, including MAN-PUL1 and MAN-PUL2, are regulated with Hybrid Two Component Systems (HTCS), which involve a multi-step phosphorylation cascade in response to an inducible factor (Lowe et al., 2012). Interestingly, upstream of BT4072, MAN-PUL4 contains a SusR (BT4069) and a sigma factor (ECF- σ) (BT4070), located next to a protein of unknown function, BT4071. BlastP search showed that BT4071 shares 64% identity with an anti- σ factor from *Bacteroides faecis*. Generally, ECF- σ is co-encoded with its own anti- σ factor (Davis et al., 2017), suggesting that it is probable that BT4071 acts as an anti- σ factor. A possible explanation for the unexpected phenotype of Bt $\Delta pul1/2/3/4$ could be that the loss of the natural target for the regulatory complex (SusR^{BT4079}-ECF- σ ^{BT4070}-anti- σ ^{BT4071}) resulted in aberrant expression of additional putative loci, mediating mannan breakdown. This hypothesis could be tested by deletion of SusR^{BT4079}-ECF- σ ^{BT4070}-anti- σ ^{BT4071} in Bt $\Delta pul1/2/3/4$ to investigate whether the unusual phenotype is lost. Alternatively, the regulatory complex could be disrupted by deletion of the anti- σ ^{BT4071} factor in Bt $\Delta pul1/2/3$ to investigate

whether this could be sufficient to rescue the ability of the strain to utilise yeast α -mannan.

Data presented in this chapter indicates that PUL4 is not essential for mannan utilisation. Deletion of this PUL did not affect the ability of Bt to grow on mannan. Recombinantly expressed proteins from PUL4 did not display activity against *C. albicans* mannan when they were assayed either individually or combined in cocktails. An extensive transcriptome analysis by Martens et al. (2008) showed that the gene region bt4080-bt4084 is upregulated *in vitro* in response to PGM and not yeast α -mannan. This was also replicated by Marcobal et al. (2011), who showed that the region bt4079-bt4084 was upregulated in response to PGM. A recent study by Zimmermann et al. (2019) demonstrated that Bt actively converts 18 drugs to 41 different metabolites, using a range of carbohydrate esterases. In this study, it was shown that BT4096, an esterase downstream of BT4094, deacylates diltiazem, a calcium channel blocker used to treat hypertension and angina. BT4075 performs metabolism of roxatidine acetate, an H₂ antagonist used to treat gastric ulcers. Protein of unknown function, BT4091, was characterised as an esterase contributing to metabolism of a topical corticosteroid, diflorasone diacetate and an antiviral drug, Famiclovir (Zimmermann et al., 2019). Genes in PULs are usually co-transcribed to facilitate efficient catabolism of the target substrates. As shown in this chapter, mannosidases BT4072^{GH38} or BT4092^{GH92}, BT4093^{GH92} or BT4073^{GH92} do not display activity against *C. albicans* mannan. Despite containing an enzyme specific to unique β -1,2 mannosyl linkages found in *C. albicans* mannan, it is likely that *C. albicans* mannan is not the target polysaccharide for the operon BT4072-BT4096. Considering the amount of esterases encoded in this PUL and the fact that it is upregulated in response to

PGM, it is possible that it could be contributing to deacetylation of sialic acid.

However, plant polysaccharides are extensively decorated with acetyl groups, and therefore it is possible that this PUL could be targeting a polysaccharide from plant origin.

Chapter 4: *Bacteroides salyersiae* deploys a non-selfish mechanism for degradation of mannan from *S. cerevisiae*.

4. 1 Introduction

Cuskin et al. (2015b) established that six *Bacteroides* species and three *Parabacteroides* species were able to utilise α -mannan from *S. cerevisiae*. *Bacteroides* species included: 34 strains of *B. thetaiotaomicron*, 25 strains of *B. ovatus*, 5 strains of *B. salyersiae*, 19 strains of *B. xylanisolvens*, 29 strains of *B. vulgatus*, and 12 strains of *B. caccae* (Cuskin et al., 2015b). *In vivo* assays showed that Bt strain $\Delta pul1/2/3$ could outcompete wild-type Bt when mice were fed a diet lacking yeast mannan. However, the fitness was shifted towards the wild-type strain when α -mannan was introduced back into the diet (Cuskin et al., 2015b). This indicates that possession of mannan-degrading loci is disadvantageous in a situation when yeast mannan is unavailable. Therefore, considering a high selective pressure of the densely populated gut, it would be logical to assume that if mannan was absent in the gut, Bt would lose PULs dedicated for its degradation to gain a competitive advantage (Cuskin et al., 2015b). However, interestingly, this is not the case as metagenomic data collected from 250 adult humans revealed that at least 1 of the mannan PULs, predominantly MAN-PUL2 and MAN-PUL3, was detected in 60% of humans (Cuskin et al., 2015b). Genome analysis revealed that MAN-PUL1 was acquired by *B. xylanisolvens* strains *NLAE-zl* P732; P352; P393; P736; P727 isolated from

the large intestine of pigs fed on distillers grain diet, which contains highly branched yeast mannan. Bx strains *NLAE-zl* P732; P352 could grow on less branched *S. cerevisiae* mannan variants *in vitro*. However, *in vitro* competition assays showed that Bt outcompetes Bx, indicating that the 'selfish' mechanism does not permit sharing (Cuskin et al., 2015b). This therefore suggests that other residents of the microbiota debranch α -mannan, making it accessible to Bx. Yeast α -mannan is a highly complex polysaccharide, depolymerisation of which is metabolically costly. Therefore, it was hypothesised the 'selfish' mechanism is retained in all mannan-utilising gut *Bacteroides* and is orchestrated by structurally similar PULs. However, some *B. salyersiae* strains were able to grow on yeast mannan to a higher OD₆₀₀ than Bt, despite lacking PULs with synteny to the mannan PULs in Bt (Cuskin et al., 2015b). This observation was contradictory to the previous hypothesis and was addressed in this chapter.

4. 2 Objectives

1. Investigate the mechanism of yeast α -mannan breakdown in *B. salyersiae*
2. Identify PULs mediating mannan degradation in *B. salyersiae*
3. Undertake biochemical characterisation of the enzymatic apparatus implementing mannan breakdown.
4. Investigate the role of yeast α -mannan breakdown by *B. salyersiae* in cross-feeding other species

4. 3 Results

4. 3. 1 Growth analysis of *Bacteroides* spp on mannan from *S. cerevisiae*

B. thetaiotaomicron VPI-5482 (*Bt*), *B. cellulolsilyticus* DSM 14838 (*Bcell*), *B. xylanisolvens* DSM 18836 (*Bx*), *B. ovatus* ATCC 8483 (*Bo*), *B. salyersiae* WAL10018 (*Bs*), *Dysgonomonas gadei* ATCC BAA-286 (*Dg*), *B. caccae* ATCC 4318 (*Bc*), *B. intestinalis* DSM 17393 (*Bint*), *B. finegoldii* DSM 17565 (*Bfine*), *B. eggerthii* ATCC 27754 (*Begg*), *B. vulgatus* ATCC 8482 (*Bv*), *B. fragilis* ATCC 25285 (*Bf*) were grown anaerobically in minimal media containing mannan from *S. cerevisiae* for 48 h. Growth analysis showed that the type strains of *Bx*, *Bo*, and *Bcell* display poor growth on yeast mannan compared to *Bt* (Figure 4. 1 a). Consistent with Cuskin et al. (2015b), *B. salyersiae* grew to a higher OD₆₀₀ on mannan from wild type *S. cerevisiae* than *Bt* (Figure 4. 1 b). Unlike *Bt*, *Bs* exhibited a 17h lag phase which was followed by a rapid exponential growth (Figure 4. 1 b), suggesting that *Bs* requires a longer period of time to upregulate the degradation apparatus than *Bt*. Cell-free supernatant collected from the stationary phase was analysed with TLC. This showed that unlike other *Bacteroides* species including *Bt*, *Bs* degrades mannan differently as bands suggestive of large manno-oligosaccharides were found in the supernatant post *B. salyersiae* growth on *S. cerevisiae* mannan (Figure 4. 1 c).

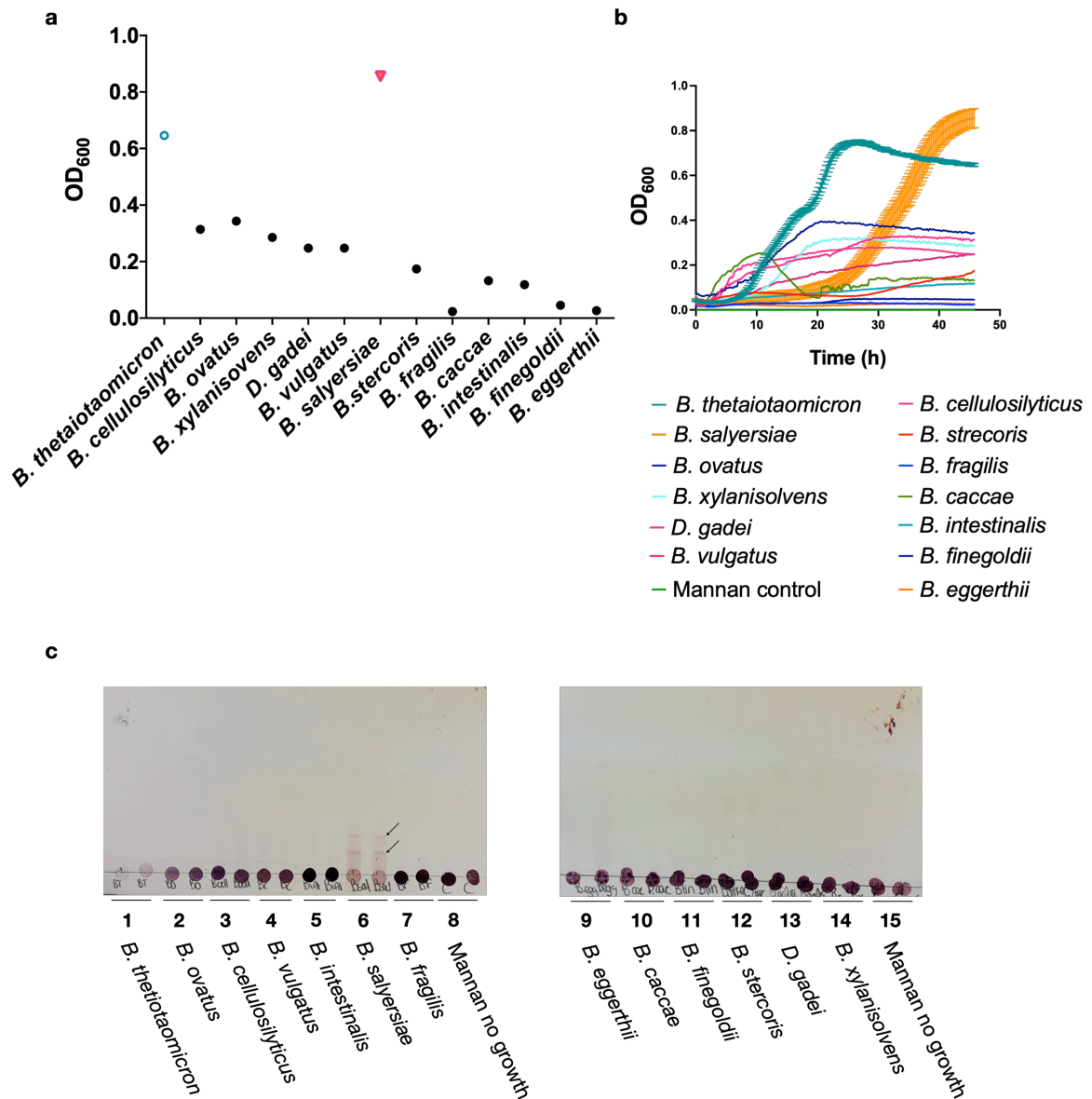


Figure 4. 1 Growth of *Bacteroides* spp. on mannan from *S. cerevisiae*. 13 different *Bacteroides* species were grown on minimal media with 10 mg ml⁻¹ *S. cerevisiae* mannan 37 °C for 48 h. Mean and error bars were generated from three technical replicates; dataset is representative of at least 2 independent experiments. Panel a: OD₆₀₀ at stationary phase taken post bacterial growth on *S. cerevisiae* mannan. Values shown on the graph are a mean of three biological replicates; Panel b: growth curves of *Bacteroides* species on *S. cerevisiae* mannan monitored at regular intervals; Panel c: TLC of cell free culture supernatant after 48 h growths. Lanes represent 2 biological replicates.

4. 3. 2 *S. cerevisiae* mannan degradation by *B. salyersiae* occurs extracellularly

The mechanism of *S. cerevisiae* mannan degradation in *B. salyersiae* was then investigated. Bs was grown in defined media with mannan and culture was collected at time points between 0 – 21 hours. Cells were separated by centrifugation at 13,000 rpm for 1 min and cell free spent media was analysed with TLC. This revealed that oligosaccharides were released in the culture supernatant as Bs was approaching early mid-exponential phase ($OD_{590}=0.49$) (Figure 4. 2 b). As the growth progressed, mannose was accumulated in the media, this was then followed by a ladder suggestive of short oligosaccharides 4 hours post inoculation (Figure 4. 2 b). As the growth continued the bands became more apparent, indicating that longer oligosaccharides were progressively released into the culture supernatant (Figure 4. 2 b). These data suggest that Bs begins mannan utilisation by gradually trimming off mannose from the side chains, making them more accessible for endo-acting mannanases. It is unusual that Bs accumulates mannose extracellularly prior to robust growth, suggesting that mannose uptake is rate-limited and takes longer than mannose can be generated at the cell surface. The ladder of manno-oligosaccharides is characteristic of activity of surface endo-acting mannanases, such as BT2623^{GH76}, BT3792^{GH76} and BT3782^{GH76} expressed by Bt. Combined, these data suggest that Bs lacks a system mediating transport of complex mannooligosaccharides inside the cell, leaving a pool of fragments in the extracellular milieu. This contrasts the selfish mechanism previously described in Bt.

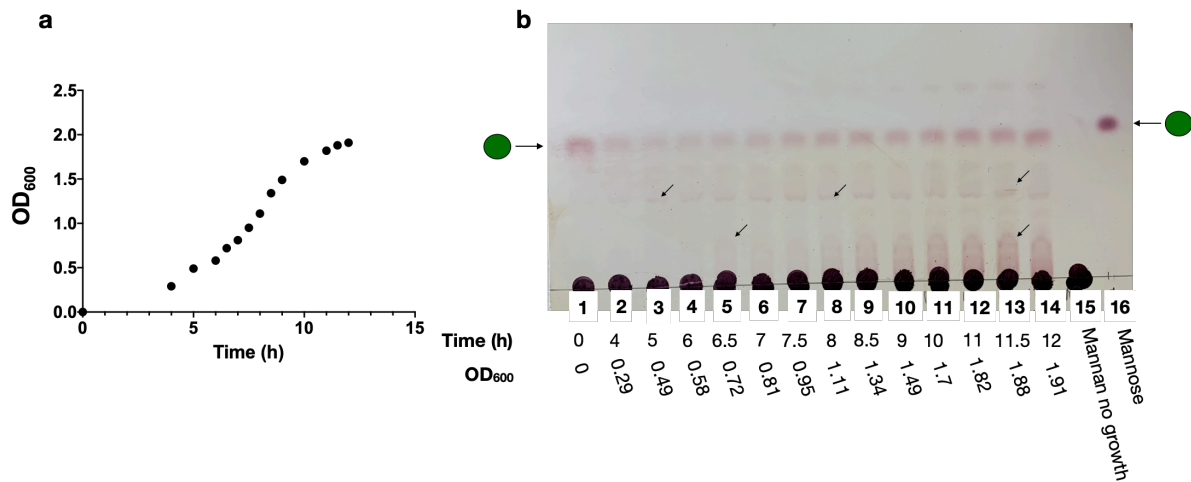


Figure 4. 2 Growth analysis of *B. salyersiae* on *S. cerevisiae* mannan. At each indicated time point, an aliquot was collected, cells were separated by centrifugation. Supernatant was analysed with TLC. Dataset is representative of at least three individual experiments. Panel a: Growth curve generated by *B. salyersiae* during growth on 10 mg ml⁻¹ *S. cerevisiae* mannan at 37 °C for 12 h. (b) TLC of cell free media. Arrows indicate oligosaccharides released into the culture supernatant by *B. salyersiae*. Substrate before bacterial growth is shown in lane 15. Mannose is shown as a green circle.

4. 3. 3 Activity of whole *B. salyersiae* cells against mannan from wild type, $\Delta mnn1$, and $\Delta mnn5$ *S. cerevisiae* strains

To investigate the location of mannan degrading enzymes in Bs, whole cell activity against mannan from *S. cerevisiae* was analysed. Bs was grown on mannan and cells from the mid-exponential phase (OD₅₉₀=0.8) were harvested, washed with sterile PBS three times, and resuspended in 1.5ml of PBS. A proportion of the cells was treated with proteinase K to degrade proteins located on the cell surface. Cells were then washed with PBS again to remove Proteinase K. Some cells were also lysed with BugBuster to investigate intracellular catabolic potential. Cells were then incubated with mannan variants aerobically, samples were taken at

regular intervals. Cells were separated by centrifugation and supernatants were analysed with TLC.

TLC analysis of this assay showed that whole cells liberate a ladder of long oligosaccharides from branched wild type mannan (Figure 4. 3 a), which were not produced by the lysed cells or the cells that were treated with Proteinase K (Figure 4. 3 b, c, d). Whole cell products were similar to the ones observed in the time-course supernatant assay (Figure 4. 2), confirming that mannan degradation was mediated by endo-mannanases localised to the surface. As the incubation time proceeded, a pool of mannose was gradually generated by the whole cells (Figure 4. 3 a). Interestingly, this was eradicated with proteinase K treatment (Figure 4. 3 b), indicating that accumulation of extracellular mannose was mediated by exo-acting enzymes localised on the cell surface. Assays with lysed cells revealed that mannan was broken down to mannose, demonstrating that *Bs* possesses a full metabolic potential to complete yeast mannan degradation intracellularly.

HPAEC-PAD analysis of supernatant also showed that mannose and a range of oligosaccharides were gradually accumulated by the whole cells (Figure 4. 4).

Overall, these data suggest that the breakdown of yeast mannan is orchestrated by exo- and endo-acting enzymes localised to the cell surface of *B. salyersiae*.

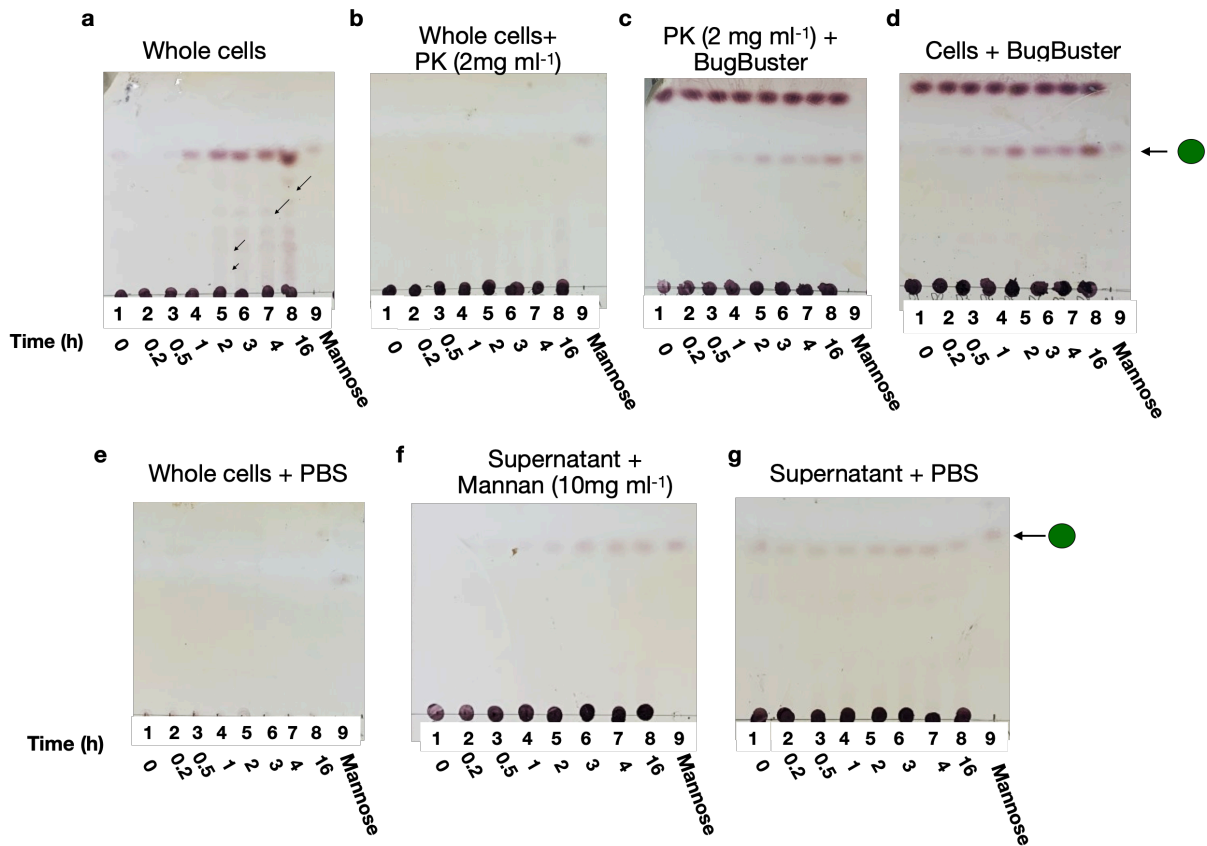


Figure 4. 3 Activity of whole *B. salyersiae* cells against *S. cerevisiae* mannan. Bs was on mannan to mid-exponential phase ($OD_{590}=0.8$). Harvested cells were washed with PBS three times and resuspended in sterile PBS. A fraction of the cells was incubated with proteinase to degrade proteins located on cell surface. Proteinase K was then washed off with PBS. Another fraction of the cells was lysed with BugBuster. Cells were incubated aerobically with 10 mg ml^{-1} *S. cerevisiae* mannan at 37°C . At each indicated time point an aliquot was taken out and supernatant was analysed with TLC and stained with Orcinol. Panel a: activity of whole cells, arrows indicate oligosaccharides. Panel b: activity of Proteinase K treated whole cells; Panel c: Activity of proteinase K treated cells lysed with BugBuster; Panel d: Activity of lysed Bs cells. A number of controls was also included: (e) activity of whole Bs cells without mannan (f) activity of supernatant against mannan (g) supernatant without a carbon source. Mannose is shown as a green circle, dataset is representative of 3 independent experiments.

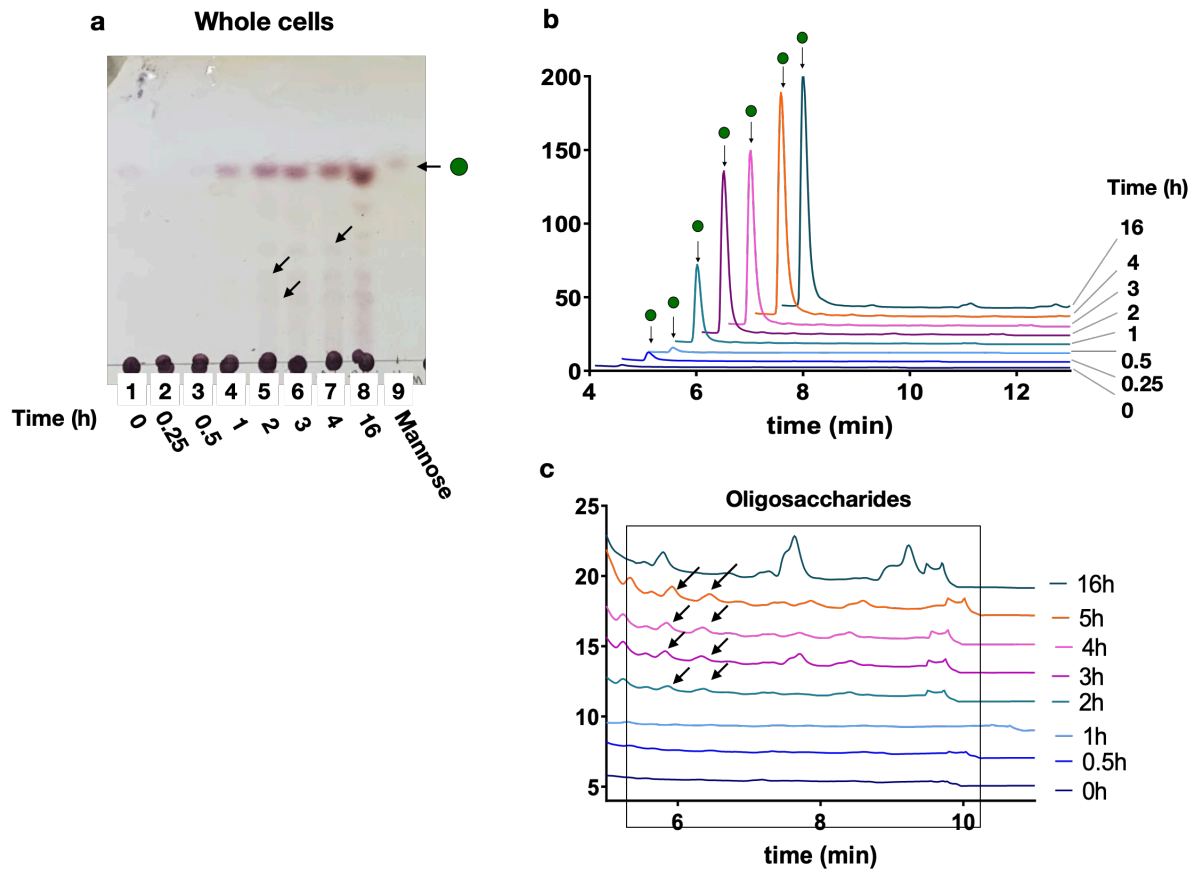


Figure 4. 4 HPAEC-PAD analysis of the whole cell assay. Products of the whole cell assay were analysed with HPAEC-PAD using CarboPac PA20 column. Mannose is shown as a green circle. Panel a: TLC analysis of the whole cell assay described in the figure 4.3. Panel b: HPAEC-PAD analysis of the whole cell assay; gradual mannose accumulation is illustrated by the increasing height of the mannose peak. Panel c: Gradual accumulation of oligosaccharides from the whole cell assay. Samples were analysed with a CarboPac PA200 column and were diluted 1:5 in distilled water.

The same assays with whole Bs cells against *mnn1* and *mnn5* *S. cerevisiae* mannan variants displayed similar activity, where a ladder indicative of manno-oligosaccharides and mannose were generated at the cell surface (Figure 4. 5 a; Figure 4. 6 a), which were eliminated with Proteinase K treatment (Figure 4. 5 b; Figure 4. 6 b). The ladder of oligosaccharides was not detected upon cell lysis, suggesting that Bs is able to complete hydrolysis of branched manno-oligosaccharides

intracellularly (Figure 4. 5 d-e; Figure 4. 6 d-e). Notably, debranching of mnn1 and mnn5 mannans by whole cells occurred more rapidly, as mannose and oligosaccharides could be detected at 30 min incubation time point (Figure 4. 5 a; Figure 4. 6 a). This is likely due to a reduced substrate complexity.

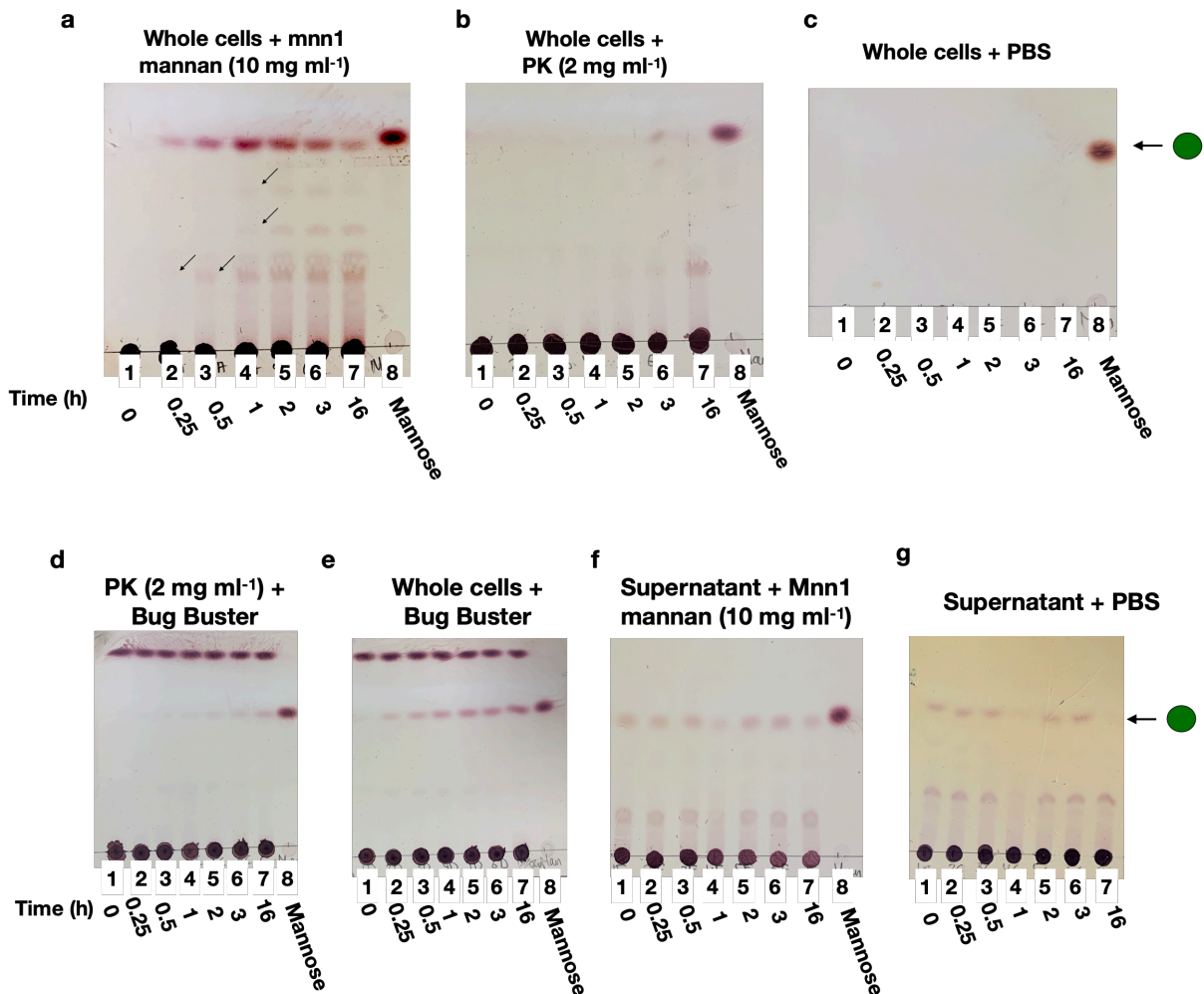


Figure 4. 5 Activity of whole *B. salyersiae* cells against mnn1 *S. cerevisiae* mannan. The experiment was conducted as described in Figure 4. 3, where the substrate was substituted for 10 mg ml⁻¹ mnn1 mannan. Panel a. Activity of whole intact cells; Panel b: activity of proteinase K treated whole cells; Panel c: whole cells without a carbon source; Panel d: activity of lysed proteinase K treated cells; Panel e: activity of lysed cells; Panel f: supernatant against mannan; g. supernatant against PBS. Mannose is shown as a green circle.

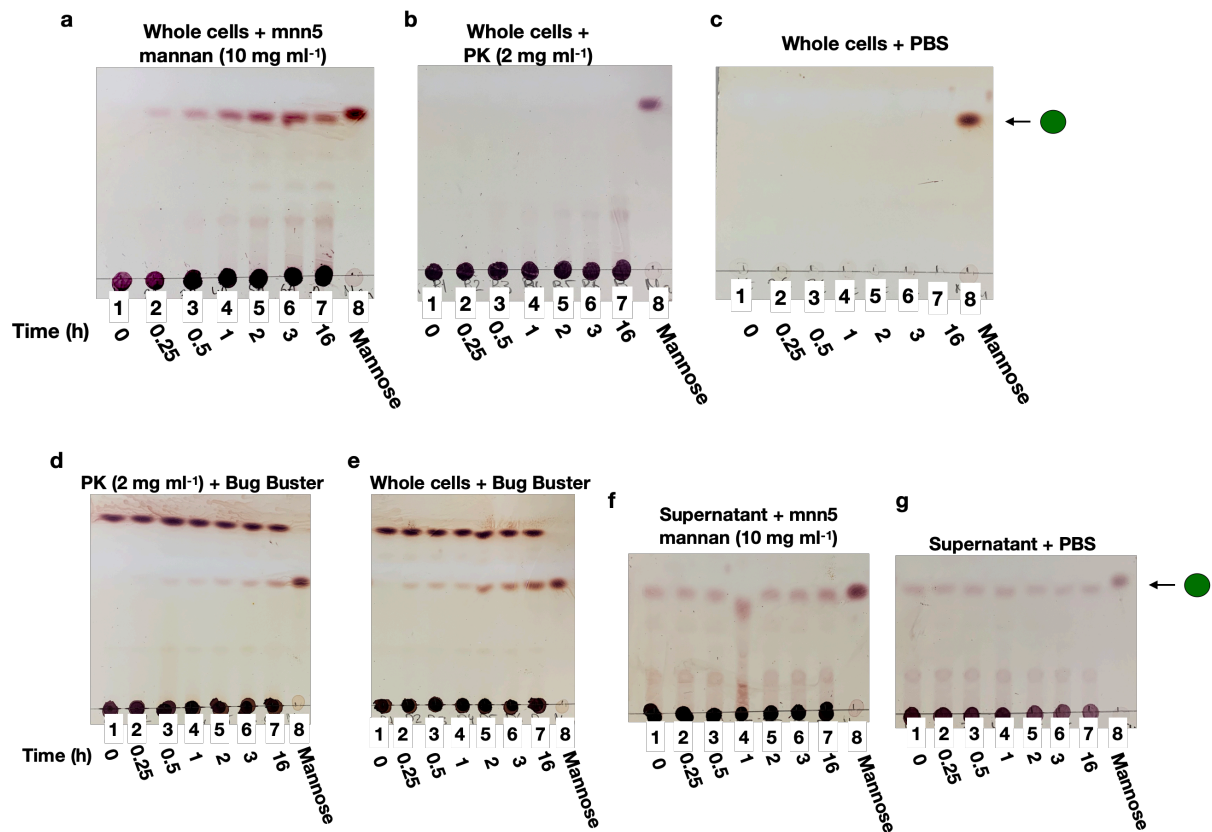


Figure 4. 6 Activity of whole *B. salyersiae* cells against *mnn5 S. cerevisiae* mannan. The experiment was conducted as described in Figure 4. 3, where the substrate was substituted for 10 mg ml⁻¹ *mnn5* mannan variant. Panel a. Activity of whole intact cells; panel b. proteinase K treated whole cells against mannan; panel c. whole cells without a carbon source; panel d. lysed proteinase K treated cells; panel e. lysed cells against *mnn5* mannan; panel f. supernatant incubated with mannan; Panel g. supernatant incubated with PBS.

4. 3. 4 Further analysis of manno-oligosaccharides generated by *B. salyersiae*.

To further investigate the nature of the oligosaccharides left in the culture supernatant by *B. salyersiae*. Cell-free media from *Bs* growth on mannan was subjected to an exo-mannosidase degradation assay. To do so, a range of previously characterised exo-mannosidases from *Bt*: BT4092^{GH92}, BT3858^{GH92}, and BT2632^{GH125}, targeting α -1,2, α -1,3, α -1,6-mannosidic bonds, respectively

(Cuskin et al., 2015b), were recombinantly expressed and used to degrade manno-oligosaccharides found in *Bs* spent media. Mannan disassembly by BT4092^{GH92}, BT3858^{GH92}, and BT2632^{GH125} is shown diagrammatically in Figure 4. 7. Endo-acting α -1,2-mannanase, BT3862^{GH99}, which produces α -1,3-mannobiose was also used to assess the extent of branching of mannan which was left in the supernatant. Enzymes were combined in order where an α -1,3-mannosidase, BT3858^{GH92}, was applied first, to remove α -1,3 sidechains (Figure 4. 7). This was then followed by BT4092^{GH92}, which can hydrolyse α -1,2-linkages and expose α -1,6 backbone to an α -1,6-mannosidase BT2632^{GH125} (Figure 4. 7).

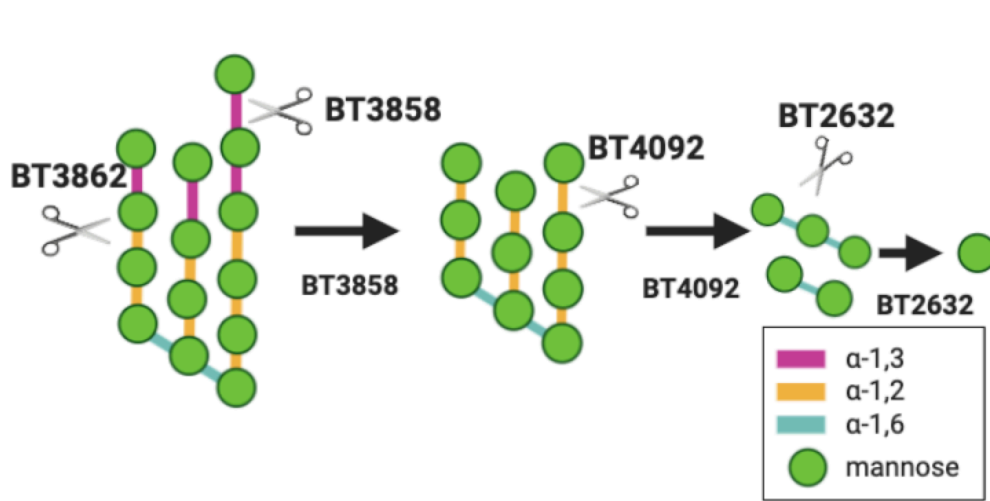










Figure 4. 7 Diagrammatic representation of exo-mannosidase degradation assay. BT3862 hydrolyses α -1,2 bond to produce an α -1,3 disaccharide. BT3858^{GH92} removes α -1,3- mannosyl caps, debranching *S. cerevisiae* mannan. This exposes α -1,2 linkages which are then removed by BT4092^{GH92}, producing long α -1,6 manno-oligosaccharides, which are hydrolysed into mannose by BT2632^{GH125}.

As shown in Figure 4.8, endo-acting α -1,2 mannanase, BT3862^{GH99} released α -1,3-mannobiose from mannan that was left in the supernatant (Figure 4. 8). This indicates that mannan that was left in the culture supernatant by *Bs* retains its α -1,3-mannosyl caps. Treatment of the supernatant with BT3858^{GH92} induced a

visible band shift and released mannose (Figure 4. 8), suggesting that the enzyme removes α -1,3-linked mannosides from the oligosaccharides left in spent media. Combining BT3858^{GH92} with BT3862^{GH99} removed α -1,3-disaccharide, demonstrating that BT3858^{GH92} indeed acts as an α -1,3-mannosidase (Figure 4. 8). This reaction did not result in any further movements of the bands, suggesting that BT3858^{GH92} releases all α -1,3-linked mannoses from mannan in the supernatant (Figure 4. 8). When the α -1,3-mannosidase, BT3858^{GH92}, was combined with BT4092^{GH92}, α -1,2 mannosidase, the band on the TLC resolved into two smaller bands (Figure 4. 8), indicating that the oligosaccharide has become smaller as more α -1,2 side chains were removed by BT4092^{GH92}. These oligosaccharides were then completely hydrolysed into mannose by BT2632^{GH125} (Figure 4. 8), demonstrating that they were joined by an α -1,6 linkage. Overall, this assay demonstrates that Bs is able to release pieces of branched oligosaccharides from *S. cerevisiae* mannan and leave them intact in the culture supernatant.

Enzyme	GH family	Mechanism	Bond	Product
BT3862	GH99	Endo	 α-1,2	α-1,3-man2 
BT4092	GH92	Exo	 α-1,2	Man 
BT3858	GH92	Exo	 α-1,3	Man 
BT2632	GH125	Exo	 α-1,6	Man 

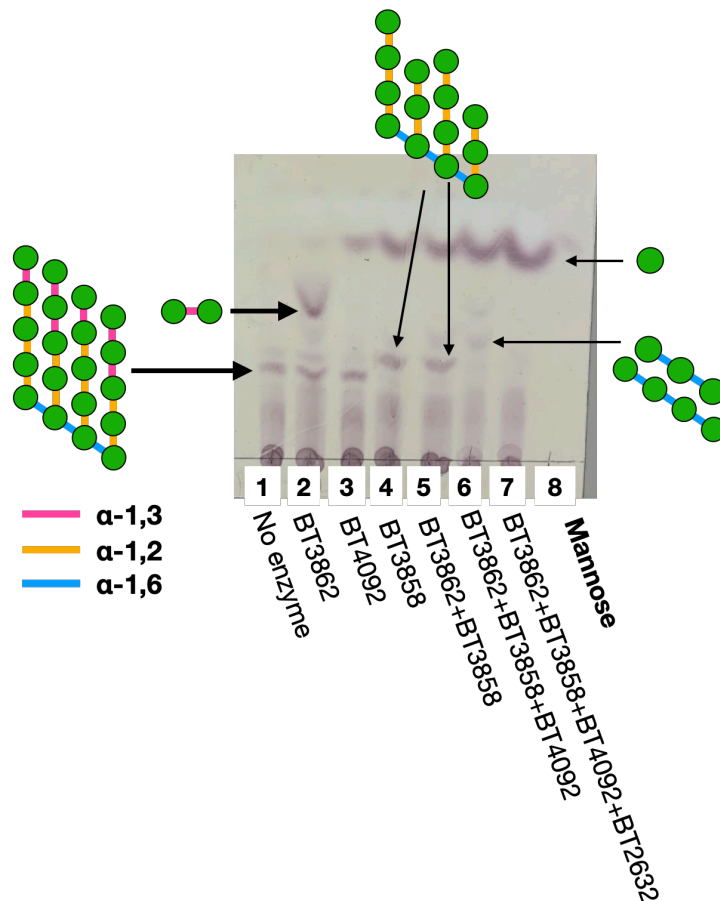
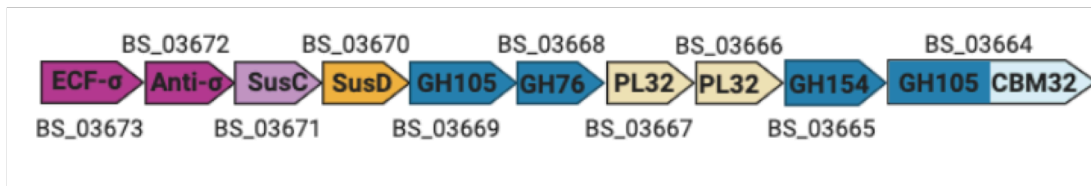


Figure 4. 8 Exo-mannosidase degradation assay of *B. salyersiae* supernatant. Bs was grown on mannan, cell free supernatant was then treated with a range of exo-mannosidases: BT3858^{GH92}; BT3862^{GH99}; BT4092^{GH92}; BT2632^{GH125} all at 1 μM, overnight at 37 °C. Lane 1: supernatant, lane 2 BT3862^{GH99} releases α-1,3 man2; lane 3 BT4092^{GH92} releases mannose; lane 4 BT3858^{GH92} removes α-1,3-linked mannose, induces a band shift; lane 5 BT3858^{GH92} and BT3862^{GH99} are combined together; lane 6 combination of BT3858^{GH92} and BT4092^{GH92} resolves the band in the supernatant into two; lane 7: BT2632^{GH125} hydrolyses products of BT4092^{GH92} and BT3858^{GH92} into mannose. Diagrammatically this assay is summarised in Figure 4.7.

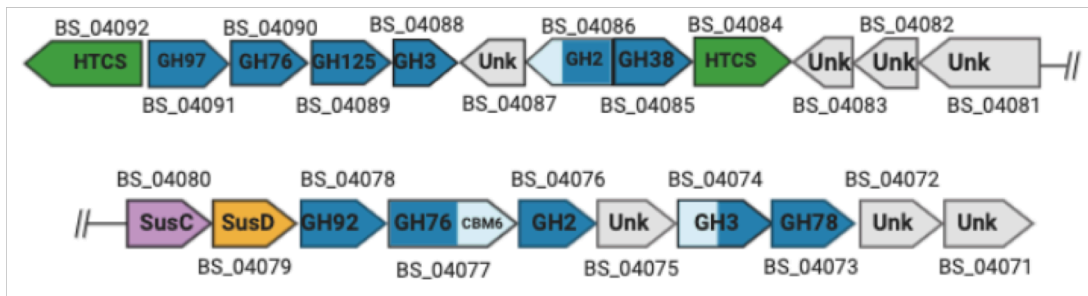
4. 3. 5 Identification of yeast α -mannan specific PULs in *B. salyersiae*

Using PULDB (<http://www.cazy.org/PULDB/>) the genome of *B. salyersiae* was searched for regions encoding endo-acting mannanases from the glycoside hydrolase 76 (GH76) family. This family includes a number of α -mannan specific endo-mannanases such as BT3782, BT3792, and BT2623, previously characterised by Cuskin et al. (2015b). This revealed that Bs possesses three GH76s: BS_03668, encoded within a predicted PUL50, labelled as Predicted Mannan PUL 2 (Figure 4. 9 a), BS_04077, enclosed in predicted PUL52, labelled as Mannan PUL 1 (Figure 4. 9 b) and BS_04090, found in a Cazyme cluster 6, adjacent to Mannan PUL 1 (Figure 4. 9 b). In addition to GH76s, the genome was searched for α -mannosidases from GH38 and GH92 families. While GH92s were scattered throughout the genome, two GH38 were found: BS_04085 grouped together with GH76 in the Cazyme cluster 6 (Figure 4. 9 b) and an orphan GH38, BS_01537, not grouped into a PUL (Figure 4. 9 c). Interestingly, BS_01537^{GH38} is positioned next to a GH2, whose family contains β -galactosidases and β -mannosidases, and a GH125, whose characterised members target α -1,6-mannosidic bonds found in the backbone of yeast mannan. Also, given the close proximity of PUL52 and Cazyme cluster 6, it could be that these two regions are a single large PUL (Figure 4. 9 b).

a Predicted Mannan PUL 2 (BS_03673 - BS_03664)



b Mannan PUL 1 (BS_04091 - BS_04071)



c not in PUL or Cluster (BS_01526 - BS_01525)

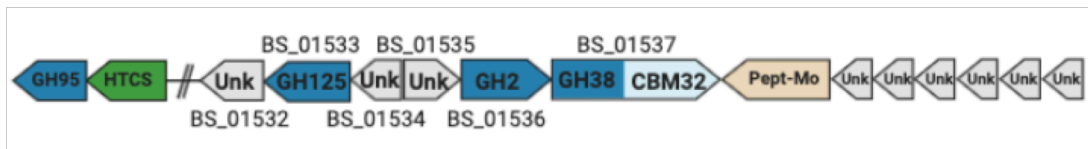


Figure 4. 9 Polysaccharide Utilisation Loci (PULs) from *B. salyersiae* WAL 10018. In the Cazy database (cazy.org) Bs WAL 10018 was predicted to possess three GH76s: BS_03668 in predicted mannan PUL 2 (a); BS_04077 and BS_04090 in Mannan PUL 1 (b). In addition, two exo-acting mannosidases from GH38 family were found: BS_04085 in Mannan PUL 1 (b) and BS_01537 in an orphan cluster (c). GH – glycoside hydrolase; unk- function unknown; SusC/SusC- transport proteins; HTCS – hybrid two component system; CBM – carbohydrate binding module; Pept-Mo – peptidase; PL – polysaccharide lyase.

To determine if any of the identified PULs were involved in mannan breakdown, protein profile upregulated in mannan-grown cells was assessed with comparative proteomics. This analysis was performed by Dr Tiaan Heunis, Newcastle University. The proteome expressed in response to *S. cerevisiae* mannan was normalised to the proteome profile of glucose-grown cells, proteins with a log₂ fold change >2 were considered upregulated, all of which passed p-value and q-value

cut off for statistical significance as described in Chapter 2 Section 2. 4. 7. In total, 582 proteins were detected, 43 of which were significantly upregulated and 45 were downregulated (Figure 4. 10). Proteins from the Mannan PUL 1 and the orphan cluster (Figure 4. 9 b and c) were located in the top 3% of the total proteome (Figure 4. 10 b) and are summarised in Table 4. 1. These included two GH76s from Mannan PUL 1: BS_04090 and BS_04077 along with GH38 BS_04085, GH92 BS_04078, and GH125 BS_04078. GH38, BS_01537, from the orphan cluster was also significantly upregulated together with GH2 and GH125, located adjacent to it. This analysis confirmed that proteins in Mannan PUL1 and the orphan cluster (Figure 4. 10 b) were likely to contribute to *S. cerevisiae* mannan degradation in *B. salyersiae*. Analysis of downregulated proteins showed that the majority of them were annotated as glucosidases.

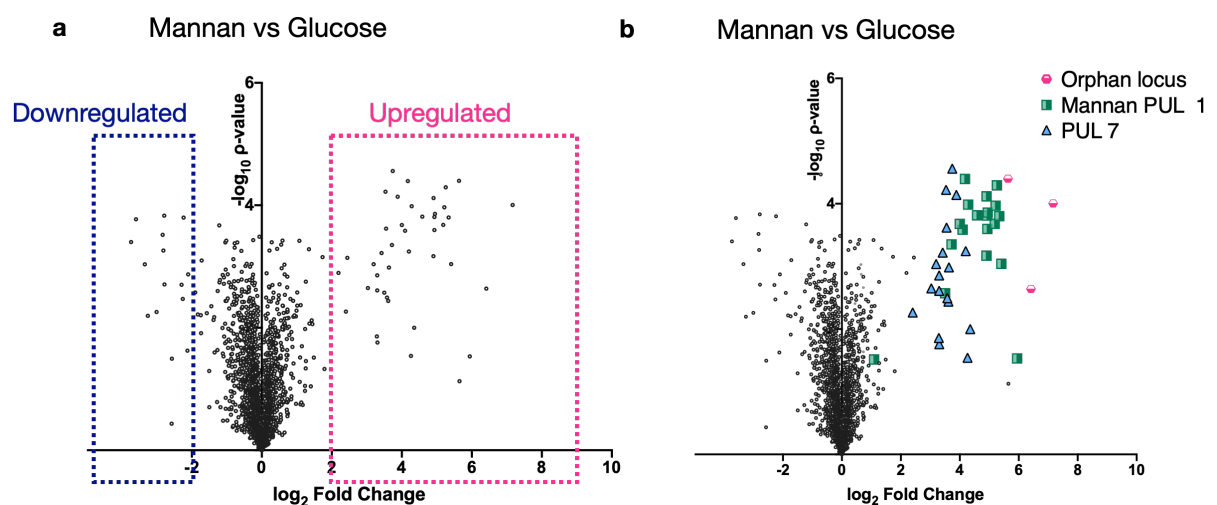


Figure 4. 10 Protein profile of *B. salyersiae* in response to yeast mannan. Comparative proteomics was performed on whole Bs cells grown on mannan and compared to glucose grown cells, all data points shown passed statistical significance. Panel a: differentially regulated proteins in response to mannan, $-2 > \log_2 > 2$ was taken as a cut off for downregulation (blue box) and upregulation (pink box), respectively; Panel b: Position of proteins from the orphan cluster, mannan PUL 1, and PUL 7 in the profile.

Protein	Locus tag in <i>B. salyersiae</i> WAL10018	Function	log2FC	p-value	protein FC
Orphan Cluster					
I8YYK1	HMPREF1532_01537	GH38	7.1656	0.00010	143.57
I8YX09	HMPREF1532_01535	unknown	6.4148	0.00230	85.32
I9TES1	HMPREF1532_01536	GH2	5.6353	0.02936	49.70
I8YYJ6	HMPREF1532_01532	epimerase	3.7429	0.00003	13.39
I9TFB4	HMPREF1532_01533	GH125	3.6137	0.00366	12.24
Mannan PUL-1					
I8YOL1	HMPREF1532_04090	GH76	5.9438	0.02936	61.55
I9SJA9	HMPREF1532_04076	GH2	5.4096	0.00091	42.51
I9SIM4	HMPREF1532_04089	GH125	5.3383	0.00016	40.46
I8XY58	HMPREF1532_04078	GH92	5.2571	0.00005	38.24
I9SJB8	HMPREF1532_04091	GH97	5.2153	0.00011	37.15
I9H857	HMPREF1532_04077	GH76	5.1851	0.00021	36.38
I9SIL7	HMPREF1532_04079	SusD	4.9469	0.00014	30.84
I9H853	HMPREF1532_04072	unknown	4.9325	0.00025	30.54
I8YOJ6	HMPREF1532_04075	unknown	4.9295	0.00016	30.47
I8YOK1	HMPREF1532_04080	SusC	4.9081	0.00008	30.03
I9SIL2	HMPREF1532_04074	GH3	4.9027	0.00068	29.91
I8XY55	HMPREF1532_04073	GH78	4.5863	0.00015	24.02
I9SJB6;I8YQM0	HMPREF1532_04086	GH2	4.1730	0.00004	18.04
I8YOK6	HMPREF1532_04085	GH38	4.0932	0.00026	17.07
I9H863	HMPREF1532_04087	esterase	4.0001	0.00021	16.00
I9SIM2	HMPREF1532_04084	HTCS	3.7172	0.00045	13.15
I9SJA4	HMPREF1532_04071	unknown	3.4998	0.00268	11.31
I9H868	HMPREF1532_04092	HTCS	1.0933	0.03058	2.13
I9SJB3	HMPREF1532_04081	unknown	4.2824	0.00010	19.46
PUL7					
I9TLQ8	HMPREF1532_00849	GH92	4.3521	0.01002	20.42
I8Z5C0	HMPREF1532_00843	unknown	4.2631	0.02877	19.20
I9IAJ9	HMPREF1532_00850	GH92	4.2021	0.00057	18.41
I9TLQ3	HMPREF1532_00844	unknown	3.8837	0.00007	14.76
I9IAJ2	HMPREF1532_00845	unknown	3.6311	0.00104	12.39
I8Z5C5	HMPREF1532_00848	unknown	3.5772	0.00322	11.94
I8Z3V1	HMPREF1532_00846	SusD	3.5509	0.00024	11.72
I9TL57	HMPREF1532_00847	SusC	3.5323	0.00006	11.57
I8Z3V7	HMPREF1532_00851	GH43	3.4193	0.00060	10.70
I9IAR0	HMPREF1532_00839	PUL7	3.3035	0.01741	9.87
I9TLX8	HMPREF1532_00838	unknown	3.2988	0.00139	9.84
I9TL53	HMPREF1532_00842	GH92	3.2981	0.00246	9.84
I8Z419	HMPREF1532_00840	GH78	3.2875	0.01386	9.76
I9TLY4	HMPREF1532_00837	GH51	3.1959	0.00092	9.16
I9TLB7	HMPREF1532_00841	GH78	3.0321	0.00224	8.18
I8Z4K0	HMPREF1532_00836	unknown	2.4019	0.00544	5.29

Table 4. 1 Table of upregulated proteins in *B. salyersiae* in response to *S. cerevisiae* mannan. Proteins listed are enclosed in either Mannan PUL 1 or the orphan cluster (Figure 4. 9). Colours correspond to: blue - characterised in this chapter, purple and orange - SusC and SusD from mannan PUL 1, pink - characterised in Chapter 5.

4. 3. 6 Domain analysis of GH76s: BS_04090^{GH76}, BS_04077^{GH76}, and BS_03668^{GH76}

Amino acid sequences of GH76s were analysed with a range of bioinformatics tools (SMART, SignalP 5.0, LipoP 1.0, and Psortb). This showed that BS_04090 contained a single GH76 domain and an N-terminal Signal Peptidase II (SPII) cleavage site (Figure 4. 11 a), indicating that it is a lipoprotein. Psortb results were inconclusive about cellular localisation of this protein. Using Clustal Omega (ebi.ac.uk/Tools/msa/clustalo/) it was identified that BS_04090 shared 44%, 36%, and 36% sequence identity with previously characterised surface GH76s from Bt: BT3782, BT2623, and BT3792, respectively (Figure 4. 11 d). Most proteins with SPII signals are lipoproteins, located on the cell surface. It was interesting to discover that BS_04090 also shared 76% sequence identity with another GH76 from Bt, BT3301. BT3301 was not upregulated in Bt in response to yeast α -mannan (Cuskin et al., 2015b), and is encoded outside the known mannan PULs in the genome of Bt.

BS_03668 protein was predicted to contain a GH76 and SCOP domain (Figure 4. 11 b), both Psortb or SignalP suggested that BS_03668 could contain a SPII cleavage site, however this prediction was inconclusive (SPI – 0.68 vs SPII – 0.23). Its closest orthologue (30% identity) in Bt was found to be BT2949 (Figure 4. 11 d), another GH76 not encoded in the mannan PULs. Despite not being detected in the proteomics data, it was decided to clone and express this protein to investigate how its activity differs from the two GH76s in the mannan PUL

BlastP search revealed that the third GH76 from Bs, BS_04077, was divergent from any proteins in Bt or other *Bacteroides spp* (Figure 4. 11 d), with closest homologues found in other Bacteroidales: *Porphyramonadaceae bacterium* and *Prevotella spp.*, sharing roughly 40% sequence identity with both. SMART analysis of BS_04077 showed that the protein contained a GH76 domain as well as carbohydrate binding motif 6 (CBM6), C-terminus was predicted to fold into a Pfam_F5_F8_type C (Figure 4. 11 c). In addition, it was predicted to contain a RICIN domain (Figure 4. 11), which was shown to mediate carbohydrate binding (Hirabayashi et al., 1998). In PULDB this protein was described as targeted for a “por secretion system”. IMG (img.jgi.doe.gov) also confirmed that the C-terminal domain of BS_04077 belonged to the TIGR04183 family, which is comprised of proteins directed to the secretion by the type 9 system (T9SS) (Discussed in Chapter 5). Both LipoP and SignalP analyses suggested that BS_04077 had a signal peptidase I site at the N-terminus, however Psortb identified BS_04077 as an outer membrane protein with a score of 9.49. Type 9 secretion system has never been described in *Bacteroides species* before and is further discussed in Chapter 5.

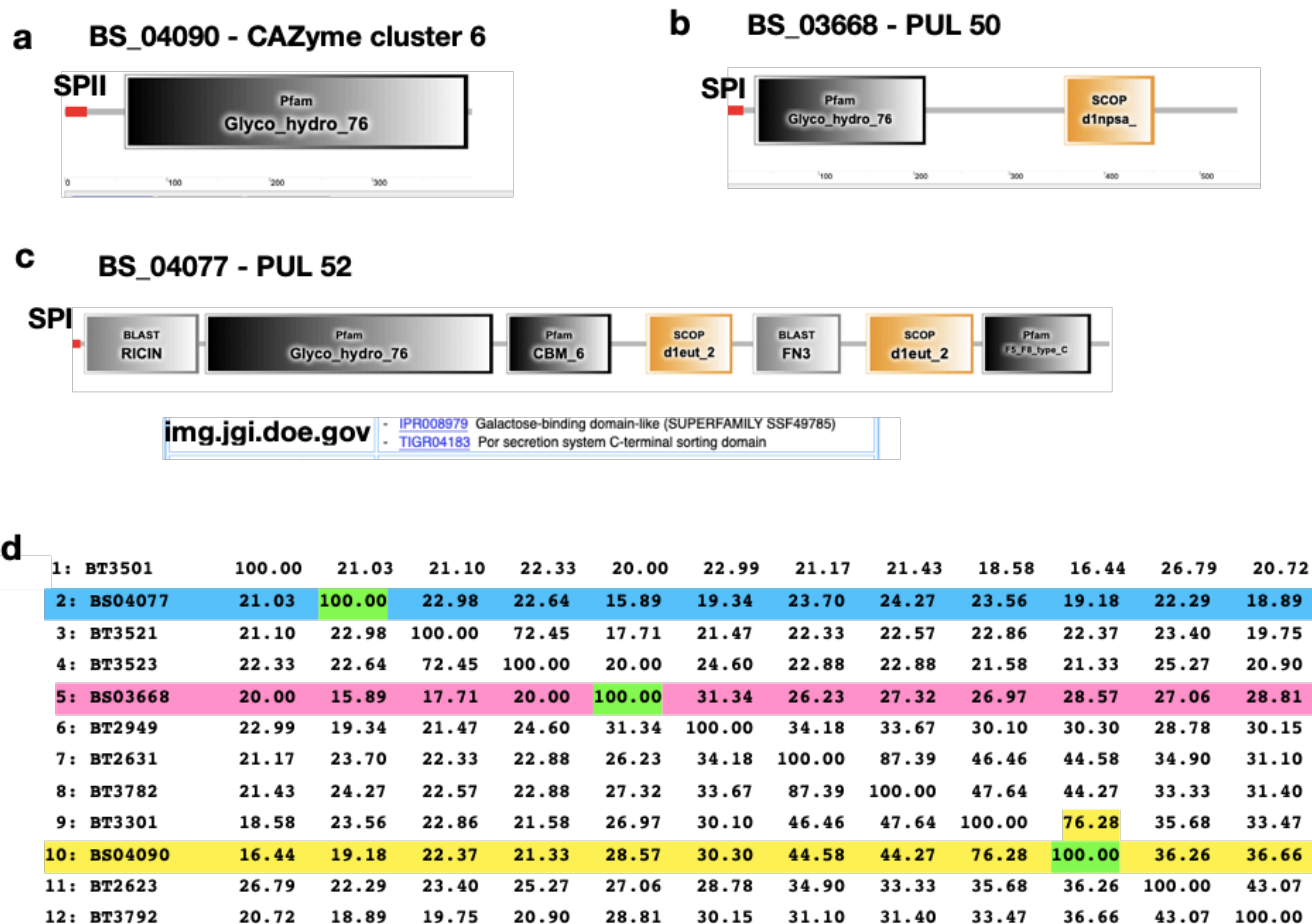


Figure 4. 11 Analysis of GH76s from *B. salyersiae*. Domain organisation of BS_04090 (a), BS_03668 (b), and BS_04077 (c) were analysed with SMART (smart.embl-heidelberg.de). Nature of the N-terminal Signal Peptides was determined with SignalP 5.0 (cbs.dtu.dk/services/SignalP/) (d) Identity matrix of GH76 from Bs and Bt. Amino acid sequences corresponding to GH76 domains of the proteins from of Bs and Bt were aligned and compared using Clustal Omega (ebi.ac.uk/Tools/msa/clustalo/).

4. 3. 7 Biochemical characterisation of Glycoside Hydrolases 76 from *Bacteroides salyersiae*

It was then investigated whether *B. salyersiae* GH76s, BS_04090, BS_03668, and BS_04077, were involved in the degradation of mannan from *S. cerevisiae*. For

unknown reasons, BS_04077 was refractory to any of the following types of cloning: Restriction enzyme cloning (both blunt and sticky end) into pET28b, pET22b, or pBAD-His(A) vectors; Hi-Fi PCR cloning, Gibson assembly cloning, In-Fusion cloning. Cloning of individual domains into either pET28b or pBAD-His (A) vectors was not achieved, synthesis of a codon optimised version by Twist Biosciences also failed.

BS_04090 and BS_03668 were amplified by PCR, cloned into pET28a vector, and recombinantly expressed in TUNER cells. Proteins were purified with IMAC and analysed with SDS-PAGE. Two soluble proteins of 45kDa and 53kDa for BS_04090 and BS_03668, respectively, were obtained (Figure 4. 12).

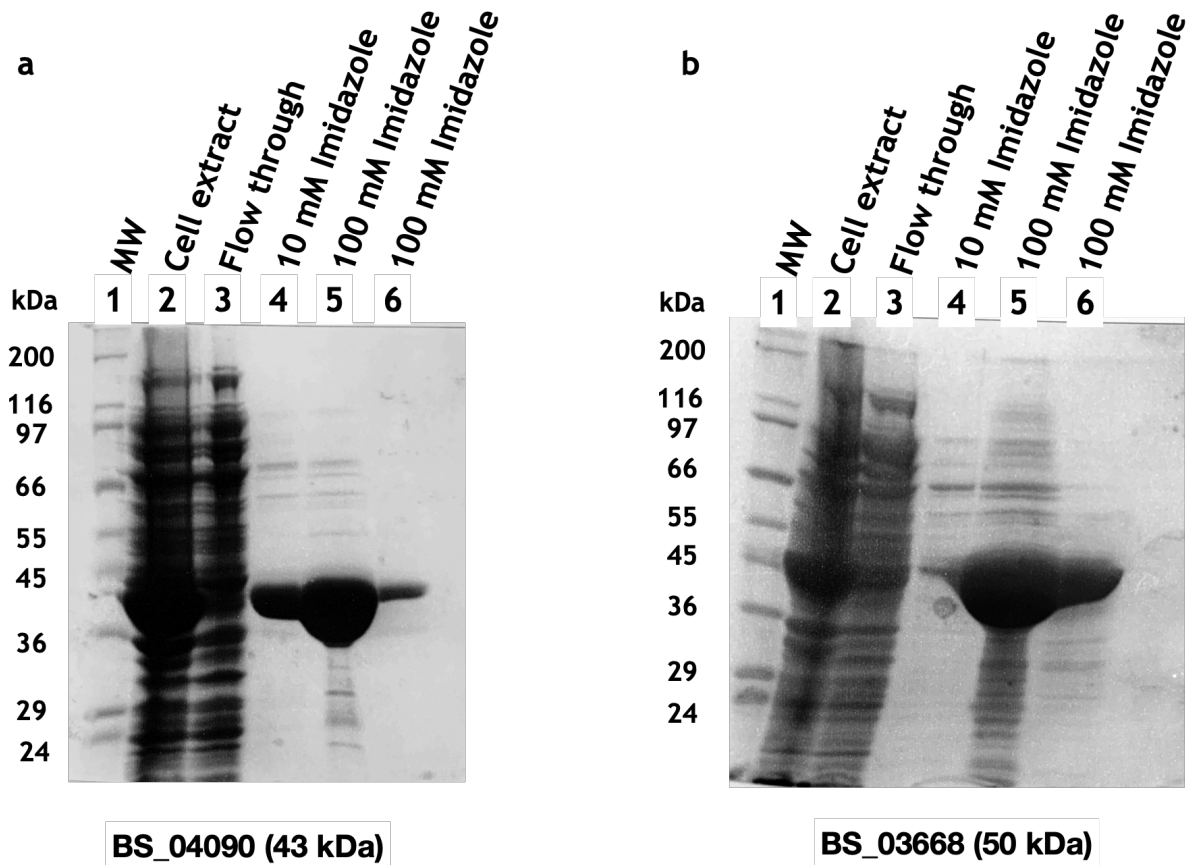


Figure 4. 12 SDS-PAGE analysis of BS_04090 and BS_03668. Indicated fractions were collected and resolved on 12.5% SDS-PAGE. Unstained protein MW ladder (Sigma, UK) was used to identify sizes. Soluble proteins were eluted with 100 mM Imidazole in TALON buffer (20 mM Tris-HCl 300 mM NaCl). Panel a: purification of recombinant BS_04090; Panel b: purification of recombinant BS_03668; soluble proteins were obtained in lane 5 in both panels.

4. 3. 7. 1 Characterisation of BS_04090^{GH76}

Activity of BS_04090 against yeast mannan was then investigated. BS_04090 was assayed against 5 mg ml⁻¹ mannan from wild type *S. cerevisiae* and *C. albicans*. Enzyme was also assayed against undecorated α -1,6-mannan backbone, extracted from $\Delta mnn2$ *S. cerevisiae* strain, and also mannan which retains two or one α -1,2 -linked mannoses attached to the backbone, derived from $\Delta mnn1$ and $\Delta mnn5$ *S. cerevisiae* strains, respectively. BT3774, α -1,2 – α -1,3- mannosidase, was also used to remove α -1,3 and α -1,2 linked side chains, exposing the α -1,6-

linked backbone, a predicted target for BS_04090. β -1,2-mannosyl caps make *C. albicans* mannan refractory to the degradation by α -mannosidases, therefore BT3780 was applied to expose alpha-mannan in these assays. The closest BS_04090 homologue in Bt, BT3301, sharing 76% sequence similarity, was also tested alongside against all substrates for comparison. BT3780, BT3301, and BT3774 cloned into pET28a plasmid were provided by Dr Fiona Cuskin. TLC analysis of these assays showed that BS_04090 could hydrolyse highly branched wild type *S. cerevisiae* mannan (Figure 4. 13 a). Products released from mnn2 mannan by BS_04090 were predominantly comprised of a disaccharide, a trisaccharide as well as mannose (Figure 4. 13 a). BT3774^{GH38} exposed the α -mannan backbone, resulting in a more extensive mannan hydrolysis by BS_04090, as indicated by the ladder of oligosaccharides (Figure 4. 13 a). The ladder of oligosaccharides produced on the wild type mannan (Figure 4. 13 a) differs from the one released from the mnn2 mannan (Figure 4. 13 a), indicating that BT3774^{GH38} does not completely remove α -1,2 mannosides from the sidechains. Further assays with mnn1 and mnn5 mannan showed that BS_04090 can perform hydrolysis of branched mannan (Figure 4. 13 a). In contrast, BT3301 was less active against wild-type *S. cerevisiae* mannan (Figure 4. 13 b) and required presence of BT3774^{GH38} to display activity (Figure 4. 13 b). Unlike BS_04090, BT3301 did not hydrolyse mnn1 or mnn5 mannan, suggesting that the endo-processing activity of the enzyme requires a certain level of backbone exposure. BT3301 displayed different activity against mnn2 mannan compared to BS_04090, generating a pool of longer oligosaccharides, some of which were longer than 5 mannose units (Figure 4. 13 b).

Neither BT3301 nor BS_04090 were active against *C. albicans* mannan (Figure 4. 13 b). Removal of the side chains with a β -1,2-mannosidase, BT3780^{GH130}, alone or in combination with BT3774^{GH38} was not sufficient to expose the backbone for either BS_04090 or BT3301 to act (Figure 4. 13 c)

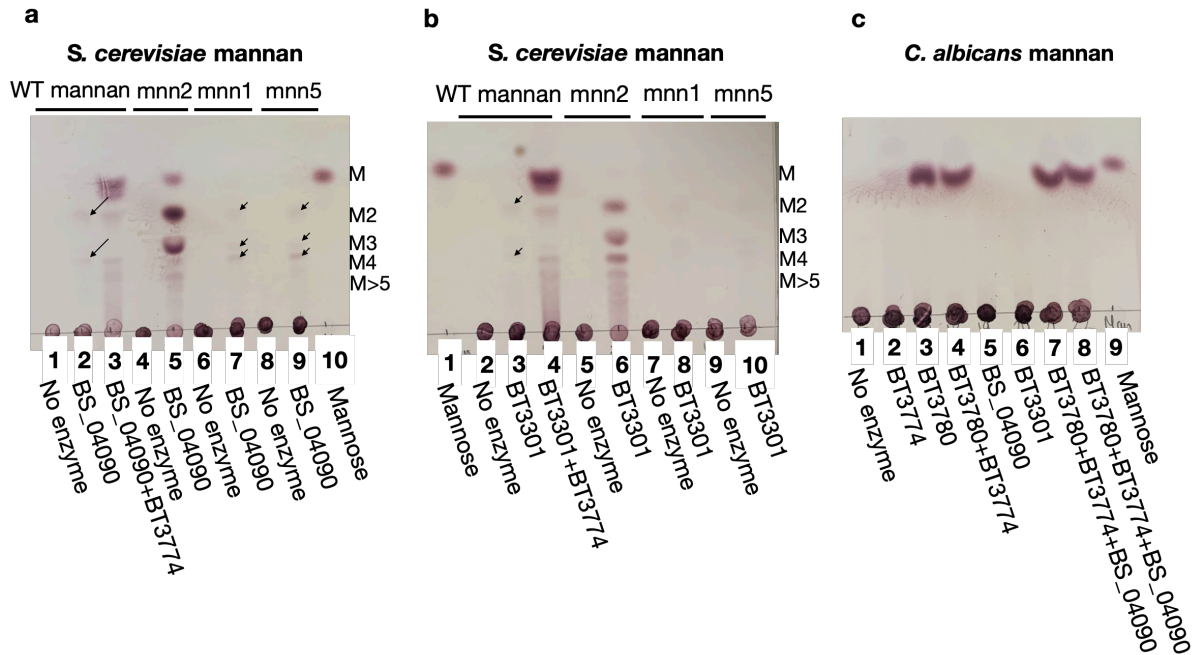


Figure 4. 13 TLC analysis of BS_04090 and BT3301 assayed against different types of yeast mannan. All enzymes at 1 μ M were incubated with 5 mg ml⁻¹ yeast mannan at 37°C overnight. Panel a: Activity of BS_04090 against indicated mannans. Panel b: Activity of BT3301 against indicated mannans. Panel c: Enzyme assays with mannan from *C. albicans*.

The activity of BS_04090 was further analysed. Enzyme at 20 nM was assayed against mnn2 mannan for 30 mins. Aliquots were taken at regular intervals, boiled and analysed with TLC. This time course assay showed that at 20nM BS_04090 could initiate hydrolysis of mnn2 at 1 min incubation time point, producing long oligosaccharides first (Figure 4. 14 a). At 5 min incubation point, the bands were more defined, and these were gradually resolved (Figure 4. 14 a). After an hour BS_04090 generated three distinct bands corresponding to a tetra-, tri-, and di-

saccharide (Figure 4. 14 a). This demonstrates that, as the reaction progressed, longer manno-oligosaccharides were processed into shorter length polymers. Activity of BS_04090 was also tested on α -1,6 manno-tetraose. Enzyme was incubated with 1 mM manno-tetraose for 60 mins. Aliquots were taken at 10-minute intervals, boiled and analysed with TLC. This showed that the enzyme requires 10 minutes to begin processing manno-tetramer into a disaccharide (Figure 4. 14 b). A very faint band suggestive of a trisaccharide was detected at 60 min time point, indicating that BS_04090 can process tetrasaccharide into mannotriose and mannose (Figure 4. 14 b). BS_04090 broke down α -1,6-tetrasaccharide at a slower rate than α -1,6 mannan backbone, demonstrating that BS_04090 has a preference for longer oligosaccharides. At higher concentrations, BS_04090 (10 μ M) was able to degrade manno-tetraose into a trisaccharide and mannose, which was then converted to a disaccharide and mannose (data not shown)

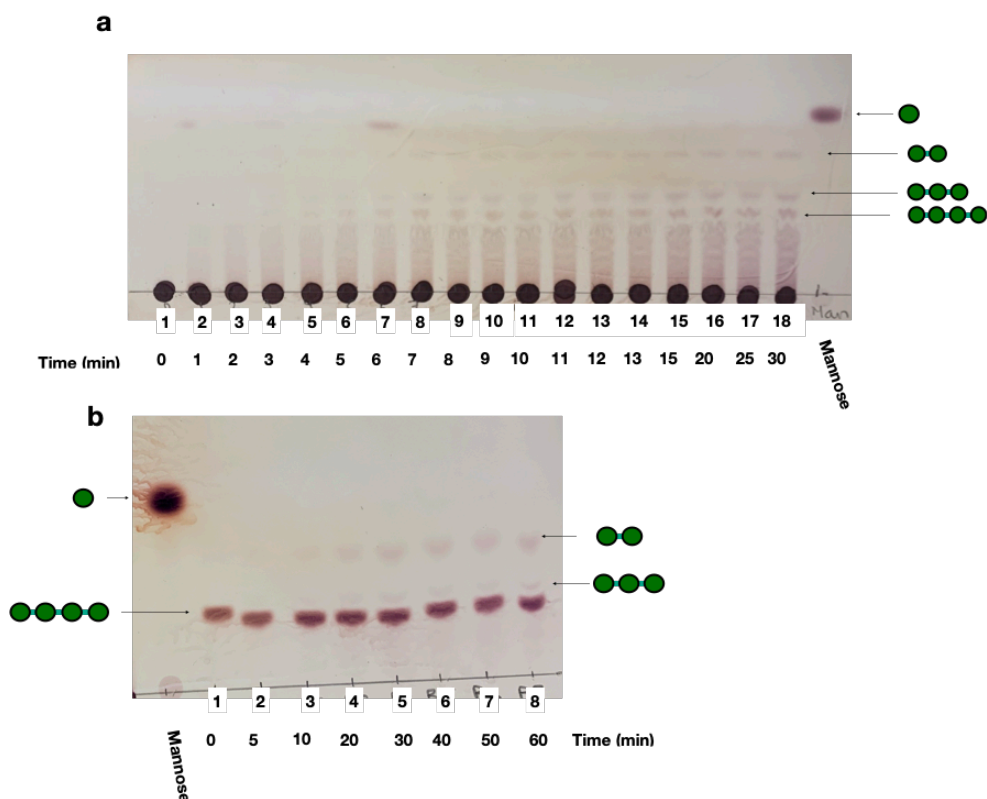


Figure 4. 14 Time course assay with BS_04090 against unbranched α -1,6-linked backbone from mnn2 *S. cerevisiae* strain (a) and α -1,6 mannotetraose (b). BS_04090 at 20 nM was incubated with 5 mg ml⁻¹ mnn2 mannan (a) and 1 mM α -1,6 mannotetraose at 37°C for 60 mins. Aliquots were taken at indicated time points; reactions were stopped by boiling.

4. 3. 7. 2 Characterisation of BS_03668^{GH76}

Activity of another GH76 from *B. salyersiae*, BS_03668, against mannan was then analysed. *S. cerevisiae* mannan was treated with a range of mannosidases from Bt, namely BT3862^{GH99}, BT409^{2GH92}, BT3774^{GH38}, to trim α -1,2 and α -1,3 side chains, revealing the α -1,6 backbone to the enzyme. Enzymes all at 1 μ M were combined and tested against *S. cerevisiae* mannan at 37°C overnight. Assays were then analysed with TLC. This showed that, similar to BS_04090, BS_03668 displayed low activity against highly branched wild type mannan (Figure 4. 15 a). In the presence of BT3862^{GH99} and BT409^{2GH92}, which remove an α -1,3 and α -1,2-

linked mannosides, activity of BS_03668 was enhanced (Figure 4. 15 a). Addition of α -1,3 mannosidase, BT3858^{GH92}, to the BT3862^{GH99}, BT4092^{GH92}, BS_03668 cocktail, improved activity of BS_03668 against mannan (Figure 4. 15 a).

BT3774^{GH38}, a broad specificity α -1,3; α -1,2 mannosidase, also exposed the backbone to BS_03668 (Figure 4. 15 a). These data demonstrate that, despite of being able to hydrolyse highly branched wild type *S. cerevisiae* mannan, BS_03668 has a preference for less complex mannan variants.

BT3774^{GH38} was also combined with BS_04090 to compare activities of the two GH76s from *B. salyersiae*. This showed that BS_03668 and BS_04090 display different activities against *S. cerevisiae* mannan (Figure 4. 15 a), where BS_04090 is able to release more products than BS_03668 from mannan in the presence BT3774 (Figure 4. 15 a). This demonstrates that α -linked side chains impose steric constraints for BS_03668, while BS_04090 is a more generalist endo-mannanase which can perform breakdown of branched polymers.

Activity of BS_03668 against *C. albicans* mannan was also analysed. *C. albicans* mannan was also treated with BT3780^{GH130} and BT3774^{GH38} to remove β -1,2-mannosyl caps and α -1,2- α -1,3-linkages from the sidechains, respectively. This showed that despite the removal of β and α -side chains, BS_03668 was not able to access *C. albicans* mannan (Figure 4. 15 b). Presence of BS_04090 in the BT3774^{GH38}, BT3780^{GH130}, BS_03668 cocktail was not sufficient to initiate backbone breakdown (Figure 4. 15 b). These data show that the architecture of side chains composing *C. albicans* mannan is more complex compared to the sidechains of mannan from *S. cerevisiae*.

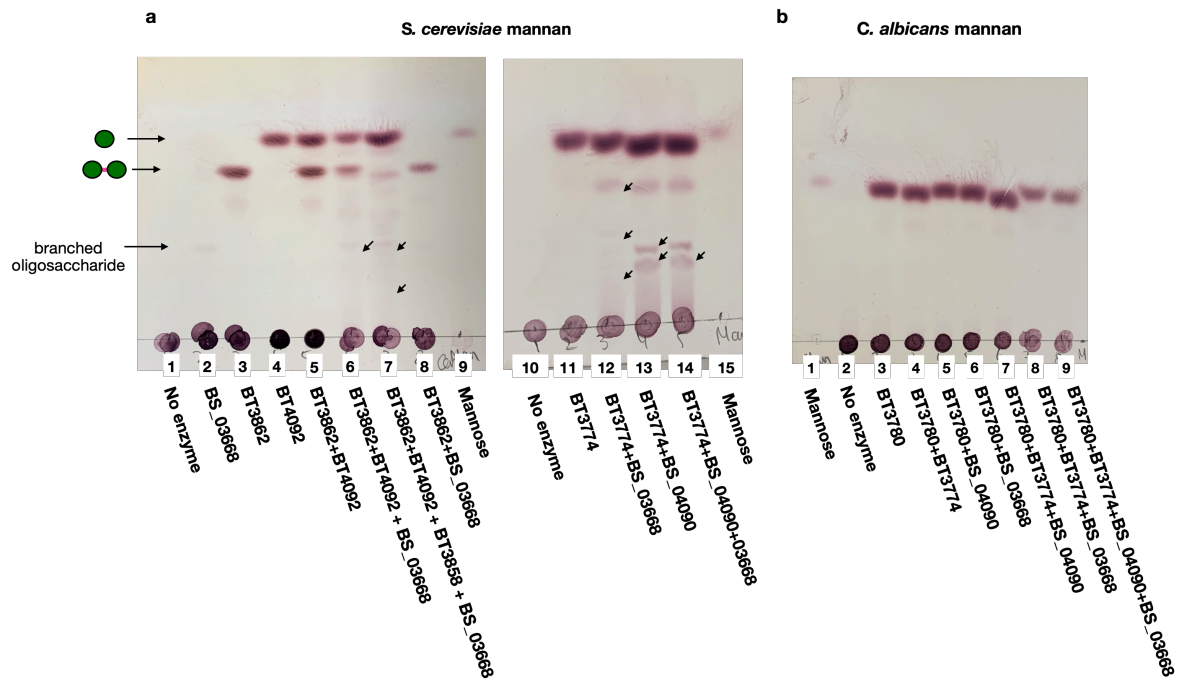


Figure 4.15 Activity of BS_03668 on yeast mannan. Enzymes at $1\mu\text{M}$ were incubated with 5 mg ml^{-1} either mannan from the wild type *S. cerevisiae* or *C. albicans* at 37°C overnight. Panel a: TLC of *S. cerevisiae* mannan degradation by a range of mannosidases. Panel b: enzymatic degradation of *C. albicans* mannan.

Activity of BS_03668 was further assessed against mnn2 mannan as well as α -1,6 manno-tetraose. BS_03668 at $1\mu\text{M}$ was incubated with mnn2 mannan for 16 hours. Aliquots were taken at 10 min intervals for 60 mins, then at 2, 3, and 16 hours. This assay showed after 10 minutes enzyme generated a smear suggestive of oligosaccharides (Figure 4.16 a), which gradually became more pronounced as reaction proceeded. It took 3 hours for BS_03668 to complete reaction on mnn2 mannan. No noticeable difference could be observed between 3 and 16 hour time points (Figure 4.16 a). The final products of this reaction were predominantly comprised of oligosaccharides longer than 4 sugars, a shadow suggestive of a disaccharide and a trisaccharide could also be observed (Figure 4.

16 a). This assay showed that BS_03668 generated a pool of long α -1,6 manno-oligosaccharides, which were then further processed into shorter polymers. To further assess the ability of BS_03668 to process shorter manno-oligosaccharides, enzyme was incubated with 1 mM α -1,6-mannotetraose for 16 hours. Samples were collected at regular intervals. This showed that the tetra-saccharide remained intact although a shadow suggestive of a disaccharide could be detected 3 hours post incubation (Figure 4. 16 b). This indicates that a mannotetraose is not a preferred substrate for BS_03668, and the enzyme indeed has a preference for oligosaccharides composed of more than 4 sugars. The concentration of BS_03668 was 150 times higher than that in the assays with BS_04090. This suggests that despite displaying activity against yeast α -mannan, it is probably not the true substrate for BS_03668.

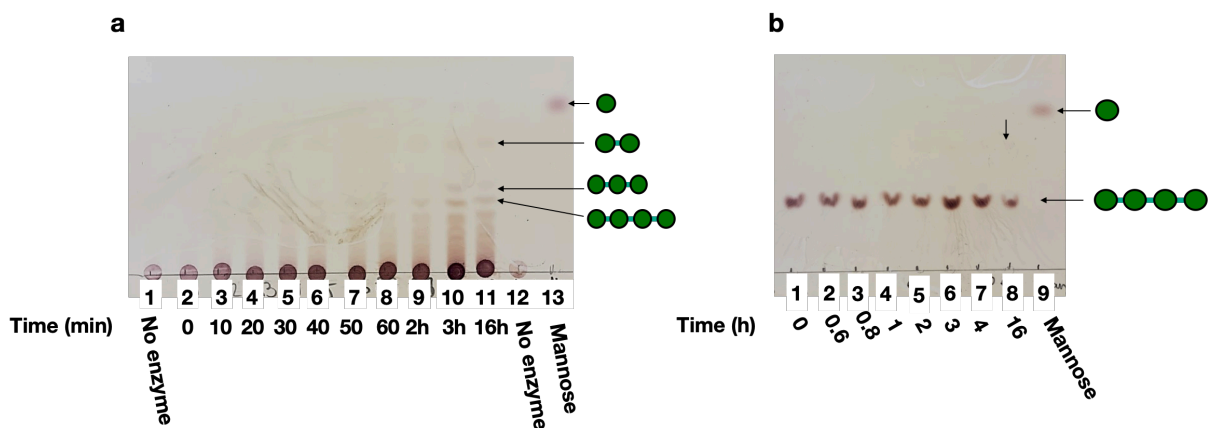


Figure 4. 16 Activity of BS_03668 against undecorated α -1,6-mannan from *mnn2 S. cerevisiae* (a) and α -1,6 manno-tetraose (b). 1μ M BS_03668 was incubated with either 5 mg ml^{-1} *mnn2* mannan or 1 mM α -1,6 manno-tetraose. Aliquots were collected at indicated time points.

4. 3. 7. 3 Characterisation of Glycoside Hydrolases 38 (GH38) from *B. salyersiae*.

Bt encodes for two GH38s, BT3774 and BT4072. As shown in Chapter 3, BT4072 displayed activity against HMNG and not yeast mannan, Cuskin and colleagues demonstrated that depolymerisation of mannan in Bt was orchestrated by BT3774. BT3774 was shown to be the only enzyme in Bt which exhibited broad specificity against α -linked mannosides and could also deconstruct phosphomannan (Cuskin et al., 2015b)

The genome search identified two GH38s in Bs: BS_04085, enclosed in the Cazyme cluster 6, and BS_01537, positioned as an orphan gene, both of these proteins were upregulated in Bs in response to yeast mannan (Table 4. 1).

BS_01537 and BS_04085 were both cloned into pET28a, expressed in TUNER cells, purified with IMAC, and analysed with SDS-PAGE. Two recombinant proteins of 148kDa and 137kDa in soluble forms for BS_04085 and BS_01537, respectively, were obtained (Figure 4. 17).

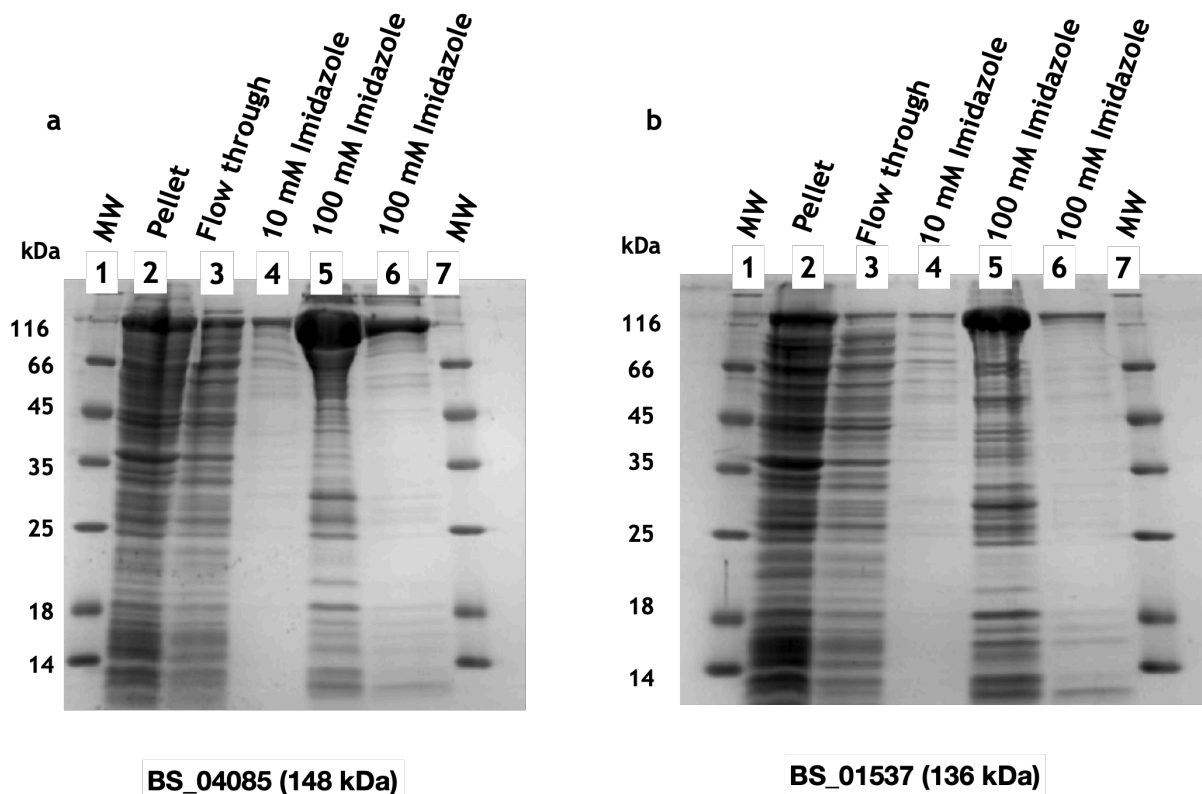


Figure 4. 17 SDS-PAGE analysis of BS_04085 and BS_01537. Proteins were purified with IMAC and indicated fractions were resolved on 12.5% SDS-PAGE. Protein sizes were identified with Wide MW Protein ladder (Sigma, UK). Panel a: recombinant BS_04085; Panel b: recombinant BS_01537, soluble proteins were eluted with 100 mM Imidazole in TALON (20 mM Tris-HCl, 300 mM NaCl).

To determine linkage specificities of these enzymes, both BS_04085 and BS_01537 were tested against α -1,2-; α -1,3; α -1,4; α -1,6 mannobioses as well as mannose-1-phosphate and mannose-6-phosphate. A previously characterised GH38 from Bt, BT3774, was also tested against mannose-1-phosphate alongside for comparison, as it is the only known α -mannosidase capable of removing phosphate from mannophosphate substrates. Reactions were analysed with TLC. This showed that, similar to BT3774, BS_01537 displayed broad specificity against α -linked disaccharides (Figure 4. 18 a), whereas BS_04085 exhibited preference for α -1,2- and α -1,3 -mannosidic linkages (Figure 4. 18 b) and

incomplete activity against α -1,6 and α -1,4-mannobioses (Figure 4. 18 b). Neither of the enzymes showed activity against mannose-6-phosphate (Figure 4. 18 c). Both BT3774 and BS_01537 performed partial hydrolysis of mannose-1-phosphate, however BS_04085 was the only enzyme capable of completely cleaving this substrate (Figure 4. 18 d).

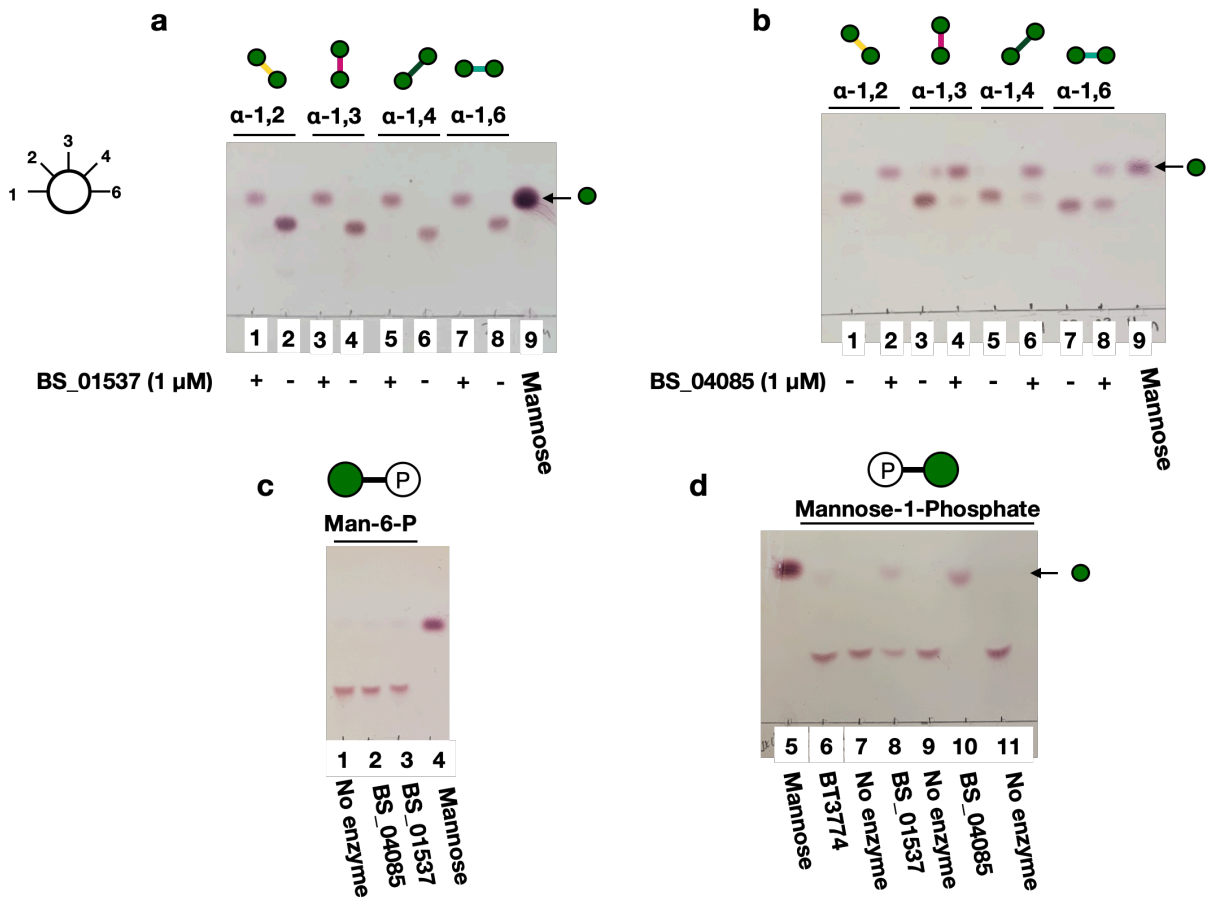


Figure 4. 18 Activity of GH38s, BS_04085 and BS_01537, against a range of substrates.

BS_04085 (a) and BS_01537 (b) at 1 μ M were incubated with 1 mM α -1,2- α -1,3- α -1,4- α -1,6-mannobioses, and 1 mM mannose-6-phosphate (c), mannose-1-phosphate (d) overnight.

Reactions were analysed with TLC. Mannose is shown with a green circle, “-” indicates substrate without enzyme, “+” with added enzyme. Panel a: BS_01537 against mannobioses; Panel b: BS_04085 against α -mannobiose substrates; Panel c: BS_01537 and BS_04085 against Man-6-phosphate; Panel d: BT3774, BS_01537, and BS_04085 against Man-1-phosphate.

It was then investigated whether BS_04085 and BS_01537 display activity against mannan from the wild type *S. cerevisiae* and *C. albicans* as well as mannan from mnn1, mnn5, mnn2 *S. cerevisiae* strains. Reactions were analysed with TLC. This showed that both BS_04085 and BS_01537 released mannose from wild-type *S. cerevisiae* mannan (Figure 4. 19 c) as well as *S. cerevisiae* mannan variants which retain α -1,2 linkage, mnn1 and mnn5 (Figure 4. 19 a, b). BS_04085 generated a small amount of mannose from mnn2 mannan, whereas BS_01537 released more mannose from mnn2 mannan (Figure 4. 19 b). This is in line with previous data, indicating that BS_01537 is a broad specificity α -mannosidase. Both BS_04085 and BS_01537 could release mannose from *C. albicans* mannan (Figure 4. 19 d), indicating that β -1,2-linkages do not cap the side chains uniformly and a proportion of α -mannan is exposed.

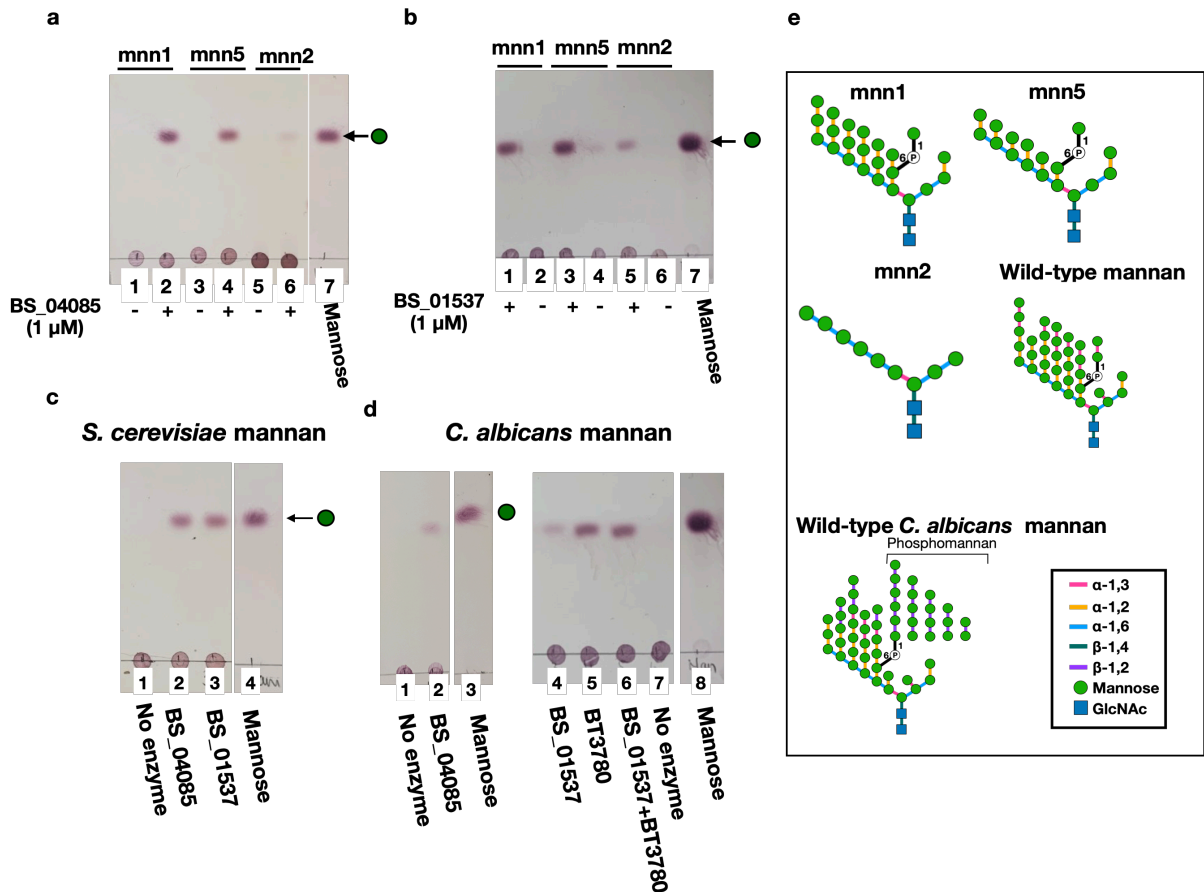


Figure 4. 19 Activity of GH38s, BS_04085 and BS_01537, against mannan from mnn1, mnn5, mnn2 *S. cerevisiae* strains and wild type *S. cerevisiae* and *C. albicans* (Panel e). Enzymes at 1 μ M were incubated with 5mgml⁻¹ substrates at 37 °C overnight. “-” indicates substrate without enzyme, “+” with added enzyme, unless specified. Panel a: BS_04085 and BS_01537 against mannan variants, respectively. Panel c: BS_04085 and BS_01537 against wild type *S. cerevisiae* mannan Panel d: BS_04085 and BS_01537 against mannan from *C. albicans*.

To investigate substrate specificities of these GH38s in more detail, their kinetic parameters were assessed. Enzymatic rates of both BS_01537 and BS_04085 were measured against varying concentrations of α -1,2- α -1,3, α -1,4, and α -1,6-linked mannobioses as well as mannan from the wild type, mnn1, and mnn5 *S. cerevisiae* strains.

This analysis showed that BS_01537 displays a strong preference for a less complex mnn5 mannan variant ($K_m = 0.77$ mg ml⁻¹ and $k_{cat}/K_m = 92.62$ min⁻¹ mg⁻¹

ml) (Figure 4. 20), which contains a single α -1,2-linked mannose attached to the backbone. BS_04085 presented the same $K_m=0.98 \text{ mg ml}^{-1}$ for mnn5 mannan as BS_01537, however its enzymatic rate, k_{cat} , was higher, giving a greater $k_{cat}/K_m = 142.23 \text{ min}^{-1} \text{ mg}^{-1} \text{ ml}$. Both BS_04085 and BS_01537 displayed similar activity against mnn1 mannan, which contains two α -1,2-linked mannoses attached to the backbone (Figure 4. 20 c, d). This also revealed that highly branched mannan, which retains α -1,3 decorations, is not a preferred substrate for BS_01537 ($k_{cat}/K_m = 1.3 \text{ min}^{-1} \text{ mg}^{-1} \text{ ml}$). In contrast, BS_04085 was capable of degrading wild-type mannan, displaying lower K_m and higher catalytic efficiency ($k_{cat}/K_m = 14.46 \text{ min}^{-1} \text{ mg}^{-1} \text{ ml}$) than BS_01537 (Figure 4. 20 a, b).

BS_01537 or BS_04085 did not display strong activity against α -linked mannobioses (Figure 4. 21). Consistent with previous observations, BS_04085 was able to act on α -1,2 and α -1,3 mannobioses, while BS_01537 exhibited broader specificity against mannosidic linkages (Figure 4. 21). k_{cat}/K_m values are summarised in Table 4. 2.

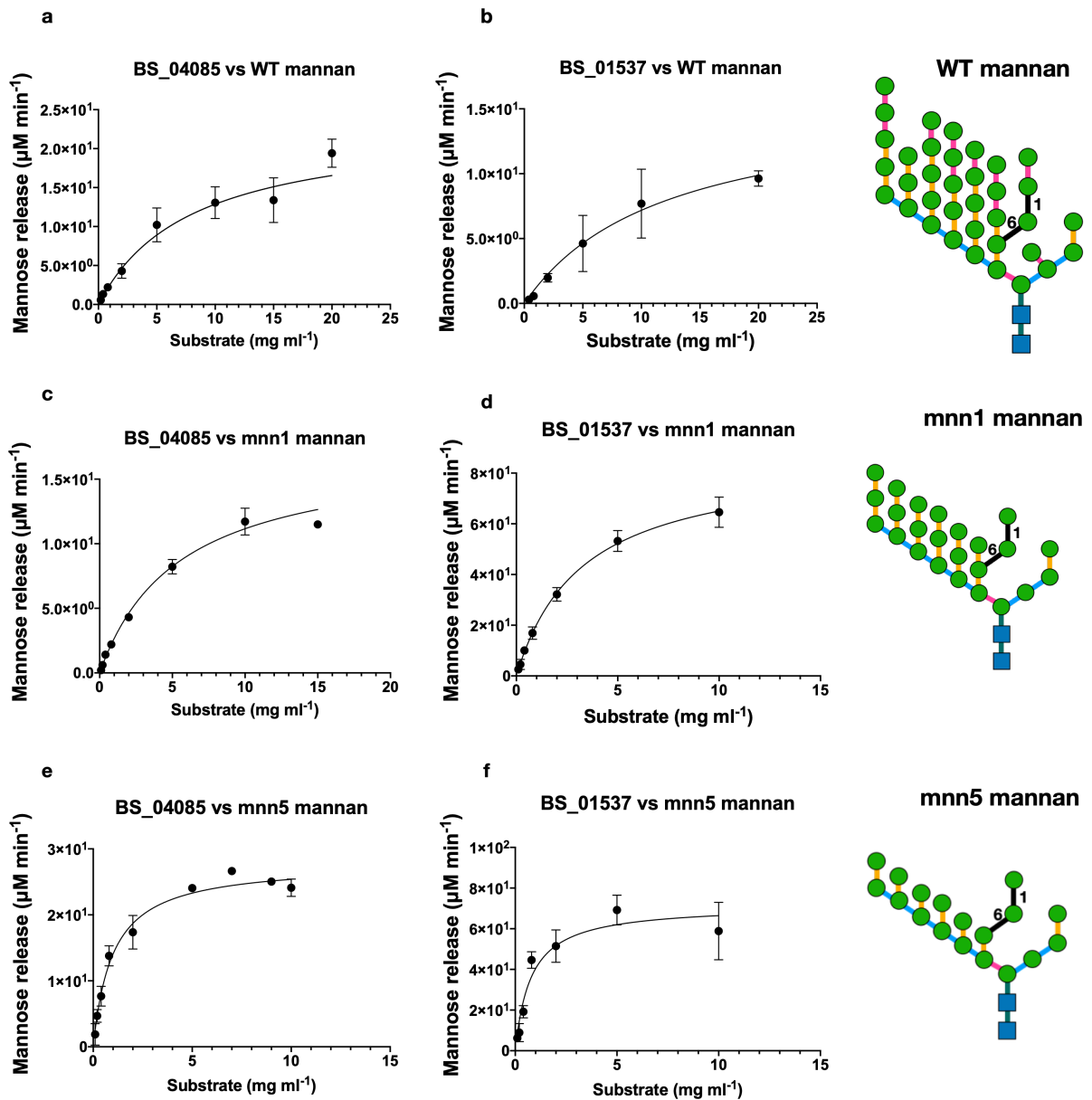


Figure 4. 20 Kinetic analysis of the two GH38s from *B. salyersiae*: BS_04085 and BS_01537 against mannan from the wild type, mnn1, mnn5 *S. cerevisiae* strains. Reactions were carried out in 40 mM MOPS containing 2mM CaCl_2 at 37°C, mannose release was monitored at 340nm using Mannose detection kit. Kinetics were determined using concentrations below and above K_m . Error bars are representative of at least 3 biological replicates. Data are representative of 2 technical repeats

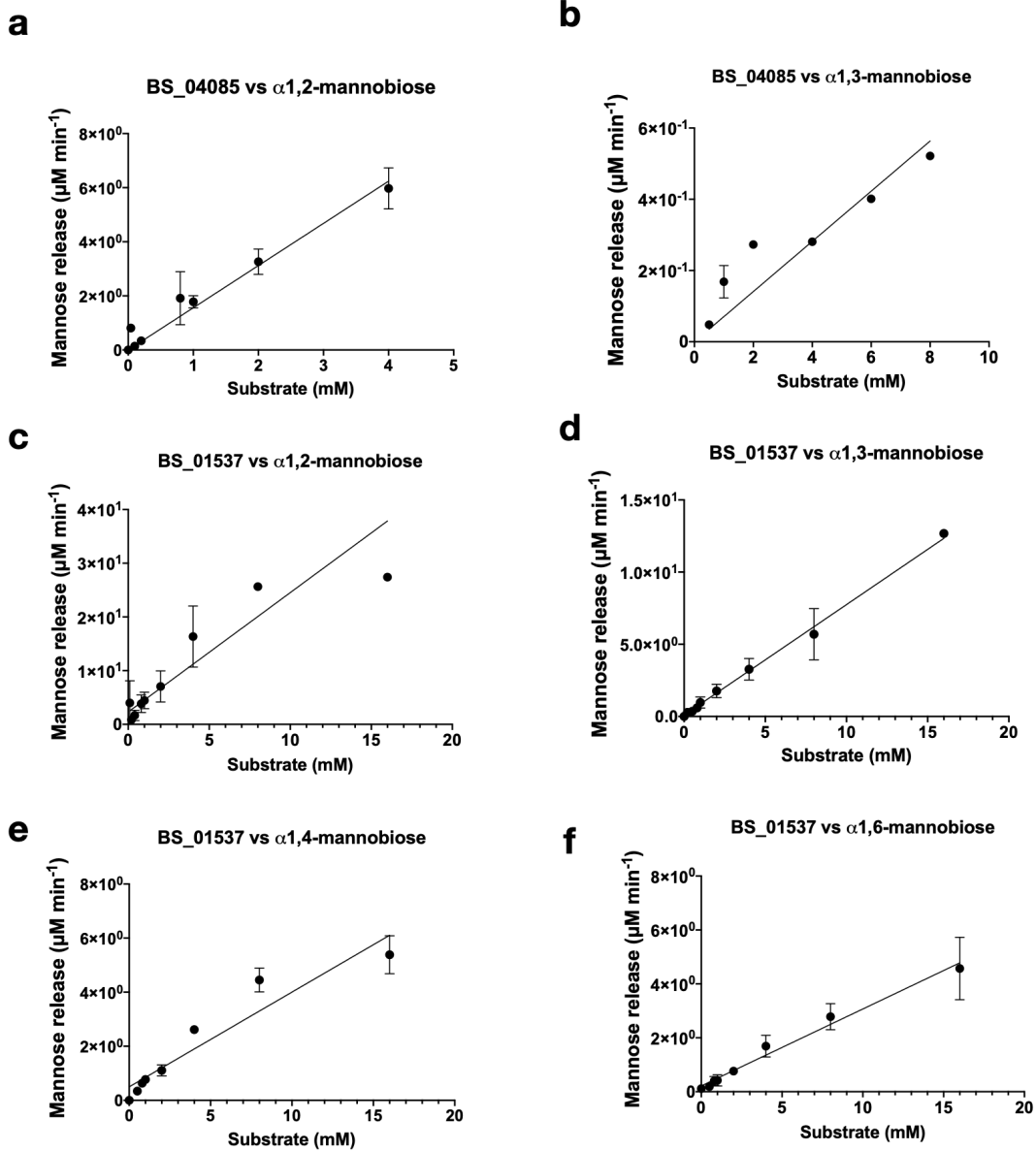


Figure 4. 21 Kinetic analysis of GH38s: BS_01537 and BS_04085 against α -linked mannobioses. Reactions were carried out in 40 mM MOPS containing 2 mM CaCl_2 at 37°C, mannose release was monitored at 340 nm using Mannose detection kit. Kinetics were determined using concentrations below K_m . Error bars are representative of at least 3 biological replicates. Data are representative of 2 technical repeats.

a

Substrate	K_m (mg ml⁻¹)	k_{cat} (min⁻¹)	k_{cat}/K_m (min⁻¹ mg⁻¹ ml)
BS_04085			
WT mannan	8.006 ± 2.8	115.8 ± 15.8	14.46
mnn1	5.4 ± 0.7	86.33 ± 5.1	15.98
mnn5	0.98 ± 0.1	139.4 ± 4.8	142.25
BS_01537			
WT mannan	12.04 ± 4.9	15.8 ± 3.2	1.31
mnn1	3.2 ± 0.4	86.158 ± 3.7	26.92
mnn5	0.772 ± 0.2	71.56 ± 4.9	92.69

b

Disaccharide	Slope	Et (μM)	k_{cat}/K_m (μM⁻¹ min⁻¹)
BS_04085			
α-1,2-man2	1.56 ± 0.06	0.2	7.8
α-1,3-man2	0.07 ± 0.007	0.2	0.35
BS_01537			
α-1,2-man2	2.23 ± 0.19	1	2.23
α-1,3-man2	0.765 ± 0.03	1	0.77
α-1,4-man2	0.35 ± 0.03	1	0.35
α-1,6-man2	0.285 ± 0.02	1	0.29

Table 4. 2 Kinetic parameters of BS_01537^{GH38} and BS_04085^{GH38}. Panel a: against *S. cerevisiae* mannan variants: mnn1, mnn5, and wild type mannan. K_m and k_{cat} were determined from Michaelis-Menten equation. Panel b: against α-linked mannobioses, K_m/k_{cat} were determined using linear regression. Error represents SEM.

It was then investigated whether BS_04085 and BS_01537 differ in their ability to deconstruct mannan. To do so, excess enzyme concentration is used with a limited amount of substrate, allowing reactions to run to completion. The total

amount of mannose released by BS_04085 and BS_01537 was quantified with a spectrophotometric assay. BS_04085 at 0.5 μM or BS_01537 at 5 μM were assayed against 10 μg of wild type, *mnn1*, and *mnn5* mannan and continuous mannose release was monitored with a spectrophotometer using a mannose detection kit. These assays showed BS_04085 released more mannose from *mnn1* mannan (40 μM) than BS_01537 (14 μM) (Figure 4. 22 a and b). Similarly, BS_04085 generated double the amount of mannose from *mnn5* mannan (45 μM) than BS_01537 (18 μM) (Figure 4. 22 a and b). In line with kinetics data, BS_04085 was capable of generating mannose from wild type mannan, while activity of BS_01537 was undetectable (Figure 4. 22 a and b).

The preference of BS_01537 was further demonstrated with a tetra-manooligosaccharide, which is composed of α -1,6-linked trisaccharide with a single α -1,3 mannosyl unit attached to the middle mannose. Both BS_04085 and BS_01537 at 1 μM were incubated with 1 mM of tetrasaccharide at 37 °C overnight, reactions were analysed with TLC. BS_01537 processed tetrasaccharide into a trisaccharide and mannose but also produced a small amount of α -1,6-disaccharide, whose identify was confirmed with a recombinant GH125. (Figure 4. 22 c). BS_04085 did not exhibit activity on this substrate (Figure 4. 22 c).

Combined these data indicate that BS_01537 acts as a broad specificity α -mannosidase, displaying preference for less complex and shorter manno-oligosaccharides. Specificity of BS_04085 is narrower but, unlike BS_01537, it is capable of depolymerising complex mannan substrates. Given these substrate specificities, it would be logical to assume that *in vivo* BS_01537 performs mannan degradation in the periplasmic space, while BS_04085 could be initiating

mannan breakdown at the cell surface, generating a pool of extracellular mannose observed in the whole cell assays.

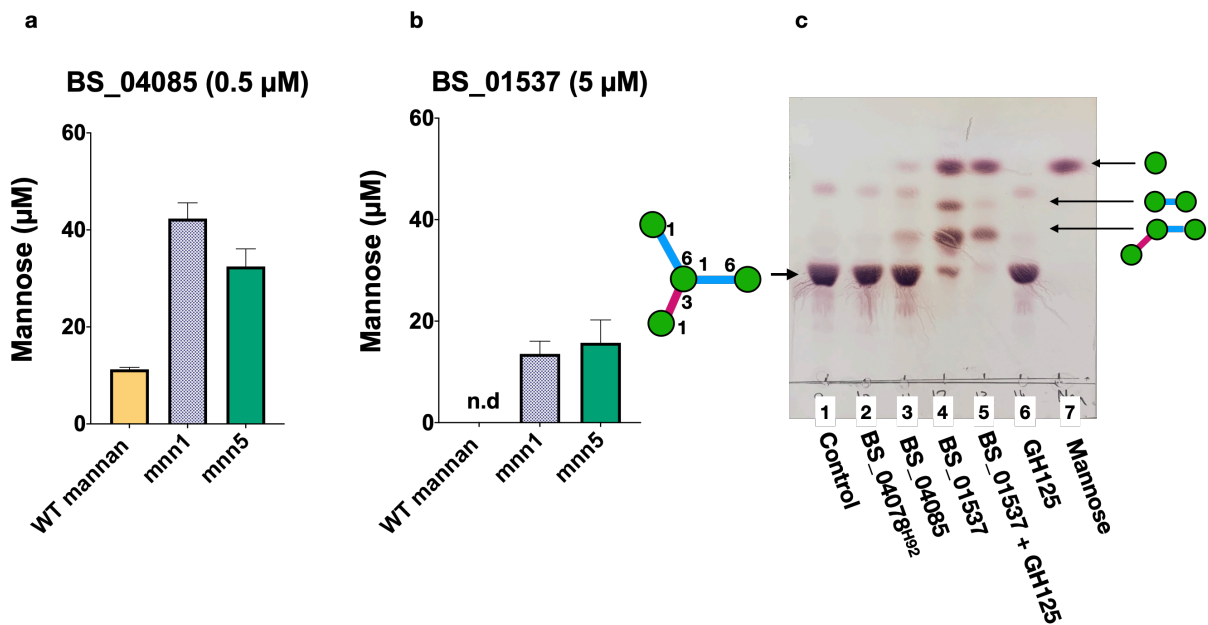


Figure 4.22 Activities of BS_04085 and BS_01537 against mannan substrates.

10 µg of wild type, mnn1, or mnn5 mannan were treated with BS_04085 at 0.5 µM and BS_01537 at 5 µM in 40 mM MOPS with 2mM CaCl₂ at 37 °C, mannose release was monitored in end point reactions continuously in a spectrophotometer using mannose detection kit. Panel a: total amount of mannose released by BS_04085 from mannan substrates. Panel b: total amount of mannose released by BS_01537 from mannan substrates, Panel c: Activity of BS_04085 and BS_01537 against manno-tetrasaccharid. Enzymes at 1 µM were assayed against 1 mM substrate overnight. BS_04078^{GH92} was used a negative control; GH125, BS_04089, was used to determine the nature of the disaccharide in lane 4.

4.3.8 Yeast α-mannan breakdown by *B. salyersiae*

Besides BS_04090^{GH76} and BS_04085^{GH38}, Mannan PUL 1 contains two additional α-mannosidases, BS_04078^{GH92} and BS_04089^{GH125} (Figure 4.9). Both BS_04078^{GH92} and BS_04089^{GH125} were cloned and expressed in *E. coli*. SDS-PAGE analysis confirmed that both proteins were soluble and had correct

molecular weight, 83 kDa for BS_04078^{GH92} and 58 kDa for BS_04089^{GH125} (Figure 4. 23).

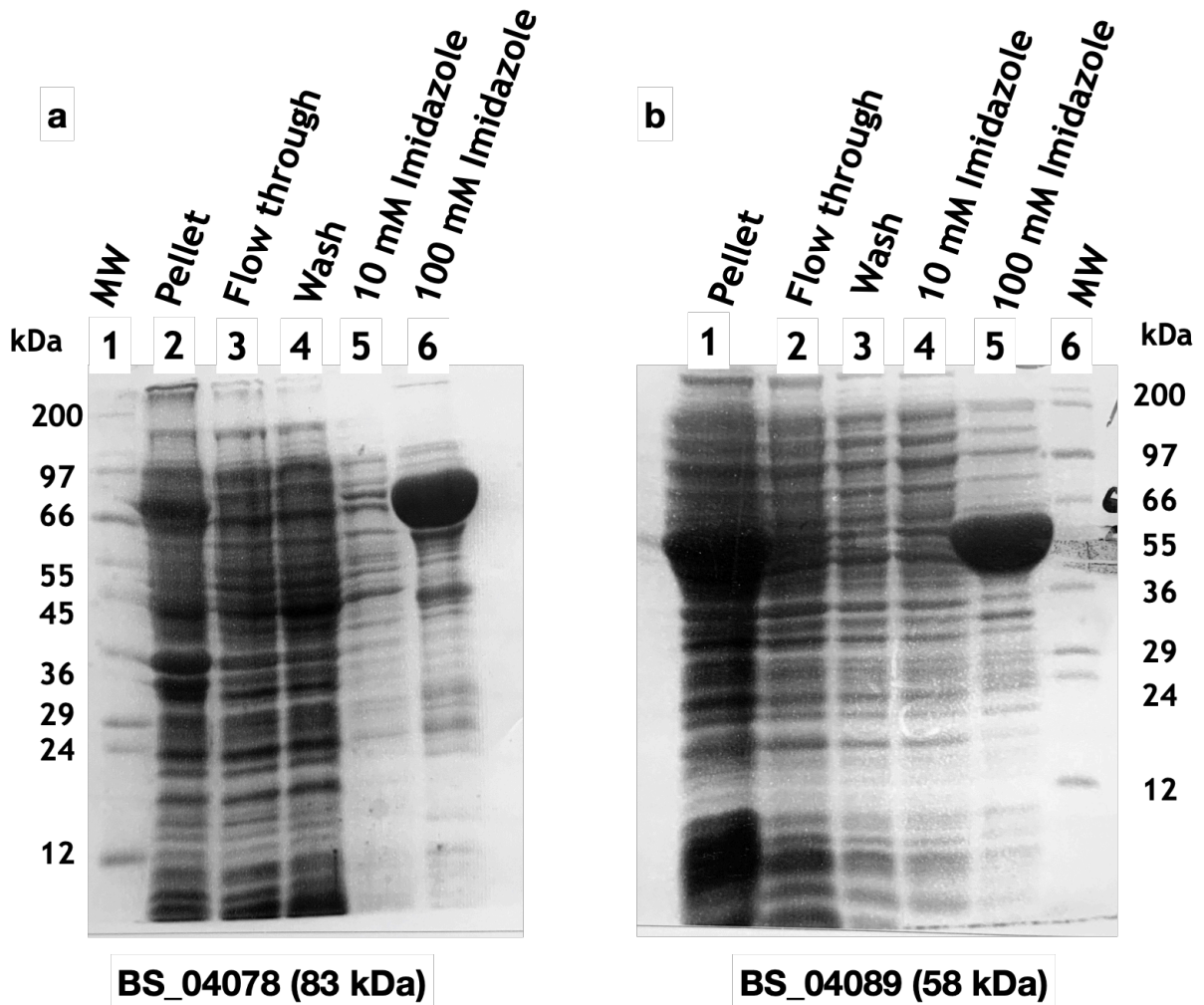


Figure 4. 23 SDS-PAGE analysis of BS_04078^{GH92} and BS_04089^{GH125}. Indicated IMAC fractions were analysed with 12.5% SDS-PAGE. Panel a: expression of recombinant BS_04078 – GH92; Pane; b: recombinant BS_04089 – GH125. Soluble proteins were eluted with 100 mM Imidazole in TALON.

Recombinant BS_04078^{GH92} and BS_04089^{GH125} at 1 μ M were then incubated with 1 mM α -1,2-, α -1,3, α -1,4, and α -1,6 mannobioses. Reactions were then analysed with TLC. BS_04079^{GH92} displayed activity against α -1,2 and α -1,6-linked disaccharides (Figure 4. 24 a). As expected, BS_04089^{GH125} was active against α -1,6-mannobiose only (Figure 4. 24 b).

Cloning and expression of BS_04078 and BS_04089, and assays against disaccharides, presented in Figure 4. 23 and Figure 4. 24, were conducted by Curtis Cottam as part of his MRes degree under my supervision.

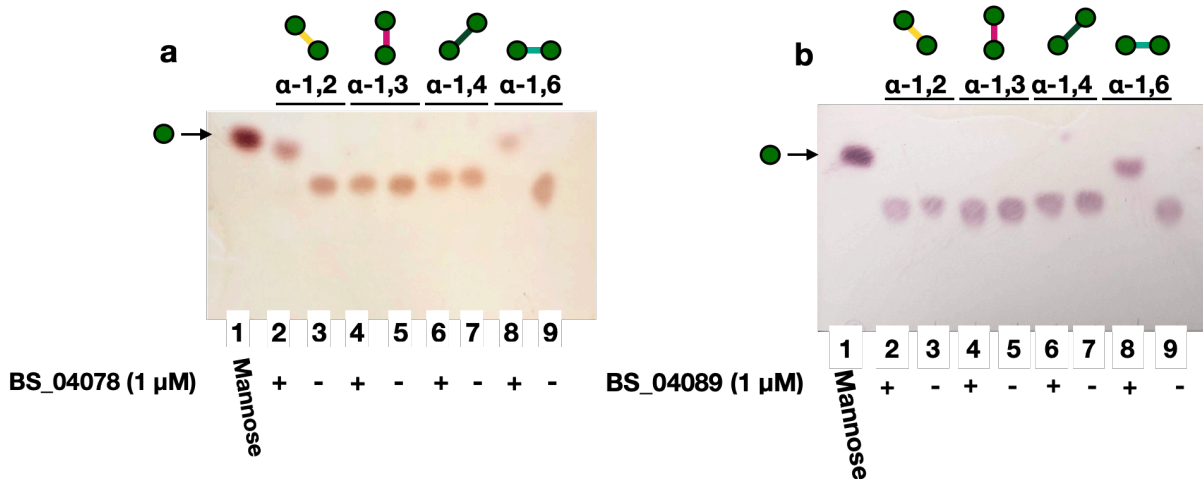


Figure 4. 24 Activity of BS_04078^{GH92} and BS_04089^{GH125} against α -linked mannobioses. Enzymes at 1 μ M were incubated with indicated substrates at 37 °C overnight. Panel a: BS_04078^{GH92} shows activity against α -1,2 and α -1,6-linked mannobioses. Panel b: BS_04089^{GH125} is active against α -1,6-mannobiose.

4. 3. 8. 1 Activity of BS_04078^{GH92}, BS_04089^{GH125}, BS_04085^{GH38}, BS_01537^{GH38}, BS_04090^{GH76} against *mnn2*, *mnn5*, and *mnn1* mannan variants.

To elucidate biological functions of BS_04078^{GH92} and BS_04089^{GH125}, they were combined in cocktails with BS_04090^{GH76}, BS_04085^{GH38}, and BS_01537^{GH38} against mannan variants (*mnn2*, *mnn1*, *mnn5*). This provided an insight into the mechanism of enzymatic breakdown of α -mannan from wild type *S. cerevisiae*. Activity of BS_04078^{GH92} and BS_04089^{GH125} was tested against the simplest mannan variant, *mnn2*, which is composed of a linear α -1,6 linked backbone (Figure 4. 25 a). BS_04085^{GH38} was assayed alongside for visual comparison. BS_04090^{GH76} was used to induce mannan hydrolysis to identify maximum substrate length for BS_04089^{GH125}. TLC analysis showed that both

BS_04078^{GH92} and BS_04089^{GH125} released mannose from mnn2 mannan (Figure 4. 25 b), confirming their α -1,6-mannosidic activity. Consistent with previous observations, BS_04090^{GH76} hydrolysed mnn2 mannan into a pool of fragments, predominantly consisting of di-, tri-, and tetra-oligosaccharides (Figure 4. 25 b). In a combination with BS_04090^{GH76}, BS_04089^{GH125} mediated breakdown on the di-, tri-, and tetra-saccharides (Figure 4. 25 b), demonstrating that an α -1,6-linked tetramer is the longest substrate for this GH125.

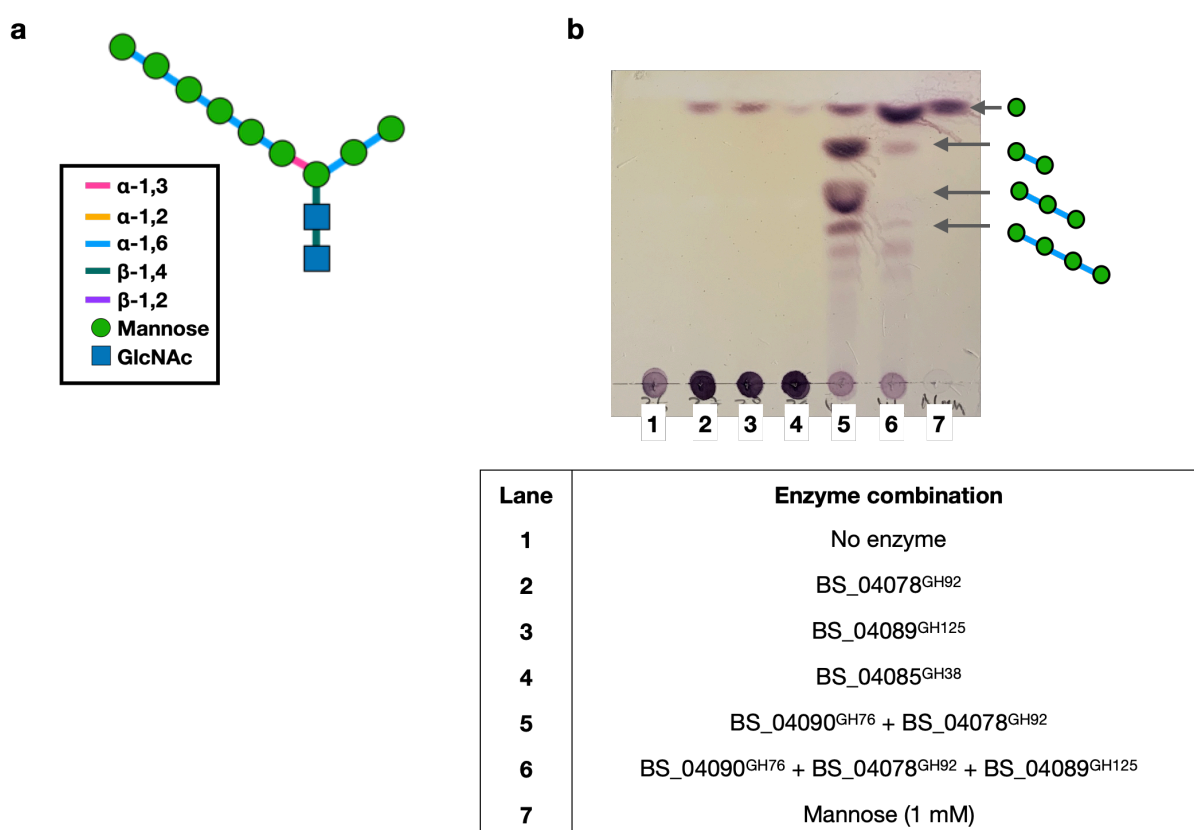


Figure 4. 25 Enzymatic degradation of mnn2 mannan. Panel a: diagram showing structure of mnn2 mannan; Panel b: activity of BS_04078^{GH92}, BS_04089^{GH125}, BS_04085^{GH38}, and BS_04090^{GH76} against mnn2 mannan. Table summarising enzymatic cocktails is shown, reactions were incubated overnight at 37 °C.

To dissect the enzymatic pathway further, BS_04078^{GH92}, BS_04089^{GH125}, BS_04090^{GH76}, BS_04085^{GH38}, and BS_01537^{GH38} were mixed in different

combinations and assayed against a more complex mannan substrate, extracted from mnn5 *S. cerevisiae* strain (Figure 4. 26). BS_04078^{GH92} released mannose from mnn5 mannan (Figure 4. 26 b). This indicates that consistent with its activity on α -1,2-disaccharide, enzyme is able to remove α -1,2-linked mannosides from mnn5 mannan. BS_04090^{GH76} mediated breakdown of mnn5 mannan, producing fragments, that are most likely complex α -1,2-; α -1,6-linked oligosaccharides (Figure 4. 26 a). Addition of other mannosidases disassembled these oligosaccharides further (Figure 4. 26 b). Fading of the sample spot at the origin highlights the extent of mannan degradation (Figure 4. 26 b). This indicates that these six enzymes are able to hydrolyse mnn5 mannan almost completely, leaving a pool of inaccessible substrates.

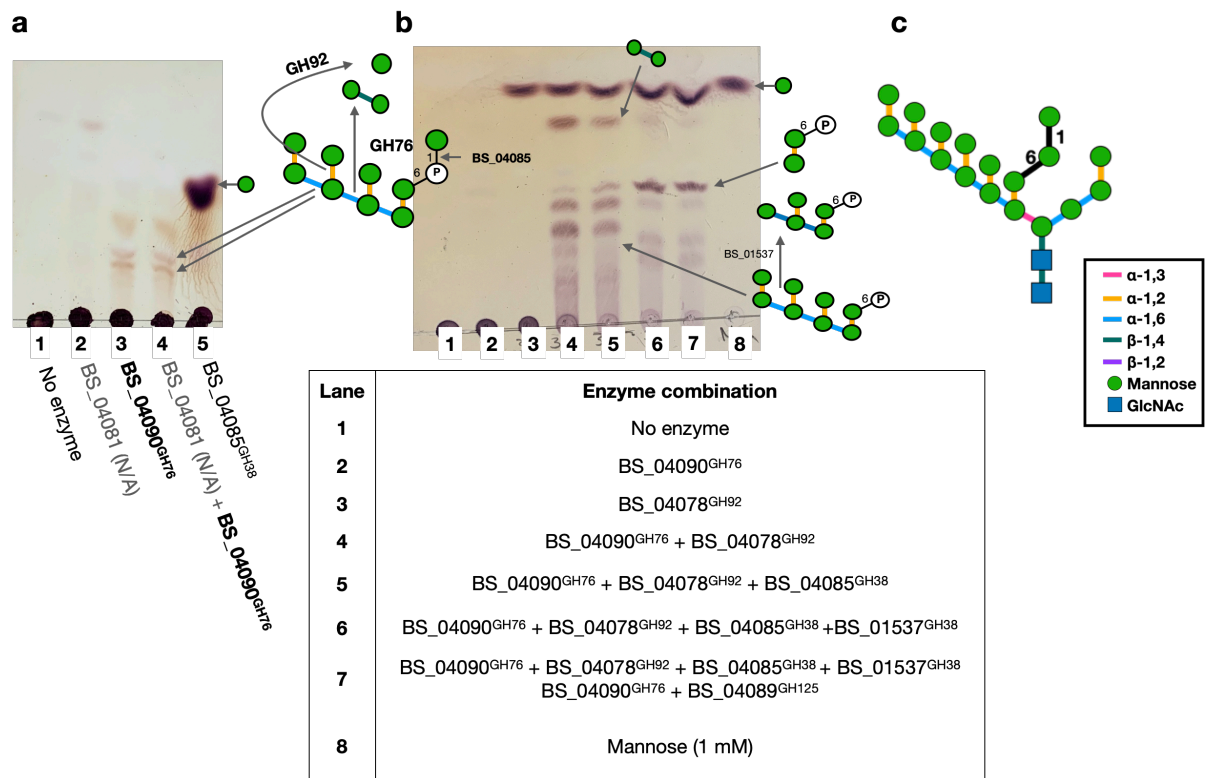


Figure 4. 26 Enzymatic degradation of mnn5 mannan. Panel b: activity of BS_04090^{GH76} against mnn5 mannan, 9 μ l of reaction was spotted onto TLC plate to visualise oligosaccharides; panel c: activity of BS_04078^{GH92}, BS_04090^{GH76}, BS_04085^{GH38}, BS_01537^{GH38}, and BS_04089^{GH125}, mixed in combinations as shown in the table, 6 μ l of reaction was resolved. Panel c: structure of mnn5 mannan. All reactions were incubated with 5 mg ml⁻¹ mnn5 mannan at 37 °C overnight

The complexity of the substrate was then increased, and enzymes were tested against mnn1 mannan, which is composed of two α -1,2-linked mannosides attached to the backbone (Figure 4. 27). This showed that BS_04090^{GH76} was able to initiate breakdown of mnn1 mannan (Figure 4. 27 b), releasing branched oligosaccharides. Combined, Bs enzymes performed further breakdown of mnn1 mannan (Figure 4. 27 c, d).

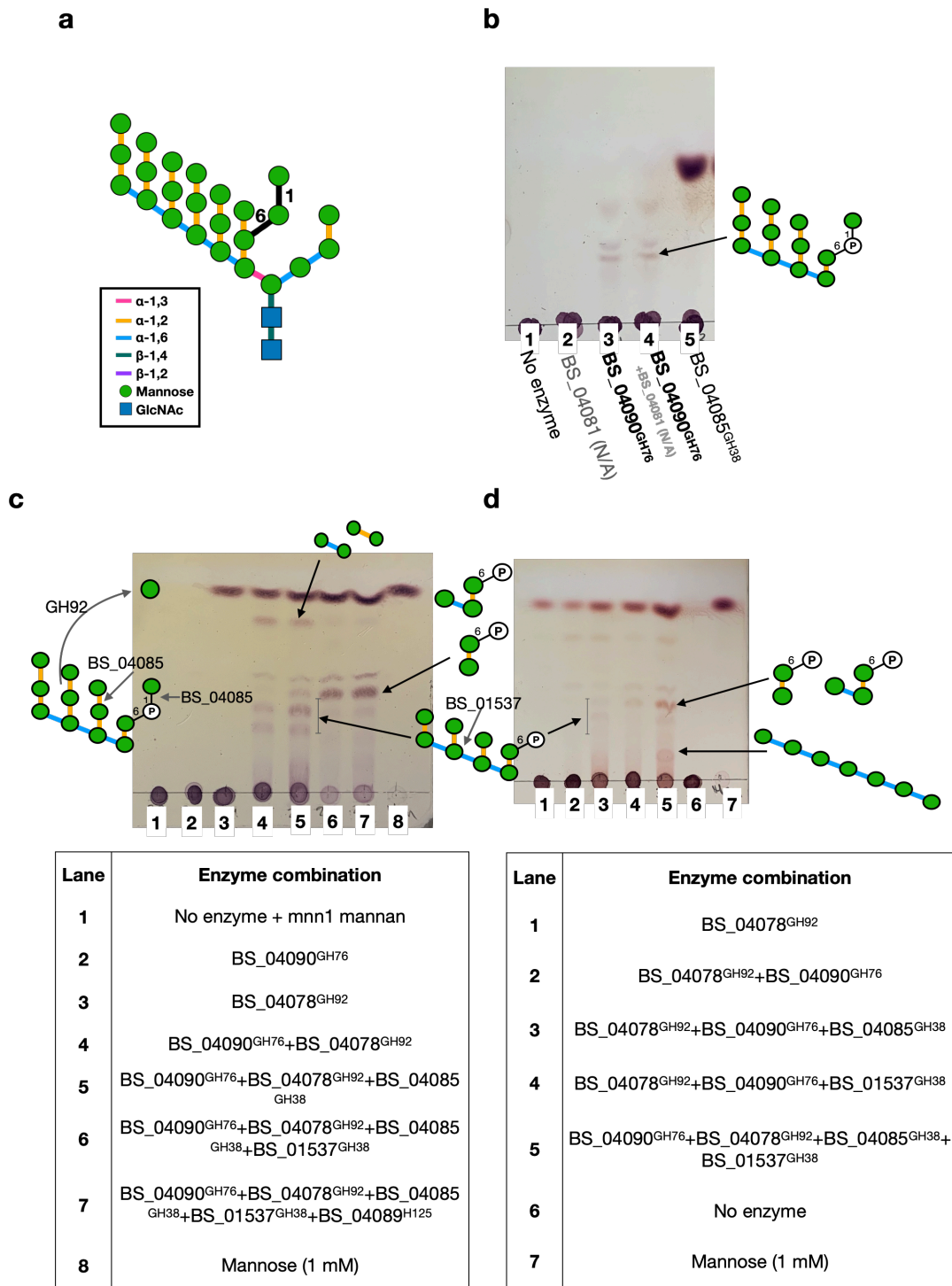


Figure 4. 27 Enzymatic degradation of mnn1 mannan. Panel a: structure of mnn1 mannan; Panel b: activity of BS_04090^{GH76} against mnn1 mannan, TLC shows 9 μ l of reaction; Panel c: activity of BS_04078^{GH92}, BS_04090^{GH76}, BS_04085^{GH38}, BS_01537^{GH38}, and BS_04089^{GH125} against mnn1 mannan in combinations shown; Panel d: enzymatic degradation of mnn1 mannan by indicated enzymes. All reactions were performed at 37 °C overnight.

4. 3. 8. 2 Activity of BS_04078^{GH92}, BS_04089^{GH125}, BS_04085^{GH38}, BS_01537^{GH38}, BS_04090^{GH76} against α -mannan from wild type *S. cerevisiae*.

It was then investigated whether exo-acting mannosidases: BS_01537^{GH38}, BS_04085^{GH38}, BS_04078^{GH92}, BS_04098^{GH125} work in concert with BS_04090^{GH76} to depolymerise mannan from wild type *S. cerevisiae* (Figure 4. 28 a). This showed that in the presence of BS_04085^{GH38}, BS_04090^{GH76} liberated a ladder of oligosaccharides (Figure 4. 28 b), indicating BS_04085^{GH38} alone is able to debranch wild type α -mannan, making it more accessible for BS_04090^{GH76}. BS_04090^{GH76} was also able to access the backbone in the presence of BS_01537^{GH38} (Figure 4. 28 b), however the products generated by BS_04090^{GH76} differ to the ones seen in the presence of BS_04085^{GH38} (Figure 4. 28 b). This demonstrates that the two GH38s indeed target different bonds in the sidechains. Similarly, BS_04078^{GH92} alone and in a combination with BS_04085^{GH38} and BS_04090^{GH76} performed efficient debranching of α -mannan (Figure 4. 28 c). The products of this reaction further resolved in the presence of BS_04089^{GH125} (Figure 4. 28 c). This indicates that together BS_04078^{GH92} and BS_04085^{GH38} are able to debranch wild type yeast α -mannan enough to expose its α -1,6-linked backbone. This set of assays demonstrates that *B. salyersiae* possesses an efficient enzymatic apparatus to implement breakdown of *S. cerevisiae* α -mannan.

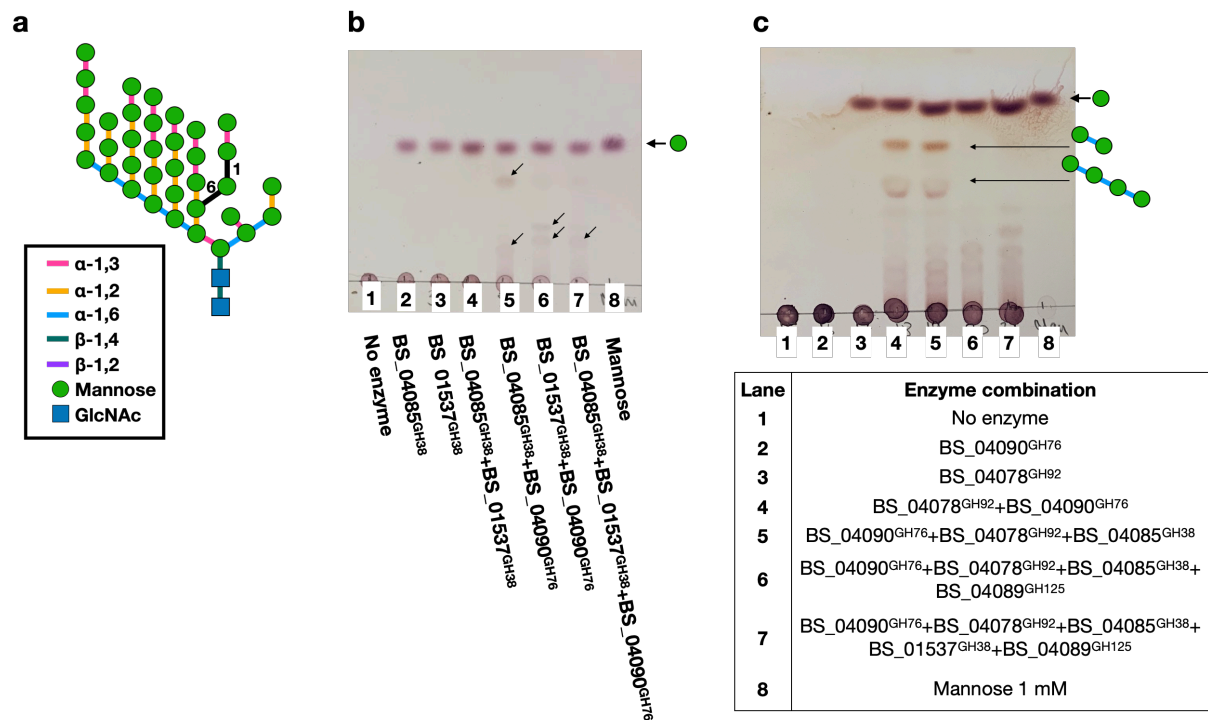


Figure 4.28 Enzymatic degradation of mannan from wild type *S. cerevisiae*. Panel a: Structure of wild type α -mannan. Panel b: activity of exo-acting BS_04085^{GH38} and BS_01537^{GH38} in incubated in combinations with endo-acting BS_04090^{GH76} against wild type yeast mannan, Panel c: activity of BS_04078^{GH92}, BS_04090^{GH76}, BS_04085^{GH38}, BS_01537^{GH38}, and BS_04089^{GH125} against yeast mannan in combinations shown. Reactions were incubated at 37 °C overnight.

4.3.9 *B. salyersiae* enables ‘sharing’ of mannan from *S. cerevisiae*.

Previously, it was shown that Bt deploys a selfish mechanism for mannan utilisation (Cuskin et al., 2015b). Unlike Bs, Bt did not leave long oligosaccharides in the culture supernatant when it is grown on mannan from *S. cerevisiae*. In *in vitro* competition assays where *S. cerevisiae* was given as a sole carbon source Bt outcompeted *B. cellulosilyticus* WH2 or *B. xylanisolvens* NLAE-zl P352 (Cuskin et al., 2015b), strongly demonstrating that Bt does not share or make the polysaccharide more accessible to other member of the gut microbiota. It was

then investigated whether the alternative mechanism for *S. cerevisiae* mannan degradation employed by *B. salyersiae* permits sharing of the polysaccharide. To address this, our *Bacteroides* library was screened against α -mannan by-products generated by Bs. *B. salyersiae* was grown in minimal media containing 15 mg ml⁻¹ *S. cerevisiae* mannan to mid-exponential phase OD₆₀₀=1.0. Cells were separated by centrifugation at 6,000 rpm and collected supernatant was sterilised by autoclaving. Defrosted supernatant was filter-sterilised using a 0.2 μ m filter and diluted 1:2 with fresh 2X minimal media to replenish nutrients necessary for growth. This produced conditioned media, which contained approximately 7 mg ml⁻¹ of digested *S. cerevisiae* mannan. The strains from the library were grown in conditioned media anaerobically at 37 °C, as described in Chapter 2 Section 2. 5. 1. Glucose or mannose at 10 mg ml⁻¹ were used alongside as a positive control. For every non-mannan-degrading strain, with the exception of Bt and Bs, *S. cerevisiae* mannan was used as a negative control. Both Bt and Bs displayed robust growth in conditioned media but to a lower OD₆₀₀ as compared to conditions where wild type mannan is used as a sole carbon source. This was expected, as conditioned media contained a smaller amount of available substrate. Conditioned media induced differential growth of a set of poor mannan degraders, which included *B. xylanisolvans*, *B. ovatus*, and *B. finegoldii*, however this effect was not ubiquitous and the remaining *Bacteroides* species were unable to grow (Figure 4. 29). To ensure that this effect was mediated by the by-products of Bs, a similar set of assays was repeated using conditioned media produced by Bt. None of the tested strains except for Bs were able to utilise Bt conditioned media (Figure 4. 30), indicating that only Bs was capable of inducing robust growth on mannan of other *Bacteroides* species.

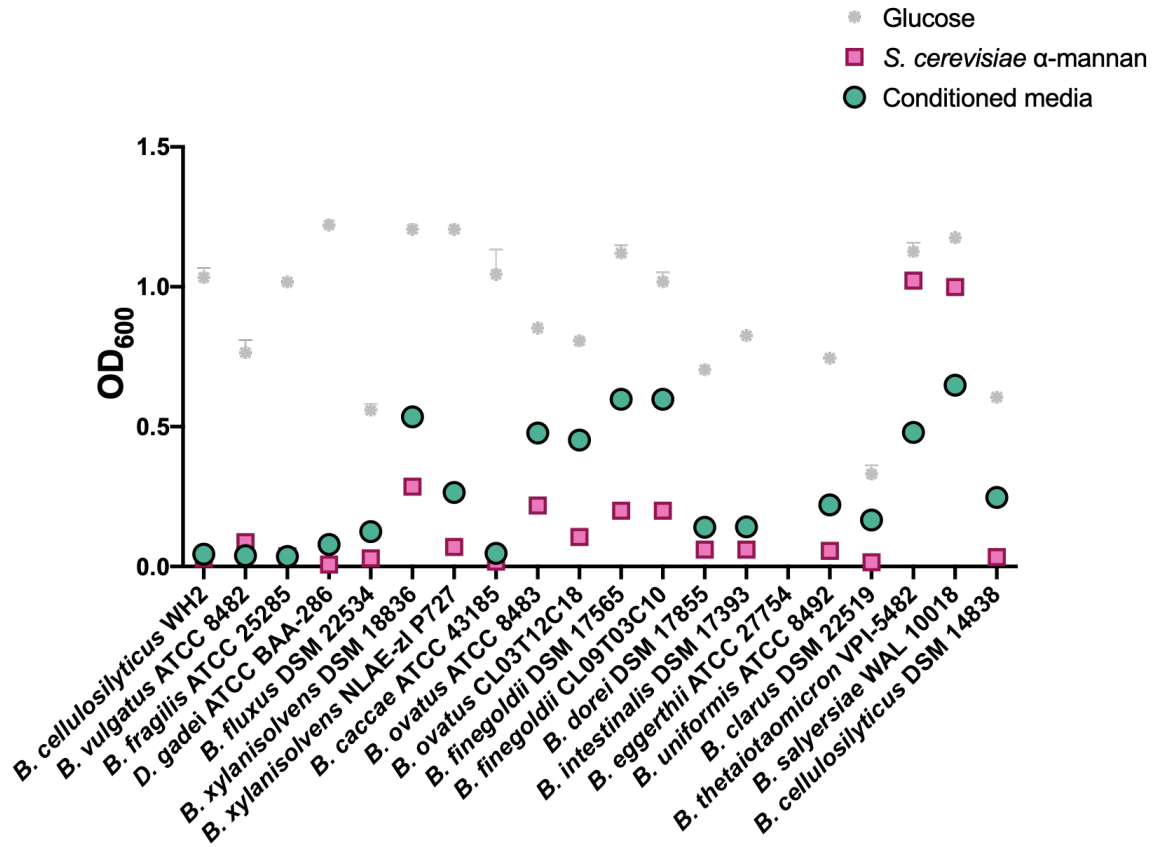


Figure 4. 29 Utilisation of *B. salyersiae*-digested *S. cerevisiae* mannan by *Bacteroides* strains. Strains of *Bacteroides* species were inoculated into Bs conditioned media and grown anaerobically at 37 °C for 28 h, maximum OD₆₀₀ was recorded (green circle). Growth on glucose (grey star) and *S. cerevisiae* mannan (pink square) were used as positive and negative controls, respectively. Dataset is representative of 3 biological repeats from at least 3 technical replicates, error bars show standard deviation.

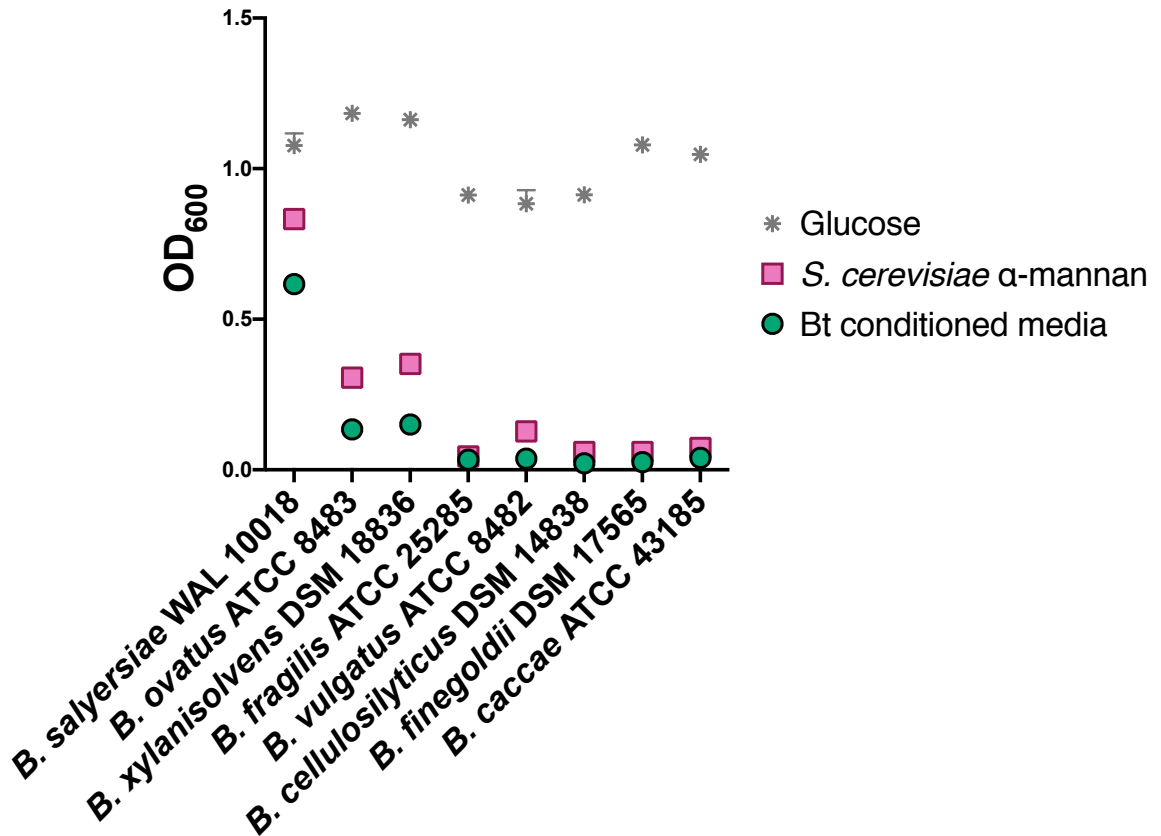
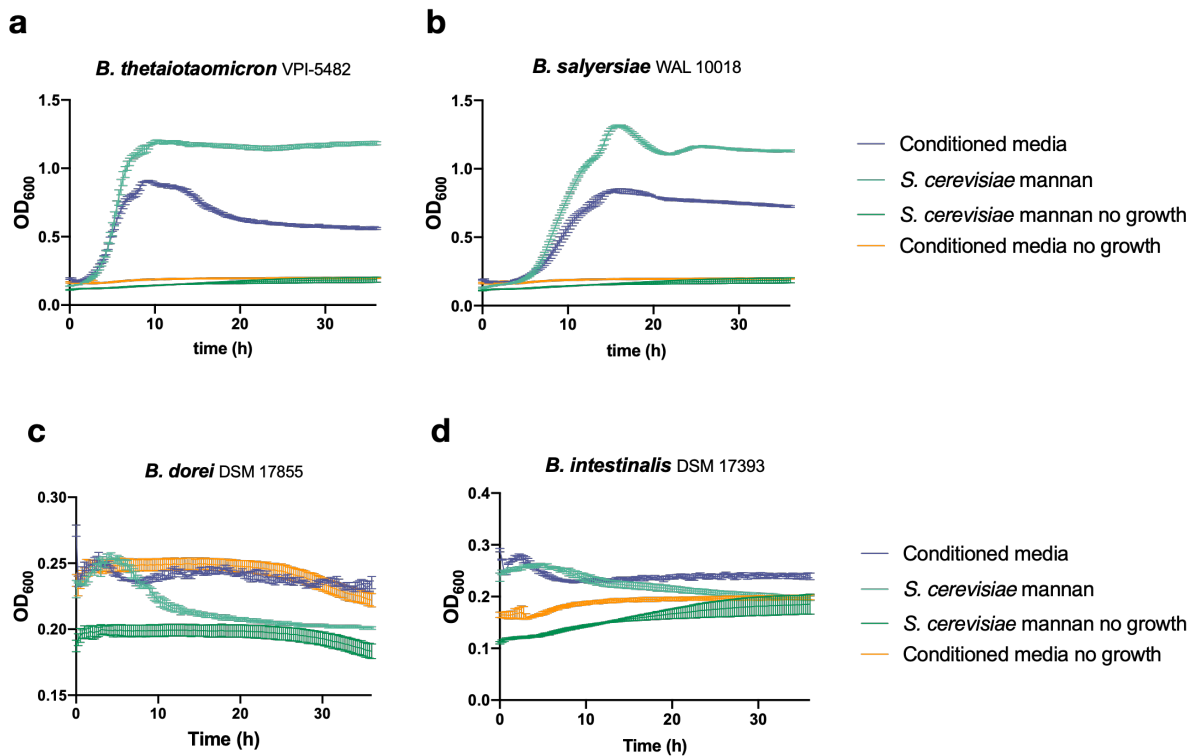


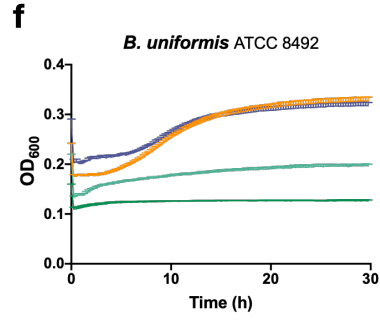
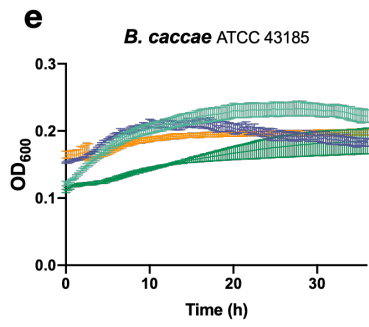
Figure 4. 30 Utilisation of Bt-digested α-mannan but *Bacteroides* species. Strains were inoculated into Bt-conditioned media (green circle) and OD₆₀₀ was recorded after 28 hours. Growths on glucose (grey star) and mannan (pink square) were included as controls. Error bars show standard error from 3 biological repeats.

To analyse the use of Bs-conditioned media more closely, change in OD₆₀₀ was monitored continuously. Both Bt and Bs grew to a lower OD₆₀₀ (Figure 4. 31 panels a and b). No apparent growth in conditioned media was observed for any of the following type strains: *B. dorei*, *B. intestinalis*, *B. caccae*, *B. uniformis*, *B. cellulosilyticus*, *B. vulgatus*, *B. fragilis*, *B. clarus*, or *B. fluxus* (Figure 4. panels c – h; o – r) In contrast, growth of *B. ovatus*, *B. xylanisolvans*, and *B. finegoldii* was profoundly enhanced (Figure 4. 31 panels i – n).

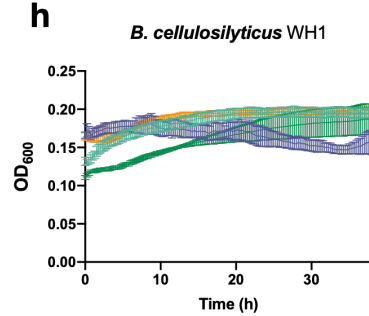
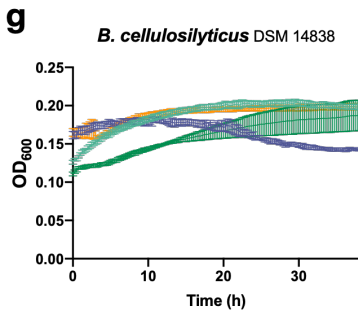
Differential substrate utilisation is a common phenomenon observed in different strains of the same species, therefore the ability to grow in conditioned media was

also analysed for another human isolate of *B. cellulosilyticus* WH1 and and a porcine strain of *B. xylanisolvens* NLAE-zl P727. For the same reason, growth of the type *B. ovatus* ATCC 8483 and *B. finegoldii* DSM 17565 strains was compared to closely related strains: *B. ovatus* CL03T12C18 and *B. finegoldii* CL09T03C10, which unlike the type strains, contain components of the anti-fungal type 6 secretion system (Verster et al., 2017). Interestingly, *B. ovatus* CL03T12C18, *B. finegoldii* CL09T03C10, *B. xylanisolvens* NLAE-zl P727 displayed poor growth on branched *S. cerevisiae* mannan compared to their type clonemates (Figure 4. 31 panels j, l, n), however their ability to utilise mannan pre-digested by Bs was still retained (Figure 4. 31 panels j, l, n). This difference is particularly striking between *B. finegoldii* CL09T03C10 and DSM 17565 strains (Figure 4. 31 panels m and n). Human *B. cellulosilyticus* isolate, WH1, was still unable to grow in conditioned media (Figure 4. 31 panel h).

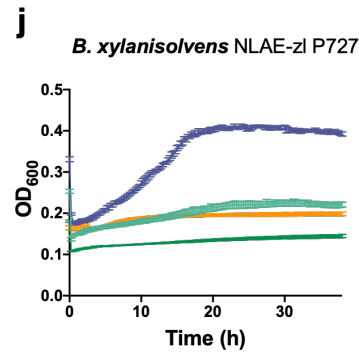
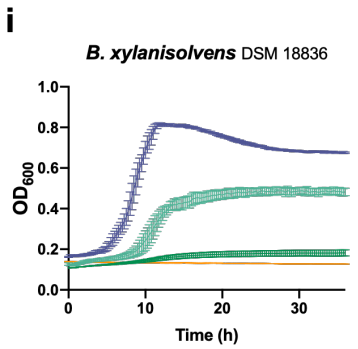




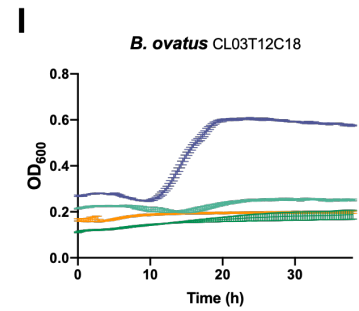
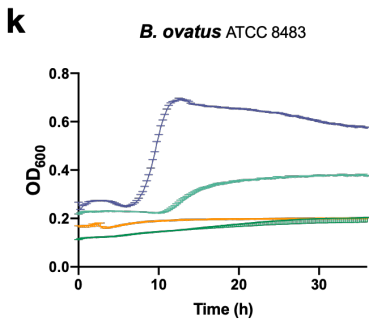
- Conditioned media
- *S. cerevisiae* mannan
- *S. cerevisiae* mannan no growth
- Conditioned media no growth



- Conditioned media
- *S. cerevisiae* mannan
- *S. cerevisiae* mannan no growth
- Conditioned media no growth



- Conditioned media
- *S. cerevisiae* mannan
- *S. cerevisiae* mannan no growth
- Conditioned media no growth



- Conditioned media
- *S. cerevisiae* mannan
- *S. cerevisiae* mannan no growth
- Conditioned media no growth

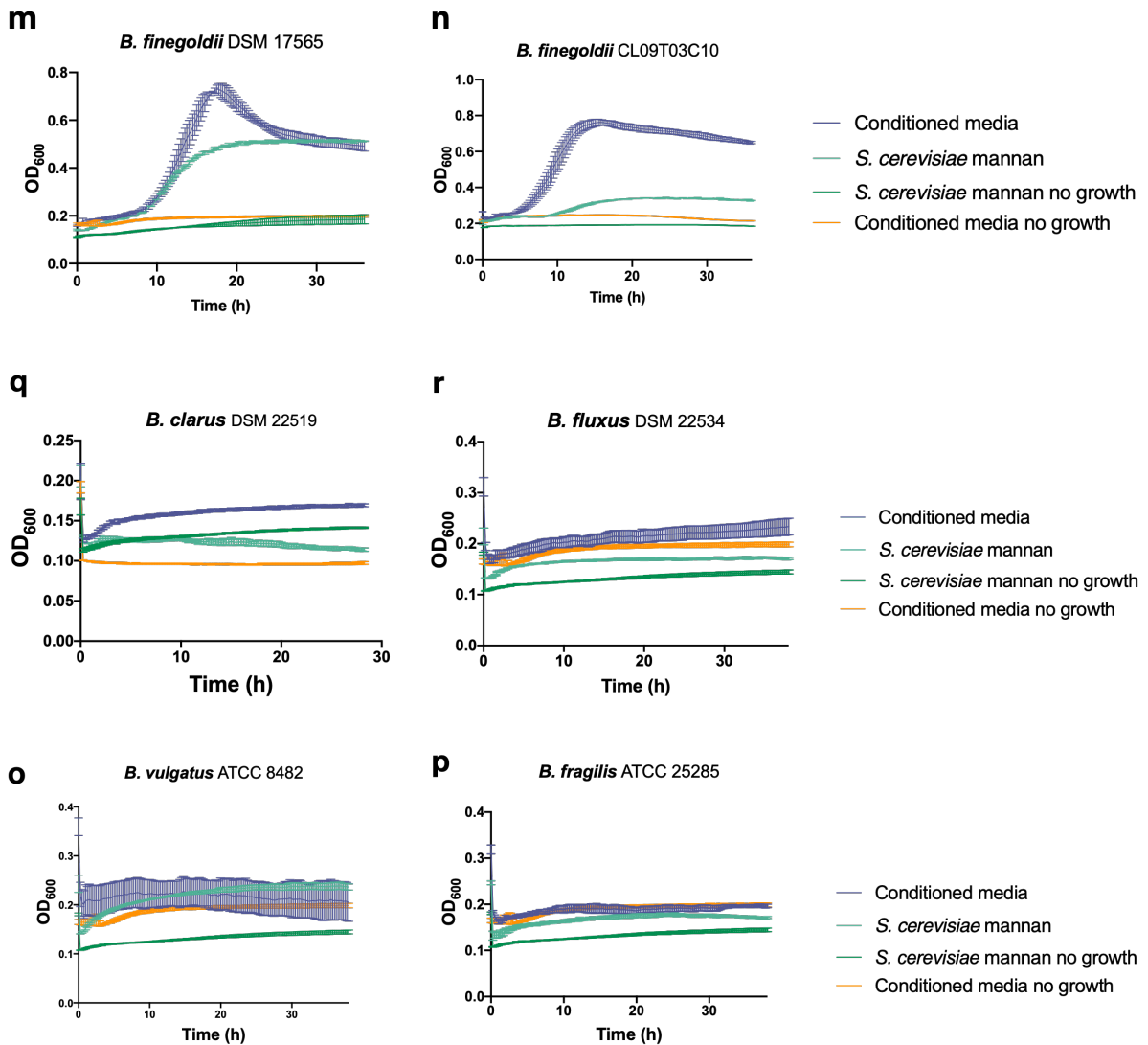


Figure 4.31 Utilisation of either native or pre-digested *S. cerevisiae* mannan by *Bacteroides* species. 18 different *Bacteroides* strains were inoculated into Bs-conditioned media (purple trace) or minimal media with mannan (teal trace). Strains were grown anaerobically at 37 °C for 38 h. Conditioned media and mannan minimal media without bacterial growth are shown in orange and green traces, respectively. Error bars show standard deviation. Dataset is representative of 3 biological replicates from 6 technical repeats

Differential growth of a certain subset of *Bacteroides* species and complete absence of growth in the others was counter-intuitive, as previous data showed that a substantial amount of extracellular mannose was accumulated by Bs as a result of its growth on *S. cerevisiae* mannan (Figure 4.2 and Figure 4.3). Mannose is

a monosaccharide, which could be expected to promote growth of a range of bacterial species. Utilisation of extracellular mannose in conditioned media by *Bacteroides* species was then analysed. Bacterial strains were grown in conditioned media as described above. Cultures were collected at the 38-hour time point and cells were separated by centrifugation at 13,000 rpm. The supernatant was collected and stored at -20 °C until analysis. The concentration of available mannose in collected supernatant was measured using a mannose detection kit. This assay showed that prior to bacterial inoculation conditioned media contained 310 µM of mannose (Figure 4. 32). Interestingly, mannose was used by the species that did not display growth in conditioned media (such as *B. caccae*, *B. fragilis*, *B. vulgatus*, and *B. intestinalis*) (Figure 4. 32), whereas species that thrive in conditioned media such as *B. xylanisolvens* or *B. fingoldii* do not completely deplete the mannose pool available to them in the media (Figure 4. 32). These data suggest that the amount of mannose in conditioned media is not sufficient to support bacterial growth and that the robust growth is promoted by complex manno-oligosaccharides. Interestingly, mannose was almost undetectable after growth of *B. ovatus* in conditioned media.

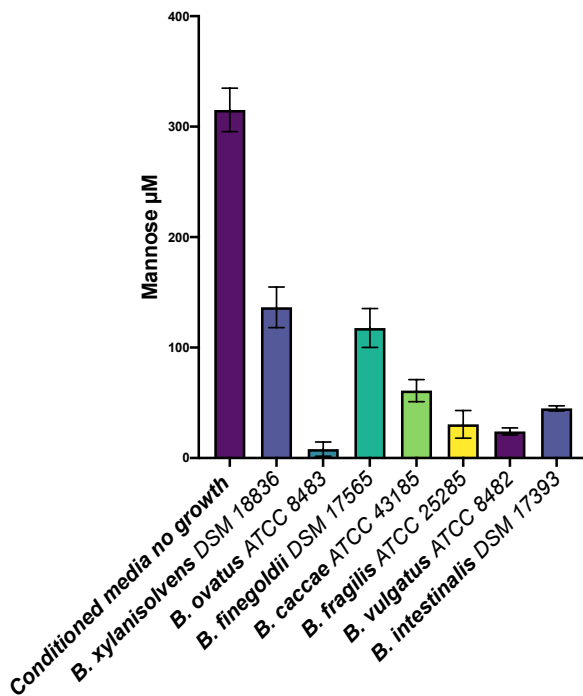


Figure 4. 32 Mannose concentration in conditioned media before and after bacterial growth. *Bacteroides* strains were grown in conditioned media and supernatant was collected after 38 hours. Mannose concentrations were measured with a linked enzyme assay using a Mannose detection kit. Error bars show SD. Dataset was generated from 3 biological replicates and 3 technical repeats.

4. 3. 10 Cross-feeding of *S. cerevisiae* mannan between *B. salyersiae* and *B. xylanisolvans* *in vitro*.

Cross-feeding of manno-oligosaccharides with the non-mannan users was further investigated. Here, *B. salyersiae* and *B. xylanisolvans* were co-cultured together, having mannan as a sole carbon source. Both *B. salyersiae* WAL 10018 and *B. xylanisolvans* DSM 18836 were grown on glucose, cells were collected from the mid-exponential phase $\text{OD}_{600}=0.7$, washed three times with sterile PBS, and resuspended in 10 ml PBS. Equal amounts of both strains (6% v/v) were inoculated into tubes containing fresh minimal media supplemented with either *S.*

cerevisiae mannan or mannose. Mono-culture controls, where Bs or Bx were grown individually on either mannan or mannose were also included. Cultures were then grown anaerobically at 37 °C, and OD₆₀₀ was monitored hourly. For the Bs-Bx co-cultures on mannan, growth of *B. salyersiae* on mannan in monoculture was used as comparator, and 1 ml of mono- and co-cultures was collected at the following growth phases: start (OD₆₀₀=0), early exponential (OD₆₀₀=0.6), mid-exponential (OD₆₀₀=1.0), stationary (OD₆₀₀=2.0) (Figure 4. 34 panel a). For co-cultures on mannose, samples were collected with the reference to the growth curve of Bs on mannose: start (OD₆₀₀=0), early exponential (OD₆₀₀=0.5), mid-exponential (OD₆₀₀=0.8), stationary (OD₆₀₀=2.0) (Figure 4. 33 a). To monitor change in CFU ml⁻¹, a series of 10-fold dilutions was plated out at each growth phase. In addition, at each time point genomic DNA was extracted from all co-culture samples and relative abundance of each strain was determined by qPCR, using unique marker genes, Bs_04085^{GH38} and BX_2930^{GH10}, to identify *B. salyersiae* and *B. xylanisolvens*, respectively (Chapter 2 Section 2. 5. 5).

4. 3. 10. 1 Competition for mannose

As expected, both Bs and Bx utilised mannose as a carbon source in monoculture. Both Bs and Bx monocultures as well as Bs-Bx co-culture presented similar growth patterns, reaching the same maximum O₆₀₀ (Figure 4. 33 a). In co-culture, the abundance of Bs and Bx remained constant throughout the experiment (Figure 4. 33 b), with the exception of the stationary phase, where Bx began to dominate over Bs (Figure 4. 33 b). However, CFU ml⁻¹ data indicate that neither Bs nor Bx impaired the ability of each other to grow in co-culture (Figure 4. 33 c, d), suggesting that mannose is shared between the two species.

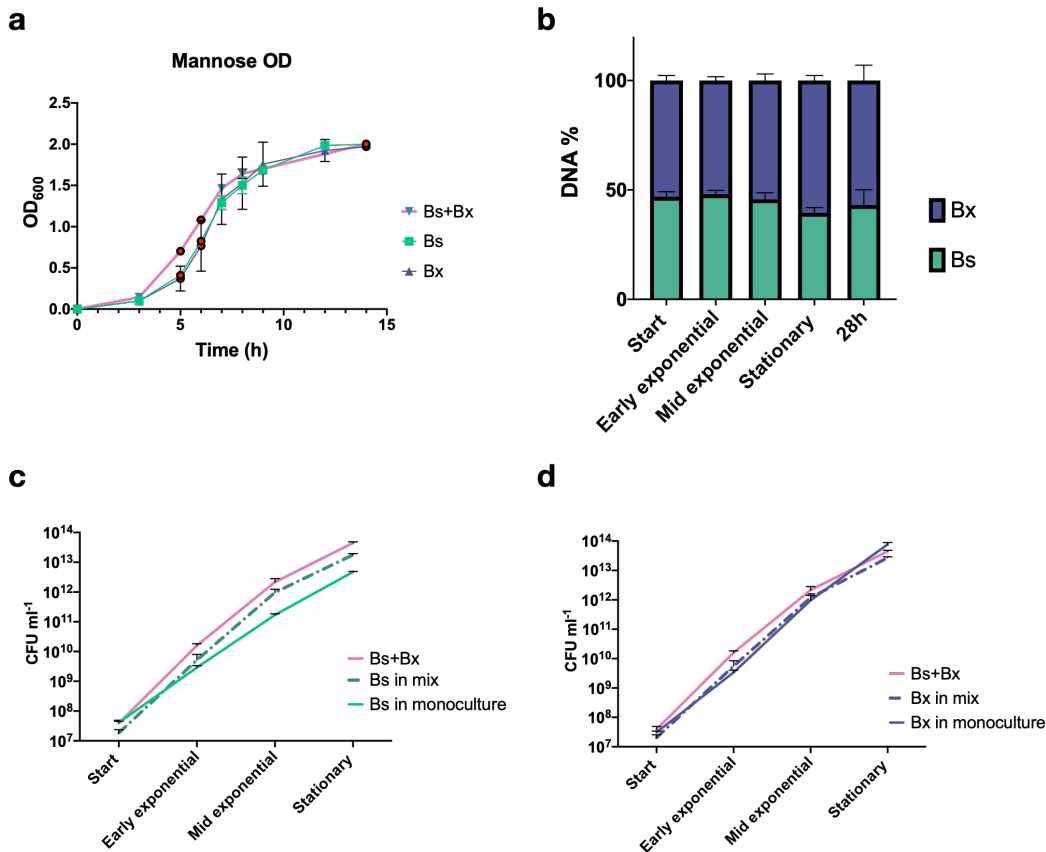


Figure 4.33 Sharing of mannose between *B. salyersiae* and *B. xylanisolvens*. *B. salyersiae* WAL 10018 and *B. xylanisolvens* DSM 18836 were co-cultured on mannose as a sole carbon source in anaerobic environment at 37 °C. Independent Bs and Bx monocultures were also included as controls. OD₆₀₀ was monitored hourly Panel a: OD₆₀₀ of Bs-Bx co-culture (pink trace), Bs monoculture (green trace), Bx monoculture (purple trace), red circles indicate time points when samples were collected; Panel b: ratio of Bs (green) to Bx (purple) in co-culture, identified by qPCR using species-specific genetic markers; Panel c: CFU ml⁻¹ of Bs in monoculture (green trace) and co-culture (dashed teal trace); Panel d: CFU ml⁻¹ of Bx in monoculture (purple) and co-culture (dashed purple trace). Pink trace in panels c and d shows total co-culture CFU ml⁻¹, all CFU ml⁻¹ were determined by colony counts. Error bars show SD. Data are representative of 3 biological replicates from 2 independent experiments.

4. 3. 10. 2 Competition for *S. cerevisiae* mannan

Consistent with previous observations, Bs displayed robust growth (max $OD_{600}=2.0$) on branched mannan from *S. cerevisiae* (Figure 4. 34 a), achieving 10^7 -fold change in $CFU\ ml^{-1}$ at the stationary phase (Figure 4. 34 c). In contrast, Bx presented poor growth on mannan in monoculture (max $OD_{600}=0.5$), which was preceded by a 10-hour lag phase (Figure 4. 34 a). This resulted in a 10^3 -fold increase in $CFU\ ml^{-1}$ (Figure 4. 34 d). Interestingly, Bs-Bx co-culture reached the same maximum $OD_{600} = 2.1$ as Bs alone (Figure 4. 34 a). Genomic DNA analysis showed that the co-culture was inoculated with Bs and Bx at equal proportions at the beginning of experiment (Figure 4. 34 b). At the early- and mid-exponential phases the ratio was shifted, and the co-culture comprised of 70% Bs and 30% Bx. This shift was then reverted at the stationary phase, where the co-culture again contained equal amounts of both Bt and Bs (Figure 4. 34 b). This ratio was maintained at the 28-hour time point (Figure 4. 34 b). This indicates that Bs is able to utilise mannan first, initiating mannan breakdown and therefore outcompeting Bx at the early growth phases. Bs-mediated mannan depolymerisation results in accumulation of less complex polymers in the media, which are used as substrates for Bx growth. Sharing was further demonstrated by the $CFU\ ml^{-1}$ data, which showed that the growth of Bs was unimpeded by the presence of Bx, as it continued to replicate in co-culture the same way as in monoculture (Figure 4. 34 c). In contrast, despite being outcompeted by Bs at the early and mid-exponential phases, Bx still managed to undergo $10^4 - 10^5$ -fold increase in $CFU\ ml^{-1}$ during these initial growth phases (Figure 4. 34 d). Bx reached its highest $CFU\ ml^{-1}$ at the stationary phase, which was at least 100-times higher than $CFU\ ml^{-1}$ achieved by Bx in monoculture (Figure 4. 34 d).

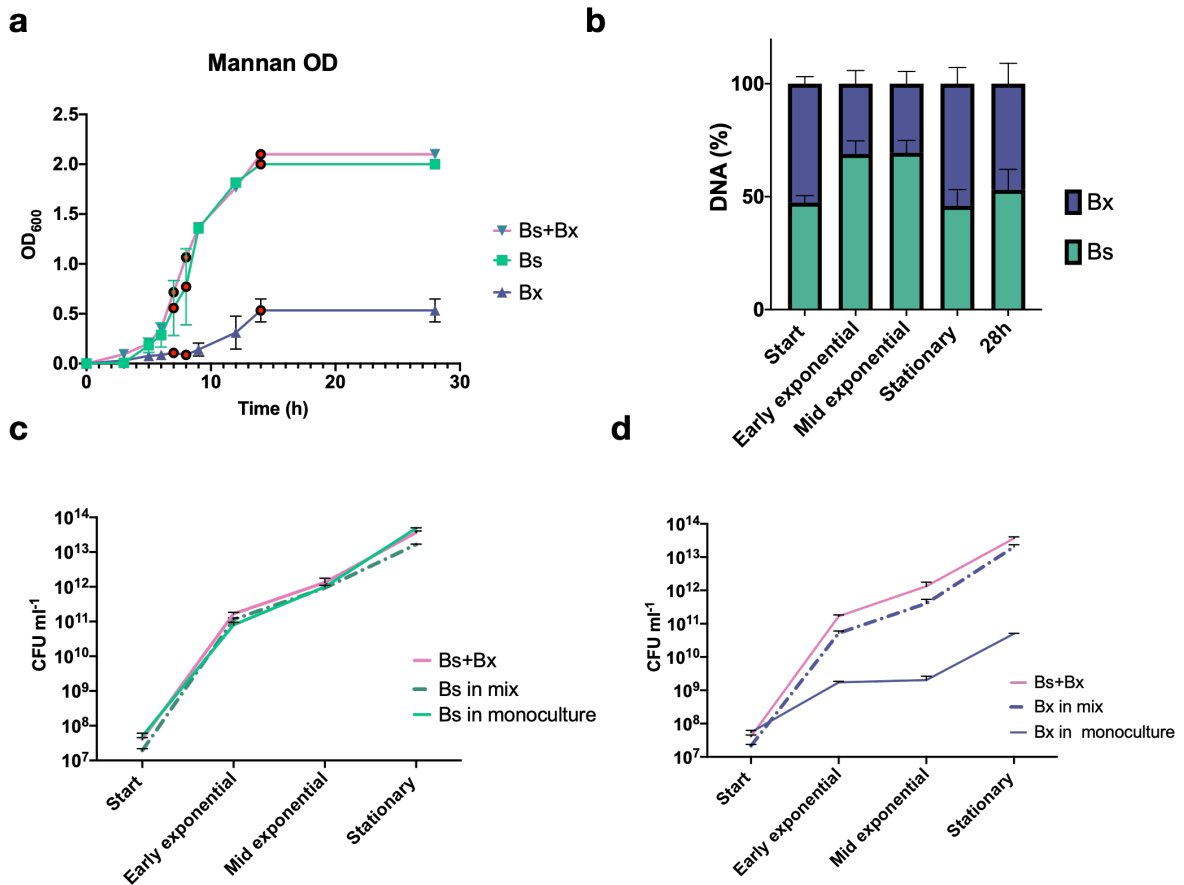


Figure 4. 34 Sharing of Mannan from *S. cerevisiae* between *B. salyersiae* and *B. xylanisolvens*. *B. salyersiae* WAL 10018 and *B. xylanisolvens* DSM 18836 were co-cultured on *S. cerevisiae* mannan as a sole carbon source anaerobically at 37 °C. Both Bs and Bx were also cultured on mannan independently. OD₆₀₀ was monitored hourly. Panel a: OD₆₀₀ of Bs-Bx co-culture (pink trace), Bs monoculture (green trace), Bx monoculture (purple trace), red circles indicate time points when samples were collected; Panel b: abundance of Bs (green) and Bx (purple) in co-culture, identified by qPCR using species-specific genetic markers; Panel c: CFU ml⁻¹ of Bs in monoculture (green trace) and co-culture (dashed green trace); Panel d: CFU ml⁻¹ of Bx in monoculture (purple) and co-culture (dashed purple trace). Pink trace in panels c and d shows total co-culture CFU ml⁻¹, all CFU ml⁻¹ were determined by colony counts. Error bars show SD. Data represent 3 biological replicates and 2 technical repeats.

To investigate the mechanism of yeast mannan breakdown in Bs-Bx co-culture, cell free spent media was analysed with TLC. Co-culture and mono-culture samples were collected at time points as indicated in Figure 4. , the time course

spanned different growth phases (Figure 4. 35 a and b). Supernatant from each time point was analysed with TLC. As shown in Figure 4. c, Bs continued to accumulate manno-oligosaccharides and mannose in the co-culture with Bx. Interestingly, degradation of mannan seemed more extensive in co-culture (Figure 4. 35 c) than in monoculture with Bs (Figure 4. 35 e). Bx did not release manno-oligosaccharides when grown on mannan independently (Figure 4. 35 d). TLC analysis of co-culture supernatant demonstrated that a pool of oligosaccharides gradually accumulated in the media, peaking at the mid exponential phase (Figure 4. 35 c lanes 5-7). This ladder then resolved as the growth progressed into early-stationary phase (Figure 4. 35 c lanes 8-9), indicating that it was consumed by either Bs or Bx. Combined with the data in Figure 4. 34, this suggests that both species utilise mannan in co-culture, where Bs plays a key role in debranching the sidechains to make structures, which are more accessible to Bx. Overall, the data presented in this section demonstrates that the alternative strategy of yeast mannan utilisation deployed by Bs facilitates growth and survival of species unable to degrade polymeric mannan, such as *B. xyloxylicans*.

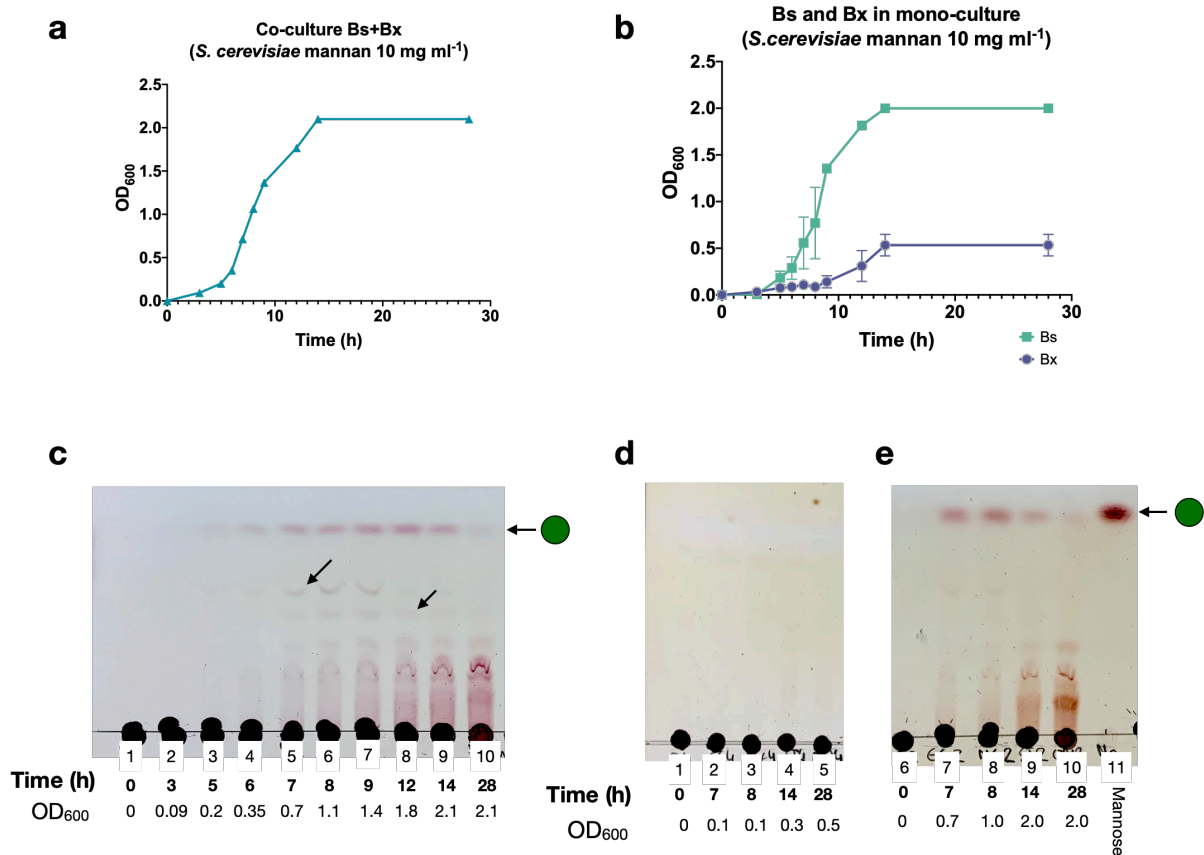


Figure 4.35 Analysis of cell free spent media. Supernatant was collected from Bs-Bx co-culture (a) and their independent monocultures (b) on *S. cerevisiae* mannan at indicated time points. Panel a: OD₆₀₀ of Bs-Bx co-culture on mannan, Panel b: OD₆₀₀ of growth of Bs on mannan (green trace), growth of Bx on mannan. Panel c: Bs-Bx co-culture, arrows indicate manno-oligosaccharides; Panel d: Bx growth on mannan; Panel e: Bs growth on mannan. Green circle shows mannose. Data are representative of 3 biological replicates and 2 technical repeats.

4.3.11 *In vitro* sharing of *S. cerevisiae* mannan between *B. thetaiotaomicron* and *B. salyersiae*, ‘selfish’ versus ‘non-selfish’.

It was previously shown by Cuskin et al. (2015b) that the selfish mechanism of yeast mannan utilisation deployed by *B. thetaiotaomicron* did not permit sharing with other non-mannan users such as *B. xylanisolvens* NLAE-zl-P352 or *B. cellulosilyticus* WH2. It was therefore investigated whether Bs could resist the competition imposed by Bt.

To address this, Bt and Bs were cultured together on *S. cerevisiae* mannan. As described in Section 4. 3. 10, Bt and Bs were both grown on glucose in minimal media, washed, and were then inoculated in equal amounts into minimal media supplemented with either *S. cerevisiae* mannan or mannose. A set of independent monoculture controls was also included. Cultures were grown anaerobically at 37°C, OD₆₀₀ was monitored hourly. Culture samples were collected from 4 growth phases: lag (OD₆₀₀=0), early-exponential (OD₆₀₀=0.5), mid-exponential (OD₆₀₀=0.8), and stationary (OD₆₀₀=1.8), respective to the growth of Bt on *S. cerevisiae* mannan. However, due to the fact that both species in this experiment are mannan users, a fifth time point was collected when Bs reached its maximum OD₆₀₀=2.1. Similarly, a range of 10-fold serial dilutions was plated out to determine CFU ml⁻¹ by colony counts. In addition, at each time point DNA was extracted from both mannan and mannose Bt-Bs co-cultures and proportion of each bacteria was determined with qPCR using unique species-specific genes, BT3780^{GH130} and BS_04085^{GH38}, to identify Bt and Bs, respectively (Chapter 2 Section 2. 5. 5).

4. 3. 11. 1 Competition assay for mannose

As expected, both Bt and Bs were able to grow on mannose in monocultures (Figure 4. 36 a), displaying similar growth patterns. Interestingly, bacterial growth in co-culture was noticeably rapid, as suggested by a sharp increase in OD₆₀₀ (Figure 4. 36 a). This behaviour was unique to Bs-Bt co-culture as it was not observed when Bs was co-cultured with Bx (Figure 4. 33 and Figure 4. 34). Bt-Bs ratio determined by qPCR showed that Bt was able to gradually dominate in the co-culture, however Bs persisted and was able to survive in the presence of Bt (Figure 4. 36 b). CFU ml⁻¹ data are suggestive of a strong competition for the carbon source, as CFU ml⁻¹ in co-culture are 100 and 1000 times lower than when

Bs and Bt, respectively, are grown on mannose on their own (Figure 4. 36 c and d).

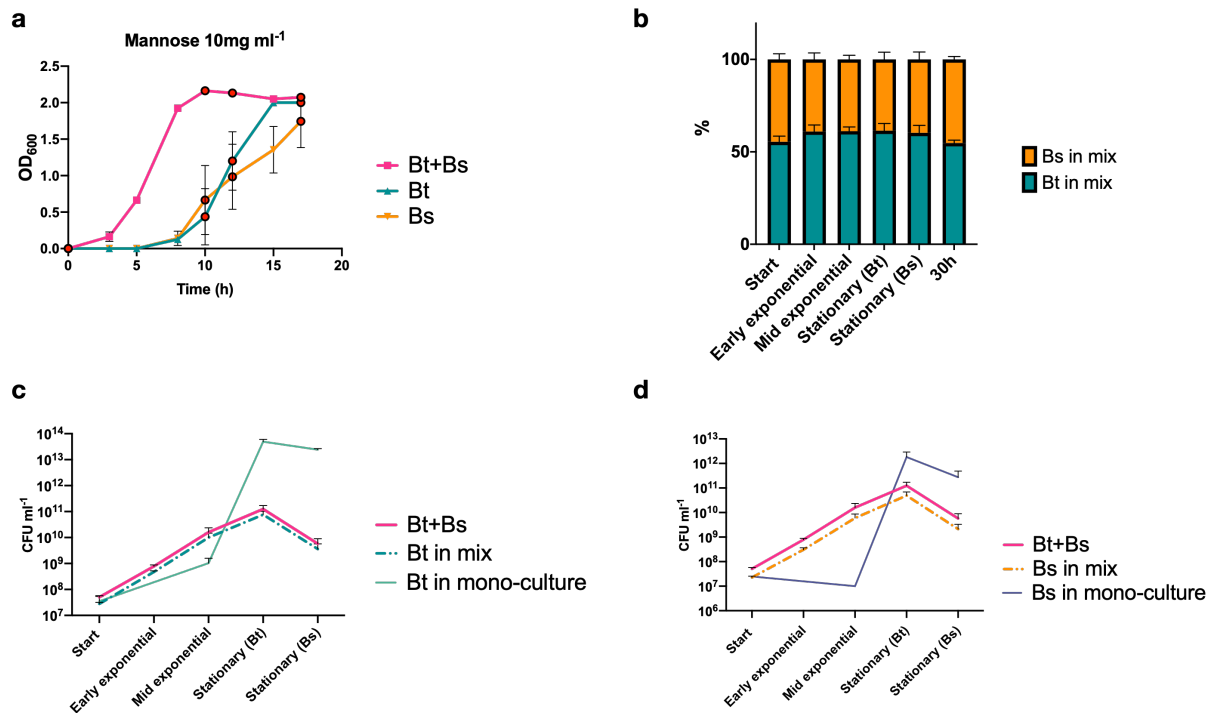


Figure 4. 36 Competition for mannose between *B. salyersiae* and *B. thetaiotaomicron*. *B. thetaiotaomicron* VPI-5482 and *B. salyersiae* WAL10018 were co-cultured on mannose as a sole carbon source anaerobically at 37 °C. Monocultures, where Bt and Bs were grown on mannose individually were included as controls. OD₆₀₀ was monitored at regular intervals. Samples were collected at the specified time points. Panel a: shows OD₆₀₀ of cultures: pink trace – Bt+Bs; teal trace – Bt, orange trace – Bs; Panel b: shows abundance of Bt (teal) and Bs (orange) in co-culture determined by qPCR and unique marker genes; Panel c: shows CFU ml⁻¹ data of Bt in monoculture (teal trace) and co-culture (dashed teal trace); Panel d: shows CFU ml⁻¹ data of Bs in monoculture (purple trace) and co-culture (dashed orange trace). Pink trace in panels c and d shows total CFU ml⁻¹ in co-culture. Error bars show SD, data are representative of 3 biological and technical replicates.

4. 3. 11. 2 Competition for *S. cerevisiae* mannan

Consistent with previously established phenotypes, Bt grew on mannan more rapidly than Bs, who displayed a 10-hour lag phase, which was then followed by robust growth (Figure 4. 37 a). Consistent with previous observations, Bt-Bs co-culture underwent a sharp increase in OD₆₀₀ (Figure 4. 37 a), indicating that bacterial growth was accelerated in co-culture. This was also reflected in the CFU ml⁻¹ data (Figure 4. 37 c and d), which demonstrated that in co-culture Bs (Figure 4. 37 d) lost its characteristic long lag phase and was able to replicate the same way as Bt (Figure 4. 37 c). This is an interesting trait which could suggest that the presence of Bs in co-culture promotes growth of Bt, or vice versa. DNA analysis showed that at the beginning of experiment co-culture comprised of equal amounts of Bt and Bs (Figure 4. 37 b). However, the ratio was quickly shifted to 70% Bt and 30% Bs and remained constant throughout the experiment (Figure 4. 37 b). This shows that Bt dominates the co-culture, demonstrating its strong competitive fitness to mannan utilisation, however Bs is still able to survive in this highly competitive environment better than a non-mannan degrader.

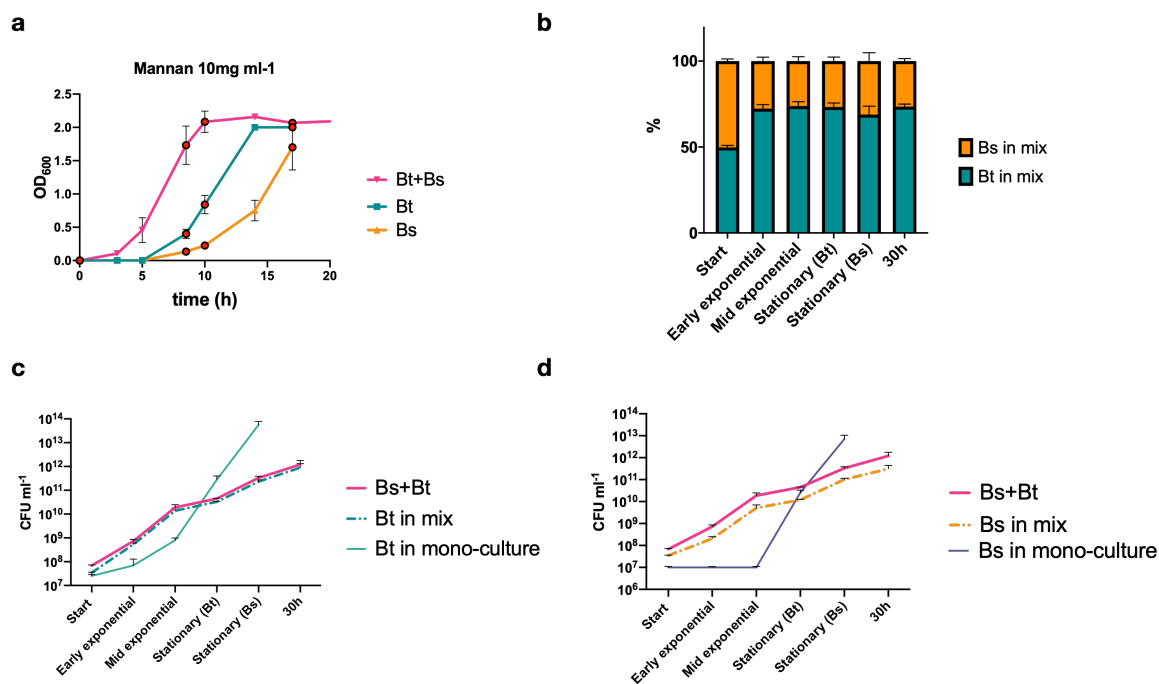


Figure 4.37 Competition for mannan between *B. salyersiae* and *B. thetaiotaomicron*. *B. thetaiotaomicron* VPI-5482 and *B. salyersiae* WAL10018 were co-cultured anaerobically at 37 °C on mannan as a sole carbon source. Monocultures, where Bt and Bs were grown on mannan individually were included as controls. OD₆₀₀ was monitored at regular intervals. Samples were collected at indicated time points. Panel a: OD₆₀₀ of cultures: pink trace – Bt+Bts; teal trace – Bt, orange trace – Bs, red circles indicate time points for sample collection; Panel b: abundance of Bt (teal) and Bs (orange) in co-culture determined by qPCR and unique marker genes; Panel c: CFU ml⁻¹ data of Bt in monoculture (teal trace) and co-culture (dashed teal trace); Panel d: CFU ml⁻¹ data of Bs in monoculture (purple trace) and co-culture (dashed orange trace). Pink trace in panels c and d shows total CFU ml⁻¹ in co-culture. Error bars show SD. Data are generated from 3 biological replicates and 3 independent experiments.

To investigate mannan degradation in Bt-Bs co-culture, cell free spent media was collected from different time points and analysed with TLC. This showed that manno-oligosaccharides and mannose began to appear in the media 5 hours post inoculation (Figure 4.38 a) and continued to accumulate extracellularly at later time points (Figure 4.38 a lanes 4-8). As previously shown by Cuskin et al. (2015b), the selfish mechanism deployed by Bt does not result in accumulation of

oligosaccharides in the extracellular milieu, as these are immediately transported into the periplasmic space (Cuskin et al., 2015b). Accumulation of manno-oligosaccharides is indicative of a 'non-selfish' mechanism implemented by Bs, however usually Bs requires at least 8 hours to initiate mannan breakdown (Figure 4. 2). These data therefore further demonstrate that, despite being outcompeted by Bt, in a co-culture with Bt, Bs manages to continue to utilise mannan in a non-selfish way. Bt-Bs co-culture reached OD₆₀₀ of 0.4 in 3 hours and this growth rapidly continued, reaching mid-exponential growth OD₆₀₀=1.0 in 7 hours (Figure 4. 38 b). At this time point, the independent monoculture of Bt just entered an early exponential growth, while the monoculture of Bs was still in its lag phase (Figure 4. 38 b). However, TLC of the co-culture supernatant (Figure 4. 38 a) is indicative of metabolically active Bs cells, suggesting that Bs was able to grow faster in a co-culture with Bt. This also suggests that mannan degradation occurs in concert, where perhaps Bt alleviates steric constraints, making mannan easier to access for Bs.

In addition to oligosaccharides, gradual accumulation of mannose in the culture supernatant was also observed, which peaked at the 10-hour time point and declined at the later time points (Figure 4. 38 a). Spectrophotometric assays showed that roughly 400 µM of mannose is accumulated in the co-culture extracellular milieu (Figure 4. 38 c). To compare this to the total amount of mannose composing 10 mg ml⁻¹ of mannan from *S. cerevisiae*, mannan was acid hydrolysed and the total amount of available mannose was also measured. This showed that in co-culture with Bt, Bs is able to release approximately 10% of available mannose extracellularly (Figure 4. 38 d), which is then consumed at the stationary phase. Extracellular mannose accumulation is counterintuitive as given

the competitiveness of Bt, it was expected that Bt would rapidly consume available monosaccharides.

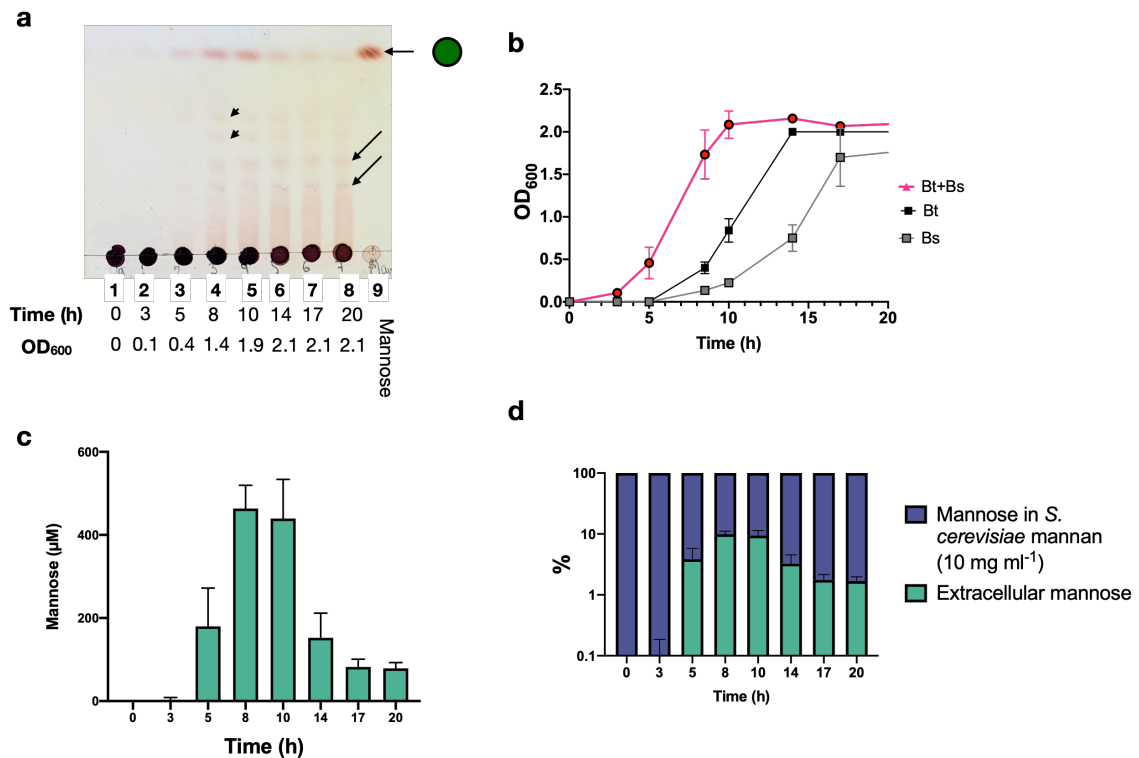


Figure 4.38 Analysis of cell free supernatant taken from Bt-Bs co-culture on mannan from *S. cerevisiae*. Panel a: TLC of cell free supernatant taken from specified time points during the Bt-Bs growth on mannan. Arrows indicate a pool manno-oligosaccharides, green circle shows mannose standard; Panel b: Growth curves (OD₆₀₀) of Bs (grey trace), Bt (black trace), and Bt-Bs (pink trace) on mannan; Panel c: mannose concentration accumulated in the co-culture supernatant. Error bars show SD. Data are representative of 3 biological replicates from 2 independent experiments.

4. 4 Discussion

The human gut is highly populated with a vast microbial community, which harbours an immense metabolic capacity to digest a wide range of complex carbohydrates. Microbes have therefore developed a few strategies to co-exist in the densely populated ecosystem of the gut. In one model, microbes occupy their

distinctive niches whilst displaying strict preference for a set of carbon sources and, thereby, avoiding direct competition with the others. As an example, Bt is the only species within the *Bacteroides* genus that can utilise levan (β -2,6-fructose polymer) (Sonnenburg et al., 2010).

However, given the complexity of microbial population in the human gut, it is likely that these substrate-specific species perform primary stages of glycan degradation and initiate sharing of complex substrates between the members of the microbiota. This was demonstrated by Rakoff-Nahoum et al. (2014) where a range of *Bacteroides spp* was screened against multiple complex carbohydrates, consequently splitting them into two groups: utilisers and non-utilisers of a particular carbon source. When a utiliser is grown on its preferred substrate, it liberates a pool of simpler by-products, which are rapidly consumed by the non-utiliser strains (Rakoff-Nahoum et al., 2014). Here, it was shown that Bt produced a range of shorter carbohydrates as a result of its growth on levan, which then supported growth of the other *Bacteroides species* (Rakoff-Nahoum et al., 2014). Another example of glycan sharing was demonstrated by Rakoff-Nahoum et al. (2016), where *B. ovatus* was shown to receive reciprocal benefits from *B. vulgatus* in exchange for a pool of fructo-oligosaccharides generated as a result of its metabolic activity on inulin. Moreover, glycan sharing also occurs at the inter-phylum level, as a member of the Firmicutes phylum, *Ruminococcus bromii*, was shown to play a critical role in the initiation of breakdown of resistant starch, facilitating cross-feeding with other Bacteroidetes such as Bt (Ze et al., 2012). Recently, cross-feeding of glycans was suggested to be central for establishing a diverse community at birth, as members of the gut microbiota in the breast-fed

infants actively share Human Milk Oligosaccharides (HMO), promoting each other's growth (Lawson et al., 2020).

As previously discussed, degradation of yeast α -mannan is limited to a number of *Bacteroidetes* (Cuskin et al., 2015b). Bt was found to possess a range of exo- and endo- acting enzymes, binding, and transport proteins, that are grouped into three mannan PULs. Proteins from these mannan PULs assemble a machinery, where large pieces of yeast α -mannan are released, transported into the periplasmic space and degraded intracellularly. Bt did not share mannan with other poor α -mannan utilisers, such as *B. xylanisolvens*, nor it made mannan more accessible to non-utilisers, such as *B. cellulosilyticus*. Therefore, the mechanism of mannan utilisation in Bt was termed "selfish" (Cuskin et al., 2015b).

In this chapter, it was demonstrated that the strategy of mannan utilisation deployed by Bs is contrasting to the 'selfish' mechanism, previously described in Bt. Unlike Bt, Bs releases large manno-oligosaccharides in the culture supernatant using enzymes localised to the cell surface. Interestingly, in addition to oligosaccharides, Bs accumulates a substantial amount of mannose extracellularly when it is grown *in vitro* on *S. cerevisiae* α -mannan or when the whole cells are incubated with this substrate. This strongly suggests the presence of a highly efficient exo-mannosidase localised on the surface. The accumulation of a simple sugar in the extracellular milieu seems counter-intuitive, however, similarly, *Ruminococcus bromii* liberates glucose by its surface amylases, to promote growth of other species in co-culture, when grown on starch (Ze et al., 2012). *R. bromii* was shown to play a central role in mediating sharing of resistant starch with the other members of the microbiota (Ze et al., 2012), this gave a suggestion that Bs promotes microbial diversity via acting as a producer of shorter manno-

oligosaccharides and simple mannose, which could be cross-fed to non-mannan users.

4. 4. 1 Mannan-degrading apparatus in *B. salyersiae*

As we were dissecting the mechanism of mannan utilisation in Bs, a genetic cluster (BS_04071-BS_04092) containing mannan-specific enzymes was identified. Biochemical characterisation of this locus showed that BS_04090^{GH76} acts as a highly efficient surface endo-mannosidase, which, unlike any of the GH76s from the three mannan PULS in Bt, is able to perform hydrolysis of highly branched α -mannan. Closest orthologue of BS_04090, sharing 76% sequence identity, in Bt was found to be BT3301^{GH76}, which is encoded outside mannan PULs and was not upregulated in response to yeast α -mannan in Bt (Cuskin et al., 2015). Despite being similar, BT3301^{GH76} was not able to hydrolyse branched mannan and both, BT3301^{GH76} and BS_04090^{GH76}, displayed different activities against mannan composed of α -1,6-linked backbone. This genetic locus also contains a second GH76, BS_04077. For unknown reasons, we were unable to clone its gene into pET28a or pBAD-HisA expression vectors, as well as a pET22b vector, which enables periplasmic expression. As discussed in Section 4.3.7 this protein possesses a multi-modular organisation, being composed of a catalytic GH76 domain as well as potential binding domains CBM6 and F5/8-type-C, a RICIN domain and other domains of unknown function. Cloning of individual domains into either pET28a, pET22b, or pBAD-HisA also failed. RICIN is a toxic lectin isolated from castor bean seeds, which binds sugars at the cell surface and inhibits protein synthesis (Yao 2011). RICIN-like lectins have been proposed to possess at least 3 glycan binding sites which recognise galactose moieties (Fu et al., 1996, Yao et al., 2011). A Ricin-like domain in a GH10 from *Luteimicrobium*

xylanilyticum isolated from the gut of a long-horned beetle has been suggested to mediate binding to a variety of hemicellulose substrates, contributing to the processivity of the enzyme (Kim et al., 2018). It is possible the presence of the RICIN-like domain precluded cloning of BS_04077^{GH76}, however cloning of the GH76 domain alone was also unattainable, indicating that the catalytic domain itself is toxic for *E. coli*, the reason for which is unknown. BlastP search for homologues showed that BS_04077^{GH76} was strictly specific to Bs, whereas GH76 domain shared 50% identity with putative proteins from *B. fingoldii* and a few *Prevotella* species. BS_04077^{GH76} contains a C-terminal domain targeting it for the Type 9 Secretion System (T9SS). The T9SS is an alternative method of translocating proteins to the cell surface and is described in more detail in Chapter 5. It is therefore possible that BS_04077 contributes to mannan degradation at the cell surface, generating a pool of branched oligosaccharides.

A possible candidate for the enzyme, which drives accumulation of extracellular mannose could be BS_04085^{GH38}, encoded in the same genetic cluster as BS_04090^{GH76} and BS_04077^{GH76}. The closest homologue of BS_04085^{GH38} in Bt is BT3774^{GH38} (40% identity) (Figure 4. 39 a). BT3774^{GH38} was shown to localise in the periplasmic space, where it orchestrates mannan breakdown in Bt (Cuskin et al., 2015b). BT3774^{GH38} shares close homology (69%) with a second GH38 characterised in this chapter, BS_01537^{GH38} (Figure 4. 39 a). BS_01537^{GH38} displayed poor activity on branched mannan from the wild type *S. cerevisiae*, showing preference for shorter substrates. Similar to BT3774, it contains N-terminal SPI signal, indicating that this enzyme is most likely located in the periplasmic space. The other two mannosidases described in this chapter, BS_04089^{GH125} and BS_04078^{GH92}, displayed broad specificities against α -1,2 and

α -1,6-mannosyl substrates. Both of them carry SPI signals at the N-termini. Combined, this suggests that BS_01537^{GH38}, BS_04089^{GH125}, and BS_04078^{GH92} work in concert to depolymerise mannan periplasmically. BS_4085^{GH38} displayed strong preference for wild type and also mnn1 and mnn5 mannan variants and was able to debranch these substrates more efficiently than BS_01537^{GH38}. Interestingly, BLAST analysis showed that BS_04085^{GH38} did not share more than 40% sequence similarity with any of the known proteins from other species, strongly indicating that this mannosidase is highly specific to Bs. Analysis of the amino acid sequence in the C-terminus revealed that BS_04085^{GH38} also contains C-terminal motifs associated with the T9SS (Chapter 5), suggesting that this mannosidase probably orchestrates mannan breakdown at the cell surface. The enzymatic cocktails comprising of BS_04085^{GH38} and BS_04090^{GH76} liberated a ladder of oligosaccharides from the highly branched wild type mannan, but the nature of this ladder was not the same as the one produced by the whole cells, suggesting that other enzymes also contribute. It is possible that unknown proteins in uncharacterized PUL7 could act as endo-acting mannanases, however BS_04077 would be the most likely candidate. Combined, we propose that BS_04085^{GH38}, BS_04090^{GH76}, and possibly BS_04077^{GH76} initiate mannan breakdown at the cell surface of Bs, resulting a pool of branched oligosaccharides and mannose. Some of these oligosaccharides are then transported into the periplasmic space and their depolymerisation is completed intracellularly with BS_01537^{GH38}, BS_04078^{GH92}, BS_04089^{GH125}, and possibly uncharacterised BS_01536^{GH125}. In addition to BS_04071-BS_04092 PUL, *S. cerevisiae* mannan induced low upregulation of an additional group of genes, enclosed in a Cazy-predicted PUL 7.

This PUL contains three GH92s, two of which BS_00849 and BS_00450, were as highly upregulated as proteins in Mannan PUL 1. Analysis of amino acid sequence showed that BS_00849^{GH92} and BS_00842^{GH92} shared 51 and 59 percent of sequence similarity to BT3773^{GH92} (Figure 4. 39 a), a periplasmic α -1,3 mannosidase from Mannan PUL 2 in Bt. Unlike BT3773^{GH92}, both BS_00849^{GH92} and BS_00842^{GH92} contain SP11 sites, indicating that they are located on the cell surface. Phylogenetic analysis showed that BS_00842^{GH92} positions on the same branch as BT3773^{GH92}, while BS_00849^{GH92} creates its own separate branch (Figure 4. 39 c). This indicates, that both BS_00842^{GH92} and BS_00849^{GH92} most likely possess α -1,3-mannosidic activities, and, given their N-terminal signals, most likely also participate in debranching of wild type α -mannan on the cell surface. BS_00850^{GH92} clustered together with α -1,2 mannosidases and carries an SP1 cleavage site, suggesting that it performs its function intracellularly. Biochemical characterisation of these three GH92 was beyond the scope of this thesis due to the time constraints.

a

1:	BS_00850 ^{GH92}	100.00	33.70	30.25	31.69
2:	BS_00849 ^{GH92}	33.70	100.00	50.00	51.07
3:	BS_00842 ^{GH92}	30.25	50.00	100.00	58.87
4:	BT3773 ^{GH92}	31.69	51.07	58.87	100.00

b

1:	BT4072 ^{GH38}	100.00	21.48	21.09	20.56
2:	BS_04085 ^{GH38}	21.48	100.00	40.34	41.70
3:	BS_01537 ^{GH38}	21.09	40.34	100.00	69.42
4:	BT3774 ^{GH38}	20.56	41.70	69.42	100.00

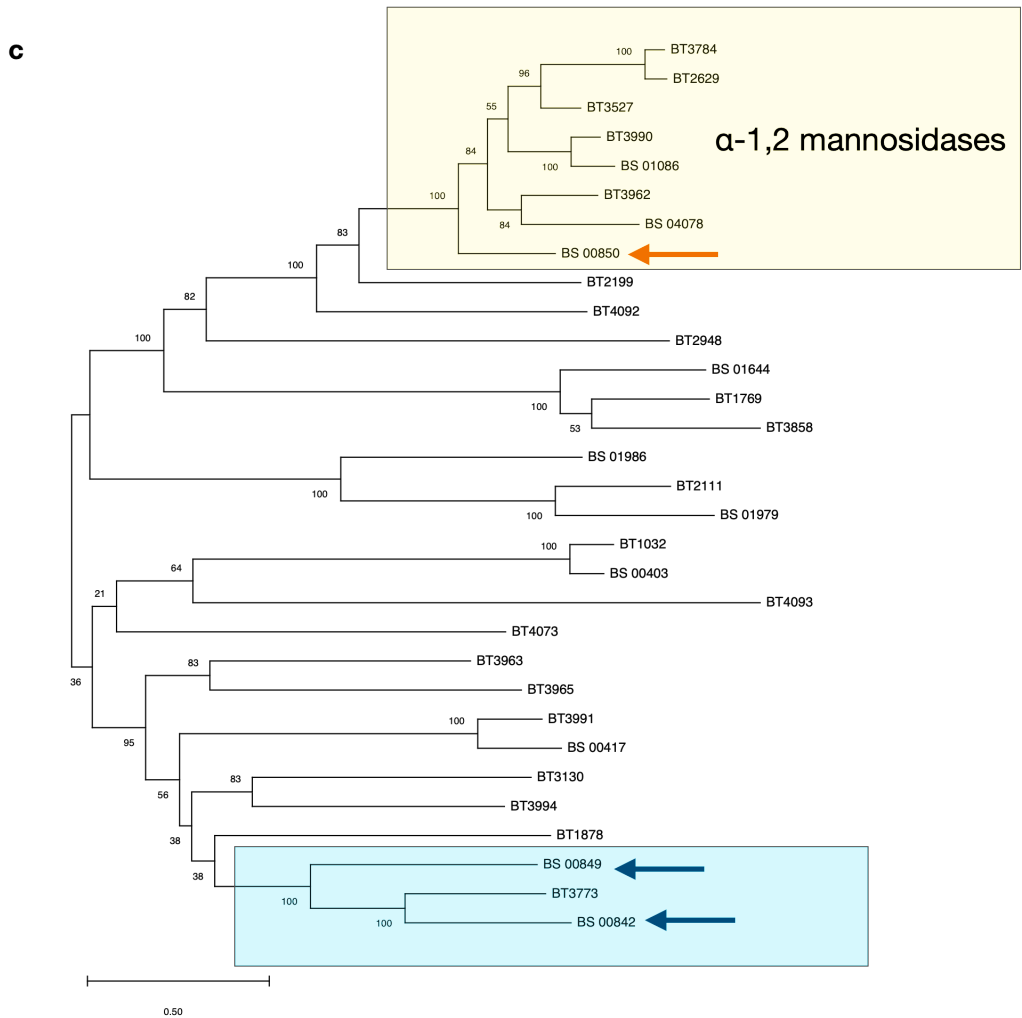


Figure 4. 39 Phylogenetic analysis of mannosidases from *Bs*. Panel a and b: Identity matrix of GH38s and GH92s, respectively, generated with Clustal Omega. Panel c: Phylogenetic tree of 31 GH92 enzymes found in *B. thetaiotaomicron* and *B. salyersiae*. The tree was generated in MegaX using the following settings: the evolutionary history was inferred by using the Maximum Likelihood method and Le Gascuel 2008 model. The percentage of trees in which the associated taxa clustered together is shown next to the branches. The tree is drawn to scale, with branch lengths measured in the number of substitutions per site.

4. 4. 2 Sharing of manno-oligosaccharides between gut *Bacteroides*

We next addressed the question of the biological role of this alternative mechanism of mannan degradation contrasting to the one deployed by Bt. We also investigated whether other *Bacteroides* species could utilise mannan by-products, using assays with conditioned media. This identified a subset of species, namely: *B. ovatus* ATCC8483 and CL03TI2C18, *B. xylanisolvens* DSM18836 and *NLAE-zl* p727, and *B. finegoldii* DSM17565 and CL09T03C10, which thrived on pre-digested mannan. These species presented inter-strain phenotypic differences when they were grown on branched wild type mannan, as a sole carbon source, however their ability to thrive on mannan by-products was consistently retained. Mannan cross-feeding was then further assessed in a set of competition assays. Previously it was shown that *B. xylanisolvens* outcompetes Bt in *in vitro* conditions, where mannose is a sole carbon source (Cuskin et al., 2015b). Unlike this, Bx shared mannose with Bs in co-culture. In a co-culture for mannan, Bs outcompeted Bx at initial growth phases, however despite this, the fitness of Bx was significantly enhanced. These assays showed that Bs and Bx co-existed in a co-culture where mannan was a sole carbon source, demonstrating that yeast mannan is actively cross fed between the members of the gut microbiota. As shown by Cuskin et al. (2015b), Bt displayed a strong competitive fitness on yeast α -mannan and did not permit sharing with other *Bacteroides*, such as Bx *NLAE-zl* p352 or *B. cellulosilyticus* WH2. Therefore, the next question addressed was whether the alternative sharing mechanism can counterpoise the competitiveness of the 'selfish' mechanism. A set of co-cultures of Bt with Bs, showed that, while sharing mannose, Bt still outcompeted Bs in the co-culture on yeast mannan, however Bs was able to survive a lot better than a non-mannan degrader.

Moreover, it was noticed that in the presence of Bt, Bs was able to digest mannan at a faster rate, suggesting that Bt shows cooperation by producing simpler substrates for Bs.

Interestingly, extracellular mannose generated by Bs was not essential for inducing growth of other *Bacteroides* species. On the contrary, extracellular mannose was primarily consumed by the species which did not display growth in conditioned media, whereas species, which thrived in conditioned media, did not show dependence on the availability of free mannose in the media. This therefore indicates that mannan cross-feeding is mediated by complex oligosaccharides rather than mannose produced by Bs. Whilst the most logical explanation would be that extracellular mannose supports growth and survival of other normal members of the gut microbiota, the alternative could be that it renders protection to the intestinal lining against pathogenic bacteria. Binding of mannosides to FimH adhesin, downregulates expression of the type 1 pili in Uropathogenic *E. coli* (UPEC), reducing its adhesion to epithelial cells and survival of UPEC in murine intestinal tracts (Spaulding et al., 2017, Schwan et al., 2018). Thus, accumulation of extracellular mannose as a result of yeast α -mannan degradation by *B. salyersiae* could possibly inhibit pathogenesis of virulent bacterial species.

It was previously discussed by Cuskin et al. (2015b), whilst presenting poor ability to grow on yeast mannan, all strains of both *B. ovatus* and *B. xylanisolvens* possess elements of mannan PUL 1 and 2 (Figure 4. 40 and Figure 4. 41).

Moreover, genome analysis showed that porcine Bx isolates (*NLAE-zl* P727, P732, P736, P393, P352) have inherited mannan PUL 1 but not mannan PUL 2 from Bt via a conjugative transposition (Cuskin et al., 2015b). Analysis of the genome of *B. finegoldii* DSM17565 showed that it contains elements of mannan

PUL 3 found in Bt, which includes a surface endo-acting α -1,3-mannanase from GH99 family, which was shown to be essential for mannan debranching in Bt (Figure 4. 41). Moreover, Bx, Bo and Bfine but not Bt or Bs share a genetic cluster, comprising of 2 GH76s and one GH92, which maintains its synteny in all three species (Figure 4. 42) This demonstrates that enzymes in these genetic regions provide Bx, Bo, and Bfine with the saccharolytic capacity to digest simplified mannan variants but not the highly branched polysaccharide from the wild-type yeast.

Combined, this chapter showed that *Bs* is able to mediate efficient breakdown of yeast α -mannan using a range of surface and periplasmic enzymes, generating a pool of oligosaccharides in the extracellular milieu as a result. In a competition with Bt, *Bs* was able to withstand the competitive pressure imposed by Bt and continued to utilise mannan using its alternative mechanism. Products of this alternative mechanism of mannan utilisation supported growth of a subset of other poor mannan-degrading *Bacteroides species*. This demonstrates that members of the gut microbiota have developed multiple strategies for accessing mannan in the gut.

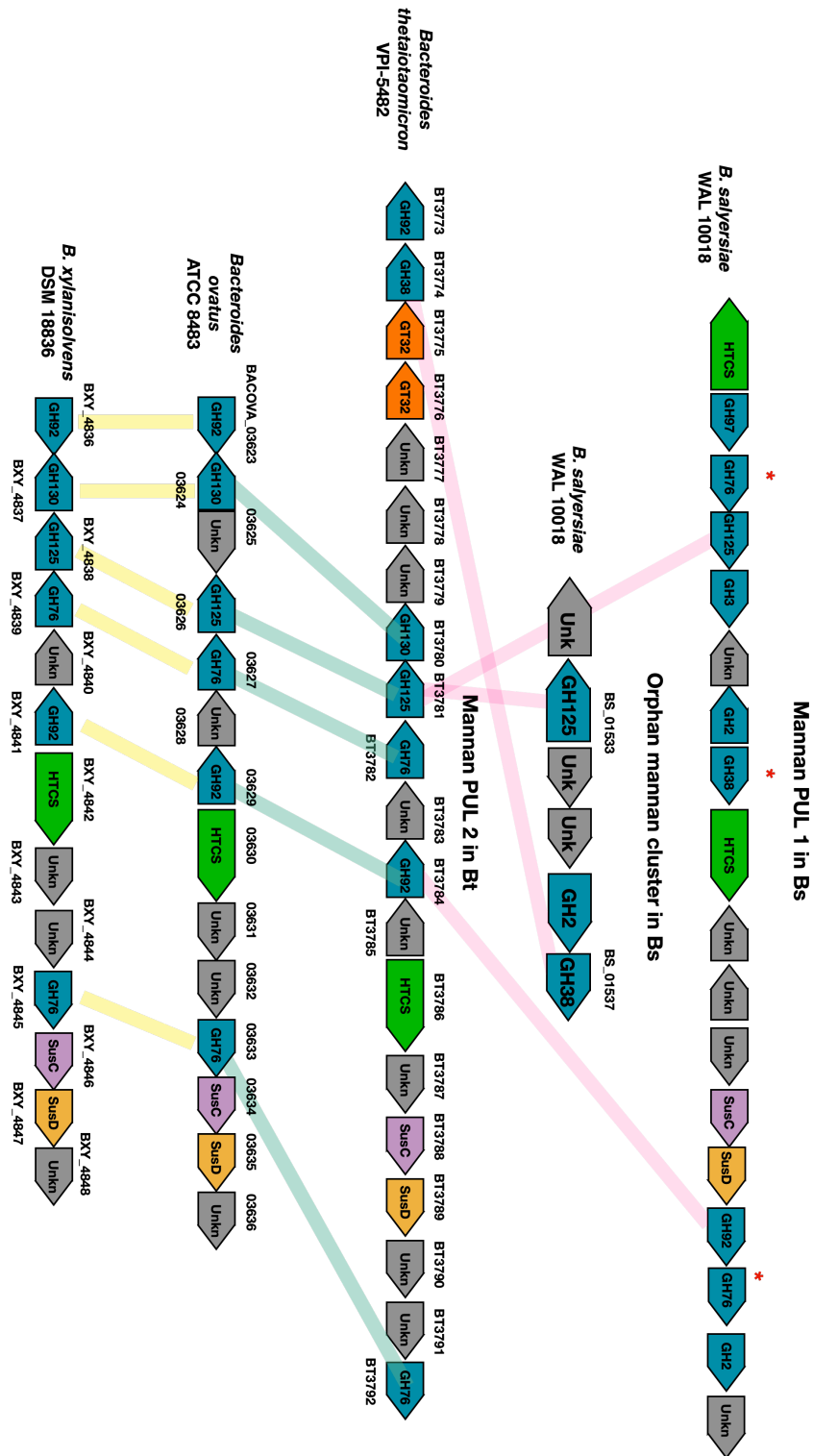


Figure 4. 40 Structural organisation of Mannan PUL 2 in *B. thetaiotaomicron* VPI-5482 and its similarity with PULs found in *B. ovatus* ATCC 8483 and *B. xylanisolvens* DSM 18836. MAN-PUL 2 shares structural synteny with PULs in Bo and Bx, but not Mannan PUL in Bs. Red stars mark enzymes unique to Bs.

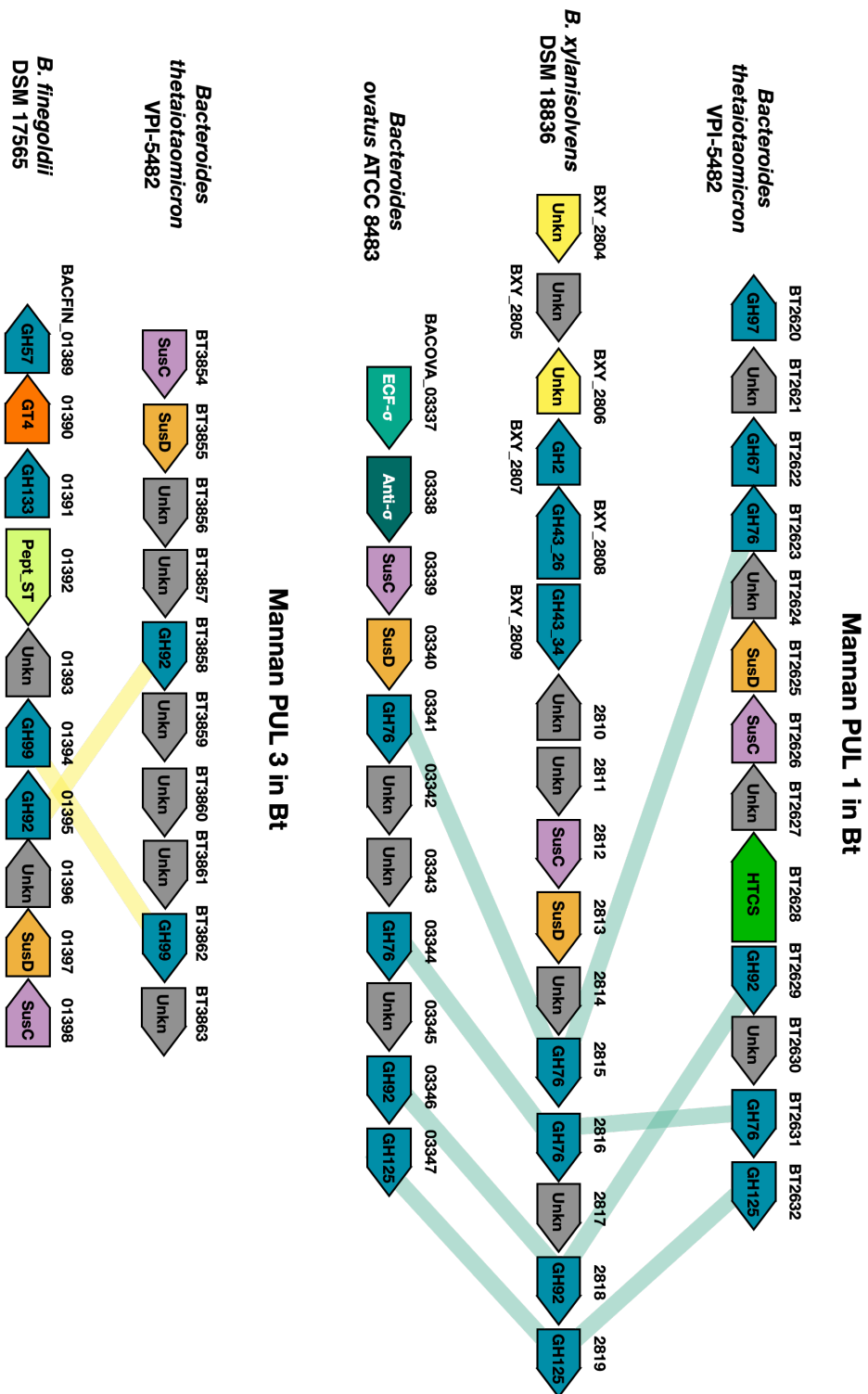


Figure 4. 41 Structural organisation of Mannan PUL 1 and Mannan PUL 3 in *B. thetaiotaomicron* VPI-5482. Elements of MAN-PUL 1 are retained in *B. xylanisolvens* DSM 18836 and *B. ovatus* ATCC 8483, elements of MAN-PUL3 are retained in *B. finegoldii* DSM 17565.

Not found in Bt or Bs

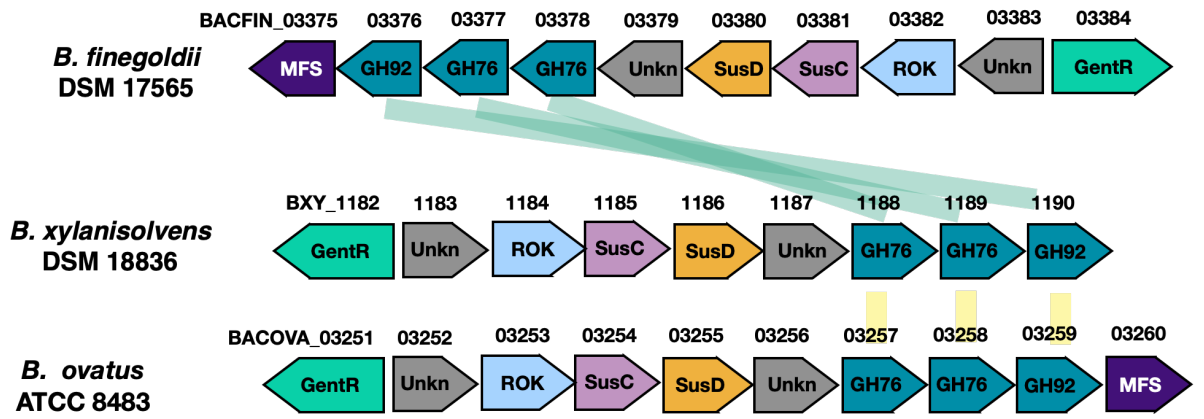


Figure 4. 42 Structural organisation of a genetic cluster shared between *B. finegoldii* DSM 17565, *B. xylanisolvens* DSM 18836, and *B. ovatus*. ATCC 8483

Chapter 5: Type 9 Secretion System in *B. salyersiae* and its role in mannan degradation

5. 1 Introduction

Biochemical characterisation of yeast α -mannan breakdown in *B. salyersiae* revealed that some proteins in Mannan PUL 1 contain Secre-tail domains (Pfam: PF18962; TIGRFAM: TIGR04183) at their C-termini, which were described to target them for the Por Secretion system (Chapter 4). Homologues of this domain were also found in *Porphyromonas gingivalis*, *Fibrobacter succinogenes*, *Flavobacterium johnsoniae*, *Cytophaga hutchinsonii*, *Gramella forsetii*, *Prevotella intermedia*, and *Salinibacter ruber*. The Por secretion system was first described in *Porphyromonas gingivalis* by Sato et al. (2005), where it was shown to mediate extracellular secretion of virulence factors, gingipain proteases (Sato et al., 2005, Sato et al., 2010). The same type of system was also shown to locate proteins to the outer membrane to implement gliding motility in *Flavobacterium johnsoniae* (Braun et al., 2005, McBride and Zhu, 2013). Orthologues of structural components of this system were restricted to the members of the Bacteroidetes phylum such as *Flavobacterium* and *Cytophaga* but were not found in human gut *Bacteroides* such as *B. thetaiotaomicron* or *B. fragilis* (McBride and Zhu, 2013, McBride, 2019). They also lacked homology with any other proteins assembling previously characterised secretion systems (I-VIII), and therefore the new system was given number 9. The spatial organisation of the proteins composing the T9SS in *P. gingivalis* has recently been proposed by Gorasia et al. (2020) (Figure 5. 1).

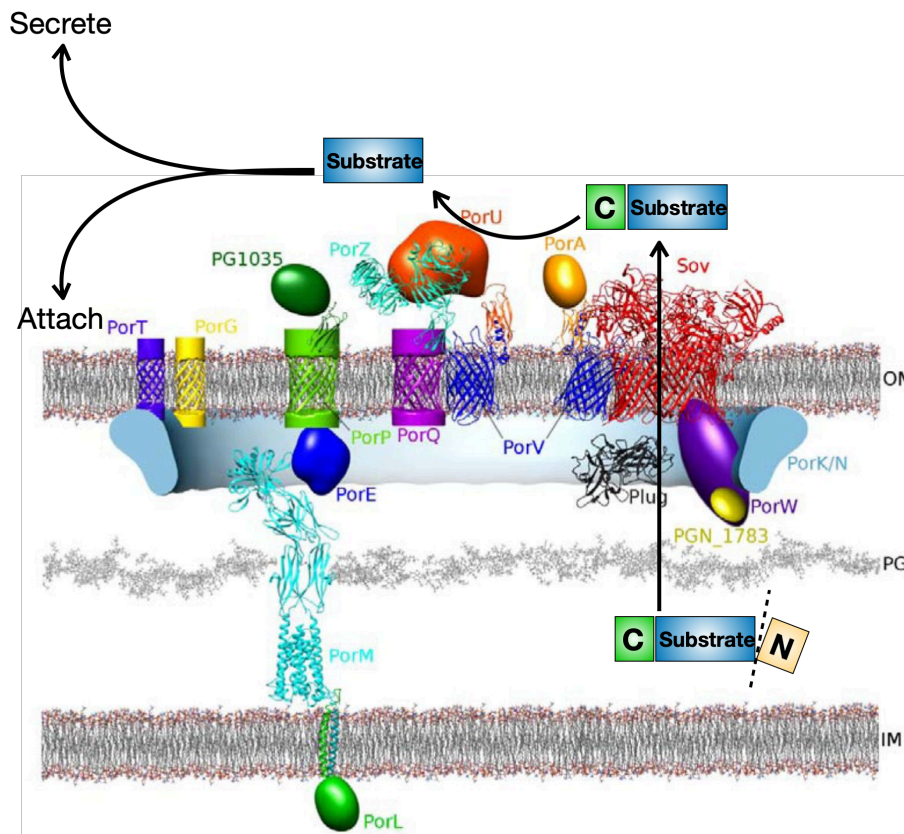


Figure 5. 1 Structural organisation of the Type 9 Secretion System in *P. gingivalis*. Model was adapted from Gorasia et al. (2020). T9SS forms a multiprotein transmembrane complex, where SprA is the main translocon, which interacts with surface sortase PorU through PorV. Signalling occurs via communication between PorK-PorN-PorE-PorM complex and intracellular transducer PorL.

5. 1. 1 Type 9 secretion system complex

5. 1. 1. 1 T9SS in *Porphyromonas gingivalis*

Sato et al. (2005) showed that secretion of gingipains was orchestrated by a periplasmic protein porT. PorT was then shown to interact with a range of other proteins, which assembled into a transmembrane complex to secrete virulent proteases (Figure 5. 1) (Sato et al., 2010, Saiki and Konishi, 2007). *P. gingivalis* mutants lacking either of these proteins failed to secrete gingipains, accumulating them at the cell surface (Sato et al., 2010). It was also discovered that closely

encoded proteins PorK, PorN, PorP, PorM, and PorL were required for export of gingipains across the inner and outer membranes, while the two orphan proteins PorX and PorY acted as signal transducers and controlled expression of the proteins within this novel secretion system (Gorasia et al., 2016, Vincent et al., 2016).

5. 1. 1. 2 T9SS in *Flavobacterium johnsoniae*

The main two extracellular adhesins, SprB and RemA, which facilitate gliding in *F. johnsoniae* were shown to be translocated to the cell surface via orthologues of the T9SS (Braun et al., 2005, Shrivastava et al., 2013, Nelson et al., 2008). The orthologue of *P. gingivalis* PorT, SprT, was found to play a central role in localising the main adhesin, SprB, at the cell surface. Cells lacking this protein exhibited defective gliding. Deletion of T9SS components, namely gldM, gldK, gldM, abrogated ability to attach to surface and resulted in completely nonmotile phenotypes in *F. johnsoniae* (Shrivastava et al., 2013, Rhodes et al., 2010).

Interestingly, strains deficient in T9SS components were also unable to hydrolyse GlcNAc substrates, which was shown to be dependent on secretion of an enzyme from the GH18 family, ChiA^{GH18} ((Rhodes et al., 2010, Kharade and McBride, 2014). The ability to break down GlcNAc substrates was found to be independent of gliding Kharade and McBride (2014), suggesting that T9SS performs multiple functions in *F. johnsoniae*. (McBride and Zhu, 2013) showed that T9SS also mediated gliding in a range of members of the Bacteroidetes phylum.

5. 1. 2 Organisation and mechanism

Currently T9SS is comprised of 19 proteins assembled into a transmembrane complex (Figure 5. 1), however its precise organisation remains unknown (Gorasia

et al., 2020). The transport of the T9SS substrates is mediated through the SprA (Sov) β -barrel protein, which forms a large pore in the outer membrane (Saiki and Konishi, 2007, Lauber et al., 2018). SprA co-expresses with the Plug and PPI proteins, while the function of the PPI protein is currently unknown, the Plug protein is believed to act as a barrier, which controls the passage of small molecules through the pore (Lauber et al., 2018). These further associate into an extremely large transmembrane complex with other proteins: PorK, PorN, PorW, and PGN_1783 (Lauber et al., 2018). Lauber and colleagues also showed that SprA co-expresses with PorV, which interacts with sortase PorU, the main peptidase orchestrating extracellular secretion or attachment of target proteins to the outer membrane (Glew et al., 2012, Gorasia et al., 2015). The PorV-PorU complex localises in close proximity with a PorZ-PorQ complex, which also has been suggested to play a role in sorting of T9SS substrates (Gorasia et al., 2015, Gorasia et al., 2020).

The export of cargo proteins across the membranes occurs in a two-step mechanism. Targets are first translocated into the periplasmic space via the Sec-pathway through the N-terminal SPI signals. Then, structural components of the T9SS, mainly PorW-PorV, recognise conserved amino acid domains at the C-termini (CTDs) of target proteins and guide them through the SprA pore to be processed by sortase PorU (Figure 5. 1) (Saiki and Konishi, 2014, Kulkarni et al., 2017). PorU removes the CTDs and either conjugates mature proteins to the anionic LPS, anchoring them in the outer membrane, or releases them into the extracellular milieu (Figure 5. 1) (Shoji et al., 2002, Gorasia et al., 2015). The sortase-like mechanism is similar to the one seen in Gram-positive *S. aureus*

(Mazmanian et al., 2001), however T9SS machinery is restricted to the Bacteroidetes phylum.

5. 1. 3 Conserved C-terminal domains

Gingipains and 682 other proteins from 87 Bacteroidetes species were found to contain a highly conserved region at the C-terminus (Seers et al., 2006, Veith et al., 2013). C-terminal domains reside in the last 100-80 amino acids and fold into a β -sandwich, forming a separate structural domain (De Diego et al., 2016). There are two types of CTDs, which have been split into two respective Pfam families, TIGR04183 (Type A) and TIGR04131 (Type B) (Kulkarni et al., 2017, Kulkarni et al., 2019). The underlying mechanism of processing of Type B CTD carrying proteins is unknown (Gorasia et al., 2020). Type A CTDs in both *F. johnsoniae* and *P. gingivalis* are characterised by a number of conserved motifs: B, D, and E. The motif B contains a conserved Glycine (G) residue, motif D is characterised by a conserved Glycine-Leucine-Tyrosine (GLY) repeat, and a motif E contains a conserved Lysine-xxx-Lysine (KxxxK) fragment at the very end of the protein (Figure 5. 2) (Veith et al., 2017, Kulkarni et al., 2017). Substrates of the T9SS are required to retain conserved amino acids residues in all three motifs simultaneously (Veith et al., 2017). Shoji et al. (2011) showed that the last two motifs D and E are crucial for efficient translocation of CTD-proteins to the outer membrane. In addition, deletion of the last few residues of the CTD in RgpB gingipain resulted in aberrant protein glycosylation, dysfunction, and accumulation of the protein intracellularly (Nguyen et al., 2007). As demonstrated by (Kharade and McBride, 2014), *F. johnsoniae* ChiA also contains a CTD, which was shown to be essential for secretion of chitinase. The removal of this C-terminal signal

aborted extracellular secretion of the enzyme as it remained bound to the cell surface. A fluorescent protein conjugated to a ChiA-derived CTD was actively secreted by *F. johnsoniae*, indicating that a CTD functions as an export signal directing proteins for the secretion by the T9SS (Kharade and McBride, 2014). Some of mannan degrading enzymes in *B. salyersiae* were predicted to contain T9SS-associated CTDs. This type of domain has never been described to be involved in glycan metabolism in gut *Bacteroides* before and therefore the contribution of the T9SS to the breakdown of yeast mannan was investigated in this chapter.

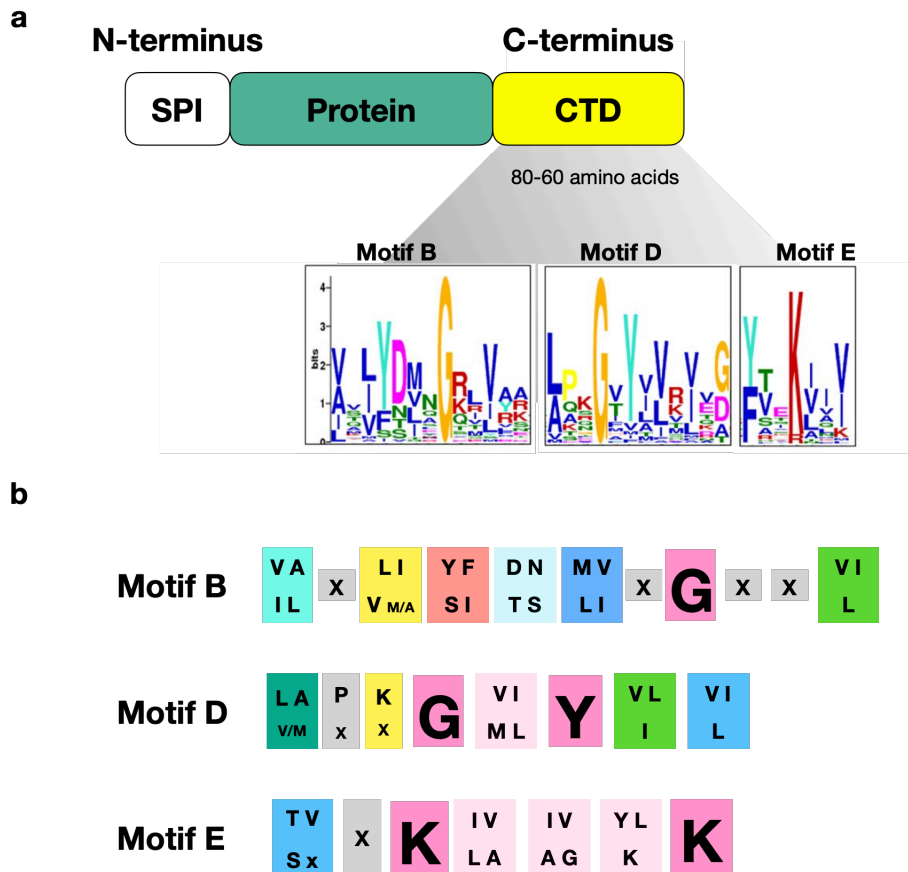


Figure 5. 2 Type 9 Secretion System associated C-terminal domains. Panel a: T9SS substrates carry N-terminal SPI signal and conserved C-terminal domain with motifs B, D, and E, Motifs are conserved in Type A substrates in *F. johnsoniae* and *P. gingivalis*, as determined by Veith et al. (2013) and Veith et al. (2017), diagram was adapted from Veith et al. (2017). Panel (b) Summary of main amino acid residues associated with T9SS C-terminal motifs; residues highlighted in pink are absolutely conserved in all T9SS substrates.

5. 2 Objectives

1. Begin characterisation of the T9SS in *B. salyersiae*
2. Identify proteins directed to the T9SS in *B. salyersiae*
3. Investigate the role of the T9SS in the breakdown of mannan from *S. cerevisiae*
4. Perform biochemical characterisation of T9SS proteins in Mannan PUL 1

5. 3 Results

5. 3. 1 Type 9 Secretion system in *B. salyersiae*.

Using BlastP, the genomes of *B. salyersiae* WAL 10018 and CL02T12C01 were searched for homologues of proteins assembling T9SS in *P. gingivalis* and *F. johnsoniae*. This analysis revealed that *B. salyersiae* WAL100018 and *B. salyersiae* CL02T12C01 possess orthologues of the main structural proteins of the T9SS (Table 5. 1). These proteins however were not enclosed in PULs and were found as orphan genes scattered throughout the genome. The exception was *porP-porK-porL-porM-porN*, which were found to be closely encoded, this is in line with (Sato et al., 2010), who showed that these genes are co-transcribed in *P. gingivalis*. Components of the T9SS in *B. salyersiae* showed relatively low sequence similarities with the proteins assembling the T9SS in either *P. gingivalis* or *F. johnsoniae*, however, overall, they were more similar to ones found in *P. gingivalis* (Table 5. 1)

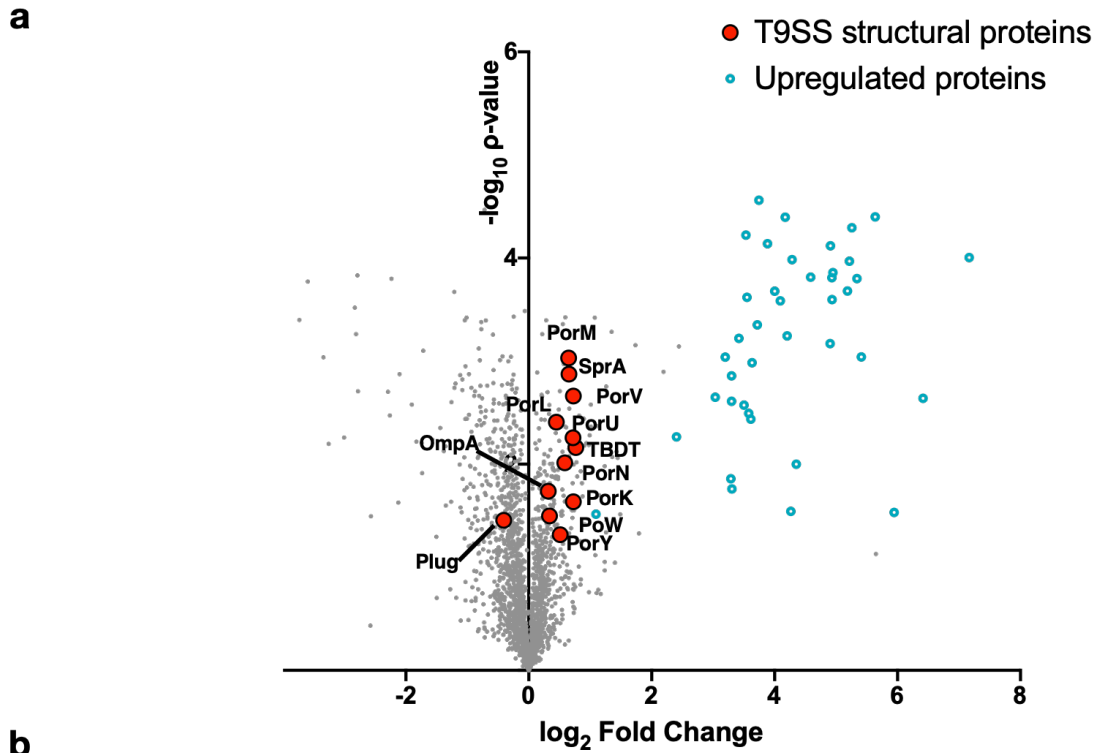
<i>Porphyromonas gingivalis</i> W83 T9SS Protein	Function	<i>P. gingivalis</i> locus tag	<i>Bacteroides salyersiae</i> WAL10018	Percentage identity (%)	<i>Flavobacterium johnsonae</i> UW101	Percentage identity (%)
Cytoplasmic and Inner membrane Components						
PorX	Chemotactic Protein	PG0928	HMPREF1532_01109	59.35	Fjoh_2906	49.43
PorY	Sensor Histidine Kinase - Signal transducer	PG0052	HMPREF1532_04120	48.27	Fjoh_1592	41.86
PorL	Motor Stator	PG0289	HMPREF1532_02242	27.5	Fjoh_1854	-
PorM	Rotor and Shaft	PG0290	HMPREF1532_02243	47	Fjoh_1855	28.92
Periplasmic components						
PorK	Associates with PorN	PG0288	HMPREF1532_02241	57.58	Fjoh_1856	35.52
PorN	Associates with PorK	PG0291	HMPREF1532_02244	39.35	Fjoh_1853	24
PorW	unknown/ Associates with PorV	PG1947	HMPREF1532_01108	34.92	Fjoh_1051	23.05
Outer membrane and Surface components						
Sov	SprA - Translocon	PG0809	HMPREF1532_03761	49.13	Fjoh_1653	37.17
PorQ	Transposase; Anchors PorZ	PG0602	No homologues	-	Fjoh_2755	
PorP	Binds PorE	PG0287	HMPREF1532_02240	32.59	Fjoh_3477	not found?
PorT	β -barrel protein , unknown	PG0751	HMPREF1532_01279	45.73	Fjoh_1466	28.51
PorV	Shuttle cargo proteins, associates with PorU	PG0027	HMPREF1532_04018	52.03	Fjoh_1555	43.52
Hypothetical Protein	β -barrel protein	PG0189	HMPREF1532_01419	35.92	Fjoh_1692	Not found?
TonB dependent receptor	β -barrel protein	PG0534	HMPREF1532_02510	43.83	Fjoh_0118	39.93
PorU	Sortase/C-terminal peptidase	PG0026	HMPREF1532_04019	35.56	Fjoh_1556	30.28
PorZ	Anchors cargo proteins	PG1604	HMPREF1532_01909	27.83	Fjoh_0707	29.94
unknown	PPI-co-expresses with SprA	PG0708	HMPREF1532_01500	30	Fjoh_1759	-
unknown	Plug-protein-SprA co-expressed	PG2092	HMPREF1532_03526	32	Fjoh_4997	-
PorE	OmpA-protein	PG1058	HMPREF1532_03848	43.1	Fjoh_1647	27.3

Table 5. 1 Table of homologues of structural T9SS proteins found in *B. salyersiae* WAL 10018.

Proteins were identified using BLASTP and IMG search engines, percentage identity was assessed by BLAST.

Analysis of the comparative proteomics performed in Chapter 4 showed that some of the proteins composing the T9SS were not upregulated but present at the amounts, where they could be detected in both glucose and mannan grown cells (Figure 5.). These included the main pore-forming translocon protein, SprA (HMPREF1532_03761), and its Plug protein (HMPREF1532_03526). It was also possible to detect proteins, which recognise T9SS targets, PorK (HMPREF1532_02241), PorN (HMPREF1532_02244), PorM (HMPREF1532_02243), and the signal transducers, PorL (HMPREF1532_02242)

and PorY (HMPREF1532_04120) (Figure 5.). The main complex, orchestrating extracellular cleavage of CTDs from the cargo proteins, which comprises of sortase PorU (HMPREF1532_04019), its anchoring protein PorV (HMPREF1532_04018), and their stabilising protein PorW (HMPREF1532_01108), was also present (Figure 5.). In addition, two other proteins, a Ton-B dependent transporter (HMPREF1532_02510, Ton-B-dependent transporter) and OmpA protein (HMPREF1532_03848), were also detected, however their function in the T9SS complex is unclear (Figure 5.). Combined these proteins assemble into a transmembrane complex as shown in Figure 5. . After normalising data to glucose, protein fold change of T9SS components remained between 0 and 1 (Figure 5. b), indicating that they are produced in equal amounts in response to yeast mannan as well as glucose. This suggests that T9SS is ubiquitously expressed in *B. salyersiae* and is independent of a nutrient source.



Protein	Locus tag in <i>B. salyersiae</i> WAL10018	Function	log ₂ FC	p-value	Protein FC
I9HG79	HMPREF1532_02510	TBDT	0.76	0.007	1.70
I8XYK7	HMPREF1532_04018	PorV	0.73	0.002	1.65
I9T6W1	HMPREF1532_02241	PorK	0.73	0.023	1.65
I9HVP1	HMPREF1532_02242	PorL	0.72	0.006	1.65
I8XZ14	HMPREF1532_03761	SprA	0.65	0.001	1.57
I8YMW4	HMPREF1532_02243	PorM	0.65	0.001	1.57
I9T6A3	HMPREF1532_02244	PorN	0.59	0.010	1.50
I8Y0P3	HMPREF1532_04120	PorY	0.51	0.048	1.42
I9SJ04	HMPREF1532_04019	Sortase - PorU	0.45	0.004	1.36
I9TKP5	HMPREF1532_01108	PorW	0.34	0.032	1.26
I8Y008	HMPREF1532_03848	OmpA	0.32	0.018	1.25
I8YF86	HMPREF1532_03526	Plug protein - DUF5103	-0.41	0.035	0.75

Figure 5. 3 Proteome of *B. salyersiae* in response to yeast α -mannan. Panel a: Volcano plot shows differentially regulated proteins in response to mannan. T9SS structural proteins are highlighted in red, summarised in panel b. Log₂ ≥ 2 was taken as a cut off for upregulation, highlighted in blue.

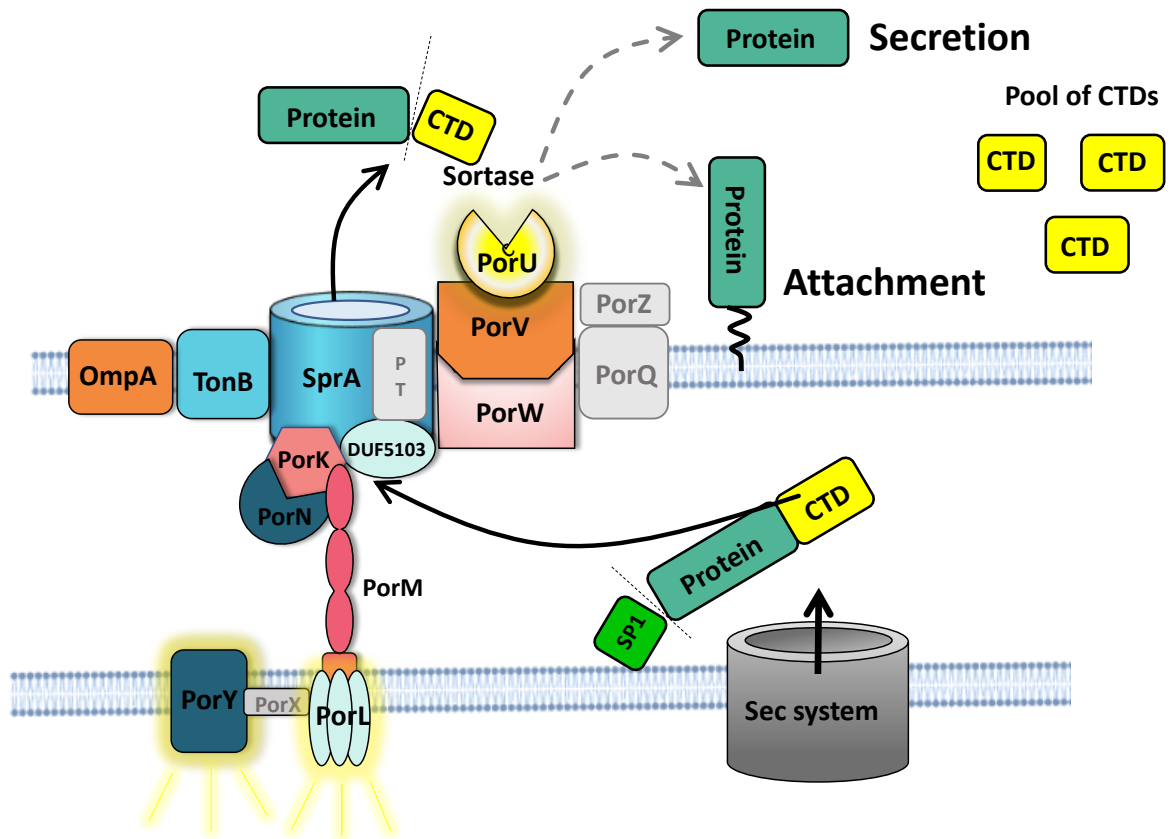


Figure 5. 4 Diagram of T9SS in *B. salyersiae*. Structural components shown in colour were detected upon proteomics analysis, proteins shown in grey: PorP, PorT, PorX, PorQ, and PorZ were not detected. T9SS substrates are translocated to the periplasmic space through the Sec pathway via SP1 N-terminal signals. In the periplasmic space, structural T9SS proteins recognise CTDs. PorW-PorV guide targets through the SprA pore to sortase PorU, which cleaves CTDs and either attaches targets to the outer membrane or secretes them extracellularly. PorY and PorL are signal transducers, which control expression of the components in the system

5. 3. 2 Proteins targeted for the secretion by the Type 9 system carry C-terminal domains.

5. 3. 2. 1 Structural components

Recently, it has been suggested that in *P. gingivalis* PorZ associates with PorQ to process proteins with type B CTDs (Lasica et al., 2016, Gorasia et al., 2020).

Moreover, *P. gingivalis* strain lacking PorZ accumulates A-LPS in the periplasmic

space (Madej et al., 2021). PorZ was shown to form complexes with PorU and directly bind phosphomannan component of A-LPS, implicating its role in the shuttle of the T9SS substrates (Madej et al., 2021). Interestingly, genome analysis showed that *B. salyersiae* possesses a homologue of PorZ but not PorQ (Table 5. 1). However, PorZ was not detected in the proteomics analysis, indicating that PorQ-PorZ complex do not form in *B. salyersiae* (Figure 5.). This suggests that all target proteins are directed to the T9SS via Type A CTD signals.

The sortase (PG0026) in *P. gingivalis* retains its CTD signal despite being embedded in the outer membrane (Glew et al., 2012). It was then investigated whether structural components of the T9SS in *B. salyersiae* carry CTDs, which would distinguish them from other proteins. Amino acid sequences of all proteins were retrieved from IMG (<https://img.jgi.doe.gov>), the last 80 amino acids were aligned in Clustal Omega (<https://www.ebi.ac.uk/Tools/msa/clustalo/>). The sortase from *P. gingivalis* shares 35% sequence similarity with *B. salyersiae* sortase (HMPREF1532_04019), last 80 amino acids of PG0026 were still aligned alongside as a positive control. This analysis showed that out of 17 structural proteins, the sortase PorU (HMPREF1532_04019) and PorZ (HMPREF1532_01909) were the only two proteins which contained conserved residues characteristic of motif B, motif D, and motif E of T9SS CTDs, others retained fragments of these motifs (Figure 5.). The CTD motifs aligned with the residues in *P. gingivalis* sortase (Figure 5.). This finding is consistent with the hypothesis that PorZ and PorU both mediate processing of CTDs, where PorU recognises Type A CTDs, while PorZ is specific for the signals in Type B CTDs. The mechanism of PorU-mediated removal of CTDs is somewhat characterised in

P. gingivalis, however the exact cleavage site still remains unknown (Glew et al., 2012). The mechanism of sorting proteins containing type B CTDs is unknown.

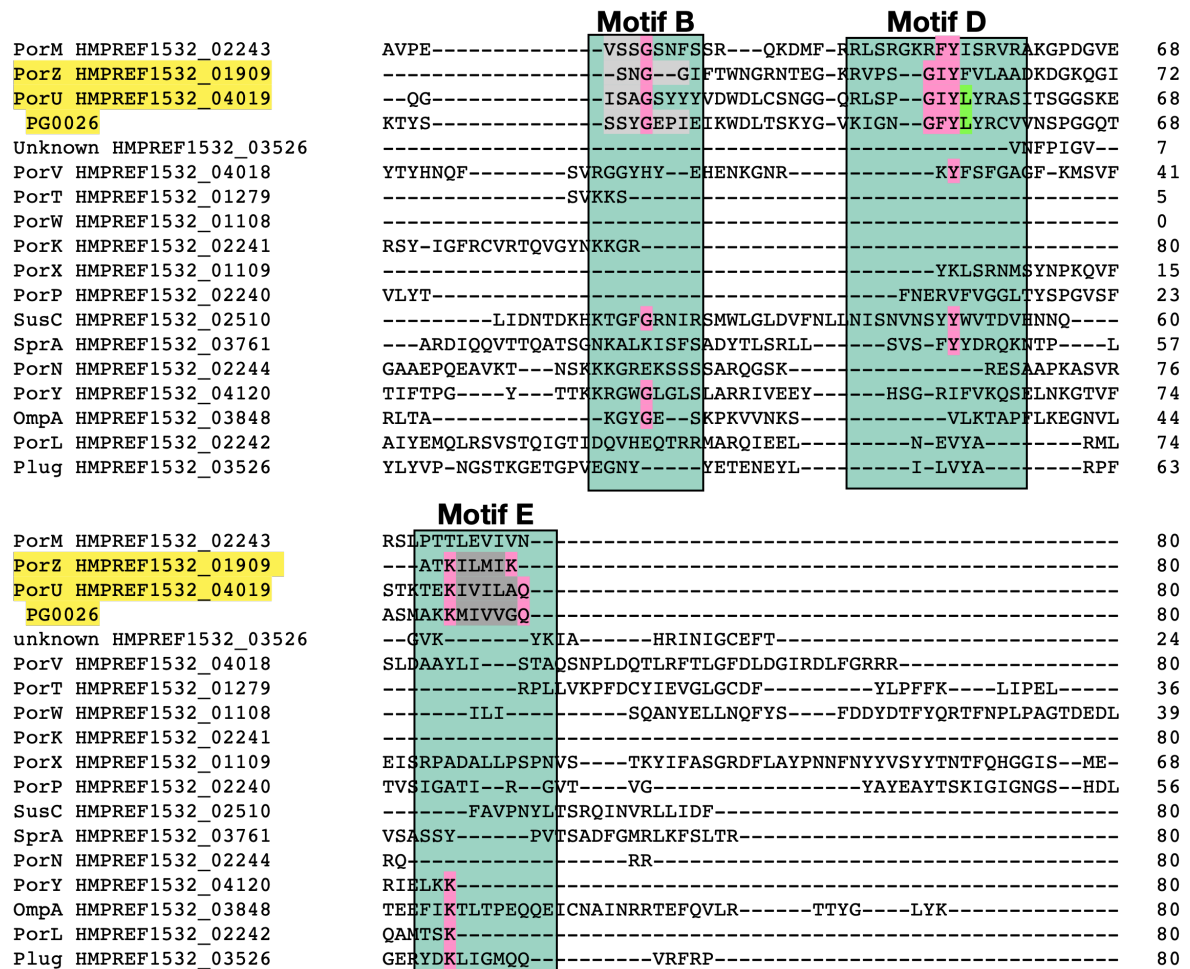


Figure 5. 5 CTDs in T9SS structural proteins. Last 80 amino acid residues were aligned in Clustal Omega. CTD in PG0026, PorU sortase in *P. gingivalis*, was used to identify position of conserved motifs. Position of conserved motifs is highlighted in green and conserved amino acid residues are highlighted in pink. 2 out of 17 structural proteins, PorZ and PorU, contain conserved residues of T9SS CTDs.

5. 3. 2. 2 Type A CTD-carrying proteins in *B. salyersiae* and other gut *Bacteroides*.

The number of proteins targeted for the T9SS in *B. salyersiae* was then investigated. This analysis was performed by Curtis Cottam as part of his MRes

project under my supervision. Figures and data from his work are indicated in figure legends. The genome of *B. salyersiae* WAL10018 was searched for proteins predicted to contain TIGR04183 domain, which is found in Type A CTDs, using Integrated Microbial Genomes systems (<https://img.jgi.doe.gov>). This analysis identified 99 proteins, 19 of which were assigned to a range of glycoside hydrolase families, while 80 had other or unknown functions (Figure 5.). For comparison, the same analysis was performed in *F. johnsoniae* as well Bt and other common gut *Bacteroides*. This showed that, unlike *B. salyersiae*, *F. johnsoniae* possessed only 40 proteins, carrying TIGR04183 domain, 8 of which were predicted to function as glycoside hydrolases (GHs) and 30 were assigned to have “other” functions (Figure 5. a). Proteins with TIGR04183 domain were not identified in most *Bacteroides species*, with the exception of *B. nordii*, which was found to possess 120 proteins: 11 GHs and 99 “other” (Figure 5. a). A very small number of TIGR04183 domain containing proteins was also found in *B. intestinalis* (2 GHs and 5 “other”), and *B. xylanisolvens* (1GH) (Figure 5.). Analysis of GHs in *B. salyersiae*, carrying T9-associated CTDs, revealed that they belonged to 12 different GH families, showing a wide range of substrate specificities (Figure 5. b). Interestingly, all (5) GH85s, a family of endo-acting β -N-acetylglucosaminidases, which cleave a range of branched N-glycans from a variety of glycosylated proteins, in *B. salyersiae* contained TIGR04183 domain in their C-termini (Figure 5. b). This demonstrates that the T9SS is restricted to a very small subset of gut *Bacteroides species*. Proteins directed to the secretion by the T9 system exert a range of functions, demonstrating that T9SS plays a number of roles in *B. salyersiae* rather than being limited to yeast mannan breakdown.

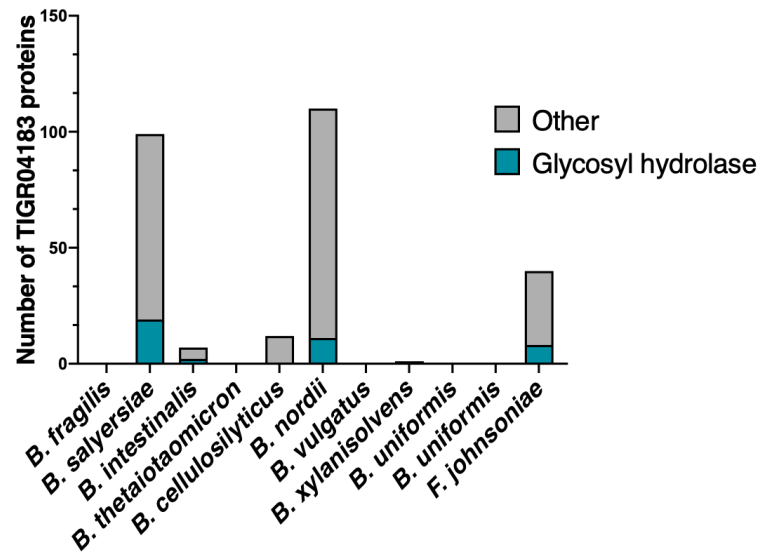
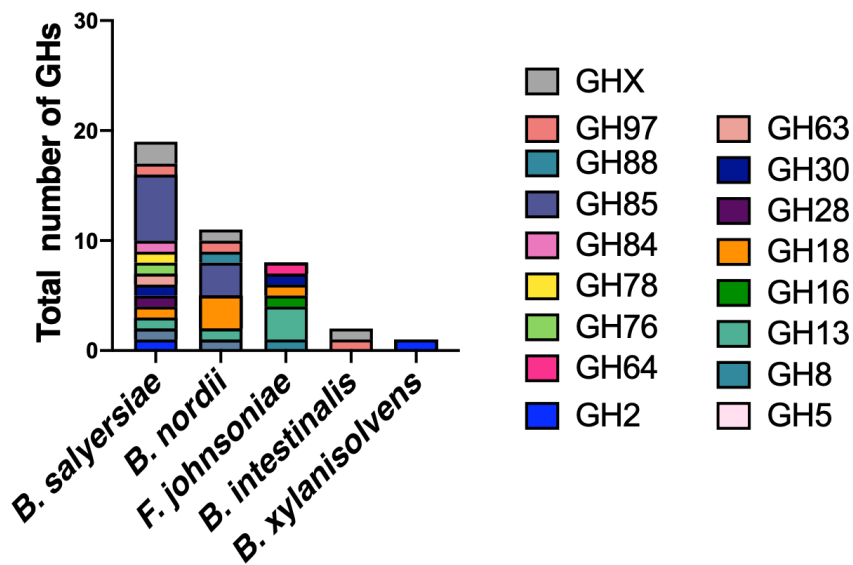
a**b**

Figure 5. 6 Number of proteins, containing Type A (TIGR04183) CTDs, among a range of Bacteroidetes. Panel a: total number of proteins predicted to contain TIGR04183 domain by species, bars coloured in teal show predicted Glycoside Hydrolases, bars coloured in grey show all other proteins with TIGR04183 domain (Type A CTD). Panel b: Total number of glycoside hydrolases predicted to contain T9SS-associated CTDs in gut *Bacteroides* and *F. johnsoniae*. GH families are colour coded, GHX includes proteins with possible GH activity but family is unknown. Figures in panels in a and b were generated by Curtis Cottam.

5. 3. 2. 3 CTDs in Mannan PUL

Biochemical characterisation of proteins from *B. salyersiae* Mannan PUL 1 revealed that BS_04077^{GH76} was described to contain a Por-SecE tail in its C-terminus (Chapter 4). The IMG analysis of the proteins composing the mannan PUL revealed that, in addition to BS_04077^{GH76}, at least 6 other proteins were predicted to contain T9SS-associated CTDs (Figure 5. a). To investigate whether conserved motifs were present in these domains, last 70 amino acids of 14 proteins in the PUL were aligned in Clustal Omega.

Contrasting to the IMG analysis, conserved amino acid residues associated with the T9SS CTDs were found in 9 out of 14 proteins (Figure 5.). This included GH38, BS_04085, which displayed specificity for highly branched mannan polymers.

Motifs were also found in three proteins of unknown functions: BS_04072,

BS_04075, BS_04081 (Figure 5.). Proteins which did not carry CTDs were

BS_04091^{GH97}, BS_04089^{GH125}, BS_04090^{GH76}, BS_04078^{GH92}, whilst

BS_04088^{GH3} only seemed to possess elements of motif E but not B or D (Figure 5.

b). GH97, BS_04091, is a predicted α -glucosidase or α -galactosidase, other three

participate in yeast mannan degradation (Chapter 4). Both BS_04089^{GH125} and

BS_04078^{GH92} displayed activities characteristic of periplasmic enzymes (Chapter

4). Interestingly, among all proteins in the PUL BS_04090^{GH76} is the only one

carrying a Signal Peptidase II (SPII) cleavage site, indicating that it is a lipoprotein, which is probably located on the cell surface.

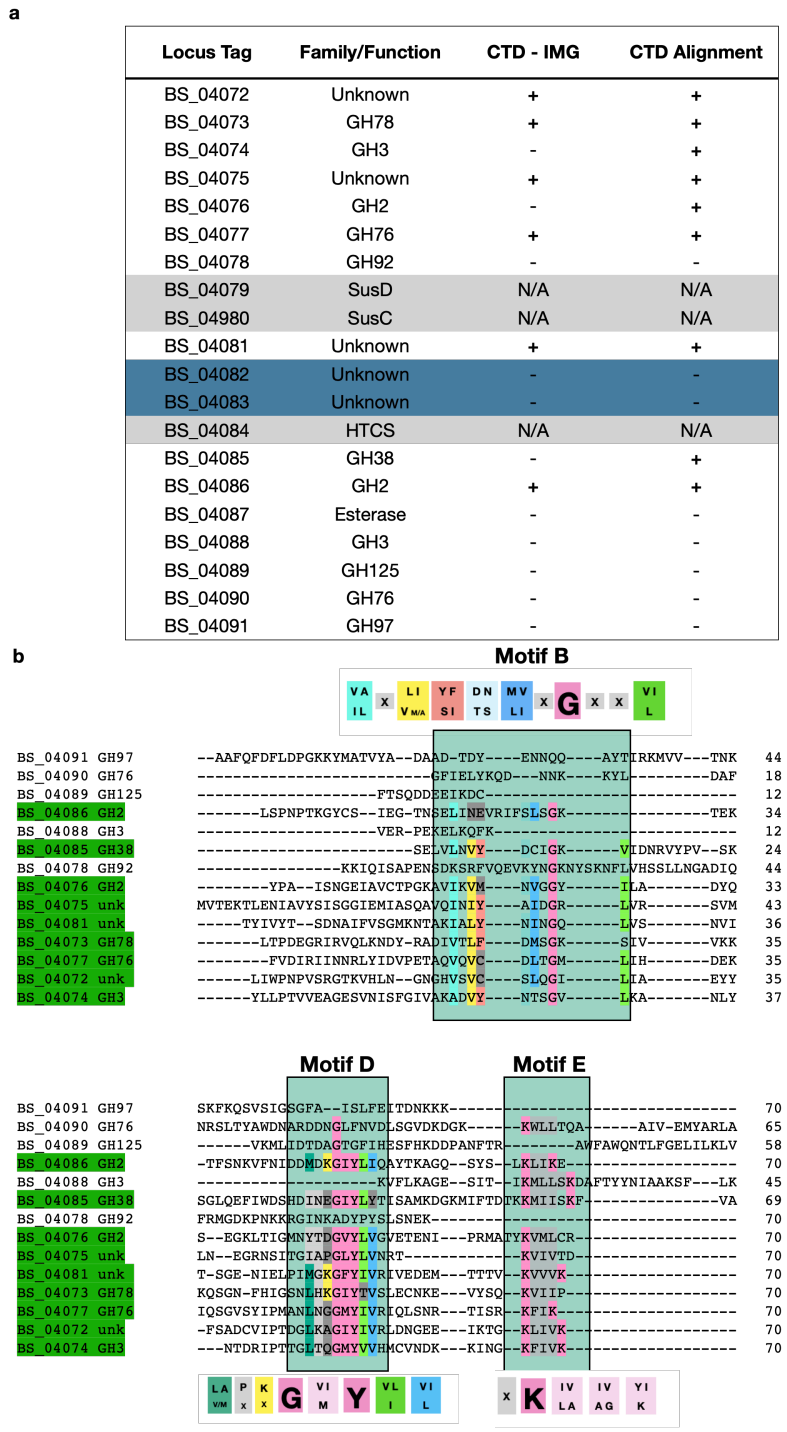


Figure 5. 7 T9SS CTD in *B. salyersiae* Mannan PUL -1. Panel a: Table of proteins from Mannan PUL 1, IMG prediction for the presence of T9SS is indicated with '+', shaded in blue were not detected in the proteomics data. Panel b: alignment of C-terminal amino acid residues of proteins in the Mannan PUL -1. Motifs B, D, and E are shaded in green, strictly conserved amino acid residues are highlighted in pink, other residues are colour-coded to match the residues shown in panel b. 9 out of 14 proteins in Mannan PUL 1 contain motifs B, D, and E of the T9SS CTDs.

5. 3. 3 Role of T9SS in yeast α -mannan breakdown.

The data in Chapter 4 showed that the enzymatic activity was associated with the cell surface of Bs and not the supernatant. This suggests that the T9SS does not secrete the enzymes into the milieu as soluble proteins, but instead, probably conjugates them to a surface structure such as LPS, as described in *P. gingivalis* (Gorasia et al., 2015, Madej et al., 2021). Nevertheless, we still investigated whether *B. salyersiae* deploys the T9SS to secrete proteins into the extracellular milieu during growth on mannan. Bs was grown on *S. cerevisiae* mannan and aliquots were collected for 13 hours to include lag, early-, mid-, and late-exponential, and stationary phases. At each time point, supernatant was concentrated 7 times with 10,000 Da Vivaspin™ spin column for 20 mins at 4,000 rpm at 4 °C. Supernatant was analysed with SDS-PAGE. To ensure cells were actively growing, a range of 10-fold serial dilutions was plated out to determine CFU ml⁻¹ by colony counts.

Consistent with previous observations, Bs displayed a lag phase, which was followed by a rapid mid-exponential growth (Figure 5. a). CFU ml⁻¹ data reflected this (Figure 5. b), indicating that Bs was rapidly growing and dividing, and therefore cell death was limited. SDS-PAGE analysis showed that bands were detected in the supernatant which was collected from the mid-exponential phase and their intensity increased as growth continued (Figure 5. c). At 24h time point, Bs entered a very late stationary phase, the ladder of proteins was a result of extensive cell lysis. This suggests *B. salyersiae* could be secreting proteins extracellularly in response to *S. cerevisiae* mannan.

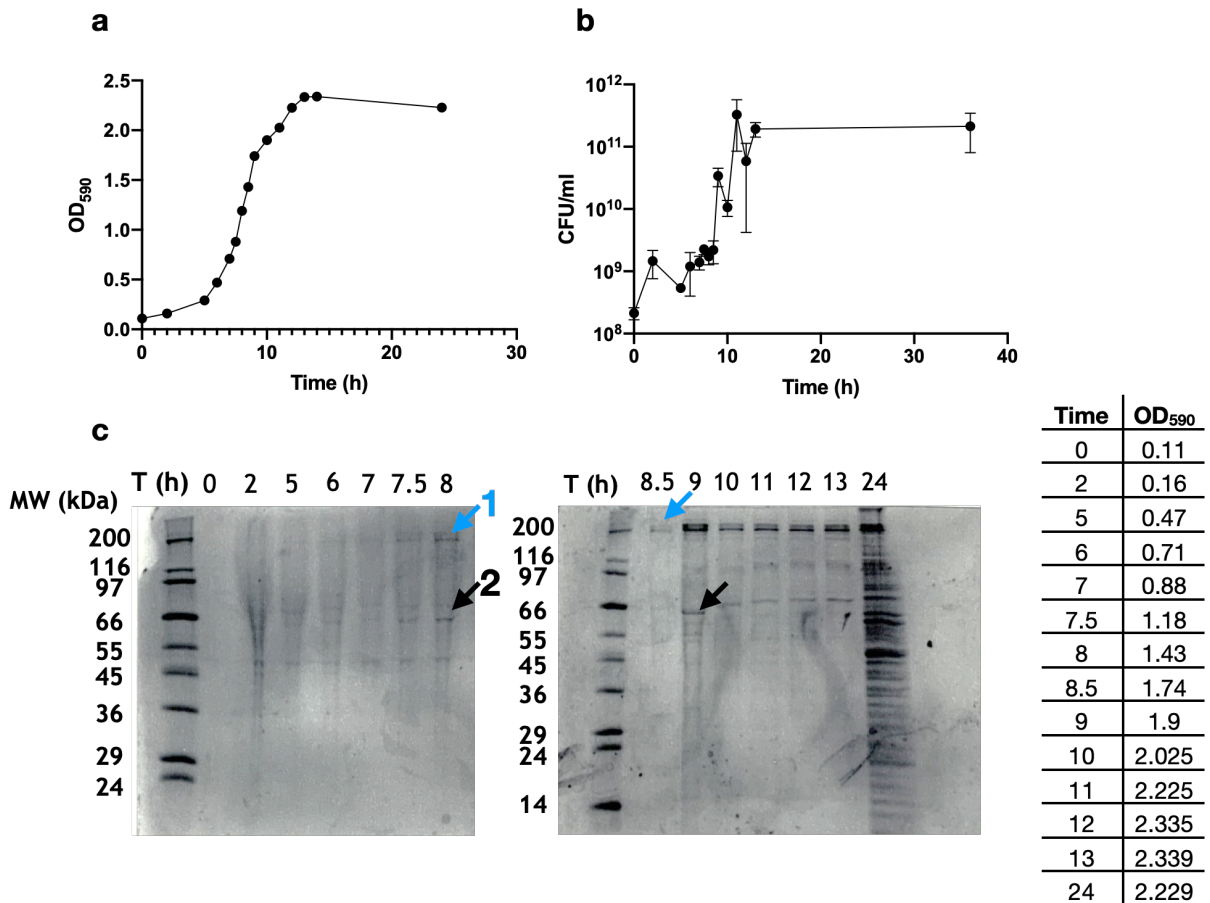


Figure 5. 8 Growth of *B. salyersiae* on mannan from *S. cerevisiae*. *Bs* was grown on 10 mg ml⁻¹ *S. cerevisiae* mannan anaerobically at 37 °C, cultures were collected at indicated time points. Panel a: OD₅₉₀; Panel b: CFU ml⁻¹; Panel c: SDS-PAGE analysis of concentrated supernatant from indicated growth phases. 13µl was resolved on 12.5% polyacrylamide gel, stained with Coomassie Blue. Wide Molecular Weight Ladder (Sigma, UK) was used as reference to identify protein sizes. Dataset represents 3 technical replicates

To identify these proteins, the clearest two bands indicated with blue and black arrows (Figure 5. c) were excised from the gel and subjected to analysis by mass spectrometry, performed by the Proteomics facility at the University of York, UK. Briefly, the procedure involved protein trypsinisation followed by analysis of peptides by matrix assisted laser desorption ionisation tandem time of flight mass spectrometry (MALDI-TOF/MS). The mass spectral data were matched to *B. salyersiae* CL02T12C01 genome available in the NCBI database using Mascot.

Threshold for the associated expect value was set to 0.05, fragment mass tolerance was set at 0.5 Da, a minimum of 2 matched peptides was required for protein identification. This analysis identified the largest band (1) as HMPREF1071_04522, 138 kDa protein, which was described as T9SS Type A sorting protein of unknown function (Figure 5. 9 a). The lower band (2) was identified as HMPREF1071_04520, 76 kDa protein, annotated as SusD (Figure 5. b).

HMPREF1071_04522 and HMPREF1071_04520 are 100% identical to HMPREF1532_04081 and HMPREF1532_04079 in *B. salyersiae* WAL10018 strain used in our lab. They are referred to here as BS_04081^{unknown} and BS_04079^{SusD} as in the Mannan PUL 1 characterised in Chapter 4 (Figure 5. c).

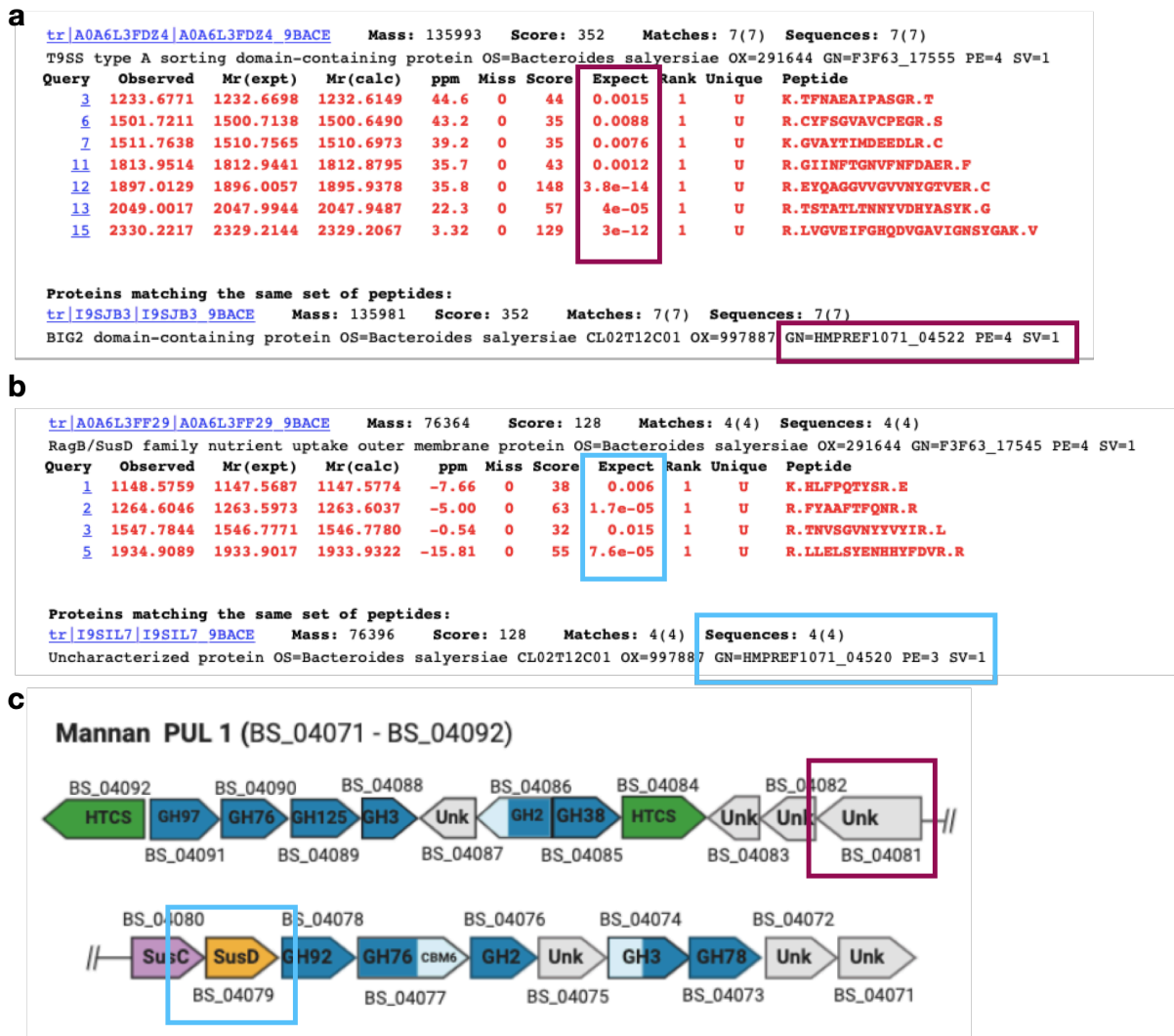


Figure 5. 9 Mass spectrometric analysis of proteins found in cell free supernatant. Bands were analysed with MALDI-TOF. Mass spectral data were searched in Mascot against *B. salyersiae* CL02T12C01 genome available in the NCBI database. Fragment mass tolerance was set at 0.5 Da, a minimum of 2 peptides with expect value lower than 0.05 were required for protein identification. Data represent two biological replicates. Panel a: Mascot analysis of band 1, identified as HMPREF1701_04522; Panel b: Mascot analysis band 2, identified as HMPREF1071_04520; Panel c: Location of newly identified proteins in Mannan PUL 1 in *B. salyersiae* WAL10018, HMPREF1701_04522 corresponds to BS_04081 – unknown, HMPREF1071_04520 – BS_04079 – SusD.

5. 3. 4 *B. salyersiae* produces Outer Membrane Vesicles (OMVs)

The presence of soluble proteins in the supernatant during the mid-exponential growth is unusual for gut *Bacteroides*. As shown in Figure 5.8, the protein of unknown function BS_04081 contains a CTD targeting it to the T9SS, suggesting that it could be secreted in a soluble form. However, the second protein identified by MALDI-MS was SusD (BS_04079), a binding protein which is usually associated with SusC in the outer membrane to mediate import of oligosaccharides into the periplasmic space (Glenwright et al., 2017, Gray et al., 2021). It could therefore be possible that the two proteins are associated with the outer membrane vesicles (OMVs), rather than being solubly secreted. Bt was previously shown to produce OMVs when grown in rich media, which were enriched in homologues of SusD and a range of other putative binding proteins (Valguarnera et al., 2018). Therefore, we looked for the presence of OMVs in the supernatant collected after growth of Bs on mannan and glucose.

Bs was grown in 50 ml of defined medium with yeast mannan or glucose for 16 hours. Supernatant was separated by centrifugation at 15,000 rpm for 30 min and filter sterilised. Potential OMVs were isolated by ultracentrifugation at 100,000 g for 2 hours and resuspended in 150 µl of sterile PBS. Samples were analysed with transmission electron microscopy (TEM), using negative staining, by Tracey Davey in the EM Research Services unit, Newcastle University.

TEM revealed that Bs produces uniform OMVs in response to both glucose and yeast mannan (Figure 5. a and b). Diameters of the OMVs were then measured using Fiji software. This showed that the OMVs produced in response to glucose varied between 30-80 nm in size, while OMVs produced in the response to yeast mannan ranged between 20-60 nm in diameter (Figure 5. d), these were harder to

measure due to electron dense contaminants in the sample, likely, originating from yeast mannan itself. Overall, OMVs generated in response to glucose were significantly larger (unpaired t-test p -value 0.0001) than the ones produced in response to yeast mannan (Figure 5. c). These data do not prove that SusD (BS_04079) and BS_04081 are released associated with OMVs but suggests that this could be possible and aligns with the data showing surface associated enzyme activity.

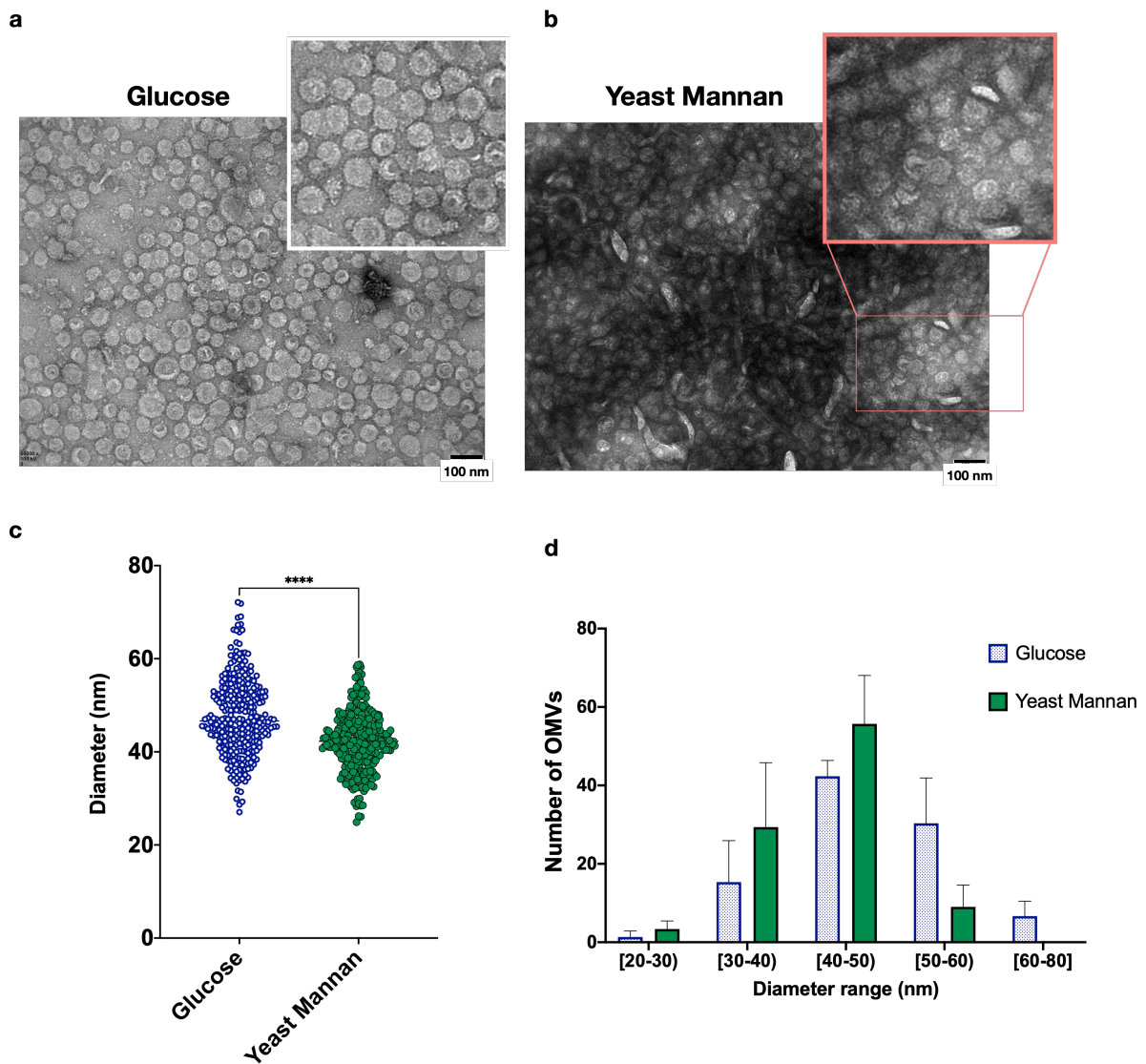


Figure 5. 10 *B. salyersiae* produces OMVs in response to glucose (a) or yeast mannan (b). OMVs were purified as described in Methods and analysed with Transmission Electron Microscopy using negative stain. Pictures were taken at 20,000 x magnification with 100 kV accelerating voltage, 100 nm scale is shown. Panel c: Diameters of OMVs from glucose (blue) and mannan (green) samples. Sample size equals 300 per treatment, diameters were measured in Fiji, using the scale bar provided. Unpaired t-test was performed to test for statistical significance, **** - $p < 0.0001$. Panel d: Representation of OMVs by their diameter range in glucose (blue) in mannan (green) samples. Error bars show SEM.

5. 3. 5 Biochemical characterisation of BS_04081^{unknown}

To elucidate the potential function of BS_04081, the encoding gene was cloned into pET28b vector by Carl Morland and recombinantly expressed in *E. coli*.

Protein was purified with IMAC, soluble protein of 138 kDa was obtained (Figure 5. a).

Prior to assays, amino acid sequence of BS_04081 was analysed with InterPro and Smart. This showed that BS_04081 was composed of a pectate lyase-like domain and a Big-2 domain, which overlapped with an invasin/intimin domain (Figure 5. b). As expected, BS_04081 also contained T9SS Secre_tail domain in the C terminus (Figure 5. b). Pectin lyase domains are characteristic of polysaccharide lyases, which target polysaccharides containing uronic sugars, however a similar fold can also be found in glycoside hydrolases and other proteins, therefore this prediction is not definite (Lombard et al., 2010, Garron and Cygler, 2014). In contrast, Bacterial-immunoglobulin (BIG)-like domains mediate cell adhesion to biotic and abiotic surfaces, contributing to pathogenesis species such as *E. coli* (Bodelón et al., 2013, Kelly et al., 1999).

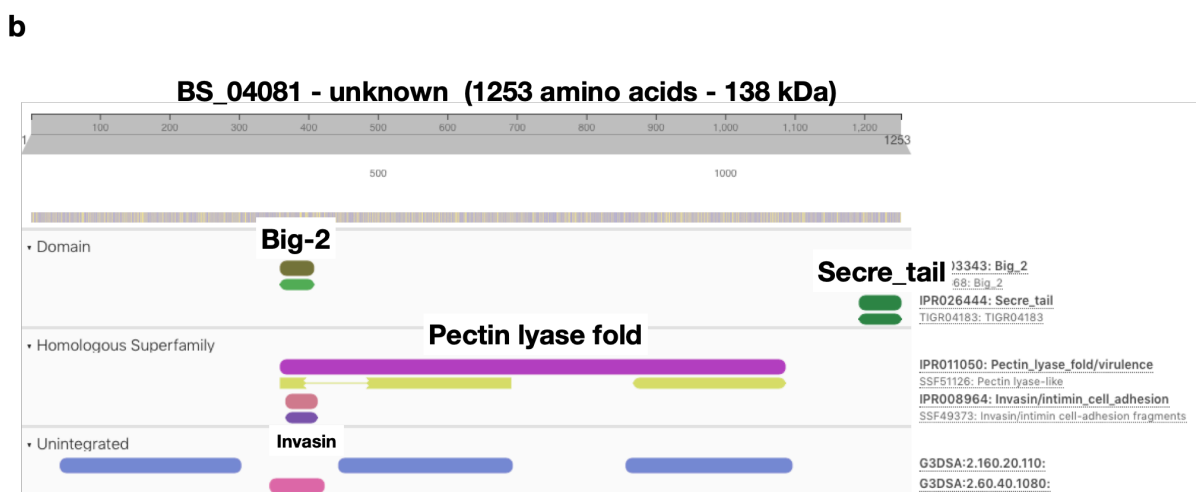
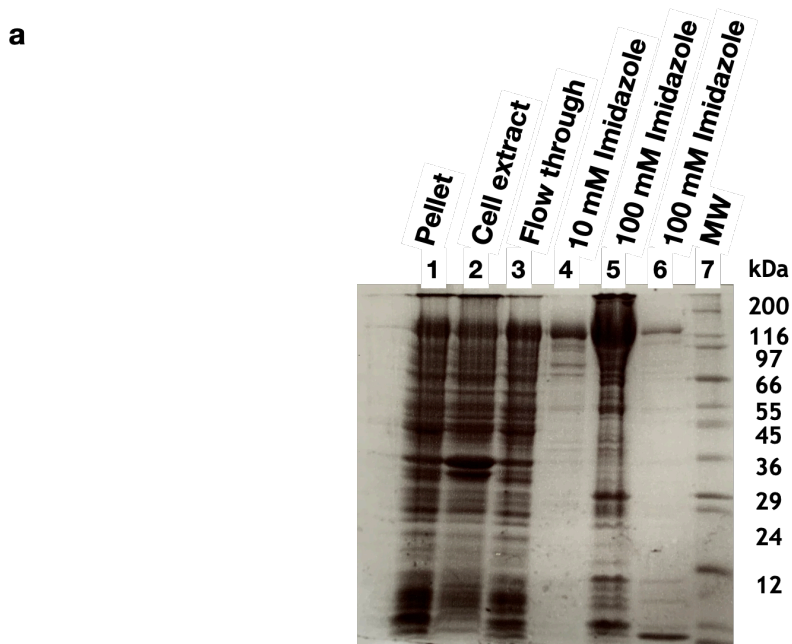


Figure 5. 11 Analysis of BS_04081^{unknown} from *B. salyersiae*. Panel a: SDS-PAGE analysis of recombinant BS_04081 purified with IMAC. Indicated fractions were collected and resolved on 12.5% (w/v) polyacrylamide gel, protein was stained with Coomassie. Soluble protein of 136 kDa was eluted with the first wash of 100 mM imidazole in TALON buffer (20 mM Tris-HCl, 300 mM NaCl, pH=0.8). Wide Molecular Weight Ladder (Sigma, UK) was used to identify protein sizes. Panel b: InterPro domain analysis of BS_04081. BS_04081 is predicted to contain a Big2 domain, overlapping with an Invasin domain, as well as pectin lyase domain and Secre-tail CTD.

To test for enzymatic activity, BS_04081 was assayed against 4 mg ml⁻¹ of mannan from wild type, *mnn1*, *mnn5*, and *mnn2* *S. cerevisiae* strains. BS_04081 was also incubated with 5 mM Ribonuclease B, which is decorated with Man₈₋₉GlcNAc₂ N-glycan, and 1 mM α-1-Acid Glycoprotein, which is glycosylated with a complex N-glycan. No activity against any of the substrates could be detected (data not shown). To investigate whether activity of BS_04081 could be metal dependent, it was treated with 1 mM EDTA at 4 °C, EDTA was washed off and metals: MnCl₂, MgCl₂, CoCl₂, CaCl₂, NiCl₂, ZnCl₂, CuCl₂ in excess were reintroduced in 100 mM MOPS. Again, no activity of BS_04081 could be detected against wild type, *mnn1*, or *mnn5* mannans (data not shown), indicating that BS_04081 is not a mannan-degrading enzyme.

PULs often contain at least one surface glycan protein, while the Sus system contains several: SusE and F, which capture glycans, potentiating their degradation at the cell surface (Koropatkin et al., 2008). The presence of a Big/intimin-like domain (Figure 5.) suggested that BS_04081 could function as a binding protein, therefore its ability to bind yeast mannan was assessed with NATIVE-PAGE affinity gels. Gels were prepared and run as described in Chapter 2 Section 2. 4. 9, where migration of the protein on a native gel is compared to the one, which contains 1 mg ml⁻¹ polysaccharide, in this case yeast mannan. If the protein binds to the substrate, its migration through the gel is retarded. Each lane was loaded with 5 µg of protein and Bovine serum albumin (BSA) (Sigma, UK) was used as a standard. This showed that without a substrate BS_04081 localised between bands indicative of a monomer and a dimer of BSA (Figure 5. a). Addition of mannan from wild type *S. cerevisiae* induced a visible shift of the protein (Figure 5. b), suggesting formation of protein-substrate complexes and indicating mannan

binding. This shift was more enhanced in the presence of mnn1 or mnn5 mannan variants (Figure 5. c and e). Upon addition mnn2 mannan, band level was comparable to that induced by mannan from the wild type yeast (Figure 5. a and f). These data demonstrated BS_04081 was able to bind all types of yeast mannan, displaying preference for mnn1 and mnn5 mannan variants, whose sidechains lack α -1,3 mannosyl caps. This suggested that BS_04081 recognises and binds α -1,2-linked mannosides with strong affinity.

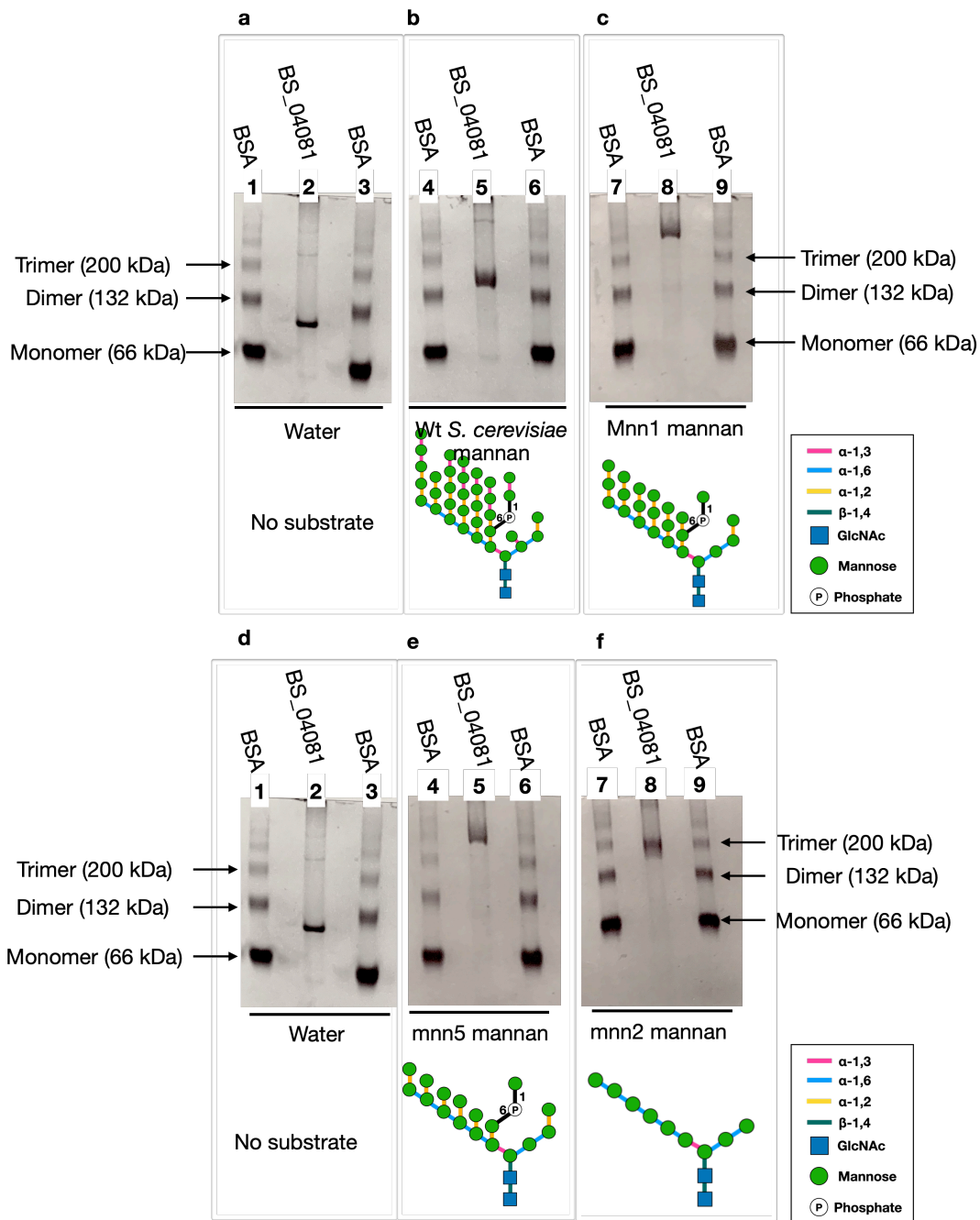


Figure 5. 12 NATIVE-PAGE affinity gels of BS_04081 against *S. cerevisiae* mannan variants. Each lane contains 5 μ g of protein, final concentration of substrate was 0.1% (w/v), BSA (Sigma, UK) was used as a ladder. Panel a and d: BS_04081 no substrate; Panels b-c and e-f: BS_04081 against indicated substrates. Structural differences between all mannans are illustrated.

Binding affinity of BS_04081 for mannan variants was quantified with isothermal titration calorimetry (ITC). Protein was dialysed in 50 mM HEPES, 150 mM NaCl (pH 7) overnight at 4 $^{\circ}$ C, substrates were prepared in dialysis buffer. BS_04081 at

20-25 μM was loaded into reaction cell and was repeatedly injected 27 times with 10 μl aliquots of substrate, cell temperature was maintained at 25 $^{\circ}\text{C}$. K_d and ΔH values were determined from the resulting heats using Microcal PEAQ-ITC software v1.30 (Malvern Panalytical), where concentration of ligand was adjusted such that number of binding sites was equal to 1.

In agreement with the data obtained from NATIVE-PAGE analysis, ITC demonstrated that BS_04081 exhibits strong affinity for mnn1 and mnn5 mannan variants, giving K_d values of 1.18 and 1.38 mM, respectively (Figure 5.). This indicates that, while recognising α -1,2 mannosidic linkages in mnn5 mannan, BS_04081 prefers repeated α -1,2-linked mannosyl units such as those found in mnn1 mannan. BS_04081 still displayed strong binding to mannan from the wild type *S. cerevisiae* ($K_d = 2.5$ mM) (Figure 5. a), suggesting that α -1,3-mannosyl caps do not interfere with binding. Binding of BS_04081 to mnn2 mannan is 10 times lower ($K_d = 31.6$ mM) compared to mannan from the wild-type, and 20 and 25 times lower than that to mnn5 and mnn1 mannan, respectively (Figure 5. d). Thermodynamic parameters are summarised in Table 5. 2.

Overall, NATIVE-PAGE together with ITC analysis show that BS_04081 is a binding protein which prefers branched mannose polymers over linear, displaying strong affinity for α -1,2-mannosidic linkages.

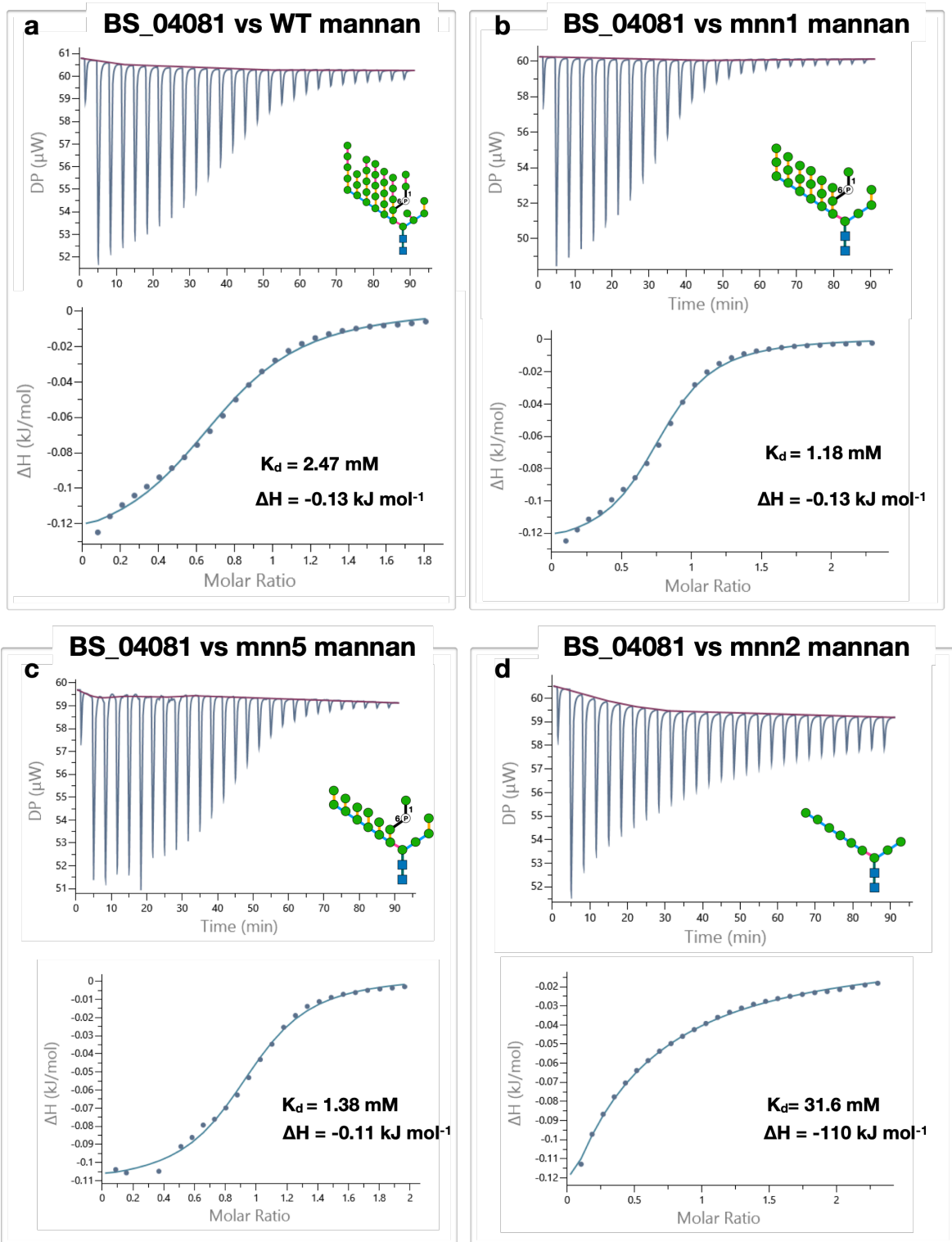


Figure 5. 13 Binding of BS_04081 to mannan from wild type, mnn1, mnn5, and mnn2 *S. cerevisiae* strains by ITC. Mannans were titrated into BS_04081 at 20-25 μM in 50 mM HEPES 150 mM NaCl pH 7. The stoichiometry was fitted to a one-site binding model to determine K_d and ΔH .

Substrate	K_d (mM)	ΔH (kJ mol ⁻¹)	ΔG (kJ mol ⁻¹)	$T \Delta S$ (kJ mol ⁻¹)
WT mannan	2.47	-0.13	-14.9	14.77
mnn5 mannan	1.38	-0.131	-16.3	16.169
mnn1 mannan	1.18	-0.11	-16.7	16.59
mnn2 mannan	31.60	-110	-8.57	-101.43

Table 5. 2 Table of thermodynamic parameters of BS_04081 against different mannan substrates. Parameters were determined using Microcal PEAQ-ITC software v1.30 (Malvern Panalytical). Second law of thermodynamics $\Delta G = \Delta H - T\Delta S$, where ΔG – Gibbs free energy, ΔH – change in enthalpy, $T\Delta S$ – change in entropy over time, was used to calculate $T\Delta S$. K_d stands for binding affinity

5. 3. 6 Biochemical characterisation of BS_04072^{unknown}

Based on the binding properties of BS_04081, it was investigated whether other unknown proteins with T9SS CTDs from the Mannan PUL contain any of the similar domains. InterPro analysis revealed that another protein from this PUL, BS_04072 was predicted to possess Big_2 domain as well as FA58C and cadherin domains (Figure 5. a), both of which are characteristic of binding proteins (Bodelón et al., 2013). GDSL domain is frequently found in esterases (Chepyshko et al., 2012) (Figure 5. a).

Gene encoding for BS_04072 was cloned into pET28b and recombinantly expressed by Carl Morland. Protein was purified with IMAC and analysed with SDS-PAGE, soluble protein of approximately 240 kDa was obtained (Figure 5. b).

t

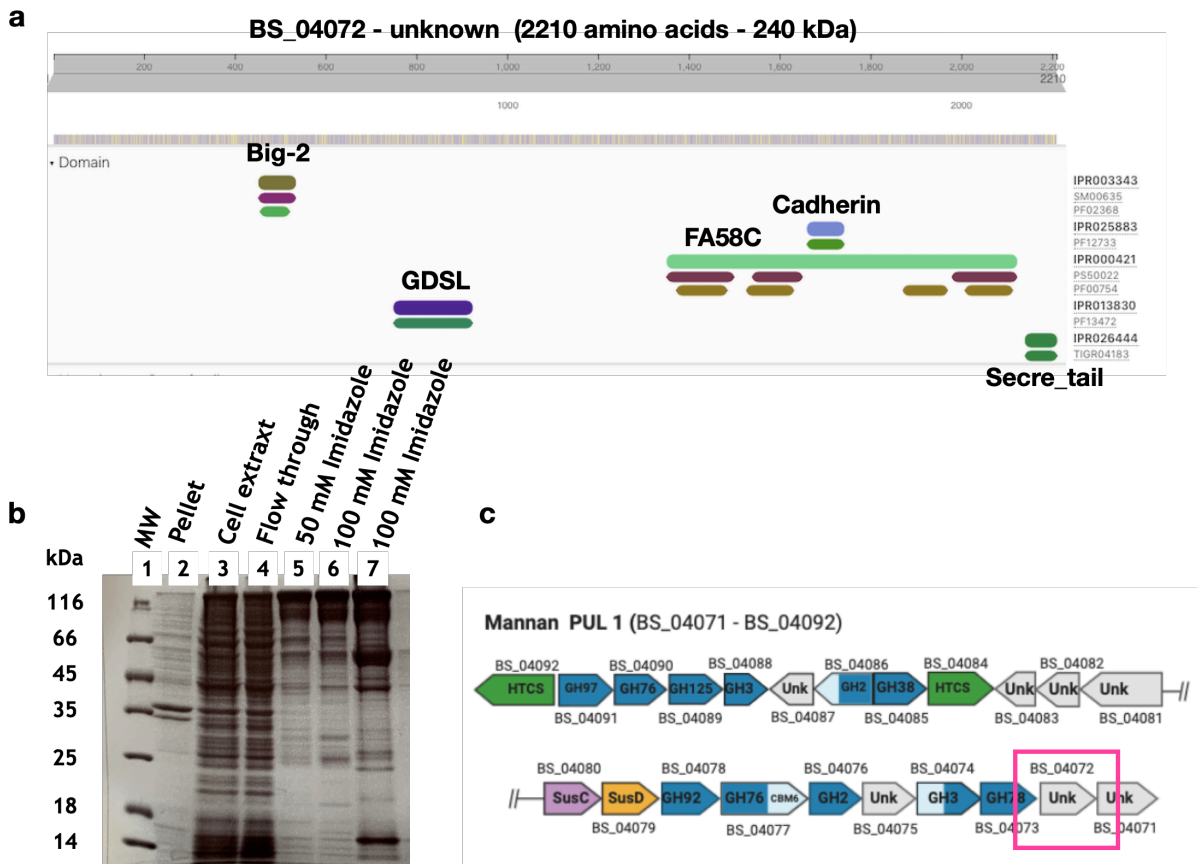


Figure 5. 14 Analysis of BS_04072^{unknown}. Panel a: Domain organisation of BS_04072 analysed in InterPro. Panel b: SDS-PAGE analysis of recombinant BS_04081. Elutions were resolved on 12.5 % gel, soluble protein was eluted with 100 mM Imidazole in TALON buffer. Panel c: location of BS_04072 in the Mannan PUL 1

Enzymatic activity BS_04072 against wild type, mnn1, and mnn5 mannans with or without metals was not detected (data not shown). Binding ability of BS_04072 was analysed with NATIVE-PAGE affinity gel, containing 1 mg ml⁻¹ wild type yeast mannan or water as negative control. This showed that the presence of wild type yeast mannan induces a visible, though small shift of BS_04072 (Figure 5.), indicating that this protein is also able to bind yeast mannan. We also analysed binding ability of BS_04072 with ITC and were able to detect heat peaks, indicative of binding. However, due to the time constraints, this was performed in a

single experiment and we were unable to fit the curve to a one-site binding model and therefore the data is not presented in this thesis.

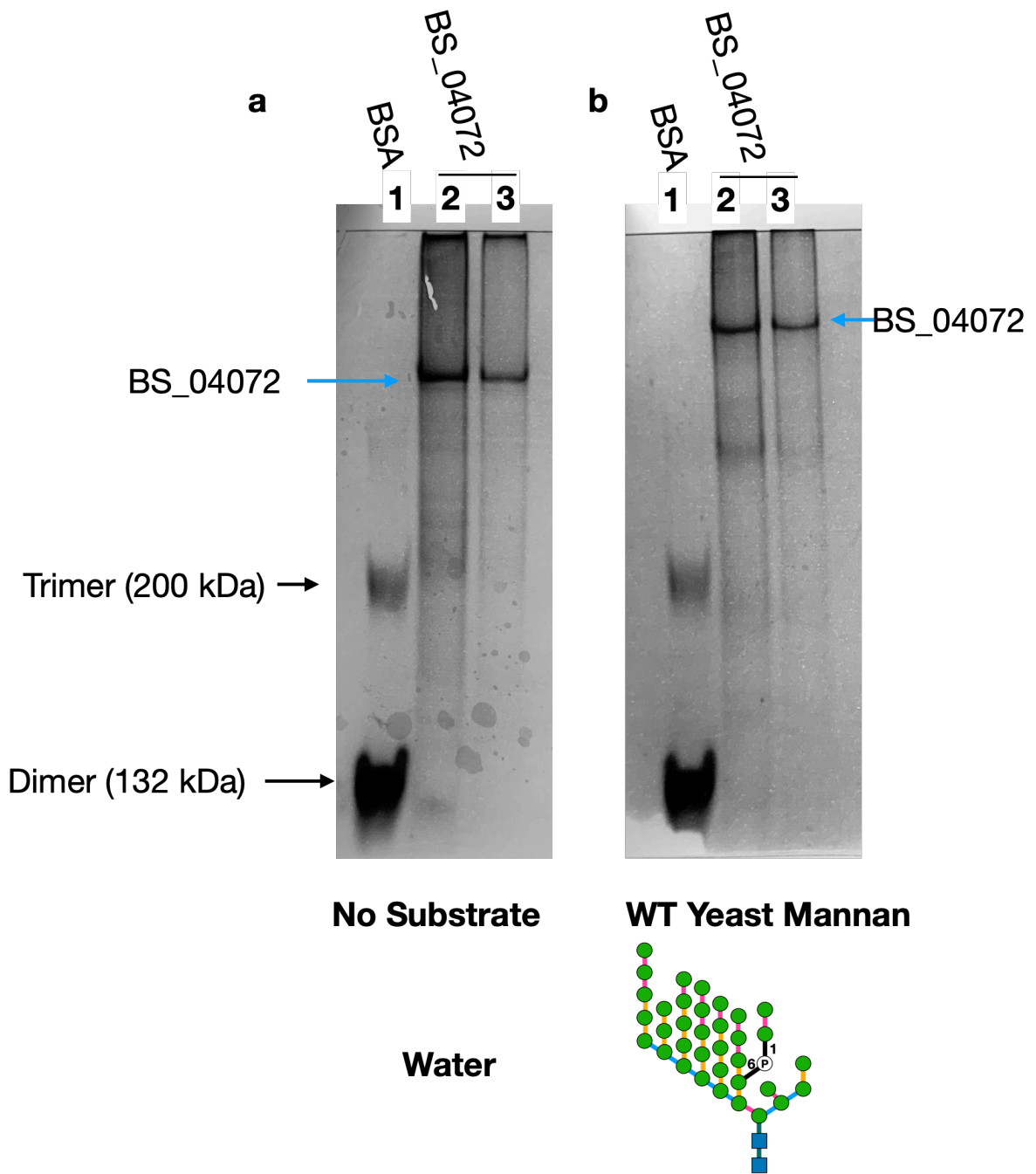


Figure 5. 15 NATIVE-PAGE affinity gel of BS_04072 against 0.1% (w/v) yeast mannan. Lanes were loaded with 5 μ g of BSA or BS_04072. Panel a: BS_04081 in a gel without substrate; Panels b: BS_04081 in a mannan containing gel.

5. 4 Discussion

T9SS is composed of at least 20 different proteins, which assemble into trans-membrane complex, which is used to either attach proteins to the outer membrane or secrete them extracellularly (Larsbrink and Mckee, 2020). It is well characterised in environmental and oral Bacteroidetes, such as *P. gingivalis* and *F. johnsoniae*, where it mediates expression of virulence associated proteases and gliding motility, respectively (Lasica et al., 2016, McBride and Zhu, 2013). In addition to gliding motility, T9SS was shown to implement extracellular secretion of a glycoside hydrolase, ChiA^{GH18}, in *F. johnsoniae* (Kharade and McBride, 2014). Unexpectedly, in the process of biochemical characterisation of the enzymatic apparatus mediating yeast α -mannan breakdown in *B. salyersiae* (Chapter 4), we found that one of the glycoside hydrolases (BS_04077^{GH76}) was described to be directed to the secretion by the Type 9 system. To date however, none of the members of the *Bacteroides* genus has been described to utilise T9SS, and therefore this was investigated further.

BlastP search (version 2020) revealed that the genome of Bs possesses homologues of all structural components of the T9SS. This was confirmed with comparative proteomics, which showed that 12 T9SS structural proteins were produced by Bs during growth on glucose and mannan. These included all of the essential T9SS proteins such as the main porin SprA and its plug, intracellular regulators PorY and PorX as well as the PorP-PorK-PorL-PorM-PorN complex, which connects the regulators with the outer membrane. The main sortase PorU and its membrane stabilising protein PorV were also detected. These proteins were not upregulated but expressed at equal amounts in response to glucose as

well as yeast mannan, indicating that T9SS is ubiquitously expressed in Bs and processing of proteins via this system is nutrient source independent.

Proteins targeted for the T9SS carry a unique signal in their C-termini, which is recognised by the components of the T9SS. The C-terminal domains (CTDs) guide T9SS substrates through the SprA pore, where they are cleaved by sortase PorU. The presence of CTDs in target proteins is pivotal for the secretion by the T9SS (Kharade and McBride, 2014, De Diego et al., 2016). T9SS CTDs are split into two Pfam Families: Type A (TIGR04183) and Type B (TIGR04131) (Veith et al., 2017, Larsbrink and Mckee, 2020), based on the conservation of amino acid residues. Type B associated motifs are not well established; however, it has been suggested that the main protein implementing gliding motility, SprB, in *F. johnsoniae* carries a Type B CTD (Kulkarni et al., 2017). Type A CTDs are characterised by their hallmark amino acid motifs B, D, E, which are conserved in an array of T9SS substrates from both *P. gingivalis* and *F. johnsoniae* (Veith et al., 2017). Here, we found that *B. salyersiae* possesses at least 109 proteins, containing Type A CTDs, 20 of these proteins were predicted to belong to a range of GH families and the rest did not have functions assigned. In addition to *B. salyersiae*, TIGR04183 domain containing proteins were also found in *B. nordii* and a small number was detected in *B. intestinalis* and *B. cellulosilyticus* but not other gut *Bacteroides*. Characterisation of T9SS in these species was beyond the scope of this thesis.

The role of the T9SS in the degradation of yeast α -mannan was then investigated. Here, we found that 9 out of 20 proteins enclosed in Mannan PUL 1 contained conserved amino acid motifs associated with Type A CTDs. Two of these proteins were mannan degrading enzymes BS_04085^{GH38} and uncharacterized

BS_04077^{GH76}. A number of T9SS proteins in this PUL did not possess assigned functions. Despite not being able to detect enzymatic activity associated with the supernatant in Chapter 4, we still investigated whether any of the proteins were secreted into the extracellular space. This showed that indeed a few proteins accumulated in the cell free supernatant during growth on yeast mannan. In-gel analysis of these proteins by MALDI-MS identified the two most abundant of them as BS_04081 (unknown) and BS_04079 (SusD). As discussed in Section 5.3.4, SusD is a binding protein, which pairs with SusC to mediate import of oligosaccharides into the periplasmic space (Glenwright et al., 2017, Gray et al., 2021). Secretion of SusD as a sole soluble protein into the extracellular space seemed unlikely but suggested that it could originate from OMVs. OMVs are membranous structures, which are produced by *Bacteroides* species such as *B. fragilis* and *B. thetaiotaomicron* (Elhenawy et al., 2014). The exact biological role of OMVs is unknown, however, they have been shown to be enriched with SusD-like and other putative binding proteins as well as GHs (Valguarnera et al., 2018, Jones et al., 2020). TEM revealed that Bs produces OMVs in response to glucose and yeast mannan, indicating that this biological process is also independent of the nutrient source. Overall, OMVs released in response to glucose were larger than the ones produced in response to yeast mannan.

In addition to SusD, MALDI-MS identified a putative Type-A T9SS protein, BS_04081. Biochemical characterisation of this protein did not reveal any enzymatic activity against yeast mannan that could be associated with this protein. In contrast, it was found that BS_04081 acts as a binding protein, displaying strong affinity for branched α -mannan substrates rather than linear. ITC demonstrated that BS_04081 exhibited particular preference for repeatedly linked

α -1,2- mannosides, such as those found in mnn1 mannan. BS_04081 does not share homology with any other proteins in gut *Bacteroides* with the closest homologue, sharing 35 % identity, found in *Prevotella spp.* The presence of OMVs suggests that BS_04081 and SusD could be packed together into or the surface of the membranous vesicles thus be released into the extracellular milieu to bind yeast mannan, somehow granting a better access to the substrate. It is still however possible that BS_04081 could be secreted as a soluble extracellular protein. One of the ways of testing this would be to raise antibodies against BS_04081 and investigate its presence in the ultracentrifuged supernatant collected from the OMV purification with Western Blot, while using OMVs as a control. Another way of testing this would be to concentrate the ultracentrifuged OMV-free supernatant and analyse it again on SDS-PAGE. This would show whether BS_04081 could be eliminated from the liquid fraction by ultracentrifugation together with OMVs or it remains in the OMV-free supernatant as a soluble protein.

We then found another protein of unknown function, BS_04072, in Bs Mannan PUL 1, which also contained the Secre-tail CTD. Domain organisation of this protein suggested that it mediates binding, which was indeed confirmed with affinity gels and ITC, however the enzymatic activity against any mannan substrates could not be detected. Alignment of BS_04072 with BS_04081 in Clustal Omega showed that they shared only 20% sequence similarity. InterPro analysis, however, showed that both BS_04081 and BS_04072 contain a Big-2 domain (IPR003343, pfam 02368). Bacterial immunoglobulin-like domains are commonly found in a variety of binding proteins in pathogenic *E. coli* strains and others such as *Citrobacter* and *Yersinia spp.* (Bodelón et al., 2013). In *E. coli*

these domains compose fimbrial adhesins and non-fimbrial proteins, such as intimins and invasins and other intracellular glycan binding proteins (Bodelón et al., 2013). In *E. coli* intimins are composed of Big_1 or Big_2 domains, which form β -stranded outer membrane proteins. These are used to interact with the host, mediating bacterial adhesion to enterocytes and the epithelial lining of the urinary tract, invasion of the Payer's patches, collectively contributing to pathogenesis (Bodelón et al., 2013). Investigations into the crystal structure of intimins revealed that binding sites are located in the C-terminus of the domain (Batchelor et al., 2000). Generally, CAZymes from gut *Bacteroides* contain a catalytic module, and some may contain a carbohydrate binding module (CBM), which does not confer catalytic activity, but instead facilitates binding to the target substrates. Currently, there are 88 CBM families listed in CAZy database

(<http://www.cazy.org/Carbohydrate-Binding-Modules.html>). CBMs display differential specificities for a range of plant cell wall carbohydrates, some of which recognise long and complex structures, whereas others bind smaller oligosaccharide fragments (Gilbert et al., 2013). Binding of CBMs to polysaccharides has been suggested to disturb the integrity of the substrates, augmenting enzyme processivity (Gilbert et al., 2013). CBM27 and CBM23 have been identified to bind complex plant β -mannans such as konjac glucomannan and carob galactomannan, whereas CBM32 exhibited binding to fragmented galactomannan (Boraston et al., 2003, Mizutani et al., 2012, La Rosa et al., 2019). CBMs binding yeast α -mannan have not yet been identified. The binding ability of both BS_04081 and BS_04072, which only share a Big-2 domain in common, was unexpected. IMG analysis showed that, in addition to BS_04081 and BS_04072, Bs possesses 4 more proteins containing a Big-2 domain, all of which are targeted

for the T9SS. In contrast, Bt was found to possess only two proteins with a potential Big 2 domain. Interestingly, *Cytophaga hutchinsonii* upregulates a range of GH9s and GH8s during growth on crystalline cellulose, majority of which contain repeating Big domains as well as T9SS CTDs (Taillefer et al., 2018). Of note, only a small number of these enzymes contained CBMs (Taillefer et al., 2018). The role of Big 2 domains in glycan metabolism is currently unknown and to investigate its contribution, binding ability of BS_04081 and BS_04072, lacking this domain, could be reassessed.

Investigations into the crystal structure of this domain may help identify residues mediating binding, which could then be mutated, providing insights into the mechanism of substrate recognition. It still should be said that Big 2 domain is only 200 amino acids long, whilst the full length of BS_04072 is 2200 amino acids, resulting in a 240 kDa protein. In addition to Big 2 domain, BS_04072 contains a F5/8C domain, which overlaps with a cadherin domain. F5/8C domains are more common in glycoside hydrolases than Big 2, *in vitro* characterisation of this type of domain from a *Paenibacillus* GH16 revealed its ability to bind a set of β -glucan substrates as well as chitin (Cheng et al., 2009). Therefore, it is possible that in BS_04072 this domain also contributes to glycan binding. Production of a 240 kDa binding protein must come at a huge metabolic cost as, for comparison, the main pore-forming protein in the T9SS, SprA, is approximately 270 kDa and it is used to control the traffic of all T9SS substrates. This therefore heightens the role of BS_04072 in the breakdown of not only mannan layer per se but the fungal cell wall. It is possible that *in vivo* this protein grants access to multiple sugar layers of the cell wall, potentiating its enzymatic degradation. The impact of such binding on fungal physiology would also be interesting to address.

Environmental Bacteroidetes utilise T9SS to express a range of lectins and adhesins, which implement gliding and allow for nutrient scavenging in the soil (Larsbrink and Mckee, 2020). In *F. johnsonii* gliding was shown to be independent from the ability to utilise chitin, but not in *Cytophaga hutchinsonii*, in which motility is tightly linked with cellulose metabolism (Rhodes et al., 2010, Zhu and McBride, 2014). Bs did not display motility, however it will be interesting to investigate whether the T9SS contributes to the 'sharing' mechanism of mannan utilisation and whether binding to mannan using proteins directed to the T9SS allows Bs to resist the competitiveness of Bt in the gut. This could be tested experimentally using genetic knock outs. The current genetic models used in our lab rely on antibiotic sensitivity, Bs, however, was found to be resistant to most antibiotics used in *Bacteroides* genetics, which made gene deletions difficult to achieve. To overcome this, we are developing a different genetic model which confers resistance to potassium tellurite. Tellurite is a highly toxic compound, which is used as a selection marker in multi-drug resistant *E. coli* and *Pseudomonas* strains (Sanchez-Romero et al., 1998, Cunrath et al., 2019). This required a construction of a novel conjugative plasmid, carrying thiopurine methyltransferase from *Acinetobacter*, which detoxifies tellurite to dimethyl ditelluride, giving colonies a black pigment. Introduction of gene knockouts in Bs is ongoing and was not described in this thesis.

The current question that remains unanswered is why *B. salyersiae* maintains two types of systems, the lipoprotein pathway and the T9SS, to locate proteins on the outer membrane, when the majority of gut *Bacteroides* do not require the T9SS for effective glycan degradation. It was noticed as an observation that all proteins targeted to the T9SS in Bs are generally much larger than the typical *Bacteroides*

surface enzymes. Interestingly, majority of the T9SS substrates in Bs, including enzymes from the Mannan PUL, obtain a multi-modular organisation, comprising of CBMs, lectin and other glycan binding domains as well as domains of unknown functions. While the molecular weight of BS_04072 is 240 kD, the largest T9SS substrate we have identified in Bs was BS_00277, which folds into a 340 kDa protein. This protein is not grouped into a PUL and the InterPro analysis revealed that it contains at least 6 domains, one of which was predicted as a hydrolase domain, however the exact function of this protein is unknown. Similarly, secreted chitinase, ChiA, from *F. johnsonii*, contains a GH18 domain, which is followed by 3 potential glycan binding domains, forming a 180 kDa protein. Cellulases from *C. hutchinsonii*, CHU_1075 and CHU_1335, display a similar organisation, where a catalytic domain is followed by multiple glycan binding modules, resulting in proteins of 2600 and 2200 amino acids long. Therefore, we hypothesise that the structural organisation and ultimately the size of a protein acts as a determinant for the secretion by the Type 9 system. Perhaps retaining the T9SS allows Bs to secrete enzymes with additional glycan binding modules, which augment their specificity, providing Bs an advantage in the competitive environment of the gut. In contrast, smaller proteins, containing a single catalytic module, are still secreted by the lipoprotein system, though how this system operates in *Bacteroides* is unknown.

Another question is why T9SS is retained only in a subset of gut *Bacteroides* and it would be interesting to investigate how common these species are in human populations.

Chapter 6: Final Discussion

The human gut is densely populated with a community of microbes, which is represented by both bacterial and fungal species (Turnbaugh et al., 2007, Underhill and Iliev, 2014). Bacteroidetes is one of the two dominant phyla of gut bacteria. These provide a range of beneficial attributes to the host, however their primary role is to degrade complex carbohydrates of dietary, host, and microbial origins (Koropatkin et al., 2012). While the capacity of the host to digest complex carbohydrates is limited, Bacteroidetes have been estimated to encode thousands of CAZymes capable of deconstructing a vast number of glycans (Lapébie et al., 2019). CAZymes are co-encoded with binding and transport proteins to form saccharolytic systems, termed polysaccharide utilisation loci (PULs). Each PUL is designed to depolymerise a specific subset of glycans and its structural organisation often reflects the complexity of the target substrate (Martens et al., 2008). Moreover, degradation of complex carbohydrates is not always orchestrated by a single PUL and often requires a number of loci to work in concert. These glycan-specific PULs are often conserved across a range of *Bacteroides species*, indicating that members can cooperate to degrade complex substrates. Gut bacteria rapidly adjust their metabolomes in response to dietary changes, where each member of the community has developed its own hierarchy for the utilisation of glycans (Rogers et al., 2013, Patnode et al., 2019). In addition to this differential prioritisation of food sources, members also deploy diverse strategies for the acquisition of glycans. Some members display strong competitiveness and utilise glycans in a 'selfish' mechanism, allowing them to occupy their respective niche (La Rosa et al., 2019, Sonnenburg et al., 2010). Whilst others, possess surface endo and exo-acting enzymes to initiate the

breakdown of complex glycans and generate a pool of simpler structures, which can be accessed by species of the same or different genera or even phyla (Rogowski et al., 2015, Rakoff-Nahoum et al., 2016).

Fungi are also normal residents of the gut microbiota, whose abundance and diversity are dictated by the bacterial community (Richard and Sokol, 2019).

Aberrant fungal growth is often associated with a range of disease states, which are tightly linked to the microbial dysbiosis in the gut (Hoarau et al., 2016). The fungal cell wall is composed of three layers of polysaccharides, where α -mannan forms the superficial layer, covering β -glucan and chitin layers. In addition to dietary carbohydrates, microbial polysaccharides, such as those in the fungal cell wall, serve as substrates for gut bacteria. *B. thetaiotaomicron* dedicates 4 different genetic loci to access fungal cell wall polysaccharides (Temple et al., 2017, Cuskin et al., 2015b). Whilst utilisation of fungal β -1,6-linked glucan is restricted to a single locus, which contains only 2 enzymes, the degradation of fungal mannan is mediated by a range of enzymes necessary to hydrolyse its diverse mannosidic bonds (Cuskin et al., 2015b, Temple et al., 2017). In fact, Bt has been estimated to dedicate about 15% of its total glycoside hydrolases to catabolism of α - and β -mannosidic bonds found mostly in fungal mannans or N-glycans.

In Bt mannan degrading proteins are arranged into 3 distinct PULs, which combine to create a system, where surface endo-acting mannanases release large manno-oligosaccharides, which are then transported into the periplasmic space and degraded intracellularly (Figure 6. 1) (Cuskin et al., 2015b). Elements of these PULs were retained by a number of strains of *B. ovatus* and *B. xylanisolvens*, who could utilise simplified mannan variants but not the complex polymer produced by wild type *S. cerevisiae* (Cuskin et al., 2015b). This presence

of mannan-specific PULs in species other than Bt strongly indicates that one species would initiate the breakdown, allowing others to cooperate and thrive on yeast mannan. In contrast, Bt was shown to deploy a 'selfish' mechanism of mannan utilisation and outcompete non-mannan degrading species in co-cultures *in vitro*. Based on the structural similarity of mannan PULs in Bo and Bx with Bt mannan PULs, it was hypothesised that all *Bacteroides species* would deploy a similar strategy of mannan utilisation. *In vivo* assays however showed that Bt strain lacking these mannan PULs outcompetes wild type Bt, when mice are fed a diet lacking yeast mannan. This therefore indicates that in the absence of mannan, the presence of mannan PULs provides a competitive disadvantage, and if mannan is unavailable to Bo and Bx *in vivo*, it is unclear why they retain these loci. Here it was also noticed that another gut bacterium, *B. salyersiae*, was able to grow on mannan to a higher OD₆₀₀ than Bt, despite lacking PULs with structural synteny to Bt mannan PULs.

This thesis aimed to further investigate the mechanism of mannan degradation by gut *Bacteroides*. Here it was found that, unlike Bt, Bs uses a range of exo- and endo-acting enzymes, which are grouped into a large PUL, to produce a pool of branched manno oligosaccharides and mannose at the cell surface (Figure 6. 1). A proportion of these oligosaccharides were then utilised by the poor-mannan degraders such as *B. ovatus*, *B. xylanisolvens*, and also *B. fingoldii* (Figure 6. 1). *In vitro* co-cultures also confirmed that the presence of Bs promoted growth and survival of Bx on yeast mannan. It was previously demonstrated that Bx outcompetes Bt in a co-culture where mannose is a sole carbon source, however experiments presented in this thesis demonstrate that Bs was able to share mannose with both Bt and Bx. Moreover, in a competition for yeast mannan with

Bt, Bs was able to survive a lot better than a non-mannan degrader. Analysis of cell free supernatant collected throughout the co-culture of Bt with Bs, indicated that manno-oligosaccharides, which are characteristic of the metabolic activity of Bs, began to appear in the media a lot sooner, than when Bs is grown on mannan on its own. This suggests, that while establishing dominance in the co-culture, either the metabolic activity or just the presence of Bt promoted growth of Bs on mannan. This was also reflected on the rapidly increasing OD₆₀₀ of the co-culture as well as the CFU ml⁻¹ numbers of Bs. The sharing phenotype was found to be specific to Bs, as, in line with the selfish strategy, mannan which was pre-digested with Bt did not promote growth of other *Bacteroides* species.

Biochemical characterisation of proteins in Bs mannan PUL revealed that 10 of them were directed for the secretion by the Type 9 System (T9SS). The T9SS has been characterised in environmental Bacteroidetes, such as *Flavobacterium johnsoniae* and *Cytophaga hutchinsonii*, as well an oral pathogen from this phylum, *Porphyromonas gingivalis* (Larsbrink and Mckee, 2020). In these species components of the secretion system arrange into a multi-protein complex, which mediates attachment of proteins to the cell surface or their extracellular secretion. While in *P. gingivalis* the primary role of the T9SS is secretion of virulent proteases, in *F. johnsoniae* it implements gliding motility as well as extracellular secretion of a chitinase from the family GH18 (Larsbrink and Mckee, 2020). Chitin metabolism was shown to be independent of gliding in *F. johnsoniae*. In contrast, T9SS-mediated motility is coupled to the ability of *C. hutchinsonii* to degrade cellulose. Nonetheless, this type of secretion system has never been described in gut *Bacteroides* before.

Our analysis revealed that indeed the T9SS is present only in a small subset of gut *Bacteroides*, which included *B. salyersiae*, *B. nordii*, *B. intestinalis*, and *B. cellulosilyticus*. Investigations into the T9SS in species other than Bs were beyond the scope of this thesis and would require further investigation. Bs was found to possess all of the essential structural components of the T9SS, which were not upregulated but expressed at the same level during growth on glucose or mannan. It was also found that Bs directs over 100 proteins to the secretion by this system, only half of which were associated with PULs and 20 were predicted to function as glycoside hydrolases. Interestingly, Bs also directs all of its GH85s, which release N-glycans from the surface of glycoproteins, to the T9SS. These data suggest that, in addition to yeast mannan metabolism, T9SS probably contributes to metabolism and acquisition of other glycans.

We next addressed the contribution of the T9SS in the breakdown of yeast mannan. Here, we discovered that Bs may potentially use the T9SS to secrete a mannan binding protein (BS_04081) into the extracellular milieu either in a soluble form or as part of the Outer Membrane Vesicles (OMVs). The role of the extracellular secretion of binding proteins is unclear and one possible hypothesis is that this high molecular weight protein could be used to opsonise yeast mannan, potentiating its degradation through the distortion of the integrity of the polysaccharide. This alleviation of steric constraints might also make mannan more accessible to Bt, explaining the rapidly increasing OD₆₀₀ when Bt and Bs are grown together. Conversely, another hypothesis is that mannan opsonisation prevents it from being degraded by other species, such as Bt, and this is what allows Bs to withstand the strong competitiveness of Bt. BS_04081 was found to possess a Big-2 domain, which, as discussed in Chapter 5, not only

uncharacteristic of proteins in gut *Bacteroides*, but also commonly found in pathogenic bacteria, contributing to their virulence (Bodelón et al., 2013). Here, we found another Big-2-domain-containing protein (BS_04072) in mannan PUL, which was also targeted for the T9SS. This protein also displayed mannan binding properties but is most likely localised to the cell surface contributing to mannan acquisition.

As an observation it was noticed that the majority of the T9SS substrates in Bs are composed of multiple putative glycan binding domains, giving these proteins a very high molecular weight. Generally, gut *Bacteroides* encode a single surface glycan binding protein (SGBP) per PUL, with the exception of the Sus-operon, which contains two, SusE and F (Foley et al., 2016). Some glycoside hydrolases contain Carbohydrate Binding Modules (CBMs), which bind substrates to assist hydrolysis. CBMs which bind yeast α -mannan have not been characterised yet. In Bt, mannan degrading system was proposed to contain a single SGBP across three PULs, BT3791, estimated to fold into a 60 kDa protein (Cuskin et al., 2015b). In contrast, both binding proteins, BS_04081 and BS_04072, in Bs are 150 and 240 kDa in size, where Big-2 domain constitutes only 200 amino acids and the rest of the proteins is formed by other putative domains. While it was assumed that they contain a single binding site, considering their size and structural organisation, this may not be true. It is possible that *in vivo* both of these proteins are able to bind multiple components of the fungal cell wall, providing Bs a competitive advantage.

In addition to these binding proteins, mannan PUL in Bs contains a T9SS-directed GH76 (BS_04077), which is most likely central to mannan breakdown in Bs.

Unfortunately, for unknown reasons we were unable to clone this protein. InterPro

analysis showed that this GH76 contains CBM6 as well as numerous other putative binding modules, where the catalytic domain occupies only 30% of the protein. We did not attempt to clone just the CMB6 on its own or other putative domains, whose role in binding yeast mannan will be interesting to investigate in the future. It is also possible that, in addition to binding, this enzyme allows Bs to compete with Bt and orchestrates mannan sharing between other gut *Bacteroides*. Bs strain lacking this GH76 will shed more light on the role of this protein in mannan metabolism and cross-feeding. In addition to mannan PUL, an uncharacterised locus, annotated as PUL7 in PULDB, was upregulated in Bs in response to yeast mannan. Some proteins in this locus are also directed to the T9SS and their contribution to mannan breakdown has not yet been investigated. We propose that Bs deploys the T9SS to secrete glycan binding proteins, providing it a strong competitive advantage in a highly populated gut. We were unable to introduce mutations into Bs due to its resistance to all antibiotics used in *Bacteroides* genetics. We are currently developing a novel genetic model which relies on the resistance to a toxic metal, which will allow us to introduce mutations into the T9SS in Bs and dissect its contribution to mannan metabolism as well as acquisition of other glycans.

B. salyersiae is not a well characterised representative of gut *Bacteroides*. A study, which used multi-omics data to associate microbial abundance with cytokine profiles, showed that the presence of *B. salyersiae* negatively correlated with the INF- γ response elicited by *C. albicans* hyphae (Schirmer et al., 2016). INF- γ is the central cytokine driving the pathogenesis of inflammatory bowel diseases (IBD), such as Crohn's disease (CD), and is produced in response to a range of inflammatory stimuli, including bacterial LPS (Langer et al., 2019). C.

albicans hyphal state, its overgrowth, and general microbial dysbiosis with decreased abundance of *Bacteroides* is highly associated with CD. Moreover, antibodies recognising man- α -1,3-man- α -1,2-man epitopes of fungal mannan are the hallmark of CD (Israeli et al., 2005, Young et al., 1998). These antibodies are called Anti-*Saccharomyces cerevisiae* Antibodies (ASCA) and are generated in the sera of CD patients in response to both mannan from *S. cerevisiae* as well as *C. albicans* (Standaert-Vitse et al., 2006). β -mannosylation has also been proposed to contribute to the production of these antibodies. The extent to which fungal mannan is degraded by gut bacteria is unknown, however, it is possible that generation of extracellular manno-oligosaccharides by Bs could contribute to the pathogenesis of CD (Figure 6. 1). Moreover, while being only partially addressed in this thesis, both *C. albicans* mannan-specific β -mannosidases contain SP11 signals, indicating that they are probably located on the cell surface of Bt. Our preliminary data show that Bs displays a very slow growth on *C. albicans* mannan but eventually reaches the same OD₆₀₀ as Bt. Given that gut *Bacteroides* cooperate to degrade yeast α -mannan, it is therefore possible that Bt uncaps *C. albicans* mannan with its surface β -1,2-mannosidases, generating substrates for Bs and other species. The cell wall of *C. albicans* is highly dynamic and responds to environmental stresses, such as oxidative stress, changes in temperature, pH, and carbon source via rearranging its sugar layers (Ballou et al., 2016, Sherrington et al., 2017, Pradhan et al., 2018), suggesting that it will most likely react to bacterial degradation of its constituents. It will be interesting to investigate whether such degradation contributes to the 'GUT' phenotype of *C. albicans* (Pande et al., 2013) and results in increased incorporation of mannose into the cell wall, masking its highly immunogenic β -glucan, or, conversely,

results in its enhanced exposure. Studying these *Bacteroides*-Fungi interactions *in vivo* will provide insights into how fungal commensalism is achieved and whether it contributes to the progression of diseases states.

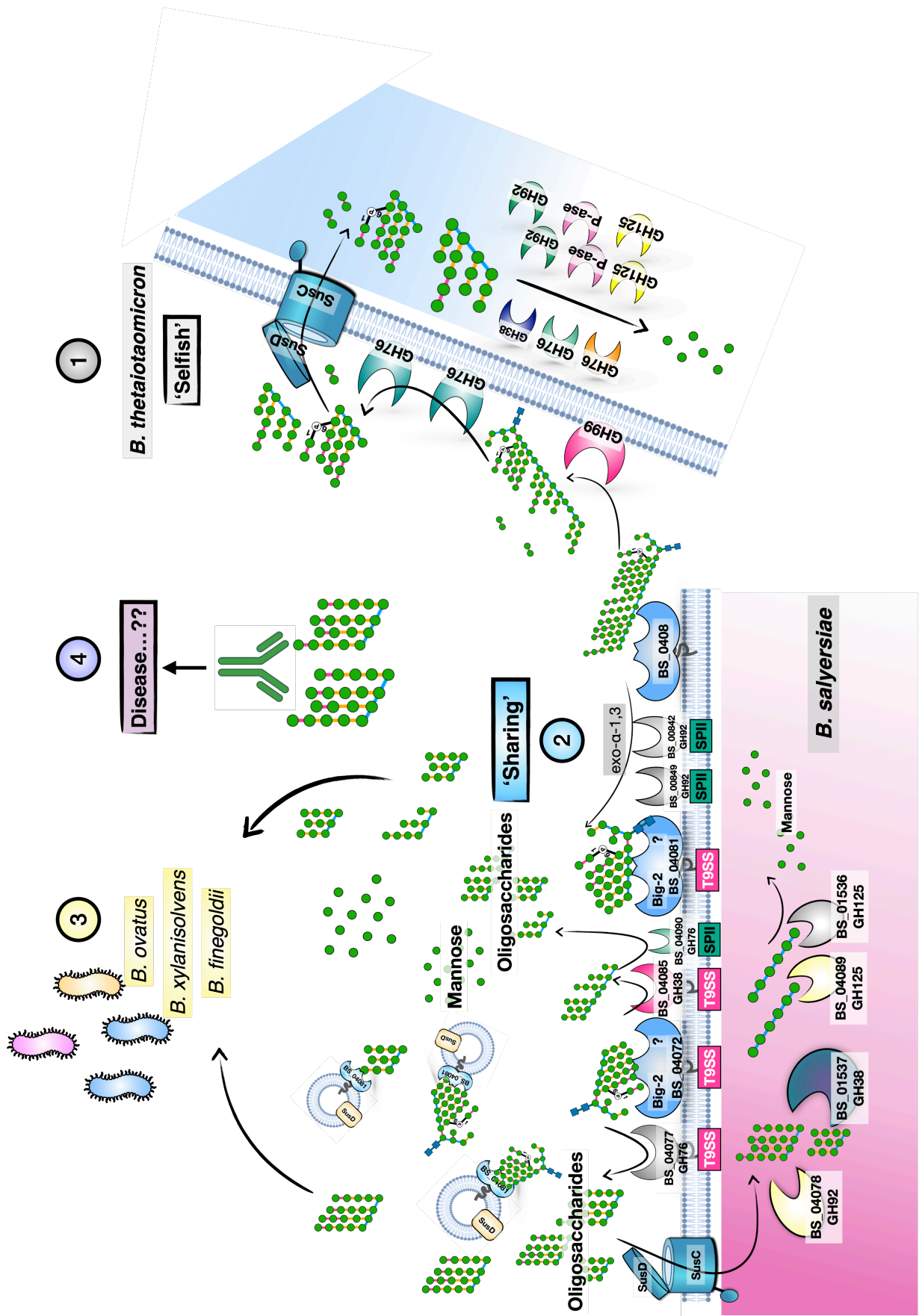


Figure 6. 1 Summary of utilisation of fungal mannan between gut *Bacteroides*

References

- Almagro Armenteros, J. J., Tsirigos, K. D., Sønderby, C. K., Petersen, T. N., Winther, O., Brunak, S., Von Heijne, G. & Nielsen, H. 2019. SignalP 5.0 improves signal peptide predictions using deep neural networks. *Nature Biotechnology*, 37, 420-423.
- Alonso-Gil, S., Males, A., Fernandes, P. Z., Williams, S. J., Davies, G. J. & Rovira, C. 2017. Computational Design of Experiment Unveils the Conformational Reaction Coordinate of GH125 α -Mannosidases. *Journal of the American Chemical Society*, 139, 1085-1088.
- Anderson, K. L. & Salyers, A. A. 1989a. Biochemical evidence that starch breakdown by *Bacteroides thetaiotaomicron* involves outer membrane starch-binding sites and periplasmic starch-degrading enzymes. *Journal of bacteriology*, 171, 3192-3198.
- Anderson, K. L. & Salyers, A. A. 1989b. Genetic evidence that outer membrane binding of starch is required for starch utilization by *Bacteroides thetaiotaomicron*. *Journal of bacteriology*, 171, 3199-3204.
- Ardèvol, A. & Rovira, C. 2015. Reaction Mechanisms in Carbohydrate-Active Enzymes: Glycoside Hydrolases and Glycosyltransferases. Insights from ab Initio Quantum Mechanics/Molecular Mechanics Dynamic Simulations. *Journal of the American Chemical Society*, 137, 7528-7547.
- Arumugam, M., Raes, J., Pelletier, E., Le Paslier, D., Yamada, T., Mende, D. R., Fernandes, G. R., Tap, J., Bruls, T., Batto, J.-M., Bertalan, M., Borruel, N., Casellas, F., Fernandez, L., Gautier, L., Hansen, T., Hattori, M., Hayashi, T., Kleerebezem, M., Kurokawa, K., Leclerc, M., Levenez, F., Manichanh, C., Nielsen, H. B., Nielsen, T., Pons, N., Poulain, J., Qin, J., Sicheritz-Ponten, T., Tims, S., Torrents, D., Ugarte, E., Zoetendal, E. G., Wang, J., Guarner, F., Pedersen, O., De Vos, W. M., Brunak, S., Doré, J., Antolín, M., Artiguenave, F., Blottiere, H. M., Almeida, M., Brechot, C., Cara, C., Chervaux, C., Cultrone, A., Delorme, C., Denariáz, G., Dervyn, R., Foerstner, K. U., Friss, C., Van De Guchte, M., Guedon, E., Haimet, F., Huber, W., Van Hylckama-Vlieg, J., Jamet, A., Juste, C., Kaci, G., Knol, J., Kristiansen, K., Lakhdari, O., Layec, S., Le Roux, K., Maguin, E., Mérieux, A., Melo Minardi, R., M'rini, C., Muller, J., Oozeer, R., Parkhill, J., Renault, P., Rescigno, M., Sanchez, N., Sunagawa, S., Torrejon, A., Turner, K., Vandemeulebrouck, G., Varela, E., Winogradsky, Y., Zeller, G., Weissenbach, J., Ehrlich, S. D., Bork, P. & Meta, H. I. T. C. 2011. Enterotypes of the human gut microbiome. *Nature*, 473, 174-180.

- Auchtung, T. A., Fofanova, T. Y., Stewart, C. J., Nash, A. K., Wong, M. C., Gesell, J. R., Auchtung, J. M., Ajami, N. J. & Petrosino, J. F. 2018. Investigating Colonization of the Healthy Adult Gastrointestinal Tract by Fungi. *mSphere*, 3, e00092-18.
- Azadmanesh, J., Gowen, A. M., Creger, P. E., Schafer, N. D. & Blankenship, J. R. 2017. Filamentation Involves Two Overlapping, but Distinct, Programs of Filamentation in the Pathogenic Fungus *Candida albicans*. *G3 (Bethesda)*, 7, 3797-3808.
- Bågenholm, V., Reddy, S. K., Bouraoui, H., Morrill, J., Kulcinskaja, E., Bahr, C. M., Aurelius, O., Rogers, T., Xiao, Y., Logan, D. T., Martens, E. C., Koropatkin, N. M. & Stålbbrand, H. 2017. Galactomannan Catabolism Conferred by a Polysaccharide Utilization Locus of *Bacteroides ovatus*: ENZYME SYNERGY AND CRYSTAL STRUCTURE OF A β -MANNANASE. *The Journal of biological chemistry*, 292, 229-243.
- Ballou, C. 1976. Structure and biosynthesis of the mannan component of the yeast cell envelope. *Adv Microb Physiol*, 14, 93-158.
- Ballou, C. E. 1990. Isolation, characterization, and properties of *Saccharomyces cerevisiae* mnn mutants with nonconditional protein glycosylation defects. *Methods Enzymol*, 185, 440-70.
- Ballou, C. E., Lipke, P. N. & Raschke, W. C. 1974. Structure and immunochemistry of the cell wall mannans from *Saccharomyces chevalieri*, *Saccharomyces italicus*, *Saccharomyces diastaticus*, and *Saccharomyces carlsbergensis*. *Journal of bacteriology*, 117, 461-467.
- Ballou, E. R., Avelar, G. M., Childers, D. S., Mackie, J., Bain, J. M., Wagener, J., Kastora, S. L., Panea, M. D., Hardison, S. E., Walker, L. A., Erwig, L. P., Munro, C. A., Gow, N. a. R., Brown, G. D., Maccallum, D. M. & Brown, A. J. P. 2016. Lactate signalling regulates fungal β -glucan masking and immune evasion. *Nature Microbiology*, 2, 16238.
- Ballou, L., Cohen, R. E. & Ballou, C. E. 1980. *Saccharomyces cerevisiae* mutants that make mannoproteins with a truncated carbohydrate outer chain. *J Biol Chem*, 255, 5986-91.
- Batchelor, M., Prasannan, S., Daniell, S., Reece, S., Connerton, I., Bloomberg, G., Dougan, G., Frankel, G. & Matthews, S. 2000. Structural basis for recognition of the translocated intimin receptor (Tir) by intimin from enteropathogenic *Escherichia coli*. *The EMBO journal*, 19, 2452-2464.
- Blom, N., Sicheritz-Pontén, T., Gupta, R., Gammeltoft, S. & Brunak, S. 2004. Prediction of post-translational glycosylation and phosphorylation of proteins from the amino acid sequence. *Proteomics*, 4, 1633-49.

- Bodelón, G., Palomino, C. & Fernández, L. Á. 2013. Immunoglobulin domains in *Escherichia coli* and other enterobacteria: from pathogenesis to applications in antibody technologies. *FEMS Microbiology Reviews*, 37, 204-250.
- Boraston, A. B., Revett, T. J., Boraston, C. M., Nurizzo, D. & Davies, G. J. 2003. Structural and Thermodynamic Dissection of Specific Mannan Recognition by a Carbohydrate Binding Module, TmCBM27. *Structure*, 11, 665-675.
- Braun, T. F., Khubbar, M. K., Saffarini, D. A. & McBride, M. J. 2005. *Flavobacterium johnsoniae* gliding motility genes identified by mariner mutagenesis. *J Bacteriol*, 187, 6943-52.
- Briliūtė, J., Urbanowicz, P. A., Luis, A. S., Baslé, A., Paterson, N., Rebello, O., Hendel, J., Ndeh, D. A., Lowe, E. C., Martens, E. C., Spencer, D. I. R., Bolam, D. N. & Crouch, L. I. 2019. Complex N-glycan breakdown by gut *Bacteroides* involves an extensive enzymatic apparatus encoded by multiple co-regulated genetic loci. *Nature Microbiology*, 4, 1571-1581.
- Brockhausen, I. & Stanley, P. 2015. O-GalNAc Glycans. *In: Varki, A., Cummings, R. D., Esko, J. D., Stanley, P., Hart, G. W., Aebi, M., Darvill, A. G., Kinoshita, T., Packer, N. H., Prestegard, J. H., Schnaar, R. L. & Seeberger, P. H. (eds.) Essentials of Glycobiology.* Cold Spring Harbor (NY): Cold Spring Harbor Laboratory Press
Copyright 2015-2017 by The Consortium of Glycobiology Editors, La Jolla, California. All rights reserved.
- Brody, J. R. & Kern, S. E. 2004. History and principles of conductive media for standard DNA electrophoresis. *Anal Biochem*, 333, 1-13.
- Brown, G. D., Herre, J., Williams, D. L., Willment, J. A., Marshall, A. S. J. & Gordon, S. 2003. Dectin-1 mediates the biological effects of beta-glucans. *The Journal of experimental medicine*, 197, 1119-1124.
- Bry, L., Falk, P. G., Midtvedt, T. & Gordon, J. I. 1996. A model of host-microbial interactions in an open mammalian ecosystem. *Science*, 273, 1380-3.
- Cambi, A., Netea, M. G., Mora-Montes, H. M., Gow, N. a. R., Hato, S. V., Lowman, D. W., Kullberg, B.-J., Torensma, R., Williams, D. L. & Figdor, C. G. 2008. Dendritic cell interaction with *Candida albicans* critically depends on N-linked mannan. *The Journal of biological chemistry*, 283, 20590-20599.
- Cantarel, B. L., Coutinho, P. M., Rancurel, C., Bernard, T., Lombard, V. & Henrissat, B. 2009. The Carbohydrate-Active EnZymes database (CAZy): an expert resource for Glycogenomics. *Nucleic acids research*, 37, D233-D238.

- Cartmell, A., Lowe, E. C., Baslé, A., Firbank, S. J., Ndeh, D. A., Murray, H., Terrapon, N., Lombard, V., Henrissat, B., Turnbull, J. E., Czjzek, M., Gilbert, H. J. & Bolam, D. N. 2017. How members of the human gut microbiota overcome the sulfation problem posed by glycosaminoglycans. *Proceedings of the National Academy of Sciences of the United States of America*, 114, 7037-7042.
- Cathey, S. S., Sarasua, S. M., Simensen, R., Pietris, K., Kimbrell, G., Sillence, D., Wilson, C. & Horowitz, L. 2019. Intellectual functioning in alpha-mannosidosis. *JIMD reports*, 50, 44-49.
- Chen, F., Ren, C.-G., Zhou, T., Wei, Y.-J. & Dai, C.-C. 2016. A novel exopolysaccharide elicitor from endophytic fungus *Gilmaniella* sp. AL12 on volatile oils accumulation in *Atractylodes lancea*. *Scientific Reports*, 6, 34735.
- Cheng, Y.-M., Hsieh, F.-C. & Meng, M. 2009. Functional analysis of conserved aromatic amino acids in the discoidin domain of *Paenibacillus* β -1,3-glucanase. *Microbial Cell Factories*, 8, 62.
- Chepyshko, H., Lai, C.-P., Huang, L.-M., Liu, J.-H. & Shaw, J.-F. 2012. Multifunctionality and diversity of GDSL esterase/lipase gene family in rice (*Oryza sativa* L. japonica) genome: new insights from bioinformatics analysis. *BMC Genomics*, 13, 309.
- Chiku, K., Nihira, T., Suzuki, E., Nishimoto, M., Kitaoka, M., Ohtsubo, K. I. & Nakai, H. 2014. Discovery of two β -1,2-mannoside phosphorylases showing different chain-length specificities from *Thermoanaerobacter* sp. X-514. *PloS one*, 9, e114882-e114882.
- Cho, K. H., Cho, D., Wang, G. R. & Salyers, A. A. 2001. New regulatory gene that contributes to control of *Bacteroides thetaiotaomicron* starch utilization genes. *Journal of bacteriology*, 183, 7198-7205.
- Chung, C. Y., Majewska, N. I., Wang, Q., Paul, J. T. & Betenbaugh, M. J. 2017. SnapShot: N-Glycosylation Processing Pathways across Kingdoms. *Cell*, 171, 258-258.e1.
- Cochet, F. & Peri, F. 2017. The Role of Carbohydrates in the Lipopolysaccharide (LPS)/Toll-Like Receptor 4 (TLR4) Signalling. *International journal of molecular sciences*, 18, 2318.
- Corbacho, I., Olivero, I. & Hernández, L. M. 2010. Identification of the MNN3 gene of *Saccharomyces cerevisiae*†. *Glycobiology*, 20, 1336-1340.
- Cosgrove, D. J. 2005. Growth of the plant cell wall. *Nature Reviews Molecular Cell Biology*, 6, 850-861.

- Couldrey, C. & E Green, J. 2000. Metastases: the glycan connection. *Breast Cancer Research*, 2, 321.
- Crouch, L. I., Liberato, M. V., Urbanowicz, P. A., Baslé, A., Lamb, C. A., Stewart, C. J., Cooke, K., Doona, M., Needham, S., Brady, R. R., Berrington, J. E., Madunic, K., Wuhrer, M., Chater, P., Pearson, J. P., Glowacki, R., Martens, E. C., Zhang, F., Linhardt, R. J., Spencer, D. I. R. & Bolam, D. N. 2019. Prominent members of the human gut microbiota express endo-acting O-glycanases to initiate mucin breakdown. *bioRxiv*, 835843.
- Cunrath, O., Meinel, D. M., Maturana, P., Fanous, J., Buyck, J. M., Saint Auguste, P., Seth-Smith, H. M. B., Körner, J., Dehio, C., Trebosc, V., Kemmer, C., Neher, R., Egli, A. & Bumann, D. 2019. Quantitative contribution of efflux to multi-drug resistance of clinical *Escherichia coli* and *Pseudomonas aeruginosa* strains. *EBioMedicine*, 41, 479-487.
- Cuskin, F., Baslé, A., Ladevèze, S., Day, A. M., Gilbert, H. J., Davies, G. J., Potocki-Véronèse, G. & Lowe, E. C. 2015a. The GH130 Family of Mannoside Phosphorylases Contains Glycoside Hydrolases That Target β -1,2-Mannosidic Linkages in Candida Mannan. *The Journal of biological chemistry*, 290, 25023-25033.
- Cuskin, F., Lowe, E. C., Temple, M. J., Zhu, Y., Cameron, E. A., Pudlo, N. A., Porter, N. T., Urs, K., Thompson, A. J., Cartmell, A., Rogowski, A., Hamilton, B. S., Chen, R., Tolbert, T. J., Piens, K., Bracke, D., Vervecken, W., Hakki, Z., Speciale, G., Munõz-Munõz, J. L., Day, A., Peña, M. J., Mclean, R., Suits, M. D., Boraston, A. B., Atherly, T., Ziemer, C. J., Williams, S. J., Davies, G. J., Abbott, D. W., Martens, E. C. & Gilbert, H. J. 2015b. Human gut Bacteroidetes can utilize yeast mannan through a selfish mechanism. *Nature*, 517, 165-169.
- D'elia, J. N. & Salyers, A. A. 1996a. Contribution of a neopullulanase, a pullulanase, and an alpha-glucosidase to growth of *Bacteroides thetaiotaomicron* on starch. *Journal of bacteriology*, 178, 7173-7179.
- D'elia, J. N. & Salyers, A. A. 1996b. Effect of regulatory protein levels on utilization of starch by *Bacteroides thetaiotaomicron*. *Journal of bacteriology*, 178, 7180-7186.
- Da Silva, C. A., Hartl, D., Liu, W., Lee, C. G. & Elias, J. A. 2008. TLR-2 and IL-17A in Chitin-Induced Macrophage Activation and Acute Inflammation. *The Journal of Immunology*, 181, 4279-4286.
- Davies, G. & Henrissat, B. 1995. Structures and mechanisms of glycosyl hydrolases. *Structure*, 3, 853-859.
- Davies, G. J., Wilson, K. S. & Henrissat, B. 1997. Nomenclature for sugar-binding subsites in glycosyl hydrolases. *The Biochemical journal*, 321 (Pt 2), 557-559.

- Davis, M. C., Kesthely, C. A., Franklin, E. A. & Maclellan, S. R. 2017. The essential activities of the bacterial sigma factor. *Can J Microbiol*, 63, 89-99.
- De Diego, I., Ksiazek, M., Mizgalska, D., Koneru, L., Golik, P., Szmigielski, B., Nowak, M., Nowakowska, Z., Potempa, B., Houston, J. A., Enghild, J. J., Thøgersen, I. B., Gao, J., Kwan, A. H., Trehwella, J., Dubin, G., Gomis-Rüth, F. X., Nguyen, K.-A. & Potempa, J. 2016. The outer-membrane export signal of *Porphyromonas gingivalis* type IX secretion system (T9SS) is a conserved C-terminal β -sandwich domain. *Scientific Reports*, 6, 23123.
- De Groot, P. W., Hellingwerf, K. J. & Klis, F. M. 2003. Genome-wide identification of fungal GPI proteins. *Yeast*, 20, 781-96.
- Dereeper, A., Guignon, V., Blanc, G., Audic, S., Buffet, S., Chevenet, F., Dufayard, J. F., Guindon, S., Lefort, V., Lescot, M., Claverie, J. M. & Gascuel, O. 2008. Phylogeny.fr: robust phylogenetic analysis for the non-specialist. *Nucleic Acids Res*, 36, W465-9.
- Derrien, M., Vaughan, E. E., Plugge, C. M. & De Vos, W. M. 2004. *Akkermansia muciniphila* gen. nov., sp. nov., a human intestinal mucin-degrading bacterium. *Int J Syst Evol Microbiol*, 54, 1469-1476.
- Edgar, R. C. 2004. MUSCLE: a multiple sequence alignment method with reduced time and space complexity. *BMC Bioinformatics*, 5, 113.
- Elhenawy, W., Debelyy, M. O. & Feldman, M. F. 2014. Preferential packing of acidic glycosidases and proteases into *Bacteroides* outer membrane vesicles. *mBio*, 5, e00909-14.
- Ene, I. V., Adya, A. K., Wehmeier, S., Brand, A. C., Maccallum, D. M., Gow, N. a. R. & Brown, A. J. P. 2012. Host carbon sources modulate cell wall architecture, drug resistance and virulence in a fungal pathogen. *Cellular microbiology*, 14, 1319-1335.
- Erwig, L. P. & Gow, N. a. R. 2016. Interactions of fungal pathogens with phagocytes. *Nature Reviews Microbiology*, 14, 163-176.
- Esteban, A., Popp, M. W., Vyas, V. K., Strijbis, K., Ploegh, H. L. & Fink, G. R. 2011. Fungal recognition is mediated by the association of dectin-1 and galectin-3 in macrophages. *Proceedings of the National Academy of Sciences of the United States of America*, 108, 14270-14275.
- Evans, D. F., Pye, G., Bramley, R., Clark, A. G., Dyson, T. J. & Hardcastle, J. D. 1988. Measurement of gastrointestinal pH profiles in normal ambulant human subjects. *Gut*, 29, 1035-1041.

- Fan, D., Coughlin, L. A., Neubauer, M. M., Kim, J., Kim, M. S., Zhan, X., Simms-Waldrup, T. R., Xie, Y., Hooper, L. V. & Koh, A. Y. 2015. Activation of HIF-1 α and LL-37 by commensal bacteria inhibits *Candida albicans* colonization. *Nat Med*, 21, 808-14.
- Foley, M. H., Cockburn, D. W. & Koropatkin, N. M. 2016. The *Sus* operon: a model system for starch uptake by the human gut Bacteroidetes. *Cellular and molecular life sciences : CMLS*, 73, 2603-2617.
- Fradin, C., Poulain, D. & Jouault, T. 2000. β -1,2-Linked Oligomannosides from *Candida albicans* Bind to a 32-Kilodalton Macrophage Membrane Protein Homologous to the Mammalian Lectin Galectin-3. *Infection and Immunity*, 68, 4391-4398.
- Fu, T., Burbage, C., Tagge, E., Chandler, J., Willingham, M. & Frankel, A. 1996. Double-Lectin Site Ricin B Chain Mutants Expressed in Insect Cells Have Residual Galactose Binding: Evidence for More Than Two Lectin Sites on the Ricin Toxin B Chain. *Bioconjugate Chemistry*, 7, 651-658.
- Fuchs, K., Cardona Gloria, Y., Wolz, O.-O., Herster, F., Sharma, L., Dillen, C. A., Täumer, C., Dickhöfer, S., Bittner, Z., Dang, T.-M., Singh, A., Haischer, D., Schlöffel, M. A., Koymans, K. J., Sanmuganatham, T., Krach, M., Roger, T., Le Roy, D., Schilling, N. A., Frauhammer, F., Miller, L. S., Nürnberger, T., Leibundgut-Landmann, S., Gust, A. A., Macek, B., Frank, M., Gouttefangeas, C., Dela Cruz, C. S., Hartl, D. & Weber, A. N. 2018. The fungal ligand chitin directly binds TLR2 and triggers inflammation dependent on oligomer size. *EMBO reports*, 19, e46065.
- Gantner, B. N., Simmons, R. M., Canavera, S. J., Akira, S. & Underhill, D. M. 2003. Collaborative induction of inflammatory responses by dectin-1 and Toll-like receptor 2. *J Exp Med*, 197, 1107-17.
- Gantner, B. N., Simmons, R. M. & Underhill, D. M. 2005. Dectin-1 mediates macrophage recognition of *Candida albicans* yeast but not filaments. *The EMBO journal*, 24, 1277-1286.
- Garrido, D., Nwosu, C., Ruiz-Moyano, S., Aldredge, D., German, J. B., Lebrilla, C. B. & Mills, D. A. 2012. Endo- β -N-acetylglucosaminidases from infant gut-associated bifidobacteria release complex N-glycans from human milk glycoproteins. *Molecular & cellular proteomics : MCP*, 11, 775-785.
- Garron, M.-L. & Cygler, M. 2014. Uronic polysaccharide degrading enzymes. *Current Opinion in Structural Biology*, 28, 87-95.
- Gasteiger, E., Hoogland, C., Gattiker, A., Duvaud, S. E., Wilkins, M. R., Appel, R. D. & Bairoch, A. 2005. Protein Identification and Analysis Tools on the EXPASY Server.

In: Walker, J. M. (ed.) *The Proteomics Protocols Handbook*. Totowa, NJ: Humana Press.

Gilbert, H. J., Knox, J. P. & Boraston, A. B. 2013. Advances in understanding the molecular basis of plant cell wall polysaccharide recognition by carbohydrate-binding modules. *Current Opinion in Structural Biology*, 23, 669-677.

Glenwright, A. J., Pothula, K. R., Bhamidimarri, S. P., Chorev, D. S., Baslé, A., Firbank, S. J., Zheng, H., Robinson, C. V., Winterhalter, M., Kleinekathöfer, U., Bolam, D. N. & Van Den Berg, B. 2017. Structural basis for nutrient acquisition by dominant members of the human gut microbiota. *Nature*, 541, 407-411.

Glew, M. D., Veith, P. D., Peng, B., Chen, Y.-Y., Gorasia, D. G., Yang, Q., Slakeski, N., Chen, D., Moore, C., Crawford, S. & Reynolds, E. C. 2012. PG0026 is the C-terminal signal peptidase of a novel secretion system of *Porphyromonas gingivalis*. *The Journal of biological chemistry*, 287, 24605-24617.

Goonatilleke, E., Huang, J., Xu, G., Wu, L., Smilowitz, J. T., German, J. B. & Lebrilla, C. B. 2019. Human Milk Proteins and Their Glycosylation Exhibit Quantitative Dynamic Variations during Lactation. *The Journal of nutrition*, 149, 1317-1325.

Gorasia, D. G., Veith, P. D., Chen, D., Seers, C. A., Mitchell, H. A., Chen, Y. Y., Glew, M. D., Dashper, S. G. & Reynolds, E. C. 2015. *Porphyromonas gingivalis* Type IX Secretion Substrates Are Cleaved and Modified by a Sortase-Like Mechanism. *PLoS Pathog*, 11, e1005152.

Gorasia, D. G., Veith, P. D., Hanssen, E. G., Glew, M. D., Sato, K., Yukitake, H., Nakayama, K. & Reynolds, E. C. 2016. Structural Insights into the PorK and PorN Components of the *Porphyromonas gingivalis* Type IX Secretion System. *PLOS Pathogens*, 12, e1005820.

Gorasia, D. G., Veith, P. D. & Reynolds, E. C. 2020. The Type IX Secretion System: Advances in Structure, Function and Organisation. *Microorganisms*, 8, 1173.

Gow, N. a. R., Latge, J. P. & Munro, C. A. 2017. The Fungal Cell Wall: Structure, Biosynthesis, and Function. *Microbiol Spectr*, 5.

Gow, N. a. R., Van De Veerdonk, F. L., Brown, A. J. P. & Netea, M. G. 2012. *Candida albicans* morphogenesis and host defence: discriminating invasion from colonization. *Nature Reviews Microbiology*, 10, 112-122.

Graf, K., Last, A., Gratz, R., Allert, S., Linde, S., Westermann, M., Gröger, M., Mosig, A. S., Gresnigt, M. S. & Hube, B. 2019. Keeping *Candida* commensal: how lactobacilli antagonize pathogenicity of *Candida albicans* in an in vitro gut model. *Dis Model Mech*, 12.

- Graham, C. E., Cruz, M. R., Garsin, D. A. & Lorenz, M. C. 2017. Enterococcus faecalis bacteriocin EntV inhibits hyphal morphogenesis, biofilm formation, and virulence of *Candida albicans*. *Proceedings of the National Academy of Sciences of the United States of America*, 114, 4507-4512.
- Gray, D. A., White, J. B. R., Oluwole, A. O., Rath, P., Glenwright, A. J., Mazur, A., Zahn, M., Baslé, A., Morland, C., Evans, S. L., Cartmell, A., Robinson, C. V., Hiller, S., Ranson, N. A., Bolam, D. N. & Van Den Berg, B. 2021. Insights into SusCD-mediated glycan import by a prominent gut symbiont. *Nature Communications*, 12, 44.
- Gregg, K. J., Zandberg, W. F., Hehemann, J.-H., Whitworth, G. E., Deng, L., Vocadlo, D. J. & Boraston, A. B. 2011. Analysis of a new family of widely distributed metal-independent alpha-mannosidases provides unique insight into the processing of N-linked glycans. *The Journal of biological chemistry*, 286, 15586-15596.
- Guo, Y., Feinberg, H., Conroy, E., Mitchell, D. A., Alvarez, R., Blixt, O., Taylor, M. E., Weis, W. I. & Drickamer, K. 2004. Structural basis for distinct ligand-binding and targeting properties of the receptors DC-SIGN and DC-SIGNR. *Nature Structural & Molecular Biology*, 11, 591-598.
- Hall, B. G. 2013. Building Phylogenetic Trees from Molecular Data with MEGA. *Molecular Biology and Evolution*, 30, 1229-1235.
- Hall, R. A. & Gow, N. a. R. 2013. Mannosylation in *Candida albicans*: role in cell wall function and immune recognition. *Molecular microbiology*, 90, 1147-1161.
- Heikinheimo, P., Helland, R., Leiros, H. K., Leiros, I., Karlsen, S., Evjen, G., Ravelli, R., Schoehn, G., Ruigrok, R., Tollersrud, O. K., Mcsweeney, S. & Hough, E. 2003. The structure of bovine lysosomal alpha-mannosidase suggests a novel mechanism for low-pH activation. *J Mol Biol*, 327, 631-44.
- Henrissat, B. 1991. A classification of glycosyl hydrolases based on amino acid sequence similarities. *The Biochemical journal*, 280 (Pt 2), 309-316.
- Henrissat, B., Callebaut, I., Fabrega, S., Lehn, P., Mornon, J. P. & Davies, G. 1995. Conserved catalytic machinery and the prediction of a common fold for several families of glycosyl hydrolases. *Proceedings of the National Academy of Sciences of the United States of America*, 92, 7090-7094.
- Henrissat, B. & Davies, G. 1997. Structural and sequence-based classification of glycoside hydrolases. *Current Opinion in Structural Biology*, 7, 637-644.
- Herrero, M., De Lorenzo, V. & Timmis, K. N. 1990. Transposon vectors containing non-antibiotic resistance selection markers for cloning and stable chromosomal insertion of foreign genes in gram-negative bacteria. *J Bacteriol*, 172, 6557-67.

- Herscovics, A. 2001. Structure and function of Class I alpha 1,2-mannosidases involved in glycoprotein synthesis and endoplasmic reticulum quality control. *Biochimie*, 83, 757-62.
- Higel, F., Seidl, A., Sörgel, F. & Friess, W. 2016. N-glycosylation heterogeneity and the influence on structure, function and pharmacokinetics of monoclonal antibodies and Fc fusion proteins. *European Journal of Pharmaceutics and Biopharmaceutics*, 100, 94-100.
- Hirabayashi, J., Dutta, S. K. & Kasai, K.-I. 1998. Novel Galactose-binding Proteins in Annelida: CHARACTERIZATION OF 29-kDa TANDEM REPEAT-TYPE LECTINS FROM THE EARTHWORM *LUMBRICUS TERRESTRIS* *. *Journal of Biological Chemistry*, 273, 14450-14460.
- Hoarau, G., Mukherjee, P. K., Gower-Rousseau, C., Hager, C., Chandra, J., Retuerto, M. A., Neut, C., Vermeire, S., Clemente, J., Colombel, J. F., Fujioka, H., Poulain, D., Sendid, B. & Ghannoum, M. A. 2016. Bacteriome and Mycobiome Interactions Underscore Microbial Dysbiosis in Familial Crohn's Disease. *mBio*, 7, e01250-16.
- Hoffmann, C., Dollive, S., Grunberg, S., Chen, J., Li, H., Wu, G. D., Lewis, J. D. & Bushman, F. D. 2013. Archaea and fungi of the human gut microbiome: correlations with diet and bacterial residents. *PLoS One*, 8, e66019.
- Hooper, L. V., Xu, J., Falk, P. G., Midtvedt, T. & Gordon, J. I. 1999. A molecular sensor that allows a gut commensal to control its nutrient foundation in a competitive ecosystem. *Proceedings of the National Academy of Sciences of the United States of America*, 96, 9833-9838.
- Huttenhower, C., Gevers, D., Knight, R., Abubucker, S., Badger, J. H., Chinwalla, A. T., Creasy, H. H., Earl, A. M., Fitzgerald, M. G., Fulton, R. S., Giglio, M. G., Hallsworth-Pepin, K., Lobos, E. A., Madupu, R., Magrini, V., Martin, J. C., Mitreva, M., Muzny, D. M., Sodergren, E. J., Versalovic, J., Wollam, A. M., Worley, K. C., Wortman, J. R., Young, S. K., Zeng, Q., Aagaard, K. M., Abolude, O. O., Allen-Vercoe, E., Alm, E. J., Alvarado, L., Andersen, G. L., Anderson, S., Appelbaum, E., Arachchi, H. M., Armitage, G., Arze, C. A., Ayvaz, T., Baker, C. C., Begg, L., Belachew, T., Bhonagiri, V., Bihan, M., Blaser, M. J., Bloom, T., Bonazzi, V., Paul Brooks, J., Buck, G. A., Buhay, C. J., Busam, D. A., Campbell, J. L., Canon, S. R., Cantarel, B. L., Chain, P. S. G., Chen, I. M. A., Chen, L., Chhibba, S., Chu, K., Ciulla, D. M., Clemente, J. C., Clifton, S. W., Conlan, S., Crabtree, J., Cutting, M. A., Davidovics, N. J., Davis, C. C., Desantis, T. Z., Deal, C., Delehaunty, K. D., Dewhirst, F. E., Deych, E., Ding, Y., Dooling, D. J., Dugan, S. P., Michael Dunne, W., Scott Durkin, A., Edgar, R. C., Erlich, R. L., Farmer, C. N., Farrell, R. M., Faust, K., Feldgarden, M., Felix, V. M., Fisher, S., Fodor, A. A., Forney, L. J., Foster, L., Di Francesco, V., Friedman, J., Friedrich, D. C., Fronick, C. C., Fulton, L. L., Gao, H., Garcia, N., Giannoukos, G., Giblin, C., Giovanni, M. Y., Goldberg, J. M., Goll, J., Gonzalez, A., Griggs, A., et al.

2012. Structure, function and diversity of the healthy human microbiome. *Nature*, 486, 207-214.
- Ifrim, D. C., Quintin, J., Courjol, F., Verschueren, I., Van Krieken, J. H., Koentgen, F., Fradin, C., Gow, N. a. R., Joosten, L. a. B., Van Der Meer, J. W. M., Van De Veerdonk, F. & Netea, M. G. 2016. The Role of Dectin-2 for Host Defense Against Disseminated Candidiasis. *Journal of interferon & cytokine research : the official journal of the International Society for Interferon and Cytokine Research*, 36, 267-276.
- Iliev, I. D., Funari, V. A., Taylor, K. D., Nguyen, Q., Reyes, C. N., Strom, S. P., Brown, J., Becker, C. A., Fleshner, P. R., Dubinsky, M., Rotter, J. I., Wang, H. L., MCGovern, D. P. B., Brown, G. D. & Underhill, D. M. 2012. Interactions between commensal fungi and the C-type lectin receptor Dectin-1 influence colitis. *Science (New York, N.Y.)*, 336, 1314-1317.
- Israeli, E., Grotto, I., Gilburd, B., Balicer, R. D., Goldin, E., Wiik, A. & Shoenfeld, Y. 2005. Anti-Saccharomyces cerevisiae and antineutrophil cytoplasmic antibodies as predictors of inflammatory bowel disease. *Gut*, 54, 1232-1236.
- Jackson, M. A., Verdi, S., Maxan, M.-E., Shin, C. M., Zierer, J., Bowyer, R. C. E., Martin, T., Williams, F. M. K., Menni, C., Bell, J. T., Spector, T. D. & Steves, C. J. 2018. Gut microbiota associations with common diseases and prescription medications in a population-based cohort. *Nature Communications*, 9, 2655.
- Jelinek-Kelly, S. & Herscovics, A. 1988. Glycoprotein biosynthesis in Saccharomyces cerevisiae. Purification of the alpha-mannosidase which removes one specific mannose residue from Man9GlcNAc. *J Biol Chem*, 263, 14757-63.
- Johnson, M., Zaretskaya, I., Raytselis, Y., Merezhuk, Y., MCGinnis, S. & Madden, T. L. 2008. NCBI BLAST: a better web interface. *Nucleic Acids Res*, 36, W5-9.
- Jones, D. R., Xing, X., Tingley, J. P., Klassen, L., King, M. L., Alexander, T. W. & Abbott, D. W. 2020. Analysis of Active Site Architecture and Reaction Product Linkage Chemistry Reveals a Conserved Cleavage Substrate for an Endo-alpha-mannanase within Diverse Yeast Mannans. *Journal of Molecular Biology*, 432, 1083-1097.
- Joshi, H. J., Narimatsu, Y., Schjoldager, K. T., Tytgat, H. L. P., Aebi, M., Clausen, H. & Halim, A. 2018. SnapShot: O-Glycosylation Pathways across Kingdoms. *Cell*, 172, 632-632.e2.
- Kanehisa, M., Goto, S., Kawashima, S. & Nakaya, A. 2002. The KEGG databases at GenomeNet. *Nucleic Acids Res*, 30, 42-6.

- Kaoutari, A. E., Armougom, F., Gordon, J. I., Raoult, D. & Henrissat, B. 2013. The abundance and variety of carbohydrate-active enzymes in the human gut microbiota. *Nature Reviews Microbiology*, 11, 497-504.
- Kapteyn, J. C., Ter Riet, B., Vink, E., Blad, S., De Nobel, H., Van Den Ende, H. & Klis, F. M. 2001. Low external pH induces HOG1-dependent changes in the organization of the *Saccharomyces cerevisiae* cell wall. *Molecular Microbiology*, 39, 469-480.
- Karson, E. M. & Ballou, C. E. 1978. Biosynthesis of yeast mannan. Properties of a mannosylphosphate transferase in *Saccharomyces cerevisiae*. *J Biol Chem*, 253, 6484-92.
- Kawaguchi, K., Senoura, T., Ito, S., Taira, T., Ito, H., Wasaki, J. & Ito, S. 2014. The mannobiose-forming exo-mannanase involved in a new mannan catabolic pathway in *Bacteroides fragilis*. *Archives of Microbiology*, 196, 17-23.
- Kelly, G., Prasannan, S., Daniell, S., Fleming, K., Frankel, G., Dougan, G., Connerton, I. & Matthews, S. 1999. Structure of the cell-adhesion fragment of intimin from enteropathogenic *Escherichia coli*. *Nat Struct Biol*, 6, 313-8.
- Kéry, V., Křepinský, J. J. F., Warren, C. D., Capek, P. & Stahl, P. D. 1992. Ligand recognition by purified human mannose receptor. *Archives of Biochemistry and Biophysics*, 298, 49-55.
- Kharade, S. S. & McBride, M. J. 2014. *Flavobacterium johnsoniae* chitinase ChiA is required for chitin utilization and is secreted by the type IX secretion system. *J Bacteriol*, 196, 961-70.
- Kim, D. Y., Lee, S. H., Lee, M. J., Cho, H.-Y., Lee, J. S., Rhee, Y. H., Shin, D.-H., Son, K.-H. & Park, H.-Y. 2018. Genetic and functional characterization of a novel GH10 endo- β -1,4-xylanase with a ricin-type β -trefoil domain-like domain from *Luteimicrobium xylanilyticum* HY-24. *International Journal of Biological Macromolecules*, 106, 620-628.
- Klis, F. M., Boorsma, A. & De Groot, P. W. 2006. Cell wall construction in *Saccharomyces cerevisiae*. *Yeast*, 23, 185-202.
- Kobayashi, H., Takahashi, S., Shibata, N., Miyauchi, M., Ishida, M., Sato, J., Maeda, K. & Suzuki, S. 1994. Structural modification of cell wall mannans of *Candida albicans* serotype A strains grown in yeast extract-Sabouraud liquid medium under acidic conditions. *Infection and immunity*, 62, 968-973.
- Kocourek, J. & Ballou, C. E. 1969. Method for fingerprinting yeast cell wall mannans. *Journal of bacteriology*, 100, 1175-1181.

- Koh, A., De Vadder, F., Kovatcheva-Datchary, P. & Bäckhed, F. 2016. From Dietary Fiber to Host Physiology: Short-Chain Fatty Acids as Key Bacterial Metabolites. *Cell*, 165, 1332-1345.
- Koh, A. Y., Köhler, J. R., Coggshall, K. T., Van Rooijen, N. & Pier, G. B. 2008. Mucosal damage and neutropenia are required for *Candida albicans* dissemination. *PLoS Pathog*, 4, e35.
- Kohatsu, L., Hsu, D. K., Jegalian, A. G., Liu, F. T. & Baum, L. G. 2006. Galectin-3 induces death of *Candida* species expressing specific beta-1,2-linked mannans. *J Immunol*, 177, 4718-26.
- Koropatkin, N. M., Cameron, E. A. & Martens, E. C. 2012. How glycan metabolism shapes the human gut microbiota. *Nature reviews. Microbiology*, 10, 323-335.
- Koropatkin, N. M., Martens, E. C., Gordon, J. I. & Smith, T. J. 2008. Starch catabolism by a prominent human gut symbiont is directed by the recognition of amylose helices. *Structure (London, England : 1993)*, 16, 1105-1115.
- Koropatkin, N. M. & Smith, T. J. 2010. SusG: a unique cell-membrane-associated alpha-amylase from a prominent human gut symbiont targets complex starch molecules. *Structure*, 18, 200-15.
- Kulkarni, S. S., Johnston, J. J., Zhu, Y., Hying, Z. T. & McBride, M. J. 2019. The Carboxy-Terminal Region of *Flavobacterium johnsoniae* SprB Facilitates Its Secretion by the Type IX Secretion System and Propulsion by the Gliding Motility Machinery. *J Bacteriol*, 201.
- Kulkarni, S. S., Zhu, Y., Brendel, C. J. & McBride, M. J. 2017. Diverse C-Terminal Sequences Involved in *Flavobacterium johnsoniae* Protein Secretion. *Journal of Bacteriology*, 199, e00884-16.
- La Rosa, S. L., Leth, M. L., Michalak, L., Hansen, M. E., Pudlo, N. A., Glowacki, R., Pereira, G., Workman, C. T., Arntzen, M. Ø., Pope, P. B., Martens, E. C., Hachem, M. A. & Westereng, B. 2019. The human gut Firmicute *Roseburia intestinalis* is a primary degrader of dietary β -mannans. *Nature Communications*, 10, 905.
- Ladevèze, S., Cioci, G., Roblin, P., Mourey, L., Tranier, S. & Potocki-Véronèse, G. 2015. Structural bases for N-glycan processing by mannoside phosphorylase. *Acta crystallographica. Section D, Biological crystallography*, 71, 1335-1346.
- Ladevèze, S., Tarquis, L., Cecchini, D. A., Bercovici, J., André, I., Topham, C. M., Morel, S., Laville, E., Monsan, P., Lombard, V., Henrissat, B. & Potocki-Véronèse, G. 2013.

Role of glycoside phosphorylases in mannose foraging by human gut bacteria. *The Journal of biological chemistry*, 288, 32370-32383.

- Laemmli, U. K. 1970. Cleavage of structural proteins during the assembly of the head of bacteriophage T4. *Nature*, 227, 680-5.
- Langer, V., Vivi, E., Regensburger, D., Winkler, T. H., Waldner, M. J., Rath, T., Schmid, B., Skottke, L., Lee, S., Jeon, N. L., Wohlfahrt, T., Kramer, V., Tripal, P., Schumann, M., Kersting, S., Handtrack, C., Geppert, C. I., Suchowski, K., Adams, R. H., Becker, C., Ramming, A., Naschberger, E., Britzen-Laurent, N. & Stürzl, M. 2019. IFN- γ drives inflammatory bowel disease pathogenesis through VE-cadherin-directed vascular barrier disruption. *The Journal of clinical investigation*, 129, 4691-4707.
- Lapébie, P., Lombard, V., Drula, E., Terrapon, N. & Henrissat, B. 2019. Bacteroidetes use thousands of enzyme combinations to break down glycans. *Nature communications*, 10, 2043-2043.
- Larsbrink, J. & Mckee, L. S. 2020. Bacteroidetes bacteria in the soil: Glycan acquisition, enzyme secretion, and gliding motility. *Adv Appl Microbiol*, 110, 63-98.
- Larsbrink, J., Rogers, T. E., Hemsworth, G. R., Mckee, L. S., Tauzin, A. S., Spadiut, O., Klintner, S., Pudlo, N. A., Urs, K., Koropatkin, N. M., Creagh, A. L., Haynes, C. A., Kelly, A. G., Cederholm, S. N., Davies, G. J., Martens, E. C. & Brumer, H. 2014. A discrete genetic locus confers xyloglucan metabolism in select human gut Bacteroidetes. *Nature*, 506, 498-502.
- Larsson, J. M., Karlsson, H., Sjövall, H. & Hansson, G. C. 2009. A complex, but uniform O-glycosylation of the human MUC2 mucin from colonic biopsies analyzed by nanoLC/MSn. *Glycobiology*, 19, 756-66.
- Lasica, A. M., Goulas, T., Mizgalska, D., Zhou, X., De Diego, I., Ksiazek, M., Madej, M., Guo, Y., Guevara, T., Nowak, M., Potempa, B., Goel, A., Sztukowska, M., Prabhakar, A. T., Bzowska, M., Widziolak, M., Thøgersen, I. B., Enghild, J. J., Simonian, M., Kulczyk, A. W., Nguyen, K. A., Potempa, J. & Gomis-Rüth, F. X. 2016. Structural and functional probing of PorZ, an essential bacterial surface component of the type-IX secretion system of human oral-microbiomic Porphyromonas gingivalis. *Sci Rep*, 6, 37708.
- Lattimer, J. M. & Haub, M. D. 2010. Effects of dietary fiber and its components on metabolic health. *Nutrients*, 2, 1266-89.
- Lauber, F., Deme, J. C., Lea, S. M. & Berks, B. C. 2018. Type 9 secretion system structures reveal a new protein transport mechanism. *Nature*, 564, 77-82.

- Lawson, M. a. E., O’neill, I. J., Kujawska, M., Gowrinadh Javvadi, S., Wijeyesekera, A., Flegg, Z., Chalklen, L. & Hall, L. J. 2020. Breast milk-derived human milk oligosaccharides promote Bifidobacterium interactions within a single ecosystem. *The ISME Journal*, 14, 635-648.
- Lee, S. J., Zheng, N.-Y., Clavijo, M. & Nussenzweig, M. C. 2003. Normal host defense during systemic candidiasis in mannose receptor-deficient mice. *Infection and immunity*, 71, 437-445.
- Lenardon, M. D., Sood, P., Dorfmüller, H. C., Brown, A. J. P. & Gow, N. a. R. 2020. Scalar nanostructure of the *Candida albicans* cell wall; a molecular, cellular and ultrastructural analysis and interpretation. *The Cell Surface*, 6, 100047.
- Levin, D. E. 2011. Regulation of cell wall biogenesis in *Saccharomyces cerevisiae*: the cell wall integrity signaling pathway. *Genetics*, 189, 1145-1175.
- Lloyd-Price, J., Arze, C., Ananthakrishnan, A. N., Schirmer, M., Avila-Pacheco, J., Poon, T. W., Andrews, E., Ajami, N. J., Bonham, K. S., Brislawn, C. J., Casero, D., Courtney, H., Gonzalez, A., Graeber, T. G., Hall, A. B., Lake, K., Landers, C. J., Mallick, H., Plichta, D. R., Prasad, M., Rahnavard, G., Sauk, J., Shungin, D., Vázquez-Baeza, Y., White, R. A., Bishai, J., Bullock, K., Deik, A., Dennis, C., Kaplan, J. L., Khalili, H., Mciver, L. J., Moran, C. J., Nguyen, L., Pierce, K. A., Schwager, R., Sirota-Madi, A., Stevens, B. W., Tan, W., Ten Hove, J. J., Weingart, G., Wilson, R. G., Yajnik, V., Braun, J., Denson, L. A., Jansson, J. K., Knight, R., Kugathasan, S., McGovern, D. P. B., Petrosino, J. F., Stappenbeck, T. S., Winter, H. S., Clish, C. B., Franzosa, E. A., Vlamakis, H., Xavier, R. J., Huttenhower, C. & Investigators, I. 2019. Multi-omics of the gut microbial ecosystem in inflammatory bowel diseases. *Nature*, 569, 655-662.
- Lombard, V., Bernard, T., Rancurel, C., Brumer, H., Coutinho, Pedro m. & Henrissat, B. 2010. A hierarchical classification of polysaccharide lyases for glycogenomics. *Biochemical Journal*, 432, 437-444.
- Lombard, V., Golaconda Ramulu, H., Drula, E., Coutinho, P. M. & Henrissat, B. 2014. The carbohydrate-active enzymes database (CAZy) in 2013. *Nucleic acids research*, 42, D490-D495.
- Lowe, E. C., Baslé, A., Czjzek, M., Firbank, S. J. & Bolam, D. N. 2012. A scissor blade-like closing mechanism implicated in transmembrane signaling in a *Bacteroides* hybrid two-component system. *Proceedings of the National Academy of Sciences*, 109, 7298.
- Lozupone, C. A., Stombaugh, J. I., Gordon, J. I., Jansson, J. K. & Knight, R. 2012. Diversity, stability and resilience of the human gut microbiota. *Nature*, 489, 220-230.

- Luis, A. S., Briggs, J., Zhang, X., Farnell, B., Ndeh, D., Labourel, A., Baslé, A., Cartmell, A., Terrapon, N., Stott, K., Lowe, E. C., Mclean, R., Shearer, K., Schückel, J., Venditto, I., Ralet, M.-C., Henrissat, B., Martens, E. C., Mosimann, S. C., Abbott, D. W. & Gilbert, H. J. 2018. Dietary pectic glycans are degraded by coordinated enzyme pathways in human colonic *Bacteroides*. *Nature microbiology*, 3, 210-219.
- Madej, M., Nowakowska, Z., Ksiazek, M., Lasica, A. M., Mizgalska, D., Nowak, M., Jacula, A., Bzowska, M., Scavenius, C., Enghild, J. J., Aduse-Opoku, J., Curtis, M. A., Gomis-Rüth, F. X. & Potempa, J. 2021. PorZ, an Essential Component of the Type IX Secretion System of *Porphyromonas gingivalis*, Delivers Anionic Lipopolysaccharide to the PorU Sortase for Transpeptidase Processing of T9SS Cargo Proteins. *mBio*, 12.
- Marcobal, A., Barboza, M., Sonnenburg, Erica d., Pudlo, N., Martens, Eric c., Desai, P., Lebrilla, Carlito b., Weimer, Bart c., Mills, David a., German, J. B. & Sonnenburg, Justin I. 2011. *Bacteroides* in the Infant Gut Consume Milk Oligosaccharides via Mucus-Utilization Pathways. *Cell Host & Microbe*, 10, 507-514.
- Markowitz, V. M., Chen, I. M. A., Palaniappan, K., Chu, K., Szeto, E., Grechkin, Y., Ratner, A., Jacob, B., Huang, J., Williams, P., Huntemann, M., Anderson, I., Mavromatis, K., Ivanova, N. N. & Kyrpides, N. C. 2012. IMG: the Integrated Microbial Genomes database and comparative analysis system. *Nucleic acids research*, 40, D115-D122.
- Martens, E. C., Chiang, H. C. & Gordon, J. I. 2008. Mucosal glycan foraging enhances fitness and transmission of a saccharolytic human gut bacterial symbiont. *Cell host & microbe*, 4, 447-457.
- Martens, E. C., Koropatkin, N. M., Smith, T. J. & Gordon, J. I. 2009a. Complex glycan catabolism by the human gut microbiota: the *Bacteroidetes* Sus-like paradigm. *The Journal of biological chemistry*, 284, 24673-24677.
- Martens, E. C., Lowe, E. C., Chiang, H., Pudlo, N. A., Wu, M., McNulty, N. P., Abbott, D. W., Henrissat, B., Gilbert, H. J., Bolam, D. N. & Gordon, J. I. 2011. Recognition and degradation of plant cell wall polysaccharides by two human gut symbionts. *PLoS biology*, 9, e1001221-e1001221.
- Martens, E. C., Roth, R., Heuser, J. E. & Gordon, J. I. 2009b. Coordinate regulation of glycan degradation and polysaccharide capsule biosynthesis by a prominent human gut symbiont. *The Journal of biological chemistry*, 284, 18445-18457.
- Maruyama, Y., Nakajima, T. & Ichishima, E. 1994. A 1,2- α -D-mannosidase from a bacillus sp.: purification, characterization, and mode of action. *Carbohydrate Research*, 251, 89-98.

- Matsuda, K., Kurakata, Y., Miyazaki, T., Matsuo, I., Ito, Y., Nishikawa, A. & Tono-zuka, T. 2011. Heterologous Expression, Purification, and Characterization of an α -Mannosidase Belonging to Glycoside Hydrolase Family 99 of *Shewanella amazonensis*. *Bioscience, Biotechnology, and Biochemistry*, 75, 797-799.
- Maurer, M., Gresnigt, M. S., Last, A., Wollny, T., Berlinghof, F., Pospich, R., Cseresnyes, Z., Medyukhina, A., Graf, K., Gröger, M., Raasch, M., Siwczak, F., Nietzsche, S., Jacobsen, I. D., Figge, M. T., Hube, B., Huber, O. & Mosig, A. S. 2019. A three-dimensional immunocompetent intestine-on-chip model as in vitro platform for functional and microbial interaction studies. *Biomaterials*, 220, 119396.
- Mazmanian, S. K., Ton-That, H. & Schneewind, O. 2001. Sortase-catalysed anchoring of surface proteins to the cell wall of *Staphylococcus aureus*. *Molecular Microbiology*, 40, 1049-1057.
- Mcbride, M. J. 2019. Bacteroidetes Gliding Motility and the Type IX Secretion System. *Microbiol Spectr*, 7.
- Mcbride, M. J. & Zhu, Y. 2013. Gliding Motility and Por Secretion System Genes Are Widespread among Members of the Phylum *Bacteroidetes*. *Journal of Bacteriology*, 195, 270.
- Mcgreal, E. P., Rosas, M., Brown, G. D., Zamze, S., Wong, S. Y. C., Gordon, S., Martinez-Pomares, L. & Taylor, P. R. 2006. The carbohydrate-recognition domain of Dectin-2 is a C-type lectin with specificity for high mannose. *Glycobiology*, 16, 422-430.
- Mercure, S., Sénéchal, S., Auger, P., Lemay, G. & Montplaisir, S. 1996. *Candida albicans* serotype analysis by flow cytometry. *Journal of clinical microbiology*, 34, 2106-2112.
- Mille, C., Bobrowicz, P., Trinel, P.-A., Li, H., Maes, E., Guerardel, Y., Fradin, C., Martínez-Esparza, M., Davidson, R. C., Janbon, G., Poulain, D. & Wildt, S. 2008. Identification of a New Family of Genes Involved in β -1,2-Mannosylation of Glycans in *Pichia pastoris* and *Candida albicans*. *Journal of Biological Chemistry*, 283, 9724-9736.
- Mille, C., Fradin, C., Delplace, F., Trinel, P.-A., Masset, A., François, N., Coddeville, B., Bobrowicz, P., Jouault, T., Guerardel, Y., Wildt, S., Janbon, G. & Poulain, D. 2012. Members 5 and 6 of the *Candida albicans* BMT family encode enzymes acting specifically on β -mannosylation of the phospholipomannan cell-wall glycosphingolipid. *Glycobiology*, 22, 1332-1342.
- Miranda, L. N., Van Der Heijden, I. M., Costa, S. F., Sousa, A. P., Sienna, R. A., Gobara, S., Santos, C. R., Lobo, R. D., Pessoa, V. P., Jr. & Levin, A. S. 2009. *Candida* colonisation as a source for candidaemia. *J Hosp Infect*, 72, 9-16.

- Mitchell, A. L., Attwood, T. K., Babbitt, P. C., Blum, M., Bork, P., Bridge, A., Brown, S. D., Chang, H.-Y., El-Gebali, S., Fraser, M. I., Gough, J., Haft, D. R., Huang, H., Letunic, I., Lopez, R., Luciani, A., Madeira, F., Marchler-Bauer, A., Mi, H., Natale, D. A., Necci, M., Nuka, G., Orengo, C., Pandurangan, A. P., Paysan-Lafosse, T., Pesseat, S., Potter, S. C., Qureshi, M. A., Rawlings, N. D., Redaschi, N., Richardson, L. J., Rivoire, C., Salazar, G. A., Sangrador-Vegas, A., Sigrist, C. J. a., Sillitoe, I., Sutton, G. G., Thanki, N., Thomas, P. D., Tosatto, S. C e., Yong, S.-Y. & Finn, R. D. 2019. InterPro in 2019: improving coverage, classification and access to protein sequence annotations. *Nucleic Acids Research*, 47, D351-D360.
- Mizutani, K., Fernandes, V. O., Karita, S., Luís, A. S., Sakka, M., Kimura, T., Jackson, A., Zhang, X., Fontes, C. M. G. A., Gilbert, H. J. & Sakka, K. 2012. Influence of a Mannan Binding Family 32 Carbohydrate Binding Module on the Activity of the Appended Mannanase. *Applied and Environmental Microbiology*, 78, 4781.
- Mora-Montes, H. M., Ponce-Noyola, P., Villagómez-Castro, J. C., Gow, N. A., Flores-Carreón, A. & López-Romero, E. 2009. Protein glycosylation in *Candida*. *Future Microbiol*, 4, 1167-83.
- Muegge, B. D., Kuczynski, J., Knights, D., Clemente, J. C., González, A., Fontana, L., Henrissat, B., Knight, R. & Gordon, J. I. 2011. Diet drives convergence in gut microbiome functions across mammalian phylogeny and within humans. *Science*, 332, 970-4.
- Mullis, K. B. & Faloona, F. A. 1987. Specific synthesis of DNA in vitro via a polymerase-catalyzed chain reaction. *Methods Enzymol*, 155, 335-50.
- Murciano, C., Moyes, D. L., Runglall, M., Islam, A., Mille, C., Fradin, C., Poulain, D., Gow, N. A. & Naglik, J. R. 2011. *Candida albicans* cell wall glycosylation may be indirectly required for activation of epithelial cell proinflammatory responses. *Infect Immun*, 79, 4902-11.
- Naas, A. E., Mackenzie, A. K., Dalhus, B., Eijsink, V. G. H. & Pope, P. B. 2015. Structural Features of a Bacteroidetes-Affiliated Cellulase Linked with a Polysaccharide Utilization Locus. *Scientific reports*, 5, 11666-11666.
- Naas, A. E., Mackenzie, A. K., Mravec, J., Schückel, J., Willats, W. G. T., Eijsink, V. G. H. & Pope, P. B. 2014. Do Rumen & Bacteroidetes Utilize an Alternative Mechanism for Cellulose Degradation? *mBio*, 5, e01401-14.
- Nakajima, T., Maitra, S. K. & Ballou, C. E. 1976. An endo- α 1 leads to 6-D-mannanase from a soil bacterium. Purification, properties, and mode of action. *J Biol Chem*, 251, 174-81.

- Nash, A. K., Auchtung, T. A., Wong, M. C., Smith, D. P., Gesell, J. R., Ross, M. C., Stewart, C. J., Metcalf, G. A., Muzny, D. M., Gibbs, R. A., Ajami, N. J. & Petrosino, J. F. 2017. The gut mycobiome of the Human Microbiome Project healthy cohort. *Microbiome*, 5, 153.
- Naumoff, D. G. 2011. Hierarchical classification of glycoside hydrolases. *Biochemistry (Moscow)*, 76, 622-635.
- Ndeh, D., Baslé, A., Strahl, H., Yates, E. A., Mcclurgg, U. L., Henrissat, B., Terrapon, N. & Cartmell, A. 2020. Metabolism of multiple glycosaminoglycans by *Bacteroides thetaiotaomicron* is orchestrated by a versatile core genetic locus. *Nature Communications*, 11, 646.
- Ndeh, D., Rogowski, A., Cartmell, A., Luis, A. S., Baslé, A., Gray, J., Venditto, I., Briggs, J., Zhang, X., Labourel, A., Terrapon, N., Buffetto, F., Nepogodiev, S., Xiao, Y., Field, R. A., Zhu, Y., O'neil, M. A., Urbanowicz, B. R., York, W. S., Davies, G. J., Abbott, D. W., Ralet, M.-C., Martens, E. C., Henrissat, B. & Gilbert, H. J. 2017. Complex pectin metabolism by gut bacteria reveals novel catalytic functions. *Nature*, 544, 65-70.
- Nelson, S. S., Bollampalli, S. & McBride, M. J. 2008. SprB is a cell surface component of the *Flavobacterium johnsoniae* gliding motility machinery. *J Bacteriol*, 190, 2851-7.
- Netea, M. G., Brown, G. D., Kullberg, B. J. & Gow, N. a. R. 2008. An integrated model of the recognition of *Candida albicans* by the innate immune system. *Nature Reviews Microbiology*, 6, 67-78.
- Netea, M. G., Gow, N. a. R., Munro, C. A., Bates, S., Collins, C., Ferwerda, G., Hobson, R. P., Bertram, G., Hughes, H. B., Jansen, T., Jacobs, L., Buurman, E. T., Gijzen, K., Williams, D. L., Torensma, R., Mckinnon, A., Maccallum, D. M., Odds, F. C., Van Der Meer, J. W. M., Brown, A. J. P. & Kullberg, B. J. 2006. Immune sensing of *Candida albicans* requires cooperative recognition of mannans and glucans by lectin and Toll-like receptors. *The Journal of clinical investigation*, 116, 1642-1650.
- Nguyen, K. A., Travis, J. & Potempa, J. 2007. Does the importance of the C-terminal residues in the maturation of RgpB from *Porphyromonas gingivalis* reveal a novel mechanism for protein export in a subgroup of Gram-Negative bacteria? *J Bacteriol*, 189, 833-43.
- Nihira, T., Suzuki, E., Kitaoka, M., Nishimoto, M., Ohtsubo, K. I. & Nakai, H. 2013. Discovery of β -1,4-D-mannosyl-N-acetyl-D-glucosamine phosphorylase involved in the metabolism of N-glycans. *The Journal of biological chemistry*, 288, 27366-27374.

- Noble, S. M., French, S., Kohn, L. A., Chen, V. & Johnson, A. D. 2010. Systematic screens of a *Candida albicans* homozygous deletion library decouple morphogenetic switching and pathogenicity. *Nat Genet*, 42, 590-8.
- Noinaj, N., Guillier, M., Barnard, T. J. & Buchanan, S. K. 2010. TonB-dependent transporters: regulation, structure, and function. *Annual review of microbiology*, 64, 43-60.
- Numao, S., Kuntz, D. A., Withers, S. G. & Rose, D. R. 2003. Insights into the Mechanism of *Drosophila melanogaster* Golgi α -Mannosidase II through the Structural Analysis of Covalent Reaction Intermediates. *Journal of Biological Chemistry*, 278, 48074-48083.
- O'Neill, E. C. & Field, R. A. 2015. Enzymatic synthesis using glycoside phosphorylases. *Carbohydr Res*, 403, 23-37.
- Odds, F. C., Brown, A. J. P. & Gow, N. a. R. 2004. *Candida albicans* genome sequence: a platform for genomics in the absence of genetics. *Genome biology*, 5, 230-230.
- Ottman, N., Smidt, H., De Vos, W. & Belzer, C. 2012. The function of our microbiota: who is out there and what do they do? *Frontiers in Cellular and Infection Microbiology*, 2.
- Owczarzy, R., Tataurov, A. V., Wu, Y., Manthey, J. A., Mcquisten, K. A., Almabrazi, H. G., Pedersen, K. F., Lin, Y., Garretson, J., Mcentaggart, N. O., Sailor, C. A., Dawson, R. B. & Peek, A. S. 2008. IDT SciTools: a suite for analysis and design of nucleic acid oligomers. *Nucleic acids research*, 36, W163-W169.
- Pande, K., Chen, C. & Noble, S. M. 2013. Passage through the mammalian gut triggers a phenotypic switch that promotes *Candida albicans* commensalism. *Nature genetics*, 45, 1088-1091.
- Panpetch, W., Hiengrach, P., Nilgate, S., Tumwasorn, S., Somboonna, N., Wilantho, A., Chatthanathon, P., Prueksapanich, P. & Leelahavanichkul, A. 2020. Additional *Candida albicans* administration enhances the severity of dextran sulfate solution induced colitis mouse model through leaky gut-enhanced systemic inflammation and gut-dysbiosis but attenuated by *Lactobacillus rhamnosus* L34. *Gut microbes*, 11, 465-480.
- Pareek, S., Kurakawa, T., Das, B., Motooka, D., Nakaya, S., Rongsen-Chandola, T., Goyal, N., Kayama, H., Dodd, D., Okumura, R., Maeda, Y., Fujimoto, K., Nii, T., Ogawa, T., Iida, T., Bhandari, N., Kida, T., Nakamura, S., Nair, G. B. & Takeda, K. 2019. Comparison of Japanese and Indian intestinal microbiota shows diet-dependent interaction between bacteria and fungi. *NPJ Biofilms Microbiomes*, 5, 37.

- Park, C., Meng, L., Stanton, L. H., Collins, R. E., Mast, S. W., Yi, X., Strachan, H. & Moremen, K. W. 2005. Characterization of a human core-specific lysosomal {alpha}1,6-mannosidase involved in N-glycan catabolism. *J Biol Chem*, 280, 37204-16.
- Patnode, M. L., Beller, Z. W., Han, N. D., Cheng, J., Peters, S. L., Terrapon, N., Henrissat, B., Le Gall, S., Saulnier, L., Hayashi, D. K., Meynier, A., Vinoy, S., Giannone, R. J., Hettich, R. L. & Gordon, J. I. 2019. Interspecies Competition Impacts Targeted Manipulation of Human Gut Bacteria by Fiber-Derived Glycans. *Cell*, 179, 59-73.e13.
- Pradhan, A., Avelar, G. M., Bain, J. M., Childers, D. S., Larcombe, D. E., Netea, M. G., Shekhova, E., Munro, C. A., Brown, G. D., Erwig, L. P., Gow, N. a. R. & Brown, A. J. P. 2018. Hypoxia Promotes Immune Evasion by Triggering β -Glucan Masking on the *Candida albicans* Cell Surface via Mitochondrial and cAMP-Protein Kinase A Signaling. *mBio*, 9, e01318-18.
- Pudlo, N. A., Urs, K., Kumar, S. S., German, J. B., Mills, D. A. & Martens, E. C. 2015. Symbiotic Human Gut Bacteria with Variable Metabolic Priorities for Host Mucosal Glycans. *mBio*, 6, e01282-15.
- Rakoff-Nahoum, S., Coyne, M. J. & Comstock, L. E. 2014. An ecological network of polysaccharide utilization among human intestinal symbionts. *Curr Biol*, 24, 40-49.
- Rakoff-Nahoum, S., Foster, K. R. & Comstock, L. E. 2016. The evolution of cooperation within the gut microbiota. *Nature*, 533, 255-259.
- Ralton, J. E., Naderer, T., Piraino, H. L., Bashtannyk, T. A., Callaghan, J. M. & Mcconville, M. J. 2003. Evidence that intracellular beta1-2 mannan is a virulence factor in *Leishmania* parasites. *J Biol Chem*, 278, 40757-63.
- Raman, R., Venkataraman, M., Ramakrishnan, S., Lang, W., Raguram, S. & Sasisekharan, R. 2006. Advancing glycomics: implementation strategies at the consortium for functional glycomics. *Glycobiology*, 16, 82r-90r.
- Raschke, W. C., Kern, K. A., Antalis, C. & Ballou, C. E. 1973. Genetic Control of Yeast Mannan Structure: ISOLATION AND CHARACTERIZATION OF MANNAN MUTANTS. *Journal of Biological Chemistry*, 248, 4660-4666.
- Ravcheev, D. A., Godzik, A., Osterman, A. L. & Rodionov, D. A. 2013. Polysaccharides utilization in human gut bacterium *Bacteroides thetaiotaomicron*: comparative genomics reconstruction of metabolic and regulatory networks. *BMC genomics*, 14, 873-873.

- Reddy, S. K., Bågenholm, V., Pudlo, N. A., Bouraoui, H., Koropatkin, N. M., Martens, E. C. & Stålbbrand, H. 2016. A β -mannan utilization locus in *Bacteroides ovatus* involves a GH36 α -galactosidase active on galactomannans. *FEBS letters*, 590, 2106-2118.
- Reeves, A. R., Wang, G. R. & Salyers, A. A. 1997. Characterization of four outer membrane proteins that play a role in utilization of starch by *Bacteroides thetaiotaomicron*. *Journal of bacteriology*, 179, 643-649.
- Rhodes, R. G., Samarasam, M. N., Shrivastava, A., Van Baaren, J. M., Pochiraju, S., Bollampalli, S. & McBride, M. J. 2010. *Flavobacterium johnsoniae* gldN and gldO are partially redundant genes required for gliding motility and surface localization of SprB. *J Bacteriol*, 192, 1201-11.
- Richard, M. L. & Sokol, H. 2019. The gut mycobiota: insights into analysis, environmental interactions and role in gastrointestinal diseases. *Nat Rev Gastroenterol Hepatol*, 16, 331-345.
- Rogers, T. E., Pudlo, N. A., Koropatkin, N. M., Bell, J. S. K., Moya Balasch, M., Jasker, K. & Martens, E. C. 2013. Dynamic responses of *Bacteroides thetaiotaomicron* during growth on glycan mixtures. *Molecular microbiology*, 88, 876-890.
- Rogowski, A., Briggs, J. A., Mortimer, J. C., Tryfona, T., Terrapon, N., Lowe, E. C., Baslé, A., Morland, C., Day, A. M., Zheng, H., Rogers, T. E., Thompson, P., Hawkins, A. R., Yadav, M. P., Henrissat, B., Martens, E. C., Dupree, P., Gilbert, H. J. & Bolam, D. N. 2015. Glycan complexity dictates microbial resource allocation in the large intestine. *Nature communications*, 6, 7481-7481.
- Roth, J., Ziak, M. & Zuber, C. 2003. The role of glucosidase II and endomannosidase in glucose trimming of asparagine-linked oligosaccharides. *Biochimie*, 85, 287-294.
- Rye, C. S. & Withers, S. G. 2000. Glycosidase mechanisms. *Current Opinion in Chemical Biology*, 4, 573-580.
- Saijo, S., Fujikado, N., Furuta, T., Chung, S.-H., Kotaki, H., Seki, K., Sudo, K., Akira, S., Adachi, Y., Ohno, N., Kinjo, T., Nakamura, K., Kawakami, K. & Iwakura, Y. 2007. Dectin-1 is required for host defense against *Pneumocystis carinii* but not against *Candida albicans*. *Nature Immunology*, 8, 39-46.
- Saijo, S., Ikeda, S., Yamabe, K., Kakuta, S., Ishigame, H., Akitsu, A., Fujikado, N., Kusaka, T., Kubo, S., Chung, S.-H., Komatsu, R., Miura, N., Adachi, Y., Ohno, N., Shibuya, K., Yamamoto, N., Kawakami, K., Yamasaki, S., Saito, T., Akira, S. & Iwakura, Y. 2010. Dectin-2 Recognition of β -1-Mannans and Induction of Th17 Cell Differentiation Is Essential for Host Defense against *Candida albicans*. *Immunity*, 32, 681-691.

- Saiki, K. & Konishi, K. 2007. Identification of a *Porphyromonas gingivalis* novel protein required for the secretion of gingipains. *Microbiol Immunol*, 51, 483-91.
- Saiki, K. & Konishi, K. 2014. *Porphyromonas gingivalis* C-terminal signal peptidase PG0026 and HagA interact with outer membrane protein PG27/LptO. *Mol Oral Microbiol*, 29, 32-44.
- Sanchez-Romero, J. M., Diaz-Orejas, R. & De Lorenzo, V. 1998. Resistance to tellurite as a selection marker for genetic manipulations of *Pseudomonas* strains. *Appl Environ Microbiol*, 64, 4040-6.
- Sato, K., Naito, M., Yukitake, H., Hirakawa, H., Shoji, M., McBride, M. J., Rhodes, R. G. & Nakayama, K. 2010. A protein secretion system linked to bacteroidete gliding motility and pathogenesis. *Proceedings of the National Academy of Sciences*, 107, 276.
- Sato, K., Sakai, E., Veith, P. D., Shoji, M., Kikuchi, Y., Yukitake, H., Ohara, N., Naito, M., Okamoto, K., Reynolds, E. C. & Nakayama, K. 2005. Identification of a new membrane-associated protein that influences transport/maturation of gingipains and adhesins of *Porphyromonas gingivalis*. *J Biol Chem*, 280, 8668-77.
- Schirmer, M., Smeekens, S. P., Vlamakis, H., Jaeger, M., Oosting, M., Franzosa, E. A., Ter Horst, R., Jansen, T., Jacobs, L., Bonder, M. J., Kurilshikov, A., Fu, J., Joosten, L. a. B., Zhernakova, A., Huttenhower, C., Wijmenga, C., Netea, M. G. & Xavier, R. J. 2016. Linking the Human Gut Microbiome to Inflammatory Cytokine Production Capacity. *Cell*, 167, 1125-1136.e8.
- Schultz, J., Copley, R. R., Doerks, T., Ponting, C. P. & Bork, P. 2000. SMART: a web-based tool for the study of genetically mobile domains. *Nucleic acids research*, 28, 231-234.
- Schwan, W. R., Beck, M. T., Hung, C. S. & Hultgren, S. J. 2018. Differential Regulation of *Escherichia coli* fim Genes following Binding to Mannose Receptors. *Journal of pathogens*, 2018, 2897581-2897581.
- Seers, C. A., Slakeski, N., Veith, P. D., Nikolof, T., Chen, Y.-Y., Dashper, S. G. & Reynolds, E. C. 2006. The RgpB C-terminal domain has a role in attachment of RgpB to the outer membrane and belongs to a novel C-terminal-domain family found in *Porphyromonas gingivalis*. *Journal of bacteriology*, 188, 6376-6386.
- Serneer, M. F., Ralton, J. E., Nero, T. L., Sobala, L. F., Kloehn, J., Vieira-Lara, M. A., Cobbold, S. A., Stanton, L., Pires, D. E. V., Hanssen, E., Males, A., Ward, T., Bastidas, L. M., Van Der Peet, P. L., Parker, M. W., Ascher, D. B., Williams, S. J., Davies, G. J. & Mcconville, M. J. 2019. A Family of Dual-Activity Glycosyltransferase-

Phosphorylases Mediates Mannogen Turnover and Virulence in Leishmania Parasites. *Cell Host & Microbe*, 26, 385-399.e9.

- Sherrington, S. L., Sorsby, E., Mahtey, N., Kumwenda, P., Lenardon, M. D., Brown, I., Ballou, E. R., Maccallum, D. M. & Hall, R. A. 2017. Adaptation of *Candida albicans* to environmental pH induces cell wall remodelling and enhances innate immune recognition. *PLoS pathogens*, 13, e1006403-e1006403.
- Shibata, N., Arai, M., Haga, E., Kikuchi, T., Najima, M., Satoh, T., Kobayashi, H. & Suzuki, S. 1992. Structural identification of an epitope of antigenic factor 5 in mannans of *Candida albicans* NIH B-792 (serotype B) and J-1012 (serotype A) as beta-1,2-linked oligomannosyl residues. *Infect Immun*, 60, 4100-10.
- Shibata, N., Suzuki, A., Kobayashi, H. & Okawa, Y. 2007. Chemical structure of the cell-wall mannan of *Candida albicans* serotype A and its difference in yeast and hyphal forms. *The Biochemical journal*, 404, 365-372.
- Shipman, J. A., Cho, K. H., Siegel, H. A. & Salyers, A. A. 1999. Physiological characterization of SusG, an outer membrane protein essential for starch utilization by *Bacteroides thetaiotaomicron*. *Journal of bacteriology*, 181, 7206-7211.
- Shoji, M., Ratnayake, D. B., Shi, Y., Kadowaki, T., Yamamoto, K., Yoshimura, F., Akamine, A., Curtis, M. A. & Nakayama, K. 2002. Construction and characterization of a nonpigmented mutant of *Porphyromonas gingivalis*: cell surface polysaccharide as an anchorage for gingipains. *Microbiology (Reading)*, 148, 1183-1191.
- Shoji, M., Sato, K., Yukitake, H., Kondo, Y., Narita, Y., Kadowaki, T., Naito, M. & Nakayama, K. 2011. Por Secretion System-Dependent Secretion and Glycosylation of *Porphyromonas gingivalis* Hemin-Binding Protein 35. *PLOS ONE*, 6, e21372.
- Shrivastava, A., Johnston, J. J., Van Baaren, J. M. & McBride, M. J. 2013. *Flavobacterium johnsoniae* GldK, GldL, GldM, and SprA are required for secretion of the cell surface gliding motility adhesins SprB and RemA. *Journal of bacteriology*, 195, 3201-3212.
- Sievers, F. & Higgins, D. G. 2018. Clustal Omega for making accurate alignments of many protein sequences. *Protein Science*, 27, 135-145.
- Singh, R. K., Chang, H. W., Yan, D., Lee, K. M., Ucmak, D., Wong, K., Abrouk, M., Farahnik, B., Nakamura, M., Zhu, T. H., Bhutani, T. & Liao, W. 2017. Influence of diet on the gut microbiome and implications for human health. *J Transl Med*, 15, 73.
- Skorupski, K. & Taylor, R. K. 1996. Positive selection vectors for allelic exchange. *Gene*, 169, 47-52.

- Sonnenburg, E. D., Sonnenburg, J. L., Manchester, J. K., Hansen, E. E., Chiang, H. C. & Gordon, J. I. 2006. A hybrid two-component system protein of a prominent human gut symbiont couples glycan sensing in vivo to carbohydrate metabolism. *Proceedings of the National Academy of Sciences of the United States of America*, 103, 8834-8839.
- Sonnenburg, E. D., Zheng, H., Joglekar, P., Higginbottom, S. K., Firbank, S. J., Bolam, D. N. & Sonnenburg, J. L. 2010. Specificity of polysaccharide use in intestinal bacteroides species determines diet-induced microbiota alterations. *Cell*, 141, 1241-1252.
- Sonnenburg, J. L., Xu, J., Leip, D. D., Chen, C.-H., Westover, B. P., Weatherford, J., Buhler, J. D. & Gordon, J. I. 2005. Glycan Foraging in Vivo by an Intestine-Adapted Bacterial Symbiont. *Science*, 307, 1955.
- Spaulding, C. N., Klein, R. D., Ruer, S., Kau, A. L., Schreiber, H. L., Cusumano, Z. T., Dodson, K. W., Pinkner, J. S., Fremont, D. H., Janetka, J. W., Remaut, H., Gordon, J. I. & Hultgren, S. J. 2017. Selective depletion of uropathogenic *E. coli* from the gut by a FimH antagonist. *Nature*, 546, 528-532.
- Spiro, M. J., Bhojroo, V. D. & Spiro, R. G. 1997. Molecular cloning and expression of rat liver endo-alpha-mannosidase, an N-linked oligosaccharide processing enzyme. *J Biol Chem*, 272, 29356-63.
- Standaert-Vitse, A., Jouault, T., Vandewalle, P., Mille, C., Seddik, M., Sendid, B., Mallet, J. M., Colombel, J. F. & Poulain, D. 2006. *Candida albicans* is an immunogen for anti-*Saccharomyces cerevisiae* antibody markers of Crohn's disease. *Gastroenterology*, 130, 1764-75.
- Suits, M. D. L., Zhu, Y., Taylor, E. J., Walton, J., Zechel, D. L., Gilbert, H. J. & Davies, G. J. 2010. Structure and kinetic investigation of *Streptococcus pyogenes* family GH38 alpha-mannosidase. *PloS one*, 5, e9006-e9006.
- Swidergall, M. 2019. *Candida albicans* at Host Barrier Sites: Pattern Recognition Receptors and Beyond. *Pathogens (Basel, Switzerland)*, 8, 40.
- Taillefer, M., Arntzen, M. Ø., Henrissat, B., Pope, P. B. & Larsbrink, J. 2018. Proteomic Dissection of the Cellulolytic Machineries Used by Soil-Dwelling &em>Bacteroidetes. *mSystems*, 3, e00240-18.
- Tamura, K., Hemsworth, G. R., Déjean, G., Rogers, T. E., Pudlo, N. A., Urs, K., Jain, N., Davies, G. J., Martens, E. C. & Brumer, H. 2017. Molecular Mechanism by which Prominent Human Gut Bacteroidetes Utilize Mixed-Linkage Beta-Glucans, Major Health-Promoting Cereal Polysaccharides. *Cell reports*, 21, 417-430.

- Temple, M. J., Cuskin, F., Baslé, A., Hickey, N., Speciale, G., Williams, S. J., Gilbert, H. J. & Lowe, E. C. 2017. A Bacteroidetes locus dedicated to fungal 1,6- β -glucan degradation: Unique substrate conformation drives specificity of the key endo-1,6- β -glucanase. *The Journal of biological chemistry*, 292, 10639-10650.
- Terrapon, N., Lombard, V., Drula, É., Lapébie, P., Al-Masaudi, S., Gilbert, H. J. & Henrissat, B. 2018. PULDB: the expanded database of Polysaccharide Utilization Loci. *Nucleic Acids Research*, 46, D677-D683.
- Thompson, A. J., Cuskin, F., Spears, R. J., Dabin, J., Turkenburg, J. P., Gilbert, H. J. & Davies, G. J. 2015. Structure of the GH76 α -mannanase homolog, BT2949, from the gut symbiont *Bacteroides thetaiotaomicron*. *Acta Crystallogr D Biol Crystallogr*, 71, 408-15.
- Thompson, A. J., Williams, R. J., Hakki, Z., Alonzi, D. S., Wennekes, T., Gloster, T. M., Songsrirote, K., Thomas-Oates, J. E., Wrodnigg, T. M., Spreitz, J., Stütz, A. E., Butters, T. D., Williams, S. J. & Davies, G. J. 2012. Structural and mechanistic insight into N-glycan processing by endo- α -mannosidase. *Proceedings of the National Academy of Sciences of the United States of America*, 109, 781-786.
- Townsend, G. E., Raghavan, V., Zwir, I. & Groisman, E. A. 2013. Intramolecular arrangement of sensor and regulator overcomes relaxed specificity in hybrid two-component systems. *Proceedings of the National Academy of Sciences*, 110, E161.
- Trunk, K., Peltier, J., Liu, Y.-C., Dill, B. D., Walker, L., Gow, N. a. R., Stark, M. J. R., Quinn, J., Strahl, H., Trost, M. & Coulthurst, S. J. 2018. The type VI secretion system deploys antifungal effectors against microbial competitors. *Nature Microbiology*, 3, 920-931.
- Turnbaugh, P. J., Ley, R. E., Hamady, M., Fraser-Liggett, C. M., Knight, R. & Gordon, J. I. 2007. The Human Microbiome Project. *Nature*, 449, 804-810.
- Tuson, H. H., Foley, M. H., Koropatkin, N. M. & Biteen, J. S. 2018. The Starch Utilization System Assembles around Stationary Starch-Binding Proteins. *Biophysical journal*, 115, 242-250.
- Underhill, D. M. & Iliev, I. D. 2014. The mycobiota: interactions between commensal fungi and the host immune system. *Nature Reviews Immunology*, 14, 405-416.
- Valguarnera, E., Scott, N. E., Azimzadeh, P. & Feldman, M. F. 2018. Surface Exposure and Packing of Lipoproteins into Outer Membrane Vesicles Are Coupled Processes in *Bacteroides*. *mSphere*, 3, e00559-18.

- Vallée, F., Lipari, F., Yip, P., Sleno, B., Herscovics, A. & Howell, P. L. 2000. Crystal structure of a class I alpha1,2-mannosidase involved in N-glycan processing and endoplasmic reticulum quality control. *The EMBO journal*, 19, 581-588.
- Van Den Elsen, J. M., Kuntz, D. A. & Rose, D. R. 2001. Structure of Golgi alpha-mannosidase II: a target for inhibition of growth and metastasis of cancer cells. *The EMBO journal*, 20, 3008-3017.
- Vautier, S., Drummond, R. A., Redelinghuys, P., Murray, G. I., Maccallum, D. M. & Brown, G. D. 2012. Dectin-1 is not required for controlling *Candida albicans* colonization of the gastrointestinal tract. *Infect Immun*, 80, 4216-22.
- Veith, P. D., Glew, M. D., Gorasia, D. G. & Reynolds, E. C. 2017. Type IX secretion: the generation of bacterial cell surface coatings involved in virulence, gliding motility and the degradation of complex biopolymers. *Molecular Microbiology*, 106, 35-53.
- Veith, P. D., Nor Muhammad, N. A., Dashper, S. G., Likić, V. A., Gorasia, D. G., Chen, D., Byrne, S. J., Catmull, D. V. & Reynolds, E. C. 2013. Protein Substrates of a Novel Secretion System Are Numerous in the Bacteroidetes Phylum and Have in Common a Cleavable C-Terminal Secretion Signal, Extensive Post-Translational Modification, and Cell-Surface Attachment. *Journal of Proteome Research*, 12, 4449-4461.
- Venkatesan, M., Kuntz, D. A. & Rose, D. R. 2009. Human lysosomal alpha-mannosidases exhibit different inhibition and metal binding properties. *Protein science : a publication of the Protein Society*, 18, 2242-2251.
- Verster, A. J., Ross, B. D., Radey, M. C., Bao, Y., Goodman, A. L., Mougous, J. D. & Borenstein, E. 2017. The Landscape of Type VI Secretion across Human Gut Microbiomes Reveals Its Role in Community Composition. *Cell host & microbe*, 22, 411-419.e4.
- Vincent, M. S., Durand, E. & Cascales, E. 2016. The PorX Response Regulator of the *Porphyromonas gingivalis* PorXY Two-Component System Does Not Directly Regulate the Type IX Secretion Genes but Binds the PorL Subunit. *Frontiers in cellular and infection microbiology*, 6, 96-96.
- Vincze, T., Posfai, J. & Roberts, R. J. 2003. NEBcutter: A program to cleave DNA with restriction enzymes. *Nucleic Acids Res*, 31, 3688-91.
- Vuong, T. V. & Wilson, D. B. 2010. Glycoside hydrolases: catalytic base/nucleophile diversity. *Biotechnol Bioeng*, 107, 195-205.
- Wang, Y.-C., Peterson, S. E. & Loring, J. F. 2014. Protein post-translational modifications and regulation of pluripotency in human stem cells. *Cell Research*, 24, 143-160.

- Wexler, A. G., Bao, Y., Whitney, J. C., Bobay, L.-M., Xavier, J. B., Schofield, W. B., Barry, N. A., Russell, A. B., Tran, B. Q., Goo, Y. A., Goodlett, D. R., Ochman, H., Mougous, J. D. & Goodman, A. L. 2016. Human symbionts inject and neutralize antibacterial toxins to persist in the gut. *Proceedings of the National Academy of Sciences*, 113, 3639.
- Witchley, J. N., Penumetcha, P., Abon, N. V., Woolford, C. A., Mitchell, A. P. & Noble, S. M. 2019. Candida albicans Morphogenesis Programs Control the Balance between Gut Commensalism and Invasive Infection. *Cell Host Microbe*, 25, 432-443.e6.
- Xu, J., Mahowald, M. A., Ley, R. E., Lozupone, C. A., Hamady, M., Martens, E. C., Henrissat, B., Coutinho, P. M., Minx, P., Latreille, P., Cordum, H., Van Brunt, A., Kim, K., Fulton, R. S., Fulton, L. A., Clifton, S. W., Wilson, R. K., Knight, R. D. & Gordon, J. I. 2007. Evolution of symbiotic bacteria in the distal human intestine. *PLoS Biol*, 5, e156.
- Yan, L., Xia, K., Yu, Y., Miliakos, A., Chaturvedi, S., Zhang, F., Chen, S., Chaturvedi, V. & Linhardt, R. J. 2020. Unique Cell Surface Mannan of Yeast Pathogen Candida auris with Selective Binding to IgG. *ACS Infectious Diseases*, 6, 1018-1031.
- Yao, J., Nellas, R. B., Glover, M. M. & Shen, T. 2011. Stability and Sugar Recognition Ability of Ricin-like Carbohydrate Binding Domains. *Biochemistry*, 50, 4097-4104.
- Young, M., Davies, M. J., Bailey, D., Gradwell, M. J., Smestad-Paulsen, B., Wold, J. K., Barnes, R. M. R. & Hounsell, E. F. 1998. Characterization of oligosaccharides from an antigenic mannan of Saccharomyces cerevisiae. *Glycoconjugate Journal*, 15, 815-822.
- Ze, X., Duncan, S. H., Louis, P. & Flint, H. J. 2012. Ruminococcus bromii is a keystone species for the degradation of resistant starch in the human colon. *The ISME journal*, 6, 1535-1543.
- Zechel, D. L. & Withers, S. G. 2000. Glycosidase mechanisms: anatomy of a finely tuned catalyst. *Acc Chem Res*, 33, 11-8.
- Zhou, W., Sailani, M. R., Contrepois, K., Zhou, Y., Ahadi, S., Leopold, S. R., Zhang, M. J., Rao, V., Avina, M., Mishra, T., Johnson, J., Lee-Mcmullen, B., Chen, S., Metwally, A. A., Tran, T. D. B., Nguyen, H., Zhou, X., Albright, B., Hong, B.-Y., Petersen, L., Bautista, E., Hanson, B., Chen, L., Spakowicz, D., Bahmani, A., Salins, D., Leopold, B., Ashland, M., Dagan-Rosenfeld, O., Rego, S., Limcaoco, P., Colbert, E., Allister, C., Perelman, D., Craig, C., Wei, E., Chaib, H., Hornburg, D., Dunn, J., Liang, L., Rose, S. M. S.-F., Kukurba, K., Piening, B., Rost, H., Tse, D., Mclaughlin, T., Sodergren, E., Weinstock, G. M. & Snyder, M. 2019. Longitudinal multi-omics of host-microbe dynamics in prediabetes. *Nature*, 569, 663-671.

- Zhu, Y. & McBride, M. J. 2014. Deletion of the *Cytophaga hutchinsonii* type IX secretion system gene *sprP* results in defects in gliding motility and cellulose utilization. *Appl Microbiol Biotechnol*, 98, 763-75.
- Zhu, Y., Suits, M. D. L., Thompson, A. J., Chavan, S., Dinev, Z., Dumon, C., Smith, N., Moremen, K. W., Xiang, Y., Siriwardena, A., Williams, S. J., Gilbert, H. J. & Davies, G. J. 2010. Mechanistic insights into a Ca²⁺-dependent family of alpha-mannosidases in a human gut symbiont. *Nature chemical biology*, 6, 125-132.
- Zimmermann, M., Zimmermann-Kogadeeva, M., Wegmann, R. & Goodman, A. L. 2019. Mapping human microbiome drug metabolism by gut bacteria and their genes. *Nature*, 570, 462-467.
- Zmora, N., Suez, J. & Elinav, E. 2019. You are what you eat: diet, health and the gut microbiota. *Nature Reviews Gastroenterology & Hepatology*, 16, 35-56.
- Znaidi, S., Van Wijlick, L., Hernández-Cervantes, A., Sertour, N., Desseyn, J.-L., Vincent, F., Atanassova, R., Gouyer, V., Munro, C. A., Bachellier-Bassi, S., Dalle, F., Jouault, T., Bognoux, M.-E. & D'enfert, C. 2018. Systematic gene overexpression in *Candida albicans* identifies a regulator of early adaptation to the mammalian gut. *Cellular microbiology*, 20, e12890-e12890.

Appendix A

Ingredients composing Defined medium used throughout this study are listed in the table below.

Media	Component	Amount per litre	Details
Defined Medium	10X Bacteroides Salts	200 ml	Bring volume to 1 L with distilled water, filter sterilise
	Balch's Vitamins	20 ml	
	Trace Mineral Solution	20 ml	
	Purine/Pyrimidine Solution	20 ml	
	Amino acid solution	20 ml	
	Vitamin K solution, 1 mg ml ⁻¹	2 ml	
	0.8% CaCl ₂	2 ml	
	FeSO ₄ , 0.4 mg ml ⁻¹	2 ml	
	MgCl ₂ , 0.1 M	2 ml	
	Hematin Histidine	2 ml	
	Vitamin B ₁₂ , 0.01 mg ml ⁻¹	1 ml	
	L-Cysteine (Sigma-Aldrich)	2 g	
Balch's Vitamins	p-Aminobenzoic acid	5 mg	Dissolve in distilled water, pH 7.0. Keep in the dark at 4 °C
	Folic Acid	2 mg	
	Biotin	2 mg	
	Nicotinic acid	5 mg	
	Calcium pantothenate	5 mg	
	Riboflavin	5 mg	

Media	Component	Amount per litre	Details
	Thiamine HCl	5 mg	
	Pyridoxine HCl	10 mg	
	Cyanocobalamin	0.1 mg	
	Thioctic acid	5 mg	
Amino Acid solution	Alanine, Arginine, Asparagine, Aspartic Acid, Cysteine, Glutamic Acid, Glutamine, Glycine, Histidine, Isoleucine, Leucine, Lysine, Methionine, Phenylalanine, Proline, Serine, Threonine, Tryptophan, Tyrosine, Valine	250 mg each	Dissolve in distilled water, filter sterilise
Trace Mineral Supplement	EDTA	0.5 g	Dissolve in distilled water, filter sterilise
	MgSO ₄ *7H ₂ O	3 g	
	MnSO ₄ *H ₂ O	0.5 g	
	NaCl	1 g	
	FeSO ₄ *7H ₂ O	0.1 g	
	CaCl ₂	0.1 g	
	ZnSO ₄ *7H ₂ O	0.1 g	
	CuSO ₄ *5H ₂ O	10 mg	

Media	Component	Amount per litre	Details
	$H_3BO_3 \cdot 2H_2O$	10 mg	
	$Na_2MoO_4 \cdot 2H_2O$	10 mg	
	$NiCl_2 \cdot 6H_2O$	20 mg	
10X Bacteroides Salts	KH_2PO_4	544 g	Dissolve in distilled water and pH to 7.2, filter sterilise
	NaCl	35 g	
	$(NH_4)_2SO_4$	45 g	
Purine/Pyrimidine solution	Adenine, Guanine, Thymine, Cytosine, Uracil	200 mg each	Dissolve in distilled water, pH 7.0, filter sterilise

